THE CHEMICAL COMPOSITION OF FOGS AND CLOUDS IN SOUTHERN CALIFORNIA

Thesis by

James William Munger

In Partial Fulfillment of the Requirements
for the Degree of
Doctor of Philosophy

California Institute of Technology
Pasadena, California
1989

(submitted July 25, 1988)

Dedicated to my children, Missy and Michael

I've looked at clouds from both sides now,
but still somehow it's clouds' illusions I recall
I really don't know clouds at all.

from "Both sides now"
by Joni Mitchell (1968)

ACKNOWLEDGEMENTS

This research has been supported by the California Air Resources Board.

I thank my wife, Marcia, my parents, and my in–laws for their support and encouragement, and understanding when my patience was worn thin. I thank my many colleagues at Caltech for their help and friendship throughout my years there. I extend special thanks to my comrades on the Fog Squad (Daniel Jacob and Jed Waldman who with myself were the original crew and Jeff Collett, Bruce Daube, and Dieter Gunz, the current members) who shared many lonely nights in search of fog and spent long tedious hours in the lab analyzing thousands of samples over the years. I thank the research assistants who have helped us over the years; Carol Choy, Gary Gibb, Walter Chong, and Aram Kaloustian. Eric Betterton and Terri Olson shared their ideas on the chemistry of aldehyde–bisulfite adducts. I thank my advisor Michael Hoffman for getting me to come to Caltech, encouraging me to stay, and providing his guidance over the years. I thank my committee members, Jim Morgan, John Seinfeld, Fred Shair, and Yuk Yung, for their inputs. I thank Rayma Harrison, Gunilla Hastrup, and Jeanne Meyer for their help in the library. I thank Sandy Brooks and Elaine Granger for their secretarial assistance. I thank Nancy Tomer for her drafting.

The Air Resources Board, the South Coast Air Quality Management District, and the Ventura County Air Pollution Control District provided pollutant concentration and emission data. Weather forecasts and meteorological data were provided by the National Weather Service and the Air Resources Board.

The field studies that make up this thesis could not have been done without the cooperation of many individuals and organizations who allowed us access to sampling sites. These include Bob Musselman of U.C. Riverside, the South Coast Air Quality Management District, The California Air Resources Board, Monitoring Division, the U. S. Navy, Pacific Missile Test Center, the Federal Aviation

Administratiön, Santa Barbara and Los Angeles Offices, and Avenue Cable TV of Ventura.

Abstract

Fogs and clouds are frequent occurrences in Southern California. Their chemical composition is of interest due to their potential role in the transformation of sulfur and nitrogen oxides to sulfuric and nitric acid and in the subsequent deposition of those acids. In addition, cloud and fog droplets may be involved in the chemistry of low–molecular–weight carboxylic acids and carbonyl compounds.

The major inorganic species in cloud and fogwater samples were NH_4^+, H^+, NO_3^-, and SO_4^{2-}. Concentrations in fogwater samples were $1 - 10 \times 10^{-3}$ **M**; pH values ranged from ≃2 to 6. Nitrate usually exceeded sulfate. Acidity depended on the availability of of NH_3 from agricultural operations. Stratus cloudwater had somewhat lower concentrations; pH values were in the range 3 – 4. The major factors accounting for variation in fog– or cloudwater composition were the preexisting aerosol and gas concentrations and variations in liquid water content. Deposition and entrainment or advection of different air masses were also important during extended cloud or fog episodes.

The droplet size dependence of cloudwater composition was investigated on one occasion in an intercepted coastal stratus clouds. The observations were consistent with the hypothesis that small droplets form on small secondary aerosol composed of H_2SO_4, HNO_3, and their NH_4^+ salts, while large droplets form on large sea–salt and soil–dust aerosol. Species that can exist in the gas phase, such as HCl and HNO_3, may be found in either droplet–size fraction.

Concentrations of S(IV) and CH_2O in the range 100 – 1000 μ**M** were observed in fogwater from urban sites in Southern California. Lower concentrations were observed in stratus clouds. The high levels of S(IV) and CH_2O were attributed to the formation of hydroxymethanesulfonate (HMSA), the S(IV) adduct of CH_2O. Direct measurement of HMSA in fogwater samples from Bakersfield, CA were made by ion–pairing chromatography. Glyoxal and methylglyoxal were observed at concentrations comparable to CH_2O in fogwater samples from Riverside, CA and in stratus cloudwater samples from sites along the Santa Barbara Channel.

TABLE OF CONTENTS

List of Figures

Figure

List of Tables

Table

CHAPTER 1

INTRODUCTION: CHEMICAL AND PHYSICAL PROCESSES IN STRATUS CLOUDS AND FOGS

The chemical composition of non–precipitating clouds and fogs is of considerable interest. Fogs have been implicated as a contributing factor in adverse human health effects, materials damage, and plant injury from air pollution. For example, many of the most disastrous pollution episodes have been associated with fogs (Hoffmann, 1984). In some coastal and mountain areas, deposition of moisture and solutes by intercepted clouds is often comparable to that of precipitation in forests (Azvedo and Morgan, 1974; Cowling, 1985; Johnson and Siccama, 1983; Lovett, 1984). On a global basis, clouds are the principal site for the oxidation of SO_2 to SO_4^{2-} and the concomitant production of acidity. On a local scale, S(IV) to S(VI) oxidation in the Los Angeles basin appears to be linked to the occurrence of fogs and high humidity (see Figure 1.1) (Cass and Shair, 1984). Field studies at Great Dun Fell (Chandler et al., 1988) have shown that SO_2 is oxidized rapidly in clouds by hydrogen peroxide.

The chemical composition of clouds and fogs is controlled by a combination of chemical and physical processes. On the scale of an individual droplet, the important processes are mass transfer across the droplet interface, mixing within the droplet, chemical equilibrium speciation, and kinetics of transformation. Mass transfer by turbulence and advection, heat transfer, droplet deposition, pollutant emissions, and chemical reactions must be considered on the scale of an entire cloud or fog bank.

Theoretical Considerations

Clouds (or fogs) consist of water droplets, which are typically 2 – 50 μm in diameter, suspended in air. The liquid water content (LWC) ranges from 0.1 to 1.0 g m^{-3} in clouds and 0.01 to 0.5 g m^{-3} in fogs. Stratiform clouds, which are the focus of this discussion, have LWC at the low end of the range for clouds. Chemical species in clouds exist in three phases; inside the droplets, as gases, and as interstitial aerosol. The total concentration of species i in a cloud or fog is given by

$$[C_i]_T = [C_i]_l \cdot L + P_i(RT)^{-1} + [C_i]_a \qquad (1)$$

where $[C_i]_T$ is the total concentration of species i (mol m^{-3}) in the atmosphere, $[C_i]_l$ is the concentration of species i in the droplet phase (**M**), L is the LWC (dm^3 m^{-3}), P_i is the partial pressure of species i in the gas phase (atm), R is the universal gas constant (m^3atm $K^{-1}mol^{-1}$), T is the absolute temperature (K), and $[C_i]_a$ is the concentration of species i in the aerosol.

The overall process of nucleation scavenging and gas dissolution is depicted in Figure 1.2. Much of the solute mass in a cloud or fog droplet is derived from the nuclei it formed on. Gases are assumed to partition into the droplet according to chemical equilibria.

Aerosol Scavenging

The partitioning of species i among the phases depends on its physical and chemical characteristics. For species that are normally present as aerosol, particle size is critical. When droplets form, they condense on preexisting particles, known as condensation nuclei. The condensation of water is described by the droplet growth equation (Table 1.1). A droplet at equilibrium with its surroundings maintains a constant size (ie. $dD_o/dt = 0$). The equilibrium solutions of the droplet growth equation for different size particles yields the Köhler curves (Figure 1.3) Hygroscopic aerosol are activated and form droplets when the supersaturation exceeds a critical value (SS_{CR}), corresponding to the maximum in the Köhler curve. The value of (SS_{CR}) depends on aerosol size; (SS_{CR}) increases for smaller aerosol. For the supersaturations typically encountered in clouds and fogs the minimum aerosol size to be activated is about 0.1 μm (Pruppacher and Klett, 1978). Aerosol smaller than this will not grow into droplets. The unactivated aerosol may be incorporated into droplets via diffusion or impaction. Diffusion is important for very small aerosol; impaction affects large aerosol more strongly.

Saturation with respect to water vapor in a cloud or fog is controlled by the rate and extent of cooling, which in turn is determined by the turbulence and radiation budget of the cloud or fog. Adiabatic cooling from vertical motion in the atmosphere leads to higher supersaturations. Radiation cooling is much slower and leads to lower supersaturations. Once an air parcel exceeds saturation, droplet growth will tend to reduce the supersaturation. The removal rate for water vapor will be limited by the surface area available for condensation, which is a function of aerosol size and number concentration.

The number of cloud condensation nuclei, CCN, in the atmosphere is highly variable (Pruppacher and Klett, 1978) Over the oceans and at high elevation the number of CCN is usually ≤ 100 cm^{-3}, while values ≥ 1000 cm^{-3} are observed in continental air masses. On a global scale the majority of the CCN in the atmosphere are thought to be ammonium sulfate salts. Even over the remote oceans, the production of sea salt aerosol is insufficient to account for the number of CCN present. Measurements of aerosol volatility (Clarke et al., 1987) are further evidence for the unimportance of NaCl as CCN. Natural emissions of reduced sulfur gases such as $(CH_3)_2S$ are considered to be the source of background CCN. A variety of primary and secondary aerosol are present in urban and near urban areas. The nature of CCN over continents will reflect local and regional emission characteristics.

The difference in CCN number between urban and remote air masses and with elevation affects the characteristics of the clouds and fogs that form there. When the number of CCN is small condensation of water is limited by the available surface area, which results in higher supersaturation. When the number of CCN is large, however, condensation of water will be sufficient to keep the supersaturation low, and some of the smallest nuclei may remain unactivated. Clouds that formed under low CCN conditions have been observed to have broad droplet-size distributions weighted towards large diameters. Furthermore, these clouds tended to be broken (Allbrecht et al. 1985). In polluted or continental air, which has higher numbers of CCN, clouds have narrower droplet size distributions that are skewed towards smaller drop size (Allbrecht et al., 1985; Barrett et al., 1979; Noonkester, 1984). Because the droplet–size spectra influences cloud optical properties (Noonkester, 1985), the distribution of CCN in the atmosphere has implications for the global radiation balance.

Equilibrium Gas Scavenging

Scavenging of gaseous species depends on their equilibrium dissolution. Mass transfer will govern the time required to reach equilibrium, however (Schwartz and Frieberg, 1981). The equilibrium concentration of species i in the droplet is governed by

$$[C_i]_l = P_i \cdot H_i \tag{2}$$

where H_i is the Henry's Law coefficient (**M** atm^{-1}). The total concentration of dissolved gas is increased if it undergoes further reaction such as acid dissociation, hydration, or complexation.

Acid–base equilibria can be described by

$$HA \overset{K_{a1}}{\rightleftharpoons} H^+ + A^- \tag{3}$$

where HA and A^- are any acid and its conjugate base, respectively, and K_{a_1} is the acid dissociation constant. The equilibrium dissolution of acidic (or basic) species is given by

$$[C_i]^*_l = P_i \cdot H_i(\alpha_{0_i})^{-1} \tag{4}$$

where the * denotes total concentration and α_{0_i} is the fraction of undissociated species i that is in direct equilibrium with the gas phase. The product $H_i(\alpha_{0_i})^{-1}$ can be replaced by an effective Henry's Law coefficient, H^*.

Carbonyl compounds hydrate in aqueous solution according to

$$RCHO + H_2O \overset{K_H}{\rightleftharpoons} RCH(OH)_2 \tag{5}$$

where K_H is the hydration constant. Equilibrium dissolution of carbonyls is governed by the effective Henry's Law coefficient $H^* = H \cdot K_H$.

Formation of hydroxyalkyl sulfonates from the addition of S(IV) to carbonyls appears to be an important set of reactions in clouds and fogs:

$$RCHO + HSO_3^- \overset{k_1}{\rightleftharpoons} RCH(OH)SO_3^- \tag{6}$$

$$RCHO + SO_3^{2-} \overset{k_2}{\rightleftharpoons} RCH(O^-)SO_3^- \tag{7}$$

$$RCH(OH)SO_3^- \overset{K_{a2}}{\rightleftharpoons} H^+ + RCH(O^-)SO_3^- \tag{8}$$

At the pH normally encountered in clouds and fogs sulfonates are present in the monoprotic form. The intrinsic equilibrium expression for sulfonate formation is given by

$$K_{s1} = \frac{[RCH(OH)SO_3^-]}{[RCHO]\,[HSO_3^-]} \tag{9}$$

where [RCHO] is the concentration of unhydrated carbonyl. A linear free energy relationship has been observed between K_{s1} and K_H (Olson and Hoffmann, 1988a). The most soluble carbonyls also have the largest sulfonate stability constants.

The overall fraction of species i in the liquid phase is given by

$$X_i = \frac{[C_i]_l^*}{[C_i]_T} = \frac{RTH_i^*L}{[1 + RTH_i^*L]^{-1}} \tag{10}$$

where H_i^* includes the effect of all reactions that species i participates in. For strong acids like HNO_3, the fraction in the liquid phase approaches 1. Likewise, for a weak acid such as NH_3 in neutral to acid droplets, scavenging approaches 100%. The scavenging of weakly acidic species such as SO_2 or HCOOH depends strongly on the pH of the solution. In acidic clouds (or fogs) ($pH < 3$), which are frequently observed in urban and near urban environments (Jacob et al.,1985; Munger et al., 1983; 1989a;b; Waldman et al., 1982; 1985), the liquid phase will be a weak sink. Above pH 5, which can be encountered in fogs that form near NH_3 sources (Jacob et al., 1986; Munger et al., 1989a), droplets will scavenge nearly all the available SO_2 or weak acid.

Chemical Reactions

Species dissolved in cloud or fog droplets can undergo chemical transformations. Hoffmann and Calvert (1985) have evaluated recent data regarding aqueous-phase reactions relevant to acid formation. Recommended rate laws and rate constants for the oxidation of S(IV) are given in Table 2.1. In polluted environments the important oxidants for transformation of S(IV) to S(VI) are H_2O_2, O_3, and trace-metal catalysis. The formation of acidity by oxidation of S(IV) tends to be self limiting. Oxidation by O_3 and trace metal catalysis are pH-dependent; at low pH the reactions are very slow. Oxidation by H_2O_2 is rapid at low pH, but H_2O_2 is quickly depleted in the presence of SO_2 in clouds. Cloud chemistry models (Chameides, 1984; Jacob, 1986) predict that oxidation by $OH\cdot$ is important in the remote troposphere, where both SO_2 and the other oxidants are in low concentration.

In the presence of carbonyls, the formation of sulfonates (equations 6-8) could compete with S(IV) oxidation. The kinetics of this reaction have been studied for a variety of carbonyls (Boyce and Hoffmann, 1984; Betterton and Hoffman 1987; Betterton et al., 1988; Deister et al., 1986; Kok et al., 1986; Olson and Hoffmann, 1988a;b). Because SO_3^{2-} is a better nucleophile the addition of SO_3^{2-} proceeds more rapidly than the addition of HSO_3^-. As a consequence, the rate of sulfonate formation increases with pH. In a droplet, sulfonate formation and S(IV) oxidation will proceed in parallel, at a rate governed by their intrinsic rate constants, until one of the reactants is depleted. The total consumption of S(IV) cannot exceed the rate for mass transfer at the droplet interface or diffusion through the droplet, however. Because the kinetics of sulfonate dissociation are extremely slow in acid conditions (Hoigne et al, 1985; Kok et al., 1986), the sulfonates are metastable in in clouds with low P_{RCHO} and P_{SO_2}.

Because nitrogen oxides are very insoluble in water (Lee and Schwartz 1981) aqueous–phase production of HNO_3 is relatively unimportant. Formation of HNO_3 may proceed in clouds at night via the gas–phase production of N_2O_5, which would hydrolyze at the droplet surface.

$$NO_2 + O_3 \rightarrow NO_3 + O_2 \tag{11}$$

$$NO_2 + NO_3 \rightarrow N_2O_5 \tag{12}$$

$$N_2O_5 + H_2O \rightarrow 2HNO_3 \tag{13}$$

The presence of NO prevents N_2O_5 formation by reaction with NO_3.

$$NO + NO_3 \rightarrow 2NO_2 \tag{14}$$

The stable layer above a fog or cloud, which is isolated from NO emissions and often has high concentrations of O_3 compared to the boundary layer, is a favorable environment for production of N_2O_5 (Russel et al., 1985).

Model calculations have identified the potential importance of the reaction of $OH\cdot$ with CH_2O and HCOOH in remote clouds (Chameides, 1984; Jacob, 1986). These reactions may be a source or sink of HCOOH in the atmosphere, depending on cloudwater pH (Jacob, 1986).

Mass Transport Considerations

Aqueous–phase reaction of a dissolved gas involves a series of steps in which mass transport could become limiting. These steps are:

(a) Diffusion or convection within the gas phase to the droplet surface.

(b) Establishment of solubility equilibria at the droplet surface.

(c) Establishment of local hydration, dissociation and complexation equilibria.

(d) Diffusion or convection within the droplet.

(e) Chemical reaction.

(f) Readjustment of the hydration, dissociation, and complexation equilibria.

(g) Diffusion or convection induced by the concentration gradients resulting from steps (e) and (f).

Schwartz and Freiberg (1981) consider mass transport for aqueous-phase SO_2 oxidation. Seinfeld (1986) presents a general treatment. Steps (a) – (g) can be compared in terms of their characteristic times, τ, (see Table 1.3) which are the times required to reach equilibrium or establish a steady-state concentration profile. The step with the longest τ will limit the overall rate of reaction.

Physical Processes in Clouds

The physical processes important on the scale of a cloud or fog bank are horizontal advection, vertical mixing (by turbulence or convection), deposition, and emission. These processes are shown schematically in Figure 1.4. They are represented in differential form by

$$\frac{dC_i}{dt} = \vec{u}\cdot\nabla C_i + w\frac{dC_i}{dz} + \frac{E_i}{H} - \frac{C_iV_{d,i}}{H} \qquad (15)$$

where C_i is the concentration of species i, $\vec{u}$ is the horizontal wind vector, w is the vertical wind component, E_i is the emission flux, H is the height of the mixed layer, and $V_{d,i}$ is the species dependent deposition velocity. Heat and moisture fluxes need to be considered as well because they control liquid water content and vertical mixing. All the phases that a species can exist in must be considered together. Clearly this becomes a very complex system of equations even when one considers only the major species found in clouds and fogs (NH_4^+, H^+, NO_3^-, SO_4^{2-}) and their precursors.

Horizontal advection is not affected by the presence of cloud or fog and will not be discussed further. Determining the vertical fluxes of heat and moisture is a major focus of microphysical studies in cloud and fog. In general fogs and stratiform clouds form within a mixed layer that is capped by a temperature inversion. A principal difference between fogs and clouds is the depth of the mixed layer. An important feature of cloud or fog layers is that they are radiatively cooled at the top (Deardroff, 1976; 1981; Lilly and Schubert, 1980; Oliver et al., 1978). This cooling promotes turbulent mixing within the cloud and entrainment of air parcels from above the cloud layer (Caughey et al., 1982; Oliver et al., 1978; Randall, 1980a,b; Slingo et al., 1982). Additional cooling due to evaporation results from the entrainment of dry air from aloft. In a study of nocturnal stratocumulus over England, using a tethered balloon, Roach et al. (1982) calculated an entrainment velocity of ≈ 0.5 cm s^{-1}. Similar values have been observed elsewhere in stratus clouds. Shear instability across the inversion may also produce turbulence in the cloud layer (Brost et al., 1982; Caughey et al., 1982). As yet, turbulent fluxes of chemical species have not been directly measured in fogs and stratiform clouds.

Variations in the inversion height are described by

$$\frac{\partial z_i}{\partial t} + U_i\frac{\partial z_i}{\partial x} + V_i\frac{\partial z_i}{\partial y} = W_e + W_i \qquad (16)$$

where U_i and V_i are the average horizontal wind components at the inversion height, W_i is the mesoscale vertical motion, and W_e is the entrainment velocity. As noted above, typical values for W_e are ≈ 0.5 cm s^{-1}. Mesoscale subsidence induced by subtropical highs is on the order of 0.25 cm s^{-1}. The balance between subsidence and entrainment supports a periodic steady state. Oliver et al. (1978) observe a diurnal cycle in the mixed layer depth in a model of turbulent and radiative transport that is patterned after mean conditions off the California coast. The predicted maximum depth in the early morning and minimum depth in the late afternoon agree with field observations. For a 500 m mixed layer, the vertical velocities reported above give a ventilation time ($\tau_v = z_i/W$) on the order of a day. In fogs, which are much thinner than stratus clouds, the effect of entrainment would be even greater. The importance of entrainment from aloft in actual fogs is indicated by observations that H_2O_2 concentrations in a cap cloud at Great Dun Fell increased with altitude (Chandler et al., 1988).

Deposition is an important term in the water budget of clouds and fogs. Drizzle in stratus clouds can transfer significant amounts of moisture from the cloud to the subcloud layer even though no drizzle reaches the ground (Brost et al., 1982a;b). Likewise, in fogs, droplet deposition significantly affects the water budget (Brown and Roach, 1976). For a fog droplet sedimentation results in permanent removal of solutes from the layer, assuming they are retained by the ground. Solutes that are transferred to the below-cloud layer by drizzle can be mixed back into the cloud by turbulence. Waldman and Hoffmann (1987) report deposition velocities for major ions in fog of 1 – 5 cm s^{-1}, with a median value of ≈ 2 cm s^{-1}. The deposition velocities for submicron aerosol are on the order of 0.1 cm s^{-1}. Deposition velocities for gases that react with surfaces (e.g. HNO_3, NH_3) are controlled by mass transfer; typical values are on the order of 1 cm s^{-1} (Huebert and Robert, 1985). The characteristic time for removal by droplet deposition from a 100 to 500 m thick fog layer is 1.4 to 7 hours. Because they are thinner, fogs are more rapidly affected by emission and deposition than clouds. For long duration fog and cloud events removal by droplet sedimentation can significantly deplete the concentration of solutes if they are not replenished by other processes.

Because the deposition velocity for submicron aerosol is small relative the deposition of gases or fog droplets, chemical speciation in the atmosphere strongly affects a species residence time and concentration. The behavior of NO_3^- and NH_4 in a simple box model illustrate this effect. In a model patterned after the situation in Riverside, California, Munger et al. (1989a) observe high levels of NH_4^+ and NO_3^- in both aerosol and fog. Deposition during nocturnal fogs and wind reversal reduced the concentrations at night. Reduction of the NH_3 emissions would increase the proportion of N(V) present as HNO_3. However, because HNO_3 is deposited rapidly, the total concentration of N(V) would actually decrease. Similar behavior is predicted for the San Joaquin Valley (Jacob et al., 1986).

REFERENCES

Allbrecht, B. A., Penc, R. S., and Schubert, W. (1985) An observational study of cloud–topped mixed layers. *J. Atmos. Sci.* **42**, 800–822.

Azvedo, J. and Morgan, D. L. (1974) Fog precipitation in coastal California forests. *Ecology* 55,1135–1141.

Barrett, E. W., Parungo, F. P. and Pueschel, R. F. (1979) Cloud modification by urban pollution: A physical demonstration. *Meteorol. Rdsch.* **32**, 136–149.

Betterton, E. and Hoffmann, M. R. (1987) The kinetics, mechanism, and thermodynamics of the reversible reaction of methylglyoxal (CH_3COCHO) with S(IV), *J. Phys. Chem.* **91**, 3011–3020.

Betterton, E. A., Erel, Y., and Hoffmann, M. R. (1988) Aldehyde–bisulfite adducts: Prediction of some of their thermodynamic and kinetic properties, *Environ. Sci. Technol.* **22**, 92–97.

Boyce, S. D. and Hoffmann, M. R. (1984) Kinetics and mechanisms of the formation of hydroxymethanesulfonic acid at low pH, *J. Phys. Chem.* **88,** 4740–46.

Brost, R. A., Lenschow, D. H., and Wyngaard, J. C. (1982a) Marine stratocumulus layers. Part I: Mean conditions. *J. Atmos. Sci.* **39**, 800–817.

Brost, R. A., Wyngaard, J. C., and Lenschow, D. H. (1982b) Marine stratocumulus layers. Part II: Turbulence budgets. *J. Atmos. Sci.* **39**, 818–836.

Brown, R. and Roach, W. T. (1976) The physics of radiation fog: II. A numerical study. *Q. J. R. Met. Soc.* **102**, 335–354.

Cass, G. R. (1975) Envoronmental Quality Laboratory Memo #5, California Institute of Technology, Pasadena California.

Cass, G. R., and Shair, F. H. 1984. Sulfate accumulation in a sea breeze/land breeze circulation system. *J. Geophys. Res.* **89**, 1429–1438.

Caughey, S. J., Crease, B. A., and Roach, W. T. (1982) A field study of nocturnal stratocumulus: II. Turbulence structure and entrainment. *Quart J. R. Met. Soc.* **108**, 125–144.

Chameides, W. L. (1984) The photochemistry of a remote marine stratiform cloud, *J. Geophys. Res.* **89,** 4739–4755.

Chandler, A. S., Choularton, T. W., Dollard, G. J., Gay, M. J., Hill, T. A., Jones, A., Jones, B. M. R., Morse, A. P., Penkett, S. A., and Tyler, B. J. (1988) A field study of the cloud chemistry and cloud microphysics at Great Dun Fell. *Atmos. Environ.* **22**, 683–694.

Clarke, A. D., Ahlquist, N. C., and Covert, D. S. (1987) The Pacific marine aerosol: Evidence for natural acid sulfates. *J. Geophys. Res.* **92**, 4179–4190.

Cowling, E. B. (1985) *J. Air Pollut. Cont. Assoc.* **35**, 916–919.

Deardroff, J. W. (1976) On the entrainment rate of a stratocumulus–topped mixed layer. *Quart. J. R. Met. Soc.* **102**, 563–582.

Deardroff, J. W. (1981) On the distribution of mean radiative cooling at the top of a stratocumulus–capped mixed layer. *Quart. J. R. Met. Soc.* **107**, 191–202.

Deister, U., Neeb, R., Helas, G. and Warneck, P. (1986) Temperature dependence of the equilibrium $CH_2(OH)_2 + HSO_3^- = CH_2(OH)SO_3^- + H_2O$ in aqueous solution, *J. Phys. Chem.* **90**. 3213–3217.

Hoffmann, M. R. (1984) Comment on acid fog. *Environ. Sci. Technol.* 18, 61–64.

Hoffmann, M. R. and Calvert, J. G. (1985) *Chemical Transformation Modules for Eulerian Acid Deposition Models Vol. II: The Aqueous–Phase Chemistry.* EPA/NCAR Report DW 930237, March, 1985.

Hoigne, J., Bader, H., Haag, W. R., and Staehelin, J. (1985) Rate constants of reactions of ozone with organic and inorganic compounds in water–III. Inorganic compounds and radicals *Water Research* **19**, 993–1004.

Huebert, B. J. and Robert, C. H. (1985) The dry deposition of nitric acid to grass. *J. Geophys. Res.* **90**, 2085–2090.

Jacob., D. J. (1986) The chemistry of OH in remote clouds and its role in the production of formic acid and peroxymonosulfate, *J. Geophys. Res.* **91**, 9807–9826.

Jacob, D. J., Waldman, J. M., Munger, J. W., and Hoffmann, M. R. (1985) Chemical composition of fogwater collected along the California coast. *Environ. Sci. Technol.* **19**, 730–736.

Jacob, D. J., Munger, J. W., Waldman, J. M., and Hoffmann, M. R. 1986. The H_2SO_4–HNO_3–NH_3 system at high humidities and in fogs: I. Spatial and temporal patterns in the San Joaquin Valley of California. *J. Geophys. Res.* **91**, 1073–1088.

Johnson, A. H., and Siccama, T. G. (1983) Acid deposition and forest decline. *Environ. Sci. Technol.* **17**, 294A–305A.

Kok, G. L., Gitlin, S., N., and Lazrus, A. L. (1986) Kinetics of the formation and decomposition of hydroxymethanesulfonate, *J. Geophys. Res.* **91**, 2801–2804.

Lee, Y.–N. and Scwartz, S. E. (1981) Evaluation of the rate of uptake of nitrogen dioxide by atmospheric and surface liquid water. *J. Geophys. Res.* **86**, 11,971–11,983.

Lilly, D. K, and Schubert, W. H. (1980) The effects of radiative cooling in a cloud–topped mixed layer. *J. Atmos. Sci.* **37**, 482–487.

Lovett, G. M. (1984) Rates and mechanisms of cloud water deposition to a subalpine balsam fir forest. *Atmos. Environ.* **18**, 361–371.

Munger, J. W., Jacob, D. J., Waldman, J. M., and Hoffmann, M. R. (1983) Fogwater chemistry in an urban atmosphere. *J. Geophys. Res.* **88**, 5109–5121.

Munger, J. W., Collett, J., Daube, B., Jr., and Hoffmann, M. R. (1989a) Fogwater chemistry at Riverside California. *Atmos. Environ.* (in press)

Munger, J. W., Collett, J., Jr., Daube, B. C., Jr. and Hoffmann, M. R. (1989b) Chemical composition of intercepted stratus cloud along the Santa Barbara Channel Coast. (submitted to *Environ. Sci. Technol.*)

Noonkester, V. R. (1984) Droplet spectra observed in marine stratus cloud layers. *J. Atmos. Sci.* **41**, 829–845.

Noonkester, V. R. (1985) Profiles of optical extinction coefficients calculated from droplet spectra observed in marine stratus cloud layers. *J. Atmos. Sci.* **41**, 1161–1171.

Oliver, D. A., Lewellen, W. S., and Williamson, G. G. (1978) The interaction between turbulent and radiative transport in the development of fog and low–level stratus. *J. Atmos. Sci.* **35**, 301–316.

Olson, T. M., and Hoffmann, M. R. (1988a) The formation kinetics, mechanism, and thermodynamics of glyoxylic acid–S(IV) adducts. *J. Phys Chem.* **92**, 000–000.

Olson, T. M., and Hoffmann, M. R. (1988b) Kinetics, mechanism, and thermodynamics of glyoxal–S(IV) adduct formation. *J. Phys. Chem.* **92**, 533–540.

Pruppacher, H. R. and Klett, J. D. (1978) *Microphysics of clouds and precipitation*, pp. 139–140. D. Reidel, Dordrecht.

Randall, D. R (1980a) Conditional instability of the first kind upside–down. *J. Atmos. Sci.* **37**, 125–130.

Randall, D. R. (1980b) Entrainment into a stratocumulus layer with distributed radiative cooling. *J. Atmos. Sci.* **37**, 148–159.

Roach, W. T., Brown, R., Caughey, S. J., Crease, B. A., and Slingo, A. (1982) A field investigation of nocturnal stratocumulus: I. Mean structure and budgets. *Q. J. R. Met. Soc.* **108**, 102–123.

Russell, A. G., McRae, G. J., and Cass, G. R. (1985) The dynamics of nitric acid production and the fate of nitrogen oxides. *Atmos. Environ.* **19**, 893–903.

Schwartz, S. E. and Freiberg, J. E. (1981) Mass–transport limitation to the rate of reaction of gases in liquid droplets: Application to oxidation of SO_2 in aqueous solutions. *Atmos. Environ.* **15**, 1129–1144.

Seinfeld, J. H. (1986) *Atmospheric Chemistry and Physics of Air Pollution*, John Wiley, New York, 738 pp..

Slingo, A., Nicholls, S. and Schmetz, J. (1982) Aircraft observations of marine stratocumulus during JASIN. *Q. J. R. Met. Soc.* **108**,833–838.

Waldman, J. M. and Hoffmann, M. R. (1987) Depositional aspects of pollutant behavior if fog and intercepted clouds. In *Sources and Fates of Aquatic Pollutants* edited by Hites, R. A., and Eisenriech, S. J., Am. Chem. Soc., Wash. D. C. pp. 79–129

Waldman, J. M., Munger, J. W., Jacob, D. J., Flagan, R. C., Morgan, J. J. and Hoffmann, M. R. (1982) Chemical composition of acid fog. *Science* **218**, 677–680.

Waldman, J. M., Munger, J. W., Jacob, D. J., and Hoffmann, M. R. (1985) Chemical characterization of stratus cloudwater and its role as a vector for pollutant deposition in a Los Angeles pine forest. *Tellus* **37**, 91–108.

Table 1.1 The droplet growth equation, expressed in terms of droplet diameter

$$D_0 \frac{dD_0}{dt} = \frac{S_v - a_w \exp(B)}{C + E\,(A-1)\ a_w \exp((B)}$$

$$A = \frac{M_W L}{RT} \qquad B = \frac{4M_w \sigma}{\rho_w D_0 RT} \qquad C = \frac{\rho_S RT}{4\mathcal{D}_m M_W e_s(t)} \qquad E = \frac{\rho_S L}{4kT}$$

$$a_w = \exp(-\Phi \frac{n_s}{n_w})$$

Activation point:

$$\frac{dD_0}{dt} = 0; \quad D_0 = D_{act}; \quad \text{and, } S_v = 1 + SS_{cr}$$

gives:

$$D_{act} = \left[\frac{3\ LNA}{B}\right]^{1/2} \qquad \text{where,} \quad LNA = \frac{M_w \rho_s}{M_s \rho_w} D_{dry}^3$$

$$SS_{cr} = \frac{2}{3\sqrt{3}} \left[\frac{B^3}{LNA}\right]^{1/2}$$

$$= K\, D_{dry}^{-1.5}$$

Solute	K for D_{dry} (in μm, 10 °C)
$(NH_4)_2SO_4$	4.93×10^{-5}
NH_4HSO_4	4.59×10^{-5}
NH_4NO_3	4.82×10^{-5}
H_2SO_4	4.21×10^{-5}
NaCl	3.68×10^{-5}

Table 1.1 Parameters:

D_0, D_{act} = droplet diameter, diameter at activation point.

D_{dry} = dry diameter for hygroscopic aerosol.

e, $e_s(T)$ = ambient, saturation water vapor pressure at T.

S_v = ambient water vapor saturation ratio, $e/e_s(T)$.

ρ_w, ρ_s = density of pure water, solute salt

R = Universal gas constant.

T = Temperature (K).

L = latent heat of evaporation

$\mathcal{D}_m$ = molecular diffusivity of water vapor in air

k = heat conductivity of air

σ_w = surface tension of water

M_w, M_s = molecular weight of water, solute ions.

n_w, n_s = number of moles of water, solute in droplet.

a_w = activity of water in droplet.

Φ = osmotic coefficient of water in solution (assumed = 1)

Table 1.2 . Recommended rate laws and rate constants according to Hoffmann and Calvert (1985) for the oxidation of S(IV) in aqueous solution at 25° C.

$$\nu = \frac{-d[S(IV)]}{dt}$$

OXIDANT	RATE LAW & RATE CONSTANTS
O_3	$\nu = (k_0\alpha_0 + k_1\alpha_1 + k_2\alpha_2)[O_3][S(IV)]$ $k_0 = 2.40 \times 10^4$ $(M^{-1}s^{-1})$ $k_1 = 3.70 \times 10^5$ $(M^{-1}s^{-1})$ $k_2 = 1.50 \times 10^9$ $(M^{-1}s^{-1})$
H_2O_2	$\nu = k[H^+][H_2O_2][S(IV)]\alpha_1(1 + K[H^+])^{-1}$ $k = 7.50 \times 10^7$ $(M^{-2}s^{-1})$ $K = 13\ M^{-1}$
$\cdot OH$	$\nu = (k_1\alpha_1 + k_2\alpha_2)[OH][S(IV)]$ $k_1 = 9.50 \times 10^9$ $(M^{-1}s^{-1})$ $k_2 = 5.50 \times 10^9$ $(M^{-1}s^{-1})$
HONO	$\nu = k[H^+][HSO_3^-][NO_2^-]$ $k = 1.75 \times 10^7$ $(M^{-1}s^{-1})$
CH_3OOH	$\nu = k[H^+][CH_3OOH][S(IV)]\alpha_1$ $k = 1.75 \times 10^7$ $(M^{-1}s^{-1})$
CH_3CO_3H	$\nu = (k_3[H^+] + k_2)[HSO_3^-][CH_3CO_3H]$ $k_3 = 3.64 \times 10^7$ $(M^{-1}s^{-1})$ $k_2 = 6.01 \times 10^2$ $(M^{-1}s^{-1})$
PAN	$\nu = k[PAN][S(IV)]\alpha_2$ $k = 1.0 \times 10^5$ $(M^{-1}s^{-1})$
$Fe(III)/O_2$	$\nu = k[Fe(III)][S(IV)]\alpha_2$ $k = 1.20 \times 10^6$ $(M^{-1}s^{-1})$
Mn/O_2	$\nu = k_2[Mn(II)][S(IV)]\alpha_1 + k_1K_1[Mn(II)]^2$ $k_2 = 3.40 \times 10^3$ $(M^{-1}s^{-1})$ $k_1 = 2.0 \times 10^9$ $(M^{-1}s^{-1})$ $K_1 = 1.26 \times 10^{-10}$

Table 1.3 Characteristic times for aqueous–phase reaction of soluble gases

Process	τ	value (s)*
Diffusion, gas	$\frac{R^2}{\pi^2 D_g}$	1×10^{-6}
Phase equilibrium	$D_l \left[\frac{4H^*RT}{\bar{v}\alpha}\right]^2$	$10^{-9}MH$
$A \underset{k_r}{\overset{k_f}{\rightleftharpoons}} B + C$	k_f^{-1}, $(k_r[C])^{-1}$	—
Diffusion, aqueous	$\frac{R^2}{\pi^2 D_l}$	1×10^{-2}
$A + B \overset{k_f}{\rightleftharpoons} C$	$(k_f[C])^{-1}$	—

---

* Values of τ (in seconds) are evaluated at $T = 25°C$; $D_g = 0.1$ cm^{2}s^{-1}; $D_l = 10^{-5}$ cm

$R = 8.314$ JK^{-1}mol^{-1}

$\bar{v}$ = mean speed = $\left[\frac{8RT}{\pi M}\right]^{\frac{1}{2}}$

M = molecular weight (g)

α = accommodation coefficient (assumed 1)

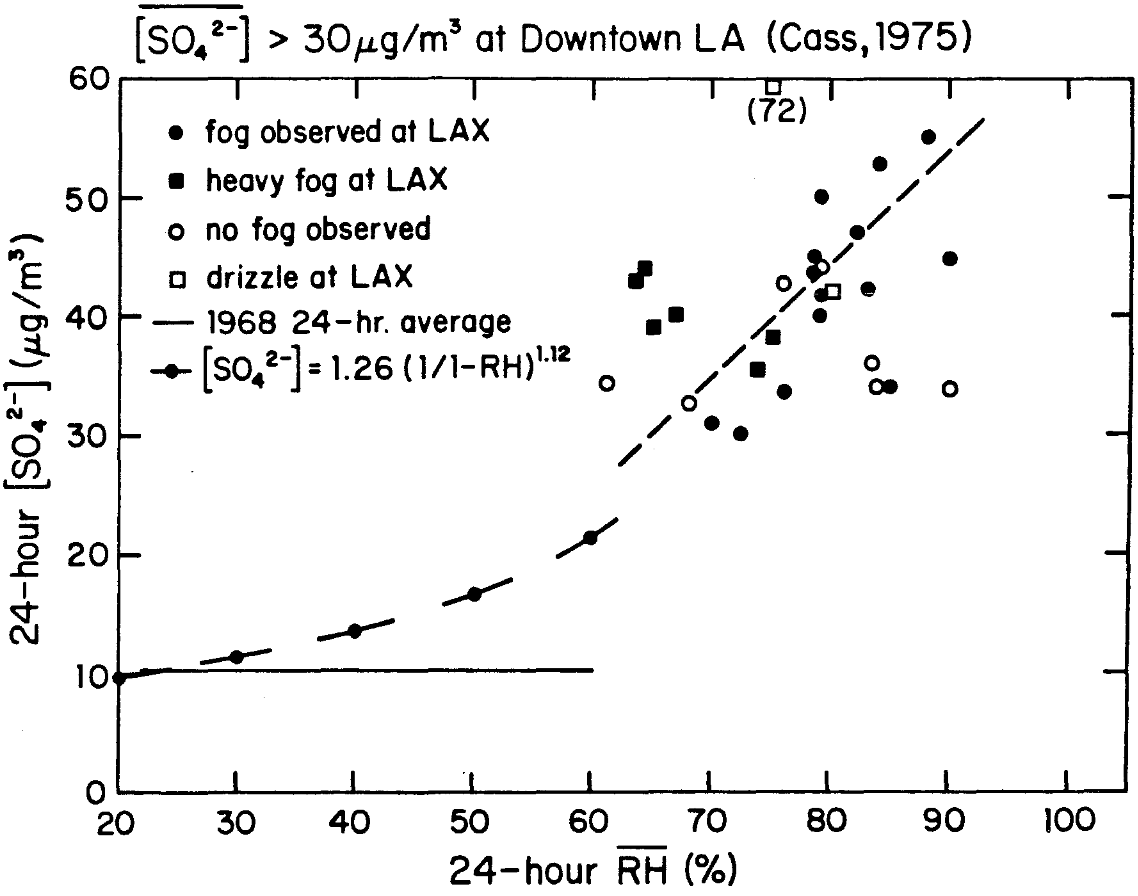

Figure 1.1 Average SO_4^{2-} concentrations in Los Angeles plotted vs average relative humidity. Data from Cass (1975)

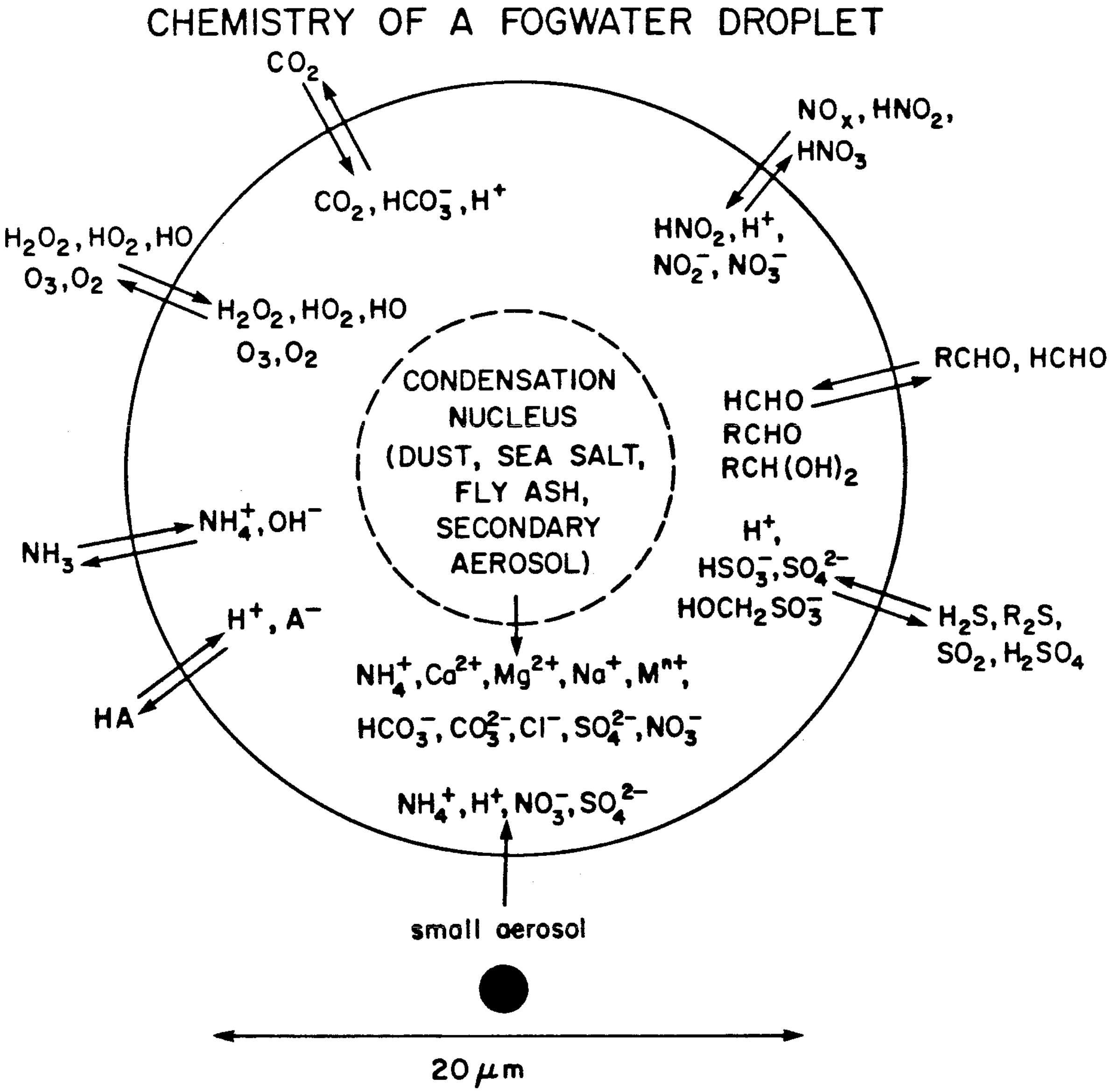

Figure 1.2 Schematic diagram of the processes of nucleation scavenging and gas dissolution that influence the chemical composition of a fog or cloud droplet.

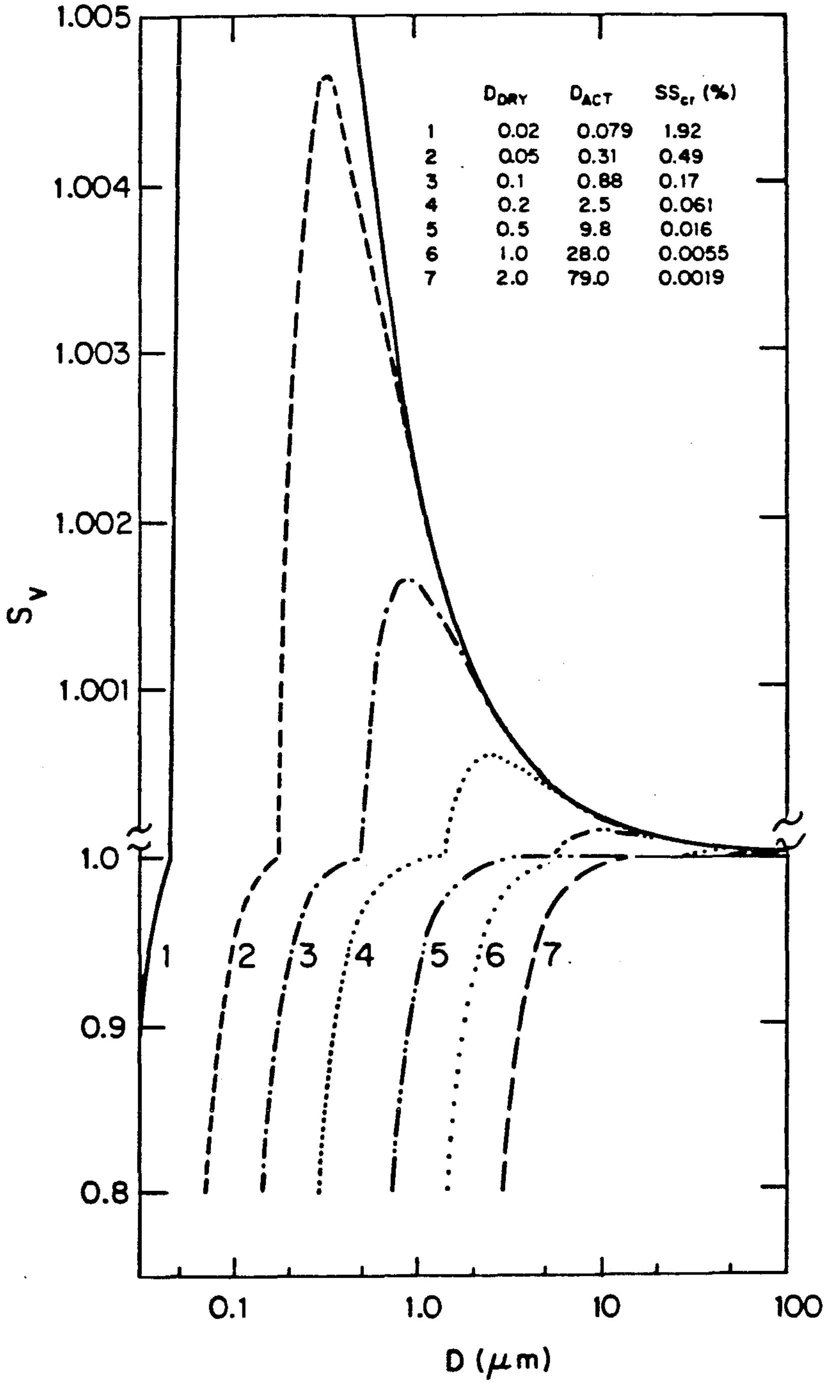

Figure 1.3 The Köhler curves. The equilibrium water vapor pressure over droplets as a function of drop diameter is plotted for a series of initial diameters. The solute is ammonium sulfate.

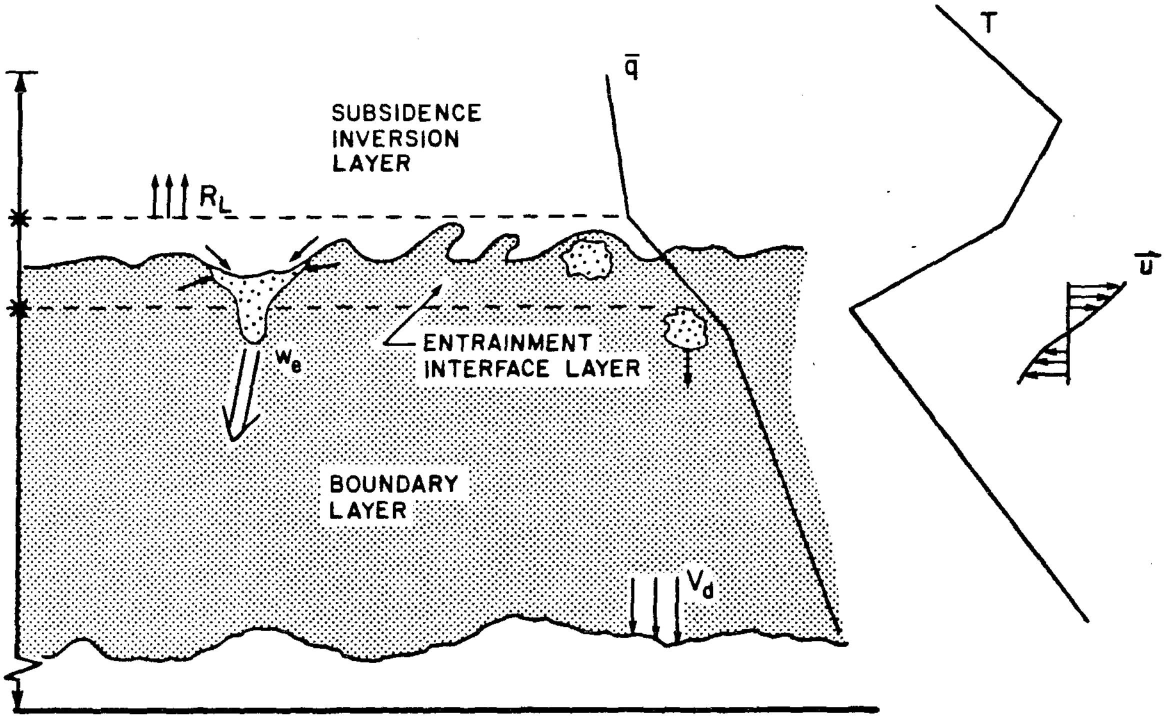

Figure 1.4 The processes of advection, entrainment, emission and deposition from a cloudy mixed layer are shown schematically. Turbulence in the cloud layer is generated by wind shear and radiative cooling at the top.

Chapter 2

The Chemistry of Carboxylic Acids and Carbonyls in Clouds and Fogs: A Review

INTRODUCTION

The importance of soluble organic carbon species in the atmosphere is well known. Liljestrand and Morgan (1981) observed that organic carbon was the dominant component by mass of rainwater collected in Los Angeles. Likens et al. (1983) reported that a large fraction of the soluble organic carbon, which was not derived directly from plants or soil, consisted of carbonyl compounds and carboxylic acids.

Carboxylic acids are a major source of acidity in precipitation from remote locations (Keene et al., 1983); even in North America, where inorganic acids are more concentrated, organic acids still make a measurable contribution to acidity (Keene and Galloway, 1984). Because carboxylate salts are weak bases, they contribute alkalinity to the atmosphere (Jacob et al., 1986a).

In the gas phase, carbonyls are highly reactive and are important precursors of photochemical smog (Finlayson–Pitts and Pitts, 1986; Seinfeld, 1986). Hydration of the carbonyl bond reduces photolysis in the aqueous phase. However, Chameides (1984) has pointed out the potential for $OH\cdot$ to attack formaldehyde in droplets. Formic acid generated via this reaction will either react with $OH\cdot$ or volatilize, depending on the pH of the droplet (Jacob 1986). Carbonyls are also potentially important in the aqueous phase because they react readily with dissolved SO_2 to form α–hydroxyalkanesulfonates (Munger et al., 1984; 1986).

Despite its importance, the speciation of soluble organic carbon in the atmosphere has not been thoroughly determined. Data on the atmospheric abundance of the simplest soluble organic species, formaldehyde, acetaldehyde, formic and acetic acid, are the most extensive. However, chemical reaction models predict that dicarbonyls and a variety of OH–substituted and unsaturated carbonyls and ketoacids should also be present in the atmosphere. Very little attention has been paid to these compounds. Methods for collection and analysis of carbonyl compounds and carboxylic acids have not been adequately evaluated or standardized, thus the validity of existing data is uncertain. Furthermore, most existing data are for individual compounds or classes of compounds, often in only one phase. A thorough evaluation of current models of organic chemistry in the atmosphere requires concurrent data on all the major compounds present in the gas, aerosol, and droplet phase. This is lacking for the carbonyls and carboxylic acids.

Sources and Sinks

Short–chain organic compounds are released as primary emissions and produced from the breakdown of hydrocarbon precursors. The major sources of primary aldehyde emissions are internal combustion engines, oil refineries, utility boilers, and aircraft (Rogozen et al., 1984). Emissions of organic acids are not well characterized. Organic acids are emitted directly from vegetation and produced by combustion (Graedel et al., 1986; Talbot et al., 1988). Bacterial metabolism produces a variety of short–chain organic acids, such as formate, acetate, lactate, and pyruvate; thus decomposing organic matter (e.g. soils, manure) could be important sources of organic acids. Bacteria living on plant surfaces may produce organic acids that would be mis–identified as direct vegetative emissions.

Secondary sources are more important contributors of carbonyls and carboxylic acids. The major classes of hydrocarbons, alkanes, alkenes, and aromatics, each react via different mechanisms, which will be summarized below. Simple molecules such as CH_2O are produced in all cases, but higher carbonyls and carboxylic acids and substituted analogs are formed as well. These products are characteristic of the precursor species or reaction mechanism.

Alkanes react with OH· via hydrogen abstraction. The rate constant for oxidation of CH_4 by OH· is 1.1 x 10^{-14} cm^3 s^{-1}. Rate constants for the higher alkanes are 1 to 3 orders of magnitude higher (Atkinson et al., 1979). The alkyl radical reacts rapidly with O_2 to form an alkyl peroxy radical, which decomposes via a series of steps to form an aldehyde or ketone and another alkyl peroxy radical (Calvert and Madronich, 1987). Alkoxy radicals from alkanes with carbon chains longer than 4 can isomerize to form γ–hydroxy carbonyls. Alkoxy radicals also react with O_2 to form aldehydes or ketones and HO_2·. This path dominates for short chain primary and secondary alkoxy radicals (Calvert and Madronich, 1987). Calvert and Madronich (1987) predict that γ–hydroxy aldehydes and ketones, which have not been considered in the troposphere, may be the largest class of carbonyls formed from alkane oxidation.

Under low NO conditions, the RO_2· radicals will react with other RO_2· or HO_2·. Collision of two RO_2· molecules produces 2 alkoxy radicals or a carbonyl and an alcohol. For a hypothetical mixture of alkanes Calvert and Madronich (1987) predict that the major products will be alkyl hydroperoxides. The initial non–hydroperoxy products will be dominated by simple ketones; the remainder would be distributed about equally among simple aldehydes, alcohols, and γ–OH substituted carbonyls.

Alkenes react with OH· by addition to the double bond. Typical rate constants for OH· addition to alkenes are 5 – 300 x 10^{-12} cm^3 s^{-1} (Atkinson et al., 1979). The OH–adduct subsequently reacts with O_2 to form a peroxy radical and ultimately a hydroxy-alkoxy radical if NO is present. This radical decomposes to form two aldehydes or reacts with O_2 resulting in an α–hydroxy carbonyl (RC(O)CH(OH)R′) (Calvert and Madronich, 1987).

Alkenes also react with O_3 by addition across the double bond to form an unstable ozonide. Typical rate constants are in the range 1 – 200 x 10^{-18} cm^3 s^{-1}

(Atkinson and Lloyd, 1984). Ozonides decompose via either of the pathways shown below to produce carbonyl compounds and a reactive Criegee biradical. The Criegee biradicals react further to form a variety of products, as shown in reactions 2 – 4. Carboxylic acids are formed when one of the substituents adjacent to the double bond is H. In the presence of high NO_x levels, reaction 3 will be favored over reaction 4 resulting in a greater yield of carbonyls at the expense of carboxylic acid.

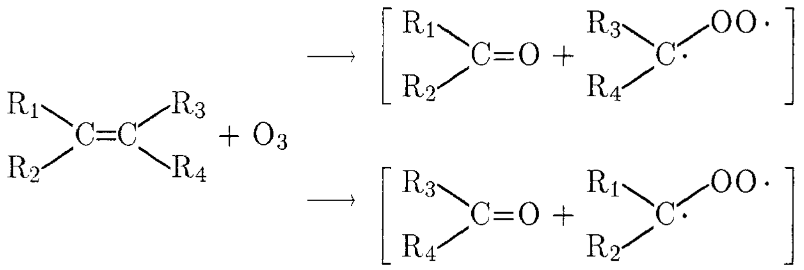

(1)

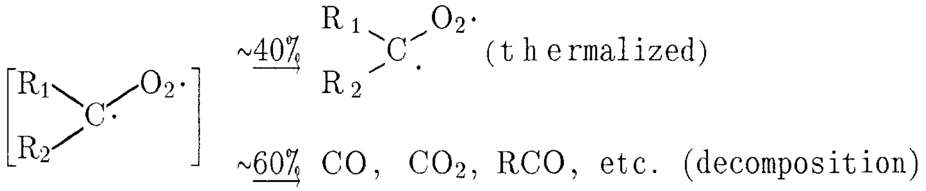

(2)

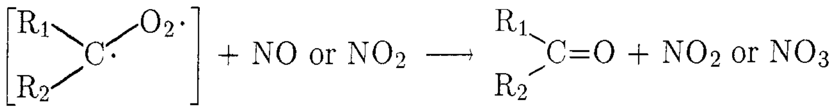

(3)

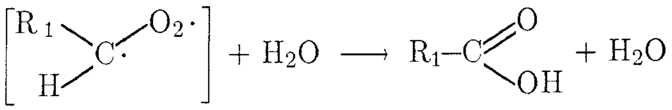

(4)

Near urban areas ethylene and propylene are the dominant alkenes (Grosjean and Fung, 1984). The predicted products of simple alkene oxidation are dominated by aldehydes. Organic acids and the characteristic α–hydroxy–carbonyls are formed as well (Calvert and Madronich, 1987). A shift to hydroxyhydroperoxides is expected in NO_x–free environments. Away from urban areas, terpenes emitted by vegetation assume greater importance. The expected initial products of isoprene–O_3 reaction include pyruvic acid, methyl glyoxal, methyl vinyl ketone, and methacrolein in addition to the products noted above (Lloyd et al., 1983; Jacob and Wofsy, 1988).

The major pathway for removal of aromatic hydrocarbons is reaction with $OH\cdot$. Typical rate constants are $1 - 50 \times 10^{-12}$ cm^3 s^{-1} (Atkinson et al., 1979). Both H abstraction and $OH\cdot$ addition are involved, although the complete mechanisms are not known. Hydrogen abstraction from the alkyl side groups results in aromatic aldehydes or nitrates. $OH\cdot$ addition to the ring is the dominant reaction channel. Fragmentation of the intermediates lead to various dicarbonyls such as glyoxal, methyl glyoxal or biacetyl and δ–dicarbonyl compounds (Tuazon et al., 1986). Phenols should also be formed from aromatic hydrocarbons, but experimental yields are less than predicted (Calvert and Madronich, 1987).

The various products noted above are susceptible to attack by oxidants. Carbonyls are sensitive to photolysis (Su et al., 1979). At zenith angles of $20 - 50^o$ the overall rate constant for CH_2O decomposition is $\simeq 5 \times 10^{-5}$ s^{-1}. Higher aldehydes have photodecomposition rate constants in the range $0.01 - 1 \times 10^{-5}$ s^{-1} (NRC, 1981). Simple aldehydes and ketones react rapidly with $OH\cdot$; rate constants are of the order $1 - 10 \times 10^{-12}$ cm^3 s^{-1} (Atkinson et al., 1979). For the conditions of their simulation, Calvert and Madronich (1987) estimate the atmospheric lifetime of CH_2O to be 0.2 days. Hydroxy substituted aldehydes would have comparable lifetimes. The α–dicarbonyl compounds have lifetimes < 0.1 days. Both simple and hydroxy–substituted ketones have lifetimes on the order of several days. Simple alcohols and organic acids likewise would have lifetimes of several days to weeks.

Chemical reaction models all indicate that a variety of substituted and difunctional carbonyls should form from oxidation of hydrocarbons. The yield and stability of these compounds is comparable to that of formaldehyde, which is routinely observed in the atmosphere. Thus they ought to be present as well. The most reactive of these species may be restricted to emission source regions. However, ketones, carboxylic acids, and alcohols are sufficiently long lived to be affected by transport and deposition processes. Sources of the important precursor hydrocarbons include both urban areas and vegetation.

Thermodynamics and kinetics in the aqueous phase

The partitioning of organic acids between vapor and particle phase in the presence of liquid water should follow the Henry's law and acid-base equilibria shown below, where HA is any organic acid and A^- is its conjugate anion.

$$HA_{(g)} \overset{H_A}{\rightleftharpoons} HA_{(aq)} \qquad (5)$$

$$HA_{(aq)} \overset{K_{a,A}}{\rightleftharpoons} H^+ + A^- \qquad (6)$$

Table 2.1 presents the Henry's Law and acidity constants for several short-chain organic acids. By substituting the equilibrium expressions into the mass balance equations, speciation of organic acid can be calculated as a function of $[H^+]$. As examples, Figs. 2.1A and 2.2A present the distribution coefficients for formic and acetic acid defined as:

$$\alpha_0 = \frac{[HA]}{[HA] + [A^-]} \quad \text{and} \quad \alpha_1 = \frac{[A^-]}{[HA] + [A^-]} \tag{7}$$

The effect of this speciation on equilibrium partial pressure is indicated in Figs. 2.1B and 2.2B. Partial pressure, computed from equation (8), increases dramatically below the pK_a for the acid.

$$P_{HA} = \frac{C_{T,A}}{\alpha_0^{-1} H_A} \tag{8}$$

$C_{T,A}$ is the total concentration of acid in the aqueous phase. The fraction of organic acid in the gas phase is given by

$$X = [1 + RTLH_A \cdot \alpha_0^{-1}]^{-1} \tag{9}$$

where R is the universal gas constant in appropriate units, T is the absolute temperature in Kelvin, and L is the liquid water content (LWC). In Figs. 2.1C and 2.2C this fraction is plotted for formic and acetic acid vs pH at a high LWC typical of a cloud, and a lower LWC typical of a haze aerosol. In cloud or fog the fraction of acid in the gas phase drops sharply as pH increases beyond the pK_a of the acid. At lower LWC, nearly all the organic acid is present in the gas phase except at very

Table 2.1. Equilibrium constants for short–chain carboxylic acids

Reaction	K^{298} (**M** or **M** atm^{-1})	ΔH (kJ mole^{-1})	Reference
$CHOOH_{(g)} \rightleftharpoons CHOOH_{(aq)}$	3.7×10^{3}	–46.9	Wagaman et al. (1982)
$CHOOH_{(aq)} \rightleftharpoons CHOO^- + H^+$	1.80×10^{-4}	0.17	Martell and Smith (1977)
$CH_3COOH_{(g)} \rightleftharpoons CH_3COOH_{(aq)}$	8.83×10^{3}	–53.5	Wagaman et al. (1982)
$CH_3COOH_{(aq)} \rightleftharpoons CH_3COO^- + H^+$	1.75×10^{-5}	0.42	Martell and Smith (1977)
$C_2H_5COOH_{(aq)} \rightleftharpoons C_2H_5COO^- + H^+$	1.34×10^{-5}	0.84	ibid.
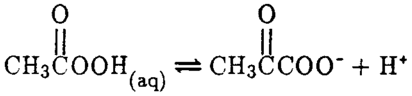 $CH_3\overset{\overset{O}{\Vert}}{C}OOH_{(aq)} \rightleftharpoons CH_3\overset{\overset{O}{\Vert}}{C}COO^- + H^+$	2.82×10^{-3}	–12.13	ibid.
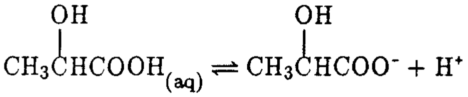 $CH_3\overset{\overset{OH}{\vert}}{C}HCOOH_{(aq)} \rightleftharpoons CH_3\overset{\overset{OH}{\vert}}{C}HCOO^- + H^+$	1.38×10^{-4}	0.33	ibid.
$HOCH_2COOH_{(aq)} \rightleftharpoons HOCH_2COO^- + H^+$	1.48×10^{-4}	–.67	ibid.
$HO_2CCO_2H_{(aq)} \rightleftharpoons HO_2CCOO^- + H^+$	5.6×10^{-2}	3.77	ibid.
$HO_2CCOO^-_{(aq)} \rightleftharpoons {}^-OOCCOO^- + H^+$	5.42×10^{-5}	6.69	ibid

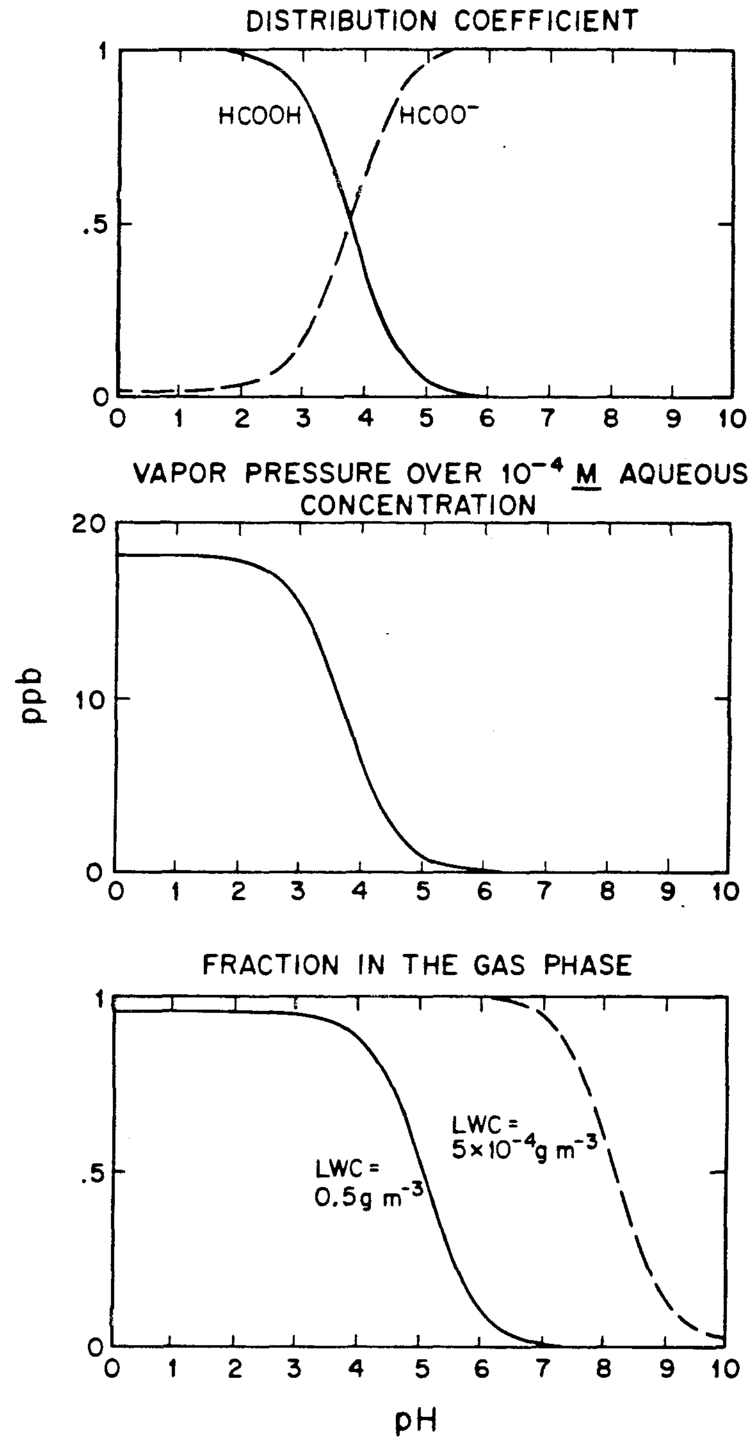

Figure 2.1 A. Distribution coefficient for formic acid as a function of pH; (——) α_0, (– – –) α_1.
B. Vapor pressure of formic acid in equilibrium with 10^{-4} **M** total aqueous formic acid as a function of pH.
C. Fraction of formic acid in the gas phase as a function of pH at two liquid water contents.

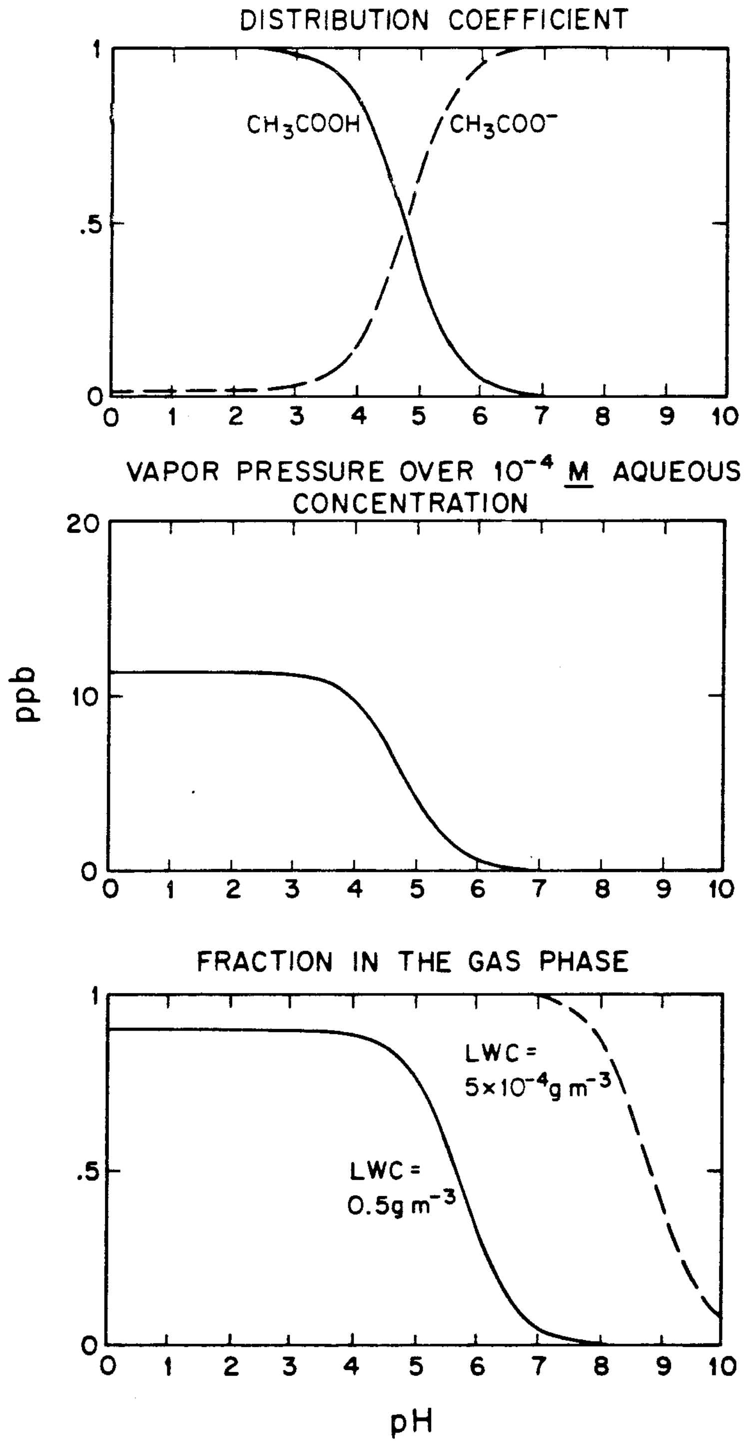

Figure 2.2 A. Distribution coefficient for acetic acid as a function of pH (——) α_0, (– – –) α_1.
B. Vapor pressure of acetic acid in equilibrium with 10^{-4} **M** total aqueous acetic acid as a function of pH.
C. Fraction of acetic acid in the gas phase as a function of pH at two liquid water contents.

high pH. Note that the fraction in the gas phase increases with increasing pK_a. Any differences in aqueous–phase concentrations of organic acids should be interpreted in light of these equilibrium considerations. When sufficient base, such as NH_3 is present to maintain pH above 7, organic acid scavenging by droplets is nearly 100%. In a haze aerosol, however, most organic acid will be in the gas phase unless the aerosol is very alkaline. Addition of acid to the aerosol by HNO_3 scavenging or S(IV) oxidation will drive organic acids into the gas phase.

The above description only qualitatively describes organic acid partitioning in aerosol. Although most aerosols can be considered to be aqueous at relative humidities above their deliquescence point (about 60%) they will have such high ionic strengths that activity corrections must be made. Below the deliquescence point the individual solid (or pure liquid) phases for the acids and their salts must be considered. The vapor pressure of each phase must be known. For very small aerosol the Kelvin effect (Pruppacher and Klett, 1978) must also be considered.

The partitioning of carbonyls between gas and aqueous phase depends on Henry's law and hydration equilibria:

$$RCHO_{(g)} \overset{H_R}{\rightleftharpoons} RCHO_{(aq)} \tag{10}$$

$$RCHO_{(aq)} + H_2O \overset{K_{h,R}}{\rightleftharpoons} RCH(OH)_2 \tag{11}$$

Glyoxal is hydrated at both carbonyl groups, but it is difficult to determine separate constants for the two hydration steps (Wasa and Musha, 1970). Measured hydration constants for carbonyls correlate well with the polarizability of the molecule as measured by the Taft parameter (σ^*) of the R group (Greenzaid et al., 1967; Buschmann et al., 1980) (see Fig. 2.3). Aldehydes and ketones have the same slope, but ketones have a lower intercept. Formaldehyde has an anomalously high hydration constant for its σ^*, which may be related to the high symmetry of the gem diol $H_2C(OH)_2$ and the possibility of extensive hydrogen bonding. Greenzaid et al. (1967) explain the difference in intercepts by the difference in number of C–H bonds on the carbonyl carbon. Unknown hydration constants can be predicted from the Taft correlation for measured constants of related compounds (see Tables 2.2 – 2.3) (Betterton et al., 1988).

The parameter of interest in atmospheric chemistry is the combined Henry's Law and hydration constant, which determines the overall solubility in droplets. Measured values of the intrinsic Henry's law constants are in the range 1–10; hydroxyacetaldehyde ($CH_2(OH)CHO$), however appears to have an unusually large Henry's law constant (Betterton and Hoffmann, 1988). Thus the magnitude of K_h controls the overall solubility of carbonyls. Based on the Taft correlation, dicarbonyls and halogenated carbonyls should be the most soluble; α–OH substituted and unsaturated carbonyl compounds would be somewhat less. Hydroxy substitution in γ position should have little effect on the hydration constant. The saturated alkanals should all be relatively insoluble.

Aqueous–Phase Reactions

Scavenging by droplets isolates carbonyls from the aforementioned removal mechanisms. Reaction with $OH\cdot_{(aq)}$ (eq 12–15) is the most important sink for carboxylic acids and carbonyl compounds in droplets (e.g. Chameides, 1984).

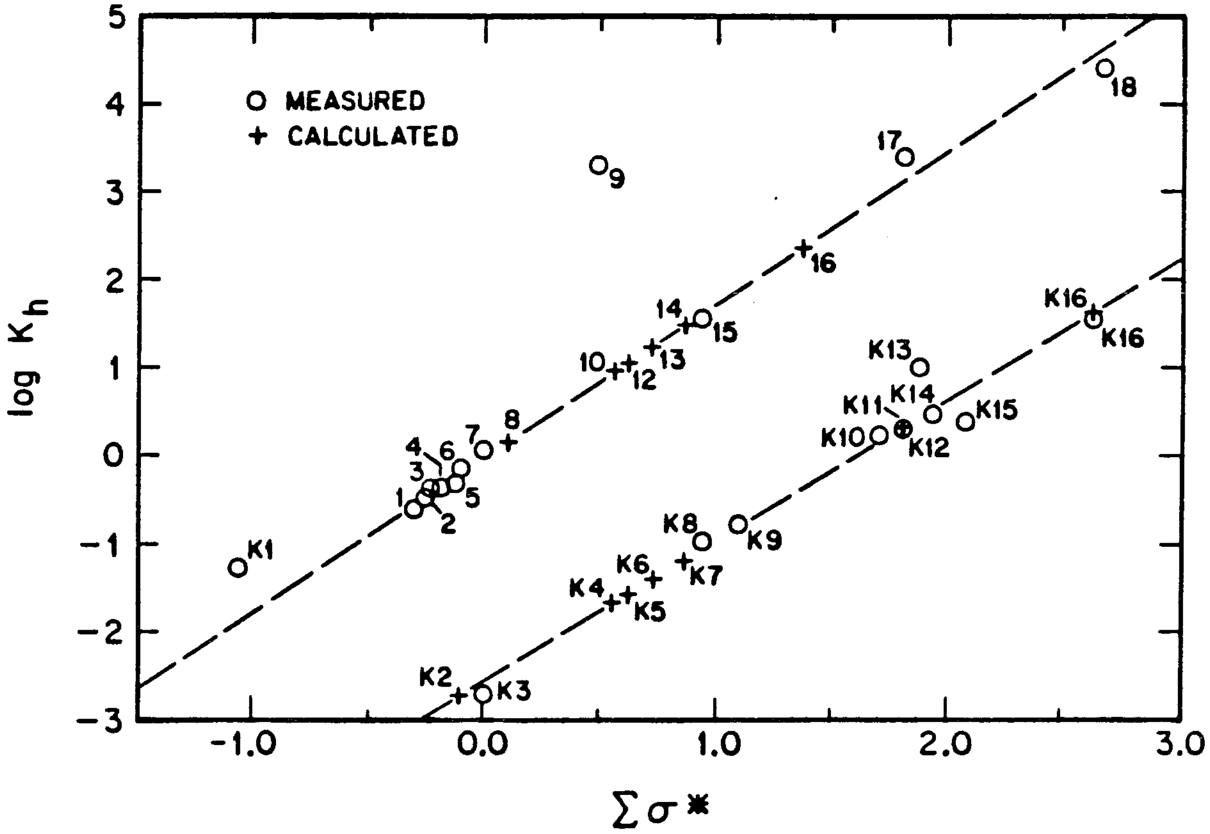

Figure 2.3. Plot of carbonyl hydration constants $K_{h,R}$ vs the Taft parameter σ^*. The numbers refer to compounds listed in Tables 2.2 and 2.3. The dashed line is the linear regression line through the measured points.

Table 2.2. Equilibrium constants for aldehydes

			log K_h		log K_{s1}	
#	R–CHO	σ^*[1]	calc	meas	calc	meas
	^-OOCCHO	−1.06	—	1.23[10]	—	6.72[11]
1	$(CH_3)_3CCHO$	−0.3	—	−0.61[2]	3.96	—
2	C_4H_9CHO	−0.25	—	−0.47[3]	4.07	—
3	$C_5H_{11}CHO$	−0.23	—	−0.39[3]	4.12	—
4	$(CH_3)_2CHCHO$	−0.19	—	−0.36[2]	—	4.68[6]
5	C_3H_7CHO	−0.12	—	−0.32[2]	—	4.45[7]
6	C_2H_5CHO	−0.1	—	−0.15[2]	—	4.08[7]
7	CH_3CHO	0	—	0.08[4]	—	5.84[9]
8	$CH_2(OH)C_2H_4CHO$	0.1	0.16	—	4.90	—
9	HCHO	0.49	—	3.30[2]	—	9.82[8]
10	$CH_2{=}CHCHO$	0.56	0.96	—	5.98	—
11	$CH_2{=}CH(CH_3)CHO$	0.56	0.96	—	5.98	—
12	$CH_2(OH)CHO$	0.62	1.06	—	6.12	6.30[9]
13	$CH_3COCH{=}CHCHO$	0.72	1.23	—	6.36	—
14	$CHOCH{=}CHCHO$	0.86	1.48	—	6.69	—
15	CH_2ClCHO	0.94	—	1.57[2]	6.88	—
16	$(OH)_2CHCHO$	1.37	2.36	—	7.89	—
17	CH_3COCHO	1.81	—	3.40[5]	—	8.91[5]
18	CCl_3CHO	2.65	—	4.40[2]	10.91	—
	HO_2CCHO	2.08	—	2.48	8.18	7.85[11]

---

[1] Taft parameter for R, obtained from Perrin et al. (1981)

[2] Greenzaid et al. (1967)

[3] Buschmann et al. (1980)

[4] Buschmann et al. (1982)

[5] Betterton and Hoffmann (1987)

[6] Bell (1966)

[7] Gubareva (1947)

[8] Skrabal and Skrabal (1936)

[9] Betterton et al. (1988)

[10] Sørensen et al (1974)

[11] Olson and Hoffmann (1988b)

Table 2.3 Equilibrium constants for ketones

#	$R-\overset{\overset{O}{\|}}{C}-R'$	sigma[1]	log K_h calc	log K_h meas	log K_{s1} calc	log K_{s1} meas
K1	CH_3COCOO^-	–1.06	—	–1.27[2]	–0.26	3.68[5]
K2	$CH_3COC_2H_5$	–0.1	–2.72	—	—	1.79[3]
K3	CH_3COCH_3	0	—	–2.70[2]	—	2.46[3]
K4	$CH_3COCH{=}CH_2$	0.56	–1.67	—	3.56	—
K5	$CH_2OHCOCH_3$	0.62	–1.57	—	3.70	—
K6	$(CH_3COCH)_2$	0.72	–1.41	—	3.94	—
K7	$CH_3COCH{=}CHCHO$	0.86	–1.19	—	4.27	—
K8	$CH_2ClCOCH_3$	0.94	—	–0.96[2]	4.46	—
K9	CH_2FCOCH_3	1.1	—	–0.78[4]	4.83	—
K10	$CH_3COCOC_2H_5$	1.71	—	0.23[4]	6.27	—
K11	"	1.81	0.34	—	6.51	—
K12	$CH_3COCOCH_3$	1.81	—	0.30[2]	6.51	—
K13	$(CH_2Cl)_2CO$	1.88	—	1.00[2]	6.67	—
K14	$Cl_2CHCOCH_3$	1.94	—	0.46[2]	6.81	—
K15	$CH_3COCOOH$	2.08	—	0.38[2]	7.14	4.66[5]
K16	CF_3COCH_3	2.61	1.62	1.54[4]	8.39	—

---

[1] Sum of Taft parameters for R and R′, obtained from Perrin et al. (1981)
[2] Greenzaid et al. (1967)
[3] Gubareva (1947)
[4] Buschmann et al. (1982)
[5] Burroughs and Sparks (1974)

$$RCH(OH)_2 + OH\cdot \longrightarrow R\dot{C}(OH)_2 + H_2O \tag{12}$$

$$R\dot{C}(OH)_2 + O_2 \longrightarrow RCOOH + HO_2\cdot \tag{13}$$

$$RCOOH + OH\cdot \xrightarrow{O_2} H_2O + CO_2 + RO_2\cdot \tag{14}$$

$$RCOO^- + OH\cdot \xrightarrow{H^+,\ O_2} H_2O + CO_2 + RO_2\cdot \tag{15}$$

The rates for the above reactions approach the diffusion control limit. Jacob (1986) notes that the fate of HCOOH formed in reaction 13 depends on droplet pH. In acid droplets the HCOOH will volatilize more rapidly than it is oxidized and the droplet will be a source of HCOOH to the gas phase. At high pH, however, HCOOH dissociates and remains in the droplet where it can be further oxidized.

Carbonyls react readily with dissolved SO_2 to form α–hydroxyalkyl sulfonates. The kinetics and thermodynamics of these reactions have been recently studied for CH_2O (Boyce and Hoffmann, 1984; Kok et al., 1986; Deister et al., 1986), benzaldehyde (Olson et al., 1986) methyl glyoxal ($CH_3C(O)CHO$) (Betterton and Hoffmann, 1987), glyoxal (Olson and Hoffmann, 1988a), and glyoxylic acid (Olson and Hoffmann, 1988b). The proposed mechanism for sulfonate formation is illustrated for the reaction of methylglyoxal and S(IV) (see Figure 2.4). Other carbonyl–S(IV) reactions will follow an analogous pathway (Olson et al., 1986). Because sulfonates are the conjugate bases of strong acids, the monoprotic form is dominant at the pH levels encountered in atmospheric droplets. Sulfite is a stronger nucleophile than bisulfite, so k_2 is greater than k_1. As a result the rate of sulfonate formation increases with pH. Among the carbonyl–S(IV) adducts studied, formaldehyde and methylglyoxal have the largest rate constants.

The dissociation of sulfonates is also pH dependent. Data from Deister et al. (1986) and Kok et al. (1986) indicate that the decomposition of HMSA is a second order reaction in the pH range 4 – 5.6. Their data lead to the following empirical rate law:

$$\frac{d[\mathrm{HMSA}]}{d\,t} = -k_d\,[\mathrm{HMSA}]\,[\mathrm{OH}^-] \tag{16}$$

the value of k_d obtained from their data is 3.6×10^3 $\mathbf{M}^{-1}s^{-1}$. The decomposition of other carbonyl–S(IV) adducts also has an inverse dependence on $[H^+]$ over this pH range (Betterton and Hoffmann, 1987; Olson and Hoffmann, 1988a).

The kinetics of sulfonate formation are further complicated by a possible shift in rate determining step at high pH. At low pH the addition of SO_3^{2-} or HSO_3^- is rate limiting. However, at higher pH dehydration of the diol becomes rate limiting. Olson and Hoffmann (1986) evaluated the kinetics of HMSA formation and determined that dehydration of $CH_2(OH)_2$ and S(IV) addition have equal rates between pH 5 and 6 for typical levels of SO_2 and CH_2O in the atmosphere. This crossover point may be different for other carbonyls as shown by Betterton and Hoffmann (1987) for methyl glyoxal.

The thermodynamics of sulfonate formation can be described by the stability constant

$$K_{S_1} = \frac{[\,\mathrm{RCH(OH)\,SO_3^-}]}{[\mathrm{RCHO}]\ \ [\,\mathrm{HSO_3^-}]} = \frac{k_1}{k_{-1}} \tag{17}$$

This constant has been determined for a number of carbonyls (see Tables 2.2–2.3). Constants for the aldehydes correlate well with the Taft parameter, σ^*, which is a measure of the molecules polarizability. The predicted values in Tables 2.2 and 2.3

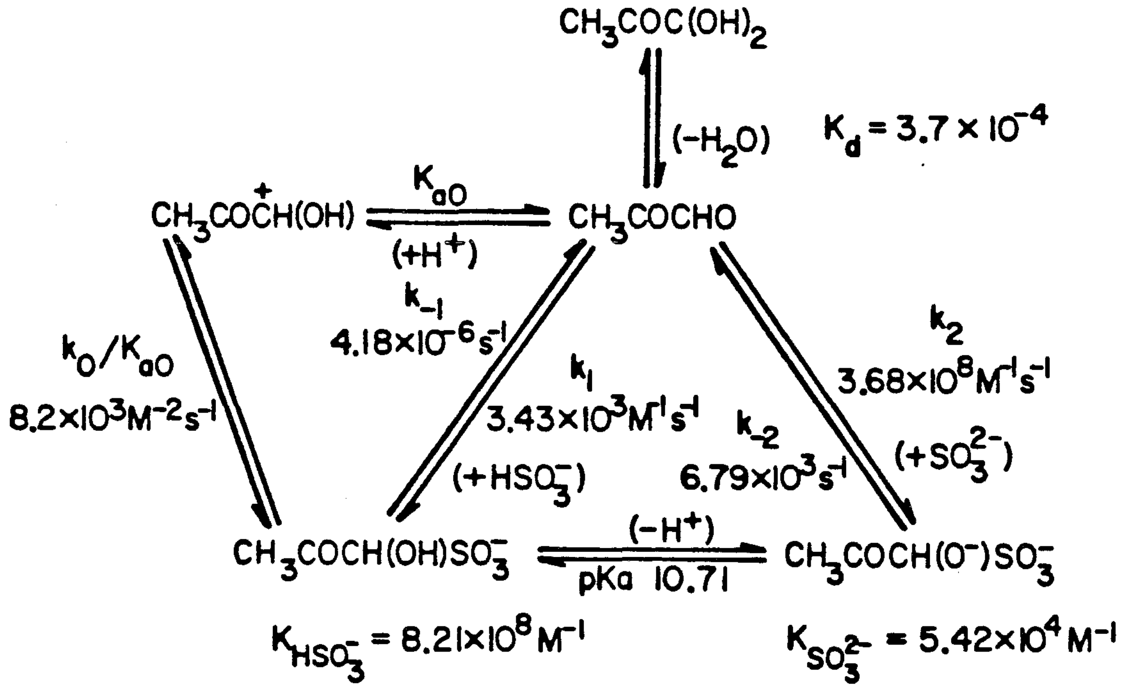

Figure 2.4. Reaction mechanism for the formation of hydroxyacetylmethanesulfonate. The reaction of other carbonyls to form analogous hydroxyalkanesulfonates follows the same pathway (Olson et al., 1986).

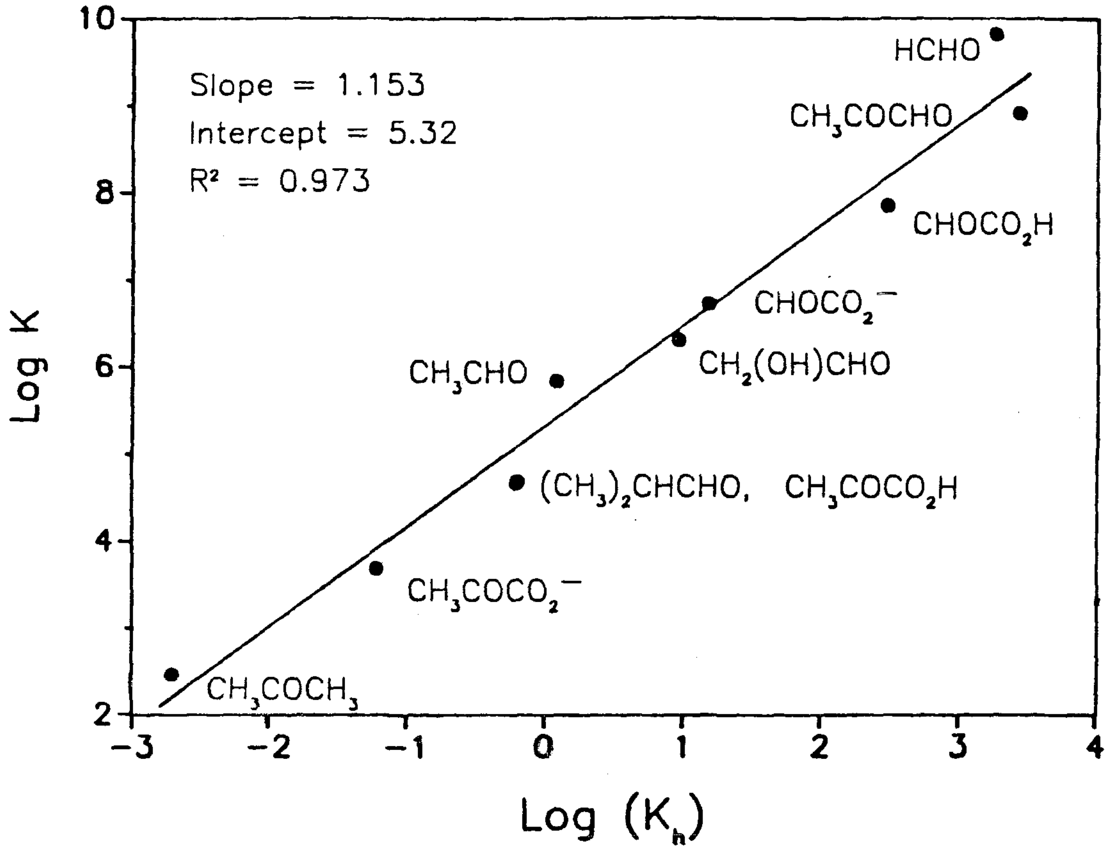

Figure 2.5. Linear free energy correlation of carbonyl–bisulfite adduct stabilities, K_{s1}, with carbonyl hydration constants, K_h. Solid line is a least-square regression fit.

are derived from a regression on measured aldehyde constants. Ketones are assumed to have the same slope, but a different intercept. Chloral (CCl_3CHO) has the highest predicted sulfonate stability constant. Dicarbonyls should also have large sulfonate stability constants. The α–OH substituted and unsaturated aldehydes will probably form sulfonates with stability similar to CH_2O. Even ketones may be activated by an adjacent acetyl or carboxyl group. Biacetyl is predicted to have a large sulfonate formation constant. The Taft correlation predicts some interesting behavior for keto acids such as pyruvic or glyoxylic acid. The protonated carboxyl group is strongly electron withdrawing (large σ^*), so the sulfonate stability constant should be large. Dissociation of the carboxyl group decreases the electron withdrawing (small σ^*) and should weaken the sulfonate formation constant. The formation constants turn out to be larger than predicted for the unprotonated acids (Table 2.2–2.3). Substituent effects are rapidly attenuated by intervening $-CH_2-$ groups. γ–OH substituted carbonyls should have smaller sulfonate formation constants than their α–OH substituted analogs.

Because both the hydration and sulfonate stability constants are correlated with the Taft parameter, a linear relation exists between them as well (Fig. 2.5). In the comparison of K_{S1} with K_h both aldehydes and ketones plot on the same line. In this plot the deprotonated forms of carbonyl–carboxylic acids do not exhibit anomalous behavior. Figure 2.5 also illustrates that the most soluble carbonyls will form the the strongest S(IV) adducts.

Measurement of an apparent supersaturation of CH_2O and S(IV) in fog and cloud samples provided circumstantial evidence for the existence of the formaldehyde–S(IV) adduct (HMSA) (Munger et al., 1983a; 1984). Direct measurements of HMSA were made in fog samples from Bakersfield California using ion–pairing chromatography (Munger et al., 1986). HMSA did not always account for the measured S(IV). The Taft correlations discussed above point out other carbonyls that are potentially present in the atmosphere, should be very soluble, and should form stable sulfonates.

The presence or absence of sulfonates will depend on the pH history of the droplets. The optimum conditions for sulfonates to form appear to be in source plumes. High levels of SO_2 and RCHO are present and the acidity may be low initially. Sulfonate formation proceeds at an initially rapid rate, but slows as the droplets are acidified by dissociation of $SO_2 \cdot H_2O$, S(IV) oxidation, and HNO_3 formation. The increased acidity also retards the decomposition reaction so that the sulfonates will not break down once the precursors are reduced by dilution or other reactions.

Sampling Methods

The most widely used methods of collecting gas–phase aldehydes are dinitrophenylhydrazine (DNPH) filled bubblers (e.g. Fung and Grosjean, 1981; Grosjean, 1982; Lowe et al., 1980), or coated resin cartridges (Kuwata et al., 1983). DNPH reacts with carbonyls at low pH to form hydrazone derivatives. These are subsequently extracted and analyzed by HPLC. A two phase system is sometimes employed to enhance the extent of derivatization by isolating the products from the reactants (Fung and Grosjean, 1981). The low pH required for derivatization minimizes negative interference due to sulfonate formation if SO_2 is present. DNPH–filled bubblers have proven effective for the identification of short–chain aldehydes in the atmosphere. Reported detection limits are 0.1 ppb. The collection efficiency for substituted carbonyls and dicarbonyls has not been determined.

Other approaches to carbonyl sampling have been tried. DuVal et al., (1985) used bisulfite–filled bubblers to sample carbonyls. The α–hydroxyalkanesulfonates that formed were subsequently analyzed by ion chromatography. This method will be most effective for carbonyls that readily form sulfonates. Low-molecular-weight organic species have also been collected using condensate films (Dawson et al., 1980; Snider and Dawson, 1985). This method is obviously limited to species with high overall solubility constants. Furthermore, the volume of air sampled is not directly measured, but must be calculated from the heat and mass transfer equations for laminar flow past a chilled plate. Henry's Law constants must be known for the species of interest at temperatures near 273 K.

Carboxylic Acids

Several methods of collecting organic acid from the gas phase were compared in a field test conducted in Charlottesville, VA during June 1986 (Keene et al., 1988). The methods included NaOH and Na_2CO_3 coated filters, NaOH coated denuders, GC resin cartridges, an aqueous condensate film sampler, an aqueous mist chamber, and a cryogenic trap. The charcoal trap method used by Hoshika (1982) has not been compared to other collection methods. The results indicate large disparities in collection efficiency by the various methods or serious artifact problems. The aqueous collection methods and the OH–coated denuder generally agreed with one another while the base–impregnated filters and GC resin gave higher concentrations. The cryogenic trap was plagued by ice plugs and did not produce any usable results. Subsequent laboratory testing suggests that the high values were due to reaction of gas–phase aldehyde to produce formic and acetic acids. A possible explanation is the Cannizzaro reaction (Geismann, 1943) (eqs. 18–19), which could proceed in a highly alkaline aqueous film on the collection surface.

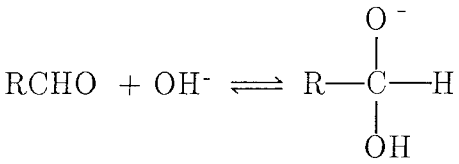

$$\mathrm{RCHO} + \mathrm{OH}^- \rightleftharpoons \mathrm{R{-}}\underset{\mathrm{OH}}{\overset{\mathrm{O}^-}{\mathrm{C}}}\mathrm{{-}H} \qquad (18)$$

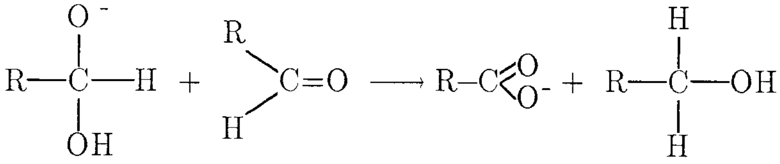

(19)

Another potential artifact on alkaline collection media is the hydrolysis of peroxyacetylnitrate, PAN, to form CH_3COO^- and NO_2^-. This is particularly important in highly polluted areas such as Los Angeles.

Previous Measurements

Formic and acetic acid are the most well studied organic acids (see Table 2.4), although some studies have included higher acids. Hoshika (1982) measured several normal and branched organic acids up to pentanoic in the gas phase. Traces of dicarboxylic acids such as citrate, oxalate, malonate and succinate have been observed in rainwater (Keene et al., 1983; Kawamura et al., 1985; Norton, 1985). Steinberg et al. (1985) report measurements of several α–ketoacids in Los Angeles rain. A number of higher monocarboxylic acids such as propanoic, lactic and butanoic have also been observed in rain, cloud and fog water (Kawamura and Kaplan, 1984; Norton, 1985; Jacob et al., 1986a; Munger, unpublished results). Concentrations of the higher acids are less than formate and acetate.

Table 2.4. Summary of atmospheric formic and acetic acid concentrations.

Site	Formic	Acetic	Reference
	(gas phase)		
	—— nmole m^{-3} ——		
Nagoya Japan	—	68	Hoshika 1982
Air near poultry manure pen	—	270	ibid.
Tucson, AZ (uncontaminated)	61	41	Dawson et al. 1980
Tucson, AZ (urban influenced)	102	163	ibid.
Saguaro National Monument, AZ	41	20	ibid.
Sells, AZ	31	24	ibid.
Ducke Reserve, Brazil (surface)	62	80	Andreae et al. 1988
(canopy top)	94	134	ibid.
Hampton, VA (growing)	84	59	Talbot et al. 1988
(non–growing)	31	31	ibid.

Table 2.4.(continued)

Site	Formic	Acetic	Reference
	(rainwater)		
	—— µM ——		
Los Angeles, CA	8.7	24	Kawamura and Kaplan (1984)
Charlottesville, VA	14	5	Keene and Galloway (1984)
Amsterdam Is.	10	4	Galloway et al. (1982)
San Carlos, Venezuela	14	3	ibid.
Katharine, Australia	22	7	ibid.
Wisconsin (spring)	10	4	Chapman et al. 1986
Hampton, VA (growing season)	7	5	Talbot et al. 1988
(non–growing)	2	2	ibid.
Ducke Reserve, Brazil	18	11	Andreae et al. 1988
	(fog and cloudwater)		
	—— µM ——		
Los Angeles, CA	92	43	Kawamura and Kaplan (1984)
Bakersfield, CA	45	155	Jacob et al. (1986)
McKittrick, CA	22	3	ibid.
Buttonwillow, CA	144	59	ibid.
Visalia, CA	53	65	ibid.

Elevated concentrations of formic and acetic acid near urban areas (Dawson et al., 1980) and correlation with NO_3^- (Norton, 1985) indicate an anthropogenic source for some organic acids. Biological activity is implicated by the elevated concentrations of organic acids near a poultry manure pen (Hoshika, 1982). A substantial background level of organic acid from biogenic sources is indicated by the levels observed at rural and remote sites (Keene et al., 1983; Keene and Galloway, 1986) Keene and Galloway (1986) note that organic acid concentrations are greatest during the growing season and sharply decline after leaf fall. Talbot et al. (1988) observe a similar seasonal trend. Formic acid decreases to a greater extent in the non–growing season than acetic acid does. Diurnal variations in formic and acetic acid concentration have been observed at both temperate (Talbot et al. 1988) and tropical sites (Andreae et al., 1988). The data imply that carboxylic acids have a vegetative source in conjunction with photochemical production. Part of the morning increase in formic and acetic acid concentrations may be due to reentrainment of air from above the nocturnal boundary layer (Jacob and Wofsy, 1988). It is not clear from the data whether acids are emitted directly from vegetation or are formed from precursors such as isoprene or other biogenic hydrocarbons. The importance of combustion as a source for carboxylic acids is indicated by their high concentrations in the haze layers derived from biomass burning in the Amazon jungle (Andreae et al. 1988), vehicle exhaust, and wood smoke (Talbot et al., 1988). Keene and Galloway (1986) have pointed out a consistent ratio between formate and acetate concentrations in rainwater from throughout the world. The ratio of formate to acetate at continental sites during the growing season is 2.89; the ratio for rainwater from all other sites and seasons is 2.44. Absolute levels of organic acid are higher for the terrestrial sites. This ratio is independent of pH, which implies that the ratios of organic acids in the gas phase vary widely (if rainwater is in equilibrium with the gas phase), while those in the liquid phase do not. They suggest that this pattern implies a common source or control mechanism for acetic and formic acid concentrations in rainwater. This relationship does not appear to hold for samples from urban areas given in Table 2.4.

Carbonyls in the atmosphere have been more extensively studied than the carboxylic acids. Most investigations have focused on formaldehyde (Table 2.5) or acetaldehyde (Table 2.6). Measurements of higher aldehydes generally indicate they are less important than formaldehyde and acetaldehyde. Concentrations of formaldehyde at remote sites are generally consistent with predictions of background levels produced by oxidation of biogenic methane (NRC 1981). Lowe and Schmidt (1983), however, report lower than expected concentrations of CH_2O over the Atlantic. The highest concentrations of aldehydes, in both gas and aqueous phase, are found in urban areas, indicating an anthropogenic source. The importance of secondary reactions is indicated by correlation between CH_2O and O_3 diurnal patterns (Cleveland et al., 1977). Summer maxima of both CH_2O and CH_3CHO (Tanner and Meng, 1984) are further evidence of the importance of photochemical production of aldehydes. The only reports of dicarbonyls in the atmosphere are those of Steinberg and Kaplan (1984) They observed glyoxal and methylglyoxal at levels comparable to CH_2O.

Based upon observations of elevated levels of CH_2O in association with S(IV), Munger et al. (1984) postulated the presence of HMSA. Analysis of samples from

Table 2.5 Atmospheric formaldehyde concentrations.

Site	n	Range	Mean	Reference
		(gas phase)		
		—— nmole m^{-3}——		
Los Angeles, CA	36	80–160	830	Grosjean (1982)
Claremont, CA	65	120–1930	1000	ibid.
New Jersey	4*	150–260	—	Cleveland et al. (1977)
Deuselbach, F.R.G	—	130–900	420	Klippel and Warneck (1980)
"	14	16–155	69	Neitzert and Seiler (1981)
"	15	0–37	—	Platt and Perner (1980)
Julich, F.R.G	72	4–265	87	ibid.
" (ground level)	64	12–180	52	Lowe et al. (1980)
(boundary layer)	10	12–20	—	ibid.
(free troposphere)	4	0–4	—	ibid.
Julich, F.R.G	174	8–410	52	Lowe and Schmidt (1983)
Mainz, F.R.G	14	30–210	78	Neitzert and Seiler (1981)
Upton, NY (Brookhaven)	135	37–1960	306	Tanner and Meng (1984)
Schenectady, NY	71	30–1240	310	Schulam et al. (1985)
Whiteface Mt. NY	18	33–106	—	ibid.
Tucson, AZ	8	—	73	Snider and Dawson (1985)
Rural Arizona	27	—	61	ibid.

Table 2.5 (continued).

Site	n	Range	Mean	Reference
St. Louis, MO	11	≤760	460	Salas and Singh (1986)
Denver, CO (June 1980)	18	≤1170	500	ibid.
Riverside, CA	18	≤1670	775	ibid.
Staten Island, NY	17	≤1870	583	ibid.
Pittsburgh, PA	8	≤1160	754	ibid.
Chicago, IL	5	≤640	460	ibid.
Downey, CA	48	≤2760	460	ibid.
Houston, TX	11	≤920	155	ibid.
Denver, CO (April 1984)	21	≤225	94	ibid.
Urban Residential Area, Japan – (summer)	2	—	273	Kuwata et al. (1983)
(winter)	2	—	120	ibid.
Industrial area, Japan (summer)	1	—	270	ibid.
(winter)	1	—	118	ibid.
Tokyo, Japan	–	33–800	—	Fushimi Miyake (1980)
Mt. Norikura	–	33–130	—	ibid.
western north Pacific		–	33–82	— ibid.
Philippines – Borneo	–	33–450	—	ibid.
Indian Ocean				
0–20° S	–	33–204	—	ibid.
>20° S	–	≤ 33	—	ibid.

Table 2.5 (continued).

Site	n	Range	Mean	Reference
Atlantic Ocean	151	4–26	8	Lowe and Schmidt (1983)
Irish Coast	37	4–21	8	ibid.
Loophead, Ireland	5	≤ 12	—	Platt and Perner (1980)
Dagebull, F.R.G.	9	0–20	13	ibid.
Cape Point, South Africa	5	8–41	20	Neitzert and Seiler (1981)
Baring Head New Zealand	–	–	8	Lowe and Schmidt (1983)
Enewetak	7	—	16	Zafiriou et al. (1980)
		(Aerosol)		
		– nmole m^{-3} –		
Claremont, CA	14	0–9	3	Grosjean (1982)
Mainz, F.R.G.	8	—	2.1	Klippel and Warneck (1980)
Deuselbach, F.R.G.	–	—	1.3	ibid.
Irish coast	16	—	0.16	ibid.
		(Rain water)		
		—— μM ——		
Mainz, F.R.G.	38	—	5.8	Klippel and Warneck (1980)
Deuselbach	19	—	4.7	ibid.
Irish coast	16	—	4.7	ibid.
Enewetak	6	0.2–0.4	0.26	Zafiriou, et al. (1980)
Los Angeles	6	2.8–15.3	8.2	Steinberg and Kaplan (1984)
Julich, F.R.G.	–	0.4–3.5	—	Lowe and Schmidt (1983)

Table 2.5 (continued).

Site	n	Range	Mean	Reference
		(fog and cloud water)		
		— µM —		
Los Angeles 1981–82	15	93–320	190	Munger et al. (1984)
Southern California coast 1983	13	53–256	73	ibid.
Bakersfield, CA 1983	83	53–709	83	ibid.
Pt. Reyes, CA	22	0.6–18	3	ibid.
San Nicholas Is, CA	5	6.6–24	17	ibid.
Pasadena, CA (intercepted stratus)	100	12–173	55	ibid.
Los Angeles (stratus)	11	11–142	70	Richards et al. (19

---

* Medians of 24–hour averages at 4 sites.

Table 2.6 Atmospheric acetaldehyde concentrations.

Site	n	Range (gas–phase)	Mean	Reference
		——— nmole m^{-3} ———		
Los Angeles, CA	33	0–1060	360	Grosjean (1982)
Claremont, CA	66	120–1380	550	ibid.
Upton, NY	135	≤20–1430	120	Tanner and Meng (1984)
Schenectady, NY	71	0–200	—	Schulam et al. (1985)
Whiteface Mt. NY	18	8–33	—	ibid.
Tucson, AZ	17	—	940	Snider and Dawson (1985)
Rural Arizona	18	—	280	ibid.
Urban residential Area, Japan – (summer)	2	—	230	Kuwata et al. (1983)
(winter)	2	—	96	ibid.
Industrial Area, Japan – (summer)	1	—	370	ibid.
(winter)	1	—	70	ibid.
Pittsburgh, PA	8	≤106	57	Salas and Singh (1986)
Chicago, IL	5	≤140	86	ibid.
Downey, CA	48	1160	350	ibid.
Houston, TX	11	≤270	90	ibid.
Denver, CO	21	86	41	ibid.

Table 2.6 (continued).

Site	n	Range	Mean	Reference
		(aerosol)		
		——— nmole m^{-3} ———		
Claremont, CA	14	0.05–9	2.2	Grosjean (1982)
		(rain and fog water)		
		——— μM ———		
Los Angeles (rain)	6	0.2–7	1.8	Steinberg and Kaplan (1985)
(fog)	2	1–3.5	—	ibid.

the San Joaquin Valley by ion–pairing chromatography confirmed the presence of HMSA (Munger et al., 1986). Samples collected during the winter of 1985–86 in Riverside also show substantial levels of aldehydes, S(IV) and HMSA (Munger et al., unpublished data; Dong and Dasgupta,1986; Dasgupta and Yang, 1986).

SUMMARY

A variety of carbonyl compounds and carboxylic acids are formed during the oxidation of hydrocarbons. Many of these compounds are soluble in water. Their equilibrium dissolution into fog– and cloudwater depends on Henry's Law and acid dissociation or carbonyl hydration. The formation of hydroxyalkyl sulfonates is of particular importance.

The simplest aldehydes and carboxylic acids have been determined in a variety of environments. The highest concentrations of formaldehyde and acetaldehyde are observed in urban areas, implying that anthropogenic sources are their most important contributors. Formic and acetic acid are more ubiquitous. Natural sources appear to be important for these species. Seasonal and diurnal cycles in their concentration suggest that vegetation is a major source for carboxylic acids in the atmosphere.

REFERENCES

Andreae, M. O., Talbot, R. W., Andreae, T. W., and R. C. Harriss (1988) Formic and acetic acids over the central Amazon region, Brazil 1. Dry season. *J. Geophys. Res.* **93**, 1616–1624.

Atkinson, R. and Lloyd, A. C. (1984) Evaluation of kinetic and mechanistic data for photochemical smog chamber modelling, *J. Phys. Chem. Ref. Data* **13,** 315.

Atkinson, R., Darnall, K. R., Lloyd, A. C., Winer, A. M., and Pitts, J. N., Jr. (1979) Kinetics and mechanisms of the reactions of the hydroxyl radical with organic compounds in the gas phase, *Adv. Photochem.* **11,** 375–487.

Betterton, E. and Hoffmann, M. R. (1987) The kinetics, mechanism, and thermodynamics of the reversible reaction of methylglyoxal (CH_3COCHO) with S(IV), *J. Phys. Chem.* **91**, 3011–3020.

Betterton, E. A., Erel, Y., and Hoffmann, M. R. (1988) Aldehyde–bisulfite adducts: Prediction of some of their thermodynamic and kinetic properties, *Environ. Sci. Technol.* **22**, 92–97.

Betterton, E. A. and Hoffmann, M. R. (1988) Henry's law constants of some environmentally important aldehydes, *Environ. Sci. Technol.* **22**, 1415–1418

Boyce, S. D. and Hoffmann, M. R. (1984) Kinetics and mechanisms of the formation of hydroxymethanesulfonic acid a low pH, *J. Phys. Chem.* **88,** 4740–46.

Burroughs, L. F. and Sparks, A. H. (1973) *J. Sci. Fd. Agric.* **24**, 187–198.

Buschmann, H.–J., Fuldner, H.–H., and Knoche, W. (1980) The reversible hydration of carbonyl compounds in aqueous solution. Part I, The keto/gem–diol equilibrium, *Ber. Bunenges. Phys. Chem.* **84**, 41–44.

Buschmann, H.–J., Dutkiewicz, E., and Knoche, W. (1982) The reversible hydration of carbonyl compounds in aqueous solution part II: The kinetics of the keto/gem–diol transition, *Ber. Bunsenges. Phys. Chem.* **86**, 129–134.

Calvert, J. G. and Madronich, S. (1987) Theoretical study of the initial products of the atmospheric oxidation of hydrocarbons, *J. Geophys. Res.* **92**, 2211–2220.

Chameides, W. L. (1984) The photochemistry of a remote marine stratiform cloud, *J. Geophys. Res.* **89**, 4739–4755.

Chapman, E. G., Sklarew, and Flickinger, J. S. (1986) Organic acids in springtime Wisconsin precipitation samples. *Atmos. Environ.* **20**, 1717–1725.

Cleveland, W. S., Graedel, T. E. and Kleiner, B. (1977) Urban formaldehyde: Observed correlation with source emissions and photochemistry, *Atmos.Environ.* **11**, 357–360.

Dasgupta, P. K. and Yang, H.–C.(1986) Trace determination of aqueous sulfite, sulfide and methanethiolate by fluorometric flow injection analysis, *Anal. Chem.* (submitted).

Dawson, G. A., Farmer, J. C., and Moyers, J. L. (1980) Formic and acetic acids in the atmosphere of the southwest U. S. A. , *Geophys. Res. Lett* **7**, 725–728.

Deister, U., Neeb, R., Helas, G. and Warneck, P. (1986) Temperature dependence of the equilibrium $CH_2(OH)_2 + HSO_3^- = CH_2(OH)SO_3^- + H_2O$ in aqueous solution, *J. Phys. Chem.* **90**. 3213–3217.

Dong, S. and Dasgupta, P. K (1987) Fast fluorometric flow injection analysis of formaldehyde in atmospheric water, *Environ. Sci. Technol.* **21**, 581–588.

DuVal, D. L., Rogers, M, and Fritz, J. S. (1985) Determination of aldehydes and acetone by ion chromatography, *Anal. Chem.* **57**,1583–1586.

Finlayson–Pitts, B. J. and Pitts, J. N., Jr. (1986) Atmospheric Chemistry: Fundamentals and Experimental Techniques, John Wiley, New York, 1098.

Fung, K. and Grosjean, D. (1981) Determination of nanogram amounts of carbonyls as 2,4–dinitrophenylhydrazones by high performance liquid chromatography, Anal. Chem. **53**, 168–171.

Fushimi, K. and Miyake, Y. (1980) Contents of formaldehyde in the air above the surface of the ocean, *J. Geophys. Res.* **85**, 7533–7536.

Galloway, J. N., Likens, G. E., Keene, W. C. and Miller, J. M. (1982) The composition of precipitation in remote areas of the world, *J. Geophys. Res.* **87**, 8771–8786.

Geismann, T. A. (1943) The Cannizzaro reaction, *Org. React.* **2**, 94–113.

Greenzaid, P., Luz, and Samuel, D. (1967) A nuclear magnetic resonance study of the reversible hydration of aliphatic aldehydes and ketones. I. Oxygen–17 and proton spectra and equilibrium constants, *J. Am. Chem. Soc.* **89**, 749–756.

Graedel, T. E., Hawkins, D. T., and Claxton, L. D. (1986) *Atmospheric Chemical Compounds: Sources, Occurrence, and Bioassay*, Academic Press, New York.

Grosjean, D. (1982) Formaldehyde and other carbonyls in Los Angeles ambient air, *Environ. Sci. Technol.* **16**, 254–262.

Grosjean, D. and Fung, K. (1984) Hydrocarbons and carbonyls in Los Angeles air, *J. Air Pollut. Cont. Assoc.* **34**, 537–543.

Gubareva, M. A. (1947) Bisulfite compounds of aldehydes and ketones. I. Equilibrium of the addition reaction in aqueous solution, *J. Gen. Chem. USSR* **17**, 2259–2264.

Hoshika, Y. (1982) Gas chromatographic determination of lower fatty acids in air at part–per–trillion levels, *Anal. Chem.* **54**, 2433–2437.

Jacob., D. J. (1986) The chemistry of OH in remote clouds and its role in the production of formic acid and peroxymonosulfate, *J. Geophys. Res.* **91**, 9807–9826.

Jacob, D. J., Munger, J. W., Waldman, J. M., and Hoffmann, M. R. (1986) The H2SO4–HNO3–NH3 system at high humidities and in fogs: I. Spatial and temporal patterns in the San Joaquin Valley of California, *J. Geophys. Res* **91**, 1073–1088.

Jacob, D. J. and Wofsy, S. C. (1988) Photochemical production of carboxylic acids in a clean continental atmosphere, in *Acid Deposition Processes at High Elevation Sites*, edited by H. M. Dunsworth, D. Reidel, Hingham, Mass. (in press).

Kok, G. L., Gitlin, S., N., and Lazrus, A. L. (1986) Kinetics of the formation and decomposition of hydroxymethanesulfonate, *J. Geophys. Res.* **91**, 2801–2804.

Kawamura, K, Steinberg, S. and Kaplan, I. R. (1985) Capillary GC determination of short–chain acids in rain, fog and mist, *Intern. J. Environ. Anal. Chem.* **19**, 175–188.

Kawamura, K. and Kaplan, I. R. (1984) Capillary gas chromatography determination of volatile organic acids in rain and fog samples, *Anal. Chem.* **56**, 1616–1620.

Keene, W. C. and Galloway, J. N. (1984) Organic acidity in precipitation of North America, *Atmos. Environ.* **18**, 2491–2497.

Keene, W. C. and Galloway, J. N. (1986) Considerations regarding sources for formic and acetic acids in the troposphere, *J. Geophys Res.* **91**, 14466–14474.

Keene, W. C., Galloway, J. N., and Holden, J. D. (1983) Measurement of weak organic acidity in precipitation from remote areas of the world, *J. Geophys. Res.* **88**, 5122–5130.

Keene, W. C., Talbot, R. W., Andreae, M. O., Beecher, K., Berresheim, J. Castro, M., Farmer, J. C., Galloway, J. N., Hoffmann, M. R., Li. S.–M., Maben, J. R., Munger, J. W., Norton, R. B., Pszenny, A. A. A. P., Puxbaum, H. Westberg, H., and Winiwarter, W. (1988) An intercomparison of measurement systems for vapor and particulate phase concentrations of formic and acetic acids, *J. Geophys. Res.* (in press).

Klippel, W. and Warneck, P. (1978) Formaldehyde in rain water and on the atmospheric aerosol, *Geophys. Res. Lett.* **5,** 177–179.

Klippel, W. and Warneck, P. (1980) The formaldehyde content of the atmospheric aerosol, *Atmos. Environ.* **14,** 809–818.

Kuwata, K., Uebori, M., Yamasaki, H., Kuge, Y., and Kiso, Y. (1983) Determination of aliphatic aldehydes in air by liquid chromatography, *Anal. Chem.* **55,** 2013–2016.

Likens, G. E., Edgerton, E. S., and Galloway, J. N. (1983) The composition and deposition of organic carbon in precipitation, *Tellus* **35,** 16–24.

Liljestrand, H. M. and Morgan, J. J. (1981) Spatial variations of acid precipitation in Southern California, *Environ. Sci. Technol.* **15,** 333–338.

Lloyd, A. C., Atkinson, R., Lurmann, F. W., and Nitta, B. (1983) Modelling potential ozone impacts from natural hydrocarbons — I. Development and testing of a chemical mechanism for the NO_x–air photooxidations of isoprene and α–pinene under ambient conditions, *Atmos. Environ.* **17**, 1931–1950.

Lowe, D. C. and Schmidt, U. (1983) Formaldehyde measurements in the nonurban atmosphere, *J. Geophys Res.* **88,** 10844–10858.

Lowe, D. C., Schmidt, U. and Ehhalt, E. H. (1980) A new technique for measuring troposheric formaldehyde [CH2O], *Geophys. Res. Lett.* **7,** 825–828.

Martell,A. E. and Smith, R. M. (1977) *Critical Stability Constants, vol. 3*, Plenum, New York.

Munger, J. W., Jacob, D. J., and Hoffmann, M. R. (1984) The occurrence of bisulfite–aldehyde adducts in fog– and cloudwater, *J. Atmos. Chem.* **1**, 335–350.

Munger, J. W., Tiller, C. T., and Hoffmann, M. R. (1986) Determination of hydroxymethanesulfonate in fog water, *Science* **231**, 247–249.

National Research Council (1981) *Formaldehyde and other aldehydes,* National Academy Press Washington, D. C., 340 pp.

Neitzert, V. and Seiler, W. (1981) Measurement of formaldehyde in clean air, *Geophys. Res. Lett.* **8**, 79–82.

Norton, R. B. (1985) Measurement of formate and acetate in precipitation at Niwot Ridge and Boulder, Colorado, *Geophys. Res. Lett.* **12**, 769–772.

Olson, T. M., Boyce, S. D., and Hoffmann, M. R. (1986) Kinetics, thermodynamics, and mechanism of the formation of benzaldehyde–S(IV) adducts, *J. Phys. Chem.* 90, 2482–2488.

Olson, T. M. and Hoffmann, M. R. (1986) On the kinetics of formaldehyde–S(IV) adduct formation in slightly acidic solution, *Atmos. Environ.* **20**, 2277–2278.

Olson, T. M., and Hoffmann, M. R. (1988a) Kinetics, mechanism, and thermodynamics of glyoxal–S(IV) adduct formation. *J. Phys. Chem.* **92**, 533–540.

Olson, T. M., and Hoffmann, M. R. (1988b) The formation kinetics, mechanism, and thermodynamics of glyoxylic acid–S(IV) adducts. *J. Phys Chem.* **92**, 4246–4253.

Perrin, D. D., Dempsey, B., and Serjeant, E. P. (1981) *pK_a Prediction for Organic Acids and Bases*, Chapman and Hall Ltd, London, 143 pp.

Platt, U. and Perner, D. (1980) Direct measurement of atmospheric CH_2O, HNO_2, O_3, and SO_2 by differential optical absorption in the near UV, *J. Geophys. Res.* **85**, 7453–7458.

Pruppacher, H. R. and Klett, J. D. (1978) *Microphysics of clouds and precipitation,* D. Reidel, Dordrecht, 139–140.

Richards, L. W., Anderson, J. A., Blumenthal, D. L., McDonald, J. A., Kok, G. L., and Lazrus, A. L. (1983) Hydrogen peroxide and sulfur (IV) in Los Angeles cloud water, *Atmos. Environ.* **17**, 911–914.

Rogozen, M. B., Maldonado, G. , Grosjean, D., Shochet, A., and Rapoport, R. (1984) Formaldehyde: A survey of airborne concentrations and sources. Final Report to California Air Resources Board, Sacramento, CA.

Salas, L. J. and Singh, H. B. (1986) Measurements of formaldehyde and acetaldehyde in urban ambient air, *Atmos. Environ.* **20**, 1301–1304.

Schulam, P., Newbold, R. and Hull, L. A. (1985) Urban and rural Ambient air aldehyde levels in Schenectady, New York and on Whiteface Mountain, New York, *Atmos. Environ.* **19**, 623–626.

Seinfeld, J. H. (1986) *Atmospheric Chemistry and Physics of Air Pollution,* John Wiley, New York, 738 pp..

Skrabal, A. and Skrabal, R. (1936) Die dynamik der formaldehyde–bisulfit reacktion, *Sitz Akad. Wirs.* Wien. **145,** 617–647.

Snider, J. R. and Dawson, G. A. (1985) Troposheric light alcohols, carbonyls, and acetonitrile: Concentrations in the southwestern United States and Henry's law data, *J. Geophys. Res.* **90,** 37973805.

Sørensen, P. E,, Bruhn, K., Lindeløv, F. (1974) *Acta Chem. Scand.* **28**,162–168.

Steinberg, S. and Kaplan, I. R. (1984) The determination of low molecular weight aldehydes in rain, fog, and mist by reversed phase liquid chromatography of the 2,4–dinitrophenylhydrazone derivatives, *Intern. J. Environ. Anal. Chem.* **18**, 253–266.

Steinberg, S., Kawamura, K., and Kaplan, I. R. (1985) The determination of α–keto acids and oxalic acid in rain, fog and mist by HPLC, *Intern. J. Environ. Anal. Chem.* **19**, 251–260.

Talbot, R. W., Beecher, K. M., Harriss, R. C., and Cofer, W. R., III (1988) Atmospheric geochemistry of formic and acetic acids at a mid–latitude temperate site. *J. Geophys. Res.* **93**, 1638–1652.

Tanner, R. L and Meng, Z. (1984) Seasonal variations in ambient atmospheric levels of formaldehyde and acetaldehyde, *Environ. Sci. Technol.* **18**, 723–726.

Tuazon, E. C., MacLeod, H., Atkinson, R., and Carter, W. P. (1986) α–dicarbonyl yields from the NOx–air photooxidations of a series of aromatic hydrocarbons in air, *Environ. Sci. Technol.* **20**, 383–387.

Wagaman, D. D., Evans, W. H., Parker, V. B., Schumm, R. H., Halow, I., Bailey, S. M., Churney, K. L., and Nutall, R. L. (1982) *J. Phys. and Chem. Ref. Data.* 11, supp. 2.

Wasa, T. and Musha, S. (1970) Polarographic behavior of glyoxal and its related compounds, *Bull. Univ. Osaka Prefect. Ser. A* **19**, 169–180.

Zafiriou, O. C., Alford, J. Herrera, M. Peltzer, E. T, Gagosian, R. B., and Liu, S.C. (1980) Formaldehyde in remote marine air and rain; Flux measurements and estimates, *Geophys. Res. Lett.* **7**, 341–344.

JOURNAL OF GEOPHYSICAL RESEARCH, VOL. 88, NO. C9, PAGES 5109-5121, JUNE 20, 1983

CHAPTER 3

Fogwater Chemistry in an Urban Atmosphere

J. William Munger, Daniel J. Jacob, Jed M. Waldman, and Michael R. Hoffmann

W. M. Keck Laboratories, California Institute of Technology, Pasadena, California 91125

Analyses of fogwater collected by inertial impaction in the Los Angeles basin and the San Joaquin Valley indicated unusually high concentrations of major and minor ions. The dominant ions measured were NO_3^-, SO_4^{2-}, NH_4^+, and H^+. Nitrate exceeded sulfate on an equivalent basis by a factor of 2.5 in the central and coastal regions of the Los Angeles basin but was approximately equal in the eastern Los Angeles basin and the San Joaquin Valley. Maximum observed values for NH_4^+, NO_3^-, and SO_4^{2-} were 10.0, 12.0, and 5.0, meq l^{-1}, while the lowest *p*H observed was 2.2. Iron and lead concentrations of over 0.1 m*M* and 0.01 m*M*, respectively, were observed. High concentrations of chemical components in fog appeared to correlate well with the occurrence of smog events. Concentrations in fogwater were also affected by the physical processes of condensation and evaporation. Light, dissipating fogs routinely showed the highest concentrations.

Introduction

Laboratory [*Schwartz*, 1983; *Martin*, 1983; *Hoffmann and Jacob*, 1983] and field [*Cass and Shair*, 1980; *Cox*, 1974; *McMurry et al.*, 1981; *Smith and Jeffery*, 1975; *Wilson and McMurry*, 1981] studies have indicated that droplet-phase chemistry is important in SO_2 oxidation. Droplet-phase oxidation of SO_2 occurs, in part, via the following reactions

$$SO_2(g) \overset{K_H}{\rightleftharpoons} SO_2(aq) \qquad (1)$$

$$SO_2(aq) \overset{K_{a1}}{\rightleftharpoons} H^+ + HSO_3^- \qquad (2)$$

$$2HSO_3^- + O_2 \xrightarrow[Mn(II)]{Fe(III)} 2HSO_4^- \qquad (3)$$

$$HSO_4^- \overset{K_{a2}}{\rightleftharpoons} H^+ + SO_4^{2-} \qquad (4)$$

In Los Angeles, *Cass* [1975] observed a correlation between the occurrence of high sulfate aerosol levels during the afternoon and the presence of coastal fog and low clouds in the morning. The mean SO_2 to SO_4^{2-} conversion rate during July in Los Angeles is 6% hr^{-1} [*Cass*, 1981], whereas gas-phase reactions can account for, at most, conversion rates of 4.5% hr^{-1} [*Sander and Seinfeld*, 1976]. *Morgan and Liljestrand* [1980] reported that light misting rainfalls emanating from low stratus clouds in Los Angeles resulted in *p*H values as low as 2.9 with correspondingly high SO_4^{2-} and NO_3^- concentrations. *Waldman et al.* [1982] have previously reported *p*H values near 2.2 in urban fog. Furthermore, *Hegg and Hobbs* [1981] have reported S(IV) to S(VI) conversion rates of 4.0 to 300% hr^{-1} in wave clouds over western Washington.

In addition to its importance as a chemical reaction site, fog may exert a significant influence on scavenging and deposition, on human health, and on vegetation. Fog forms in the ground layer where gases and aerosols are most concentrated. Because fog droplets are approximately 100 times smaller than rain drops, they should be more concentrated than rain, and mass transfer should not limit the kinetics of fog droplet reactions [*Schwartz*, 1983; *Baboolal et al.*, 1981].

In light of these results and the expectation that fog droplets (or the fine aerosol remaining after fog has evaporated) are sites for rapid conversion of SO_2 to SO_4^{2-} we began a study to characterize the chemical composition of fogwater. Because of the physical similarity to clouds, fog is expected to exhibit the same chemical processes occurring in clouds and, to some degree, aquated submicron aerosols. Information about the chemistry of fogwater may be applicable to the broader questions about ambient acid formation and acidic precipitation. The role of fog in the nocturnal chemistry of SO_2 has been examined by *Jacob and Hoffmann* [1983].

Methods

Fogwater was collected with a rotating arm collector (RAC), which was modified from an original design reported by *Mack and Pilie* [1975]. A 67.5-cm-long, Teflon-coated steel tube with 10 × 0.95 cm slots milled into opposite sides at each end of the tube is rotated at 1700 rpm with a 1.5-HP induction motor. This rotation imparts a relative velocity of ~ 50 m/s to the slots. Droplets impact in the slots and are driven by centrifugal force into 30-ml polyethylene bottles attached at the ends of the arms. During operation, the pivot of the arm is 1.4 m above ground level. Based upon changes in particle-size distributions measured with a laser optical particle counter during operation in a cloud chamber, the RAC was determined to have a lower-size cut of ~ 8 μm [*Jacob et al.*, 1982]. The bulk of liquid water in fogs is contributed by droplets larger than 8 μm, but droplets smaller than 8 μm may be more concentrated than those that are actually collected. Consequently, the concentration of species in fogwater may be slightly underestimated. With this design, up to 2 ml min^{-1} of fogwater has been collected during dense fog and 0.1 to 1.0 *ml* min^{-1} during lighter fog. Collection efficiency under these conditions is estimated to be greater than 80%, based on laboratory calibration. We are currently working on a fog sampler with a lower-size cut in order to characterize the chemistry of the smaller fog droplets.

Site Descriptions

Figure 1 indicates the sites at which fogwater was collected. The Pasadena site, which is located on the roof of a four-story building on the Caltech campus, is in a predominantly residential neighborhood 25 km north of downtown Los Angeles. There are no major pollutant sources in the immediate vicinity. The Lennox site was selected because of its close proximity to both industrial and mobile pollutant sources and its high frequency of marine fog in late autumn: it is situated on the roof of a one-story building at a busy intersection within 100 m of a

Paper number 3C0293.
0148-0227/83/003C-0293$05.00

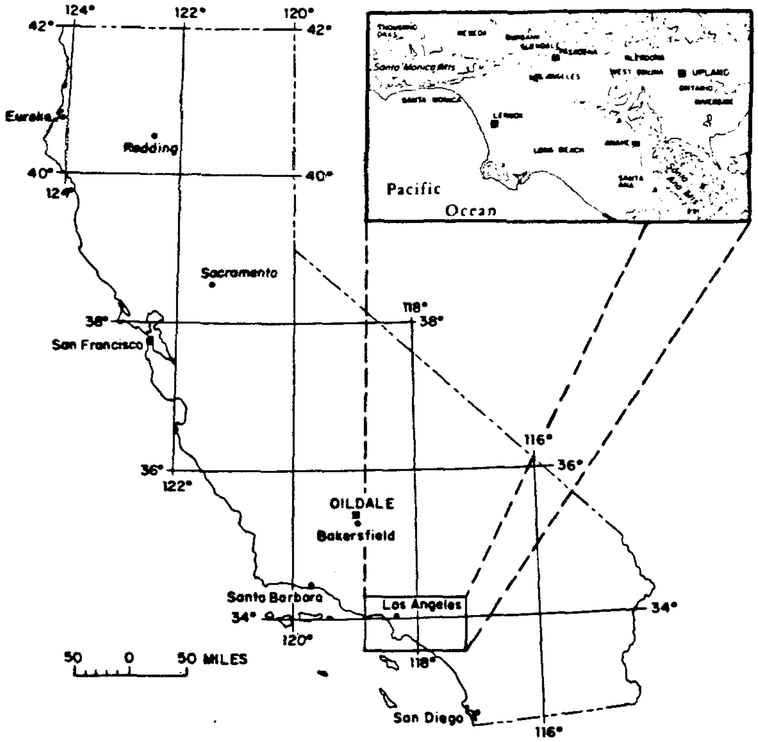

Fig. 1. Map of fog sampling sites in Southern California. Los Angeles area sites are indicated on the inset.

major freeway and 6 km from the ocean. Major point sources near the Lennox site include an oil refinery, power plant, Los Angeles International Airport, and several other industrial facilities.

The Oildale site, near Bakersfield, is in an area with higher sulfur emissions from secondary oil recovery operations and is subject to extensive fog ('Tule fog'), which persists throughout the San Joaquin Valley during the early winter. The sampler was placed on the roof of an air-quality monitoring station (about 4 m aboveground). Upland is 60 km NE of downtown Los Angeles. A steel plant and several other heavy industries are located within 30 km of this site, which is also on the roof of an air-quality monitoring station in a residential area.

FOG PATTERNS

In Los Angeles, fog generally occurs during two distinct periods: November through January and April through June. At the two inland sites, Pasadena and Upland, fog occurs sporadically in the night and early morning throughout the fog seasons. Fogs along the coast tend to form repeatedly for several nights, lifting for only part of the day. In the San Joaquin Valley, fog forms for extended periods during the early winter months and often persists throughout the day.

ANALYTICAL METHODS

The sample-handling and analytical protocol is illustrated in Figure 2. Analysis of the sample began as soon as collection ended; measurement of *p*H and separation of preserved aliquots was completed within 30 min. In the field, samples were stored over ice, then refrigerated when brought back to the laboratory; *p*H was determined in the field with a Radiometer PHM 80 meter. Sulfite was preserved by addition of CH_2O at *p*H 4 to form hydroxymethanesulfonic acid (HMSA) [*Dasgupta et al.*, 1980; *Fortune and Dellinger*, 1982]; 3,5-diacetyl-1,4-dihydrolutidine (DDL) formed by reaction of formaldehyde and acetyl acetone in the presence of NH_4^+ [*Nash*, 1953] is stable for at least 7 days [*Rietz*, 1980]. Sulfite is known to interfere with this reaction [*Nash*, 1953], but no correction was made. Addition of HNO_3 to achieve a concentration of 0.16 *M* was used to stabilize an aliquot for trace-metal analyses. Beginning with the Oildale samples, aliquots were filtered through 0.4-μm Nuclepore membranes in the field. Because of extremely high cation and anion concentrations in fogwater, samples usually had to be diluted before analysis. With sample dilution, complete analyses of volumes as small as 5 ml was practicable.

Major cations were determined on a Varian AA5 atomic absorption spectrophotometer by using an air-acetylene flame. Lanthanum was added to the entire aliquot used for AAS in order to release calcium and magnesium. Ammonium was determined by the phenol-hypochlorite method [*Solórzano*, 1967]. Anions were determined by ion chromatography (IC), using a 3-m*M* $NaHCO_3$/2.4-m*M* Na_2CO_3 eluent. Aliquots of sample were spiked to give the same HCO_3^-/CO_3^{2-} concentration as the eluent in order to eliminate the water dip that interferes with F^- and Cl^- peaks. *Galloway et al.* [1982] suggest that low molecular weight carboxylic acids are present in rainwater. Considering the high aldehyde concentrations observed in fogwater, it is likely that the corresponding acids are present as well. If present, these acids would be a positive interference with fluoride. The absorbance of DDL formed

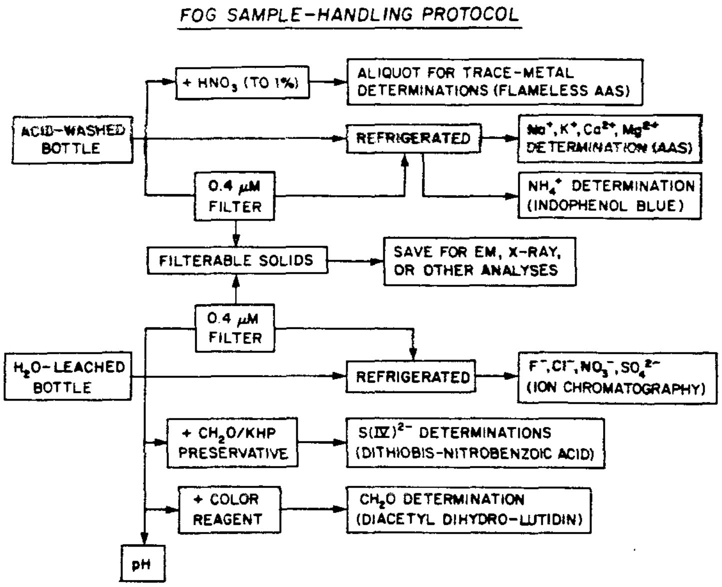

Fig. 2. A schematic flow diagram indicating fog sample-handling protocol and analytical procedures.

from CH_2O was measured at 412 nm on a Beckman Acta III spectrophotometer.

The preserved solution for S(IV) was injected into the IC and eluted with 1 m*M* KHP [*Dasgupta et al.*, 1980]. Because the F^- and Cl^- peaks coeluted with the hydroxymethanesulfonate (HMSA) using this eluent, the S(IV) in the samples could not be directly quantified. Instead, S(IV) was taken as the difference between the SO_4^{2-} concentration in the preserved aliquot and the SO_4^{2-} concentration in the unpreserved aliquot, measured by the usual IC methods. The first value would be SO_4^{2-} only, the second would be the sum of SO_4^{2-} and SO_3^{2-}. After December 7, S(IV) was measured by a colorimetric method, using 5,5′, Dithiobis-(2-nitrobenzoic acid) DTNB [*Humphrey et al.*, 1970]. Trace metals were determined by flameless atomic absorption (Varian AA6 equipped with a CRA 90 or Perkin-Elmer 360 with a HGA 2100). Gas-phase concentrations of SO_2, NO_x, O_3 were made continuously at the Lennox, Upland, and Oildale sites by conventional instrumental methods.

RESULTS

Table 1 describes the conditions before and during the fog sampling. Samples from Pasadena were collected both after

TABLE 1. Description of Conditions During and Before Fog Sample Collection

Site	Date	Sampled Interval, hr	Conditions During Fog	Prior Conditions
Pasadena	November 15, 1981	2040–0115	Light wind SSW-N; sampled beginning to end of fog.	Fair, good air quality.
Pasadena	November 23, 1981	2320–0130	Light S-SE wind; 14°–12°C; fog thickened to near drizzle; sampled beginning to end of fog.	Hazy and smoggy.
Lennox	December 7, 1981	2305–0840	Light westerly wind; traffic volume and ambient pollutants began to increase at 0530; missed first hour of fog, sampled until fog lifted.	Previous night foggy, smoggy during day, NO_x alert called (NO_x = 0.8 ppm).
Lennox	December 18, 1981	2315–0043	Light westerly wind; sampled from beginning of fog; fog persisted until morning.	Previous night foggy; high NO_x levels during day.
Pasadena	December 20, 1981	745–845	Light northerly wind; 10°C; fog began before 0700; sampled until fog lifted	Previous day was fair.
Oildale	January 14, 1982	0200–0750	Light southerly wind; 3°–4°C, thin fog.	Overcast all of preceding day; dense fog on previous night.
Pasadena	January 17, 1982	2130–2200	Sample collected as fog dissipated.	Smog and haze during the afternoon.
Upland	May 14, 1982	0630–0910	Light and variable wind, 12°C, thin fog.	Low clouds and ground haze throughout night.

TABLE 2. Concentration Ranges for Major and Minor Ions, Sulfite, and Formaldehyde Observed During Fog Events.

Location	Number of Samples in event	Date	*p*H	μeq l^{-1}											
				H^+	Na^+	K^+	NH_4^+	Ca^{2+}	Mg^{2+}	F^-	Cl^-	NO_3^-	SO_4^{2-}	SO_3	CH_2O, mg/l
Pasadena	4	Nov. 15, 1981	5.25–4.74	5.6–55	12–496	4–39	370	19–360	7–153	120	56–280	130–930	62–380	—	—
Pasadena	4	Nov. 23, 1981	4.85–2.92	14–1200	320–500	33–53	1290–2380	140–530	89–360	180–410	480–730	1220–3250	481–944	150–180	3.1–3.5
Lennox	8	Dec. 7, 1981	5.78–2.55	2–2820	28–480	6–156	1120–4060	49–4350	17–1380	115–395	111–1110	820–4560	540–2090	30–250	4.6–12.8
Lennox	3	Dec. 18, 1981	2.81–2.52	1550–3020	80–166	19–40	950–1570	73–190	43–99	180–500	90–197	2070–3690	610–1970	—	—
Pasadena	1	Dec. 20, 1981	3.75	178	51	373	1773	217	78	242	161	1000	450	—	—
Oildale	3	Jan. 14, 1982	3.07–2.90	850–1260	151–1220	39–224	4310–9750	165–1326	20–151	126–242	203–592	3140–5140	2250–5000	440–710	6.1–14.4
Pasadena	1	Jan. 17, 1982	2.25	5625	2180	500	7960	2050	1190	637	676	12000	5060	—	—
Upland	3	May 14, 1982	2.88–2.22	1320–6310	1220–5200	96–482	2329–6312	596–4218	321–1816	168–342	654–1110	4240–10660	2760–4890	446–592	6.1–8.6

clean air days and smoggy days. The fogs in Lennox followed smoggy days. Oildale samples were collected during a period of extensive and persistent fog in the San Joaquin Valley. Samples at Upland were collected after dawn, when the haze that had been present during the night thickened enough to be collected.

The high and low concentrations of major ions, sulfite, and formaldehyde in fogwater during eight fog events are presented in Table 2. Concentrations of most ions in the second set of Pasadena samples, which followed a smoggy day, were higher than in the first Pasadena fog event. At Lennox the concentrations of major ions in fog were even higher than the Pasadena samples. Some of the fog samples from Lennox contained significant amounts of suspended solids. The greatest amount was in the final sample taken from the December 7 fog event during morning rush hour as the fog was dissipating.

The present sampling method does not differentiate between particles within droplets and particles greater than 8 μm that are independent of water droplets. Because the minimum size for activating condensation nuclei in ambient fog is much smaller than the collector cutoff size, most particles collected in fog, with the exception of hydrophobic material, can be assumed to be associated with droplets.

A single fogwater sample collected in Pasadena on January 17 had exceptionally high concentrations. The sulfate and nitrate concentrations were the maximum values observed in any fog. Fogwater collected in Oildale also had very high nitrate and sulfate concentrations as well as the highest NH_4^+, CH_2O, and S(IV) concentrations. The Upland fog samples were also characterized by high levels of acidity and acidic anions.

Concentrations of trace metals in the fog samples were also elevated, as shown in Table 3. During some of the fog events, metal concentrations varied over an order of magnitude. The usual pattern was for high concentrations at the beginning and end of the event. Lead and iron concentrations exceeded 1.0 mg L^{-1} (0.01 m*M*) on occasion.

The anion-to-cation ratios were close to unity for most of the samples, but there were discrepancies in some samples. In light of the large dilutions necessary to bring high concentrations down into suitable analytical ranges, the ion balances were reasonable. There were apparent excesses of cations in some of the samples that had large quantities of particles present. Calculation of the ion balance by using the concentrations of cations in filtered aliquots yielded better results. The aliquot for anions was routinely filtered prior to injection into the IC. This does not explain the apparent anion deficiency (or cation excess) in the fogwater samples collected from Oildale. The inclusion of SO_3^{2-} in the anion sum does not completely make up the deficit either, however, sulfite in aliquots from these samples was not measured immediately. Even though preservation techniques were used, sulfite may be underestimated. Considering the high concentrations of aldehydes, it is probable that the corresponding carboxylic acids were present in the fogwater; this would account for some of the apparent anion deficiency. Other factors that may contribute to poor ionic balances are losses of ions to particle surfaces via sorption and formation of adducts and complexes of indeterminant charge.

DISCUSSION

Figure 3 presents the ionic composition of individual fog samples as a function of time. Concentrations of all ions decrease sharply during the first few hours of the fogs in Lennox; however, the ionic proportions do not change appreciably. In most cases, concentrations in the fogwater rose as the fog

TABLE 3. Ranges of Selected Trace-Metal Concentrations in Fog Samples

		$\mu g\ l^{-1}$				
Site	Date	Fe	Mn	Pb	Cu	Ni
Pasadena	Nov. 15, 1981	90–2,100	18–160	250–270	1–15	2–21
Pasadena	Nov. 15, 1981	920–1,770	34–56	1,310–2,540	88–140	8–14
Lennox	Dec. 7, 1981	356–23,700	19–810	820–2,400	9–150	2–52
Lennox	Dec. 18, 1981	1,020–2,080	25–81	1,700–2,350	84–1,400	32–54
Pasadena	Dec. 20, 1981	340	42	156	—	—
Oildale	Jan. 14, 1982	240–6,400	97–800	241–366	45–401	124–586
Upland	May 14, 1982	—	430–570	1,690–2,400	156–185	155–213

Number of samples per event is the same as for Table 2.

dissipated. The short duration fogs, which were usually very light fogs that resulted in low collection rates, also had high concentrations. Physical processes of droplet growth by accretion of water vapor, followed by evaporation, appear to account for this pattern.

Dilution by droplet growth could take place without any appreciable change in liquid water content (LWC) if the sedimentation rate was high enough to balance the condensation rate. Work by *Roach et al.* [1976] suggests that a significant portion of the liquid water formed during a fog event is lost, presumably to ground surfaces. During the periods over which concentrations were decreasing, collection rates, which are a function of LWC, remained constant. Advection of more dilute fog could account for this as well.

In Figures 4 and 5 the concentration of selected ions, normalized to their initial concentration, are depicted. If physical factors are responsible, the patterns will be nearly identical for ions that are controlled by the same factors or have common sources. The nearly hundredfold increase in Ca^{2+} and Mg^{2+}, and the concomitant drop in H^+ concentration in the final two samples collected in the December 7 fog at Lennox, coincided with morning rush hour traffic, which would generate a large amount of road dust. Concentrations of other ions were increased during that period, as a result of evaporation, but not to the extent that Ca^{2+} and Mg^{2+} increases (25 times their initial concentrations); $[Na^+]$ and $[Cl^-]$ increased by a factor of 5, and $[SO_4{}^{2-}]$, $[NO_3{}^-]$, and $[NH_4{}^+]$ returned to their initial concentrations. Acidity was nearly neutralized at the end of this fog event. In association with the increased $[Ca^{2+}]$ and $[Mg^{2-}]$, an increase in suspended particles, [Pb] and [Fe], was observed at the same time as a rise in CO levels at Lennox, coinciding with the morning traffic. Transfer of gaseous NH_3 into the droplets could account for the increase in $[NH_4{}^+]$ and simultaneous drop in $[H^+]$ during the December 7 Lennox fog event, while the other ions were maintained at constant concentrations. However, if the NH_3 had been present when the fog formed, it would have been immediately scavenged because of its high solubility at low *p*H. Unless there was a local source for NH_3, advective transport must be invoked to account for the apparent increase in $[NH_4{}^+]$.

In Pasadena, $[H^+]$ and $[NO_3{}^-]$ simultaneously increased while the other ions were decreasing. This may be evidence for the nocturnal formation of HNO_3 via the following reactions [*Graham and Johnston*, 1978]:

$$NO + O_3 \longrightarrow NO_2 + O_2 \qquad (5)$$

$$NO_2 + O_3 \longrightarrow NO_3 + O_2 \qquad (6)$$

$$NO_2 + NO_3 \longrightarrow N_2O_5 \qquad (7)$$

$$N_2O_5 + H_2O \longrightarrow 2HNO_3 \qquad (8)$$

Alternatively, the increase in HNO_3 could result from scavenging or diffusion of fine aerosol to the droplets or by advection of fog with higher $NO_3{}^-$ concentrations.

In nearly all the cases the dominant ions in the fog samples were $NO_3{}^-$, $SO_4{}^{2-}$, H^+, and $NH_4{}^+$, which are the major components of secondary aerosol in Los Angeles [*Cass*, 1979]. These ions account for over 90% of the solutes in the initial stages of the Lennox samples. The highest concentrations were observed when the fog was preceded by smoggy days. Because secondary aerosols are effective condensation nuclei [*Barrett et al.*, 1979], they will exert a considerable influence on the composition and concentration in fogwater. When the concentration of secondary aerosol is high, the subsequent fogwater will also have high concentrations. The fraction of $NO_3{}^-$ and $SO_4{}^{2-}$ neutralized by NH_3 (measured in terms of $NH_4{}^+$) will largely determine the free acidity of the fog that first deliquesces. In this connection it is noteworthy that the initial fogwater samples collected at Lennox are the most acidic, and subsequent samples during the event are progressively more neutral, while at Pasadena and Upland the converse is true.

If HNO_3 and NH_3 were present when the fog initially formed, they would be scavenged rapidly as well and influence the fogwater composition [*Jacob and Hoffmann*, 1983]. However, the combination of cooler temperatures and higher humidity before the onset of fog will probably force NH_3 and HNO_3 to condense into the particulate phase [*Stelson and Seinfeld*, 1982; *Stelson*, 1982], which can be scavenged via nucleation or diffusion as the fog forms.

Figure 6 is a conceptualization of the condensation evaporation cycle for fog droplets and illustrates the link between fogwater chemistry and the chemistry of smog and haze aerosol. High atmospheric concentrations of aerosol precursors appear to result in highly concentrated fogwater. Likewise, dissipation of highly concentrated fog results in very concentrated and reactive aerosol. The high trace-metal content in fogs would catalyze SO_2 oxidation. This link between fog and the subsequent aerosol can be seen in the correlation reported by *Cass* [1975] between morning fog and high humidity and high aerosol sulfate concentrations in the afternoon.

THE ROLE OF ALDEHYDES IN FOG DROPLETS

Aldehydes are released as primary emissions from combustion sources and are generated photochemically from hydrocarbons [*National Research Council*, 1981]. The peroxide radical is an important byproduct of these reactions. Aldehydes are photochemically destroyed, with $OH\cdot$ and $HO_2\cdot$ as byproducts. Intermediates in aldehyde reaction pathways also play a role in the gas-phase reaction networks of SO_2 and NO_x.

Concentrations of formaldehyde as high as 0.5 m*M* were present in the Los Angeles fogwater samples. Other aldehydes,

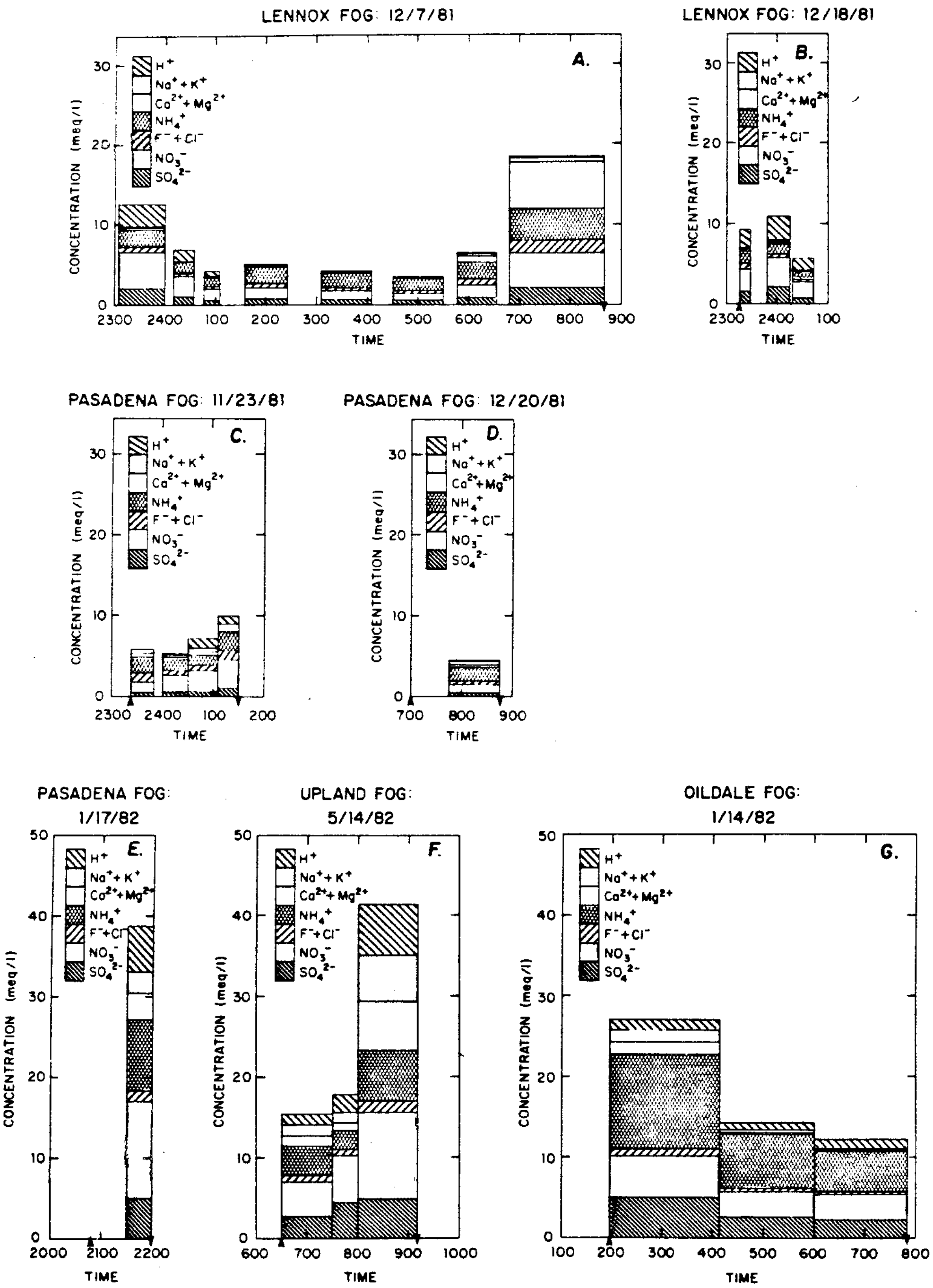

Fig. 3. Ionic composition as a function of time in sequential fog samples. Sampling interval is indicated by the width of each bar. The times of fog formation and dissipation are indicated by arrows.

such as acetaldehyde and benzaldehyde, are present in the Los Angeles atmosphere [*National Research Council*, 1981; *Grosjean*, 1982], and their presence in fogwater samples at comparable concentrations has been confirmed by the hydrazone derivative method [*Fung and Grosjean*, 1981]. Aldehydes react with HSO_3^- according to the following general stoichiometry:

$$HSO_3^- + RCHO \rightleftharpoons RHOCHSO_3^- \qquad (9)$$

The formation constant for the formaldehyde-bisulfite addition complex, HMSA, has a maximum of about 10^5 between

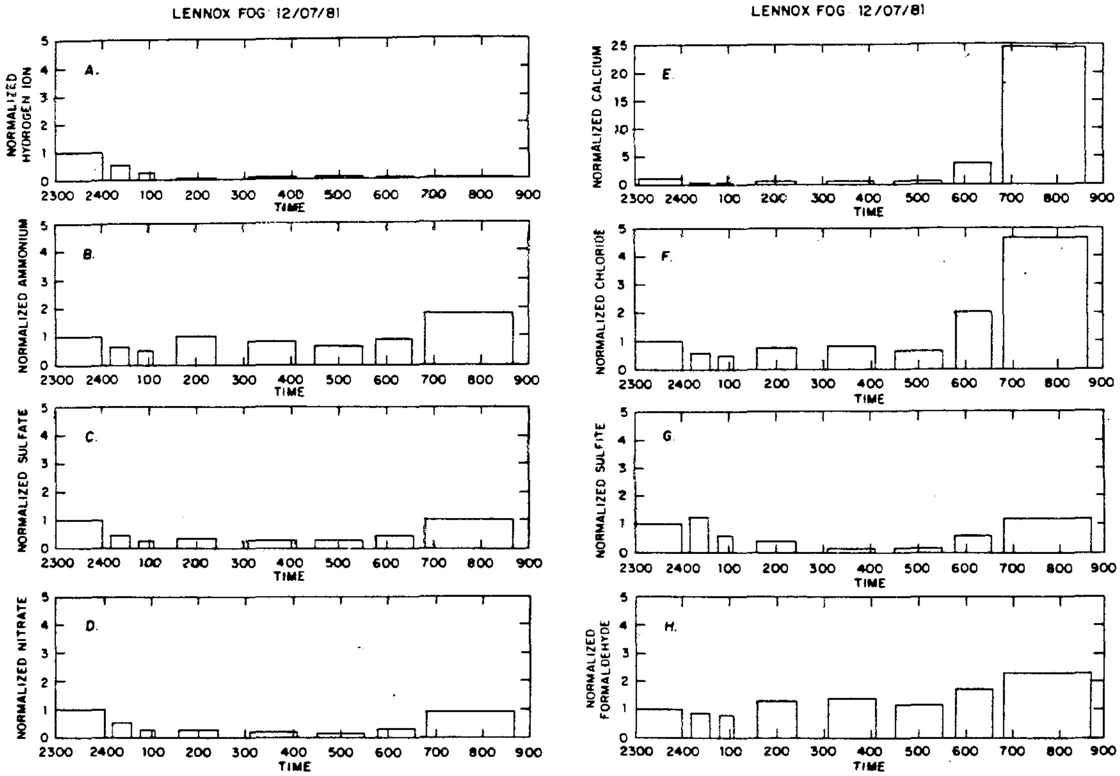

Fig. 4. (a–h) Nondimensional concentrations of individual ions in fog collected on December 7–8, 1981, at the Lennox sampling site. Concentrations are normalized for each component with respect to the concentrations in the initial sample (i.e., $\hat{C}_i = C_i/C_{i,0}$). Note the differences in scale. Sampling interval indicated by the width of each bar. NA indicates that a sample was not analyzed. Magnesium and sodium, which are not shown, were nearly identical to Ca^{2+} and Cl^-, respectively.

pH 4 and 6 and drops to 10^3 at pH 9 [*Dasgupta et al.*, 1980]. *Stewart and Donnally* [1932] observed a similar pattern for the formation of the benzaldehyde-S(IV) adduct. They also observed an interaction between temperature and pH. At low pH the temperature dependence of the equilibrium was stronger than at high pH. Low temperature increased the stability of the complex. The molar ratio of formaldehyde to S(IV) in the fog samples ranged from 0.9 to 17. Using Dasgupta's constants, the free S(IV) concentration in the fog ranges from 5% to 60% of the total. The equilibrium partial pressures of SO_2 and CH_2O, required to achieve the S(IV) and CH_2O values measured in the fogwater, were calculated from the following mass balance relationships:

$$[\mathrm{S(IV)}] = [\mathrm{SO_2(aq)}] + [\mathrm{HSO_3}^-] + [\mathrm{SO_3}^{2-}] + \sum_{i=1}^{n} [R_i\mathrm{CHOHSO_3}^-] + \sum_{j=1}^{m} [M_j\mathrm{SO_3}] \qquad (10)$$

$$[R_i\mathrm{CHO}]_T = [R_i\mathrm{CHO}] + [R_i\mathrm{CHOHSO_3}^-] \qquad (11)$$

where R_iCHO represents aldehydes forming sulfonic acid adducts, and M_j represents first-row transition metals forming stoichiometric sulfite complexes. Using the appropriate conditional equilibrium expressions for the concentration of the sulfonic acid adducts of CH_2O, CH_3CHO, C_7H_6O, and the sulfitoiron(III) complex, and ignoring other S(IV) adducts and complexes because of their low potential concentrations, gives

$$[\mathrm{S(IV)}] = K_H P_{\mathrm{SO_2}}\left(1 + \frac{K_{a1}}{[\mathrm{H^+}]} + \frac{K_{a1}K_{a2}}{[\mathrm{H^+}]^2} + \frac{K_{a1}K_{a2}\beta}{[\mathrm{H^+}]^2}\,\mathrm{Fe(III)}] + \sum_{i=1}^{n} \frac{K_{a1}}{[\mathrm{H^+}]}[R_i\mathrm{CHO}]K_{Ai}\right) \qquad (12)$$

$$[R_i\mathrm{CHO}]_T = K_H{}^i P_{R_i\mathrm{CHO}}\left(1 + \frac{K_{a1}K_H P_{\mathrm{SO_2}}}{[\mathrm{H^+}]}K_{Ai}\right) \qquad (13)$$

$$[\mathrm{Fe(III)}]_T = [\mathrm{Fe(III)}] + [\mathrm{Fe(III)SO_3}^-] \qquad (14)$$

where β is the formation constant for an Fe(III) – S(IV) complex; $K_H{}^i$ is Henry's Law constant for R_iCHO; K_H is Henry's Law constant for SO_2; K_{a1} and K_{a2} are acid dissociation constants; K_{Ai} is the bisulfite adduct formation constant, $P_{R_i\mathrm{CHO}}$ and $P_{\mathrm{SO_2}}$ are partial pressures.

Substitution of the aldehyde and metal mass balances into (12) gives

$$[\mathrm{S(IV)}] = \frac{K_H P_{\mathrm{SO_2}}}{[H^+]^2}\left[[\mathrm{H^+}]^2 + K_{a1}[\mathrm{H^+}] + \frac{K_{a1}K_{a2}\beta[\mathrm{Fe(III)}]_T[\mathrm{H^+}]^2}{([\mathrm{H^+}]^2 + \beta K_{a1}K_{a2}K_H P_{\mathrm{SO_2}})} + \sum_{i=1}^{n} \frac{K_{a1}K_{Ai}[\mathrm{H^+}]^2[R_i\mathrm{CHO}]_T}{(\mathrm{H^+} + K_{a1}K_{Ai}K_H P_{\mathrm{SO_2}})}\right] \qquad (15)$$

The appropriate equilibrium constants are given in Table 4.

In the absence of adduct formation the equilibrium partial pressures of CH_2O calculated from fogwater data range from 16 ppb to 76 ppb, which are reasonable values for the Los Angeles atmosphere [*Grosjean*, 1982]. Adduct formation would lower the equilibrium partial pressure. The highest values of S(IV) found in some fog samples cannot be completely accounted for by aldehyde and iron-complex equilibria alone. Measured sulfite is 4–5 times higher than the predicted equilibrium value, even with P_{SO_2} as high as 30 ppb at the Los Angeles sites or 50 ppb at Oildale, which are the highest values for those sites. The lower concentrations of S(IV), however, are comparable to the values predicted from equilibrium considerations. Stable organic and inorganic sulfite species in ambient aerosols have been demonstrated to exist [*Izatt et al.*, 1978; *Eatough et al.*, 1978]. Aldehydes may play an important role in the atmospheric chemistry of S(IV) as stabilizers that retard oxidation of S(IV), and possibly as sources of peroxides and free radicals through their photochemistry. More data on the aldehyde content of the atmosphere are necessary to ascertain their role in the heterogeneous chemistry of SO_2.

NITRATE TO SULFATE EQUIVALENT RATIOS

As is indicated in Figure 7, $[NO_3^-]$ in Pasadena and Lennox was about 2.5 times $[SO_4^{2-}]$; at Oildale and Upland the ratio was closer to 1 : 1. The nitrate to sulfate ratios in fogwater differ markedly from that observed in Los Angeles area rainwater [*Liljestrand and Morgan*, 1981]. In rainwater the equivalent ratio was less than 1 for coastal and central Los Angeles sites and increased to unity at Riverside at the eastern edge of the basin. Fogwater exhibited the opposite trend: $[NO_3^-]$ exceeded $[SO_4^{2-}]$ at the coastal and central Los Angeles sites and decreased to near one at the most inland site (Upland). Beside the differences in their source strengths (NO_x emissions exceed SO_2 emissions by a factor of 2.5 in Los Angeles), there are important differences in the kinetics of their respective oxidations and scavenging processes, as is discussed by *Jacob and Hoffmann* [1983].

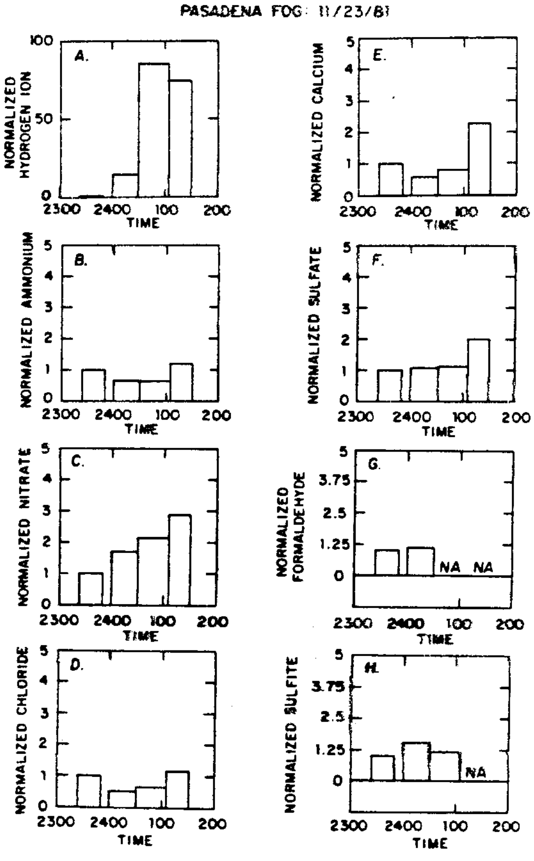

Fig. 5. (*a–h*) Nondimensional concentrations of individual ions in fog collected on November 23–24, 1981, at the Pasadena sampling site. The normalization procedure and scales are described in Figure 4.

SODIUM CHLORIDE RATIOS

As Figure 8 illustrates, most of the fogwater samples had Na:Cl ratios near that of seawater. There were a few samples with excess Cl^-, which may be due to local sources. The highest excess of Cl^- was found in Lennox fog during morning rush hour, which suggests lead bromochloride salts from automobile emissions as a possible Cl^- source. Those samples also had high [Pb]. Two of the samples with excess Na^+ were collected at the beginning of fog events and may be affected by soil and dust. However, the other samples with excess Na^+ were extremely acidic. Reaction between marine aerosol and acidic gases or aerosol may be volatilizing HCl in the fog or the preceding aerosol as suggested by *Eriksson* [1960] and *Hitchcock* [1980]. The resulting fog would be deficient in Cl^-.

COMPARISON TO OTHER DATA

Fog and cloudwater ionic concentrations as high as in some of these samples have been observed previously (see Table 5). At many of the sites, *p*H values were in the range 3 to 4, but none were as low as the most extreme values for the Los Angeles area fogs. The concentration ranges for the cations Na^+, K^+, Ca^{2+}, and Mg^{2+} in other regions overlap with the concentration ranges observed in Southern California. The extreme values reported here, which were found in light fogs and in the Lennox sample that was laden with particles, are somewhat higher. Ammonium concentrations are comparable, but the extreme values observed in this study are about 10 times the maxima for previously reported data. Sulfate concentrations are comparable to other reported values, while nitrate concentrations are considerably higher in the California fogs, which is to be expected because of the dominance of NO_x emissions. Furthermore, high concentrations of HNO_3, which can be easily scavenged by fogwater, have been measured in the Los Angeles atmosphere [*Appel*, 1981].

Dense smog as a precursor gave rise to the most highly concentrated fogwater in Los Angeles. Other areas of the world subject to intense air pollution may also prove to have highly concentrated fogwater. Although ionic composition in the 1952 London fog was not measured, approximate calculations based on SO_2 emission rates, measured SO_2 concentrations, droplet residence time, and liquid water content [*Wilkins*, 1954*a*, *b*] gives SO_4^{2-} concentrations of 11 to 46 meq l^{-1}. For comparison, the extreme value measured during the winter of 1981–1982 in Southern California was 5 meq l^{-1}.

IMPLICATIONS

Highly concentrated fogwater can have several important environmental effects. Sedimentation and impaction rates of

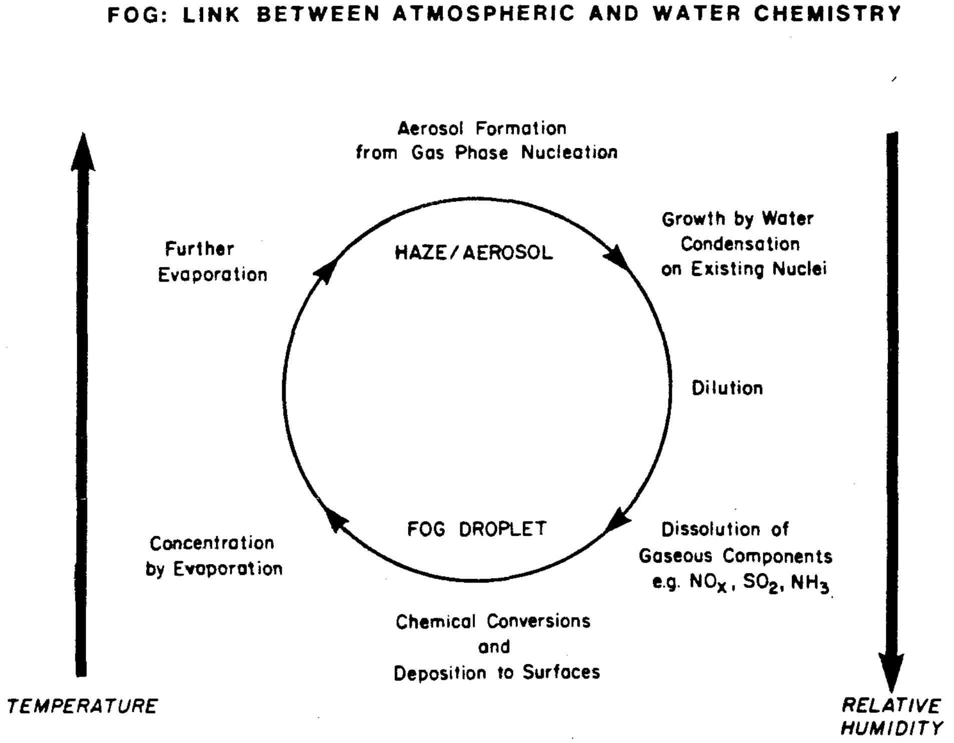

Fig. 6. A schematic diagram depicting the temperature and humidity dependence for fog formation and the apparent link between atmospheric gas phase and water phase chemistry.

TABLE 4. Equilibrium Constants Applicable to S(IV) and Aldehyde Chemistry

	K, *M* or *M* atm^{-1}	ΔH° 298, kcal mol	Reference
$SO_{2(g)} \xrightleftharpoons{K_H} SO_{2(aq)}$	1.245	−6.247	*Sillén and Martell* [1971]
$SO_{2(aq)} \xrightleftharpoons{K_{a1}} H^+ + HSO_3^-$	1.290×10^{-2}	−4.161	*Sillén and Martell* [1971]
$HSO_3^- \xrightleftharpoons{K_{a2}} H^+ + SO_3^{2-}$	6.014×10^{-8}	−2.23	*Sillén and Martell* [1971]
$CH_2O_{(g)} \xrightleftharpoons{K'_H} CH_2O_{(aq)}$	6.3×10^3	—	*Ledbury and Blair* [1925]
$CH_2O_{(aq)} + HSO_3^- \xrightleftharpoons{K_{A,1}} CH_2OHSO_3^-$	$\simeq 10^5$	—	*Dasgupta et al.* [1980]
$Fe^{3+} + SO_3^{2-} \xrightleftharpoons{\beta} FeSO_3^+$	$\simeq 10^{10} - 10^{18}$	—	*Carlyle* [1971]; *Hansen et al.* [1976]
$C_7H_6O + HSO_3^- \xrightleftharpoons{K_{A,2}} C_7H_6OHSO_3^-$	$\simeq 10^5$	—	*Stewart and Donnally* [1932]
$C_2H_4O + HSO_3^- \xrightleftharpoons{K_{A,3}} C_2H_4OHSO_3^-$	$\simeq 10^5$	—	by extrapolation

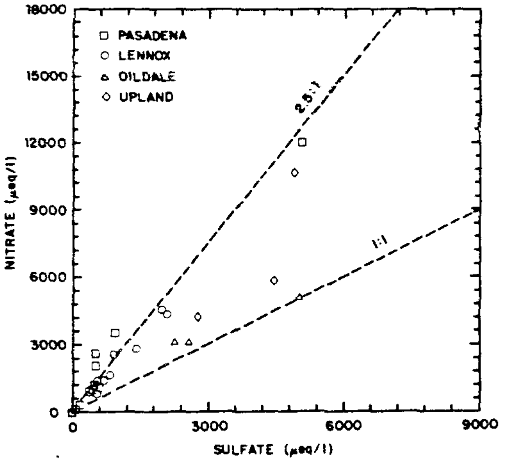

Fig. 7. Plot of nitrate and sulfate equivalent concentrations in fogwater. Dashed lines indicate 2.5 : 1 and 1 : 1 ratios.

fog droplets will be greater than for dry gas and aerosol. *Roach et al.* [1976] have calculated that up to 90% of the liquid water condensed during a fog event may sediment out on the ground. When winds accompany fog, interception of droplets by vegetation is also a major depositional pathway [*Schlesinger and Reiners*, 1974; *Lovett and Reiners*, 1982]. Measurement of rain and dry deposition fluxes alone may not adequately account for atmospheric loadings in regions where fog is frequent. Surface wetness from fog deposition may enhance deposition of SO_2 and subsequent oxidation to SO_4^{2-} (with a possible involvement of trace metals) [*Lindberg et al.*, 1979].

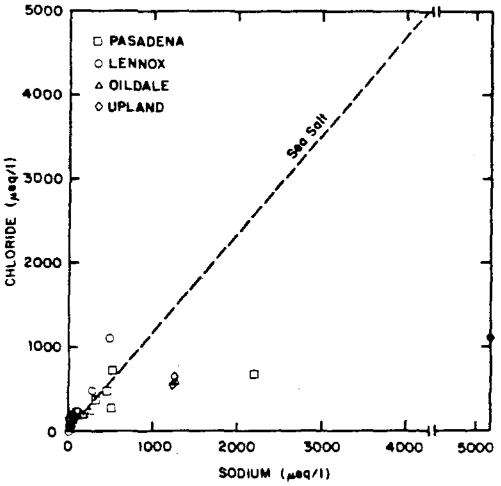

Fig. 8. Plot of sodium and chloride concentrations. Dashed line indicates the NaCl ratio in seawater.

Fogwater deposited on leaf surfaces is highly efficient in leaching ions from the leaves [*Tukey*, 1979] and may result in some plant injury. Experiments with acid mists show plant injury occurring at pH levels around 3 [*Jacobson*, 1980], which is typical of fogwater in parts of Southern California. Damage to building materials and metal surfaces is also possible from deposition of acidic fog. Corrosion of statuary and building materials has been observed in several locations throughout the world. The role of fog in this damage is not known, although research [*Metropolitan Museum of Art*, 1979] on the Horses of San Marco (ca. 100 B.C.) in Venice, Italy, indicates that fog and high SO_2 concentrations have resulted in significant damage during the last 50 years.

Historically, fogs have been implicated in a number of severe pollution episodes that caused increased human mortality [*Environmental Protection Agency*, 1971]. The most notable of these is the infamous London Fog of 1952 [*Wilkins*, 1954*a*, *b*], which caused 4000 excess deaths during the 5-day episode and 12,000 deaths over 4 months. Further research is needed to ascertain whether the fog caused mortality or was merely a consequence of the severe inversion conditions that caused a build up of toxic air pollutants, which were the true agents of mortality. Previous analysis [*Larsen*, 1970] suggested that these deaths correlated well with the product of gas-phase SO_2 and particle concentrations; however, sulfuric acid mists have been implicated [*Wilkins*, 1954*a*, *b*].

CONCLUSION

Fogwater in Southern California provides a propitious environment for the scavenging of particulate and gaseous forms of S(IV), S(VI), N(V), and N(−III); for the subsequent conversion of S(IV) to S(VI); and for the concomitant production of acidity. Unusually high concentrations of SO_4^{2-}, NO_3^-, NH_4^+, and H^+ were observed. The highest concentrations were observed during fog events preceded by smoggy days. Acidity caused by NO_3^- and SO_4^{2-} precursors was neutralized to some extent by scavenging of NH_3 and calcareous dust.

The physical processes of condensation and evaporation, along with scavenging and subsequent chemical conversion of reactive gas-phase components, appear to mutually control the temporal trends in fogwater composition. The apparent cyclical relationship between the occurrence of smog and fog in the Los Angeles basin is a manifestation of this phenomenon. The late night and early morning fogs, which form more readily in a particle-laden atmosphere, appear to accelerate and enhance smog production, visibility reduction, and particulate sulfate levels during the subsequent day. This relationship can be dubbed the smog-fog-smog cycle.

Clearly, more research is needed to elucidate the mechanisms by which fog-processed aerosols become highly reactive sites for daytime photochemical transformations. The role of aldehydes and transition metals in the transport and transformation of S(IV) in atmospheric water droplets needs to be explored more intensively. Furthermore, given the millimolar concentrations of some of the metal ions in urban fog, the effect of metal ion catalysts on important chemical transformations (e.g., S(IV) to S(VI)) needs to be considered more carefully in the development of quantitative air quality models for urban airsheds.

TABLE 5. Summary of Fog and Cloud Water Compositions

				μeq l^{-1}								
Location	Date	Type*	*p*H	SO_4^{2-}	NO_3^-	Cl^-	Na^+	K^+	Ca^{2+}	Mg^{2+}	NH_4^+	Reference
Mt. Washington, N.H.	1930–40	CF	3.0–5.9	4.2–1100		0–34						*Houghton* [1955]
Nantucket, Mass.	1930–40	MF	—	285–2600		650–5750						*Houghton* [1955]
Brooklin, Maine	1930–40	F	3.5–6.3	95–770		0–140						*Houghton* [1955]
SW of London	1960	C†	4.4–7.2	40	19	94	95	13	66	25	22	*Oddie* [1962]
Germany, Baltic Sea	1955–65	MF†	3.8	1860	900	1740	1500	240	750		2335	*Mrose* [1966]
Harz Mtn.	1955–65	CF†	5.1	775	450	205	295	85	220		710	*Mrose* [1966]
nr. Dresden	1955–65	UF†	4.2	3300	380	585			3180		2100	*Mrose* [1966]
Kiev, USSR	Dec. 1964	C	3.4–5.4	400–2060	17–200	115–325	80–215	30–130	40–535	16–160	235–1300	*Petrenchuk and Drozdova* [1966]
Mt. Noribura, Japan	July 1963	CF	3.4–4.3	230–1250	50–350	75–230	45–165	55–85			115–260	*Okita* [1968]
Mt. Tsukaba, Japan	Nov. 1963	CF	5.6–6.5	360–2065	11–75	295–1270	180–435	154			110–965	*Okita* [1968]
Puerto Rico	Nov.–Dec. 1967	C	4.9–5.4	75–190		150–1975				20–90	35–400	*Lazrus et al.* [1970]
Nova Scotia	Aug. 1975	MF		54–470		14–235	880–1240	43–50	38–69	42–77	9–72	*Mack and Katz* [1976]
Coastal California	Sep.–Oct. 1970	MF		77–490	24–235	96–1235	78–945	11–23	9–100	23–175	0–580	*Mack et al.* [1977]
Whiteface Mtn., N.Y.	Aug. 1976	CF†	3.6–3.9	52–140	140–215	1.7–3.1	2.3–11	13–20	10–20	2.2–6.1	32–89	R. A. Castillo et al. (unpublished manuscript, 1980)
	Aug. 1980	CF	3.2–4.0	32–806	7–192	1–14	1–7	1–6			4–197	*Falconer* [1981]
Los Angeles, Calif.	Jan. 80	C	4.6–6.8	5–400	0–445	1–760	2–50	1–70			0–230	*Hegg and Hobbs* [1981]

*Type of sample: F = fog; C = clouds aloft; CF = intercepted clouds; MF = marine fog; UF = urban fog

†Mean values of samples

‡Range of mean values; otherwise range of samples

Acknowledgments. We gratefully acknowledge the financial support of the California Air Resources Board and the invaluable assistance provided by its professional staff. Additional logistical support was provided by the South Coast Air Quality Management District. Special thanks are extended to R. C. Flagan, J. J. Morgan, D. Lawson, and D. Grosjean for their contributions to the success of this research.

REFERENCES

Appel, B. R., Y. Tokiwa, and M. Haik, Sampling of nitrates in ambient air, *Atmos. Environ., 15*, 283–289, 1981.

Baboolal, B., H. R. Pruppacher, and J. H. Topalian, A sensitivity study of a theoretical model of SO_2 scavenging by water drops in air, *J. Atmos. Sci., 38*, 856–870, 1981.

Barrett, E., F. P. Parungo, and R. F. Pueschel, Cloud modification by urban pollution: A physical demonstration, *Meteorol. Res., 32*, 136–149, 1979.

Carlyle, D. W., A kinetic study of the aquation of sulfitoiron(III) ion, *Inorg. Chem., 10*, 761–764, 1971.

Cass, G. R., Dimensions of the Los Angeles SO_2/sulfate problem, *Memo. 15*, Environ. Qual. Lab., Calif. Inst. Technol., Pasadena, California, 1975.

Cass, G. R., On the relationship between sulfate air quality and visibility with examples in Los Angeles, *Atmos. Environ., 13*, 1069–1084, 1979.

Cass, G. R., Sulfate air quality control strategy design, *Atmos. Environ., 15*, 1227–1249, 1981.

Cass, G. R., and F. H. Shair, Transport of sulfur oxides within the Los Angeles sea breeze/land breeze circulation system, paper presented at Joint Conference on Application of Air Pollution Meteorology, Am. Meteorol. Soc., New Orleans, March 24–27, 1980.

Cox, R. A., Particle formation from homogeneous reactions of sulfur dioxide and nitrogen dioxide, *Tellus, 26*, 235–240, 1974.

Dasgupta, P. K., K. De Cesare, and J. C. Ullrey, Determination of atmospheric sulfur dioxide without tetrachloromercurate(II) and the mechanism of the Schiff reaction, *Anal. Chem., 52*, 1912–1922, 1980.

Eatough, D. J., T. Major, J. Ryder, M. Hill, N. F. Mangelson, N. L. Eatough, L. D. Hansen, R. G. Meisenheimer, and J. W. Fischer, The formation and stability of sulfite species in aerosols, *Atmos. Environ., 12*, 263–271, 1978.

Environmental Protection Agency, Guide for Air Pollution Avoidance, Appendix B. History of Episodes, *Rep. PH-22-68-32*, pp. 123–135, Washington, D.C., 1971.

Eriksson, E., The yearly circulation of chloride and sulfur in nature: Meteorological, geochemical, and pedological implications, Part 2, *Tellus, 12*, 63–109, 1960.

Falconer, P. D., Cloud Chemistry and Meteorological Research at Whiteface Mountain: Summer 1980, *ASRC Publ. 806*, Atmos. Sci. Res. Center, State Univ. New York, Albany, 1981.

Fortune, C. R., and B. Dellinger, Stabilization and analysis of sulfur(IV) aerosols in environmental samples, *Environ. Sci. Technol., 16*, 62–66, 1982.

Fung, K., and D. Grosjean, Determination of nanogram amounts of carbonyls as 2,4-dinitrophenylhydrazones by high-performance liquid chromatography, *Anal. Chem., 53*, 168–181, 1981.

Galloway, J. N., G. E. Likens, W. C. Keene, and J. M. Miller, The composition of precipitation in remote areas of the world, *J. Geophys. Res., 87*, 8771–8786, 1982.

Graham, R. A., and H. S. Johnston, The photochemistry of NO_3 and the kinetics of the N_2O_5-O_3 system, *J. Phys. Chem., 82*, 254–268, 1978.

Grosjean, D., Formaldehyde and other carbonyls in Los Angeles ambient air, *Environ. Sci. Technol., 16*, 254–262, 1982.

Hansen, L. D., L. Whiting, D. J. Eatough, T. E. Jensen, and R. M. Izatt, Determination of sulfur(IV) and sulfate aerosols by thermometric methods, *Anal. Chem., 48*, 634–638, 1976.

Hitchcock, D. R., Sulfuric acid aerosols and HCl release in coastal atmospheres: Evidence of rapid formation of sulfuric acid particulates, *Atmos. Environ., 14*, 165–182, 1980.

Hegg, D. A., and P. V. Hobbs, Cloudwater chemistry and the production of sulfates in clouds, *Atmos. Environ., 15*, 1597–1604, 1981.

Hoffmann, M. R., and D. J. Jacob, Kinetics and mechanisms of the catalytic oxidation of dissolved sulfur dioxide in aqueous solution: An application to nighttime fog-water chemistry, in *Acid Precipitation*, vol. 6, edited by J. G. Calvert, Ann Arbor Science Publishers, Ann Arbor, Michigan, 1983.

Houghton, H. G., On the chemical composition of fog and cloud water, *J. Meteorol., 12*, 355–357, 1955.

Humphrey, R. E., M. H. Ward, and W. Hinze, Spectrophotometric determination of sulfite with 4,4-dithiopyridine and 5,5-dithiobis(2-nitrobenzoic acid), *Anal. Chem., 42*, 698–702, 1970.

Izatt, R. M., D. J. Eatough, M. L. Lee, T. Major, B. E. Richter, L. D. Hansen, R. G. Meisenheimer, and J. W. Fischer, The formation of inorganic and organic S(IV) species in aerosols, in *Proceedings of the 4th Joint Conference on Sensing Environmental Pollutants*, pp. 821–824, American Chemical Society, Washington, D.C., 1978.

Jacob, D. J., and M. R. Hoffmann, A dynamic model for the production of H^+, NO_3^-, and SO_4^{2-} in urban fog, submitted to *J. Geophys. Res.*, 1982.

Jacob, D. J., R. C. Flagan, J. M. Waldman and M. R. Hoffmann, Design and calibration of rotating-arm collectors for ambient fog sampling, paper presented at 4th International Conference on Precipitation Scavenging, Dry Deposition, and Resuspension, Nov. 29–Dec. 3, Santa Monica, Calif., 1982.

Jacobson, J. S., Experimental studies on the phytotoxicity of acidic precipitation: The United States experience in *Effects of Acid Precipitation on Terrestrial Ecosystems*, edited by T. C. Hutchinson and M. Havas, pp. 151–160, Plenum, New York, 1980.

Larsen, R. I., Relating air pollutant effects to concentration and control, *J. Air Pollut. Control Assoc., 20*, 214–225, 1970.

Lazrus, A. L., H. W. Baynton, and J. P. Lodge, Trace constituents in oceanic cloud water and their origin, *Tellus, 22*, 106–113, 1970.

Ledbury, W., and E. W. Blair, The partial formaldehyde vapour pressure of aqueous solutions of formaldehyde, Part 2, *J. Chem. Soc., 127*, 2832–2839, 1925.

Liljestrand, H. M., and J. J. Morgan, Spatial variations of acid precipitation in Southern California, *Environ. Sci. Technol., 15*, 333–338, 1981.

Lindberg, S. E., R. C. Harriss, R. R. Turner, D. S. Shriner, and D. D. Huff, Mechanism and rates of atmospheric deposition of selected trace element and sulfate to deciduous forest watershed, *Rep. ORNL/TM-6674*, Oak Ridge Nat. Lab., Oak Ridge, Tenn. 1979.

Lovett, G. M., and W. A. Reiners, Deposition of cloudwater and dissolved ions to subalpine forests of New England, paper presented at 4th International Conference on Precipitation Scavenging, Dry Deposition, and Resuspension, sponsor, Santa Monica, Calif., Nov. 29–Dec. 3, 1982.

Mack, E. J., and U. Katz, The Characteristics of Marine Fog Occurring off the Coast of Nova Scotia, *Rep. CJ-5756-M-1*, Calspan Corp., Buffalo, New York, 1976.

Mack, E. J., U. Katz, C. W. Rogers, D. W. Gaucher, K. R. Piech, C. K. Akers, and R. J. Pilié, An Investigation of the Meteorology, Physics and Chemistry of Marine Boundary Layer Processes, *Rep. CJ-6017-M-1*, Calspan Corp., Buffalo, New York, 1977.

Mack, E. J., and R. J. Pilie, Fog Water Collector, U.S. Patent 3889532, 1975.

Martin, L. R., Kinetic studies of sulfite oxidation in aqueous solution, in *Acid Precipitation: SO_2, NO, NO_2 Oxidation Mechanisms: Atmospheric Considerations*, edited by J. G. Calvert, Ann Arbor Science Publishers, Ann Arbor, Mich., 1983.

McMurry, P. H., D. J. Rader, and J. L. Smith, Studies of aerosol formation in power plant plumes, 1, Parameterization of conversion rate for dry, moderately polluted ambient conditions, *Atmos. Environ., 15*, 2315–2329, 1981.

Metropolitan Museum of Art, *The Horses of San Marco, Venice*, translated from Italian by J. and V. Wilton-Ely, New York, 1979.

Morgan, J. J., and H. J. Liljestrand, Measurement and interpretation of acid rainfall in the Los Angeles basin, *Rep. AC-2-80*, W. M. Keck Lab. Hydraul. Water Resour., Calif. Inst. Technol., Pasadena, California, 1980.

Mrose, H., Measurement of *p*H and chemical analyses of rain-, snow-, and fog-water, *Tellus, 18, 266–270, 1966.*

Nash, T., The colorimetric estimation of formaldehyde by means of the Hantzsch reaction, *Biochem. J., 55*, 416–421, 1953.

National Research Council, *Formaldehyde and Other Aldehydes*, National Academy Press, Washington, D. C., 1981.

Oddie, B. C. V., The chemical composition of precipitation at cloud levels, *Quart. J. R. Meteorol. Soc., 88*, 535–538, 1962.

Okita, T., Concentrations of sulfate and other inorganic materials in fog and cloud water and in aerosol, *J. Meteorol. Soc. Jpn., 46*, 120–126, 1968.

Petrenchuk, O. P., and V. M. Drozdova, On the chemical composition of cloud water, *Tellus, 18*, 280–286, 1966.

Rietz, E. B., The stabilization of small concentrations of formaldehyde in aqueous solutions, *Anal. Lett., 13*, 1073–1084, 1980.

Roach, W. T., R. Brown, S. J. Caughey, J. A. Garland, and C. J. Readiness, The physics of radiation fog, 1, A field study, *Quart. J. R. Meteorol. Soc.*, *10*, 313–33, 1976.

Sander, S. P., and J. H. Seinfeld, Chemical kinetics of homogeneous oxidation of sulfur dioxide, *Environ. Sci. Technol.*, *10*, 1114–1123, 1976.

Schlesinger, W. H., and W. A. Reiners, Deposition of water and cations on artificial foliar collectors in fir Krummholz of New England mountains, *Ecology*, *55*, 378–386, 1974.

Schwartz, S. E., Gas-aqueous reactions of sulfur and nitrogen oxides in liquid-water clouds, in *Acid Precipitation:* SO_2, *NO, and* NO_2 *Oxidation Mechanisms: Atmospheric Considerations*, edited by J. G. Calvert, Ann Arbor Science Publishers, Ann Arbor, Mich., 1983.

Sillén, L. G., and A. E. Martell, *Stability Constants of Metal-Ion Complexes, Suppl. 1*, 2nd ed., The Chemical Society, London, 1971.

Smith, F. B., and G. H. Jeffrey, Airborne transport of sulphur dioxide from the U.K., *Atmos. Environ.*, *9*, 643–659, 1975

Solórzano, L., Determination of ammonia in natural waters by the phenolhypochlorite method, *Limnol. Oceanogr.*, *14*, 799–801, 1967.

Stelson, A. W., Thermodynamics of aqueous atmospheric aerosols, Ph.D. thesis, 127 pp., Calif. Inst. Technol., Pasadena, California, 1982.

Stelson, A. W., and J. H. Seinfeld, Relative humidity and temperature dependence of the ammonium nitrate dissociation constant, *Atmos. Environ.*, *16*, 983–992, 1982.

Stewart, T. D., and L. H. Donnally, The aldehyde bisulfite compounds, 2, The effect of varying hydrogen ion and of varying temperature upon the equilibrium between benzaldehyde and bisulfite ion, *J. Am. Chem. Soc.*, *54*, 3555–3558, 1932.

Tukey, H. B., Jr., The leaching of substances from plants, *Ann. Rev. Plant Physiol.*, *71*, 305–324, 1970.

Waldman, J. M., J. W. Munger, D. J. Jacob, R. C. Flagan, J. J. Morgan, and M, R. Hoffmann, Chemical composition of acid fog, *Science*, *218*, 677–680, 1982.

Wilkins, E. T., Air pollution and the London fog of December 1952, *J. R. Sanit. Inst.*, *74*, 1–21, 1954*a*.

Wilkins, E. T., Air pollution aspects of the London fog of December 1952, *J. R. Meteorol. Soc.*, *80*, 267–278, 1954*b*.

Wilson, J. C., and P. H. McMurry, Studies of aerosol formation in power plant plumes, 2, Secondary aerosol formation in the Navajo generating station plume, *Atmos. Environ.*, *15*, 2329–2339, 1981.

(Received October 4, 1982;
revised February 4, 1983;
accepted February 17, 1983.)

Journal of Atmospheric Chemistry **1** (1984). 335–350. 0167-7764/84/0014-0335$02.40

CHAPTER 4

The Occurrence of Bisulfite-Aldehyde Addition Products in Fog- and Cloudwater

J. W. MUNGER, D. J. JACOB and M. R. HOFFMANN*
Environmental Engineering Science, Mail Code 138–78, California Institute of Technology, Pasadena, CA 91125, U.S.A.

(Received: 24 October 1983; in revised form: 7 February 1984)

Abstract. Elevated concentrations of S(IV) and formaldehyde were observed in fog- and cloudwater at sites in California. The highest concentrations (up to 3 m*M* S(IV) and 0.7 m*M* CH_2O) were measured at Bakersfield, during a prolonged period of repeated fog. In Bakersfield [S(IV)] generally exceeded [CH_2O], while in the Los Angeles area the reverse was observed. The lowest concentrations of both species were observed at marine and high altitude sites away from local emissions. Equilibrium computations indicate that high concentrations of S(IV) cannot be achieved without the formation of S(IV)–RCHO adducts.

Key words. Formaldehyde, sulfur (IV), sulfonic acids, sulfur oxidation, air pollution, fogwater chemistry.

1. Introduction

Formaldehyde and other aldehydes are ubiquitous in the atmosphere, especially in urban areas. Formaldehyde concentrations in three phases at sites ranging from remote to polluted are listed in Table I. In Los Angeles, Grosjean (1982) found other aldehydes at concentrations comparable to formaldehyde. Aerosol-phase concentrations are less than 1% of the gas-phase concentrations at all sites listed in Table I. Rainwater concentrations convert to air concentrations of 0.017 to 0.174 $\mu g\, m^{-3}$ in clouds with liquid water content ranging from 0.1 to 1.0 $g\, m^{-3}$. Again this value is much less than typical gas-phase concentrations.

Aldehydes are emitted directly from combustion sources, while photochemical oxidation of hydrocarbons is a source of secondary aldehydes (Table II). Oxidation of naturally-occurring CH_4 by $HO^\bullet$ leads to a background CH_2O level of 0.5–2 ppb (0.6–2.5 $\mu g\, m^{-3}$) (NRC, 1981). In urban areas, photochemical oxidation of alkanes and alkenes produce a variety of aldehydes. Because emissions of reactive hydrocarbons generally exceed direct aldehyde emissions, secondary pathways are the dominant sources of aldehydes in most urban atmospheres. Cleveland *et al.* (1977) report that diurnal patterns of CH_2O concentrations in New Jersey follow O_3 more closely than CO, suggesting a photochemical source for much of the formaldehyde.

Destruction of aldehydes occurs via photolysis and reaction with oxidants (Table III).

---

* To whom correspondence should be addressed.

Table I. *Atmospheric formaldehyde concentrations at selected sites*

Site	*n*	Range ($\mu g\ m^{-3}$)	Mean ($\mu g\ m^{-3}$)	Reference
Gas phase				
Los Angeles, CA, 1980	36	2.4–48	25	Grosjean, 1982
Claremont, CA, 1980	65	3.6–58	30	Grosjean, 1982
New Jersey, summer 1974[a]	4	4.6–7.9	–	Cleveland *et al.*, 1977
Deuselbach, West Germany, 1975–76	–	4–27	12.7	Klippel and Warneck, 1980
Enewetak, South Pacific, 1979	–	–	0.5	Zafirou *et al.*, 1980
Aerosol				
Claremont, 1980	14	0–0.26	0.081	Grosjean, 1982
Mainz, West Germany, 1976	8	–	0.063	Klippel and Warneck, 1980
Deuselbach, 1975–76		–	0.04	Klippel and Warneck, 1980
Ireland, 1975–77 (clean air)	16		0.005	Klippel and Warneck, 1980
Rainwater				
		$\mu g L^{-1}$	$\mu g L^{-1}$	
Mainz, 1976	38	–	174	Klippel and Warneck, 1980
Deuselbach, 1974–76	19	–	141	Klippel and Warneck, 1980
Ireland, 1975–76	16	–	142	Klippel and Warneck, 1980
Enewetak, 1979	6	6–11	7.9	Zafirou *et al.*, 1980
Ireland, 1977 (clean air)	5	–	111	Klippel and Warneck, 1978

[a] Medians of 25-hour averages at 4 sites.

Table II. Summary of reactions involved in the formation of aldehydes from hydrocarbon precursors[a]

No.	Reaction	Reference
(1)	$HO^{\bullet} + CH_4 \rightarrow H_2O + CH_3^{\bullet}$	NRC, 1981
(2)	$CH_3^{\bullet} + O_2 (+ N_2 \text{ or } O_2) \rightarrow CH_3O_2^{\bullet} (+ N_2 \text{ or } O_2)$	NRC, 1981
(3)	$CH_3O_2^{\bullet} + NO \rightarrow CH_3O^{\bullet} + NO_2$	NRC, 1981
(4a)	$2CH_3O_2^{\bullet} \rightarrow 2CH_3O^{\bullet} + O_2$	NRC, 1981
(4b)	$2CH_3O_2^{\bullet} \rightarrow CH_3OH + CH_2O + O_2$	NRC, 1981
(5)	$CH_3O^{\bullet} + O_2 \rightarrow CH_2O + HO_2^{\bullet}$	NRC, 1981
(6a)	$RCH_2CH_3 + HO^{\bullet} \rightarrow RCH_2CH_2^{\bullet} + H_2O$	Demerjian *et al.*, 1974
(6b)	$RCH_2CH_3 + HO^{\bullet} \rightarrow R\dot{C}HCH_3 + H_2O$	Demerjian *et al.*, 1974
(7)	$\begin{matrix} RCH_2CH_2^{\bullet} \\ \text{or} \\ R\dot{C}HCH_3 \end{matrix} + (NO, O_2, h\nu, \text{ or } HO^{\bullet}) \rightarrow \begin{matrix} CH_2O, CH_3CHO, \\ \\ RCHO, \text{etc.} \end{matrix}$	Demerjian *et al.*, 1974
(8)	$RCH = CHR' + HO^{\bullet} + (NO, O_2) \rightarrow RCHO + R'CHO + (NO_2)$	Niki *et al.*, 1978
(9)	$2RCH = CH_2 + 2O_3 \rightarrow RCHO + RCHO_2 + CH_2O + CH_2O_2$	NRC, 1981
(10)	$\begin{matrix} RCHO_2 \\ \text{or} \\ CH_2O_2 \end{matrix} + (NO \text{ or } SO_2) \rightarrow \begin{matrix} RCHO \\ \text{or} \\ CH_2O \end{matrix} + (NO_2 \text{ or } SO_3)$	NRC, 1981

[a] Only major products are shown.

Table III. Summary of reactions involved in aldehyde destruction[a]

No.	Reaction	Reference
(11a)	$RCHO + h\nu \rightarrow R^{\cdot} + HCO^{\cdot}$	Calvert and Pitts, 1966
(11b)	$\rightarrow RH + CO$	
(12)	$R^{\cdot} + O_2 + M \rightarrow RO_2^{\cdot} + M$	Calvert and Pitts, 1966
(13)	$HCO^{\cdot} + O_2 \rightarrow HO_2^{\cdot} + CO$	Calvert and Pitts, 1966
(14)	$HO^{\cdot} + CH_2O \rightarrow H_2O + HCO^{\cdot}$.	Smith, 1978
(15)	$HO. + HCO^{\cdot} \rightarrow H_2O + CO$	Smith, 1978
(16)	$NO_3^{\cdot} + CH_2O \rightarrow HNO_3 + HCO^{\cdot}$	NRC, 1981
(17)	$HO_2^{\cdot} + CH_2O \rightleftharpoons {}^{\cdot}O_2CH_2OH$	Su *et al.*, 1979
(18)	${}^{\cdot}O_2CH_2OH + HO_2^{\cdot} \rightarrow HO_2CH_2OH + O_2$	Su *et al.*, 1979
(19)	$HO_2CH_2OH + h\nu \rightarrow HCOOH + H_2O$	Su *et al.*, 1979
(20)	$2\ {}^{\cdot}O_2CH_2OH \rightarrow 2\ OCH_2OH + O_2$	NRC, 1981
(21)	$OCH_2OH + O_2 \rightarrow HCOOH + HO_2^{\cdot}$	NRC, 1981

[a] Only major products are shown.

Photolysis of CH_2O initially forms CO and H_2, and is a source for $HO_2^{\cdot}$ (Calvert, 1980). The most important oxidants for aldehydes are $HO^{\cdot}$, $HO_2^{\cdot}$, and, at night, $NO_3^{\cdot}$. Primary products are CO, HCOOH, and additional $HO_2^{\cdot}$. Nitric acid can be formed by $NO_3^{\cdot}$ attack on aldehydes. The concentration of aldehydes in the atmosphere is thus determined by a dynamic balance between production and destruction.

In the aqueous phase, aldehydes hydrolyze via reactions (22) and (23) to form gem-diols

$$RCHO_{(g)} \overset{H_A}{\rightleftharpoons} RCHO_{(aq)}\ , \tag{22}$$

$$RCHO_{(aq)} + H_2O \overset{K_H}{\rightleftharpoons} RCH(OH)_2\ ; \tag{23}$$

The combined Henry's law and hydrolysis constant, H_A, is 6.3×10^3 for CH_2O (Ledbury and Blair, 1925). The hydrolysis constant alone, K_H, is 2530, 1.2, and 1.2 for CH_2O, CH_3CHO, and C_2H_5CHO, respectively (Buschmann *et al.*, 1980). In the hydrated form, aldehydes are less sensitive to photodecomposition (NRC, 1981). Because of glycol formation and limited insolation, fog and clouds may provide ideal environments for the accumulation of aldehydes.

Aldehydes also form hydroxyalkylsulfonic acids in aqueous solutiun by addition of S(IV) to aldehyde (Bell and Evans, 1966; Boyce and Hoffmann, 1984):

$$SO_{2(g)} \overset{H_S}{\rightleftharpoons} SO_{2(aq)} \tag{24}$$

$$SO_{2(aq)} \overset{K_{a_1}}{\rightleftharpoons} H^+ + HSO_3^- \tag{25}$$

$$HSO_3^- \overset{K_{a_2}}{\rightleftharpoons} H^+ + SO_3^{2-} \tag{26}$$

$$HSO_3^- + RCHO_{(aq)} \underset{k_{-1}}{\overset{k_1}{\rightleftharpoons}} RCHOHSO_3^- \tag{27}$$

$$SO_3^{2-} + RCHO_{(aq)} \underset{k_{-2}}{\overset{k_2}{\rightleftharpoons}} {}^-O_3SRCHO^- \tag{28}$$

The addition product with formaldehyde, hydroxymethanesulfonate (HMSA) undergoes acid base equilibria shown in reactions (29) and (30):

$$HO_3SCH_2OH \overset{K_1}{\rightleftharpoons} HO_3SCH_2O^- + H^+ \tag{29}$$

$$HO_3SCH_2O^- \overset{K_2}{\rightleftharpoons} {}^-O_3SCH_2O^- + H^+ \tag{30}$$

HO_3SCH_2OH is a strong acid (Roberts *et al.*, 1971); pK_2 is 10.2 (Sørensen and Andersen 1970). At pH values found in fogs and clouds, HMSA will be in the monovalent form. Reactions (24)–(28) are an additional source of acidity in the droplet because they lead to a supersaturation with respect to S(IV) and a concomitant increase in H^+ from reactions (25) and (26). Oxidation of S(IV) to S(VI) in the presence of strong oxidants or metal catalysts via reaction (31) is a competing sink for S(IV) and an alternate pathway for the production of acidity:

$$HSO_3^- \xrightarrow{\text{oxidants}} H^+ + SO_4^{2-} \tag{31}$$

In a well-buffered, open system, reactions (27), (28), and (31) are independent of one another. If the system is not open with respect to $SO_{2(g)}$, however, (27), (28), and (31) will be in direct competition for a limited amount of S(IV).

Formation of HMSA has been suggested as a possible explanation for excess CH_2O concentrations in aerosol (Klippel and Warneck, 1980; Grosjean, 1982), and the apparent stability of S(IV) in aerosol (Izatt *et al.*, 1978). Richards *et al.* (1983) suggest that HMSA formation inhibits S(IV) oxidation by H_2O_2, but Jacob and Hoffmann (1983) predict that both reactions should proceed in parallel. Because the sources of aledehydes and their precursors are so widespread, the formation of bisulfite-aldehyde adducts could be an important reaction in atmospheric water droplets wherever SO_2 is present. In this paper we present findings of elevated CH_2O and S(IV) concentrations in fog- and cloudwater and discuss these results in light of thermodynamic and kinetic considerations.

2. Methods

As part of a study of fogwater chemistry in Southern California (Waldman *et al.*, 1982; Munger *et al.*, 1983), S(IV) and CH_2O concentrations were routinely measured. Aliquots were removed from the samples immediately after collection and preserved. Formaldehyde was preserved as 3,5-diacetyl-1,4-dihydrolutidine (DDL) (Nash, 1953; Reitz, 1980). The absorbance of the DDL was measured at 412 nm on a Beckman Acta III spectrometer. Beginning in December 1982, I_2 was added to oxidize S(IV) in the samples and eliminate its interference (Smith and Erhardt, 1975). Only for samples with an appreciable excess of S(IV) over CH_2O would this interference be a problem. Standards were made using both CH_2O and $NaCH_2OHSO_3$; with added I_2, both CH_2O sources gave an equivalent response.

Sulfur(IV) in the fog samples was preserved as the formaldehyde adduct by addition of excess CH_2O (Dasgupta *et al.*, 1980; Fortune and Dellinger, 1982) and measured by a colorimetric method using 5,5',dithio-bis(2-nitrobenzoic acid) (DTNB) under mildly alkaline conditions (Humphrey *et al.*, 1970). The samples collected at Henninger Flats during May and June 1983 were preserved by addition of EDTA and phosphate buffer at pH 7; the two methods were equally efficacious. Absorbance of the colored product was measured at 412 nm on Beckman Acta III spectrophotometer. The standard curve for both Na_2SO_3 and $NaCH_2OHSO_3$ was linear up to 250 μM; the response to $NaCH_2OHSO_3$ was 90 to 100% of the response to Na_2SO_3. The coexistence of CH_2O and S(IV) in samples complicates their analysis. Any analytical procedure used must dissociate the adduct to ensure complete recovery of both species.

Fogwater was collected at several sites in the Los Angeles Basin (Pasadena, Lennox, and Upland), at points along the California coast (Pt Reyes, San Nicholas Island, and Del Mar), and at Bakersfield (Kern County) in the San Joaquin Valley. Stratus clouds were sampled above Pasadena at Henninger Flats (elev. 800 m) and Mt Wilson (elev. 1800 m). Stratus clouds intercept Henninger Flats when the marine layer is moderately deep; clouds at Mt Wilson are associated with an even deeper mixed layer. Stratus clouds were sampled from an airplane over the Los Angeles basin in May 1982 (see Richards *et al.* for details). These samples included plume-impacted clouds and clouds over the ocean.

Bakersfield is heavily impacted by emissions from tertiary oil recovery and refining operations (Table IV, Kern County). In addition, agricultural activity in the San Joaquin valley is a source of particulate matter (CARB, 1982) and ammonia. During the sampling period SO_2 levels up to 80 ppb were observed in Bakersfield (CARB, unpublished data). In Los Angeles (Table IV, South Coast Air Basin), SO_2 emissions from petroleum refining, power production, and other industrial fuel combustion processes are comparable to those in Kern County, but emissions of hydrocarbons are greater due to the high density of mobile sources. As a result, the hydrocarbon to SO_2 mass emission ratio is much greater in the South Coast Air Basin than in Kern County. The South Coast Air Basin also has significantly higher NO_x emissions than Kern County, and O_3 levels are higher.

3. Results

The median and range of S(IV) and CH_2O liquid concentrations are presented in Table V. The highest concentrations of S(IV) were observed at the Bakersfield site during an

Table IV. Emissions of SO_2, NO_x, and reactive hydrocarbons in airsheds surrounding the sampling sites

Airshed	SO_2 (10^3 kg day^{-1})	NO_x (10^3 kg day^{-1})	RHC (10^3 kg day^{-1})	Area (km^2)
South Coast Basin	240	1123	1375	16,930
Kern County	170	171	427	14,460

Source: CARB (1982).

Table V. Concentrations of S(IV) and CH_2O in fog- and cloudwater samples collected in California

Samples series	S(IV) (μM)			CH_2O (μM)		
	Range	Median	*n*	Range	Median	*n*
Urban fog						
Los Angeles, 1981–82	15–196	90	13	93–322[a]	189	15
Southern California Coast, 1983	8–279	48	10	53–256	73	13
Bakersfield, 1983	45–2980	517	88	53–709	170	83
Marine fog						
Point Reyes	3.5–10	5	23	0.57–18[a]	3.1	22
San Nicholas Island, 1982	9–18	12	5	6.6–24	17	5
Stratus clouds						
Henninger Flats, 1982	7–60	13	35	34–132[a]	65	35
Henninger Flats, 1983	1–94	8	64	12–173	50	65
Mt Wilson	2–16	3	9	1.8–14[a]	2.4	9
Los Angeles Basin, 1982	5–365	29	11	11–142[a]	70	11

[a] I_2 was not added to prevent interference by S(IV). Some CH_2O values may be underestimated if [S(IV)] was high relative to [CH_2O].

extended stagnation episode in which fog formed almost every night for three weeks. Sulfur(IV) generally exceeded formaldehyde in these samples, especially when concentrations were highest. At sites in Los Angeles, CH_2O levels were comparable to those in Bakersfield, but S(IV) levels were lower. At coastal sites and at higher elevations (Mt Wilson), concentrations of both CH_2O and S(IV) were low and roughly equimolar. At San Nicholas Island, elevated acidity, nitrate, sulfate, and trace metal concentrations suggest that this site was influenced by anthropogenic emissions; concentrations of S(IV) and CH_2O were higher there than at Pt Reyes. Point Conception and the Santa Barbara Channel, major offshore oil exploration and production areas, were directly upwind of San Nicholas Island during the sampling period. Concentrations in the low-level clouds overlapped those found in ground-level fog in Los Angeles, but were still much higher than at Mt Wilson. The highest cloudwater concentrations were found near emission sources.

The concentrations of S(IV) and CH_2O per unit volume of air (Table VI) were calculated from the measured concentrations in the liquid phase and the liquid water content (LWC). The LWC was measured as mass on an open-faced paper filter or calculated from the collected sample volume. A sampling rate of 5 m^3 min^{-1} and a collection efficiency of 60% (Jacob *et al.*, 1984) were assumed to convert volume collected to LWC. Although the aqueous concentrations of CH_2O per volume of air are less than the gas-phase concentrations typical of urban atmospheres, they generally exceed those previously reported for aerosol (see Table I). This confirms previous findings that the gas phase is the major pool of aldehyde (Klippel and Warneck, 1980; Grosjean, 1982).

Table VI. Concentrations of S(IV) and CH_2O on an air volume basis in fog- and cloudwater samples collected in California

Sample series	S(IV) (ng m^{-3})			CH_2O (ng m^{-3})		
	Range	Average	*n*	Range	Average	*n*
Urban fog						
Southern California coast, 1983	42–725	283	9	195–1140	459	12
Bakersfield, 1983	160–9000	1980	82	45–3800	650	78
Marine fog						
Point Reyes, 1982	11–46	29	24	0.2–26	13	24
San Nicholas Island, 1982	13–26	18	4	29–40	27	4
Stratus clouds						
Henninger Flats, 1982	42–1630	144	38	142–4800	504	37
Henninger Flats, 1983	2–170	84	64	20–476	151	65
Mt Wilson, 1982	10–53	14	9	8–42	13	9
Los Angeles Basin, May 1982	75–3500	–	11	133–1440	–	11

4. Discussion

The S(IV) and CH_2O equilibria are described by the expressions given in Table VII. Other carbonyl compounds that form bisulfite adducts, such as acetaldehyde, propanal, *n*-butanal, *n*-pentanal, benzaldehyde, and acrolein (Bordwell, 1963; Grosjean, 1982) and some transition metals that may form complexes with S(IV) (Eatough and Hansen, 1983) are undoubtedly present in fog- and cloudwater. The presence of these adducts and

Table VII. Equilibria and thermodynamic data

No.	Equilibrium expression	$K_{eq_{298}}$ (M atm^{-1} or M^{-1})	ΔH_{298} (kcal mol^{-1})	Reference
(32)	$[SO_2 \cdot H_2O] = H_S P_{SO_2(g)}$	1.245	−6.247	Sillén and Martell, 1964
(33)	$[HSO_3^-] = K_{a1} \dfrac{[SO_2 \cdot H_2O]}{[H^+]}$	1.29×10^{-2}	−4.161	Sillén and Martell, 1964
(34)	$SO_3^{2-} = K_{a2} \dfrac{[HSO_3^-]}{[H^+]}$	6.014×10^{-8}	−2.23	Sillén and Martell, 1964
(35)[b]	$[CH_2O_l] = H_F^* P_{CH_2O(g)}$	6.3×10^3	−12.85	Ledbury and Blair, 1925
(36)	$[CH_2O_{aq}] = \dfrac{[CH_2(OH)_2]}{K_H}$	2.53×10^3	−8.0	Buschmann *et al.*, 1980; Bell, 1966
(37)	$[CH_2OHSO_3^-] = K_F [HSO_3^-] [CH_2O_{(l)}]$	10^5	−12.3[a]	Dasgupta *et al.*, 1981

[a] No data for HMSA are available; the ΔH for formation of benzaldehyde-bisulfite adduct (Stewart and Donnally, 1932) is used here.

[b] $CH_2O_l = CH_2O_{aq} + CH_2(OH)_2$.

complexes would contribute to the total S(IV) concentration. Sulfur(IV) concentrations in excess of that predicted from the formaldehyde-bisulfite equilibrium would suggest the presence of other adduct-forming species. We found that trace-metal concentrations were generally insufficient to contribute substantially to the total S(IV), but Grosjean and Wright (1983) report the presence of higher aldehydes in Los Angeles cloud- and fogwater at concentrations comparable to formaldehyde. Because higher aldehydes were not measured in this study, discussion will be limited to the formation of the S(IV)–CH_2O adduct, HMSA.

The appropriate mass balance relationships for the S(IV)–CH_2O equilibria are given below:

$$[\mathrm{S(IV)}]_T = [\mathrm{SO_2 \cdot H_2O}] + [\mathrm{HSO_3^-}] + [\mathrm{SO_3^{2-}}] + [\mathrm{CH_2OHSO_3^-}] \qquad (38)$$

$$[\mathrm{CH_2O}]_T = [\mathrm{CH_2O}_{(l)}] + [\mathrm{CH_2OHSO_3^-}] \qquad (39)$$

Substituting the equilibrium expressions of Table VII into the mass balance equations, (38) and (39), followed by rearrangement yields:

$$[\mathrm{S(IV)}]_T = H_\mathrm{S} P_{\mathrm{SO_2}} \left\{ 1 + \frac{K_{a1}}{[\mathrm{H^+}]} \left(1 + K_F H_F^* P_{\mathrm{CH_2O}} + \frac{K_{a2}}{[\mathrm{H^+}]} \right) \right\} \qquad (40)$$

$$[\mathrm{CH_2O}]_T = H_F^* P_{\mathrm{CH_2O}} \left(1 + K_F H_\mathrm{S} \frac{K_{a1}}{[\mathrm{H^+}]} P_{\mathrm{SO_2}} \right) \qquad (41)$$

Equations (40) and (41) show that the concentration of S(IV) and CH_2O vary inversely with pH. Because the enthalpies of reactions (32), (33), (34), (35), and (36) are negative, adduct formation will be enhanced at lower temperature. Equations (40) and (41) (Figures 1 and 2) indicate that high concentrations of S(IV) and CH_2O can exist in solution via adduct formation. Concentrations would be much lower if no adduct was formed.

Because other reactions may compete for the reactants, formation of bisulfite-aldehyde adducts is kinetically controlled. Boyce and Hoffmann (1984) report the following rate expression for the formation of HMSA via reactions (22)–(30).

$$\frac{d[\mathrm{HMSA}]}{dt} = H_\mathrm{S} H_F^* P_{\mathrm{SO_2}} P_{\mathrm{CH_2O}} \frac{1}{(1 + K_H)} \left(\frac{k_1 K_{a1}}{\mathrm{H^+}} + \frac{k_2 K_{a1} K_{a2}}{[\mathrm{H^+}]^2} \right) \qquad (42)$$

where $k_1 = 7.9 \times 10^2\ M^{-1}\ \mathrm{s}^{-1}$ and $k_2 = 2.48 \times 10^7\ M^{-1}\ \mathrm{s}^{-1}$. The activation energies for k_1 and k_2 are 5.9 and 4.8 kcal mole^{-1}, respectively. The negative temperature dependence for the acid-base and Henry's law equilibria dominate the positive temperature dependence of the kinetic constants; consequently the reaction rate increases with decreasing temperature. At CH_2O partial pressure of 5 ppb and SO_2 partial pressure of 20 ppb the formation rates at pH 3 are 0.20 at 0°C and 0.09 $\mu M\ \mathrm{h}^{-1}$ at 10°C. The rates increase to 1530 and 680 $\mu M\ \mathrm{h}^{-1}$ at pH for 0°C and 10°C, respectively. The dissociation reaction is

BISULFITE-ALDEHYDE PRODUCTS

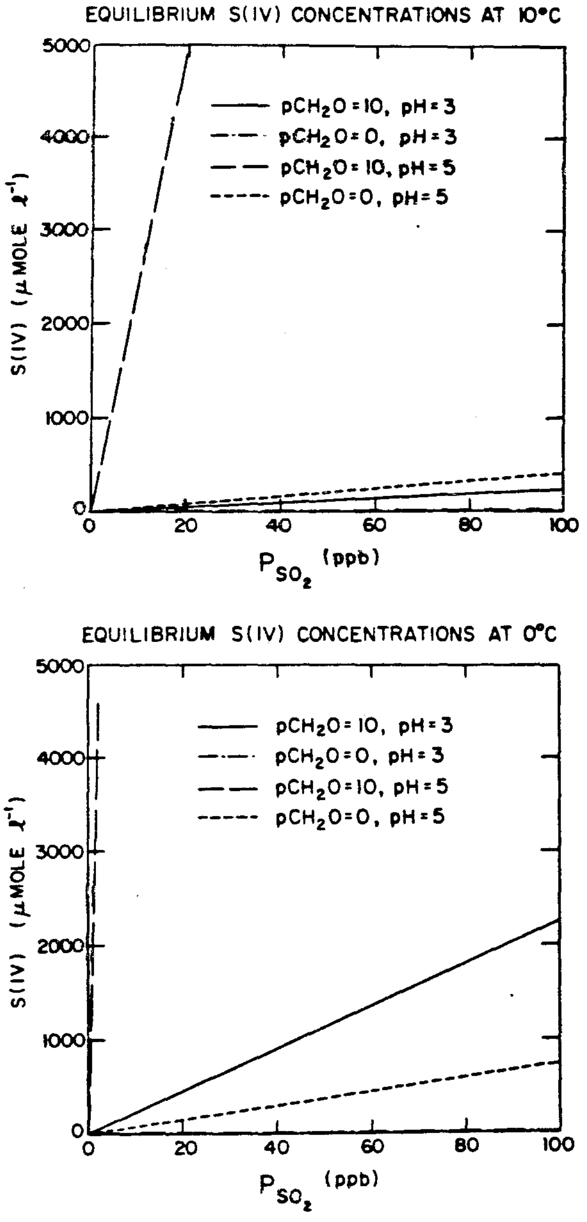

Fig. 1. Equilibrium concentrations of S(IV) with and without CH_2O present for two temperatures and two pH values. 10°C (A) is typical of Los Angeles area fog- and cloudwater; 0°C (B) is typical of Bakersfield fog. 10 ppb is an upper limit for 24-hour average CH_2O concentrations (NRC, 1982).

slower than the formation reaction by a factor of 10^5, so HMSA will not readily break down. Because the time scale for changes in ambient gas concentrations and fog formation and dissipation is much shorter than the reaction time for HMSA formation and

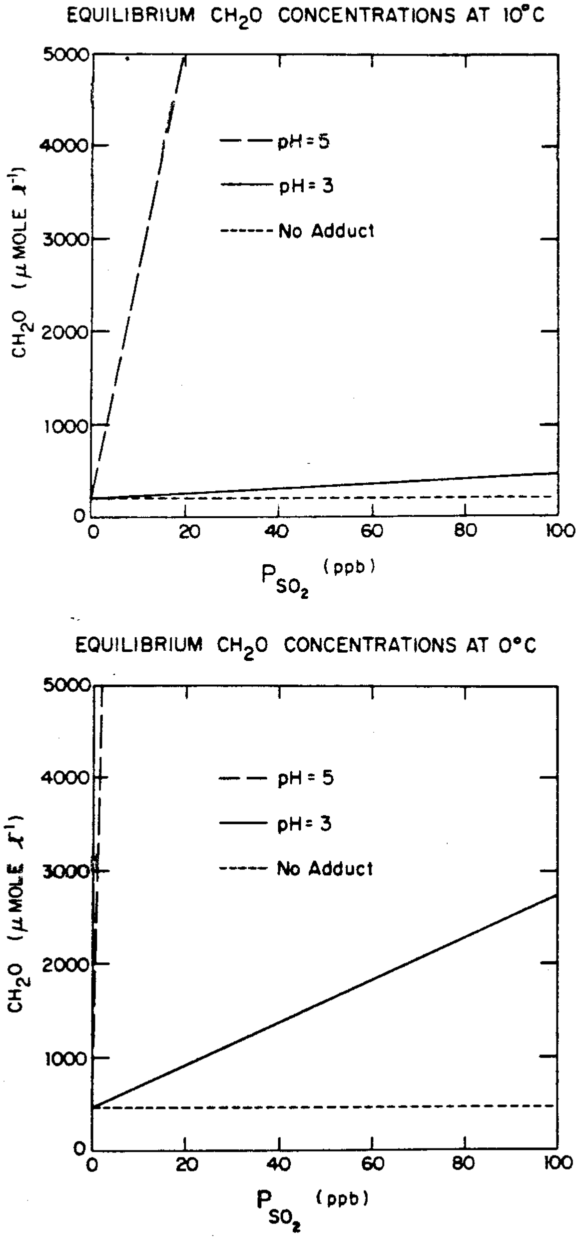

Fig. 2. Concentrations of CH_2O in equilibrium with 10 ppb CH_2O in the gas phase with and without adduct formation for two temperatures and two pH values. 10°C (A) is typical of Los Angeles area fog- and cloudwater; 0°C (B) is typical of Bakersfield fog. 10 ppb is an upper limit for 24-hour average CH_2O concentrations (NRC, 1982).

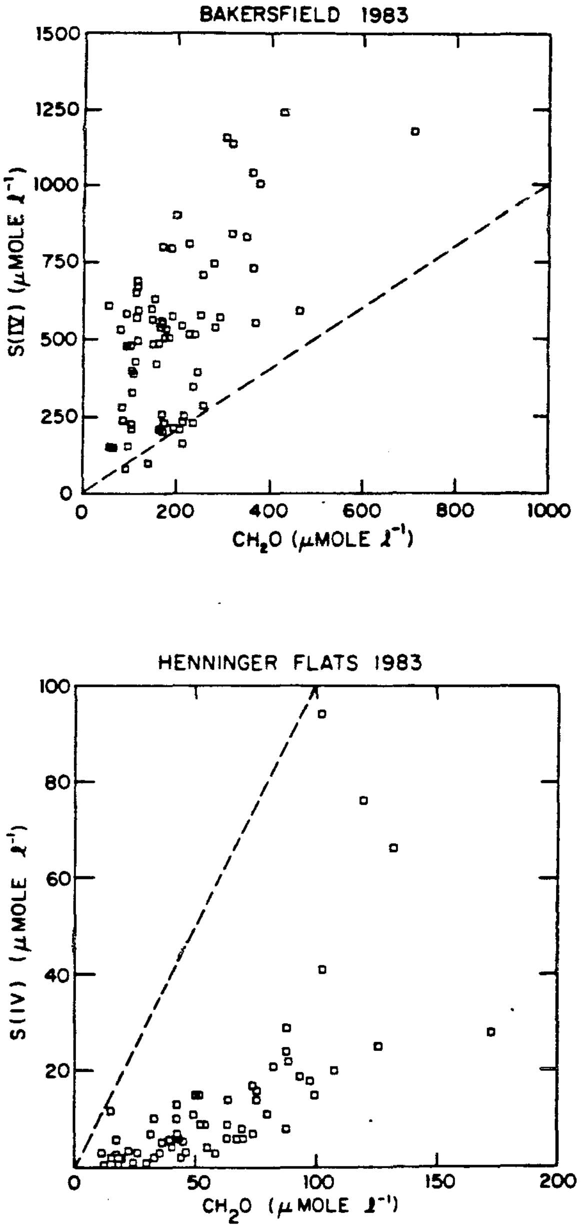

Fig. 3. S(IV) *vs.* CH_2O in fog- and cloudwater. Bakersfield (A), Los Angeles area stratus clouds (B). The line indicates equal concentrations of S(IV) and CH_2O.

dissociation at low pH, S(IV) and aldehyde concentrations may be out of equilibrium. Furthermore, S(IV) oxidation reactions, which are more rapid (McArdle and Hoffmann, 1983; Hoffmann and Boyce, 1983), may diminish the amount of substrate available for adduct formation. Once formed, however, bisulfite-aldehyde adducts would be stable towards oxidants, explaining the coexistence of S(IV) and H_2O_2 reported by Richards *et al.* (1983).

The presence of high concentrations of S(IV) and CH_2O at the onset of fog suggests that HMSA must be present in the condensation nuclei. Adducts present upon fog or cloud dissipation would likely remain as aquated aerosol and provide condensation nuclei for subsequent fogs. In addition, adducts could form in haze aerosol and in fresh plumes containing high concentrations of SO_2 and primary aldehyde. Appreciable concentrations of S(IV) and CH_2O could build up during prolonged cycles of fog and haze such as occur in many parts of Southern California.

The most favorable conditions for S(IV)–aldehyde adduct formation were found at Bakersfield, where temperatures were near 0°C, SO_2 concentrations were high, and fogwater pH was in the range 3–6 (Jacob *et al.*, 1984). Furthermore, the near-stagnant air mass associated with wintertime fog episodes in the San Joaquin Valley (Reible *et al.*, 1983) could lead to a sufficiently long residence time for the formation of appreciable adduct concentrations. In fogs and clouds investigated in the Los Angeles area, temperatures were higher (near 10°C) and pH values were mostly in the range 2–4 (Munger *et al.*, 1983; Hering and Blumenthal, 1983; Richards *et al.*, 1983). Partial pressures of SO_2 were generally lower than in Bakersfield (South Coast Air Quality Management District, unpublished data; Richards *et al.*, 1983), but gas-phase formaldehyde was probably greater because of the higher oxidant levels and abundant hydrocarbon emissions. Sulfur(IV) concentrations were lower in Los Angeles than in Bakersfield; CH_2O concentrations were comparable in the ground-level fog and slightly lower in the stratus samples. Sites more distant from local emissions had the lowest concentrations of all, but both species were measurable. The presence of nearly equimolar concentrations of S(IV) and CH_2O at Point Reyes, San Nicholas Island, and Mt Wilson suggests that S(IV) stabilization by adduct formation during long-distance transport may be an important consideration.

Sulfur(IV) and CH_2O concentrations in Bakersfield fogwater and in Los Angeles area cloudwater are compared in Figure 3. Sulfur(IV) exceeded CH_2O at Bakersfield. The individual concentrations of each S(IV) species in (38) can be calculated from pH, temperature, partial pressures, and the equilibria in Table VII. Excess S(IV) is calculated as the difference between measured S(IV) and the calculated free S(IV) (the first three terms on the right of (38)). This difference consists of HMSA and other adducts, and accounts for most of the measured S(IV) (Figure 4). The excess S(IV) increased with CH_2O concentration. Because S(IV) concentrations were higher than the corresponding CH_2O concentrations and free S(IV) was negligible, adducts with higher aldehydes were probably present as well. The presence of acetic and higher carboxylic acids, which are the products of gas-phase aldehyde destruction (Table III), in fogwater samples (J. W. Munger, unpublished results) suggests that higher aldehydes were present in the Bakersfield fogwater as well. In the stratus cloudwater samples from Los Angeles, only those collected

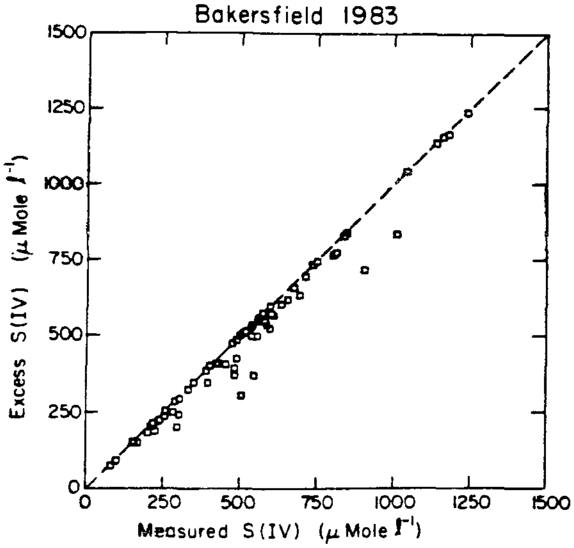

Fig. 4. "Excess" S(IV) vs. measured S(IV) in Bakersfield fogwater samples. "Excess" S(IV) is the difference between measured S(IV) and "free" S(IV) (see text). The dashed line indicates equal values for excess and measured S(IV) (i.e., no free S(IV)).

in plumes with high SO_2 concentrations had S(IV) higher than CH_2O. The remainder of the samples had more CH_2O than S(IV). The latter situation would arise if SO_2 concentrations were insufficient to saturate all the available aldehyde, or if adduct formation were very slow.

The stability of the S(IV) and CH_2O in fogwater is indicated by results illustrated in Figure 5. After a month of storage at 4°C without preservatives, appreciable concentrations of both species remain in samples from Bakersfield, often at concentrations near their original value. However, it is apparent that S(IV) undergoes the greatest depletion. In the aged samples S(IV) is nearly equal to or slightly less than CH_2O. Aldehydes, S(IV), and hydroxyalkylsulfonic acids in fog and cloud droplets may oxidize more rapidly when exposed to the atmosphere. Chameides and Davis (1983) report that CH_2O is oxidized to formic acid by $OH^\cdot$ in solution. We observe HCOOH in our fogwater samples, but we have no evidence to determine whether it is formed by gas- or liquid-phase reactions. Preliminary work in this laboratory suggests that HMSA is oxidized by aqueous-phase $OH^\cdot$. The addition of H_2O_2 and Fe(II), which form $OH^\cdot_{(aq)}$ via reaction (42), rapidly destroys HMSA.

$$\mathrm{Fe(II)} + H_2O_2 \longrightarrow \mathrm{Fe(III)} + {}^\cdot OH + {}^-OH \qquad (42)$$

5. Summary and Conclusion

The finding of appreciable levels of S(IV) and CH_2O in nearly all fogwater samples

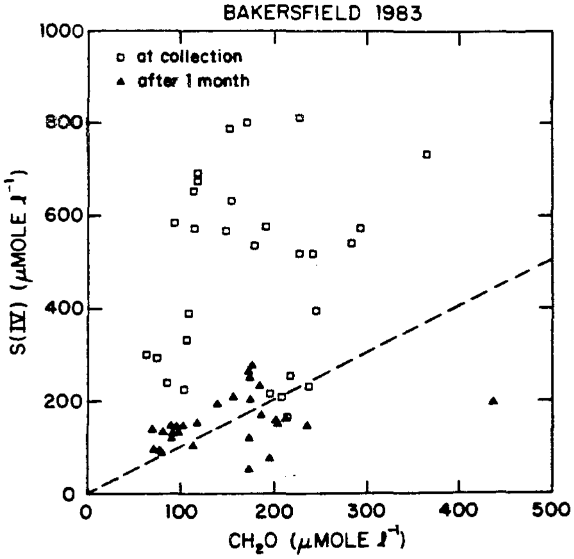

Fig. 5. S(IV) *vs.* CH_2O in Bakersfield samples at the time of collection and after one month of storage at 4°C without preservatives. The line indicates equal concentrations of S(IV) and CH_2O.

examined suggests that the formation of S(IV) aldehyde adducts is an important reaction in atmospheric water droplets. The presence of CH_2O and other aldehydes could lead to the uptake of relatively high concentrations of S(IV) into cloud and fog droplets and aquated aerosol by stabilizing reduced sulfur species. Acidity is produced via adduct formation. Because the formation and dissociation of S(IV) aldehyde adducts are slow at low pH, competition with S(IV) oxidation for substrate may limit adduct formation. The extreme slowness of the adduct dissociation rate is likely to preclude equilibrium in aged air masses (i.e., adduct concentration may exceed that supported by ambient concentrations of SO_2 and CH_2O). These data indicate that aldehyde–S(IV) adduct formation is important in S(IV) chemistry. Bisulfite-aldehyde adducts are likely to form whenever irradiated mixtures of SO_2 and hydrocarbons contact liquid water. The equilibria and kinetics of S(IV)–aldehyde adduct formation should be applied to models of sulfur uptake, transport, and transformation.

Acknowledgements

This research was supported by the California Air Resources Board (Contract A2-048-32). We thank the CARB, the South Coast Air Quality Management District, the Los Angeles County Fire Department Forestry Division, the United States Navy, the National Park Service, and the Mt. Wilson Observatories for logistical support and the use of field facilities. We also thank J. Waldman and S. Boyce for their contributions to the success of this project.

References

Bell, R. P., 1966, The reversible hydration of carbonyl compounds, in V. Gold (ed.), *Advances in Physical Organic Chemistry*, vol. 4, Academic Press, London, pp. 1–29.

Bell, R. P., Evans, F. R. S., and Evans, P. G., 1966, Kinetics of the dehydration of methylene glycol in aqueous solution, *Proc. Roy. Soc. A.* 291, 297–323.

Bordwell, F. G., 1963, *Organic Chemistry*, Macmillan, New York.

Boyce, S. D. and Hoffmann, M. R., 1984. Kinetics and mechanism of the formation of hydroxymethanesulfonic acid at low pH, *J. Phys. Chem.*, in press.

Buschmann, H. J., Fulderner, H. H., and Knoche, W., 1980, The reversible hydration of carbonyl compounds in aqueous solution. Part I, the ketol gem-diol equilibrium, *Ber. Bunsenges Phys. Chem.* 84, 41–44.

California Air Resources Board (CARB), 1982, *Emissions Inventory*, California Air Resources Board, Sacramento, California.

Calvert, J. G. and Pitts, J. N., Jr., 1966, *Photochemistry*, John Wiley, New York.

Calvert, J. G., 1980, The homogeneous chemistry of formaldehyde generation and destruction within the atmosphere, in *Proceedings of the NATO Advanced Study Institute on Atmospheric Ozone: Its Variation and Human Influences*, Federal Aviation Administration, Washington, D.C., pp. 153–190.

Chameides, W. L. and Davis, D. D., 1983, Aqueous-phase source of formic acid in clouds, *Nature* 304, 427–429.

Cleveland, W. S., Graedel, T. E., and Kleiner, B., 1977, Urban formaldehyde: Observed correlation with source emissions and photochemistry, *Atmos. Environ.* 11, 357–360.

Dasgupta, P. K., DeCesare, K., and Ullrey, J. C., 1980, Determination of atmospheric sulfur dioxide without tetrachlormercurate(II) and the mechanism of the Schiff Reactions, *Anal. Chem.* 52, 1912–1922.

Demerjian, K. L., Kerr, J. A., and Calvert, J. G., 1974, The mechanism of photochemical smog formation, *Adv. Environ. Sci. Technol.* 4, 1–262.

Eatough, D. J. and Hansen, L. D., 1983, Organic and inorganic S(IV) compounds in airborne particulate matter, *Adv. Environ. Sci. Technol.* 12, 221–268.

Fortune, C. R. and Dellinger, B., 1982, Stabilization and analysis of S(IV) aerosols in environmental samples, *Environ. Sci. Tech.* 16, 62–66.

Grosjean, D., 1982, Formaldehyde and other carbonyls in Los Angeles ambient air, *Environ. Sci. Technol.* 16, 254–262.

Grosjean, D. and Wright, B., 1983, Carbonyls in urban fog, ice fog, cloudwater and rainwater, *Atmos. Environ.* 17, 2093–2096.

Hering, S. V. and Blumenthal, D. L., 1983, Field comparison of fog/cloud water collectors: Preliminary results, *Proc. APCA Specialty Conference on the Meteorology of Acid Deposition*, Hartford, Connecticut, October, 1983.

Hoffmann, M. R. and Boyce, S. D., 1983, Catalytic autoxidation of aqueous sulfur dioxide in relationship to atmospheric systems, *Adv. Environ. Sci. Technol.* 12, 149–189.

Humphrey, R. E., Ward, M. H., and Hinze, W., 1970, Spectrophotometric determination of sulfite with 4,4-Dithiopyridine and 5,5′-Dithiobis(2-Nitrobenzoic acid), *Anal. Chem.* 42, 698–702.

Izatt, R. M., Eatough, D. J., Lee, M. L., Major, T., Richter, B. E., Hansen, L. D., Meisenheimer, R. G., and Fischer, J. W., 1978, The formation of inorganic and organic S(IV) species in aerosols, *Proc. 4th Joint Conf. on Sensing Environ. Pollutants*, Amer. Chem. Soc., Washington, D.C., pp. 821–824.

Jacob, D. J. and Hoffmann, M. R., 1983, A dynamic model for the production of H^+, NO_3^-, and SO_4^{2-} in urban fog, *J. Geophys. Res.* 88C, 6611–6621.

Jacob, D. J., Wang, R-F. T., and Flagan, R. C., 1984, Fogwater collector design and characterization, *Environ. Sci. Technol.*, in press.

Jacob, D. J., Waldman, J. M., Munger, J. W., and Hoffmann, M. R., 1984, A field investigation of physical and chemical mechanisms affecting pollutant concentrations in fog droplets, *Tellus*, in press.

Klippel, W. and Warneck, P., 1978, Formaldehyde in rain water and on the atmospheric aerosol, *Geophys. Res. Lett.* 5, 177–179.

Klippel, W. and Warneck, 1980, The formaldehyde content of the atmospheric aerosol, *Atmos. Environ.* **14**, 809–818.

Ledbury, W. and Blair, E. W., 1925, The partial formaldehyde vapour pressure of aqueous solutions of formaldehyde. Part II. *J. Am. Chem. Soc.* **127**, 2832–2839.

McArdle, J. V. and Hoffmann, M. R., 1983, Kinetics and mechanism of the oxidation of aquated sulfur dioxide by hydrogen peroxide at low pH, *J. Phys. Chem.* **87**, 5425–5429.

Munger, J. W., Jacob, D. J., Waldman, J. M., and Hoffmann, M. R., 1983, Fogwater chemistry in an urban atmosphere, *J. Geophys. Res.* **88**, 5109–5121.

Nash, T., 1953, The colorimetric estimation of formaldehyde by means of the Hantzsch Reaction, *Biochem. J.* **55**, 416–421.

National Research Council (NRC), 1981, *Formaldehyde and Other Aldehydes*, National Academy Press, Washington, D.C.

Niki, H., Maker, P. D., Savage, C. M., and Breitenbach, L. P., 1978, Mechanism for hydroxyl radical initiated oxidation of olefin-nitric oxide mixtures in parts per million concentrations, *J. Phys. Chem.* **82**, 135–137.

Reible, D. D., Shair, F. H., Smith, T.-B., Lehrman, D. E., 1983, The origin and fates of air pollutants in California's San Joaquin Valley I. Winter. *Atmos. Environ.*, in press.

Reitz, E. B., 1980, The stabilization of small concentrations of formaldehyde in aqueous solutions, *Anal. Lett.* **13**, 1073–1084.

Richards, L. W., Anderson, J. A., Blumenthal, D. L., McDonald, J. A., Kok, G. L., and Lazrus, A. L., 1983, Hydrogen peroxide and sulfur(IV) in Los Angeles cloudwater, *Atmos. Environ.* **17**, 911–914.

Roberts, J. D., Stewart, R., and Caserio, M. C., 1971, *Organic Chemistry*, W.A. Benjamin, Menlo Park, CA.

Sillén, G. L. and Martell, A. E., 1964, *Stability Constants of Metal-ion Complexes*, special publication No. 17, Chemical Society, London.

Smith, R. H., 1978, Rate constant and activation energy for the gaseous reaction between hydroxyl and formaldehyde, *Int. J. Chem. Kinet.* **10**, 519–528.

Smith, R. V. and Erhardt, P. W., 1975, Nash determination for formaldehyde in the presence of bisulfite, *Anal. Chem.* **47**, 2462–2454.

Sørensen, P. E. and Andersen, V. S., 1970, The formaldehyde-hydrogen sulphite system in alkaline aqueous solution. Kinetics, mechanisms, and equilibria, *Acta Chem. Scand.* **24**, 1301–1306.

Su, F., Calvert, J. G., and Shaw, J. H., 1979, Mechanism of the photooxidation of gaseous formaldehyde, *J. Phys. Chem.* **83**, 3185–3191.

Stewart, T. D. and Donnally, L. H., 1932, The aldehyde bisulfite compounds II. The effect of varying hydrogen ion and of varying temperature upon the equilibrium between benzaldehyde and bisulfite ion, *J. Am. Chem. Soc.* **54**, 3555–3558.

Waldman, J. M., Munger, J. W., Jacob, D. J., Flagan, R. C., Morgan, J. J., and Hoffmann, M. R., 1982, Chemical composition of acid fog., *Science* **218**, 677–680.

Zafiriou, O. C., Alford, J., Herrera, M., Peltzer, E. T., and Gagosian, R. B., 1980, Formaldehyde in remote marine air and rain: Flux measurements and estimates, *Geophys. Res. Lett.* **5**, 341–344.

Reprint Series
17 January 1986, Volume 231, pp. 247–249

SCIENCE

Identification of Hydroxymethanesulfonate in Fog Water

J. WILLIAM MUNGER, CHRISTINE TILLER, MICHAEL R. HOFFMANN*

Identification of Hydroxymethanesulfonate in Fog Water

J. William Munger, Christine Tiller, Michael R. Hoffmann*

Previous studies have suggested that hydroxymethanesulfonate ion (HMSA) can be an important species in fog and cloud water. Formation of HMSA explains observed excesses of sulfur in the S(IV) state (+4 oxidation state) and formaldehyde (CH_2O) in fogs and clouds. HMSA was determined in fog water by a novel ion-pairing chromatographic technique. Concentrations in samples collected in Bakersfield, California, within 5 kilometers of major sources of sulfur dioxide (SO_2), were as high as 300 micromoles per liter. Total CH_2O and S(IV) concentrations, which were measured independently, ranged from 10 to 200 and 5 to more than 300 micromoles per liter, respectively. Concentrations of CH_2O, S(IV), and HMSA at Buttonwillow, California, which is 15 kilometers from the nearest source of SO_2, were less than those at Bakersfield but not absent. These data confirm that HMSA forms in atmospheric water droplets and can reach appreciable concentrations. HMSA represents an important source of acidity for water droplets and may also play a role in long-distance transport and transformation of SO_2.

Hydroxymethanesulfonate, the HSO_3^- adduct of CH_2O, has been postulated as an important S(IV) species in fog and cloud water (*1*). We define $SO_{2(aq)}$ as the sum of $SO_2 \cdot H_2O + HSO_3^- + SO_3^{2-}$; we define S(IV) as the sum of $SO_{2(aq)}$ plus all other species with sulfur in the +4 oxidation state (that is, aldehyde adducts, $HORHSO_3^-$, and metal complexes, $(Me)_n(SO_3)_m^{ny-2m}$). This sum is identical to the measured concentration of S(IV), [S(IV)]. The formation of hydroxymethanesulfonate (HMSA) allows an apparent excess of S(IV) and CH_2O compared to the amounts present in Henry's law equilibrium to exist in the droplet phase. Because HMSA is a strong acid, its formation will acidify droplets without S(IV) oxidation. Furthermore, the formation of HMSA allows S(IV) to coexist with oxidants such as H_2O_2 and O_3 (*2–4*).

The thermodynamics and kinetics of reaction between CH_2O and dissolved SO_2 to form HMSA have been determined. Kerp (*5*), Donally (*6*), Deister *et al.* (*7*), and Kok *et al.* (*4*) have all reported values near $10^7 M^{-1}$ for the equilibrium constant (defined by $K = [HMSA]/[HSO_3^-][CH_2O]$. The stability of the $CH_2O{:}HSO_3^-$ adduct will be at a maximum in the *p*H range 3 to 5, where HSO_3^- is the dominant form of $SO_{2(aq)}$. The rate at which HMSA forms in a droplet can be calculated from the rate constants determined by Boyce and Hoffmann (*8*). For CH_2O and SO_2 partial pressures of 1×10^{-9} and 5×10^{-9} atm at *p*H 3, the HMSA formation rate is 1.6 n*M* hour^{-1}. It increases by about a factor of 100 for each unit increase in *p*H to 0.1*M* hour^{-1} at *p*H 7. The formation rate increases linearly with gas-phase concentration; lower temperatures also increase the formation rate somewhat because of increased gas solubility. The rate of HMSA decomposition increases with *p*H (*4, 7*); this can be expressed as $R = k_d[HMSA][OH^-]$. The value of k_d derived from the data of Kok *et al.* (*4*) and Deister *et al.* (*7*) between *p*H 4 and 5.6 is $3.6 \times 10^3 M^{-1}$ sec^{-1}. The characteristic time for HMSA dissociation (time for a 1/*e* decrease in concentration) evaluated from this expression decreases from 579 to 25 hours as *p*H varies from 4 to 5.6. Dynamic models of fog and cloud-water chemistry (*9*) indicate that HMSA could be the major S(IV) species in droplets when *p*H exceeds 5. Appreciable [S(IV] would form in the droplet phase immediately after condensation. However, the suggestion by Richards *et al.* (*2*) that the presence of CH_2O prevents oxidation of S(IV) by H_2O_2 is not substantiated by model calculations (*9*) or experiments (*3, 4*). In an open system, SO_2 will continually dissolve in the droplet and be available as $SO_{2(aq)}$ to react with H_2O_2. High [HMSA] may be found in more acidic environments if HMSA is formed before droplet acidification. Prior formation is also indicated by the coexistence of HMSA and H_2O_2.

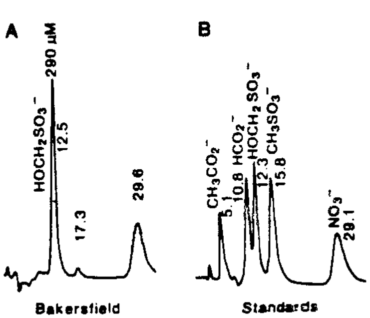

Fig. 1. Representative chromatograms for (A) a sample of fog water collected in Bakersfield, California, and (B) a solution containing formate, acetate, HMSA, methanesulfonate, and nitrate. The numbers indicate retention times in minutes. Neither methanesulfonate nor hydroxyethanesulfonate was present in the fog water samples. The peak at 17.3 minutes was present in many samples.

An interesting feature of HMSA chemistry is that the conditions most conducive to the production of HMSA are not suitable for its preservation. It forms most rapidly above *p*H 5 but will not be preserved unless the droplets are subsequently acidified. High concentrations of oxidant will compete for $SO_{2(aq)}$, but, once HMSA forms, it is fairly resistant to oxidation by H_2O_2 and O_3 (*3, 4*). We suggest that a likely environment for rapid HMSA formation is in SO_2 source plumes, where concentrations of the precursor species are high, *p*H is near neutral, and oxidant concentrations are low. As the plume is diluted, equilibrium between HMSA and its precursors may not be maintained because of the slow dissociation kinetics, especially if continued $SO_{2(aq)}$ oxidation generates additional acidity in the droplet. Equilibrium will be maintained only between gaseous SO_2 and $SO_{2(aq)}$.

The presence of HMSA in a variety of environments is indicated by circumstantial evidence. Analyses of Los Angeles fog and cloud water, which had *p*H in the range 2 to 4, indicated that total S(IV) and CH_2O were supersaturated with respect to Henry's law equilibrium with $SO_{2(g)}$ and $CH_2O_{(g)}$ (*1, 2*). Similar observations were made in the San Joaquin Valley (*1*). Warneck *et al.* (*10*) observed that $[CH_2O]$ in aerosol over Germany was supersaturated with respect to the gas phase and postulated that HMSA was present. Snider and Dawson (*11*) suggested that enhanced concentrations of carbonyls in Arizona rainwater compared to the gas phase may indicate aqueous-phase production of carbonyl. Their observations may also be accounted for by the formation of sulfonic acids. No analyses were per-

---

Environmental Engineering Science, W. M. Keck Laboratories, California Institute of Technology, Pasadena 91125.

*To whom correspondence should be addressed.

formed in these earlier studies to confirm the presence of HMSA.

The southern San Joaquin Valley of California offers an amenable environment for studying aqueous-phase atmospheric chemistry. Oil field operations supply a major source of SO_2, hydrocarbons, and NO_x, while extensive agricultural activity produces large amounts of NH_3; thus *p*H is maintained near neutral in aerosol and fog droplets. During the winter the valley is frequently capped by a temperature inversion, leading to persistent atmospheric stagnation with widespread fogs or low clouds (*12*). This combination of high concentrations of precursors, humid conditions, sufficient NH_3 to neutralize acidity, and stagnation is conducive to the formation of HMSA.

In earlier studies of fog in the San Joaquin Valley during the winters of 1982–83 and 1983–84 (*1, 12*) we have observed [S(IV)] up to $3 \times 10^{-3}M$ and $[CH_2O]$ up to $7 \times 10^{-4}M$. These values were far in excess of the Henry's law equilibrium for dissolution of SO_2 at the ambient levels of 0 to 50 parts per billion (1 ppb = 1×10^{-9} atm).

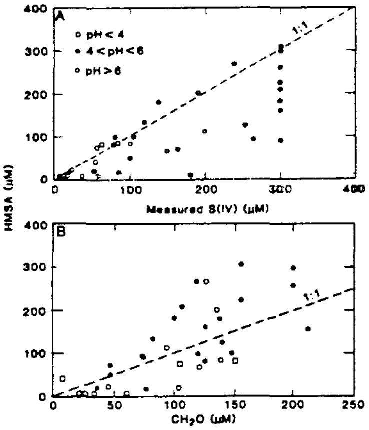

Fig. 2. (A) [HMSA] at Bakersfield plotted against measured [S(IV)]; [S(IV)] greater than 300 μM saturated the reagents used. Points plotted at 300 μM had [S(IV)] in excess of the saturation level. (B) [HMSA] at Bakersfield plotted against measured $[CH_2O]$.

During December 1984 and January 1985 we sampled fog in Bakersfield and Buttonwillow, California; the sampling sites (*13*) and fog collection procedure (*14*) have been described. Immediately after collection, the *p*H was determined with a combination electrode and individual aliquots were preserved for later determination of [S(IV)] and $[CH_2O]$ (*15, 16*). The analytical procedures are designed to measure total species. However, our results suggest that the efficiency of the Nash method for CH_2O determination is less than 100 percent when HMSA is present. HMSA was determined by ion-pairing chromatography and identified by retention time (*17*). Standards containing hydroxyethanesulfonic acid and methanesulfonic acid were also analyzed to determine their retention times. A representative chromatogram is given in Fig. 1. The difference between standard and sample retention times was less than 2 percent. We recognize that identification based on retention time is not definitive; however, other species such as formate and acetate, likely to be present in fog water, elute separately. The instability of HMSA and the difficulty of obtaining large sample volumes preclude the use of mass spectrometry for confirmation. In samples with high *p*H, some of the HMSA could have decomposed between sampling and analysis; the results presented here should be considered lower bounds for [HMSA].

Table 1. Volume-weighted average of concentrations for various species in fog water samples.

Date*	Sample *p*H	Concentration of species (μM)			*n*†
		S(IV)	CH_2O	HMSA	
		Bakersfield, California			
12/28/84	5.9	150	98	140	6
1/3/85	5.2	130	78	76	10
1/4/85	6.9	18	32	0	5
1/5/85	4.6	≥230	110	120	13
1/8/85	7.4	16	27	0	1
1/10/85	6.1	180	‡		2
1/14/85	5.9	150	120	65	3
1/19/85	4.1	89	150	79	10
1/20/85	3.0	84	160		2
		Buttonwillow, California			
1/3/85	5.1	36	55		6
1/4/85	6.2	9	28		7
1/5/85	6.1	22	33	0	11

*The date given is that of the morning on which the fog event ended. †Number of consecutive samples collected over the course of each fog event. The sampling period was generally 1 hour. ‡Not analyzed because of insufficient sample volume.

Table 1 presents the volume-weighted mean and ranges of [S(IV)], $[CH_2O]$, and [HMSA] and *p*H for each fog event sampled. Figure 2A shows the apparently linear relation between HMSA and S(IV) at Bakersfield ($r^2 = 0.65$). The residual variance is due to the presence of free $SO_{2(aq)}$ in high *p*H samples and possibly some HMSA decomposition before analysis. The highest [HMSA] was found in samples with moderate *p*H (5.5 to 6.5). Samples with higher or lower *p*H had lower [HMSA]. Low *p*H will retard the formation of adduct, while high *p*H will prevent its preservation in the atmosphere and in sample bottles.

There is also an apparently linear relation between [HMSA] and $[CH_2O]$ ($r^2 = 0.54$) (Fig. 2B). The appearance of excess HMSA as compared to total CH_2O in many samples indicates that I_2, added in order to prevent the interference of S(IV) in CH_2O analysis, is not totally effective. Appreciable concentrations of free CH_2O should exist in the droplet because of the high effective Henry's law constant.

During the sampling program, $[SO_2]$ was always less than 30 ppb and usually less than 10 ppb (*18*). This partial pressure of SO_2 was sufficient to account for all the S(IV) observed during most of the sampling periods when fog water *p*H values varied from 5 to 7. Nevertheless, HMSA was an important fraction of the S(IV) measured. In the two fog events that were in the low *p*H domain, the equilibrium of $SO_{2(aq)}$ with ambient $SO_{2(g)}$ was not sufficient to account for all the measured S(IV). During an 8-hour period in the middle of the fog event on 5 January 1985, when the *p*H varied from 5.5 to 4.8, the measured [S(IV)] was continually above the upper detection limit (250 μM). The concentration of free $SO_{2(aq)}$, as calculated from the sample *p*H and SO_2 partial pressure = 10 ppb (an upper limit for the period), was less than half the measured [S(IV)]. In terms of the Henry's law dissolution, S(IV) was supersaturated by a factor of 10 during the fog event of 19 January. The *p*H during this event was 3.7 to 4.9; [HMSA] and [S(IV)] were about 60 to 80 μM, with higher values at the beginning and end of the fog event when the liquid water content was lower. $[CH_2O]$ during this event was generally higher than [HMSA], suggesting the presence of free CH_2O.

At Buttonwillow, [S(IV)] and $[CH_2O]$ were considerably less than at Bakersfield. This is consistent with the greater distance between major pollution sources and Buttonwillow as compared to Bakersfield; $[SO_4^{2-}]$ and $[NO_3^-]$ were lower at Buttonwillow as well (*13*). The *p*H was usually in the range 5.5 to 7, although two samples had *p*H <5 with [S(IV)] less than 10 μM. HMSA was not determined in all the samples from Buttonwillow, but little or none was observed in the samples that were analyzed. As noted above, the lifetime of HMSA at *p*H 5.6 is 25 hours and should decrease further as *p*H rises. Thus HMSA may decompose during advection from SO_2 source areas to Buttonwillow. More HMSA and S(IV) is observed at Bakersfield because of its proximity to the oil fields in Oildale. If the atmosphere in the valley were not buffered by NH_3 emissions, then HMSA would have a longer residence time.

The results of this study support the hypothesis that HMSA may be an important species in fog and cloud water. The pattern of [HMSA] in the fog samples is consistent with the formation of HMSA during favorable conditions of high SO_2 and intermediate *p*H and preservation by subsequent acidification. Over the *p*H range of 5.5 to 7, which is typical of the samples from the San Joaquin Valley, the chemical lifetime of HMSA is shorter than the time for atmospheric transport within the valley (*19*). Appreciable [HMSA] or [S(IV)] was not observed at Buttonwillow. Observations of excess [S(IV)] and [CH_2O] in fog and cloud water from the more acidic Los Angeles basin indicate that other conditions may also allow the formation of HMSA.

REFERENCES AND NOTES

1. J. W. Munger, D. J. Jacob, M. R. Hoffmann, *J. Atmos. Chem.* 1, 335 (1984); J. W. Munger, D. J. Jacob, J. M. Waldman, M. R. Hoffmann, *J. Geophys. Res.* 88, 5109 (1983).
2. L. W. Richards *et al.*, *Atmos. Environ.* 17, 911 (1983).
3. J. A. McArdle and M. R. Hoffmann, *J. Phys. Chem.* 87, 5425 (1983); J. Hoigne, H. Bader, W. R. Haag, J. Staehelin, *Water Res.* 19, 993 (1985).
4. G. L. Kok, S. N. Gitlin, A. L. Lazrus, *J. Geophys. Res.*, in press.
5. W. Kerp, *Arb. Kais. Gesundh.* 421, 180 (1904).
6. L. H. Donally, *Ind. Eng. Chem. Anal. Ed.* 5, 91 (1933).
7. U. Deister, R. Neeb, G. Helas, P. Warneck, *J. Phys. Chem.*, in press.
8. The initial formation of HMSA can be expressed in terms of gas-phase concentrations as

$$\frac{d[\mathrm{HMSA}]}{dt} = H_s H_f P_{SO_2} P_{CH_2O} \frac{1}{(1 + K_h)} \times \left(\frac{k_1 K_{a1}}{[H^+]} + \frac{k_2 K_{a1} K_{a2}}{[H^+]^2}\right)$$

9. Values for the Henry's law constants for SO_2 and CH_2O at 298 K are $H_s = 1.245 M$ atm^{-1} and $H_f = 6.3 \times 10^3 M$ atm^{-1} (in terms of hydrated CH_2O). P_i is the partial pressure of species *i*. The acidity constants for S(IV) are $K_{a1} = 1.29 \times 10^{-2} M$ and $K_{a2} = 6.01 \times 10^{8} M$. The hydration constant for CH_2O is $K_h = 2.53 \times 10^3$. The original references and enthalpy data are given by Munger *et al.* (*1*). The rate constants are $k_1 = 7.9 \times 10^2 M^{-1}$ sec^{-1} (activation energy = 5.9 kcal mol^{-1}); $k_2 = 2.48 \times 10^7 M$ sec^{-1} (activation energy = 4.8 kcal mol^{-1}) [S. D. Boyce and M. R. Hoffmann, *J. Phys. Chem.* 88, 4740 (1984)].
9. D. J. Jacob and M. R. Hoffmann, *J. Geophys. Res.* 88, 6611 (1983); Y. G. Adewuyi, S-Y. Cho, R-P. Tsay, G. R. Carmichael, *Atmos. Environ.* 18, 2413 (1984).
10. P. Warneck, W. Klippel, G. K. Moortgat, *Ber. Bunsenges. Phys. Chem.* 82, 1136 (1978); W. Klippel and P. Warneck, *Atmos. Environ.* 14, 809 (1980).
11. J. R. Snider and G. A. Dawson, *J. Geophys. Res.* 90, 3797 (1985).
12. D. J. Jacob, J. M. Waldman, J. W. Munger, M. R. Hoffmann, *Tellus* 36B, 272 (1984); D. J. Jacob, thesis, California Institute of Technology, Pasadena (1985).
13. During December 1984 and January 1985 fog water was collected at a site adjacent to the Bakersfield Airport and in Buttonwillow. Sampling commenced at the onset of fog formation and continued until the fog dissipated. Major oil fields are located within 5 km of the Bakersfield Airport in the northeast quadrant. Buttonwillow is located near the center of the valley, at least 15 km southeast of oil fields on the west side of the valley. Complete results and site descriptions are given by J. M. Waldman [thesis, California Institute of Technology, Pasadena (1985)].
14. The collector is described in D. J. Jacob, R.-F. T. Wang, R. C. Flagan, *Environ. Sci. Technol.* 18, 827 (1984).
15. Total S(IV) was determined in an aliquot of sample that was preserved with CH_2O immediately after collection. Analysis was by the pararosaniline method [P. K. Dasgupta, K. DeCesare, J. C. Ullrey, *Anal. Chem.* 52, 1912 (1980); P. K. Dasgupta, *ibid.* 53, 2084 (1981)]. Standards made from Na_2SO_3 or $NaCH_2OHSO_3$ gave identical results. Analysis was complete within a week of collection; no loss of S(IV) was observed in preserved aliquots or standard solutions. Analytical error was within 5 percent.
16. Total CH_2O was determined in a separate aliquot of sample to which Nash reagent was added immediately after collection [T. Nash, *Biochem J.* 55, 416 (1953)]. Prior to color determination, I_2 was added to destroy the S(IV) in the sample [R. V. Smith and P. W. Erhardt, *Anal. Chem.* 47, 2462 (1975)]. Recovery of $NaCH_2OHSO_3$ standards was 90 to 100 percent compared to CH_2O standards. Minimal losses of CH_2O were observed during storage. Analytical error was less than 5 percent.
17. HMSA was determined by ion-pairing chromatography on a polystyrene divinylbenzene column (Dionex MPIC) followed by a suppressor column containing cation-exchange resin in the Ag^+ form (Dionex ISR), and a conductivity detector. The mobile phase contained 2 m*M* tetrabutylammonium chloride, 5 percent (by volume) CH_3OH, and $2 \times 10^{-5} M$ HCl. Analytical error was less than 5 percent. Samples to be analyzed for sulfonic acids were refrigerated, but no preservatives were used.
18. California Air Resources Board, unpublished data.
19. D. D. Reible, F. H. Shair, T. B. Smith, D. E. Lehrman, *Atmos. Environ.*, in press.

20. Supported by the California Air Resources Board (contract A4-075-32) and a summer undergraduate research fellowship from California Institute of Technology (C.T.). We thank D. Jacob, J. Waldman, D. Bucholz, and S. Hawes for their contributions to this work.

30 September 1985; accepted 30 October 1985

CHAPTER 5

Carboxylic Acids and Carbonyl Compounds in Southern California Clouds and Fogs

by

J. William Munger, Jeff Collett, Jr.,
Bruce C. Daube, Jr., and Michael R. Hoffmann

Environmental Engineering Science
W. M. Keck Laboratories, 138–78
California Institute of Technology
Pasadena, CA 91125, U.S.A.

Accepted for publication in *Tellus*

Tellus (1988), 00B, 000–000

Carboxylic acids and carbonyl compounds in southern California clouds and fogs

By J. WILLIAM MUNGER, JEFF COLLETT, Jr., BRUCE C. DAUBE, Jr. and MICHAEL R. HOFFMANN, *Environmental Engineering Science, W. M. Keck Laboratories, 138-78, California Institute of Technology, Pasadena, CA 91125, USA*

(Manuscript received 16 November 1987; in final form 1 July 1988)

ABSTRACT

Formaldehyde, formate, and acetate have been determined in fog and cloudwater from several areas of southern California. Up to 190 μM formate and acetate was seen in high pH fog samples from the San Joaquin Valley. Formaldehyde concentrations as high as 500 μM were observed there. Organic acid concentrations were much lower at an acidic site along the margin of the valley. Fog from Riverside, CA had maximum concentrations of 1500 and 500 μM formate and acetate. The highest concentrations were observed in the samples with highest pH. Formaldehyde at Riverside was as high as 380 μM. Average formate and acetate concentrations in intercepted stratus clouds from the Santa Barbara Channel coast and San Pedro Hill were 20–60 μM and 10–30 μM, respectively. Formaldehyde concentrations in stratus clouds were 10–20 μM. Because the lifetime of a cloud or fog droplet is usually much longer than the characteristic time for interfacial mass transport, hydration or dissociation, droplets can be assumed to be in equilibrium with their surroundings. The product of aqueous-phase concentration and liquid water content in the cloud (fog) is nearly always much less than the predicted equilibrium partial pressure. Only the high pH fogs from the San Joaquin Valley have the potential to deplete the gas-phase reservoir of organic acid.

1. Introduction

Soluble organic carbon is an important component of the atmosphere. Liljestrand and Morgan (1981) observed that organic carbon was the dominant component by mass of rainwater collected in Los Angeles, while Likens et al. (1983) established that carbonyl compounds and carboxylic acids contribute a major portion of the dissolved organic carbon in rainwater. Carboxylic acids can be the dominant source of free acidity in rainwater, particularly in remote regions where strong mineral acids are scarce (Galloway et al., 1982; Keene et al., 1983). At high pH the salts of carboxylic acids (e.g., $NH_4^+COO^-$) become a component of atmospheric alkalinity (Jacob et al., 1986). Carbonyls play a well known role in gas-phase photochemistry (Finlayson-Pitts and Pitts, 1986; Seinfeld, 1986). In the aqueous phase, formation of gem diols reduces their susceptibility to photolysis. However, model calculations indicate that the following reaction may be important (Chameides, 1984).

$$CH_2(OH)_2 + OH\cdot \xrightarrow{O_2} HCOOH + HO_2\cdot + H_2O.$$

The fate of HCOOH formed via this reaction is pH dependent (Jacob, 1986). At $pH > pK_a$, $HCOO^-$ is rapidly oxidized by OH·, while in acidic droplets HCOOH may be released to the surrounding atmosphere. In addition the formation of carbonyl-S(IV) adducts (hydroxyalkylsulfonates) may enhance S(IV) scavenging in droplets (Munger et al., 1984, 1986).

The equilibria that control partitioning of carbonyls and carboxylic acids between droplets and the surrounding air are shown in Table 1. Equilibrium constants have been measured for many environmentally important species; some important constants, however, have not been

Table 1. *Generalized equilibrium reactions*

Henry's Law	
aldehyde	$RCHO_{(g)} \overset{H_a}{\rightleftharpoons} RCHO_{(aq)}$
Henry's Law	
organic acid	$HA_{(g)} \overset{H_A}{\rightleftharpoons} HA_{(aq)}$
dissociation	$HA_{(aq)} \overset{K_a}{\rightleftharpoons} H^+ + A^-$
hydration	$RCHO_{(aq)} \overset{K_H}{\rightleftharpoons} RCH(OH)_2$
sulfonate formation	$RCHO_{(aq)} \overset{K_s}{\rightleftharpoons} RCH(OH)SO_3^-$

determined. In these cases, Taft correlations can be used to estimate values for carbonyl hydration constants and sulfonate stability constants (Betterton et al., 1988). Because the characteristic times for interfacial mass transfer and the equilibrium reactions in Table 1 are short compared to cloud droplet lifetimes, droplets should be in equilibrium with their surroundings (Schwartz and Freiberg, 1981). Raindrops, however, which are larger and fall through layers with different compositions may not achieve equilibrium with their surroundings.

Some general predictions may be made about the distribution of carbonyls and carboxylic acids in the presence of liquid water. Carbonyl solubility is primarily a function of the hydration constant. Formaldehyde is easily hydrated, but the longer chain carbonyls are not. Aldehydes with low hydration constants will be less important in the aqueous phase. Because electron withdrawing substituents adjacent to the carbonyl carbon enhance its hydration, dicarbonyls and halo-substituted acetaldehyde should have large hydration constants. The carbonyl group on ketoacids, such as pyruvic, should be strongly hydrated when the acid is protonated, but not when it is dissociated. Sulfonate stability is similarly enhanced by an adjacent electron withdrawing substituent, so it should follow the same trend as the hydration constants (Olson and Hoffmann, 1988).

The distribution of carboxylic acids between vapor and aqueous phase will be strongly pH dependent. At droplet pH values below the pK_a for the acid, most of it will be present in the gas phase. When the pH of the droplet is above the pK_a, the droplet will be an efficient sink for weak acids. At 25°C in a cloud with liquid water content $= 0.5$ g m^{-3}, formate and acetate are predicted to be found predominantly in the aqueous phase above $\simeq$ pH 5 and 6, respectively. The solubility of carbonyls and carboxylic acids is increased further by low temperatures.

Combustion processes are the major source of primary aldehydes (Rogozen et al., 1984). Vegetation and combustion are thought to be direct sources of carboxylic acids (Graedel et al., 1986). Acetic and formic acid have been observed in automobile exhaust and smoke from burning biomass (Kawamura et al., 1985; Talbot et al., 1988). Bacterial metabolism produces a variety of short-chain carboxylic acids; thus decomposing organic matter (e.g., soils, manure) could be sources of carboxylic acids. Atmospheric reactions, however, are thought to be the major sources of carbonyls and carboxylic acids. A wide variety of aldehydes, ketones and substituted carbonyls are formed from the oxidation of hydrocarbons. Even non-urban areas may have a strong source of carbonyls and carboxylic acids. For example, ozonolysis of isoprene, a natural hydrocarbon emitted by vegetation, is potentially a major source of HCOOH (Jacob and Wofsy, 1988). Carbonyls are sensitive to photolysis and attack by oxidants. Atmospheric residence times for aldehydes are less than a day (NRC, 1981). Carboxylic acids are generally more stable; their major sink is surface deposition.

Keene and Galloway (1986) have summarized much of the recent data on HCOOH and CH_3OOH in rainwater. However, fog and cloudwater measurements made in conjunction with gas-phase measurements are less extensive. Carlier et al. (1986) have summarized the literature on gas-phase formaldehyde. Fewer data are available on aqueous-phase formaldehyde. In this paper we present data on formaldehyde, formate and acetate concentrations in cloud and fogwater from several sites in southern California. Our objective is to establish the range of concentrations in these environments and identify differences and similarities among the various sites.

2. Methods

Samples have been collected from four regions of southern California (see Fig. 1) with a variety of meteorological and pollution characteristics.

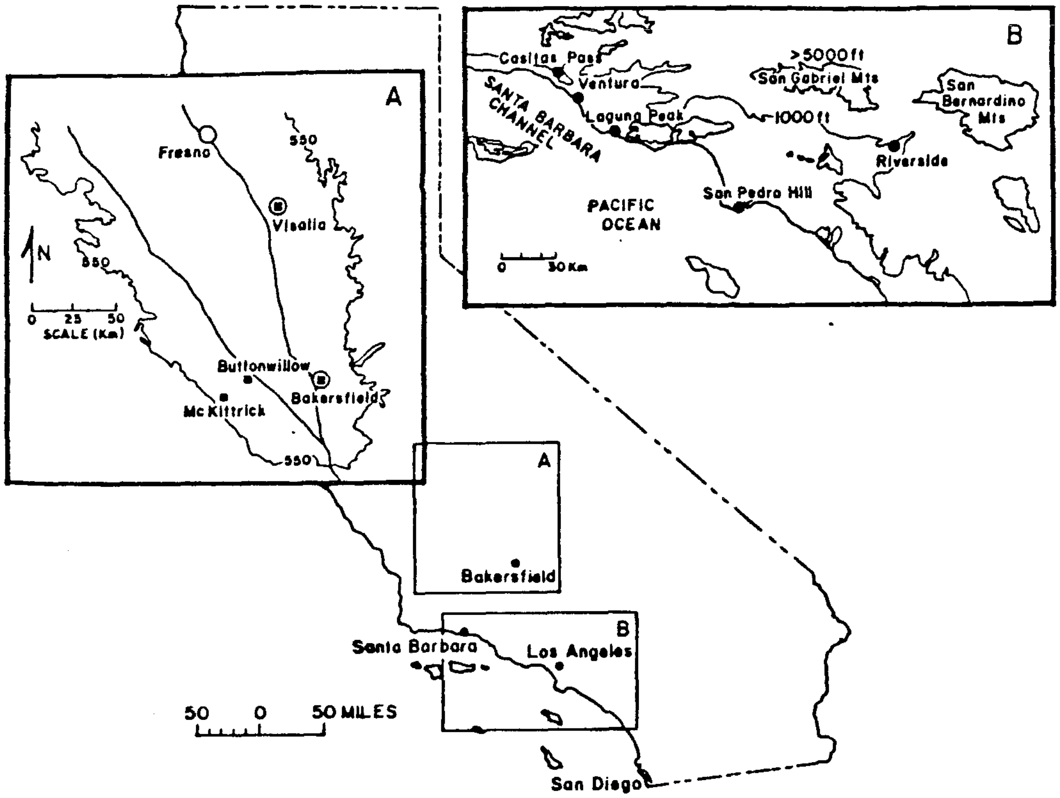

Fig. 1. Inset A shows the San Joaquin Valley outlined by the 550 m contour. The location of sampling sites (■), highways (——), and population centers (○) are indicated. Oil fields surround McKittrick and Bakersfield, livestock feedlots are centered around Visalia and Bakersfield. Inset B shows the Los Angeles Basin and Santa Barbara Channel area with sampling sites denoted by ●.

The San Joaquin Valley (inset A of Fig. 1) is subject to persistent stagnation episodes, lasting several days at a time. These are accompanied by fog or low stratus, during the early winter months. Emissions from urban centers, oil field steam generators, animal feedlots, and agricultural burning accumulate in the stagnant air mass. Crop residues are commonly burned in the San Joaquin Valley. Although air pollution control regulations prohibit burning when the valley is not well ventilated, emissions from these fires could persist in the valley and contribute to the organic species observed in the fog. Fogwater samples were collected at four locations during the period December 1983–January 1984. Bakersfield is a major population center adjacent to the oilfields on the east side of the valley. Visalia is a small city in a predominantly agricultural area. Buttonwillow is a small town surrounded by cropland. McKittrick is located on the west slope of the valley and is surrounded by oilfields; because of its high elevation it is impacted by stratus clouds that do not affect the valley floor. Details of the sampling conditions and the inorganic ion analyses are presented elsewhere (Jacob et al., 1986). Fogwater pH values in the San Joaquin Valley range from near 3 to above 6, depending on the local balance between acids and NH_3 (Jacob et al., 1986). Photochemical activity is reduced because of the cloud cover and low sun angle.

At Riverside, California (inset B of Fig. 1) radiation fogs form during the winter months. Samples were collected there during the winter of

1986. Persistent temperature inversions over the Los Angeles basin trap emissions near the ground. Prevailing winds that blow from the coast are funneled through the Riverside area during the day; nocturnal land breezes recycle the air mass back toward the coast. Very high pollutant levels are observed under these conditions. In addition to urban emissions from urban Los Angeles and Orange County, the Riverside area is affected by numerous dairy feedlots located in Chino, a few km to the west. These feedlots are a major source of NH_3 in the Los Angeles basin (Russell and Cass, 1986) and could also emit some organic compounds. Details of the sampling conditions at Riverside and complete results are given elsewhere (Munger, 1989).

Stratus clouds are frequent occurrence along the California coast. Temperature inversions associated with subsidence in the Pacific High cap the mixed layer. As noted above, sea/land breeze cycles recirculate emissions and secondary pollutants (Cass and Shair, 1984). Local emission sources include numerous offshore oil platforms and the population centers along the coastal plain. Transport of emissions from Los Angeles to the Santa Barbara Channel has been observed (Shair et al., 1982). In addition, extensive areas are covered with chaparral and forest outside the immediate urban areas; these are potential sources for natural hydrocarbons. Three sites along the Santa Barbara Channel coast were sampled in July and August of 1986 (see Fig. 1). Samples were collected from two elevations on Laguna Peak, which is at the southeastern end of the channel. The upper site is identified as Laguna Peak; the lower site is identified as Laguna Road. The Ventura site was located on a hill overlooking the city, while the third site, Casitas Pass, was located at the head of a valley. A complete description of the sampling conditions and the inorganic composition of the samples is given elsewhere (Munger, 1989).

Intercepted stratus clouds were sampled from San Pedro Hill overlooking Los Angeles Harbor (see inset B of Fig. 1) during June and July 1987. This site is affected at time by nearby refineries, as well as by the overall mix of emissions from throughout the Los Angeles basin. A complete description of the sampling conditions and the inorganic composition of the samples is given elsewhere (Munger, 1989).

The San Joaquin Valley samples were collected with a *R*otating *A*rm *C*ollector (Jacob et al., 1984). The remainder of the samples were collected with a *C*altech *A*ctive *S*trand *C*ollector (Daube et al., 1987). Although the CASC does not isolate the collected droplets from the air stream as quickly as the RAC, it collects the entire droplet size spectrum effectively, generates larger sample volumes, and its operation is automated (Daube et al., 1987). Side-by-side comparison of the two collectors does not indicate any bias in CH_2O concentrations (Collett, unpublished data). If, as we will attempt to show, dissolved carboxylic acids and carbonyls in clouds and fog are in equilibrium with the gas phase, then their concentrations will not depend on droplet size unless the pH or S(IV) concentrations of the droplets is size dependent.

In order to assess the droplet-size dependence of fog and cloud chemical composition a size-fractionating inlet was constructed for the CASC. A series of teflon rods at the mouth of the inlet collect the larger droplets. The 50% size cut for the rods is $\simeq 16$ μm diameter. The remaining droplets penetrate to the strands and are collected there. A series of cloudwater samples were collected at San Pedro Hill using this inlet on the morning of 15 July 1987.

No gas-phase concentrations with which to compare the aqueous-phase concentrations are available because the method used in our field program (NaOH impregnated filters) has been shown to produce an artifact (Keene, personal communication).

Formaldehyde in fog and cloud samples was determined by the Nash method (Nash, 1953; Reitz, 1980). The reagent mixture was added to the sample in the field to stabilize the CH_2O as 3,5-diacetyl-1,4-dihydrolutidine (DDL). Iodine was used in most cases to eliminate S(IV), which complexes with CH_2O (Smith and Erhrdt, 1975). In order to assess the efficacy of the Nash method at determining S(IV)-bound formaldehyde standards were prepared with $NaCH_2OHSO_3$ as well as 37% CH_2O solution. Recovery of CH_2O from the sulfonate standards was 90–100% compared to the CH_2O standard. The San Pedro Hill samples were analyzed according to Dong and Dasgupta's (1987) modification of the Nash method for use with an autoanalyzer. This procedure employs addition of

S(IV) to aliquots of sample shortly after collection to stabilize CH_2O as the sulfonate salt (Boyce and Hoffmann, 1984). Immediately before analysis, the samples were treated with strong base and H_2O_2 to release CH_2O.

Chloroform was added to aliquots of sample shortly after collection to retard decomposition of the carboxylic acids (Keene and Galloway, 1984). Samples were analyzed by Ion Exclusion Chromatography on a Dionex 2020i Ion Chromatograph. The San Joaquin Valley samples were analyzed with a Dionex ICE anion separator column and Ag^+ resin packed-bed suppressor. Subsequent samples were analyzed using the Dionex HPICE AS1 column preceded by an MPIC (uncharged resin) guard column. The guard column was installed to protect the separator column from nonpolar material in the samples. The eluents used in all cases were HCl at 1–5 mM concentration. A Dionex ICE AMMS suppressor was tested, but high baselines and a limited lifetime made it impractical for these analyses. Parallel analysis by normal ion chromatography using 2 mM $Na_2B_4O_7$ as eluent gave equivalent results for HCOOH concentrations, but acetate coeluted under these conditions with propionate and lactate and perhaps other acids. In addition to formate and acetate, which are reported here, several other acids were frequently observed in the chromatograms. These peaks have been tentatively identified as lactate or glyoxylate and pyruvate.

3. Results and discussion

The concentration range and mean value for each sampling site are given for formate, acetate, and formaldehyde in Tables 2–4. The vapor equivalent is the product of the aqueous-phase concentration and the liquid water content of the cloud (fog), which is estimated from the collection rate. Equilibrium partial pressures were calculated from the measured concentration and pH using Henry's Law and dissociation constants adjusted to a typical temperature for the sample group.

Among the San Joaquin Valley sites McKittrick consistently had the lowest carboxylic acid concentrations (see Fig. 2). Concentrations at Bakersfield were quite variable; the most highly concentrated samples there had large excesses of acetate relative to formate. At Buttonwillow both the formate concentrations and formate/acetate ratio were fairly high. Visalia, on the other hand had an excess of acetate. Higher levels of CH_3COO^- may indicate

Table 2. *Formate concentrations*

	Measured aqueous phase (μM)			
Site	N	Min	Max	Avg
Bakersfield	6	40	169	77
McKittrick	26	0	56	21
Visalia	11	40	187	71
Buttonwillow	2	133	157	145
Riverside	11	106	1517	627
Casitas Pass	25	16	58	27
Ventura	16	31	96	60
Laguna Peak	16	24	103	42
Laguna Road	18	21	74	39
San Pedro Hill	21	12	43	20

	Vapor equivalent (ppb)*			
Site	N	Min	Max	Avg
Bakersfield	6	0.081	0.234	0.133
McKittrick	26	0.000	0.164	0.071
Visalia	11	0.036	0.348	0.112
Buttonwillow	2	0.209	0.442	0.326
Riverside	11	0.224	2.486	0.885
Casitas Pass	25	0.032	0.145	0.081
Ventura	16	0.078	0.203	0.126
Laguna Peak	16	0.075	0.337	0.193
Laguna Road	18	0.048	0.130	0.087
San Pedro Hill	19	0.005	0.152	0.076

	Equilibrium partial pressure (ppb)			
Site	N	Min	Max	Avg
Bakersfield	6	0.001	0.75	0.16
McKittrick	26	0	1.4	0.41
Visalia	11	0.001	0.11	0.013
Buttonwillow	2	0.20	0.56	0.38
Riverside	11	1.55	33	9.3
Casitas Pass	25	0.64	5.8	1.5
Ventura	17	0.0	12	6.7
Laguna Peak	16	2.7	12	4.8
Laguna Road	18	2.0	9.7	4.5
San Pedro Hill	21	0.79	4.5	1.8

* Vapor equivalent = $C_{aq}LRT$, where L is the liquid water content (g m^{-3}), R is the gas constant and T is °K.

Table 3. *Formate concentrations*

	Measured aqueous phase (μM)			
Site	N	Min	Max	Avg
Bakersfield	6	0	244	83
McKittrick	25	0	28	3
Visalia	11	35	187	86
Buttonwillow	2	47	74	60
Riverside	11	56	581	245
Casitas Pass	25	4	14	10
Ventura	17	3	173	32
Laguna Peak	16	12	44	18
Laguna Road	17	7	34	15
San Pedro Hill	21	6	31	10

	Vapor equivalent (ppb)*			
Site	N	Min	Max	Avg
Bakersfield	6	0.048	0.498	0.185
McKittrick	25	0.0	0.046	0.007
Visalia	11	0.032	0.348	0.134
Buttonwillow	2	0.074	0.208	0.141
Riverside	11	0.108	1.026	0.353
Casitas Pass	25	0.010	0.057	0.031
Ventura	17	0.009	0.360	0.068
Laguna Peak	16	0.046	0.121	0.082
Laguna Road	18	0.000	0.101	0.034
San Pedro Hill	19	0.002	0.079	0.036

	Equilibrium partial pressure (ppb)			
Site	N	Min	Max	Avg
Bakersfield	6	0	0.33	0.11
McKittrick	26	0	0.44	0.05
Visalia	11	0.003	0.37	0.05
Buttonwillow	2	0.21	0.64	0.42
Riverside	11	1.6	8.5	4.0
Casitas Pass	25	0.20	0.74	0.44
Ventura	17	0.18	9.15	1.67
Laguna Peak	16	0.59	2.3	0.96
Laguna Road	17	0.38	1.8	0.76
San Pedro Hill	21	0.27	1.6	0.52

* Vapor equivalent = $C_{aq}LRT$, where L is the liquid water content (g m^{-3}), R is the gas constant and T is °K.

Table 4. *Formaldehyde concentrations*

	Measured aqueous phase (μM)			
Site	N	Min	Max	Avg
Bakersfield	16	27	498	168
McKittrick	49	6	93	26
Visalia	15	18	65	31
Buttonwillow	6	61	115	88
Riverside	16	65	384	236
Casitas Pass	30	3	13	7.8
Ventura	32	7	18	13
Laguna Peak	15	7	32	17
Laguna Road	20	11	15	13
San Pedro Hill	20	5	38	13

	Vapor equivalent (ppb)*			
Site	N	Min	Max	Avg
Bakersfield	16	0.035	1.24	0.281
McKittrick	49	0.009	0.180	0.069
Visalia	15	0.017	0.074	0.039
Buttonwillow	6	0.065	0.324	0.142
Riverside	16	0.090	0.793	0.378
Casitas Pass	29	0.007	0.046	0.025
Ventura	32	0.005	0.071	0.031
Laguna Peak	15	0.022	0.166	0.080
Laguna Road	20	0.011	0.064	0.033
San Pedro Hill	18	0.013	0.193	0.051

	Equilibrium partial pressure (ppb)			
Site	N	Min	Max	Avg
Bakersfield	16	1.6	30	10
McKittrick	49	0.36	5.6	1.6
Visalia	15	1.1	3.9	1.9
Buttonwillow	6	3.7	6.9	5.3
Riverside	16	12.8	30	18
Casitas Pass	30	0.31	1.2	0.78
Ventura	32	0.75	1.8	1.3
Laguna Peak	15	0.72	3.2	1.7
Laguna Road	20	1.1	1.5	1.3
San Pedro Hill	20	0.53	3.8	1.3

* Vapor equivalent = $C_{aq}LRT$, where L is the liquid water content (g m^{-3}), R is the gas constant and T is °K.

a greater contribution from fresh emissions, which are enriched in CH_3COOH (Talbot et al., 1988).

McKittrick had the lowest formaldehyde concentrations, followed by Visalia (see Fig. 3). Most of the samples from these two sites had <50 μM [CH_2O]. The Buttonwillow samples fell in the range 70–120 μM. The highest concentrations of formaldehyde (up to 500 μM) were in samples from Bakersfield.

Because the solubility of carbonyls and carboxylic acids is a function of temperature and

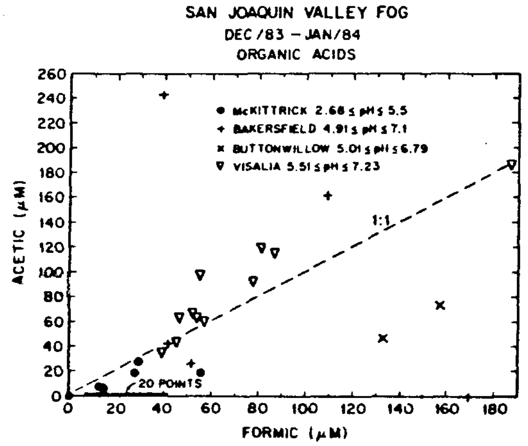

Fig. 2. Formic and acetic acid concentrations in San Joaquin Valley fog samples. The range of pH in the samples is noted in the symbol legend. Data from Jacob et al. (1986).

pH (for the acids) it may be misleading to compare aqueous-phase concentrations among samples with different pH or collected at different temperatures. We have normalized our results with respect to temperature and pH by calculating the equilibrium partial pressures. The total carboxylic acid in the aqueous phase (vapor equivalent) is comparable to or larger than the equilibrium partial pressure at Visalia, Bakersfield, and Buttonwillow. At these sites it is likely that most of the available carboxylic acid has been scavenged by the fog. Only at McKittrick, which had consistently acidic fog, was the aqueous phase concentration small compared to the calculated equilibrium. If it were at equilibrium, McKittrick would actually have had the highest total formic acid. The equilibrium concentrations of acetic acid were comparable among the sites. The observed concentration patterns were related to the proximity to sources. McKittrick and Bakersfield are adjacent to oil fields, or major urban areas. The major hydrocarbon sources, which are precursors to carboxylic acids and formaldehyde, are well to the south of Visalia. Formaldehyde and total carboxylic acid levels were low there. Bakersfield, being the largest urban area, has the highest CH_2O concentrations. The inorganic anions, NO_3^- and SO_4^{2-}, which are derived from combustion sources, were also highest at Bakersfield. The formation of the S(IV)–CH_2O adduct, hydroxymethanesulfonate, also contributes to

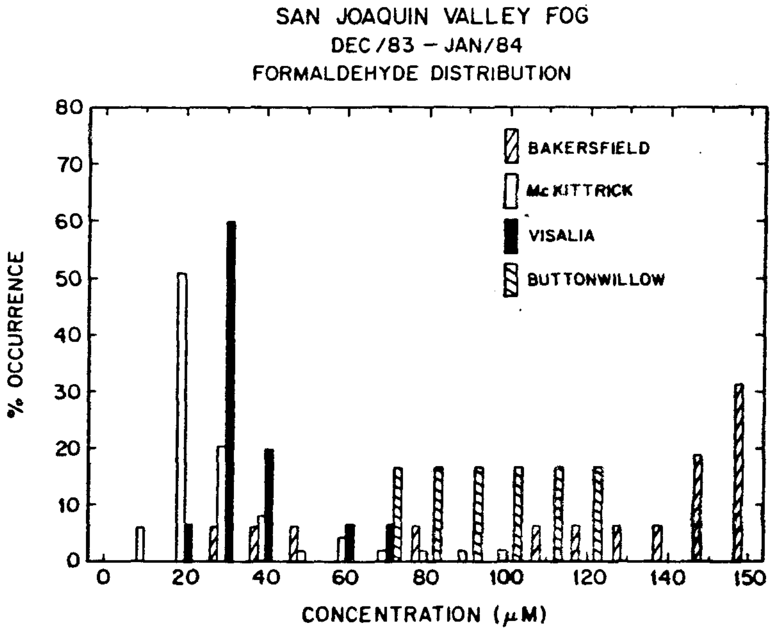

Fig. 3. Distribution of CH_2O concentrations in San Joaquin Valley fog samples. Data from Jacob et al. (1986).

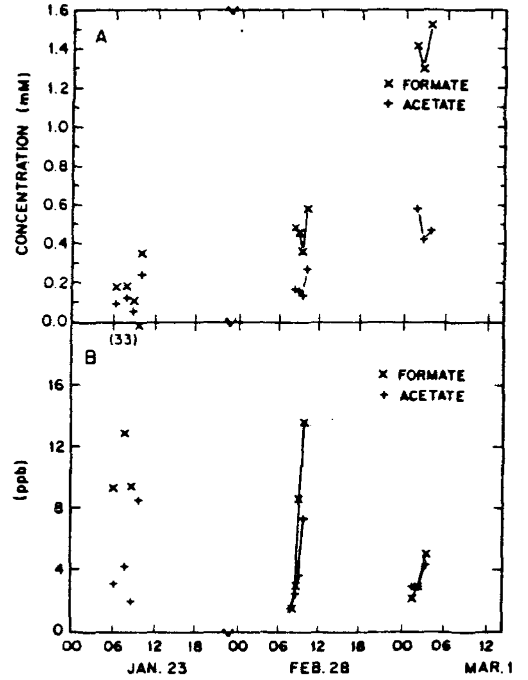

Fig. 4. Formate and acetate concentrations vs time in Riverside, CA fog samples collected during the winter of 1986. Points not connected by lines were not consecutive samples. Panel A shows the measured aqueous concentrations. Panel B shows the calculated equilibrium partial pressures at 15°C.

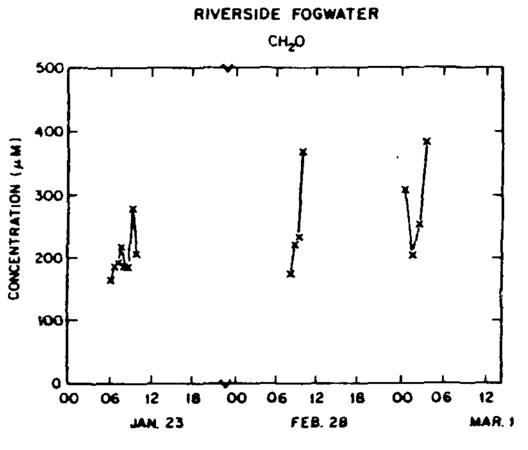

Fig. 5. Formaldehyde concentrations versus time in Riverside, CA fogwater samples collected during the winter of 1986.

high CH_2O concentrations at Bakersfield (Munger et al., 1984, 1986).

Formic and acetic acid concentrations in the Riverside fogwater samples were extremely high (see Fig. 4A). Formic acid exceeded 1000 μM during the 3 January 1986 event; acetic acid was around 500 μM. These values are a factor of 10 higher than the values reported by Kawamura and Kaplan (1984) for a single fog sample collected in Los Angeles. Formaldehyde levels (Fig. 5) ranged from 150 to near 400 μM; the variation within an event was as great as between events. Similar concentrations of CH_2O have been observed in Los Angeles coastal fogs (Munger et al., 1983). The maximum CH_2O concentration observed in Los Angeles fog and mist by Grosjean and Wright (1983) or Steinberg and Kaplan (1984) using the DNPH derivative method was 75 μM. Glyoxal and methylglyoxal were also found in the Riverside fogwater samples at concentrations comparable to the CH_2O (Munger, 1989). High concentrations of organic carbon species in the Riverside fogwater are not surprising considering its location downwind of the Los Angeles urban area, with its heavy concentration of vehicle emissions and active photochemical smog chemistry. The concentration increases at the end of the fog events coincide with morning traffic and wind reversal, which would advect fresh emissions to the site. For comparison, the range of NH_4^+, NO_3^- and SO_4^{2-} was 8.3–26 mM, 6.1–29 mM, and 1.4–6.2 mM, respectively (Munger, 1989).

The large differences in aqueous-phase carboxylic acid concentrations between the three events are due to the fogwater acidity. The range of equilibrium partial pressures of the acids for each event overlap (Fig. 4B). In all but the highest pH samples the aqueous-phase acid was much less than the potential equilibrium partial pressure. Formate always exceeded acetate in these samples, although the magnitude of the excess increased with concentration.

Figs. 6 and 7 indicate that the distributions of formate, acetate, and formaldehyde concentrations at the four Santa Barbara Channel sites have considerable overlap. Because these samples were routinely acidic the aqueous phase was a small fraction of the total acid present. Casitas Pass, which had the lowest concentrations of inorganic components, also had the lowest

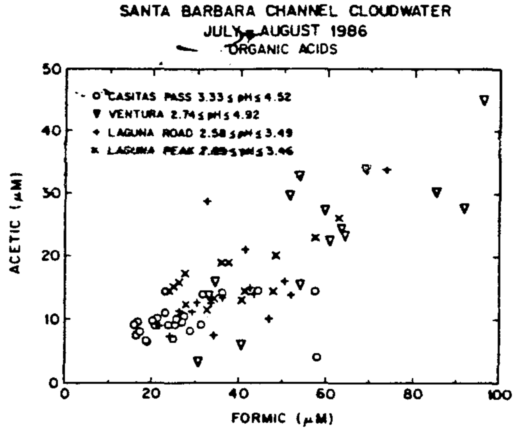

Fig. 6. Formate and acetate concentrations in intercepted stratus cloud samples from four sites along the Santa Barbara Channel coast. The range of pH in each set of samples is indicated in the symbol legend.

organic concentrations. Because of its location at the head of a valley it may be isolated from the major emission sources and is affected more by cleaner, upper level air, entrained in drainage flows from the surrounding mountains. Two features distinguished these samples form the San Joaquin Valley and Riverside samples. Formate consistently exceeded acetate and the formaldehyde concentrations were relatively low.

Fig. 8 shows an apparently linear relationship between formate and acetate at the San Pedro Hill site. The line fit through the data has a slope of about 0.5 (i.e., formate/acetate = 2). This corresponds to a $HCOOH_T/CH_3COOH_T$ ratio that is smaller than the average of 2.4 reported for marine rain samples (Keene and Galloway, 1987), but larger than the value of ≈ 1.5 reported by Talbot et al. (1988) for precipitation during the growing season at Hampton, VA. Because of the acidity in these samples, the equilibrium partial pressures were much greater than the vapor equivalent of the aqueous phase. Carboxylic acid concentrations at San Pedro Hill were generally less than at our other sites. Formaldehyde levels at San Pedro Hill (Fig. 9) were comparable to the stratus cloud samples from the Santa Barbara Channel area.

The size-fractionated samples from San Pedro Hill were collected after several hours of cloud.

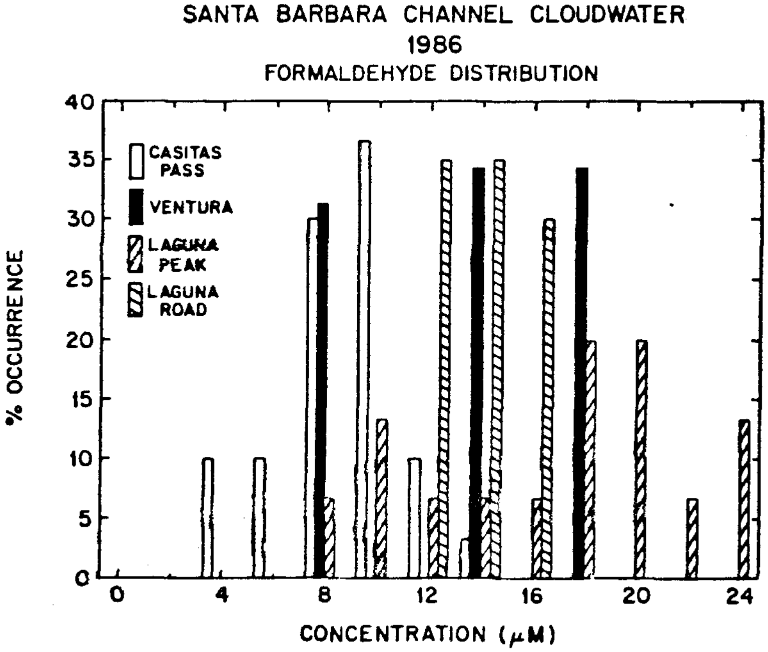

Fig. 7. Distribution of CH_2O concentrations in intercepted stratus cloud samples from four sites along the Santa Barbara Channel coast.

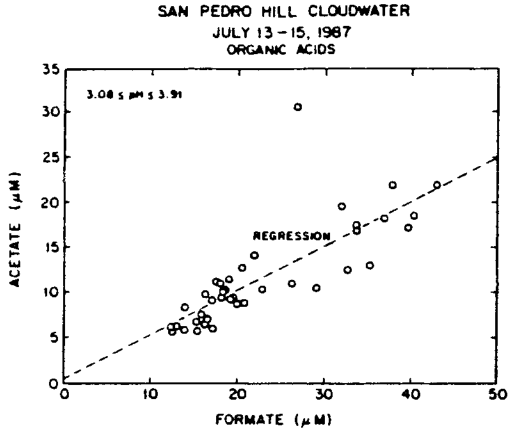

Fig. 8. Formate and acetate concentrations in samples of intercepted stratus clouds on San Pedro Hill. The range of sample pH is indicated at the upper left of the figure.

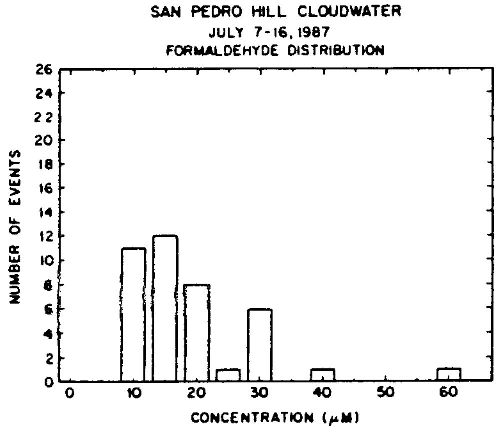

Fig. 9. Distribution of CH_2O concentrations in intercepted stratus cloud samples from San Pedro Hill.

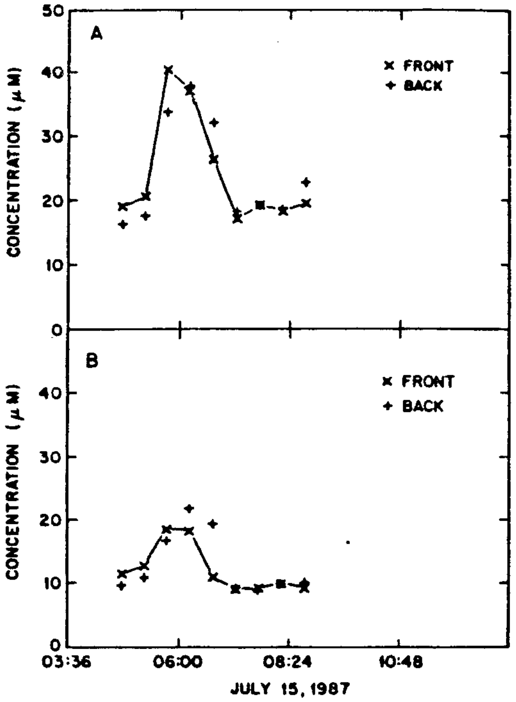

Fig. 10. Formate (A) and acetate (B) concentrations in size-fractionated cloudwater samples from San Pedro Hill. Large droplets are collected in the front fraction; small droplets are collected in the back fraction.

Cloud intercepted the hilltop around sunset the previous evening and continued throughout the night. The size-fractionated sampling began at 0400 and continued until the cloud was too thin to sample. Drizzle, falling intermittently from 0630 to 1000, contributed to the coarse fraction of the cloudwater.

Comparison of the inorganic components suggests that size-dependent differences in the composition of the precursor aerosol are retained in the droplets (Munger, 1989). The large drops had higher concentrations of soil dust and sea salt components, which would reside in the larger aerosol. The small drops had higher levels of SO_4^{2-}, NH_4^+, and H^+, which would derive from the smaller secondary aerosol. Components that exist partly in the gas phase (NO_3^- and Cl^-) did not appear to be size segregated. The difference in pH was small however. Fig. 10 shows that there is little difference in the carboxylic acid concentrations of the two cloudwater fractions, which would be expected if the cloud were in equilibrium with the surrounding air. The equilibrium partial pressures of each fraction are comparable. Over the cloudwater pH range of 3 to 3.6 most of the carboxylic acid will be in the gas phase. Even during periods of drizzle when some of the large droplets could have originated from near the top of the cloud, equilibrium appears to be maintained. The CH_2O concen-

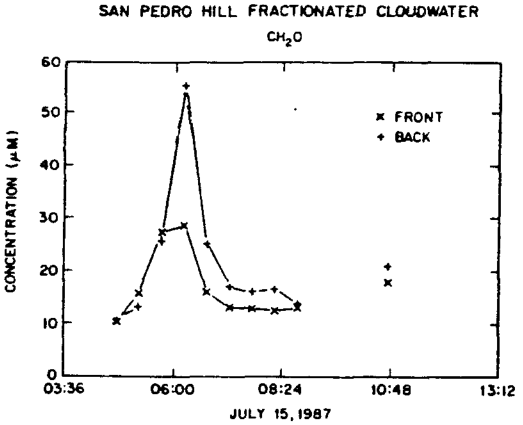

Fig. 11. Formaldehyde concentrations in the size-fractionated cloudwater samples from San Pedro Hill. Large droplets are collected in the front fraction; small droplets are collected in the back fraction.

trations (Fig. 11) in the initial fractionated samples are equivalent, which is consistent with equilibrium considerations. Beginning at 0530 there was a spike in [CH_2O], [HCOOH], and [CH_3COOH] as well as the major inorganic ions, that could not be attributed to a drop in liquid water content. The carboxylic acids appear to maintain their equilibrium; however, the small-droplet fraction has a much higher [CH_2O] during this spike. The difference decays away over the next 3 hours. The sharpness of this pulse suggests passage of a plume or a major wind shift. The CH_2O data imply that the precursor nuclei for the smaller droplets contain CH_2O that is not in equilibrium with the gas phase. The presence of the S(IV) adduct, hydroxymethanesulfonate (HMSA) (Munger et al., 1984), could account for this. At the observed pH of $\simeq 3.5$ the kinetics of HMSA dissociation would be quite slow (Boyce and Hoffmann, 1984), thus HMSA in the precursor aerosol would be retained in the droplet where it would be measured as CH_2O. Preliminary measurements of S(IV) and HMSA itself in these samples are consistent with this explanation.

Some of the cloud (fog) events exhibited a concave concentration vs time profile for the carboxylic acids. The variation over time was greatest for HCOOH; CH_3COOH changed only slightly. Formaldehyde was often constant over the same periods. In previous studies we have observed this pattern in the concentrations of inorganic ions and attributed it to dilution and concentration as liquid water content varies over the life of the cloud (fog). Carboxylic acid concentrations should be independent of liquid water content if they are in equilibrium. However, we can not determine from these data whether the concentrations are responding to liquid water or to other factors that affect both total organic concentration and liquid water content. Many of the clouds (fogs) dissipate after sunrise. Photochemical production, fresh emissions and increased mixing would all contribute to higher concentrations as the droplets were evaporating.

4. Summary and conclusions

High concentrations of carboxylic acid were observed in fogs and clouds where pH was high or near sources of precursor hydrocarbons. Riverside, where both conditions are met for some events, had the highest carboxylic acid concentrations seen in southern California. The apparent lower concentrations of carboxylic acid in stratus clouds at San Pedro Hill relative to the Santa Barbara Channel sites is surprising if urban pollution is a major source of carboxylic acids. The elevation of the sampling sites and meteorological conditions were similar for both sets of samples. A more detailed analysis of air mass histories will be required to interpret these data. Proximity to sources alone did not account for the CH_2O concentrations in fog and cloud. Bakersfield, which is adjacent to major combustion sources had high concentrations of CH_2O in fogwater, but clouds at San Pedro Hill, which is affected by Los Angeles air pollution, did not. The shallower mixed layer, weaker insolation, and higher SO_2 concentrations (which would support sulfonate formation) at Bakersfield are factors that would account for higher [CH_2O]. Furthermore, the Bakersfield samples were collected at ground level, whereas, the San Pedro sampling site was on a 450 m hill. The hilltop location and night time sampling at San Pedro Hill may account for the apparent low P_{CH_2O} compared to previous measurements of gas-phase CH_2O in Los Angeles (Grosjean, 1982). In general [HCOOH] exceeded [CH_3COOH] in these fog and cloudwater samples, which agrees with the trends noted by Keene and Galloway (1986). The San Joaquin Valley and high pH Riverside fog samples, which were the most strongly affected by feedlot emissions, were notable exceptions. If this latter observation is not due simply to coincidence, it suggests that animal wastes may be a source of CH_3COOH or that destruction of $HCOO^-$ is accelerated in high pH droplets as suggested by Jacob (1986). Alternatively, ground level fogs may be more strongly influenced by direct anthropogenic emissions, which are enriched in CH_3COOH relative to HCOOH (Talbot et al., 1988).

5. Acknowledgements

This research was supported by a contract with the California Air Resources Board contract #A4-075-32. We thank the California Air Resources Board, Avenue Cable TV of Ventura, the US Navy, the Federal Aviation Administration and Dr. R. Musselman of Univ. Calif. Riverside for the permission to use their facilities as sampling sites. This work would not have been possible without the field and laboratory assistance of C. Choy, G. Gibb, W. Chong, and A. Kaloustian.

REFERENCES

Betterton, E., Erel, Y. and Hoffmann, M. R. 1988. Aldehyde-bisulfite adducts: Prediction of some of their thermodynamic and kinetic properties. *Environ. Sci. Technol. 22*, 3011–3020.

Boyce, S. D. and Hoffmann, M. R. 1984. Kinetics and mechanism of the formation of hydroxymethanesulfonic acid at low pH. *J. Phys. Chem. 88*, 4740–4746.

Carlier, P., Hannachi, H. and Mouvier, G. 1986. The chemistry of carbonyl compounds in the atmosphere—A Review. *Atmos. Environ. 20*, 2079–2099.

Cass, G. R. and Shair, F. H. 1984. Sulfate accumulation in a sea breeze/land breeze circulation system. *J. Geophys. Res. 89*, 1429–1438.

Chameides, W. L. 1984. The photochemistry of a remote marine stratiform cloud. *J. Geophys. Res. 89*, 4739–4755.

Daube, B. C. Jr., Flagan, R. C. and Hoffmann, M. R. 1987. *Active Cloudwater Collector*. United States Patent #4,697,462, 6 October 1987.

Dong, S. and Dasgupta, P. K. 1987. Fast flourimetric flow injection analysis of formaldehyde in atmospheric water. *Environ. Sci. Technol. 21*, 581–588.

Finlayson-Pitts, B. J. and Pitts, J. N., Jr. 1986. *Atmospheric chemistry: fundamentals and experimental techniques*. New York: John Wiley, 1098.

Galloway, J. N., Likens, G. E., Keene, W. C. and Miller, J. M. 1982. The composition of precipitation in remote areas of the world. *J. Geophys. Res. 87*, 8771–8786.

Graedel, T. E., Hawkins, D. T. and Claxton, L. D. 1986. *Atmospheric chemical compounds: sources, occurrence, and bioassay*. New York: Academic Press, 732 pp.

Grosjean, D. 1982. Formaldehyde and other carbonyls in Los Angeles ambient air. *Environ. Sci. Technol. 16*, 254–262.

Grosjean, D. and Wright, B. 1983. Carbonyls in urban fog, ice fog, and cloudwater and rainwater. *Atmos. Environ. 17*, 2093–2096.

Jacob, D. J. 1986. The chemistry of OH in remote clouds and its role in the production of formic acid and peroxymonosulfate. *J. Geophys. Res. 91*, 9807–9826.

Jacob, D. J., Wang, R.-F. T. and Flagan, R. C. 1984. Fogwater collector design and characterization. *Enviorn. Sci. Technol. 18*, 827–833.

Jacob, D. J., Munger, J. W., Waldman, J. M. and Hoffmann, M. R. 1986. The H_2SO_4-HNO_3-NH_3 system at high humidities and in fogs: I. Spatial and temporal patterns in the San Joaquin Valley of California. *J. Geophys. Res. 91*, 1073–1088.

Jacob, D. J. and Wofsy, S. C. 1988. Photochemical production of carboxylic acids in a clean continental atmosphere. In: *Acid deposition processes at high elevation sites* (ed. H. M. Dunsworth). Hingham, Mass: D. Reidel (in press).

Kawamura, K., Ng, L. L. and Kaplan, I. R. 1985. Determination of organic acids (C_1–C_{10}) in the atmosphere, motor exhausts, and engine oils. *Environ. Sci. Technol. 19*, 1082–1086.

Kawamura, K. and Kaplan, I. R. 1984. Capillary gas chromatography determination of volatile organic acids in rain and fog samples. *Anal. Chem. 56*, 1616–1620.

Keene, W. C. and Galloway, J. N. 1984. Organic acidity in precipitation of North America. *Atmos. Environ. 18*, 2491–2497.

Keene, W. C. and Galloway, J. N. 1986. Considerations regarding sources for formic and acetic acids in the troposphere. *J. Geophys. Res. 91*, 14466–14474.

Keene, W. C., Galloway, J. N. and Holden, J. D. 1983. Measurement of weak organic acidity in precipitation from remote areas of the world. *J. Geophys. Res. 88*, 5122–5130.

Likens, G. E., Edgerton, E. S. and Galloway, J. N. 1983. The composition and deposition of organic carbon in precipitation. *Tellus 35*, 16–24.

Liljestrand, H. M. and Morgan, J. J. 1981. Spatial variations of acid precipitation in southern California. *Environ. Sci. Technol. 15*, 333–338.

Munger, J. W. 1989. *Chemical composition of fogs and clouds in southern California*. Ph.D. Thesis, California Institute of Technology, Pasadena, CA.

Munger, J. W., Jacob, D. J. and Hoffmann, M. R. 1984. The occurrence of bisulfite-aldehyde adducts in fog- and cloudwater. *J. Atmos. Chem. 1*, 335–350.

Munger, J. W., Tiller, C. T. and Hoffmann, M. R. 1986. Determination of hydroxymethanesulfonate in fog water. *Science 231*, 247–249.

Nash, T. 1953. The colorimetric estimation of formaldehyde by means of the Hantszch reaction. *Biochem. J. 55*, 416–421.

National Research Council, 1981. *Formaldehyde and other aldehydes*. Washington, DC: National Academy Press, 340 pp.

Olson, T. M. and Hoffmann, M. R. 1988. The formation kinetics, mechanism, and thermodynamics of glyoxylic acid-S(IV) adducts. *J. Phys. Chem. 92*, 0000–0000.

Reitz, E. B. 1980. The stabilization of small concentrations of formaldehyde in aqueous solutions. *Analyt. Lett. 13*, 1073–1084.

Rogozen, M. B., Maldonado, G., Grosjean, D., Shochet, A. and Rapoport, R. 1984. Formaldehyde: A survey of airborne concentrations and sources. Final Report to California Air Resources Board. Sacramento, CA, 311 pp.

Russell, A. G. and Cass, G. R. 1986. Verification of a mathematical model for aerosol nitrate and nitric acid formation and its use for control measure evaluation. *Atmos. Environ. 18*, 1815–1817.

Schwartz, S. E. and Freiberg, J. E. 1981. Mass-transport limitation to the rate of reaction of gases in liquid droplets: Application to oxidation of SO_2 in aqueous solutions. *Atmos. Environ. 15*, 1129–1144.

Seinfeld, J. H. 1986. *Atmospheric chemistry and physics of air pollution*. New York: John Wiley, 738 pp.

Shair, F. H., Sasaki, E. J., Carlan, D. E., Cass, G. R., Goodin, W. R., Edinger, J. G. and Schacher, G. E. 1982. Transport and dispersion of airborne pollutants associated with the land breeze–sea breeze system. *Atmos. Environ. 16*, 2043–2053.

Smith, R. V. and Erhardt, P. W. 1975. Nash determination for formaldehyde in the presence of bisulfite. *Anal. Chem. 47*, 2462–2454.

Steinberg, S. and Kaplan, I. R. 1984. The determination of low molecular weight aldehydes in rain, fog, and mist by reversed phase liquid chromatography of the 2,4-dinitrophenyl hydrazone derivatives. *Intern. J. Environ. Anal. Chem. 18*, 253–266.

Talbot, R. W., Beecher, K. M., Harriss, R. C. and Cofer, W. R., III. 1988. Atmospheric geochemistry of formic and acetic acids at a mid-latitude temperate site. *J. Geophys. Res. 93*, 1638–1652.

CHAPTER 6

Fogwater Chemistry at Riverside California

by

J. William Munger, Jeff Collett,
Bruce Daube, Jr., and Michael R. Hoffmann

Environmental Engineering Science
W. M. Keck Laboratories, 138–78
California Institute of Technology
Pasadena, CA 91125

Accepted for Publication in: *Atmospheric Environment*

March, 1988

ABSTRACT

Fog and aerosol samples were collected during the winter of 1986 at Riverside California. The dominant components of the aerosol were NH_4^+, NO_3^-, and SO_4^{2-}. Gaseous NH_3 was frequently present at levels equal to or exceeding the aerosol NH_4^+. Maximum levels were 3800, 3100, 690, and 4540 neq m^{-3} for NH_4^+, NO_3^-, SO_4^{2-}, and $NH_{3(g)}$, respectively. The fogwater collected at Riverside had very high concentrations, particularly of the major aerosol components. Maximum concentrations were 26000, 29000, and 6200 μ**N** for NH_4^+, NO_3^-, and SO_4^{2-}, respectively. pH values in fogwater ranged from 5.7 to 2.3. Formate and acetate concentrations as high as 1500 and 580 μ**M** were measured. The maximum CH_2O concentration was 380 μ**M**. Glyoxal and methylglyoxal were found in all the samples; their maximum concentrations were 280 and 120 μ**M**.

Comparison of fogwater and aerosol concentrations indicates that scavenging by fog droplets under the conditions at Riverside is less than 100% efficient.

The chemistry at Riverside is controlled by the balance between HNO_3 production from NO_x emitted throughout the Los Angeles basin and NH_3 emitted from dairy feedlots just west of Riverside. The balance is controlled by local mixing. Acid fogs result at Riverside when drainage flows from the surrounding mountains isolate the site from the NH_3 source. Continued formation of $HNO_{3(g)}$ in this air mass eventually depletes the residual $NH_{3(g)}$.

A simple box model that includes deposition, fog scavenging, and dilution is used to assess the effect of curtailing the dairy feedlot operations. The calculations suggest that in the presence of reduced NH_3 levels the total NO_3^- in the atmosphere would be less, but nearly all of it would be HNO_3. Fogwater in the basin would be uniformly acidic.

Introduction

Previous studies of fogwater chemical composition show a direct relation to ambient air quality. High aerosol and pollutant gas concentrations lead to highly concentrated fogs. Conversely, highly concentrated fog or clouds contribute to high aerosol loading. We have previously termed this relationship the "smog–fog–smog cycle" Munger et al. [1983]. In polluted locations such as Los Angeles and the southern San Joaquin Valley, nitric and sulfuric acid are the dominant anions in fog and cloud. Ammonia or hydrogen ion are the major cations. Droplet acidity depends on the balance between NH_3 emissions and NO_x and SO_2 emissions and oxidation [Jacob et al., 1986; Munger et al., 1983]. In addition to these major inorganic ions, fog and cloudwater contain important organic species derived from pollutant sources. Carbonyls such as formaldehyde, glyoxal, and methylglyoxal and organic acids such as formic and acetic acid are produced by photochemical oxidation of hydrocarbons and from direct emissions. These highly soluble species have been observed at high concentrations in fog and cloudwater [Munger et al., 1983; Steinberg and Kaplan, 1984; Kawamura et al., 1985; Jacob et al., 1986].

The combined effect of topography, meteorology, and emission distribution of the South Coast Air Basin (SCAB) leads to extreme pollutant levels in the eastern portion of the basin. Air pollution monitoring stations in and around Riverside and San Bernardino have some of the highest levels of O_3 and particulate NO_3^- and SO_4^{2-} in the SCAB [Hoggan et al., 1980]. Dairy operations around Chino (see Fig. 6.1), which are the major NH_3 source for the entire SCAB [Russell and Cass, 1986], are responsible for extreme concentrations of NH_3 gas and NH_4^+ aerosol in the the eastern basin. The predominant daytime wind advects pollutants from central and coastal Los Angeles and Orange Counties through the Santa Ana Canyon near Anaheim into the eastern basin. Temperature inversions restrict vertical mixing of pollutants. Air passing through the basin during the day is recycled at night by drainage flows from

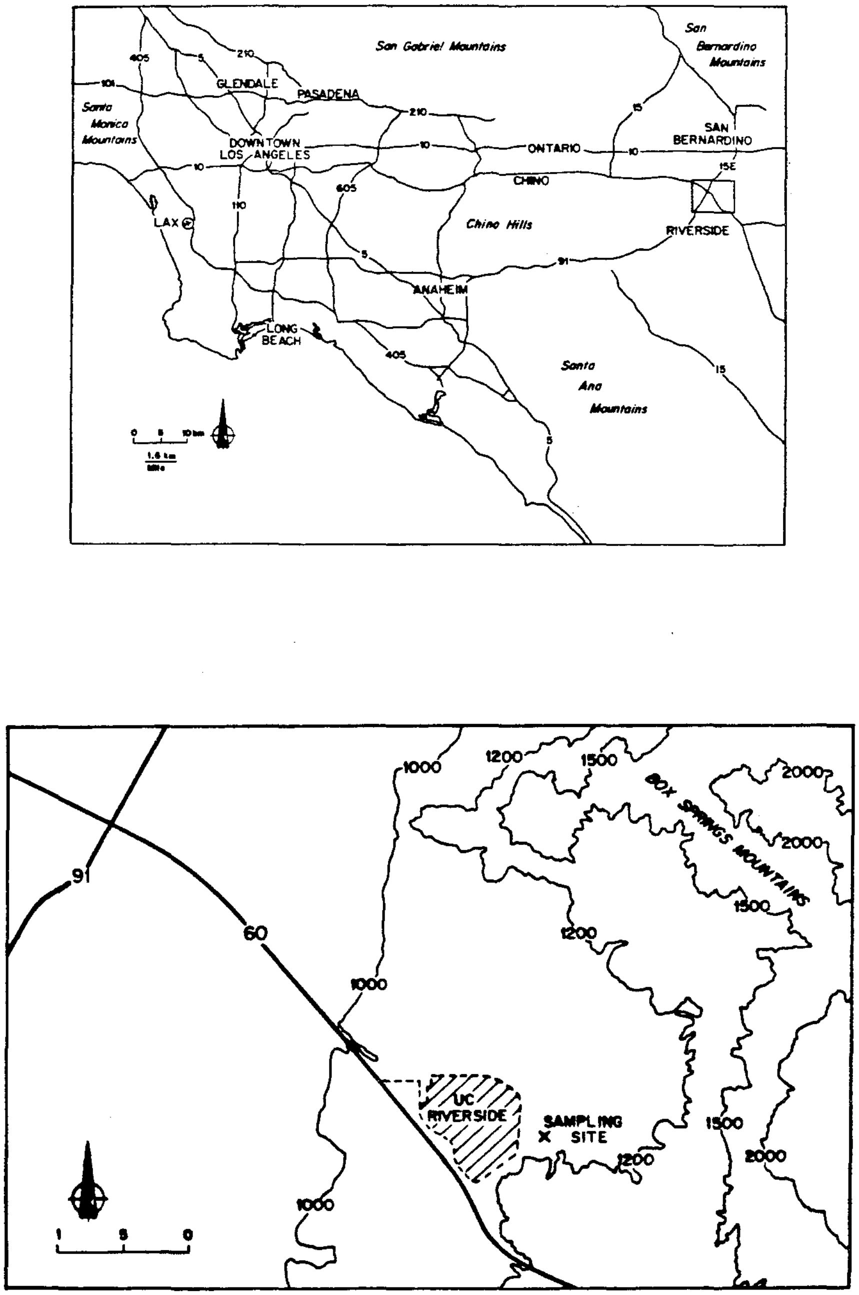

Figure 6.1. (A) Map of the South Coast Air Basin indicating the location of major freeways and the surrounding mountains. (B) Map of the Riverside sampling site and its immediate surroundings. The area of this map is outlined by the small box in panel A.

the surrounding mountains.

Fog and low clouds are frequent in the eastern SCAB. Marsh (1984) reports 60 days of fog per year in the Riverside area. The frequency of low ceilings or restricted visibility at March Air Force Base near Riverside exceeds 25% in February – June and September – October [March Air Force Base Climate summary]. Because Riverside has high pollutant levels in association with frequent fog and cloud it is an ideal location to identify smog/fog interactions. Previous results indicate a potentially wide range of pH in fog and cloud from the eastern basin [Munger et al., 1983]. A sample collected in Upland had a pH near 2.0, whereas a sample from Ontario, downwind of the feedlots in Chino, had a pH near 7. More thorough sampling is required to determine the balance between acid and base inputs and identify the interaction between fogwater and atmospheric composition. Baseline data on the chemistry of fog and clouds in the region are required to assess the impacts of future development and to identify potential health effects. Aerosol and fogwater were collected during the winter of 1985–86 to meet these objectives.

Methods

Sampling Site

Samples were collected from the roof of a one story building on the eastern edge of the University of California, Riverside campus (elevation 350 m) (see Figure 6.1 for map of the area). The site was bordered by undeveloped grass and shrub land. The Box Spring Mountains rise to nearly 1000 m to the north and east of the collection site. A major freeway passes within 600 m of the sampling site; access roads to parking lots on the campus are at least 100 m away.

Fogwater was collected using the Caltech Active Strand Collector (CASC) [Daube et al., 1987] (see Fig. 6.2). Droplets collect by inertial impaction on slanted teflon strands. Gravity and aerodynamic drag propel them into a teflon trough beneath the strands where they accumulate and drain into a collection bottle, which was emptied at 30 – 60 minute intervals. The 50% collection efficiency cutoff predicted from impaction theory is ≃ 3 µm. 24.5 m^3 of air are sampled per minute. Prior to sample collection, the strands and sample tube were rinsed thoroughly with distilled water. The first 15 minutes of sample were discarded to avoid any bias by residual rinse water.

Aerosol and selected gases were sampled using the automated filter pack illustrated in Figure 6.3. Teflon filters (Gelman Zefluor, 1µm pore size) were used to collect aerosol for inorganic analysis. HNO_3 was collected on a nylon filter (Gelman Nylasorb) placed behind a teflon filter. NH_3 was collected on two oxalic acid–impregnated glass fiber filters behind a second teflon filter. The third filter holder contained a base–impregnated quartz filter preceded by a teflon filter. Because base–impregnated filters have been shown to collect artifact organic acids [Keene et al., 1988] the results for these filters are not included here. A flow rate of 10 – 11 l s^{-1} was maintained with a critical orifice. Flow rates were checked with a calibrated rotameter. Denuder difference methods were not used in this study because liquid water collected during fog events would destroy the coating of the denuder. The interferences associated with filter pack methods [Hering et al., 1986] are minimized by the short collection times used in this study and the relative constancy of temperature and humidity during the sampling periods. Samples collected during fog contain both aerosol and fog droplets. In order to minimize loss of volatile components, wet filters were extracted immediately after collection. Sedimenting fog and rain droplets were excluded by a cover. In order to collect a sample of interstitial aerosol one of the filter cassettes was mounted at a port on the side of the CASC, downstream of the collection strands during some foggy periods. Nearly all droplets with diameter > 16 μm are excluded from this filter, however, a fraction of

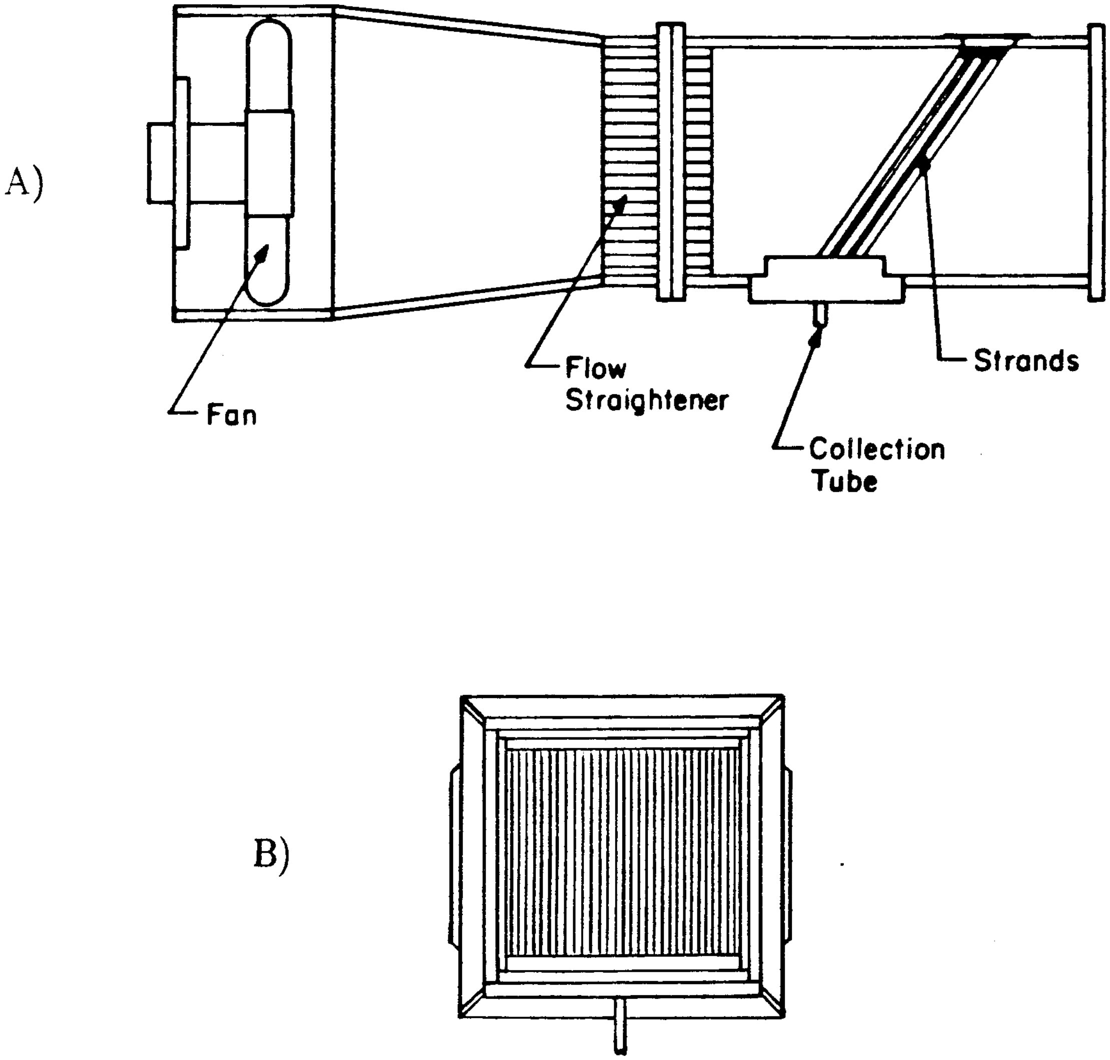

Figure 6.2 Diagram of the Caltech Active Strand Cloudwater Collector used in the Riverside sampling program. A. Side view B. Front view.

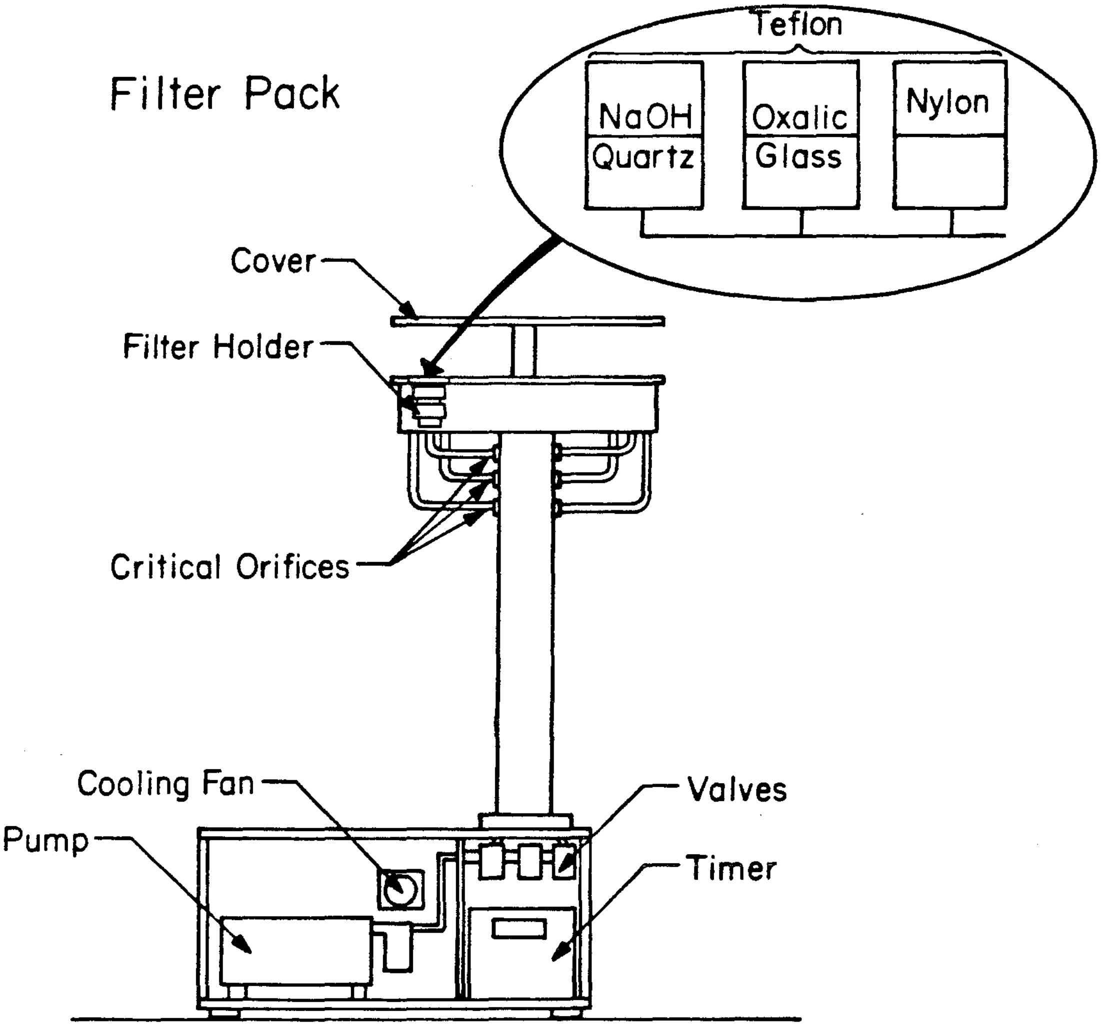

Figure 6.3. Diagram of the aerosol filter pack used in the Riverside sampling program.

the droplets $< 16\ \mu m$ will penetrate to the filter. The contribution due to small fog droplets would be greatest when the mass median diameter of the fog droplets was small, which might occur as the fog was dissipating. We estimate from Stokes Law (Friedlander, 1977) that the inlet will exclude nearly all droplets with diameters $> 16\ \mu m$. The collection efficiency for the strands upstream of the inlet (calculated from impaction theory) is 50% for 3.5 μm droplets and rises sharply to $> 80\%$ for diam. $> 10\ \mu m$. The maximum efficiency is limited by the fraction of incoming air swept by the strands. The combined action of the strands and the aerosol inlet minimizes the influence of droplets on the interstitial aerosol sample.

Analytical Procedures

At the end of each sampling interval the collected fogwater was transferred to a sample bottle and weighed. The pH of an aliquot from the sample was determined at the field site using a Radiometer pHM 80 meter with a combination electrode calibrated against pH 4 and 7 buffers. Small aliquots of sample were removed and treated to stabilize reactive species. S(IV) was stabilized as the hydroxymethanesulfonate by adding buffered CH_2O [Dasgupta et al., 1980]. CH_2O was reacted with NH_4^+–acetylacetone [Nash, 1953] to form 3,5–dihydro–1,4-dihydrolutidine (DDL), which is stable for several weeks [Reitz, 1980]. A buffered solution of p–OH phenylacetic acid (POPA) and peroxidase was used to preserve peroxides (H_2O_2 and ROOH) [Lazrus et al., 1985] by formation of the dimer. Carboxylic acids were preserved by addition of chloroform [Keene et al. 1984]. Carbonyls were derivatized with 2,4–dinitrophenylhydrazine in acidic solution [Grosjean and Wright, 1983].

The samples and preserved aliquots were stored in a refrigerator at 4° C until analysis. Major anions were determined by ion chromatography with a Dionex AS4A separator column and a micromembrane suppressor. The eluent was 2.8 mM HCO_3^-/ 2.2 mM CO_3^{2-}. The metallic cations were determined by atomic absorption spectrophotometry. An air/acetylene flame was used for Na^+ and K^+; N_2O/acetylene was used for Ca^{2+} and Mg^{2+} to minimize interferences. NH_4^+ was determined by flow injection analysis employing the indophenol blue method.

The stabilized CH_2O was determined by absorption measurement at 412 nm after addition of I_2 to accelerate the decomposition of sulfonates [Smith and Erhardt, 1975]. The results for standards prepared from hydroxymethanesulfonate (HMSA), the S(IV) adduct of CH_2O were comparable to CH_2O standards. The results from the Nash determination are therefore total CH_2O concentrations. S(IV) was analyzed by the pararosaniline method [Dasgupta, 1981], adapted for flow injection analysis. This method is also intended to give a total concentration; Na_2SO_3 and $NaCH_2OHSO_3$ fave equivalent resoponses. Peroxide was determined from the fluorescence of the POPA enzyme solution [Lazrus et al., 1985]. The method is sensitive to both H_2O_2 and some organic peroxides, however, the significantly lower Henry's law coefficients of CH_3OOH and peroxoacetic acid suggest that they will not be important in fog and cloud water [Lazrus et al., 1985]. Carboxylic acids were determined by ion exclusion chromatography (Dionex ICE–AS1) with dilute HCl as the eluent.

The dinitrophenylhydrazone derivatives of carbonyls were extracted 3 times in 60/40 hexane/dichloromethane after adding cyclohexanone 2,4–dinitrophenylhydrazone (Aldrich) as an internal standard. The organic fraction was washed with H_2O to remove excess acid and unreacted DNPH, and then evaporated to dryness under a stream of N_2. The extracted and dried hydrazones were stored in the refrigerator until analysis. Immediately before analysis the residue was dissolved in tetrahydrofuran (THF). The derivatized carbonyls were separated by HPLC on a C18 column (Alltech Spherisorb ODS–2), using 45/27.5/27.5 (v/v/v) H_2O/CH_3CN/THF as the mobile phase. Aldehydes and ketones were determined by absorbance at 365nm; each analysis was repeated at 430 nm to determine the dicarbonyls, which absorb at a higher wavelength. Stored and fresh standards gave comparable peak areas at the time of analysis, indicating that the derivatives were stable during storage. The spectra taken at the peaks of selected samples (see Figure 6.4) were compared to sample spectra to aid in identification of the compounds present. Standards were prepared from carbonyl hydrazones that were previously synthesized and purified. The DNPH determination of carbonyls is not sensitive to carbonyls bound by S(IV); only free carbonyls are measured by this method.

The α–OH alkanesulfonates were determined in selected samples by an ion–pairing chromatographic method developed by Munger et al. [1986]. Separation is accomplished on a Dionex MPIC column using tetrabutylammonium chloride/HCl in dilute aqueous CH_3OH or CH_3CN as mobile phase. Because background interferences were more pronounced in the Riverside fogwater samples than had been observed in previously sampled fogs and clouds, not all the samples were analyzed for sulfonates.

The teflon and oxalic acid filters were extracted in distilled deionized water (DDH_2O) on a shaker table. A small volume of ethanol was added to the filter prior to the water in order to more effectively wet the surface. The nylon filters were extracted in HCO_3^-/CO_3^{2-} IC eluent. Composition of the extracts was determined by the same procedures used for the fogwater samples, with the exception of additional buffer in the complexing reagent and oxalic acid in the rinse solution of the ammonia analysis to account for the effect of the oxalic acid. The precision, accuracy, and detection limits for the major analyses are given in Appendix A.

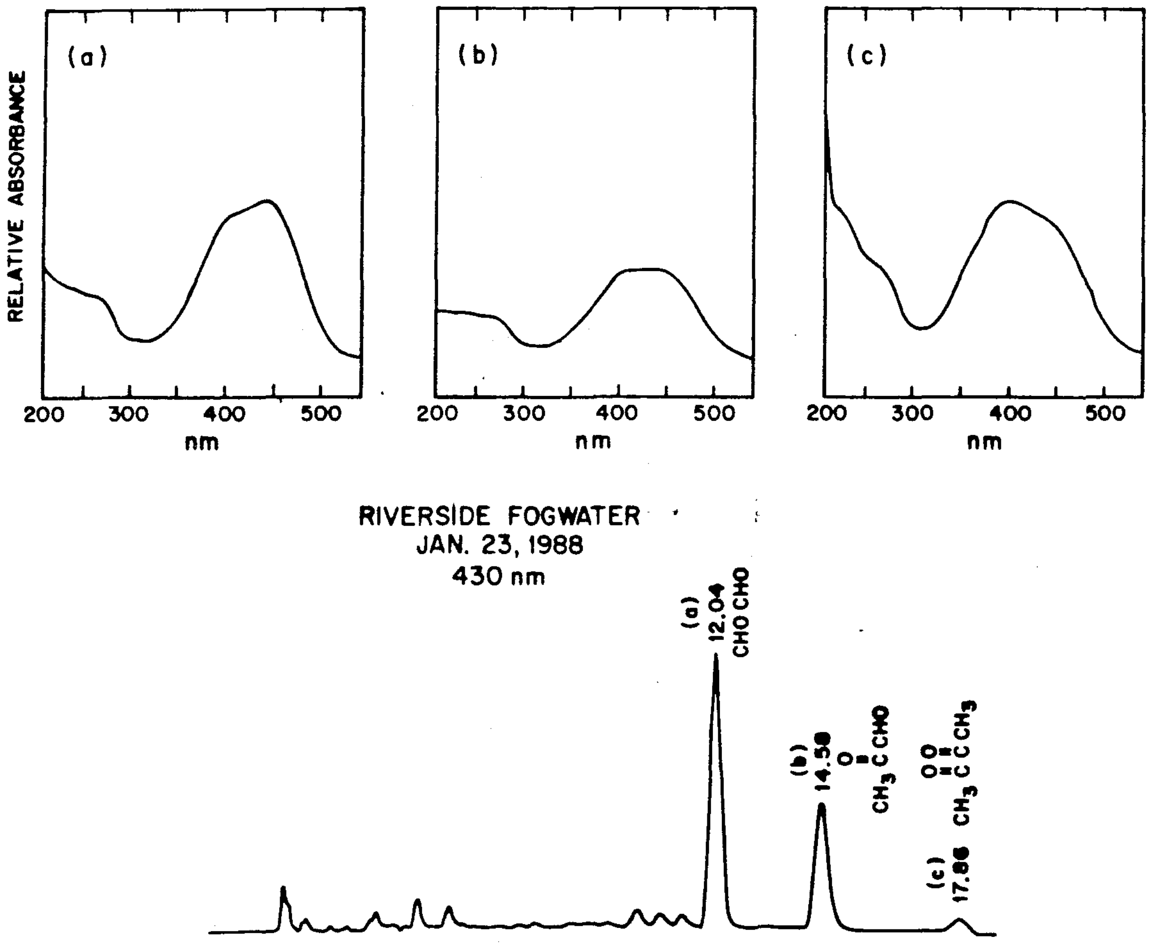

Figure 6.4. Chromatogram and peak spectra for derivatized samples of Riverside fogwater. Note the distinct spectra of glyoxal, methylglyoxal and 2,3 butanedione (biacetyl). Comparison of sample spectra with standards is an aid to identification of unknown peaks.

Results

Meteorology and Sampling Conditions

Sampling was initiated when fog was forecast for the Riverside area. During the winter of 1985–86 aerosol and fog were collected during four periods at the Riverside site. The first two sampling periods November 26 and January 16 were not foggy, though visibility was reduced by dense haze. The sampling on 26 November was preceded by light rain the previous day. Fog was present during the subsequent sampling periods, described below.

On the night of 22 January aerosol sampling began at 2230, with visibility about 2 miles in thick haze. Fog formed at the site prior to 0545. Fogwater sampling commenced at 0555 and continued until the fog dissipated at 1000. A single aerosol sample was collected during the foggy period. Two more aerosol samples were collected in the thick haze that remained after dissipation of the fog. Aerosol collection continued the following night. Visibility the second night was reduced to about 1 mile by haze. Fog formed over much of the inland basin that night, but did not penetrate as far inland or rise as high as the sampling site.

Two aerosol samples were obtained during hazy conditions in the early morning of 28 February. Fog formed between 0600 and 0730, and four fogwater samples were collected between 0744 and 1000. Two aerosol samples were taken during the fog and one post–fog aerosol sample was collected during the afternoon. Fog formed before midnight the following night. Four samples of fogwater were collected between 0000 and 0400. Light drizzle was observed during this event. After 0400 the fog layer rose above the sampling site, but it remained overcast well into the following morning. Two aerosol samples were obtained during the fog, and one post fog aerosol sample was collected immediately after fog sampling stopped. Interstitial aerosol samples were collected during the fog events on both days.

Aerosol samples were collected at Pasadena to determine the composition of aerosol away from point NH_3 sources. Samples were collected at Pasadena when fog was expected at other sampling sites in the basin. During the day Pasadena is generally upwind of the Riverside San Bernardino area. Drainage flows from the nearby mountain slopes and eastern San Gabriel Valley affect the site at night. Conditions were generally hazy or smoggy during sampling at Pasadena.

The concentrations of major air pollutants are measured by the South Coast Air Quality Management District at a network of stations throughout the SCAB. Data for two sites near the Riverside sampling site are shown in Figure 6.5 for the periods during which fog samples were obtained. Because the CO, O_3, and NO_2 concentrations are quite similar at the two sites, it is probable that these measurements are also representative of the air mass at the Riverside sampling site. Active photochemistry is indecated by the high daytime O_3 concentrations. The marked differences in the the NO concentrations at Rubidoux and Fontana may be due to their proximity to traffic. The decreasing concentrations of all species on March 1 are due to dilution by the strengthened onshore flow and deeper mixed layer, which was indicated by the rising cloud layer.

Aerosol Concentrations

The aerosol at Riverside (Table 6.1) was dominated by NH_4^+, which constituted 78–99% of the total cation loading. Calcium and sodium, the next–most important cations, were at least an order of magnitude less concentrated. Nitrate was the major anion; it exceeded SO_4^{2-} by factors ranging from 1.5 to 6. The range of nitrate concentrations was greater than that for sulfate. In the most dilute aerosol samples, those with < 1000 neq m^{-3} NH_4^+, there was a close balance between the acidic anions and basic cations. The remaining samples generally had excess NH_4^+ ($NH_4^+ > NO_3^- + SO_4^{2-}$). The two samples from Riverside with an excess of acid were both collected during the night, either with fog at the site or covering the remainder of the basin. Concentrations of NH_3 ranged from 32 – 4540 nmole m^{-3} (0.7 – 100 ppb) at Riverside. All the concentrations were well above the detection limit. The maximum observed NH_3 concentration of 4540 nmole m^{-3} exceeded the maximum NH_4^+ concentration. Nitric acid levels were comparatively low.

In general the concentrations in the Pasadena aerosol (Table 6.2) were less than at Riverside. The fraction of NH_4^+ in the Pasadena aerosol ranged from 42 – 96%. The NO_3^-:SO_4^{2-} ratio in the Pasadena samples was 0.36 – 5.0. Free HNO_3 was present at the Pasadena site. On several occasions it exceeded the aerosol NO_3^-. Gaseous NH_3 was present in Pasadena at much lower levels than in Riverside.

Fogwater Composition

Riverside fogwater samples contained such a high level of suspended solids that the collected samples appeared black. These particles were hydrophobic with an affinity for surfaces. The collector strands, sampling tubes and bottles became visibly soiled with black particulate matter during a sampling event. The fogwater composition (Table 6.3) was dominated by NH_4^+, NO_3^-, and SO_4^{2-}. The concentrations of NH_4^+ and NO_3^- exceeded 0.02 **N** in several samples. The pH of the samples ranged from 2.33 to 5.68. The first event was the most acidic; its pH dropped from 3.7 in the first sample collected to 2.33 at the end of the event. The February 28 event was only moderately acidic; its pH dropped from 5.0 to 4.25. Fog the following night was not acidic at all; it had pH > 5, even though it had some of the highest observed NO_3^- and SO_4^{2-} concentrations. The drop in pH and increase in solute concentration were partly due to the concentrating effect of droplet evaporation.

Table 6.1 Major aerosol and gas concentrations at Riverside, California

Date	Seq	Start Time	Stop Time	Na^+	NH_4^+	Ca^{2+}	Mg^{2+}	Cl^-	NO_3^-	SO_4^{2-}	NH_3	HNO_3
				neq m^{-3}								
11/26	A	22:20	02:05	36.3	791	53.8	12.2	40.8	464	319	NA	28.0
11/27	B	02:18	05:38	25.3	841	63.0	7.6	50.3	521	256	NA	17.1
01/16	A	21:30	00:00	82.6	705	81.4	29.4	73.7	519	192	507	21.0
01/17	A	00:00	04:00	39.7	1112	64.5	17.0	20.1	779	178	433	16.0
01/22	A	22:30	01:59	64.3	2564	79.4	27.5	52.6	1860	5657	1144	18.8
01/23	A	06:03	09:35	11.1	2354	20.7	4.5	42.4	1969	326	32	20.8
01/23	B	11:05	14:00	143	3779	138	42.4	202	3104	612	NA	NA
01/23	C	14:10	17:15	18.0	3648	113	23.3	67.6	2593	517	1498	76.9
01/23	D	23:00	03:00	26.8	3349	50.0	11.8	15.3	3072	550	91	28.0
02/28	A	01:45	04:00	456	3787	83.8	36.7	16.5	2922	688	69	44.6
02/28	B	04:01	06:30	402	2957	72.2	21.4	95.2	2410	430	123	24.9
02/28	C	07:36	09:26	11.7	3141	65.7	7.4	71.6	2134	599	179	20.6
02/28	D	09:33	10:42	8.1	3002	35.7	17.2	135	2278	616	183	43.7
02/28	E	13:00	16:00	168	2920	13.2	20.8	49.8	1654	406	4537	50.5
03/01	A	20:00	02:00	63.3	2051	13.2	1.7	49.8	1870	470	1097	13.9
03/01	B	02:10	04:05	56.5	2602	21.8	7.0	104	2219	443	903	8.5
03/01	C	04:15	06:15	11.0	2384	17.4	3.1	38.6	1934	309	855	15.1
Minimum				8.	704	13.	2.	15	463	178	32	8
Maximum				456	3787	139	42	202	3104	688	4537	77
Arith. Avg.				95	2470	62	17	66	1900	440	832	28

Table 6.2 Major aerosol and gas concentrations at Pasadena, California

Date	Seq	Start Time	Stop Time	Na^+	NH_4^+	Ca^{2+}	Mg^{2+}	Cl^-	NO_3^-	SO_4^{2-}	NH_3	HNO_3
				neq m^{-3}								
12/27	A	22:00	02:00	23.9	913	61.9	19.0	32.1	756	159	192	37.4
01/16	A	22:25	01:59	42.4	572	32.9	13.2	28.2	437	137	152	16.5
01/17	A	02:00	06:00	29.4	520	25.9	11.2	20.1	409	130	124	12.6
01/17	B	14:20	17:00	96.7	1859	187	56.1	61.3	2033	410	541	638
01/17	C	20:00	00:00	28.2	633	47.5	18.2	18.7	553	105	168	44.0
01/18	A	02:00	06:00	57.9	150	20.7	5.2	33.2	114	6.6	116	25.3
01/19	A	15:40	18:00	61.6	736	61.6	15.9	69.1	653	265	116	398
01/19	B	19:00	23:00	45.6	614	37.9	14.1	28.6	442	180	59	67.0
01/20	A	00:00	04:00	30.5	664	21.6	9.7	9.7	392	271	13	305
02/26	A	20:00	00:00	13.9	780	29.7	6.2	4.6	521	300	33	100
02/27	A	02:00	06:00	8.5	834	21.6	5.8	25.5	572	239	46	29.9
02/28	A	00:00	03:00	48.0	1228	24.6	15.2	42.0	624	741	5	358
02/28	B	03:01	06:00	15.4	1002	20.2	9.3	8.8	494	540	10	339
02/28	C	07:01	08:33	30.9	1521	40.0	10.9	8.6	761	810	5	771
02/28	B	08:00	10:50	4.9	894	33.8	5.5	3.8	545	223	30	190
02/28	D	04:00	17:00	38.7	1102	85.0	23.2	12.1	1312	545	64	891
03/01	A	00:00	04:00	41.9	688	40.9	9.1	3.9	219	607	10	832
03/01	B	08:00	11:31	19.8	808	31.0	8.5	5.3	379	464	16	650
03/04	A	20:00	23:00	22.1	1098	84.1	15.8	32.3	637	490	173	59.5
03/05	A	01:00	04:00	23.2	468	36.0	6.7	11.6	226	183	65	20.6
03/05	B	09:29	12:04	5.1	650	43.4	7.7	6.0	408	171	457	472
03/05	C	14:45	16:45	131	950	75.9	18.6	14.2	324	644	49	757
03/05	D	20:00	23:00	146	790	42.7	15.2	8.2	NA	654	7	268
03/06	A	01:00	04:00	159	951	39.1	11.6	21.9	415	554	5	340
Minimum				3.3		14.0	1.8	3.8	NA	3.5	5	0.0
Maximum				159		187	56.1	69.1	NA	810	541	891
Arith. Avg.				44.3		48.8	13.7	21.3	NA	330	108	283

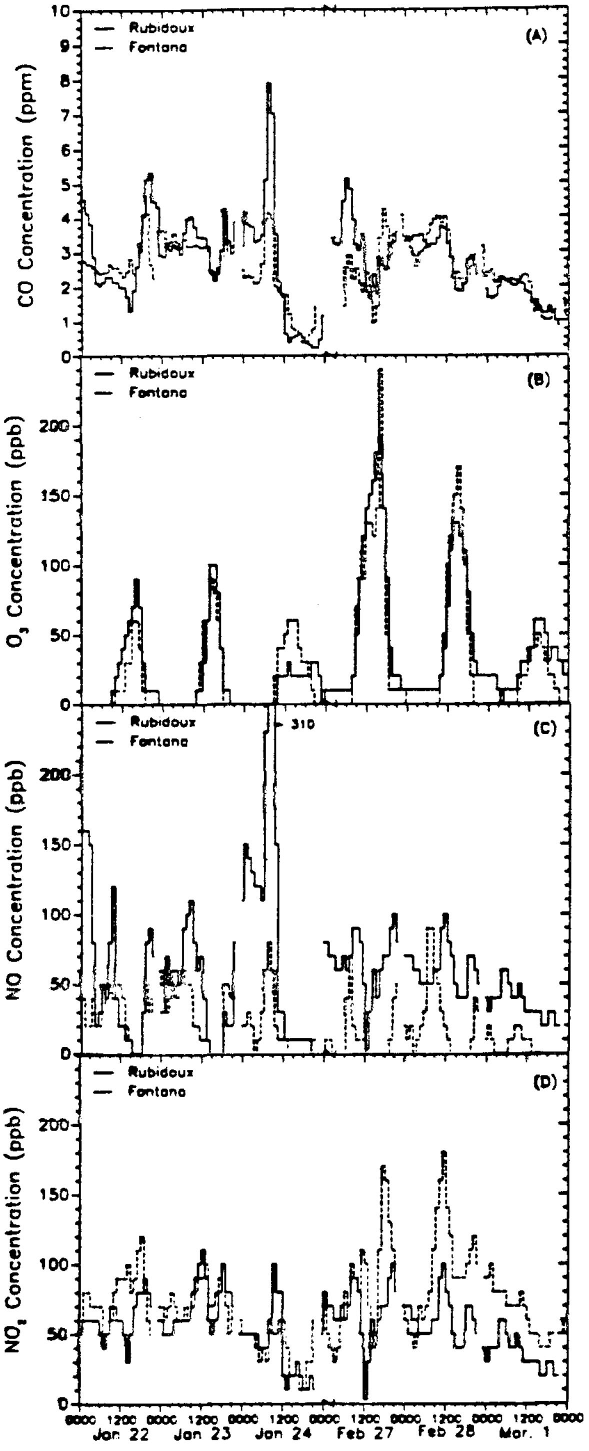

Figure 6.5. Concentration profiles of CO, O_3, NO, and NO_2 at South Coast Air Quality Management District monitoring stations near the Riverside sampling site. Rubidoux is ≈10 km W and Fontana is ≈ 20 km NW of the Riverside sampling site.

However, some of the variation occurred during periods with stable LWC (as estimated from sample collection rate).

Except for the final sample collected during the March 3 fog event the anion cation balance was between 0.99 and 1.10 which suggests that all major species were determined. It is likely that the NO_3^- determination for sample 301–D was too high or the NH_4^+ determination was too low. However, because the sample was small it could not be reanalyzed.

The concentration of CH_2O determined by the Nash method varied from 165 to 384 μ**M**. Dong and Dasgupta [1987] found similar concentrations of CH_2O in several of these samples that they analyzed by a flow–injection fluorimetric method. The S(IV) concentrations determined by the automated pararosaniline method were lower than the concentrations determined by Dasgupta and Yang [1986] in separate aliquots of several samples. The S(IV) concentrations reported here appear to be too low because of negative interference by the background matrix in the samples. This interference has not been a problem in samples from other locations.

The large number of carbonyls present in the Riverside fogwater samples is indicated by the number of peaks seen in Figure 6.6. Concentrations of the species that have been identified and quantified are given in Table 6.4. Note that the CH_2O concentrations determined by the DNPH derivatization are less than those determined by the Nash method (Table 6.3). As noted above, the Nash method determined total CH_2O, while the DNPH derivative only forms from free carbonyls. In some cases the dicarbonyl concentrations exceed the formaldehyde concentration. The samples from March 1 are the most extreme case of this. A third dicarbonyl, 2,3 butanedione (biacetyl), was also present at low levels in most of the samples.

Peroxide was not detectable in the samples from 23 January. The two fog events on 28 February and 1 March contained peroxide up to 25 μ**M**.

Table 6.3 Major ion concentrations in fogwater samples from Riverside, California.

Date	Seq	Start Time	Stop Time	Vol	pH	Na^+	NH_4^+	Ca^{2+}	Mg^{2+}	Cl^-	NO_3^-
				ml	µN						
01/23	A	05:55	06:30	58	3.70	123	10600	303	86	206	8230
01/23	B	06:30	07:00	59	3.65	37	10300	124	33	178	8290
01/23	C	07:00	07:30	55	3.08	30	8660	118	27	165	7580
01/23	D	07:30	08:00	37	3.35	41	12200	212	41	<100	9890
01/23	E	08:00	08:30	45	2.90	37	11300	158	35	<100	10900
01/23	F	08:30	09:00	48	2.78	32	10500	100	27	<100	10600
01/23	G	09:00	09:35	22	2.66	47	14000	181	45	176	12500
01/23	H	09:35	10:12	18	2.33	106	19800	362	81	371	20100
		N		8	8	8	8	8	8	8	8
		Minimum		18	2.33	30	8660	100	27	<100	7580
		Maximum		59	3.70	123	19800	362	86	371	20100
		Vol. Wt. Avg			2.99	52	11096	175	43	158	819
02/28	A	07:44	08:20	89	5.22	64	8340	131	26	130	6090
02/28	B	08:20	08:45	67	4.88	35	8380	109	23	170	6050
02/28	C	08:45	09:30	92	4.24	43	10400	106	26	190	7850
02/28	D	09:30	10:00	16	4.25	54	18100	209	55	384	13300
		N		4	4	4	4	4	4	4	4
		Minimum		16	4.24	35	8340	106	23	130	6050
		Maximum		92	5.22	64	18100	209	55	384	13300
		Vol. Wt. Avg			4.59	48	9588	122	27	178	7050
03/01	A	00:00	01:00	40	5.68	188	25800	396	103	380	18800
03/01	B	01:00	02:06	87.8	5.53	103	21200	164	49	370	15300
03/01	C	02:06	03:00	37.5	5.36	62	23200	129	37	370	17200
03/01	D	03:00	04:05	11.5	5.20	91	24000	294	73	750	28900
		N		4	4	4	4	4	4	4	4
		Minimum		11	5.20	62	21200	129	37	370	15300
		Maximum		87	5.68	188	25800	396	103	750	28900
		Vol.Wt. Avg			5.48	112	22926	217	60	396	17400

Table 6.3 continued

Date	Seq	SO_4^{2-}	S(IV)	CH_2O	H_2O_2	HFo	HAc	HMSA	-/+	LWC
		μN			μM					g m^{-3}
01/23	A	2030	57	165	0	178	95	83	0.93	0.09
01/23	B	1650	64	187	0	—*	—*	92	0.94	0.11
01/23	C	1430	33	193	0	—*	—*	49	0.95	0.10
01/23	D	1810	53	218	0	182	122	103	0.90	0.07
01/23	E	1920	32	187	0	—*	—*	66	1.00	0.08
01/23	F	1850	13	186	0	106	56	52	1.01	0.09
01/23	G	2840	20	279	0	—*	—*	64	0.94	0.04
01/23	H	3960	14	207	0	346	237	86	0.98	0.03
N		8	8	8	8	8	4	8	8	
Minimum		1430	13	165	0	106	56	49	0.90	
Maximum		3960	64	279	0	346	237	103	1.01	
Vol.Wt. Avg		1929	40	194	0	—	—	73	0.96	0.074
02/28	A	1890	5	175	6	480	167	158	0.95	0.14
02/28	B	1810	12	223	17	451	161	NA	0.94	0.15
02/28	C	2300	15	234	15	357	134	NA	0.97	0.11
02/28	D	3660	10	370	25	576	267	NA	0.94	0.03
N		4	4	4	4	4	4	NA	4	
Minimum		1810	5	175	6	357	134	NA	0.94	
Maximum		3660	15	370	25	576	267	NA	0.97	
Vol.Wt. Avg.		2096	11	221	14	444	163		0.95	0.109
03/01	A	4900	60	309	19	NA	NA	NA	0.91	0.04
03/01	B	3770	12	205	21	1408	581	NA	0.90	0.07
03/01	C	3830	11	254	0	1293	417	NA	0.91	0.04
03/01	D	6230	26	384	15	1517	462	NA	1.47	0.01
N		4	4	4	4	4	4		4	
Minimum		3770	11	205	0	NA	NA	NA	0.90	
Maximum		6230	60	384	21	NA	NA	NA	1.47	
Vol.Wt. Avg		4199	24	252	15	0	0		0.94	0.040

* —indicates invalid data
NA —indicates not anlyzed
HFo = $CHOOH + CHOO^-$
HAc = $CH_3COOH + CH_3COO^-$

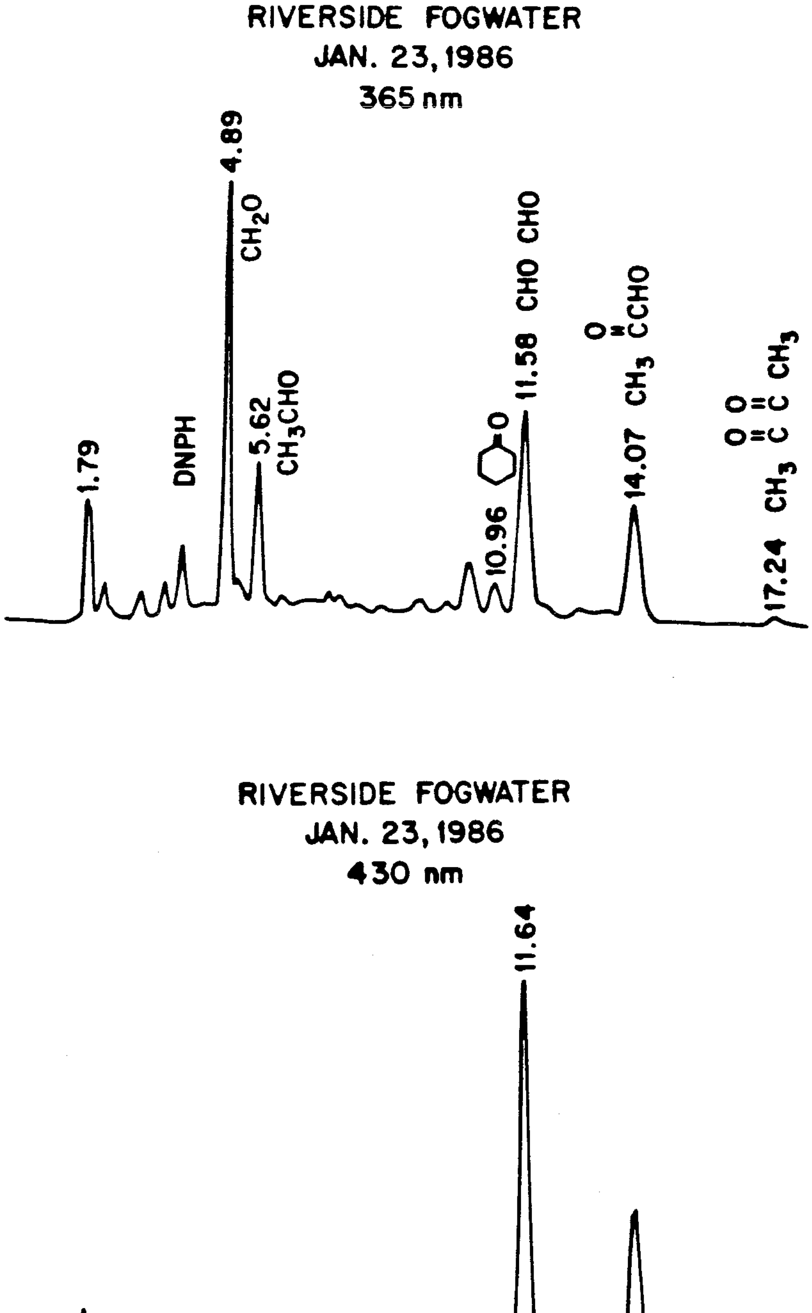

Figure 6.6. HPLC chromatograms of DNPH derivatives of Riverside fogwater at two wavelengths. Several–fold greater sensitivity for dicarbonyls is achieved monitoring the absorbance at 430 nm, which is near the absorbance maximum for these compounds.

Table 6.4 Carbonyl concentrations in Riverside fogwater samples determined by HPLC analysis of DNPH derivatives

Date	ID	Start Time	Stop Time	Vol[1]	CH_2O	CHOCHO	CH_3COCHO	$(CH_3CO)_2$
				(ml)	μM			
01/23	A	05:55	06:30	3	109	65.3	45.9	4.7
01/23	B	06:30	07:00	3	122	32.3	25.8	3.7
01/23	C	07:00	07:30	3	162	34.6	26.7	3.5
01/23	D	07:30	08:00	2	228	59.9	44.1	5.8
01/23	E	08:00	08:30	2	119	55.3	42.7	5.1
01/23	F	08:30	09:00	2	142	56.8	47.7	5.8
01/23	G	09:00	09:35	1	104	121	83.9	1.4
01/23	H	09:35	10:12	1	84	139	108	0.0
01/23		Blank		3	0.4	0.0	0.0	0.0
01/23		Blank		2	14.7	0.4	0.0	0.0
01/23		Blank		2	17.2	0.5	0.0	0.0
02/28	A	07:44	08:20	2	36.3	38.6	35.5	3.9
02/28	B	08:20	08:45	2	40.8	45.0	41.1	4.9
02/28	C	08:45	09:30	2	57.3	77.1	60.5	6.6
02/28	D	09:30	10:00	1	107	198	128	14.0
02/28		Blank		2	21.0	0.8	0.0	0.0
03/01	A	00:00	01:00	2	4.1	147.8	79.1	8.8
03/01	B	01:00	02:06	2	8.7	142.3	74.9	8.9
03/01	C	00:06	03:00	2	8.2	144.1	77.4	8.8
03/01	D	03:00	04:05	1	36.0	276.2	124	17.7
03/01		Blank		2	13	0.6	0	0

[1] Volume of sample that was derivatized

Sample Concentrations are corrected for blank concentrations. The concentrations given for the blanks are the actual concentrations in the blank.

Hydroxymethanesulfonate (HMSA) was observed in the January 23 samples at 50 – 100 μM levels. Sample "A" from February 28 had 160 μM HMSA. Unfortunately the HMSA concentration in the remaining samples, which had the higher H_2O_2, could not be determined because of interferences.

Formate and acetate had high concentrations in the Riverside fogwater. The highest concentrations, 1520 and 580 μM, were observed in the March 1 samples, which had pH > 5. Even the January 23 samples, which were quite acid had formate and acetate concentrations up to 350 and 340 μM. In all cases HCOOH exceeded CH_3COOH, though the ratio varied substantially.

Discussion

Aerosol Data

The results presented here are an example of the coincidence between severe air pollution and fog. This of course does not necessarily imply a causal relationship. The sampling periods affected by fog are extreme pollution events. The overall average SO_4^{2-} concentration of 440 neq m^{-3} is 80% of the California State Air Quality Standard for SO_4^{2-} (25 μg m^{-3} as a 24–hr average). The nitrate concentrations reported here are 6 – 10 times the monthly averages for January and February [Hoggan et al., 1980;1986]. The two sampling periods not affected by fog, Nov. 26–27 and Jan 16–17 exhibited lower aerosol concentration.

Russell and Cass [1984] performed a series of detailed aerosol measurements in the SCAB during August of 1982. Their results for Rubidoux, which is 8 km west of UC Riverside, also indicated that NH_4^+, NO_3^-, and SO_4^{2-} were the dominant components of the aerosol. The concentrations they observed were considerably less, although they also observed high NH_3 and low HNO_3 concentrations. Higher wind speeds and a deeper mixed layer during the August study could account for the difference in concentrations observed.

The acid–base balance of the aerosol is illustrated in Figure 6.7A. At Riverside, which is adjacent to the major NH_3 source region, most of the aerosol had an excess of NH_4^+. On the other hand, Pasadena appeared to have neutral aerosol. When NH_3 and HNO_3 in the gas phase were included (see Fig. 6.7B) the alkaline excess at Riverside was enhanced and the most concentrated of the Pasadena samples appeared acidic. This observation is consistent with the distribution of sources and prevailing winds in the SCAB. Emissions of NO_x are highest along the coast and over downtown Los Angeles, where traffic density is greatest. The region downwind is affected by HNO_3 formed from the oxidation of NO_x. When the air mass reaches the vicinity of Chino it is mixed with NH_3 emissions, neutralizing the HNO_3.

Scavenging Ratios

The extent to which fog is affected by the preexisting aerosol and gas–phase composition depends on the scavenging efficiency. At humidities $\geq 100\%$, nearly all hygroscopic aerosol larger than a critical size will be activated and form droplets. The critical size for nucleation decreases as the supersaturation ratio is increased [Pruppacher and Klett, 1978]. For conditions typical of fog the critical size is $\simeq 0.1$ μm. This phenomenon would allow for scavenging efficiencies < 1 if a large mass of aerosol smaller than critical size were present. Scavenging efficiency would thus be related to the degree of supersaturation. Aerosol smaller than the critical size are scavenged by existing droplets through diffusion and impaction, which are less efficient processes. Soluble gases rapidly exchange across the air–water interface. The characteristic time for mass transfer across the interface is typically less than the lifetime of droplets, thus the extent of scavenging from the gas phase can be predicted from thermodynamic considerations [Schwartz and Freiberg, 1981].

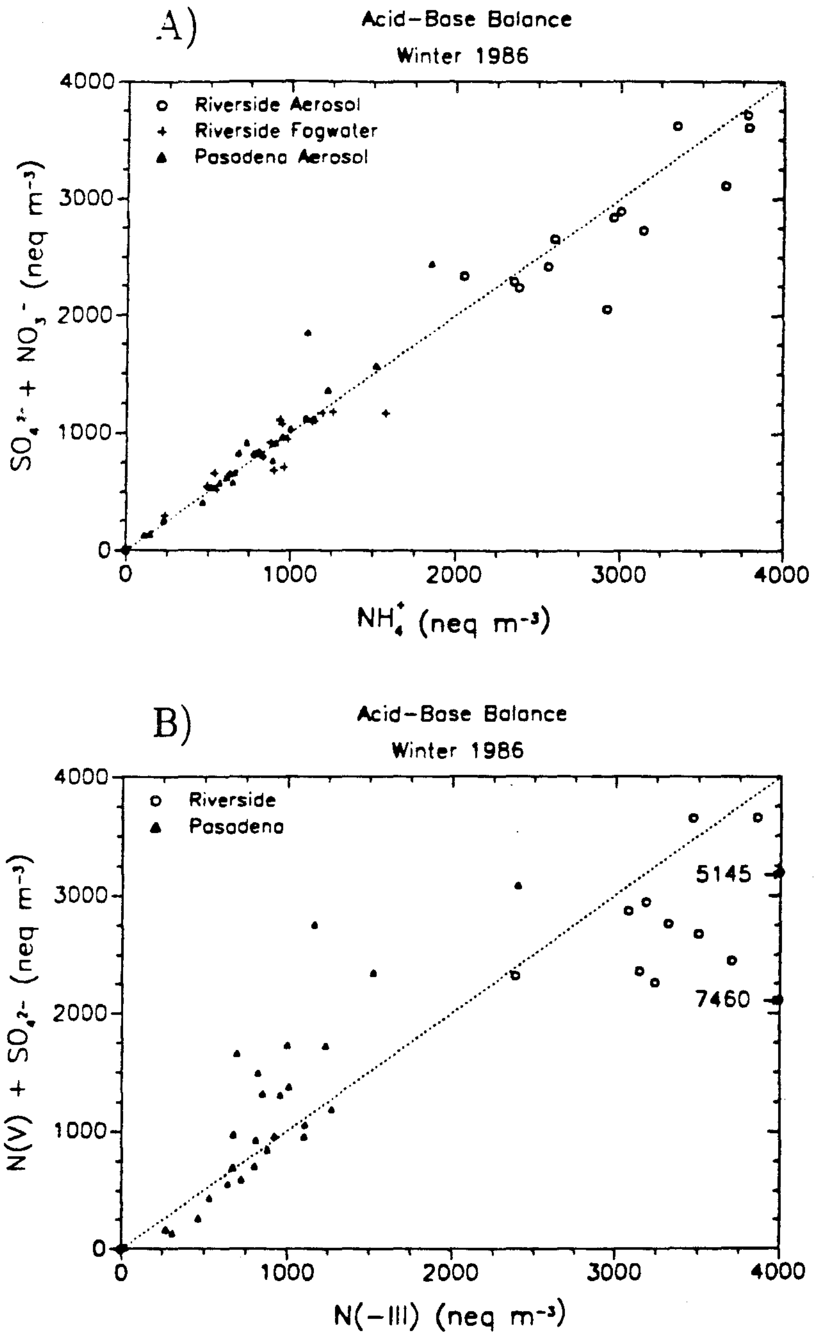

Figure 6.7. Acid – base balance in Riverside and Pasadena aerosol samples. Only the dominant species, NH_4^+, NO_3^-, and SO_4^{2-} are shown. The line indicates the condition $NH_4^+ = NO_3^- + SO_4^{2-}$. Points below and to the right of this line are alkaline, points above and to the left are acidic. A. Aerosol (or fog) only, (B) Aerosol plus gaseous NH_3 and HNO_3.

Table 6.5 Concentration of aqueous–phase solutes per volume of air [1]

Date	Seq	LWC[2]	H^+	Na^+	NH_4^+	Ca^{2+}	Mg^{2+}	Cl^-	NO_3^-
		g m^{-3}	neq m^{-3}						
01/23	A	0.09	18.5	11.4	984	28.1	7.9	19.1	764
01/23	B	0.11	24.6	4.0	1132	13.6	3.6	19.6	912
01/23	C	0.10	84.6	3.1	881	12.0	2.8	16.8	771
01/23	D	0.07	30.6	2.8	836	14.5	2.8	<6.9	678
01/23	E	0.08	106	3.2	953	13.3	3.0	<8.4	920
01/23	F	0.09	149	2.8	941	9.0	2.4	<9.0	950
01/23	G	0.04	78.1	1.7	500	6.5	1.6	6.3	446
01/23	H	0.03	128	2.9	542	9.9	2.2	10.2	551
N			8	8	8	8	8	8	8
Minimum			18.5	1.7	500	6.5	1.6	<6.3	446
Maximum			149	11.4	1132	28.1	7.9	19.6	950
02/28	A	0.14	0.8	8.9	1155	18.1	3.6	18.0	843
02/28	B	0.15	2.0	5.3	1258	16.4	3.5	25.5	908
02/28	C	0.11	6.6	4.9	1196	12.2	3.0	21.8	903
02/28	D	0.03	1.7	1.7	554	6.4	1.7	11.8	407
N			4	4	4	4	4	4	4
Minimum			0.8	1.7	554	6.4	1.7	11.8	407
Maximum			6.6	8.9	1258	18.1	3.6	25.5	908
03/01	A	0.04	0.08	7.0	963	14.8	3.8	14.2	702
03/01	B	0.07	0.22	7.7	1579	12.2	3.6	27.6	1140
03/01	C	0.04	0.17	2.4	902	5.0	1.4	14.4	669
03/01	D	0.01	0.06	0.9	238	2.9	0.7	7.4	286
N			4	4	4	4	4	4	4
Minimum			0.08	0.9	238	2.9	0.7	7.4	286
Maximum			0.22	7.7	1579	14.8	3.8	27.6	1140

Table 6.5 continued

Date	Seq	SO_4^{2-}	S(IV)	CH_2O	H_2O_2	HFo[3]	HAc[4]	HMSA
		neq m^{-3}	nmole m^{-3}					
01/23	A	188	5.3	15.3	0.0	16.5	8.8	7.7
01/23	B	181	7.0	20.6	0.0	—[5]	—	10.1
01/23	C	146	3.4	19.6	0.0	—	—	5.0
01/23	D	124	3.6	14.9	0.0	12.5	8.6	7.1
01/23	E	162	2.7	15.8	0.0	—	—	5.6
01/23	F	166	1.2	16.7	0.0	9.4	5.0	4.8
01/23	G	101	0.7	10.0	0.0	—	—	2.3
01/24	H	108	0.4	5.7	0.0	9.5	6.5	2.4
N		8	8	8	8	4	8	8
Minimum		101	0.4	5.7	0.0	2.8	0.0	2.3
Maximum		188	7.0	20.6	0.0	16.5	8.8	10.1
02/28	A	262	0.73	24.2	0.85	66.5	23.1	—
02/28	B	272	1.76	33.5	2.61	67.6	24.2	—
02/28	C	264	1.77	26.9	1.75	41.0	15.4	—
02/28	D	112	0.32	11.3	0.76	17.6	8.2	—
N		4	4	4	4	4	4	0
Minimum		112	0.32	11.3	0.76	17.6	8.2	—
Maximum		272	1.77	33.5	2.61	67.6	24.2	—
03/01	A	183	2.23	11.54	0.69	NA	NA	—
03/01	B	281	0.88	15.27	1.53	105	43.3	—
03/01	C	149	0.42	9.88	0.00	50.3	16.2	—
03/01	D	62.	0.26	3.80	0.15	15.0	4.6	—
N		4	4	4	4	4	4	0
Minimum		62	0.26	3.80	0.15	15.0	4.6	—
Maximum		281	2.23	15.27	1.53	105.0	43.3	—

[1] $C_{air} = C_{aq} L$

[2] LWC is estimated from the sample collection rate

[3] HFo = $CHOOH + CHOO^-$

[4] HAc = $CH_3COOH + CH_3COO^-$

[5] — indicates sample not analyzed

The aqueous–phase concentrations in the fogwater samples have been multiplied by the liquid water content (LWC) estimated from the collection rate to give the concentration on a mass per volume of air basis (Table 6.5). The comparison of fogwater loading (Table 6.5) with the aerosol concentration (Table 6.1) suggests that the fogwater scavenging under these conditions is not 100% efficient. It is unlikely that the estimated LWC values are too low by this amount, but we can not exclude the possibility. The existence of a significant fraction of unactivated aerosol is supported by the results for the fine aerosol filters (Table 6.6). The concentrations of fine aerosol are comparable to the fogwater. If the CASC and aerosol inlet perform as expected, considerably more than half the solute mass would have to be in the smallest droplets to account for this result without having any unactivated aerosol.

The scavenging ratios for individual events are computed by three different methods and presented in Table 6.7. The scavenging ratios computed by method 1, which compares the concentration in the fog with the concurrent total aerosol, are < 50%. The ratio decreases at the end of the fog event as the droplets are evaporating. Method 2, which compares the fog concentration to the aerosol before the fog yields similar results. In method 3 the difference between total and fine aerosol concentrations is divided by the total. The calculation by method 3 does not depend on the estimated LWC. If the fine aerosol measurement includes a significant fraction of small droplets, the scavenging ratios computed by method 3 will be underestimates. The scavenging ratios calculated by method 3 are somewhat higher than the others, but the pattern of decreased efficiency as the fog dissipates is preserved. Because of the inherent uncertainties in the scavenging calculations, these values are qualitative. However, the consistently low values suggest that radiation fogs in highly polluted air may not scavenge aerosol at 100% efficiency.

Low scavenging efficiencies were also reported by Waldman and Hoffmann [1987] in a study of radiation fog in the San Joaquin Valley. That study also showed a

Table 6.6 Fine Aerosol Concentrations at Riverside, California.

Date	Seq	Start	Stop	Na^+	NH_4^+	Ca^{2+}	Mg^{2+}	Cl^-	NO_3^-	SO_4^{2-}
				neq m^{-3}						
02/28	C	07:36	09:26	579	986	78	9	61	735	138
02/28	D	09:33	10:42	825	2338	140	20	110	1733	415
03/01	A	00:00	02:00	4	664	3	0	15	569	100
03/01	B	02:10	04:05	4	1225	6	5	11	1034	150

Table 6.7 Scavenging Ratios for Riverside Fogwater.

Method 1: $R = [C_{fog}]/[C_{aerosol}]$

Date	Seq	Start	Stop	Na^+	NH_4^+	Ca^{2+}	Mg^{2+}	Cl^-	NO_3^-	SO_4^{2-}	N(-III)[1]	N(V)[1]
01/23	A	06:03	09:35	0.38	0.38	0.68	0.78	—[2]	0.39	0.47	0.37	0.39
02/28	C	07:36	09:26	0.54	0.38	0.23	0.45	0.30	0.41	0.44	0.36	0.41
02/28	D	09:33	10:42	0.21	0.18	0.18	0.10	0.09	0.18	0.18	0.17	0.18
03/01	A	00:00	02:00	0.12	0.63	1.02	2.20	0.43	0.50	0.50	0.41	0.49
03/01	B	02:10	04:05	0.03	0.21	0.18	0.15	0.10	0.21	0.23	0.15	0.21

Method 2: $R = [C_{fog}]/[C_{aerosol}]_{pre\text{-}event}$

Date	Seq	Start	Stop	Na^+	NH_4^+	Ca^{2+}	Mg^{2+}	Cl^-	NO_3^-	SO_4^{2-}	N(-III)	N(V)
01/22	A	22:30	01:59	0.18	0.38	0.35	0.29	0.36	0.41	0.33	0.27	0.41
02/28	B	04:01	06:30	0.02	0.39	0.25	0.17	0.19	0.35	0.61	0.37	0.35

Method 3: $R = (1-[C_{fine}]/[C_{total}])$

Date	Seq	Start	Stop	Na^+	NH_4^+	Ca^{2+}	Mg^{2+}	Cl^-	NO_3^-	SO_4^{2-}	N(-III)	N(V)
02/28	C	07:36	09:26	—	0.69	—	—	0.15	0.66	0.77	0.70	0.66
02/28	D	09:33	10:42	—	0.22	—	—	0.18	0.24	0.33	0.27	0.25
03/01	A	00:00	02:00	0.93	0.68	0.74	0.82	0.69	0.70	0.79	0.79	0.70
03/01	B	02:10	04:05	0.92	0.53	0.72	0.36	0.89	0.53	0.66	0.65	0.54

[1] N(-III) = $NH_3 + NH_4^+$, N(V) = $HNO_3 + NO_3^-$

[2] —indicates data invalid for calculating scavenging ratios.

weak positive correlation between scavenging ratio and LWC. ten Brink et al. [1987], however, observed nearly complete scavenging of aerosol SO_4^{2-} and b_{scat}, a surrogate for total aerosol in clouds. We have also observed high scavenging efficiencies for intercepted marine stratus and mountain clouds [Collett et al., 1988; Munger et al., 1988]. Because the aerosol number concentration, size distribution, and saturation conditions in clouds are much different than those at the ground, we do not see a conflict in these results.

Temporal Variations

The aerosol, gas and fogwater concentrations of major ions and alkalinity are plotted together in Figs. 6.8A–C and 6.9. During the night of Jan. 22 the N(–III) concentration decreased, mostly due to a decline in NH_3. The NO_3^-concentration was constant over that period and SO_4^{2-} decreased. The following morning all three species increased as the fog dissipated. The timing of this increase coincided with the onset of a westerly wind, which advected fresh emissions to the site, and to an increase in traffic throughout the basin. Ammonium and NH_3 declined the following night, when the site was above the fog layer, but NO_3^- and SO_4^{2-} remained high. During the night of Feb. 28, NO_3^- and NH_4^+ declined. The gas–phase contributions were small. The NO_3^- concentration remained low the following morning, but NH_3 rose to its highest level during the study. The concentrations were similar the following night, but NH_3 made a larger contribution to the total N(–III). The alkalinity plot, Fig. 6.9 indicates that the gas phase is the major reservoir of alkalinity at Riverside. The acidity of the fog is not completely explained by the precursor aerosol and gas–phase species. Prior to the Jan. 23 fog the atmosphere contained over 1000 neq m^{-3} total alkalinity. This was almost completely dissipated by the time the fog formed; the atmosphere was still more alkaline than the fog, however. High alkalinity levels were

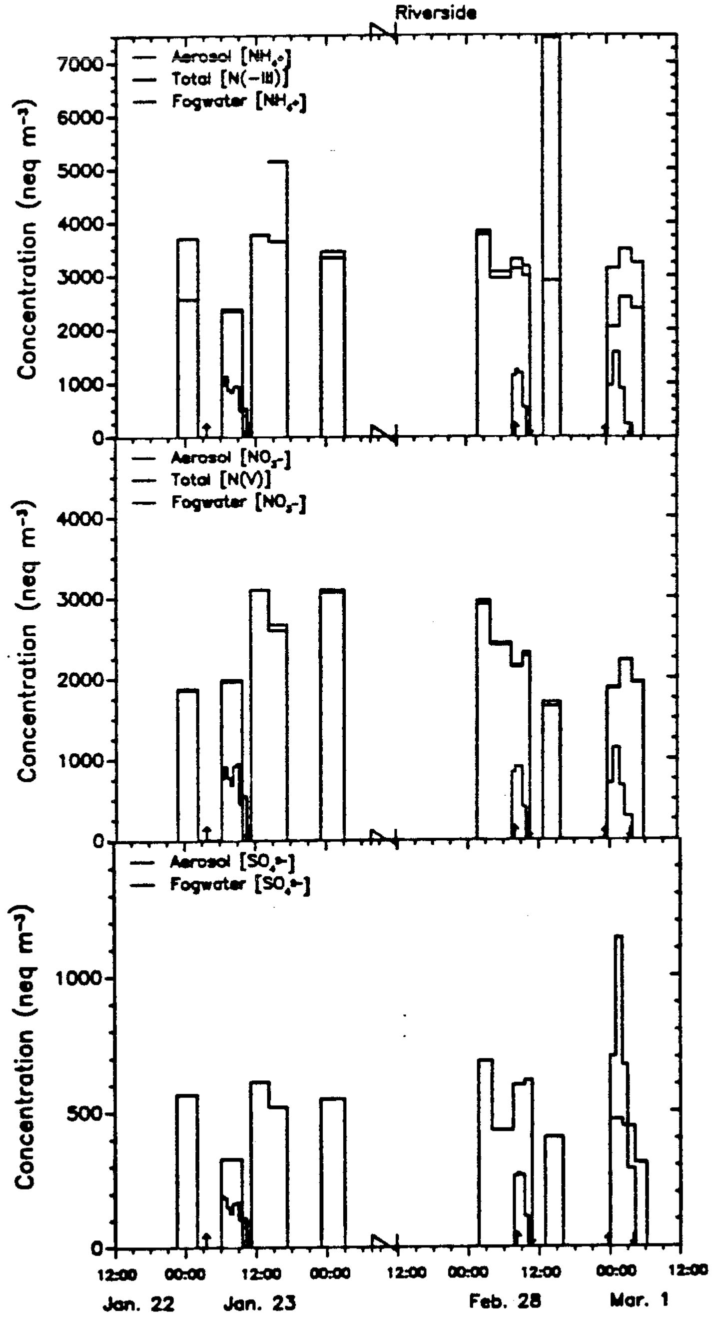

Figure 6.8. Plot of aerosol, gas and fogwater concentrations of N(−III), N(V), and SO_4^{2-} at Riverside. Fogwater concentrations are calculated from the aqueous-phase concentration and liquid water content estimated from the collection rate. The start and end of a fog event are indicated by ↑ and ↓.

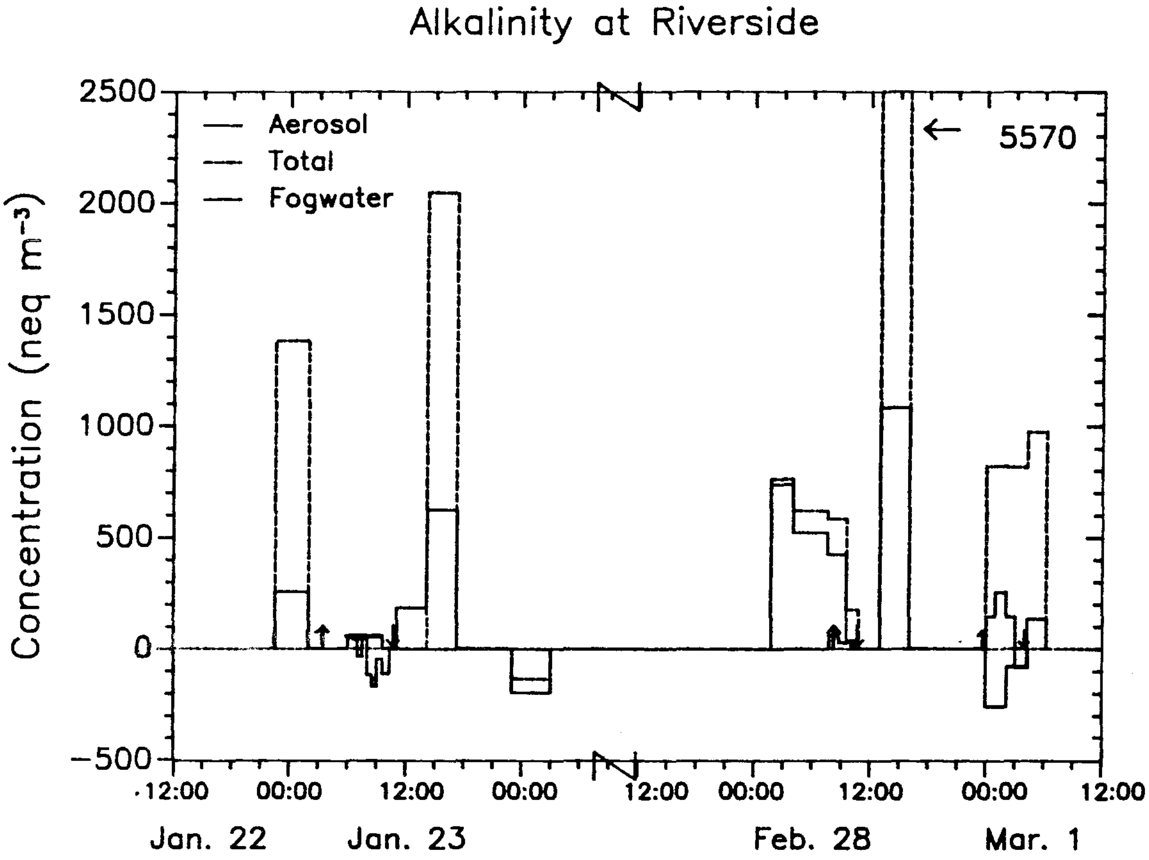

Figure 6.9. Plot of atmospheric alkalinity at the Riverside sampling site. The aerosol and fogwater lines are computed from the equation: Alk = Σcations – Σanions. The total Alkalinity is the aerosol alkalinity plus the contribution from gas–phase NH_3 and HNO_3. The start and end of a fog event are indicated by ↑ and ↓.

obtained the following afternoon. The air mass was acidic the following night. Again on Feb. 28, an alkaline air mass generated a moderately acidic fog. On March 1 the alkalinity of the fog was supported by an excess of NH_3 in the gas phase. The aerosol measurements alone would imply that the flux of NH_3 in the basin exceeds the production of HNO_3 from NO_x emissions, but the fogwater data are not consistent with this argument.

The resolution of this contradiction lies in the meteorology of the basin and the location of the emission sources relative to the sampling site. During the day the sea breeze creates a westerly flow through the basin. Nitric acid is continually produced, but NH_3 emissions near Chino are more than sufficient to neutralize the air mass by the time it reaches the Riverside sampling site. Convective mixing will distribute the NH_4NO_3 and NH_3 as well as unreacted NO_x throughout the mixed layer. At night the wind reverses direction and a shallow nocturnal inversion forms, which effectively isolates the site from the NH_3 emissions. The air now affecting the site is polluted air that was isolated from the boundary layer by the nocturnal inversion. Nitric acid is produced in this air mass via $NO_3\cdot$ and N_2O_5 mechanisms:

$$NO_2 + O_3 \rightarrow NO_3\cdot + O_2 \qquad (1)$$

$$NO_3\cdot + NO_2 \rightarrow N_2O_5 \qquad (2)$$

$$NO_3\cdot + RH \rightarrow HNO_3 + R\cdot \qquad (3)$$

$$NO + O_3 \rightarrow NO_2 + O_2 \qquad (4)$$

$$NO + NO_3\cdot \rightarrow 2NO_2 \qquad (5)$$

The concentrations of $NO_3\cdot$ and N_2O_5 are enhanced in this air mass because it is also isolated from NO emissions, which would consume O_3 and $NO_3\cdot$ via reactions 4 and 5. Over the course of the night production of HNO_3 titrates the residual NH_3 in the air mass. This is observed on the nights of Jan. 22 – 23 and February 28. The conditions on Jan. 23 are an extreme example of this. The sampling site was above the fog layer, clearly indicating that it was isolated from the NH_3 sources. This was the only sampling period that had acidic aerosol. We did not observe a decrease in alkalinity or formation of acid fog on the night of March 1 when there was no wind reversal. This scheme implies that the source of HNO_3 in the fog is above the fog layer. Its logical consequence is that acid fog may form at the margins of the basin while fog in the center is neutral or alkaline. Because the hillsides are one of the most desirable sites for housing developments this is of particular concern for assessing potential health effects of fogwater in the Riverside area.

The concentrations of carbonyls in the Riverside fogwater samples are plotted in Figure 6.10. On January 23 CH_2O reaches its maximum at the midpoint of the collection period, which is between 07:30 and 08:00. Subsequent to this time CH_2O decreases while the dicarbonyls, CHOCHO and $CH_3C(O)CHO$, increase. The increase in dicarbonyl concentrations coincides with morning rush hour, which would contribute hydrocarbon precursors, and increased sunlight. This pattern is repeated on Feb. 28. The presumed source of dicarbonyls in the atmosphere is the gas–phase oxidation of aromatic compounds, such as toluene. The observed concentrations of carbonyls and dicarbonyls are consistent with their solubilities. CH_2O, CHOCHO, and $CH_3C(O)CHO$, which have the highest concentrations, all have large effective Henry's Law constants because of their large hydration constants [Betterton et al., 1988]. Acetaldehyde, which has been reported at levels comparable to CH_2O in the Los Angeles air [Grosjean, 1982], but is 10^{-3} times as soluble, was not observed above the blank concentration in these samples.

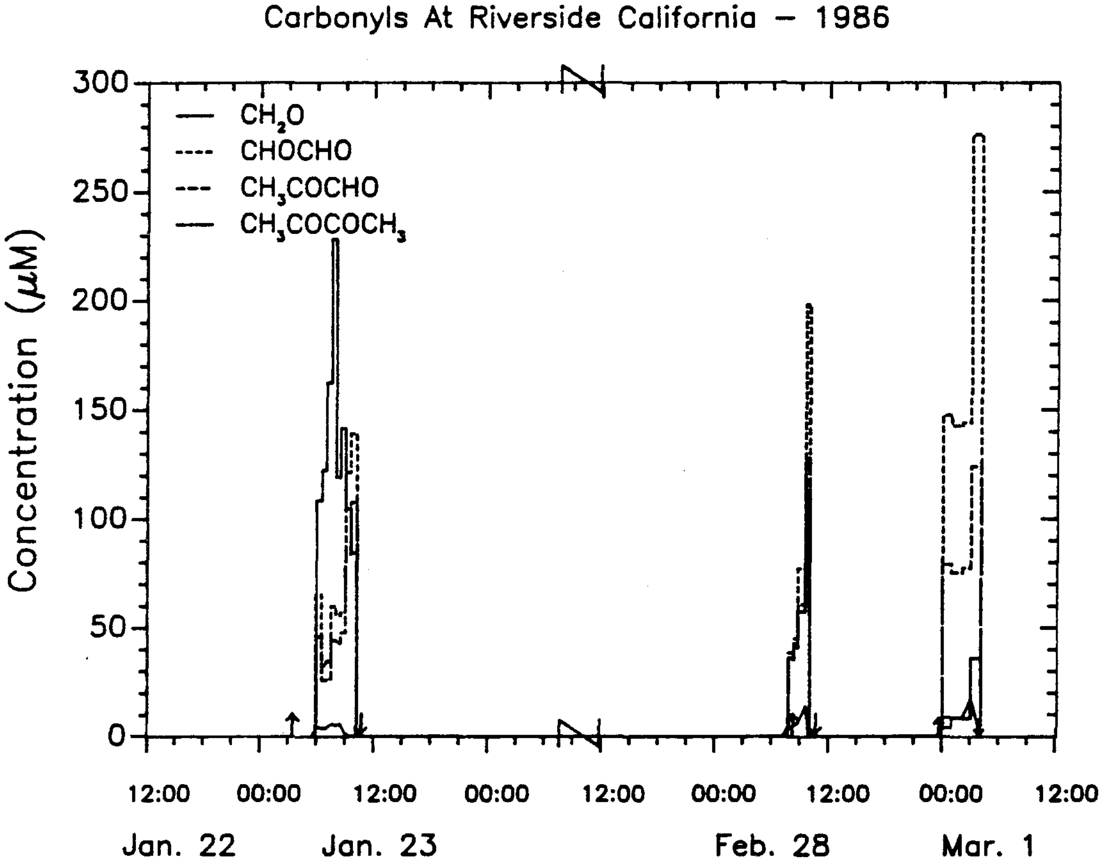

Figure 6.10. Plot of carbonyl concentrations determined by the DNPH derivatization method. The start and end of a fog event are indicated by ↑ and ↓.

Several lines of evidence indicate the importance of sulfonates in the Riverside fog. Direct measurements of HMSA in some samples indicated the presence of HMSA. The disparity between free CH_2O (DNPH measurement, Table 6.4) and total CH_2O (Nash measurement, Table 6.3) implies the presence of HMSA. Thirdly, the apparent coexistence of S(IV) with peroxide suggests that the S(IV) was present as the sulfonate [Munger et al., 1984]. HMSA was observed in the January 23 samples at 50 – 100 μM levels, and in the first sample from February 28 at 160 μ**M**. Unfortunately the HMSA concentration in the remaining samples, which had higher H_2O_2, could not be determined because of interferences.

Because the kinetics of sulfonate formation are slow compared to the reaction of S(IV) with H_2O_2 [Boyce and Hoffmann, 1984; Deister et al., 1986, Kok et al., 1986] the sulfonates probably formed prior to their scavenging by the fog. Although the dicarbonyls found in these samples could also react with S(IV) to form the corresponding sulfonates [Betterton and Hoffmann, 1987; Olson and Hoffmann, 1988] it is not clear whether they were present as sulfonates.

The physical and chemical processes that drive the observed concentration changes are horizontal advection, vertical mixing (by turbulence), deposition, emission, and chemical reaction. These processes can be represented in differential form by equation (6),

$$\frac{dC_i}{dt} - \vec{u}\cdot\nabla C_i = \kappa\frac{dC_i}{dz} + \frac{E}{H} - \frac{C_i V_{d,i}}{H} + R_i \tag{6}$$

where C_i is the concentration of species i, $\vec{u}$ is the horizontal wind vector, κ is the turbulent eddy diffusion coefficient, E is the emission flux, H is the height of the mixed layer, $V_{d,i}$ is the species dependent deposition velocity, and R_i is the net reaction rate ($R_i = \Sigma k_j C_j - k_i C_i$, where k_j and C_j are the pseudo–first order rate constants and the reactants that form species i, and k_i is the pseudo–first order rate constant for destruction of species i). Diffusion is neglected from equation (6) because it is small relative to the other terms. All the phases that a species can exist in must be considered together. Clearly this becomes a very complex system of equations even when one considers only the major species found in the fog (NH_4^+, H^+, NO_3^-, SO_4^{2-}) and their precursors. Equation 6 is presented here as a guide to evaluating the observed compositional changes, rather than as an equation to be solved.

This equation can be used to establish some bounds on the magnitude of the advection and source terms for N(–III) and N(V). This analysis is simplified for N(–III) and N(V) because $R = 0$ for N(–III) and $E = 0$ for N(V). During periods with constant concentration, the net transport equals the difference between deposition and emission (or atmospheric reaction). For sampling intervals on Jan. 22 and again on Mar. 1 the aerosol NO_3^- concentration was constant at about 2000 neq m^{-3}. Assuming a deposition velocity of 0.1 cm s^{-1} [Waldman and Hoffmann, 1987] the change in concentration due to deposition would range from 18 – 36 nmole hr^{-1} for mixing heights of 200 to 400 m. In fog, however, with an assumed deposition velocity of 1 cm s^{-1} (a lower limit reported by Waldman and Hoffmann [1987] for San Joaquin Valley fog) and a scavenging fraction = 0.5 the deposition term would increase to 180 nmole hr^{-1} for a 200 m mixing height. For an NH_4^+ concentration of 3000 neq m^{-3} the deposition term would be 27 – 54 neq m^{-3} in the absence of fog for the same mixing heights. Assuming a deposition velocity of 1 cm s^{-1} for NH_3 gives values of 90 – 180 nmole hr^{-1} for a 1000 nmole m^{-3} concentration. As was predicted for N(V), N(–III) deposition is enhanced by the formation of fog, which scavenges the NH_4^+ aerosol and deposits it at a faster rate.

Impact of Development

Because the eastern SCAB is undergoing rapid development, which is likely to force the abandonment of dairy farming in the Chino area, it is important to consider the effect on fogwater chemistry of reduced NH_3 inputs. In order to evaluate the role of fog formation, dry deposition, and changes in emissions we constructed a simple box model of the Riverside basin. It is not sufficient to merely subtract the NH_4^+ and NH_3 from the present results to predict the effect of reduced NH_3 emissions because changes in the N(V) speciation, which is partly dependent on the concentration of N(–III), will have a pronounced effect on its fate. The model is described by the following rate expression:

$$\frac{dC_i}{dt} = \frac{E_i}{H} + P_i - \frac{(\alpha_f \cdot C_i \cdot v_d^f + \alpha_a \cdot C_i \cdot v_d^a + \alpha_g \cdot C_i \cdot v_d^g)}{H} - \frac{C_i}{\tau_f} \qquad (7)$$

which is derived from equation 6 by approximating the advection and vertical mixing term as a first order dilution described by the inverse of the flushing time, τ_f. Integration was performed using a 4th–order Runge–Kutta method. The coefficients α_f, α_g, and α_a are the fractions present as fog, gas and aerosol, respectively. The corresponding v_d^i are the deposition velocities associated with each phase.

The model is allowed to run for a 2 day period from midnight to midnight. The initial conditions, deposition velocities, production and emission terms are listed in Table 6.8. At each time step the species are partitioned into aerosol and gas phases by an acid–base balance. Because either NH_3 or HNO_3 is usually in a large excess it is not necessary to explicitly include the dissociation of NH_4NO_3. Fog is formed between 0200 and 1000, and is assumed to scavenge half the aerosol and 100% of any gas present. This is valid for HNO_3 at all expected pH values and for NH_3 in acidic fog. During the period 2000 to 0800 the NH_3 source is shut off (wind reversal) and the dilution term is included. 10% of the base case was chosen for the low ammonia case because the elimination of dairy production would cut the NH_3 emissions drastically, but probably not eliminate them completely.

Although the results of the simulation (Fig. 6.11) do not exactly mimic the Riverside observations (and were not intended to) they are qualitatively similar and show a comparable range of concentration. The depletion of NH_3 by nighttime production of HNO_3 is exaggerated in the simulation. The effect of fog is to slightly enhance the deposition of NH_4NO_3 aerosol. When NH_3 emissions are decreased both N(–III) and N(V) are less than the base case (Fig. 6.12). However, nearly all the N(V) is present as HNO_3 giving a highly acid atmosphere. A balance between production of HNO_3 and its rapid dry deposition leads quickly to a steady state concentration around 1000 neq m^{-3}. A 0.1 g m^{-3} fog forming in the low NH_3 case would be uniformly acidic ($pH \simeq 2$) whereas the same fog in the base case would only approach pH 2 towards the end of the event. The variable pH levels that were observed in the fog are simulated by the base case. Without the NH_3 source the model predicts uniform acidity, unlike the present situation with highly variable fogwater acidity. Any portion of the basin that is influenced by advection from Los Angeles is likely to have acid fogwater.

Acknowledgements

This work was supported by the California Air Resources Board, Contract # A4–075–32. We thank R. Musselman of UC Riverside for permission to sample at UC Riverside.

Table 6.8 Simulation conditions

Initial Concentrations

S(VI)	750 neq m^{-3}
N(–III)	2000 neq m^{-3}
N(V)	1000 neq m^{-3}

Deposition Velocities

Aerosol $v_d{}^a =$ 0.1 cm s^{-1}
Gas $v_d{}^g =$ 1.0 cm s^{-1}
Fog $v_d{}^f =$ 1.0 cm s^{-1}

Inputs

$P =$ $NO_x \longrightarrow HNO_3$ 5.3×10^{-11} mole m^{-3} s^{-1}
$E =$ F_{NH_3} 4.0×10^{-8} mole m^{-2} s^{-1}

Mixing Height $H = 250$ m
Flushing time $\tau = 12$ hr

For Low NH_3 case, all conditions are the same except $F_{NH_3} = 0.1 \cdot F^0_{NH_3}$

A) Simulation Results : Base Case – with fog

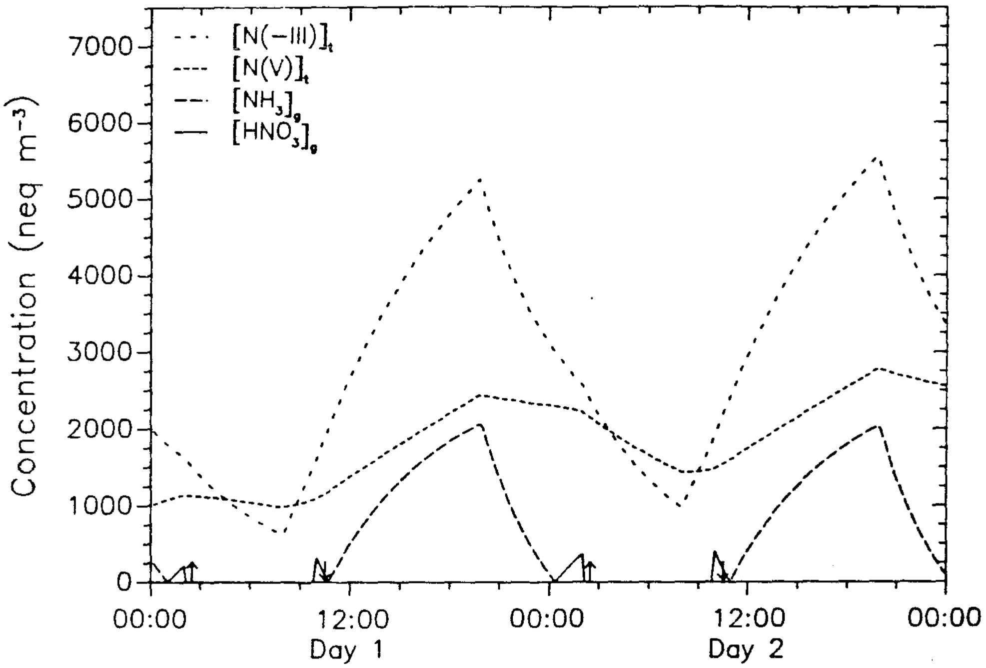

B) Simulation Results : Base Case – No fog

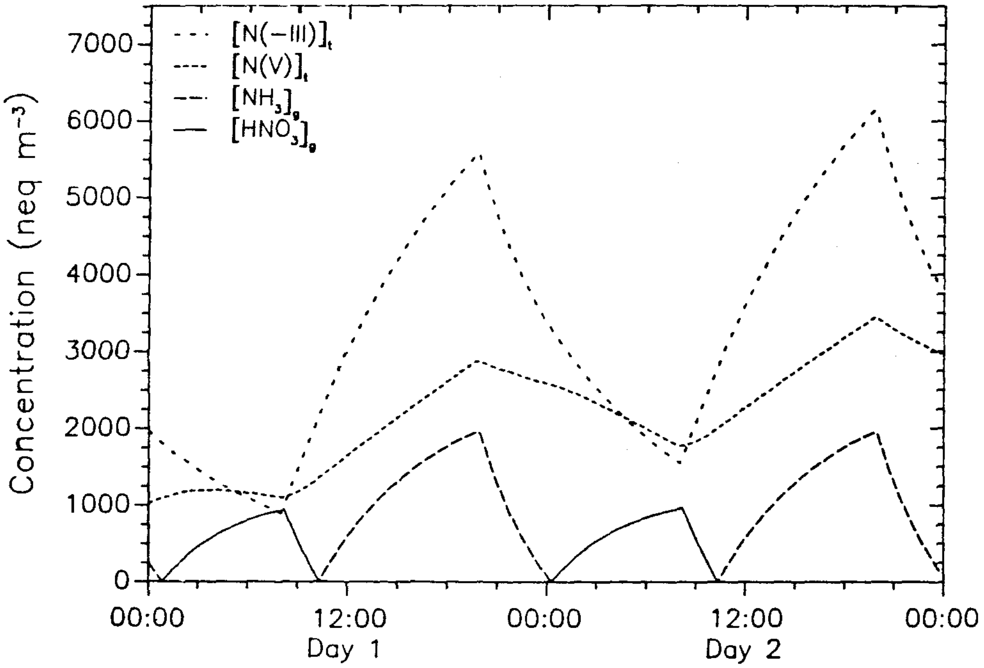

Figure 6.11. Simulation of fog and aerosol chemistry in the Riverside area. Panels A and B are with and without fog. The start and end of a fog event are indicated by ↑ and ↓.

A) Low NH_3 Case – with Fog

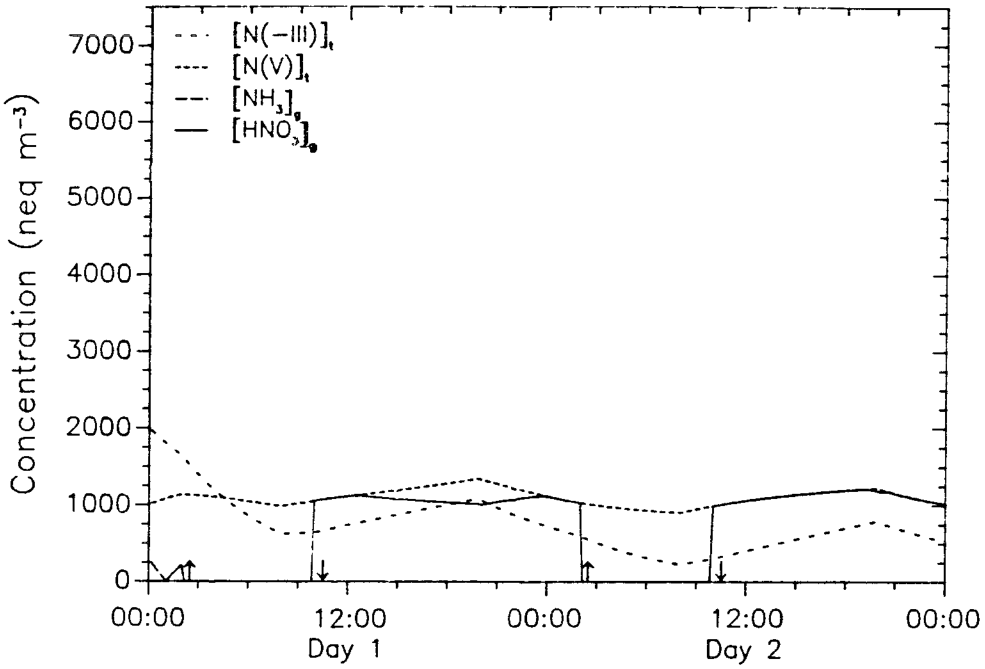

B) Low NH_3 Case – No Fog

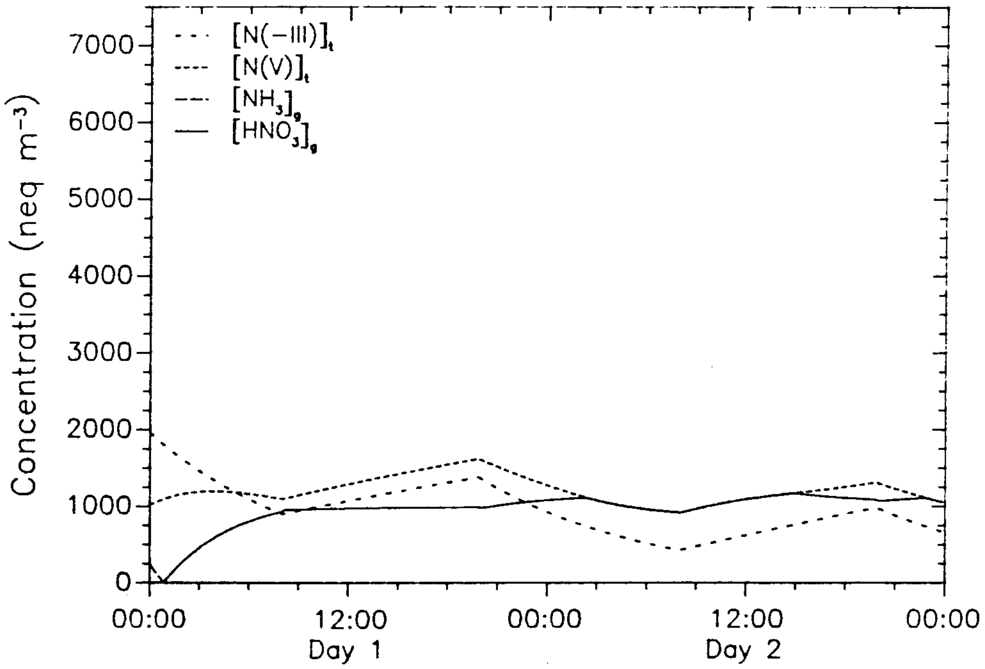

Figure 6.12. Simulation of fog and aerosol chemistry in the Riverside area under low NH_3 emissions. Panels A and B are with and without fog. The start and end of a fog event are indicated by ↑ and ↓.

References

Betterton, E. A. and Hoffmann, M. R. (1987) The kinetics, mechanism, and thermodynamics of the reversible reaction of methylglyoxal (CH_3COCHO) with S(IV). *J. Phys. Chem.* **91**, 3011–3020.

Betterton, E. A., Erel, Y, and Hoffmann, M. R. (1988) Aldehyde–bisulfite adducts: Prediction of some of their thermodynamic and kinetic properties. *Environ. Sci. Technol.* **22**, 92–99.

Boyce, S. D. and Hoffmann, M. R. (1984) Kinetics and mechanisms of the formation of hydroxymethanesulfonic acid a low pH. *J. Phys. Chem.* **88**, 4740–46.

Collett, J., Jr., Daube, B. C., Jr., Munger, J. W., and Hoffmann, M. R. (1989) Cloudwater chemistry in Sequoia National Park. *Atmos. Environ.* in press.

Dasgupta, P. K. (1981) Determination of atmospheric sulfur dioxide without tetrachloromercurate(II): Further refinements of a pararosaniline method and a field application. *J. Air Pollut. Cont. Assoc.* **31**, 779–782.

Dasgupta, P. K., DeCesare, K. and Ullrey, J. C. (1980) Determination of atmospheric sulfur dioxide without tetrachloromercurate (II) and the mechanism of the Schiff reaction. *Anal. Chem.* **52**, 1912–1922.

Dasgupta, P. K. and Yang, H.–C. (1986) Trace determination of aqueous sulfite, sulfide and methanethiolate by flourimetric flow injection analysis. *Anal. Chem.* **58**, 2839–2844.

Daube, B. C., Jr., Flagan, R. C., and Hoffmann, M. R. (1986) *Active Cloudwater Collector* United States Patent #4,697,462 Oct.6, 1987.

Deister, U., Neeb, R., Helas, G. and Warneck, P. (1986) Temperature dependence of the equilibrium $CH_2(OH)_2 + HSO_3^- = CH_2(OH)SO_3^- + H_2O$ in aqueous solution. J. *Phys. Chem.* **90**. 3213–3217.

Dong, S. and Dasgupta, P. K (1987) Fast flourimetric flow injection analysis of formaldehye in atmospheric water. *Environ. Sci. Technol.* **21**. 581–588.

Grosjean, D. (1982) Formaldehyde and other carbonyls in Los Angeles ambient air. *Environ. Sci. Technol.* **16**, 254–262.

Grosjean, D. and Wright, B. (1983) Carbonyls in urban fog, ice fog, cloudwater and rainwater. *Atmos. Environ.* **17**, 2093–2096.

Hering, S. V. et al. (1986) Field comparison of measurement methods for nitric acid, ARB Final Report #A4–164–32, California Air Resources Board, Sacramento, CA.

Hoggan, M., Davidson, A., and Shikiya, D. (1980) Seasonal and diurnal variation in air quality in California's South Coast Air Basin, South Coast Air Quality Management District, El Monte, CA. 103 pp.

Jacob, D. J., Munger, J. W., Waldman, J. M., and Hoffmann, M. R. (1986) The H_2SO_4–HNO_3–NH_3 system at high humidities and in fogs: I. Spatial and temporal terns in the San Joaquin Valley of California, *J. Geophys. Res* **91**, 1073–1088.

Kawamura, K., Steinberg, S. and Kaplan, I. R. (1985) Capillary GC determination of short–chain acids in rain, fog and mist. *Intern. J. Environ. Anal. Chem.* **19**, 175–188.

Kok, G. L., Gitlin, S., N., and Lazrus, A. L. (1986) Kinetics of the formation and decomposition of hydroxymethanesulfonate. *J. Geophys. Res.* **91**, 2801–2804.

Keene, W. C., Talbot, R. W., Andreae, M. O., Beecher, K. Berresheim, J., Castro, M., Farmer., J. C., Galloway, J. N., Hoffmann, M. R., Li, S.–M., Maben, J. R., Munger, J. W., Norton, R. B., Pszenny, A. A. A. P., and Puxbaum, H. (1988) An intercomparison of measurement systems for vapor and particulate phase concentrations of formic and acetic acids, *J. Geophys Res.* (submitted)

Lazrus, A., Kok, G. L., Gitlin, S. N., Lind, J. A., and McLaren, S. E. (1985) Automated flourometric method for hydrogen peroxide in atmospheric precipitation. Anal. *Chem.* **57**, 917–922.

Marsh, S. L., Jr. and Bergman, L. D. (1984) Meteorological factors influencing the acidity of fog in the Los Angeles Basin, Presentation at 77th Annual meeting of the Air Poll. Cont Assoc., San Francisco, CA, June 24–29, 1984.

Munger, J. W., Jacob, D. J., Waldman, J. M., and Hoffmann, M. R. (1983) Fogwater chemistry in an urban atmosphere. *J. Geophys. Res.* **88,** 5109–5121.

Munger, J. W., Jacob, D. J., and Hoffmann, M. R. (1984) The occurrence of bisulfite–aldehyde adducts in fog- and cloudwater. *J. Atmos. Chem.* **1,** 335–350.

Munger, J. W., Tiller, C. T., and Hoffmann, M. R. (1986) Determination of hydroxymethanesulfonate in fog water. *Science* **231,** 247–249.

Munger, J. W., Collett, J., Jr., Daube, B. C., Jr., and Hoffmann, M. R. (1988) Chemical composition of nocturnal marine stratus clouds along the Southern California coast. (in prep)

Nash, T. (1953) The colorimetric estimation of formaldehyde by means of the Hantszch reaction, *Biochem. J.* **55**, 416–421.

Olson, T. M. and Hoffmann, M. R. (1988) The kinetics, mechanism and thermodynamics of glyoxal–S(IV) adduct formation, *J. Phys. Chem.* **92** 533–540.

Pruppacher, H. R. and Klett, J. D. (1978) *Microphysics of clouds and precipitation*, pp. 139–140. D. Reidel, Dordrecht.

Reitz, E. B. (1980) The Stabilization of small concentrations of formaldehyde in aqueous solutions. *Anal. Lett.* **13**, 1073–1084.

Russell, A. G. and Cass, G. R. (1984) Acquisition of regional air quality model validation data for nitrate, sulfate, ammonium ion and their precursors. *Atmos. Environ.* **18**, 1815–1827.

Russell, A. G. and Cass, G. R. (1986) Verification of a mathematical model for aerosol nitrate and nitric acid formation and its use for control measure evaluation. *Atmos. Environ.* **20**, 2011–2025.

Russell, A. G., McRae, G. J., and Cass, G. R. (1985) The dynamics of nitric acid production and the fate of nitrogen oxides. *Atmos. Environ.* **19**, 893–903.

Schwartz, S. E. and Freiberg, J. E. (1981) Mass–transport limitation to the rate of reaction of gases in liquid droplets: Application to oxidation of SO_2 in aqueous solutions. *Atmos. Environ.* **15**, 1129–1144.

Smith, R. V., and Erhardt, P. W. (1975) Nash determination for formaldehyde in the presence of bisulfite. *Anal. Chem.* **47**, 2462–2454.

Steinberg, S. and Kaplan, I. R. (1984) The determination of low molecular weight aldehydes in rain, fog, and mist by reversed phase liquid chromatography of the 2,4–dinitrophenyl hydrazone derivatives. *Intern. J. Environ. Anal. Chem.* **18**, 253–266.

ten Brink, H. M., Schwartz, S. E., And Daum, P. H. (1987) Efficient Scavenging of aerosol sulfate by liquid–water clouds. *Atmos. Environ.*

Waldman, J. M. and Hoffmann, M. R. (1987) Depositional aspects of pollutant behavior in fog and intercepted clouds in *Sources and Fates of Aquatic Pollutants.* Advances in Chemistry Series **216**, 80–129.

CHAPTER 7

CHEMICAL COMPOSITION OF INTERCEPTED STRATUS CLOUD ALONG THE SANTA BARBARA CHANNEL COAST

ABSTRACT

Marine stratus clouds are frequent along the Santa Barbara Channel Coast of southern California. These clouds form at the top of an inversion–capped mixed layer. The chemical composition of clouds and precursor aerosol was investigated at elevated sites during the summers of 1985 and 1986. The airmass over the Channel has an excess of acidity. Concentrations of excess sulfate and total nitrate (NO_3^- + HNO_3) are typically 100 – 200 neq m^{-3}. Sulfate and nitrate concentrations over 1000 μN are observed in cloudwater samples. Cloudwater pH is usually less than 4. The excess acidity in the atmosphere effectively removes Cl^-, from sea–salt aerosol. Most of the chloride is rescavenged by clouds at night, however. Concentrations of acids at a site above the inversion base were as high or higher than at lower elevations. Apparent sources of acidity in the Channel area are oxidation of local emissions from urban centers and offshore oil platforms and transport from Los Angeles.

INTRODUCTION

Stratiform clouds are prevalent along the eastern coasts of the subtropical oceans. The combination of a temperature inversion induced by subsidence about quasi–stationary high pressure systems and cold sea surface temperatures, due to upwelling, is conducive to the formation of stratus and stratocumulus clouds. In addition to their influence on local climate, these stratiform clouds influence global climate and circulation because of their large areal extent. Stratus clouds process aerosol, but do not usually remove it via precipitation, thus they will influence aerosol properties.

The summertime weather at the California coast typifies these conditions. A persistent High is located over the eastern Pacific. High temperatures over the inland deserts in California and Arizona generate a region of low pressure. Northerly winds result from this pressure gradient. Subsidence about the High leads to a temperature inversion. Calculations of divergence and vertical motion (Nieburger et al., 1961) indicate that subsidence should depress the inversion. Convective mixing at the surface offsets the vertical motion, however, preventing the inversion from being pushed to the surface. The average height of the summertime inversion base along the Southern California coast is 400 – 600 m. The inversion is lowest at the coastline and slopes upward away from the coast in either direction (Neiburger et al, 1961).

The radiation, dynamic, and thermodynamic structure of the marine stratocumulus have been studied extensively off the coast of California (Allbrecht et al., 1985; Brost et al, 1982a;b; Mahrt and Paumier, 1982) to validate models of stratocumulus dynamics. Cloud–topped boundary layers are unique in that their mixing is frequently driven by radiative cooling at the top of the layer (Randall, 1980a,b; Deardroff, 1976, 1981), rather than by heating at the surface. Cool air at the cloud top tends to sink. Dry air from above the cloud is pulled in behind the descending air parcel. This process is termed entrainment. Additional cooling is caused by evaporation of droplets when dry air is mixed into the cloud. Quantification of the heat and moisture fluxes, and entrainment rates has been a major goal of the aforementioned research.

The chemistry of the marine layer and associated stratus clouds along the California coast is also of considerable interest. Dynamics and microphysics play a major role in determining cloud chemical composition. Conversely, cloud microphysics may be influenced by the chemical composition of the air mass. Cloudwater concentrations of species that are formed or transported above the inversion base are increased by entrainment. Conversely, cloudwater concentrations of species that are absent above the inversion are reduced by entrainment.

Because ventilation is limited by the temperature inversion and recirculation associated with the land/sea breeze cycle, pollutant concentrations may build up along the coast. Coastal cloudwater may be prone to acidification because sources of atmospheric alkalinity are limited (Jacob et al., 1985). The Santa Barbara Channel is of special interest in this regard because it is subject to frequent clouds, the coastal plain is undergoing rapid urban development, and there is pressure to accelerate exploration and utilization of offshore oil resources in the Channel.

During the summers of 1985 and 1986 we undertook a study of cloudwater and aerosol composition at several sites along the Santa Barbara Channel coast. The goals of this study were to determine the acid/base status of the Santa Barbara Channel air mass and observe chemical and physical mechanisms that control the chemical composition of coastal stratus clouds.

METHODS

Sampling Sites

The sampling sites used in this study are indicated in Figure 7.1, a map of the Santa Barbara Channel area. Two sites, La Jolla Peak (LJ) and Casitas Pass (CP), were used during the summer of 1985. La Jolla Peak (elev. 475 m)is located 3.4 km inland from the coast near Point Mugu, at the southeastern end of the Channel. The site, used as a Federal Aviation Administration airway beacon, was on the SE side of the hill, facing a valley; a row of 300 m high hills at the coastline separated it from the ocean. The immediate surroundings were covered by undisturbed grass and shrub. Samples were collected from the roof of a one story building, just below the top of the peak.

The Casitas Pass site was located at an Air Quality Monitoring station operated by the California Air Resources Board. The site was at a saddle point (elev. ≈ 300 m) at the head of a valley extending west toward the ocean, about 7 km away. The surroundings were avocado and citrus groves (below the pass) and chaparral or oak forest (the hillsides above the pass to the north and south). The site had excellent exposure to the west, but a water tank and the crest of the pass restricted the exposure from the east side of the pass. The sampling equipment was placed at ground level in the center of a gravel–covered clearing.

Four sites, Laguna Peak, Ventura, Casitas Pass, and El Capitan, were used during the summer of 1986 (see Fig. 7.1). The same site was used at Casitas Pass. The La Jolla Peak site was moved to Laguna Peak about 1.6 km SW at an elevation of 450 m. Laguna Peak is 2 km from the ocean, with no intervening hills. The site was located at a U. S. Navy communication and tracking facility, its surroundings were shrub and grass. The sampling equipment, a cloudwater collector and aerosol filter pack, were positioned on the roof of a building, about 5 m above the ground. A secondary site, used for cloudwater collection only, was located on the west side of Laguna Peak at an elevation of ≈ 240 m, 0.5 km from the summit. The stand for the cloudwater collector was placed on the ground on a level grassy area. The collector was operated on 12 V battery power at this site. These sites are referred to as Laguna Peak (LP) and Laguna Road (LR), respectively.

Two sites were used in Ventura. At Emma Wood State Beach (referred to as Beach site or EW) aerosol and gas samples only were collected on the roof of an air quality monitoring station operated by the Ventura County Air Pollution Control Department (APCD). The site was within 200 m of the beach. A major highway ran within 100 m of the site on the landward side and a railroad track passed between the sampling site and the beach. The second site in Ventura (referred to as Hill site or TV) was at a cable TV receiving station on a hill about 2.4 km ENE of Emma Wood (elev. 170 m). Its immediate surroundings were mostly undeveloped grass or tree covered hillsides. The cloudwater and aerosol samplers used at the Hill site were positioned on the roof of a one story building at the edge of the hill.

The El Capitan site was at an air quality monitoring station operated by the Santa Barbara County APCD. It was located in a State Park campground on a bluff immediately above the beach. Only aerosol and gas samples were collected there.

Collection Methods

Cloudwater samples during 1985 were collected with a Rotating Arm Collector (RAC), described in Jacob et al., (1984). Droplets are collected by inertial impaction in slots in a teflon coated steel rod and accumulated in polyethylene bottles attached to the ends of the rod. The RAC is mounted on a stand 1.4 m above the ground. At the La Jolla Peak site in 1985 and all sites in 1986 cloudwater was collected with the Caltech Active Strand Cloudwater Collector (CASC) (Daube et al., 1987). In operation, the CASC is mounted on a 2 m high stand. A fan draws air at 9 m s^{-1} across a bank of inclined teflon strands, which collect droplets by impaction. Gravity and aerodynamic drag propel the droplets down the strands where they accumulate in a teflon trough and drain to a collection bottle. The CASC has a theoretical 50% lower droplet–size cut of 3.5 μm (diameter), whereas the RAC appears to have a size cut near 20 μm, based on a scale model calibration (Jacob et al., 1984). Collett et al. (1989) observed in a comparison of the two collectors that samples from the RAC were enhanced in sea salt and soil dust-derived species which are predominantly present in coarse aerosol (Seinfeld, 1986). The CASC appeared to collect a more representative sample of the entire cloud droplet spectrum. A comparison of sample collection rates gave no evidence of increased evaporation on the CASC, despite the longer residence time of droplets on the strands. Because the CASC collects smaller droplets more efficiently and has a significantly higher collection rate, it sampled thin clouds more effectively.

The collection surfaces were thoroughly rinsed with distilled water before and after sampling. The samplers were kept covered when not in use to minimize contamination by dust. The first 15 minutes of sample were discarded to avoid inclusion of residual rinse water, and allow the collection surface to equilibrate with the ambient cloudwater.

Aerosol and selected gaseous compounds were collected using filter pack methods. An automatic timer was used to control the filter pack during 1986 so three samples could be obtained without operator attention. Open–faced Teflon filters (Gelman Zeflour, 1 μm pore size) were used to collect aerosol for inorganic analysis. Nitric acid was collected on a Nylon filter (Gelman Nylasorb) placed behind one Teflon filter. Ammonia was collected on an oxalic acid–impregnated glass fiber filter behind another Teflon filter. Flow rates through the filters were controlled by critical orifices, which were periodically checked with a calibrated rotameter. A rain shield above the filters excluded sedimenting droplets and large debris. Sampling the total aerosol, which includes droplets and residual aerosol, during cloud events presents special problems. In windy conditions droplet collection may be enhanced or diminished depending on the orientation of the filter. We observed non–uniform coverage by droplets on the filters during cloudy periods. Filter pack methods are recognized to produce artifacts by volatilization of collected aerosol (Appel et al., 1979; Spicer and Schumacher, 1979). We attempted to minimize this problem by using short sampling intervals and avoiding sampling during periods of rapid temperature change.

Analytical Methods

Immediately after the end of a collection interval the sample was weighed to determine its volume, and an aliquot was removed to determine its pH using a Radiometer PHM80 meter and a combination electrode (Radiometer GK2320C). The meter was calibrated using pH 4 and 7 buffers. Additional aliquots were removed from the sample and treated to preserve unstable species. S(IV) was preserved as hydroxymethanesulfonate by adding buffered CH_2O (Dasgupta et al., 1980). CH_2O was reacted with NH_4^+–acetylacetone (Nash, 1953) to form 3,5-diacetyl-1,4-dilutidine (DDL), which is stable for weeks (Reitz, 1980). A buffered solution of p–OH phenylacetic acid (POPA) and peroxidase was used to preserve peroxides (H_2O_2 and ROOH) (Lazrus et al., 1985) by formation of the dimer. Carboxylic acids were preserved from bacterial decomposition by addition of $CHCl_3$ to an aliquot of sample (Keene and Galloway, 1984). Carbonyls were derivatized with 2,4–dinitrophenylhydrazine in acidic solution (Grosjean and Wright, 1983). The samples and preserved aliquots were stored at 4° C until analysis.

The samples were analyzed by the same methods used previously (Munger et al., 1983; Jacob et al., 1986). A brief summary of the analytical methods follows. Additional details are given in Appendix A. Anions were determined by ion chromatography, metal cations were determined by atomic absorption spectrometry, and NH_4^+ was determined by colorimetric, flow–injection analysis. The stabilized CH_2O was determined spectrophotometrically at 412 nm. I_2 was added to eliminate interference by S(IV) (Smith and Erhardt, 1975). The CH_2O determined by the Nash method is total CH_2O; recovery of $NaCH_2OHSO_3$ standards was 90 – 100% compared to CH_2O. The preserved S(IV) was determined by the pararosaniline method (Dasgupta, 1981) adapted for use with a flow injection analyzer. This method determines total S(IV); standards prepared from Na_2SO_3 or $NaCH_2OHSO_3$ gave comparable responses. Peroxide was determined from the fluorescence of POPA dimer (Lazrus et al., 1985) The method is sensitive to H_2O_2 and some organic peroxides, however, because they have significantly lower Henry's Law coefficients, CH_3COOH and peroxoacetic acid are unlikely to be important in cloudwater (Lazrus et al., 1985). Carboxylic acids were determined by ion exclusion chromatography, with a 2.5 m**M** HCl eluent, and in parallel by normal ion chromatography, with a 5 m**M** $Na_2B_4O_7$ eluent. The derivatized carbonyls were extracted in CH_2Cl_2/C_6H_{14} and determined by reverse phase HPLC using a C18 column and aqueous CH_3CN/THF (tetrahydrofuran) eluent. The aldehydes and ketones were monitored at 365 nm; the analysis was repeated at 430 nm to identify dicarbonyl compounds, which have an absorbance peak at a higher wavelength.

The inorganic ions on the Teflon filters were extracted by shaking with H_2O (Corning Megapure) after wetting the filter with 200 μl of CH_3CH_2OH. The oxalic acid–impregnated filters were extracted in H_2O. The nylon filters were extracted in HCO_3^-/CO_3^{2-} solution (IC eluent). The filter extracts were analyzed by the same methods as the cloudwater samples with the exception that the buffer strength of the NH_4^+ reagents was adjusted to account for the presence of oxalic acid in the filter extract. Reported inorganic aerosol concentrations are the average of results from two separate filters.

RESULTS

Meteorology and Sampling Conditions

1985

During the summer of 1985 the La Jolla Peak site was operated from July 23 to September 18. Sampling at Casitas Pass did not begin until August 7. The stratus layer was often below the sites. Extended cloud interception events occurred at La Jolla Peak on the mornings of July 24 – 26 and on August 21. Brief cloud episodes were also sampled on the mornings of July 30, September 4 and September 17. The cloud event on July 24 was discontinuous; the stratus layer dropped after 2 hours of sampling and then lifted again after sunrise. Cloud interception was continuous the following night from 2230 until 0820. Interception was continuous the morning of July 26, but the cloud top was just above the site.

Temperature profiles measured at Pt. Mugu for the period August 4–6, 1986, which are representative of the profiles on other cloudy days, are shown in Figure 7.2. Profiles for the other sampling days are given in Appendix B. The inversion base, which is generally coincident with the cloud top, was at a maximum height near sunrise. During the day the inversion base dropped, with a concomitant heating of the inversion layer. The mixed layer also warmed slightly due to surface heating. The inversion base was highest on the morning of July 25, 1985, which was the most extensive cloud event at La Jolla Peak. Clouds briefly covered the site on the morning of July 30, but did not rise much past the top of the peak. Cloud was present below La Jolla Peak on August 20, when there was a weak surface–based temperature inversion. Over the course of the day a more pronounced inversion developed at 300 – 500 m. Stratus formed the following night and rose well above the level of La Jolla Peak. The peak was in cloud from 0000 to 0800. The cloud events on September 4 and 17 were thin and did not yield large sample volumes. Both ended before sunrise.

Intercepted clouds were sampled at Casitas Pass on the mornings of August 7, 8, 9. The site was near the top of the stratus layer on August 7 and 8; samples were collected intermittently as the cloud top moved up and down. Clouds moved back and forth between the two valleys on either side of Casitas Pass as the height of the inversion base oscillated. After sunrise on August 8 and 9 the cloud top rose well above the pass, as surface heating induced upslope winds and pushed the cloud layer upward. The largest sample volumes, which are proportional to cloud liquid water content (LWC), were obtained during an extended interception event on August 8. Even though Casitas Pass (elev. 300 m) appeared to be near the inversion base, based on cloud top observations, temperature profiles from Point Mugu for the period Aug 6 – 9 show that the inversion base exceeded 500 m each morning. Clouds were present at La Jolla Peak on the morning of August 9, but was not sampled.

1986

The summer of 1986 was noted for the frequency and persistence of the nocturnal marine stratus clouds. Clouds formed nearly every night for several weeks in July and August. Three or four day periods during three consecutive weeks were selected for intensive study. The presence of clouds at the four sampling sites and the height of the inversion base at Pt. Mugu during these periods is indicated in Figure 7.3. The temperature profiles for these periods (see Figure 7.2 and Appendix B) indicate the presence of a strong and very persistent temperature inversion. As in 1985, a diurnal cycle was observed in the height of the inversion base. At Laguna Peak sampling began at the lower site (LR). When the cloud rose above that site, sampling continued at the summit (LP). Initial samples at Laguna Peak were collected near the top of the cloud. Later samples are from the interior of the stratus layer.

The wind direction profiles at Point Mugu for the period August 4 – 6, 1986, are shown in Figure 7.4. Profiles for the other intensive sampling periods (see Appendix B) were similar. In the mixed layer, winds were controlled by the diurnally varying sea/land breeze. Westerly winds predominated in the afternoon; the direction of nighttime wind was variable. The wind in the inversion layer frequently had an easterly component, and was usually different from the surface wind. Westerly winds dominated above the inversion layer, where the flow was controlled by circulation around the Pacific High.

Chemical Composition

Aerosol

The average and range of concentrations for aerosol components are presented in Table 7.1 for day and nighttime aerosol samples collected at each site during 1985 and 1986. Concentrations are not adjusted for changes in pressure with elevation in order to allow direct comparison of cloudwater and aerosol loadings. The pressure correction term would be 1.06 at the highest sites, Laguna and La Jolla Peaks. Complete results are presented in Appendix B. Because the number of samples was small and the variability in concentration high, none of the differences between day and night were statistically significant. Consistent with the proximity to the ocean, Na^+ was a major component of the aerosol. The Na^+ concentration decreased away from the coastline. Except at the two sites adjacent to the beach (El Capitan and Emma Wood), the concentration of Cl^- was less than expected if all the Na^+ was due to sea salt. The magnitude of the apparent Cl^- deficiency was less at night than in the day. In addition to the sea salt, SO_4^{2-}, NO_3^-, and NH_4^+ had appreciable concentrations. Gaseous HNO_3 and NH_3 were major contributors to the total N(V) and N(–III) concentration. Most of the SO_4^{2-} observed in these samples was "non–sea salt" or "excess" SO_4^{2-} ($SO_{4\,xs}^{2-}$). Even at the two coastal sites sampled in 1986, the fraction of $SO_{4\,xs}^{2-}$ exceeded 60%. In 1985 the N(V) concentration exceeded that of $SO_{4\,xs}^{2-}$ at both sites. In 1986, however, neither species was clearly dominant. There was a tendency at Laguna Peak, Ventura, and Casitas Pass for $SO_{4\,xs}^{2-}$ to be higher in the day and N(V) to dominate at night.

Concentrations of $SO_{4\,xs}^{2-}$ and N(V) tended to be higher at Laguna or La Jolla Peaks than at the other sites. The other sites all had similar concentrations. When the day and nighttime means were compared to one another, the only statistically significant differences were higher concentrations of Na^+, Cl^-, and Mg^{2+} (sea salt) at El Capitan than at all other sites and higher HNO_3 at Laguna Peak than at El Capitan during the day.

Cloudwater Composition

The average chemical composition and range of values is given in Tables 7.2–7.8 for each cloud event sampled during the study. The ion balance, $\Sigma A^-/\Sigma M^+$ ($\Sigma A^- = [Cl^-] + [NO_3^-] + [SO_4^{2-}]$, $\Sigma M^+ = [H^+] + [NH_4^+] + [Na^+] + [Ca^{2+}] + [Mg^{2+}]$) {$K^+$ was excluded because it was insignificant relative to the other cations}, and liquid water content (LWC) estimated from collection rate are also given. The times listed are the period during which cloud was present at the site. Complete results are presented elsewhere (Munger, 1989 Appendix B).

Calculated ion balances indicated that a number of the 1985 La Jolla Peak samples had analytical errors. We suspect that the pH readings made at the time were erroneously low. The pH of the suspect samples was ≈ 0.5 units less than the preceding samples, but other ions had not changed dramatically. The average, minimum and maximum values reported for pH are based on a calculated pH for samples that had $\Sigma A^-/\Sigma M^+ < 0.6$, and on measured pH for all other samples.

Corrected pH was determined from the difference between measured cations (excluding H^+) and anions. The average based on corrected values is 0.1 – 0.3 units higher than the average of the measured values, which is consistent with the apparent pH discrepancy.

Cloudwater collected in this study was consistently acidic; Figures 7.5 and 7.6 present the pH distribution for the two sampling years. H^+, Na^+, NH_4^+, Cl^-, NO_3^-, and SO_4^{2-} were the other major ions in the cloudwater. Only a few samples had S(IV) concentrations above the detection limit of 1 μ**M**. CH_2O concentrations ranged from 10 – 50 μ**M**, with average values closer to 10 μ**M**. Most samples had <20 μ**M** H_2O_2. Formic (HCOOH) and acetic (CH_3COOH) acid were only measured in 1986. At the pH levels in the cloudwater most of the acid will be present in the protonated form; the measured values are total concentrations. For convenience these species are expressed as the acid. Except for one sample with 173 μ**M** CH_3COOH, which was probably contaminated, HCOOH consistently exceeded CH_3COOH.

Table 7.9 presents the concentrations of all the organic species determined in a series of samples for which carbonyls were measured. Formic acid was the dominant organic species. However, acetaldehyde (CH_3CHO) was found to exceed CH_2O. This is surprising because the solubility of CH_3CHO is three orders of magnitude less than that of CH_2O; thus it should be of much less importance than CH_2O in the aqueous phase for typical observed gas–phase concentrations. The possibility that the CH_3CHO peak is misidentified cannot be excluded. Acetic acid, glyoxal, (CHOCHO), and methylglyoxal, ($CH_3C(O)CHO$) were also found to be important. Other carboxylic acids and carbonyls were not present at detectable levels. The CH_2O concentrations determined by the Nash and DNPH derivatization methods disagree for several samples, there is no obvious explanation.

Figure 7.7 plots the concentration of the major ions against time for the July 24–26, 1985, sampling period. Cloudwater concentrations decreased over the period.

During the events on July 24 and 25 the concentrations doubled from beginning to end. On the morning of July 26, concentrations were fairly constant. The concentrations during the August 21 event were similar to those on July 24. The cloudwater concentrations at Casitas Pass followed the same pattern of increasing over the course of the event, but were lower than those observed at La Jolla Peak.

Figures 7.8 and 7.9 plot the concentrations in the two intensive sampling periods during 1986 for which samples were obtained simultaneously at several sites. The concentrations in the Laguna Road samples were appreciably higher than those in the Laguna Peak samples collected shortly thereafter. Over the course of sampling, the Laguna Peak cloudwater became more concentrated. On Aug. 5 and 6 the cloudwater concentration at Ventura were between the cloudwater concentrations at Laguna Peak and Laguna Road. The Ventura cloudwater samples also showed a pattern of increasing concentrations over the course of the event. On Aug. 13 and 14 Ventura cloudwater was more concentrated than the Laguna Peak cloudwater and concentrations decreased rather than increased over the course of the event on Aug. 14. During all cloud events Casitas Pass had lower concentrations of the principal chemical components. Cloudwater collected at the Laguna Road site on July 31 was comparable to the samples from Aug. 13 – 14. The concentration profile exhibited a concave profile, however, with the highest concentrations at the beginning and end. Similar results were observed for the cloud interception event at Ventura on August 1.

Aerosol and cloudwater loadings at Laguna Peak, Ventura, and Casitas Pass for the period August 4 – 6, 1986, are shown in Figures. 7.10 – 7.15. Plots for the other two intensive sampling periods are presented in Appendix B. Cloudwater loading (neq m^{-3}) is the product of concentration (μN) and LWC (ml m^{-3}). At Laguna Peak some of the highest aerosol concentrations of N(–III), N(V), and SO_4^{2-} occurred when the site was in the inversion layer. Lower concentrations were observed when the site was immersed in stratus. Most of the N(V) was present as HNO_3 during clear periods.

Na^+ also had its maximum values during the cloud–free periods, but Cl^- did not follow this trend. When cloud was present at Laguna Road, the cloudwater loading of N(–III), N(V) and SO_4^{2-} was usually less than the aerosol concentration in the clear air at the summit. The loading of Na^+ and Cl^- in the lower elevation cloud was often greater than in the aerosol above the cloud. Over the course of the event both aerosol and cloudwater loading decreased. When the clouds intercepted Laguna Peak, the cloudwater loading was comparable to the aerosol loading. This pattern is predicted to occur if air from the mixed layer, which is high in sea salt, is mixed with inversion layer air, which is high in NO_3^-, SO_4^{2-}, and NH_4^+. The short duration cloud events were often thin or patchy. Cloudwater loading during these events was usually less than the aerosol. Cloudwater loadings in the final LR samples were comparable to the first LP samples. The observed concentration differences were primarily due to differences in LWC.

At Ventura, N(–III), N(V), and SO_4^{2-} were well mixed from sea level up to the TV site. When there was a gradient in aerosol concentrations of these species, sea level concentrations were slightly higher. Na^+ and Cl^-, were not well mixed; their concentrations were always much higher at the beach than on the hill. The difference is more than would be caused by the difference in pressure at the two sampling sites. Aerosol concentrations at Ventura were variable, but there were no clear patterns to the variation. On several days the maximum Na^+ concentrations occurred in the early evening, which is counter to the expected maximum during the afternoon when the sea breeze is strongest. With the exception of the Aug. 5 event, the cloudwater loading was equal to the aerosol concentration during the extended cloud events. Cloudwater loading of N(–III), N(V), and SO_4^{2-} was also less than the aerosol concentration during the thin cloud event on Aug. 13.

The behavior of sea–salt aerosol is illustrated in Figures. 7.16 – 7.19. At Ventura and Casitas Pass, Cl^- was moderately depleted relative to Na^+ in the aerosol. Even at high Na^+ concentration in the Emma Wood samples, the Cl^- concentrations are $\leq$ 75% of the expected value if sea salt was the sole source of Na^+. Figure 7.18 also illustrates the Na^+ and Cl^- gradient between the beach and hill sites in Ventura. In the Ventura cloudwater, however, the $Cl^-:Na^+$ ratio was very close the the value for seawater. The aerosol at Laguna Peak was was severely depleted in Cl^-. The samples with the highest Na^+ had little or no Cl^-. The cloudwater from Laguna Road still exhibited an apparent Cl^- deficiency at high concentration, though at low concentrations the $Cl^-:Na^+$ ratio was close to the seawater value. The cloudwater collected at the summit of Laguna Peak often had a Cl^- excess.

DISCUSSION

The strongest temperature inversions were associated with the most extensive cloudiness. It is possible that persistent clouds strengthen the temperature inversion, or that the strong inversion, which implies stronger subsidence, leads to more frequent, persistent, and extensive clouds. In all of the cloud events studied, the inversion base rose during the night and lowered in the day, which is contrary to usual pattern over land. This result is in accordance with predictions from a model of radiant and turbulent heat transfer in low–level marine stratus over the ocean (Oliver et al., 1978). Turbulence, driven by radiative cooling allows the cloud top to propagate upwards during the night. Subsidence heating would continually warm the inversion layer and depress the inversion base. If the competing effect of convective mixing at night (induced by warm ocean water, relative to the air, or radiative and evaporative cooling at the cloud top) were stronger, the mixed layer would increase. The observed changes in the height of the inversion base are consistent with this explanation. The consequence of this process would be the transfer of aerosol and gases across the inversion layer.

The composition of aerosol and cloudwater over the Santa Barbara Channel is consistent with a mixture of sea salt and anthropogenic aerosol. Nitrate and non–sea salt sulfate concentrations over the Santa Barbara Channel are a factor of 10 or more higher than concentrations observed at mid–ocean sites in the North Pacific (Prospero, et al., 1985). Harrison and Pio (1983a) observed similar concentrations of the major aerosol components at a coastal site in northwestern England where ammonium nitrate and sulfate aerosol was mixed with sea–salt aerosol. Saltzmann et al. (1986) report comparable levels of $SO_{4\,xs}^{2-}$ in aerosol of the Peruvian coast that they attribute to smelter emissions. Total SO_4^{2-} concentrations observed in this study are similar to the concentrations reported at Santa Catalina Island (Cass and Shair, 1984), which is ≈ 32 km off the Los Angeles coast and is affected by advection from Los Angeles. Maximum SO_4^{2-} concentrations at two coastal stations in Los Angeles (Cass and Shair, 1984) were 3 times the highest value observed for SO_4^{2-} at Laguna Peak.

Acidic components (NO_3^- + $SO_{4\,xs}^{2-}$) in the cloudwater were found to exceed NH_4^+. This is consistent with the observations of Jacob et al. (1985). Much of the atmospheric acidity was due to HNO_3 in the gas phase. In general the excess of acidic anions over cations in the aerosol was small. In most samples from Laguna and La Jolla Peaks the concentration of N(V) exceeded that of $SO_{4\,xs}^{2-}$ on an equivalents basis. At the remaining sites, however, neither species was consistently in excess. However, NO_3^- usually exceeded $SO_{4\,xs}^{2-}$ in cloudwater. The ratios of the volume–weighted average concentrations ranged from 1.1 to 1.6. This $NO_3^-:SO_{4\,xs}^{2-}$ ratio is considerably less than the typical value of 2.5, which is commonly observed observed in clouds and fogs collected in Los Angeles (Munger et al., 1983, 1989). In the Channel area, NO_x emissions reported from stationary sources exceed SO_x emissions by a factor of 15 (California Resources Board Emission Inventory). Vehicular emissions add to this excess. Active photochemistry, which would rapidly convert NO_x to HNO_3, is indicated by peak O_3 concentrations of up to 100 ppb at the coastline and in the Channel at Anacapa Island (Ventura County APCD data); while up to 140 ppb was measured inland at Casitas Pass. Therefore, HNO_{3gas} or $NO_3^-{}_{aerosol}$ appears to be lost from the air mass at a faster rate than the SO_4^{2-}.

The distribution of Na^+, Mg^{2+} and Cl^- (with a few exceptions) in the aerosol and cloudwater is consistent with their derivation from sea spray. The high concentrations of Na^+, Mg^{2+}, and Cl^- at Emma Wood and El Capitan are probably due to a few large sea–salt aerosol or sea–spray droplets. These would not remain suspended long enough to penetrate far inland or rise more than a few meters above sea level. The deposition of large sea–salt particles could account for the large concentration gradient for sea salt–derived ions observed between Emma Wood and the TV site, a short distance away. A further decrease in sea salt–derived ions is observed between the TV site and Casitas Pass or Laguna Peak. Comparison of the Laguna Road and Laguna Peak samples indicates a sea salt gradient within the stratus layer. Concentrations (and total loading) of Na^+ and Mg^{2+} were greater near the cloud base (Laguna Road samples) than near the cloud top (Laguna Peak samples). Cl^-, however, did not follow this trend, suggesting there may be some other source for Cl^- in the air above the mixed layer. The predominance of NH_4^+, and its associated anions, over Na^+ and Mg^{2+} in cloudwater with increasing height is consistent with the observation that sea salt aerosol are not the dominant source of cloud condensation nuclei (Pruppacher and Klett, 1978), even over the remote ocean.

The highest concentrations of N(V) and $SO_{4\,xs}^{2-}$ were observed at Laguna and La Jolla Peaks, which are the sites furthest east and at the highest elevations. This pattern could be explained by transport of the polluted air mass from the Los Angeles basin, which is situated southeast of the Santa Barbara Channel, by upper level winds. As noted previously, winds in the inversion layer frequently had an easterly component. Shair et al. (1982) have documented transport from Los Angeles to sites as far north as Ventura. In that study a power plant plume was followed by means of SF_6 tracer. At night the plume was transported over the ocean by the land breeze.

The following morning it returned to shore on the sea breeze. The plume remained near the inversion base during most of the night. However, around 0500 it was dispersed throughout the mixed layer by convection over the ocean. Transport over the length of the Channel by the sea/land breeze cycle has been observed as well (Angell et al., 1966). It is unlikely that the highest concentrations of N(V) and $SO_{4\,xs}^{2-}$ would be found at Laguna or La Jolla Peak if their primary source were oxidation of locally emitted NO_x and SO_2. Furthermore, the concentrations of N(V) and $SO_{4\,xs}^{2-}$ were not higher when the inversion base was lower during the July 29 – August 1 sampling period, which might be expected if they were derived from local sources. The comparable concentrations of these species for this particular sampling periods indicate that there may have been effective mixing from one end of the channel to the other.

The volatilization of HCl from the acidification of sea salt aerosol is well known (Eriksson, 1960; Martens et al., 1973; Hitchcock et al., 1980). Theoretical calculations by Clegg and Brimblecombe (1985) indicate that the most HCl is lost from the smallest aerosol. The loss of Cl^- decreases rapidly with increasing relative humidity above 99%. Thus droplets would retain their Cl^-, even at low pH. This mechanism would account for the Cl^- deficiency observed in aerosol from the Santa Barbara Channel area. Small Cl^- deficiencies were observed at the coastal sites (Emma Wood and El Capitan) where presumably, large sea–salt aerosol and sea–spray droplets are present. Nearly complete removal of Cl^- was observed at Laguna Peak where most of the sea salt should be present as small aerosol and where the humidity was the lowest. As noted above, the atmosphere in the Santa Barbara Channel has excess acidity, mostly as gas–phase HNO_3.

HCl volatilization by HNO_3 has some important consequences for the size distribution of NO_3^- and Cl^- aerosol, which may in turn affect the fate of those species in the atmosphere. In the absence of sea salt, NO_3^- is present in the atmosphere as gas–phase HNO_3 or sub–micron aerosol (NH_4NO_3) formed by gas-to-particle conversion processes. Deposition of HNO_3 on sea salt particles, which are mainly in the size range 1 – 40 μm (diameter), transfers NO_3^- mass from the gas phase to large diameter particles; at the same time Cl^- is transferred to the gas phase. If NH_3 is available, HCl may react to form NH_4Cl aerosol (Harrison and Pio, 1983b). NO_3^- and SO_4^{2-} in polluted marine air have bimodal distributions. The portion having a mode at about 1 μm was associated with NH_4^+; a second mode around 3.5 μm was associated with Na^+ (Harrison and Pio, 1983a). The transport of both gases and particles to the surface layer is limited by turbulent transfer. The deposition velocities for small particles (0.01 μm $< d \leq 1$ μm) is typically 0.1 cm s^{-1} or less, while reactive gases such as HNO_3 have deposition velocities of 1 – 3 cm s^{-1} (Huebert and Robert, 1985). Deposition velocity for large particles (diam. > 1 μm) increases with size. Over water surfaces, particle growth in the humid boundary layer enhances deposition of large particles (diam. > 1 μm) up to the limit imposed by turbulent transfer (Slinn and Slinn, 1980).

Unless the gaseous HCl is separated from the air mass during the day, it will be rescavenged totally by cloud droplets at night. Thus the Na^+:Cl^- ratio in cloudwater will be close to the seawater ratio. Deposition of HCl_{gas} to land surfaces may slightly exceed that of the smaller sea–salt aerosol, which could account for the slight Cl^- deficiency we sometimes observed in cloudwater at Laguna Road. The Na^+ and Cl^- need not necessarily be in the same droplets, however. HCl will be scavenged during droplet activation and growth and could be present to some extent in all droplets. Droplet scavenging provides a second mechanism for the formation of Cl^- aerosol in addition to direct gas–to–particle reactions. Future studies of aerosol and gas–phase species in coastal settings should include measurements of HCl to verify that this exchange occurs.

Theoretical considerations suggest scavenging efficiency by stratus clouds should be near 100%. Hygroscopic aerosol larger than about 0.1 μm (Pruppacher and Klett, 1978) should be activated at the supersaturations observed in stratus clouds. Gaseous species should partition into the droplet phase according to their Henry's Law coefficients. At the pH observed in the Santa Barbara Channel cloudwater, both HNO_3 and NH_3 should be partitioned almost completely into the droplet phase. The characteristic time for interfacial mass transfer is seconds to minutes (Schwartz and Freiberg, 1981). Most of the aerosol mass is associated with particles larger than 0.1 μm and the residence time of air parcels in stratus clouds is several minutes. Previous studies of scavenging by stratus clouds indicate nearly 100% scavenging of SO_4^{2-} and light–scattering particles (ten Brink et al., 1987).

Scavenging ratios, defined as $R_s = [C]_{cloud} / [C]_{aerosol}$, have been calculated for the periods with concurrent (or consecutive) aerosol and cloudwater data (Table 7.10). The scavenging ratios for NH_4^+ and NO_3^- are computed from N(–III) and N(V), respectively, to eliminate the effect of gas/aerosol partitioning. Two major sources of uncertainty are inherent in this method. The sampling intervals (2 – 4 hours typically) are long relative to the time for changes in cloudwater composition or microphysics. If the cloud is inhomogeneous, or patchy, the average scavenging ratio obtained will be less than the instantaneous ratio for the cloud parcels. Secondly, the estimate of LWC derived from the sampler collection rate and theoretical collection efficiency is subject to some uncertainty, which propagates to the derived cloudwater loading. These uncertainties should affect all species in the cloud equally. Differences in scavenging ratios for different ions imply that they are affected by different processes.

The scavenging ratios at Laguna Peak and Ventura, were generally close to 1. The exceptions with low scavenging ratios were generally short–duration cloud events that were often patchy. Low scavenging ratios, however, were also observed during the first interval on August 5 at Laguna Peak, when the site was near the cloud top.

The ratio for N(V) was consistently greater than the the ratio for SO_4^{2-}. As noted previously, NO_3^- may be present as large aerosol derived from sea salt or as HNO_{3gas}, both of which will be more rapidly scavenged by droplets than the smaller SO_4^{2-} aerosol.

The scavenging ratios computed for the Casitas Pass samples were consistently less than 1. The events on July 31 and August 1 were of short duration. The others extended over several hours. Casitas Pass was usually near the top of the stratus layer. Clear patches would likely be entrained into the cloud. The sampler at Casitas Pass was only 2 m above the ground, whereas, at the other sites, the samplers were on the tops of roofs. Heating at the warm ground surface may have evaporated some of the cloud droplets at this site. Thus the material collected as aerosol may have included the freshly evaporated droplets, thereby reducing the scavenging ratio.

Because very little of the stratus cloudwater is removed at the ground the solutes in the droplets remain in the atmosphere as aerosol after the clouds dissipate. Hoppel et al. (1986) suggest that non–precipitating clouds increase the size of the aerosol by transferring small aerosol and gas to droplets, which then evaporate to form particles larger than the original condensation nuclei.

The organic species found in the Santa Barbara Channel cloudwater may arise from two sources. Formaldehyde and other carbonyls are well known primary pollutants; they are also formed from the reaction of hydrocarbons, which come from incomplete combustion, fuel and solvent evaporation, or from vegetation (Graedel et al., 1986). Toluene and related aromatic compounds are a major source of the dicarbonyls, glyoxal and methyl glyoxal. Natural emissions may account for many of the carbonyls and carboxylic acids observed in the troposphere. In particular, isoprene, a major product of plants, reacts with O_3 to give HCOOH, and $CH_3C(O)CHO$, observed in cloudwater samples, among other products, which were not observed. Anthropogenic emissions are also direct and indirect sources (Talbot et al., 1988) of these carboxylic acids. The $HCOOH/CH_3COOH$ ratio near 2 that was observed in the Santa Barbara Channel cloudwater approaches the average value of 2.4 reported for rainwater at marine sites (Keene and Galloway, 1986). The lower concentrations of carbonyls than carboxylic acids are consistent with the faster rates of photochemical degradation for carbonyls in the atmosphere.

SUMMARY

During the summers of 1985 and 1986 the composition of aerosol and cloudwater at several sites along the coast of the Santa Barbara Channel was analyzed. The aerosol there was a mixture of sea salt and ammonium nitrates and sulfates. The concentrations of NO_3^- and SO_4^{2-} were comparable on an equivalents basis. Excess N(V) was present as HNO_3. The aerosol was depleted in Cl^- via the reaction of sea salt with HNO_3 to release HCl. There was little difference in concentration at sites separated by tens of kilometers. Elevated concentrations of acidic anions were present both above and below the persistent temperature inversion that forms along the coast. The highest concentrations of sea–salt derived species were observed below the inversion. Stratus clouds form frequently beneath the inversion. Cloudwater was consistently acidic, as would be expected from the composition of the aerosol and gas preceding the cloud. Scavenging of the preexisting aerosol and gases was nearly 100% efficient when a uniform cloud was present. Formic acid and acetaldehyde were the major organic species present. Acetic acid, formaldehyde, glyoxal, and methylglyoxal were present as well.

ACKNOWLEDGEMENTS

This research was supported by the California Air Resources Board. We gratefully acknowledge the assistance and cooperation of the United States Navy Pacific Missile Test Center at Point Mugu, the Federal Aviation Administration, the California Air Resources Board, Monitoring Branch, the Ventura County Air Pollution Control District, and Avenue Cable TV for allowing us access to their facilities for use as sampling sites. Rawinsonde and meteorological data for Point Mugu were provided by the U. S. Navy. Additional meteorological data were provided by the California Air Resources Board. The CARB and Ventura County APCD provided pollutant data for the sampling periods. Assistance in the field and laboratory was provided by S. Gomez, C. Choy, and G. Gibb.

REFERENCES

Allbrecht, B. A., Penc, R. S., and Schubert, W. 1985. An observational study of cloud–topped mixed layers. *J. Atmos. Sci.* **42**, 800–822.

Angell, J. K., Pack, D. H., Holzworth, G. C., and Dickson, C. R. 1966. Tetroon trajectories in an urban atmosphere. *J. Appl. Met.* **5**, 565–572.

Appel, B. R., Wall, S. M., Tokiwa, Y., and Haik, M. 1979. Interference effects in sampling particulate nitrate in ambient air. *Atmos. Environ.* **13**,319–325.

Blanchard, D. C. and Woodcock, A. H. 1980. The production, concentration and vertical distribution of the sea–salt aerosol. *Ann. N. Y. Acad. Sci.* **338**, 330–347.

Brost, R. A., Lenschow, D. H., and Wyngaard, J. C. 1982a. Marine stratocumulus layers. Part I: Mean conditions. *J. Atmos. Sci.* **39**, 800–817.

Brost, R. A., Wyngaard, J. C., and Lenschow, D. H. 1982b. Marine stratocumulus layers. Part II: Turbulence budgets. *J. Atmos. Sci.* **39**, 818–836.

Cass, G. R., and Shair, F. H. 1984. Sulfate accumulation in a sea breeze/land breeze circulation system. *J. Geophys. Res.* **89**, 1429–1438.

Caughey, S. J., Crease, B. A., and Roach, W. T. 1982. A field study of nocturnal stratocumulus: II. Turbulence structure and entrainment. *Quart J. R. Met. Soc.* **108**, 125–144.

Clarke, A. D., Ahlquist, N. C., and Covert, D. S. 1987. The Pacific marine aerosol: Evidence for natural acid sulfates. *J. Geophys. Res.* **92**, 4179–4190.

Clegg, S. L. and Brimblecombe, P. 1985. Potential degassing of hydrogen chloride from acidified sodium chloride droplets. *Atmos. Environ.* **19**, 465–470.

Collett, J., Jr., Daube. B., Jr., Munger, J. W., and Hoffmann, M. R. 1989. A comparison of two cloudwater/fogwater collectors. *Atmos. Environ* (submitted)

Dasgupta, P. K., DeCesare, K. and Ullrey, J. C. 1980. Determination of atmospheric sulfur dioxide without tetrachloromercurate (II) and the mechanism of the Schiff reaction. *Anal. Chem.* **52**, 1912–1922.

Dasgupta, P. K. 1981. Determination of atmospheric sulfur dioxide without tetrachloromercurate (II): Further refinements of a pararosaniline method and a field application. *J. Air Pollut. Cont. Assoc.* **31**, 779–782.

Daube, B. C., Jr., Flagan, R. C., and Hoffmann, M. R. 1987. *Active Cloudwater Collector* United States Patent # 4,697,462, Oct. 6, 1987.

Deardroff, J. W. 1976. On the entrainment rate of a stratocumulus–topped mixed layer. *Quart. J. R. Met. Soc.* **102**, 563–582.

Deardroff, J. W. 1981. On the distribution of mean radiative cooling at the top of a stratocumulus–capped mixed layer. *Quart. J. R. Met. Soc.* **107**, 191–202.

Eriksson, E. 1960. The yearly circulation of chloride and sulphur in nature, meteorological, geochemical, and pedological implications. Part 2. *Tellus* **12**, 63–109.

Graedel, T. E., Hawkins, D. T., and Claxton, L. D. 1986. *Atmospheric chemical compounds: Sources, occurrence, and bioassay.* Academic Press, New York.

Grosjean, D. and Wright, B. 1983. Carbonyls in urban fog, ice fog, and cloudwater and rainwater. *Atmos. Environ.* **17**,2093–2096.

Harrison, R. M. and Pio, C. A. 1983a. Size–differentiated composition of inorganic atmospheric aerosols of both marine and polluted continental origin. *Atmos. Environ.* **17**, 1733–1738.

Harrison, R. M. and Pio. C. A 1983b. Major ion composition and chemical associations of inorganic atmospheric aerosols. *Envir. Sci. Technol.* **17**, 169–174.

Hitchcock. D. R., Spiller, L. L., and Wilson, W. E. 1980. Sulphuric acid aerosols and HCl release in coastal atmospheres: evidence of rapid formation of sulphuric acid particulates. *Atmos. Environ.* **14**, 165–182.

Hoppel, W,. A., Frick, G. M., and Larson, R. E. 1986. Effect of nonprecipitating clouds on the aerosol size distribution in the marine boundary layer. *Geophys. Res. Lett.* **13**, 125–128.

Huebert, B. J. and Robert, C. H. 1985. The dry deposition of nitric acid to grass. *J. Geophys. Res.* **90**, 2085–2090.

Jacob, D. J., Wang, R.–F. T. and Flagan, R. C. 1984. Fogwater Collector Design and characterization. *Environ. Sci., Technol.* **18**, 827–833.

Jacob, D. J., Waldman, J. M., Munger, J. W., and Hoffmann, M. R. 1985. Chemical composition of fogwater collected along the California coast. *Environ. Sci. Technol.* **19**, 730–736.

Jacob, D. J., Munger, J. W., Waldman, J. M., and Hoffmann, M. R. 1986. The H_2SO_4–HNO_3–NH_3 system at high humidities and in fogs: I. Spatial and temporal patterns in the San Joaquin Valley of California. *J. Geophys. Res.* **91,** 1073–1088.

Keene, W. C. and Galloway, J. N. 1984. Organic acidity in precipitation of North America. *Atmos. Environ.* **18,** 2491–2497.

Keene, W. C. and Galloway, J. N. 1986. Considerations regarding sources for formic and acetic acids in the troposphere. *J. Geophys. Res.* **91**, 14466–14474.

Lazrus, A., Kok, G. L., Gitlin, S. N., Lind, J. A., and McLaren, S. E. 1985, Automated fluorometric method for hydrogen peroxide in atmospheric precipitation. Anal. *Chem.* **57**, 917–922.

Mahrt, L. and Paumier, J. 1982. Cloud–top entrainment instability observed in AMTEX. *J. Atmos. Sci.* **39**, 622–634.

Martens, C. S., Wesolowski, J. J., Harriss, R. C., and Kaifer, R. 1973. Chlorine loss from Puerto Rican and San Francisco Bay area marine aerosols. *J. Geophys. Res.* **78**, 8778–8791.

Munger, J. W., Jacob, D. J., Waldman, J. M., and Hoffmann, M. R. 1983. Fogwater chemistry in an urban atmosphere. *J. Geophys. Res.* **88,** 5109–5121.

Munger, J. W., Collett, J., Daube, B., Jr., and Hoffmann, M. R. 1989. Fogwater chemistry at Riverside California. *Atmos. Environ.* (in press).

Nash, T. 1953. The colorimetric estimation of formaldehyde by means of the Hantszch reaction. *Biochem. J.* **55**, 416–421.

Nieburger, M., Johnson, D. S., and Chien. C.–W. 1961. *Studies of the structure of the atmosphere over the eastern Pacific Ocean in summer I. The inversion over the eastern North Pacific Ocean.* University of California Press, Berkeley

Oliver, D. A., Lewellen, W. S., and Wialliamson, G. G. 1978. The interaction between turbulent and radiative transport in the development of fog and low-level stratus. *J. Atm. Sci.* **35**, 301–316.

Prospero, J. M., Savoie, D. L., Nees, R. T., Duce, R. A., and Merrill, J. 1985. Particulate sufate and nitrate in the boundary layer over the North Pacific Ocean. *J. Geophys. Res.* **90**, 10,586–10,596.

Pruppacher, H. R. and Klett, J. D. 1978. *Microphysics of clouds and precipitation*, pp. 139–140. D. Reidel, Dordrecht.

Randall, D. R 1980a. Conditional instability of the first kind upside–down. *J. Atmos. Sci.* **37**, 125–130.

Randall, D. R. 1980b. Entrainment into a stratocumulus layer with distributed radiative cooling. *J. Atmos. Sci.* **37**, 148–159.

Reitz E. B. 1980. The stabilization of small concentrations of formaldehyde in aqueous solutions. *Analyt. Lett.* **13**, 1073–1084.

Saltzman, E. S., Savoie, D. L., Prospero, J. M., Zika, R. G., and Mosher, B. 1986. Elevated atmospheric sulfur levels off the Peruvian coast. *J. Geophys. Res.* **91**, 7913–7918.

Schwartz, S. E. and Freiberg, J. E. 1981. Mass–transport limitation to the rate of reaction of gases in liquid droplets: Application to oxidation of SO_2 in aqueous solutions. *Atmos. Environ.* **15**, 1129–1144.

Seinfeld, J. H. 1986. *Atmospheric Chemistry and Physics of Air Pollution,* John Wiley. New York, 738 pp..

Shair, F. H., Sasaki, E. J., Carlan, D. E., Cass, G. R., Goodin, W. R., Edinger, J. G., and Schacher, G. E. 1982. Transport and dispersion of airborne pollutants associated with the land breeze–sea breeze system. *Atmos. Environ.* **16**, 2043–2053.

Slinn, S. A. and Slinn, W. G. N. 1980. Predictions for particle deposition on natural waters. *Atmos. Environ.* **14**, 1013–1016.

Smith, R. V., and Erhardt, P. W. 1975. Nash determination for formaldehyde in the presence of bisulfite. *Anal. Chem.* **47**, 2462–2454.

Spicer, C. W. and Schumacher, P. M. 1979. Particulate nitrate: Laboratory and field studies of major sampling interferences. *Atmos. Environ.* **13**, 543–552.

Spicer, C. W., Howes, J. E., Jr., Bishop, T, A., Arnold, L. H., and Stevens, R. K. 1982. Nitric acid measurement methods: An intercomparison. *Atmos. Environ.* **16**, 1487–1500.

Talbot, R. W., Beecher, K. M., Harriss, R. C., and Cofer, W. R., III. 1988. Atmospheric geochemistry of formic and acetic acids at a mid–latitude temperate site. *J. Geophys. Res.* **93**, 1638–1652.

ten Brink, H. M., Schwartz, S. E., And Daum, P. H. 1987. Efficient scavenging of aerosol sulfate by liquid–water clouds. *Atmos. Environ.*

Table 7.1 Range and average of concentrations in aerosol samples collected at sites along the Santa Barbara Channel

	Na^+	NH_4^+	Ca^{2+}	Mg^{2+}	Cl^-	NO_3^-	SO_4^{2-}	$SO_{4\,xs}^{2-*}$	NH_3	HNO_3	N(–III)	N(V)
	neq m^{-3}								nmole m^{-3}			
La Jolla Peak 1985												
Day (N = 18)												
Min	3.9	0.0	0.0	0.8	0.0	15.7	32.0	20.5	7.0	4.3	8.4	20.0
Max	225	239	37	51	126	152	304	292	89	386	253	454
Avg	96	60	11	23	38	55	96	84	29	77	89	132
Night (N = 14)												
Min	1.2	10.7	0.0	0.0	0.0	11.4	35.8	30.2	4.4	4.7	22.5	4.7
Max	284	166	42	35	211	153	153	118	68	186	188	328
Avg	78	44	17	16	45	61	72	63	30	57	75	119
Casitas Pass 1985												
Day (N = 6)												
Min	73.4	0.0	2.9	19.0	14.6	10.3	43.5	25.8	0.0	10.6	0.0	20.9
Max	207	68	41	55	101	172	95	74	115	163	172	245
Avg	129	37	19	31	40	78	66	50	47	63	92	126
Night (N = 10)												
Min	12.3	35.2	0.0	6.2	0.0	43.1	54.3	42.3	8.0	11.2	45.9	65.3
Max	207	185	43	58	123	153	141	134	97	43	213	191
Avg	108	75	26	32	51	103	84	71	24	24	99	127
Laguna Peak 1986												
Day (N = 8)												
Min	9.2	39.2	5.0	0.9	0.0	18.1	90.1	89.0	0.0	16.3	39.2	74.5
Max	87	176	47	17	25	112	386	381	34	202	189	244
Avg	52	118	19	10	8	46	224	218	7	134	125	180
σ	23	39	7	5	8	14	90	89	11	53	39	60
Night (N = 12)												
Min	7.0	42.2	6.4	1.2	0.0	22.3	57.6	56.4	0.0	7.5	46.3	88.7
Max	49	156	49	11	45	138	193	187	101	355	182	412
Avg	22	84	19	5	17	72	128	125	19	124	102	196
σ	15	34	14	3	14	39	38	37	29	117	44	98

Table 7.1 (continued)

	Na^+	NH_4^+	Ca^{2+}	Mg^{2+}	Cl^-	NO_3^-	SO_4^{2-}	$SO_{4\,xs}^{2-*}$	NH_3	HNO_3	N(–III)	N(V)
	neq m^{-3}								nmole m^{-3}			
Ventura (Hill) 1986												
Day (N = 15)												
Min	16.1	25.0	12.8	3.9	0.0	18.0	42.4	25.7	0.0	11.6	25.0	37.9
Max	167	303	62	41	126	146	295	286	42	139	313	236
Avg	71	105	29	15	35	49	159	151	8	78	114	127
σ	41	63	14	10	38	31	63	65	11	40	66	49
Night (N = 19)												
Min	23.9	43.1	9.7	2.7	2.4	41.7	66.1	39.4	0.0	5.7	47.3	47.5
Max	239	177	52	53	200	205	169	164	19.5	51	181.4	218
Avg	105	100	22	23	77	97	113	100	2.8	20	107.5	118
σ	66	41	11	15	58	51	28	32	5	13	39	49
Ventura (Beach) 1986												
Day (N = 11)												
Min	121	42.9	4.8	21.1	73.3	37.3	108	48.2	0.0	5.6	42.9	42.9
Max	490	210	57	98	432	93	261	243	37	144	217	230
Avg	254	107	23	55	198	69	170	139	11	54	117	124
σ	118	49	12	23	119	18	50	61	15	432	45	53
Night (N = 12)												
Min	90	32.1	9.0	19	19	33	45	0.0	0.0	4.2	53	39
Max	1001	146	79	201	1051	114	176	165	82	112	167	193
Avg	396	82	34	85	348	75	132	87	16	26	99	101
σ	297	34	17	55	307	24	39	49	24	30	35	44
Casitas Pass 1986												
Day (N = 14)												
Min	4.7	42.7	11.3	0.0	0.0	28.2	55.7	44.6	0.0	0.0	20.0	66.4
Max	123	168	36	27	51	81	189	189	145	133	288	192
Avg	51	123	20	11	16	48	133	126	46	62	161	115
σ	33	28	7	8	16	13	32	34	38	30	54	32
Night (N = 21)												
Min	4.8	24.1	5.2	0.5	0.0	30.6	32.1	24.8	0.0	0.0	29.2	40.7
Max	129	201	34.5	30	101	105	156	153	74	36	222	119
Avg	45	113	13.7	9	30	65	81	75	13	12	122	78
σ	39	45	7	9	31	22	27	29	18	8	50	22

Table 7.1 (continued)

	Na^+	NH_4^+	Ca^{2+}	Mg^{2+}	Cl^-	NO_3^-	SO_4^{2-}	$SO_{4\,xs}^{2-}$*	NH_3	HNO_3	N(-III)	N(V)
	neq m^{-3}								nmole m^{-3}			
					El Capitan 1986							
					Day (N = 4)							
Min	404	18.0	27.1	87.9	422	36.7	72.0	23.0	0.0	10.2	57.0	46.9
Max	1079	106	85	215	867	133	289	159	39	29	106	162
Avg	612	74	48	133	554	92	181	107	16	22	90	114
σ	273	34	22	49	183	35	82	56	16	8	19	42
					Night (N = 8)							
Min	50.2	11.3	6.1	10.8	36.6	11.8	21.5	12.9	0.0	4.9	34.2	16.7
Max	335	136	69	73	297	140	149	114	42	22	136	162
Avg	217	76	34	48	186	64	87	61	20	11	91	76
σ	93	44	20	22	92	41	41	34	15	6	35	45

* "Excess" (non–sea salt) Sulfate $[SO_{4\,xs}^{2-}] = [SO_4^{2-}] - [Na^+]\frac{[SO_4^{2-}]_{sw}}{[Na^+]_{sw}}$

Table 7.2 1985 La Jolla Peak Cloudwater (RAC) Samples

	Vol	pH	Na^+	NH_4^+	Ca^{2+}	Mg^{2+}	Cl^-	NO_3^-	SO_4^{2-}	$SO_{4\,xs}^{2-*}$
	ml		μN							
July 24 (0235 – 0410, 0605 –0935)										
N	5	5	5	5	5	5	5	5	5	4
Min	13	2.36	193	214	62	57	196	509	370	347
Max	49	3.36	710	882	259	236	1100	2750	1980	1944
Avg	23	2.85	341	616	139	124	460	1795	1086	1045
Vol Wt. Avg		2.80	253	463	111	99	347	1306	808	777
July 25 (2230 – 0820)										
N	8	8	7	8	8	8	8	8	8	8
Min	5.5	2.81	192	192	24.7	54.1	161	370	225	167
Max	70	3.38	480	719	136	125	322	1410	1080	1042
Avg	39	3.10	326	385	70	88	239	764	608	573
Vol Wt. Avg		2.91	313	309	74	87	242	636	503	465
July 26 (0335 – 0617)										
	4	4	4	4	4	4	4	4	4	4
Min	40	3.28	30	284	11	13	70	365	322	313
Max	58	3.38	483	323	22	37	126	511	371	350
Avg	50	3.35	177	305	14	27	102	426	353	332
Vol Wt. Avg		2.98	201	303	14	28	105	418	356	332
July 30 (0500 – 0545)										
N	1	1	1	1	1	1	1	1	1	1
Avg	11	3.50	>870	310	76	816	1120	844	568	167
August 21 (0019 – 0135, 0210 – 0750)										
N	6	6	6	6	6	6	6	5	6	6
Min	16	2.55	147	109	22	34	183	201	132	111
Max	52	3.79	965	591	139	259	389	2540	1110	1046
Avg	32	3.11	408	313	65	106	242	1017	557	508
Vol Wt. Avg		3.05	313	244	49	79	243	700	404	366
September 17(0000 – 0045, 0315 – 0400)										
N	2	1	2	2	2	2	2	2	2	2
Min	4	3.46	1500	105	121	321	1030	558	358	153
Max	15	3.46	1550	>150	275	523	1210	1050	410	177
All Samples										
N	27	26	25	26	26	26	26	25	26	23
Min	1.1	2.36	30	105	10.5	12.5	70	201	132	128
Max	70	3.79	1550	882	275	816	1210	2750	1980	1792
Avg	31	3.12	396	372	83.8	143	363	973	630	582
Vol Wt Avg		2.95	301	308	57	86	247	681	472	436

Table 7.2 1985 La Jolla Peak Cloudwater (RAC) Samples (continued)

	S(IV)	CH_2O	H_2O_2	−/+	H^+	LWC
		μM			μM	g m^{-3}
		July 24				
N	5	5	5	4	5	5
Min	0	13	4.1	0.95	437	0.08
Max	2.7	50	19.1	1.19	6607	0.27
Avg	1.3	30	8.6	1.08	2428	0.14
Vol Wt Avg	0.8	24	11	0.96	1591	
		July 25				
N	7	7	7	7	8	8
Min	0	9	3.2	0.38	417	0.09
Max	6.6	21	79	1.00	4365	0.40
Avg	2	15	25	0.74	1907	0.23
Vol Wt Avg	1	14	27	0.68	1237	
		July 26				
N	4	4	4	2	4	4
Min	0	10	6	0.38	355	0.32
Max	6	17	22	1.00	1950	0.53
Avg	1	14	13	0.74	1132	0.43
Vol Wt Avg	NA	14	14	—	1055	
		July 30				
N	1	1	1	1	1	1
Avg	0	NA	21	—	316	0.08
		August 21				
N	6	0	6	5	6	6
Min	0	NA	5	0.93	162	0.09
Max	0	NA	22	1.04	2818	0.40
Avg	0	NA	14	0.99	1289	0.21
Vol Wt Avg	0	—	16	—	888	
		September 17				
N	0	0	0	1	1	2
Min	NA	NA	NA	0.80	347	0.03
Max	NA	NA	NA	0.80	346	0.11
		All Samples				
N	23	16	23	19	26	
Min	0	9	3.2	0.38	162	
Max	6.6	50	79	1.19	6607	
Avg	1.1	19.8	16.4	0.70	1788	
Vol Wt Avg	0.97	16	18	0.75	1126	

Table 7.3 1985 La Jolla Peak Cloudwater (CASC) Samples

	Vol ml	pH	Na^+	NH_4^+	Ca^{2+}	Mg^{2+}	Cl^-	NO_3^-	SO_4^{2-}	$SO_{4\,xs}^{2-*}$
			μN							
July 25 (2300 – 0820)										
N	8	6	9	9	9	9	8	8	8	8
Min	19	2.78	117	223	31	37.3	138	327	317	300
Max	143	3.26	231	888	66	86	229	1250	1190	1172
Avg	100	3.09	156	428	40	53	171	618	601	583
Vol Wt. Avg		2.65	154	362	39	55	169	547	535	516
July 26 (0330 – 0617)										
N	3	3	3	3	3	3	3	3	3	3
Min	301	3.29	46	265	16	17	94	320	329	323
Max	381	3.34	73	319	19	18	126	495	356	350
Avg	346	3.31	57	296	18	18	111	409	339	332
Vol Wt. Avg		2.95	58	294	18	18	112	401	340	333
July 30 (0500 – 0545)										
N	1	1	1	1	1	1	1	1	1	1
Avg		3.43	870	430	54	661	2200	949	717	611
August 21 (0019 – 0135, 0210 – 0750)										
N	8	7	8	7	8	8	8	8	8	8
Min	31	2.24	133	131	19	19	138	203	168	151
Max	236	3.70	781	745	158	211	1370	4730	2000	1905
Avg	134	2.92	342	421	66	80	394	1573	846	804
Vol Wt. Avg		2.77	264	355	50	56	276	1083	608	576
September 4 (2300 – 0300)										
N	3	3	3	3	3	3	3	3	3	3
Min	49	4.27	764	712	212	582	738	325	653	349
Max	56	4.94	2980	1070	370	1110	1050	732	1020	928
Avg	52	4.69	2085	859	279	822	899	478	802	550
Vol Wt. Avg		4.69	2357	812	259	756	937	422	753	468
August 17 (0000 – 0045, 0315 – 0400)										
N	2	2	2	2	2	2	2	2	2	2
Min	27	3.41	843	93	76	356	901	390	290	188
Max	71	3.47	1270	260	140	392	1190	992	448	294
All Samples										
N	26	22	26	25	26	26	25	25	25	22
Min	19.4	2.24	46.1	92.9	15.8	17.3	94	203.2	167.5	162
Max	381	4.94	2980	1070	370	1110	2200	4730	2000	1639
Avg	128	3.33	521	442	79	194	474	901	658	595
Vol Wt Avg		2.83	248	345	44	81	253	647	484	454

Table 7.3 1985 La Jolla Peak Cloudwater (CASC) Samples (Continued)

	S(IV)	CH_2O	H_2O_2	−/+	H^+	LWC
	———	μM	———		μM	gm^{-3}
July 25						
N	3	0	4	6	7	8
Min	0	NA	3.1	0.37	549.5	0.05
Max	6	NA	36	0.96	6166	0.22
Avg	3	NA	12	0.70	2799	0.15
Vol Wt Avg	—	—	—		2233	
July 26						
N	3	3	3	3	3	3
Min	0	13	5	0.37	457	0.36
Max	4	15	10	0.89	2089	0.47
Avg	1	14	8	0.63	1198	0.44
Vol Wt Avg	1	14	8		1119	
July 30						
N	1	0	1	—	1	1
Avg	0	NA	10		398	0.04
August 21						
N	8	0	8	6	7	8
Min	0	NA	3	0.64	200	0.04
Max	0	NA	2	1.02	5754	0.27
Avg	0	NA	13	0.86	2399	0.15
Vol Wt avg	0	—	15	0.81	1687	
September 4						
N	0	0	0	0	3	3
Min	NA	NA	NA	0.78	11	0.02
Max	NA	NA	NA	0.96	54	0.05
Avg	NA	NA	NA	0.90	26	0.04
Vol Wt Avg	—	—	—		21	
September 17						
N	0	0	0	2	2	2
Min	NA	NA	NA	0.89	339	0.03
Max	NA	NA	NA	1.07	389	0.09
All Samples						
N	15	3	16	20	23	
Min	0	13	2.8	0.37	11.5	
Max	5.7	15	36.3	1.07	6166	
Avg	1	14	12	0.67	1789	
Vol Wt Av	0.96	—	12	0.63	1464	

Table 7.4 1985 Casitas Pass Cloudwater (RAC) Samples

	Vol	pH	Na^+	NH_4^+	Ca^{2+}	Mg^{2+}	Cl^-	NO_3^-	SO_4^{2-}	$SO_{4\,xs}^{2-*}$
	ml		μN							
August 7										
N	2	2	2	2	2	2	2	2	2	2
Min	8	4.38	200	113	35.3	51	333	141	100	76
Max	16	4.93	480	209	68.9	131	751	299	195	137
August 8										
N	5	5	5	4	5	5	5	5	5	4
Min	10	3.28	46	170	28.2	19.1	59.8	191	84	71
Max	40	3.88	400	413	149	108	628	956	422	373
Avg	27	3.64	142	279	58	42	247	426	179	162
Vol Wt Avg		3.67	97	267	42	31	174	346	142	131
August 9										
N	3	3	3	2	3	3	3	3	3	3
Min	6	3.31	620	847	268	222	155	401	162	0
Max	13	3.57	>1000	1450	672	842	1600	2800	2150	1736
Avg	9	3.41	873	1149	434	567	722	1580	958	741
Vol Wt Avg		3.38	387	1037	385	497	705	833	942	895
All Samples										
N	10	10	10	10	8	10	10	10	10	10
Min	6	3.28	46	113	28	19	60	141	84	0
Max	40	4.93	>1000	1450	672	842	1600	>2800	2150	1736
Avg	19	3.77	401	467	169	209	448	>731	407	325
Vol Wt Avg		3.75	>218	282	71	83	315	>414	206	165

Table 7.4 1985 Casitas Pass Cloudwater (RAC) Samples (continued)

	S(IV)	CH_2O	H_2O_2	−/+	H^+	LWC
	μM				μM	g m^{-3}
			August 7			
N	0	0	0	2	2	2
Min				1.25	11.8	0.25
Max				1.32	41.7	0.27
			August 8			
N	5	0	5	4	5	5
Min	0		2.7	0.64	132	0.09
Max	0		17	1.13	525	0.33
Avg	0		8	0.93	261	0.25
Vol Wt Avg	0		6	0.99	212	
			August 9			
N	2	0	1	1	3	3
Min	0		8		269	0.03
Max	0		8		490	0.07
Avg	0				398	0.05
Vol Wt Avg	0		8	0.90	415	
N	7	0	6	7	10	10
Min	0		3	0.64	12	0.03
Max	0		17	1.32	525	0.33
Avg	0		8	1.05	255	0.19
Vol Wt Avg	0	—	6		178	

Table 7.5 1986 Laguna Peak Cloudwater Samples

	Vol	pH	Na^+	NH_4^+	Ca^{2+}	Mg^{2+}	Cl^-	NO_3^-	SO_4^{2-}	$SO_{4\,xs}^{2-*}$
	ml		μN							
					August 5					
N	6	6	6	6	6	6	6	6	6	6
Min	88	2.69	21	195	6	7	74	500	395	392
Max	327	3.14	137	599	27	39	169	1090	1110	1093
Avg	190	2.96	52	344	14	16	94	703	599	593
Vol Wt Avg		2.96	46	326	12	14	90	681	568	563
					August 6					
N	5	5	5	5	5	5	5	5	5	5
Min	16	2.71	9	143	4	3	46	345	276	275
Max	378	3.33	45	502	14	16	94	1250	1340	1335
Avg	210	3.10	26	287	8	8	72	632	633	630
Vol Wt Avg		3.18	18	217	6	6	62	470	432	430
					August 13					
N	2	2	2	2	2	2	2	2	2	2
Min	10	2.85	106	425	22.9	31.4	200	792	607	594
Max	69	3.01	318	686	73.3	88.3	350	1410	1010	972
Vol. Wt Avg		2.98	137	464	30	40	222	884	667	650
					August 14					
N	7	7	7	7	7	7	7	7	7	7
Min	113	3.01	20	171	7	8	97	344	279	277
Max	423	3.46	151	578	27	40	167	1100	888	870
Avg	249	3.19	72	304	14	21	137	637	489	480
Vol Wt Avg		3.21	56	262	12	17	128	550	417	410
					All Samples					
N		20	20	20	20	20	20	20	20	20
Min.		2.69	9	143	4	3	46	344	276	275
Max.		3.46	318	686	73	88	350	1410	1340	1335
Avg.		3.07	68	337	16	20	122	702	590	582
Vol Wt Avg.		3.16	47	276	11	15	105	579	472	466

Table 7.5 1986 Laguna Peak Cloudwater Samples (continued)

	S(IV)	CH2O	H2O2	HFo	HAc	H+	−/+	LWC
	µM							g m^{-3}
				August 5				
N	6	6	6	6	6	6	6	6
Min	0	15	0	24	14	724	0.75	0.12
Max	0	18	2	41	19	2042	1.01	0.31
Avg	0	17	1	30	16	1160	0.90	0.19
Vol Wt Avg	0	17	1	29	17	1105		
				August 6				
N	4	4	4	4	4	5	5	5
Min	0	20	2	40	13	468	1.03	0.03
Max	0	33	6	63	26	1950	1.08	0.35
Avg	0	25	4	52	19	930	1.06	0.20
Vol Wt Avg	0	23	3	49	17	657	1.06	
				August 13				
N	1	1	1	1	1	2	2	2
Min	0	7.2	1.7	37.3	18.9	977	1.02	0.022
Max	0	7.2	1.7	37.3	18.9	1413	1.07	0.128
Vol Wt Avg	—	—	—	—	—	1042		
				August 14				
N	4	4	4	5	5	7	7	7
Min	0	9	1	27	12	347	0.94	0.12
Max	0	13	4	103	44	977	1.57	0.39
Avg	0	11	3	49	20	689	1.17	0.26
Vol Wt Avg	0	10	2	41	17	614		
				All Samples				
N	15	15	15	16	16	20	20	20
Min.	0	7	0	24	12	347	0.75	0.02
Max.	0	33	6	103	44	2042	1.57	0.39
Avg.	0	17	2	42	18	941	1.05	0.21
Vol Wt Avg	0	17	1	39	17	775	1.02	

Table 7.6 1986 Laguna Road Cloudwater Samples

	Vol	pH	Na^+	NH_4^+	Ca^{2+}	Mg^{2+}	Cl^-	NO_3^-	SO_4^{2-}	$SO_{4\,xs}^{2-*}$
	ml						μN			
					July 31					
N	6	6	6	6	6	6	6	6	6	6
Min	43	3.34	151	722	33	42	160	651	425	407
Max	190	3.49	456	1350	152	109	368	1110	806	751
Avg	120	3.41	310	964	71	79	262	887	564	527
Vol Wt Avg		3.41	306	963	72	77	256	879	565	528
					August 4					
N	4	4	4	4	4	4	4	4	4	4
Min	43	2.58	655	468	80	137	548	978	1030	914
Min	43	2.58	655	468	80	137	548	978	1030	914
Max	101	2.95	1070	1780	162	247	758	2140	2630	2501
Avg	69	2.79	923	1038	129	210	675	1452	1710	1598
Vol Wt Avg		2.81	876	848	120	197	663	1294	1499	1393
					August 6					
N	6	6	6	6	6	6	6	6	6	6
Min	60	2.60	119	639	21	28	102	612	842	816
Max	204	3.13	365	1110	36	88	404	1300	1510	1489
Avg	122	2.95	193	886	28	47	198	930	1102	1079
Vol Wt Avg		2.98	223	819	28	54	239	811	1021	994
					August 14					
N	4	4	4	4	4	4	4	4	4	4
Min	81	2.90	144	445	29	44	225	790	670	651
Max	137	3.01	180	504	59	61	312	1280	925	903
Avg	99	2.96	160	470	46	51	258	986	791	772
N	20	20	20	20	20	20	20	20	20	20
Min		2.58	119	445	21	28	102	612	425	407
Max		3.49	1070	1780	162	247	758	2140	2630	2500
Avg		3.06	367	857	65	90	325	1030	1000	956
Vol Wt Avg		3.12	319	807	59	79	299	926	860	822

Table 7.6 1986 Laguna Road Cloudwater Samples (continued)

	S(IV)	CH2O	H2O2	HFo	HAc	H+	−/+	LWC
	μM							g m^{-3}
				July 31				
N	5	5	5	4	4	6	6	6
Min	0	11	17	21	9	324	1.02	0.10
Max	0	15	21	41	29	457	1.12	0.18
Avg	0	13	19	33	18	393	1.07	0.14
Vol Wt Avg	0	13	19	32	18	390	1.07	
				August 4				
N	4	4	4	4	3	4	4	4
Min	0	6	2	29	11	1122	1.01	0.04
Max	5	12	7	74	34	2630	1.09	0.09
Avg	3	9	4	48	19	1700	1.05	0.07
Vol Wt Avg	2	8	4	43	16	1551	1.05	
				August 6				
N	6	6	6	6	6	6	6	6
Min	0	7	0	24	7	741	0.97	0.06
Max	12	15	4	52	16	2512	1.31	0.19
Avg	4	11	2	40	11	1245	1.07	0.11
Vol Wt Avg	6	10	1	35	10	1043	1.05	
				August 14				
N	3	3	3	3	3	4	4	4
Min	0	4	0	26	11	977	0.81	0.09
Max	0	12	1	44	15	1259	0.96	0.13
Avg	0	9	1	37	13	1111	1	0
N	18	18	18	17	16	20	20	20
Minimum		0	4	0	21	7	324	0.81
Maximum		12	15	21	74	34	2630	1.31
Arith. Ave		2	11	7	40	15	1054	1.03
Vol Wt Avg		2	10	7	29	11	872	

Table 7.7 1986 Ventura (Hill) Cloudwater Samples

	Vol	pH	Na^+	NH_4^+	Ca^{2+}	Mg^{2+}	Cl^-	NO_3^-	SO_4^{2-}	$SO_{4\,xs}^{2-*}$
	ml		μM							
July 30										
N	2	2	2	2	2	2	2	2	2	2
Min	107	4.24	171	520	57	43	150	247	267	246
Max	188	4.92	189	539	65	47	203	284	325	302
Vol Wt Avg		4.50	179	531	61	45	173	263	292	270
August 1										
N	8	8	8	8	8	8	8	8	8	8
Min	75	3.13	548	405	48	116	482	673	554	488
Max	147	3.44	2240	966	217	519	2180	1290	998	781
Avg	103	3.28	1039	629	124	234	961	912	744	618
Vol Wt. Avg		3.24	1036	588	114	232	951	895	726	600
August 5										
N	4	4	4	4	4	4	4	4	4	4
Min	80	3.06	78	931	24	23	146	952	976	934
Max	107	3.11	349	1400	62	71	435	1200	1010	1001
Avg	98	3.09	211	1223	39	42	287	1066	999	973
Vol Wt. Avg		3.09	217	1216	40	44	293	1059	998	972
August 6										
N	6	6	6	6	6	6	6	6	6	6
Min	118	2.85	78	598	18	24	112	985	630	608
Max	182	3.06	203	1190	157	69	250	1740	1170	1145
Avg	161	2.96	154	841	46	42	186	1269	838	819
Vol Wt. Avg		2.95	151	822	40	40	182	1247	822	804
August 13										
N	2	2	2	2	2	2	2	2	2	2
Min	33	2.75	3880	1800	771	1010	3330	3730	2170	1701
Max	34	2.85	5720	2990	1400	1450	4290	6480	3220	2528
Vol Wt. Avg		2.80	4720	2343	1058	1211	3768	4985	2649	2078
August 14										
N	10	10	10	10	10	10	10	10	10	10
Min	50	2.74	74	698	31	29	104	708	387	378
Max	150	3.03	1060	1730	297	254	989	2240	1530	1402
Avg	99	2.88	381	987	122	96	397	1586	939	893
Vol Wt. Avg		2.90	294	923	89	75	326	1450	829	793
All Samples										
N	32	32	32	32	32	32	32	32	32	32
Min	33	2.74	74	405	18	23	104	247	267	246
Max	188	4.92	5720	2990	1400	1450	4290	6480	3220	2528
Avg	111	3.12	745	959	154	181	684	1430	948	858

Table 7.7 1986 Ventura (Hill) Cloudwater (continued)

	S(IV)	CH_2O	H_2O_2	HFo	HAc	H^+	−/+	LWC
	μM							$g\ m^{-3}$
				July 30				
N	2	2	2	0	0	2	2	2
Min	0	13	0	NA	NA	12	0.80	0.13
Max	0	18	1.5	NA	NA	58	0.92	0.18
Vol Wt. Avg	0	15	1	—	—	31.9	0.85	
				August 1				
N	8	8	8	6	7	8	8	
Min	0	5	0	31	3	363	0.93	0.07
Max	0	10	11	54	30	741	1.07	0.14
Avg	0	7	6	41	14	548	1.00	0.10
Vol Wt Avg	0	7	6	39	14	569		
				August 5				
N	4	4	4	0	0	4	4	4
Min	0	6	5	NA	NA	776	0.96	0.08
Max	0	13	6	NA	NA	871	1.08	0.10
Avg	0	10	6	NA	NA	819	1.00	0.09
Vol Wt Avg	0	10	6	NA	NA	816		
				August 6				
N	6	6	5	0	0	6	6	6
Min	0	12	0	NA	NA	871	1.00	0.11
Max	0	19	29	NA	NA	1413	1.06	0.17
Avg	0	14	10	NA	NA	1124	1.04	0.15
Vol Wt Avg	0	14	9	—	—	1112		
				August 13				
N	0	0	0	0	0	2	2	2
Min						1413	1.03	0.02
Max						1778	1.03	0.03
Vol Wt. Avg						1580		
				August 14				
N	10	10	10	10	10	10	10	10
Min	0	11	10	54	23	933	0.58	0.04
Max	0	27	24	96	173	1820	1.08	0.14
Avg	0	19	18	72	44	1340	0.98	0.09
Vol Wt Avg	0	18	18	67	42	1248	0.99	
				All Samples				
N	30	30	29	16	17	32	32	32
Min	0	5	0	31	3	12	0.58	0.02
Max	0	27	29	96	173	1820	1.08	0.18
Avg	0	13	11	60	32	971	0.99	0.10
Vol Wt Avg	0	13	10	56	30	896		

Table 7.8 1986 Casitas Pass Cloudwater Samples

	Vol	pH	Na^+	NH_4^+	Ca^{2+}	Mg^{2+}	Cl^-	NO_3^-	SO_4^{2-}	$SO_{4\,xs}^{2-*}$
	ml		μM							
July 31										
N	2	2	2	2	2	2	2	2	2	2
Min	130	3.87	15.9	149	9.5	7.0	34.8	147	108	106
Max	303	4.06	18.4	283	17.5	8.9	38.2	171	138	136
August 1										
N	2	2	2	2	2	2	2	2	2	2
Min	199	4.07	48	330	8.6	14.2	39.7	196	177	171
Max	212	4.26	82	358	18.4	23.4	73.1	229	211	201
August 5										
N	5	5	5	5	5	5	5	5	5	5
Min	52	3.33	19.2	612	12.2	7.6	50	402	280	278
Max	157	3.96	176	1090	48.7	49.8	110	892	523	518
Avg	114	3.72	63	805	23.9	20.4	73	610	410	402
Vol. Wt. Avg.		3.67	60	755	22	19	71	575	385	378
August 6										
N	7	7	7	7	7	7	7	7	7	7
Min	68	3.85	14.0	418	8.3	5.6	29.3	283	197	195
Max	272	4.52	83.2	930	25	27	57	474	419	414
Avg	164	4.09	36	587	14	12	45	355	293	289
Vol Wt Avg		4.00	31	537	12	10	44	338	270	266
August 13										
N	7	7	7	7	7	7	7	7	7	7
Min	26	4.06	23	354	11	9	34	209	195	192
Max	356	4.42	146	721	170	49	164	417	496	478
Avg	107.	4.22	66	571	50	23	72	315	333	325
Vol Wt Avg		4.17	57	530	42	21	65	297	307	300
August 14										
N	9	9	9	9	9	9	9	9	9	9
Min	23	3.47	12	460	13	7	22	357	204	203
Max	346	4.01	132	1130	80	52	141	649	769	753
Avg	143	3.77	34	707	33	18	55	501	383	379
Vol Wt Avg		3.77	30	680	29	16	51	478	361	357
All Samples										
N		32	32	32	32	32	32	32	32	32
Min		3.33	12	149	8	6	22	147	108	106
Max		4.52	176	1130	170	52	164	892	769	753
Avg		3.97	47	613	29	18	58	406	329	277
Vol Wt Avg		3.90	41	552	24	15	53	369	295	290

Table 7.8 1986 Casitas Pass Cloudwater Samples (continued)

	S(IV)	CH2O	H_2O_2	HFo	HAc	−/+	H^+	LWC
	μM						μM	g m^{-3}
July 31								
N	2	2	2	1	1	2	2	
Min	0	6.2	3.5	23.7	9.1	0.83	87	0.12
Max	0	7.1	4.8	23.7	9.1	0.91	135	0.28
August 1								
N	2	2	2	2	2	2	2	2
Min	0	4.7	3.3	17.2	8.0	0.85	55	0.16
Max	0	4.9	3.3	20.1	9.9	0.94	85	0.19
August 5								
N	5	5	5	5	5	5	5	5
Min	0	7.7	5.6	16.4	6.6	0.91	110	0.05
Max	0	10.9	16.2	57.3	14.4	1.01	468	0.15
Avg	0	9	9	28	11	0.96	222	0.11
Vol Wt Avg	0	9	9	27	10	0.96	216	
August 6								
N	7	7	7	7	7	7	7	7
Min	0	7.7	4.4	15.9	9.1	0.89	30	0.09
Max	0	9	7	32	14	0.99	141	0.25
Avg	0	8	6	22	10	0.94	92	0.17
Vol Wt Avg	0	8	5	20	10	0.94	101	
August 13								
N	7	5	6	5	5	7	7	7
Min	0	3	3	19	6	0.83	38	0.08
Max	0	9	8	44	15	0.98	87	0.24
Avg	0	5	5	30	9	0.91	63	0.12
Vol Wt Avg	0	5	5	27	8	0.92	68	
August 14								
N	9	9	0	5	5	9	9	9
Min	0	7		23	4	0.91	98	0.09
Max	0	13		58	14	1.02	339	0.18
Avg	0	10		34	10	0.96	183	0.12
Vol Wt Avg	0	9		32	10	0.96	170	
All Samples								
N	32	30	22	25	25	32	32	32
Min.	0	3	3	16	4	0.83	30	0.05
Max.	0	13	16	58	15	1.02	468	0.28
rith.	0	8	6	27	10	0.93	131	0.14
Vol Wt Avg	0	7	4	19	7	0.94	126	

Table 7.9 Concentrations of major dissolved organic compounds in samples of Santa Barbara Channel Stratus Cloudwater

Date	Seq	Start	Stop	Nash CH_2O	HCOOH	CH_3COOH	CH_2O	CH_3CHO	CHOCHO	$CH_3C(O)CHO$
				µM						
						Casitas Pass				
08/13	A	03:21	04:00	3	29	8	17.7	13.1	8.0	3.9
08/13	C	04:40	06:05	4	19	6	8.2	11.8	5.2	2.8
08/13	D	06:05	06:55	5	25	7	7.5	9.1	6.3	3.1
08/14	B	00:00	01:00	13	58	4	9.9	25.2	6.4	3.8
08/14	C	01:00	02:00	10	36	14	10.8	16.2	8.3	4.0
08/14	D	02:00	04:00	7	23	11	7.3	16.5	6.4	3.7
08/14	E	04:00	05:00	8	26	10	10.0	16.6	7.1	3.9
08/14	F	05:00	06:00	9	27	10	9.9	14.1	7.1	4.0
08/14	G	06:00	07:00	10	NA	NA	12.3	11.6	7.0	4.1
08/14	H	07:00	08:00	9	NA	NA	12.1	16.0	7.6	4.2
08/14	I	08:00	09:00	11	NA	NA	12.4	17.7	9.6	5.0
08/14	J	09:00	09:15	12	NA	NA	13.4	22.8	11.0	5.4
						Ventura				
08/13	A	22:45	00:00	27	92	28	15.3	37.2	11.8	4.2
08/14	B	00:00	01:00	18	85	30	14.0	41.4	14.4	3.0
08/14	C	01:00	02:00	19	74	173	16.6	33.6	5.9	5.2
08/14	D	02:00	03:00	15	69	34	19.1	33.7	11.7	5.7
08/14	E	03:00	04:00	21	64	24	16.9	31.8	8.9	5.5
08/14	F	04:00	05:00	23	61	23	15.2	31.2	27.2	7.1
08/14	G	05:00	06:00	11	64	23	15.1	24.0	11.6	5.6
08/14	H	06:00	07:00	18	54	33	11.6	18.4	9.0	4.9
08/14	I	07:00	08:00	14	60	27	12.9	1.5	8.7	4.1
						Laguna Road/Peak				
08/13	A	05:21	06:10	4	26	11	11.5	11.5	11.2	4.7
08/13	A	08:30	09:00	7	37	19	15.1	16.3	22.4	7.2

Table 7.10 Cloudwater Scavenging Ratios

Date	Start	Stop	Na$^+$	Mg^{2+}	Cl$^-$	SO$_4^{2-}$	N(–III)	N(V)
Laguna Peak								
08/05	03:33	05:30	0.39	1.17	0.29	0.54	0.45	0.65
08/05	05:30	08:30	0.72	0.87	2.71	0.69	0.79	0.98
08/06	06:40	11:10	0.42	1.32	—	1.01	1.18	1.34
08/14	02:30	05:00	0.67	1.50	1.48	1.16	1.10	1.39
08/14	05:05	07:00	3.33	1.22	0.83	1.28	1.49	1.76
08/14	07:00	09:00	0.34	0.98	1.02	0.80	0.77	1.06
Ventura								
07/30	06:30	08:15	0.48	0.95	0.74	0.59	0.70	0.60
08/01	00:20	03:20	1.12	0.86	0.79	0.74	<0.86	0.88
08/01	03:20	06:20	1.16	1.15	0.90	0.67	0.77	0.80
08/05	02:45	05:45	0.58	0.51	0.90	0.57	0.64	0.51
08/06	01:55	04:00	0.38	0.91	1.31	0.79	0.89	0.99
08/13	03:45	06:30	0.77	0.80	1.20	0.39	0.33	0.67
08/13	22:45	00:00	0.95	0.72	1.06	0.50	0.45	0.63
08/14	04:00	08:50	0.59	0.58	1.21	0.65	0.69	0.68
Casitas Pass								
07/31	06:30	06:30	0.12	0.39	0.07	0.34	0.42	0.56
08/01	02:45	05:00	0.45	0.65	0.50	0.44	0.61	0.61
08/05	02:20	03:00	0.42	0.53	0.36	0.53	0.57	0.59
08/06	02:00	06:20	0.29	0.60	4.83	0.56	0.65	0.71
08/06	06:20	07:46	0.17	0.39	1.04	0.56	0.69	0.67
08/13	03:21	06:05	1.09	5.82	—	0.48	0.44	0.60
08/13	06:05	08:40	0.36	0.89	0.19	0.37	0.29	0.41
08/14	00:00	04:00	0.51	0.64	0.46	0.45	0.50	0.51
08/14	04:00	08:05	0.44	1.03	3.90	0.57	0.64	0.65

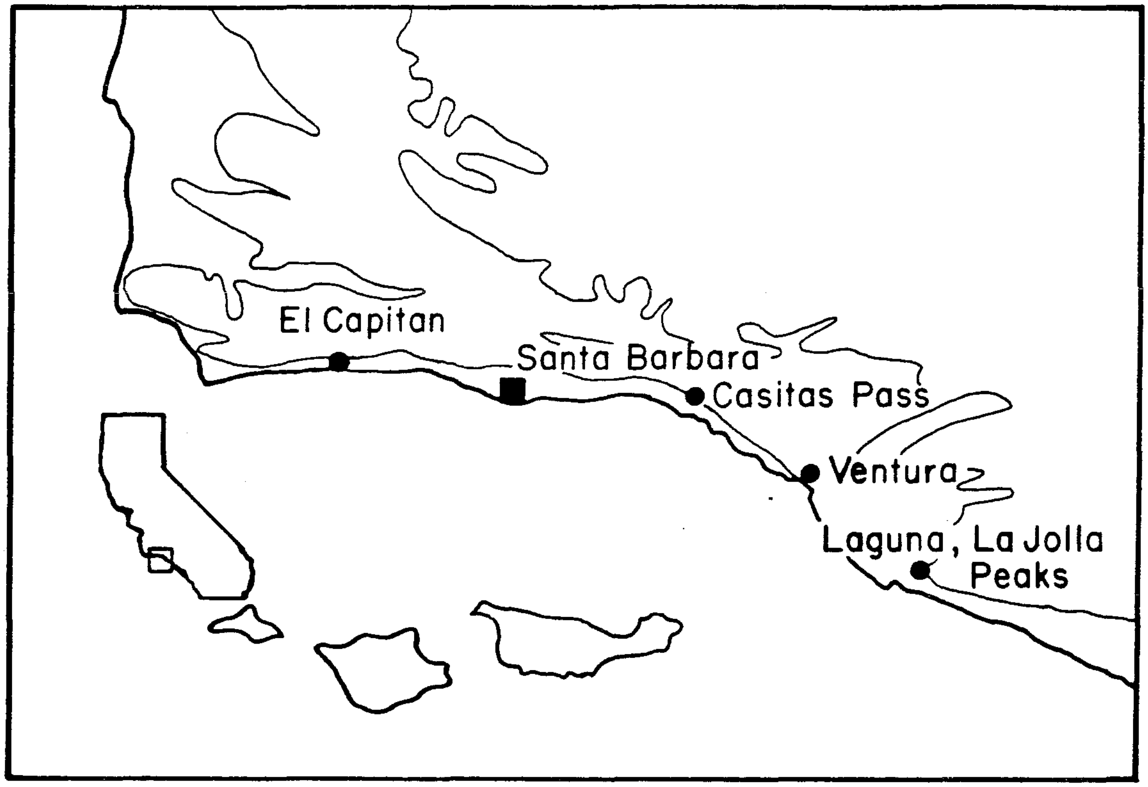

Figure 7.1. Map of the Santa Barbara Channel Area showing the location of sampling sites. La Jolla Peak and Casitas Pass were used in 1985. In 1986 the sites were Laguna Peak, Ventura, Casitas Pass and El Capitan. Two elevations were used at Laguna Peak. At Ventura one site was at the coast and a second was in the hills a few km inland.

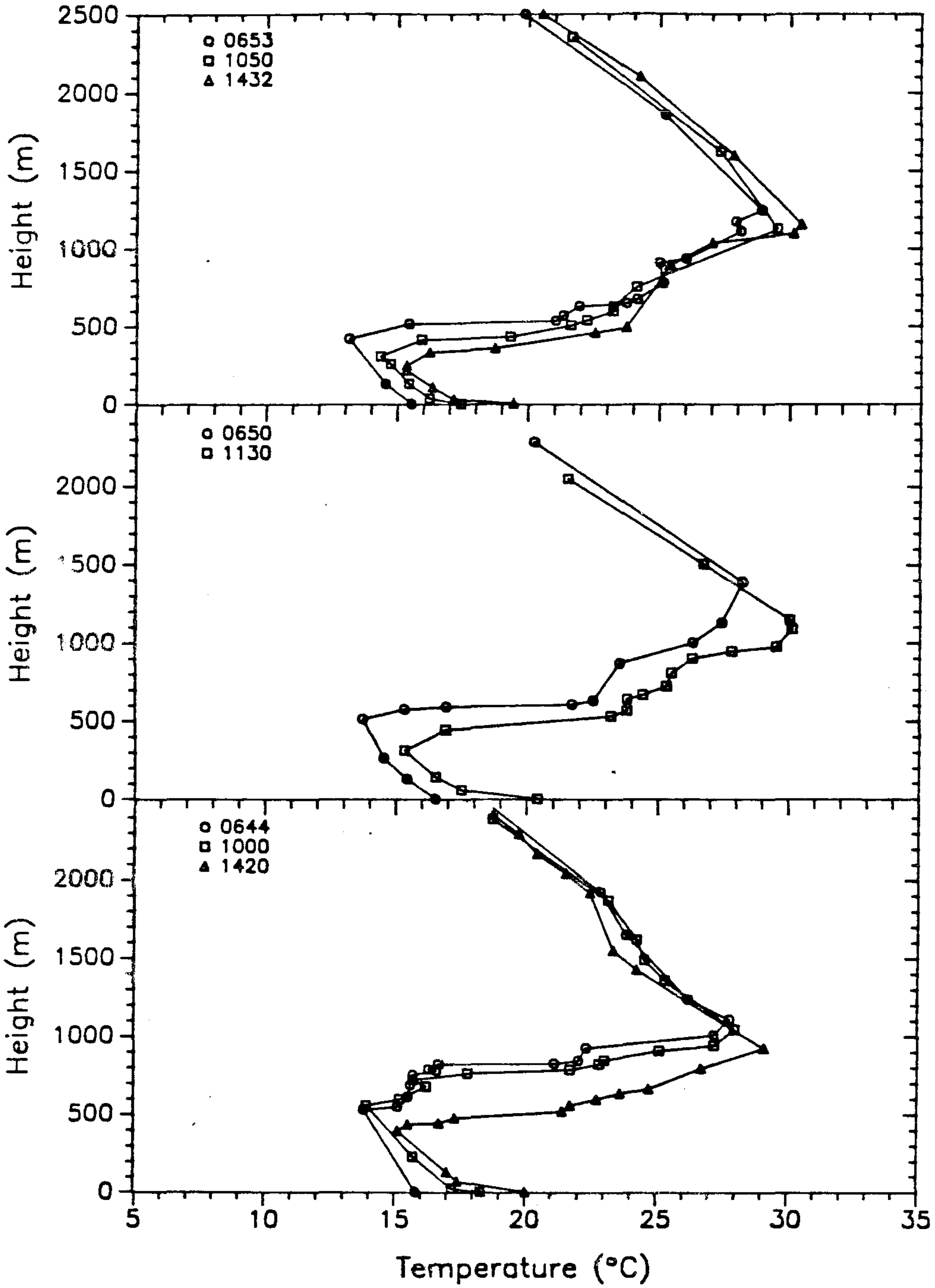

Figure 7.2 Temperature profiles for the period August 4 – August 6, 1986 taken at Point Mugu by rawinsonde.

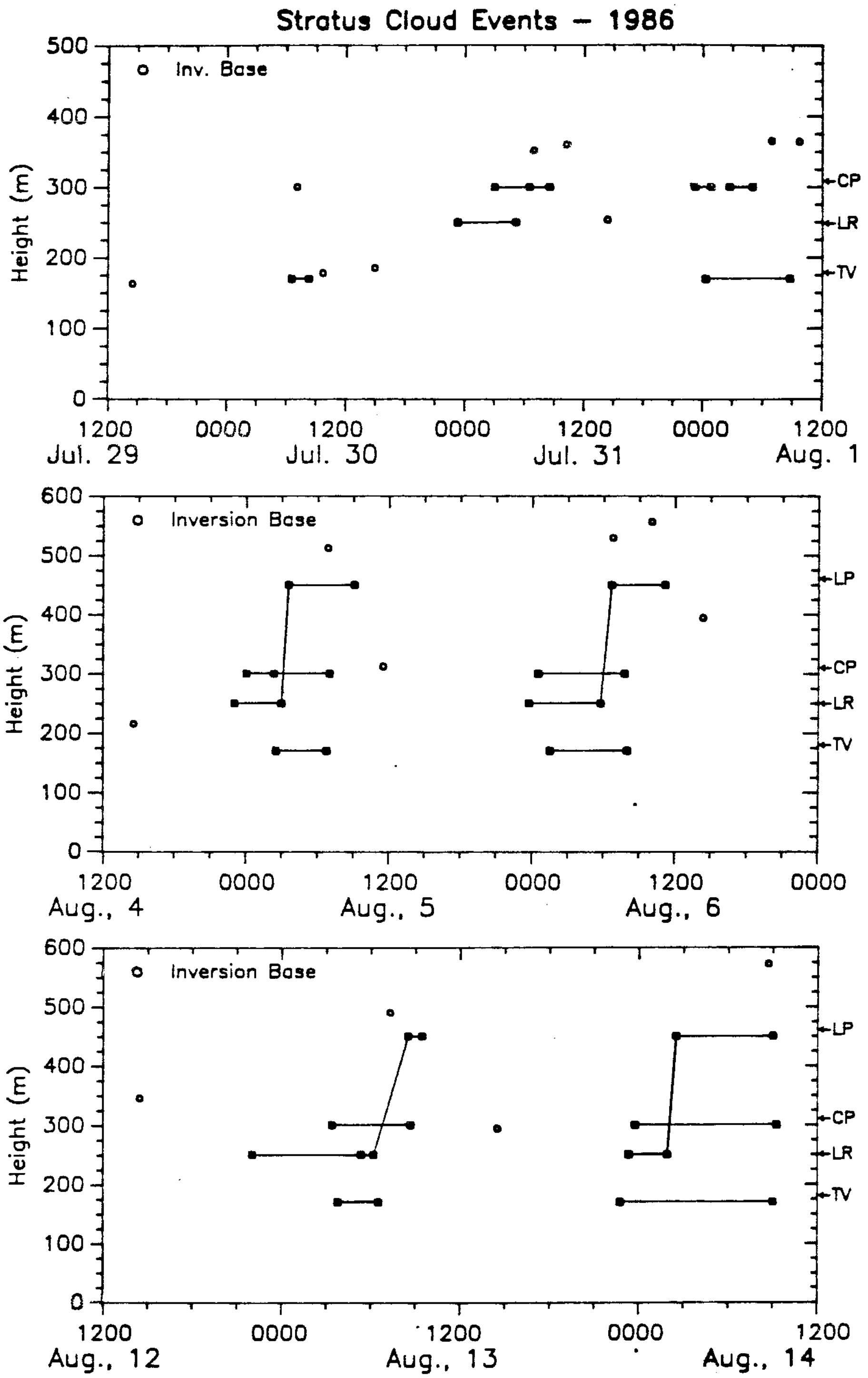

Figure 7.3 The presence of cloud at each sampling site used in 1986 is shown by a line. The symbols indicate the beginning and end of cloud impaction at the site. Open symbols indicate that cloud was present, but not sampled; the closed symbol shows the beginning of sampling. The heights of the inversion base derived from the Point Mugu rawinsonde data are shown by open circles.

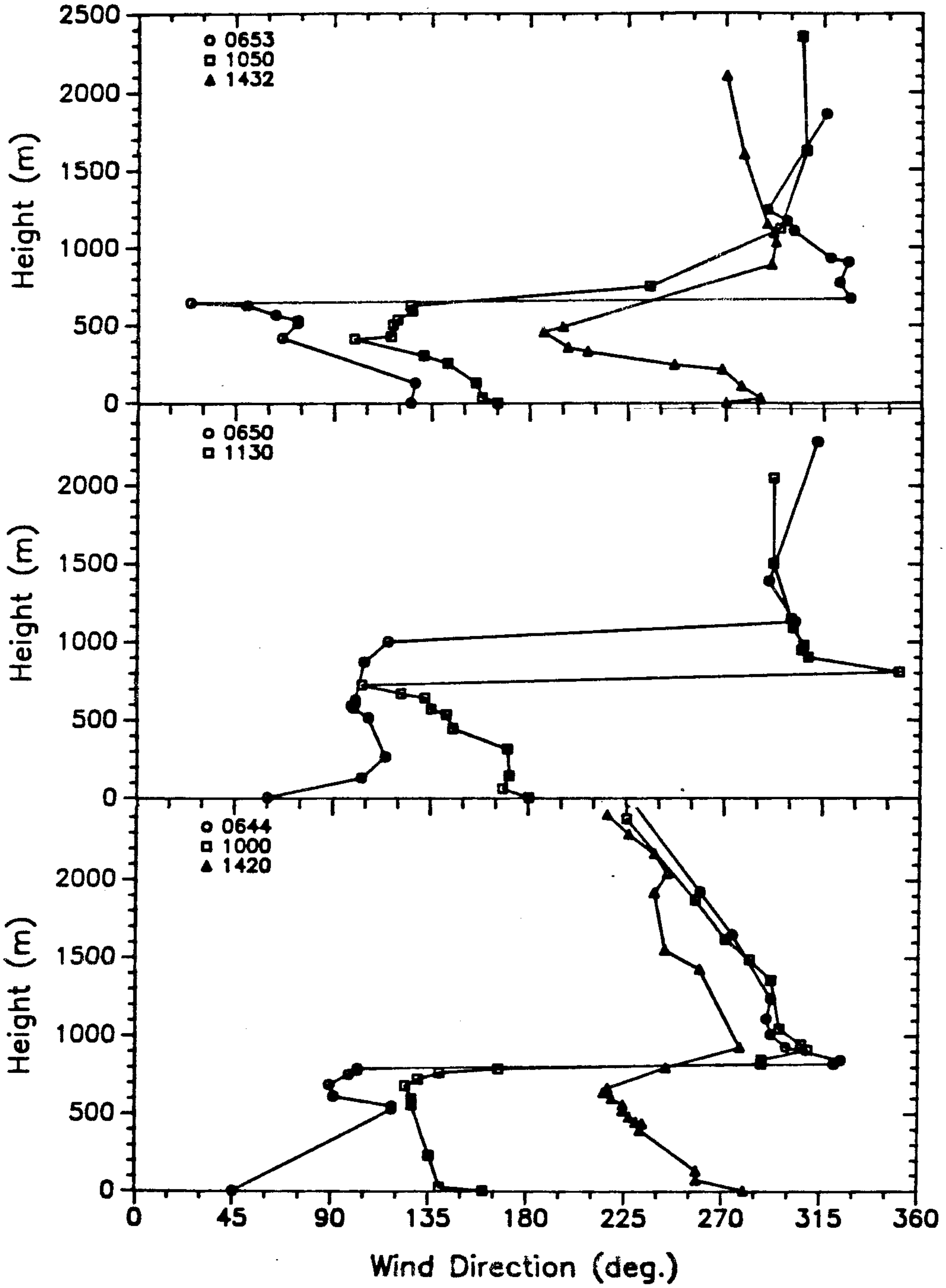

Figure 7.4 Wind direction profiles taken at Point Mugu for the period August 4 – August 6, 1986.

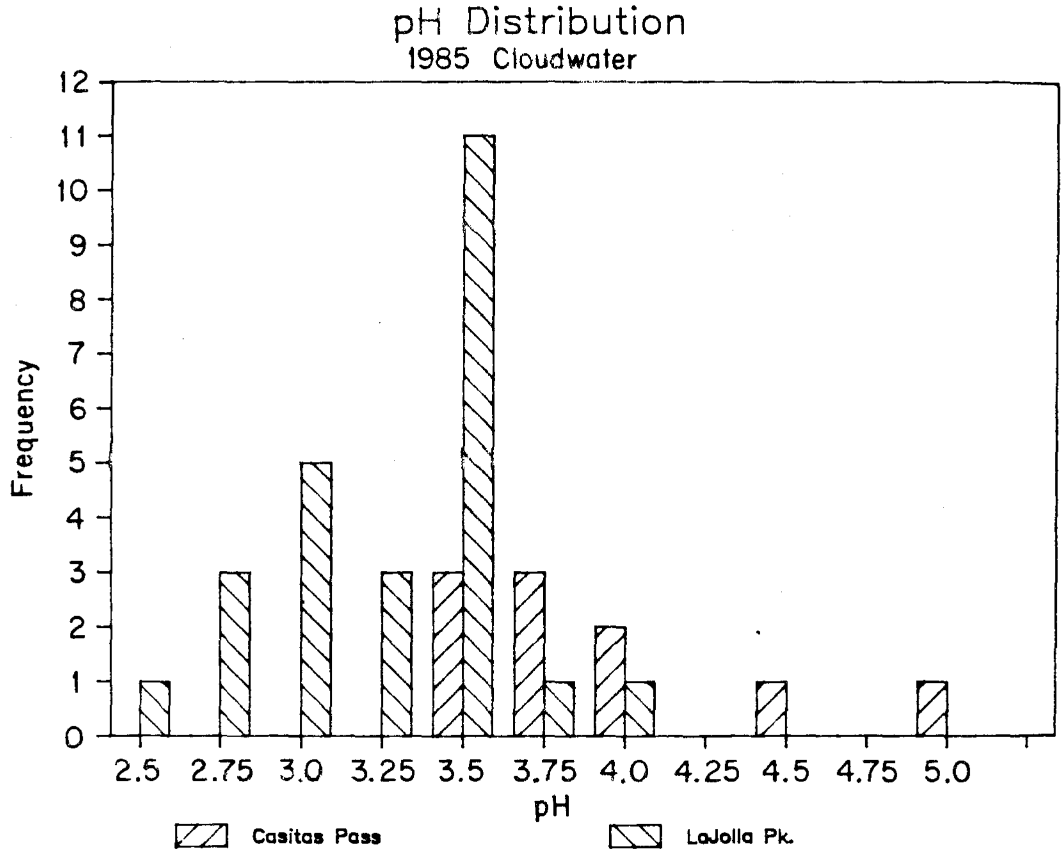

Figure 7.5 Distribution of cloudwater pH in samples collected at La Jolla Peak and Casitas Pass during the summer of 1985. The pH of suspect samples from La Jolla Peak has been adjusted to achieve a proper ion balance.

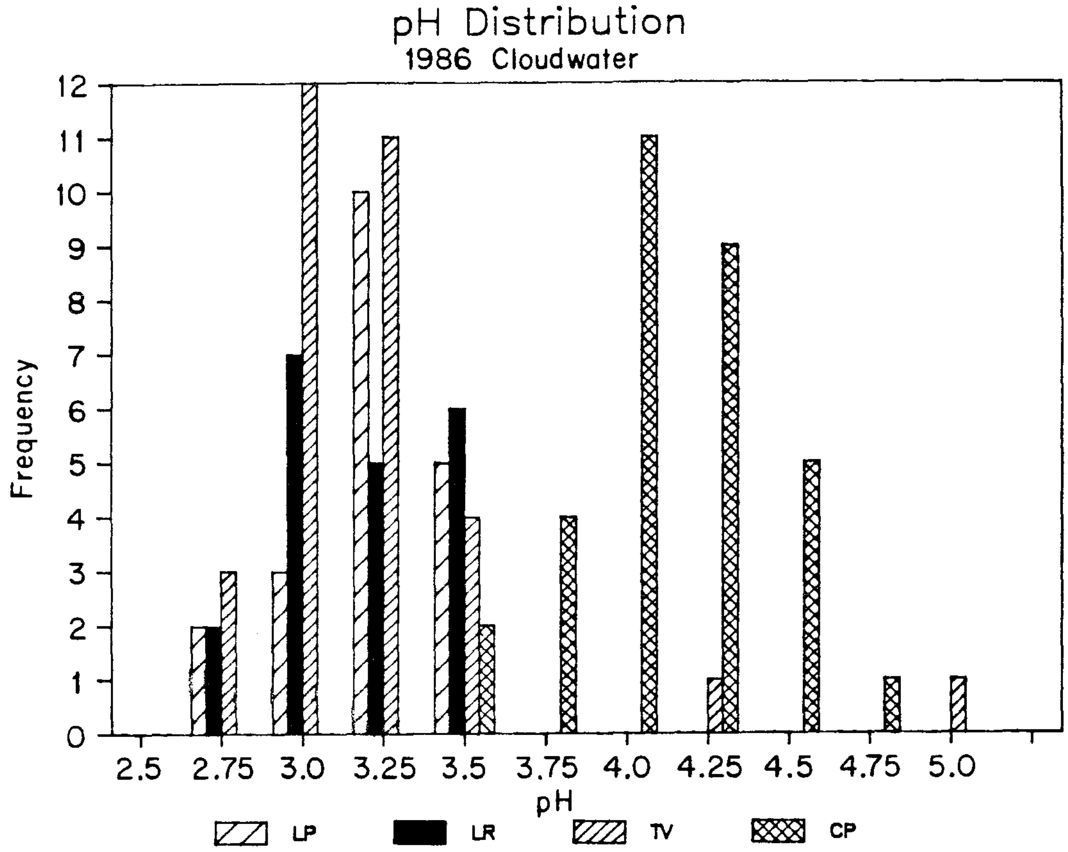

Figure 7.6 Distribution of cloudwater pH in samples collected at four sites along the Santa Barbara Channel coast during the summer of 1986. LP is Laguna Peak, LR is Laguna Road, TV is the hill site in Ventura, CP is Casitas Pass.

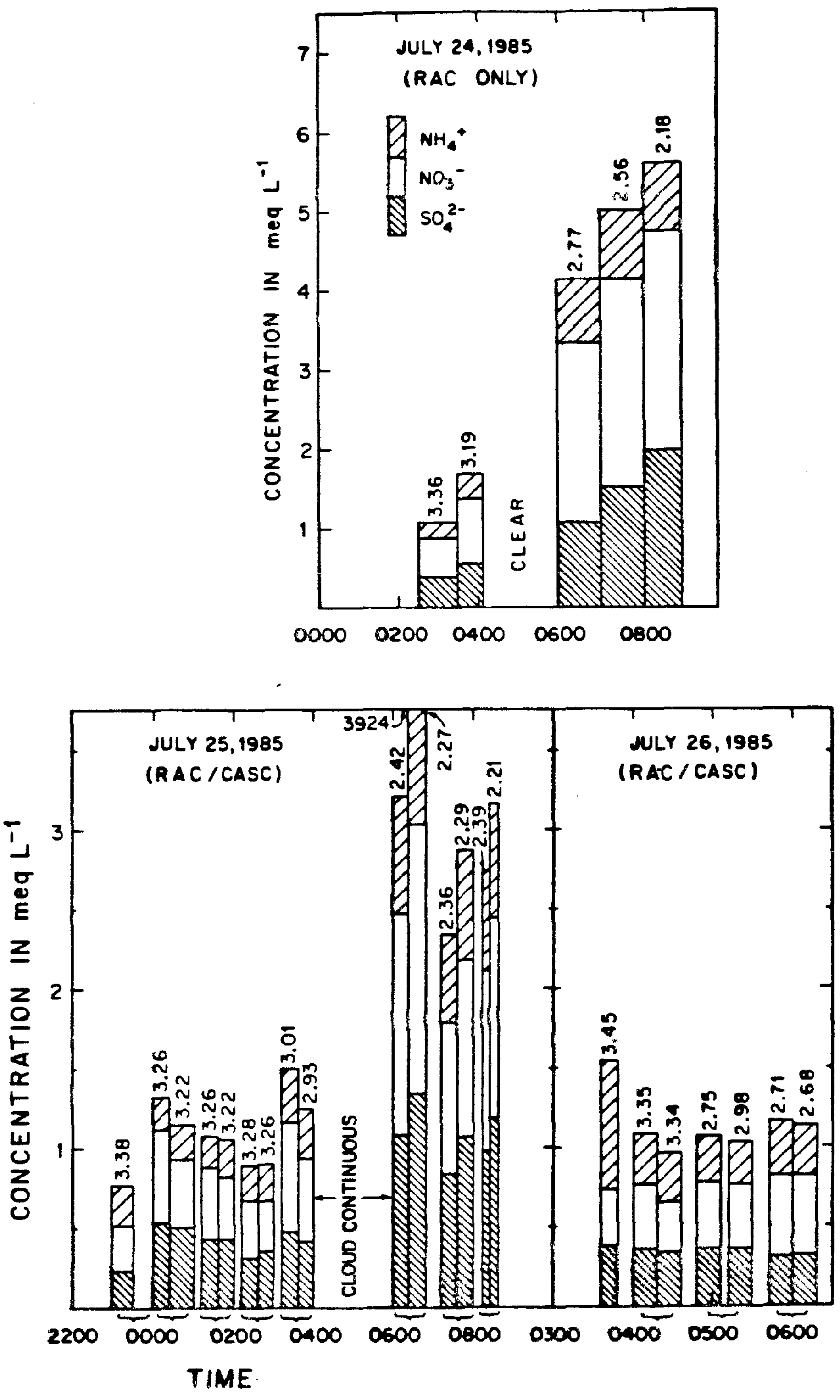

Figure 7.7 Concentrations of major ions in cloudwater collected at La Jolla Peak in July 1985. Cloudwater pH is indicated by the number above each bar. RAC and CASC samples were collected simultaneously; the point of the brace indicates the time of collection. Sample duration is indicated by the width of each bar.

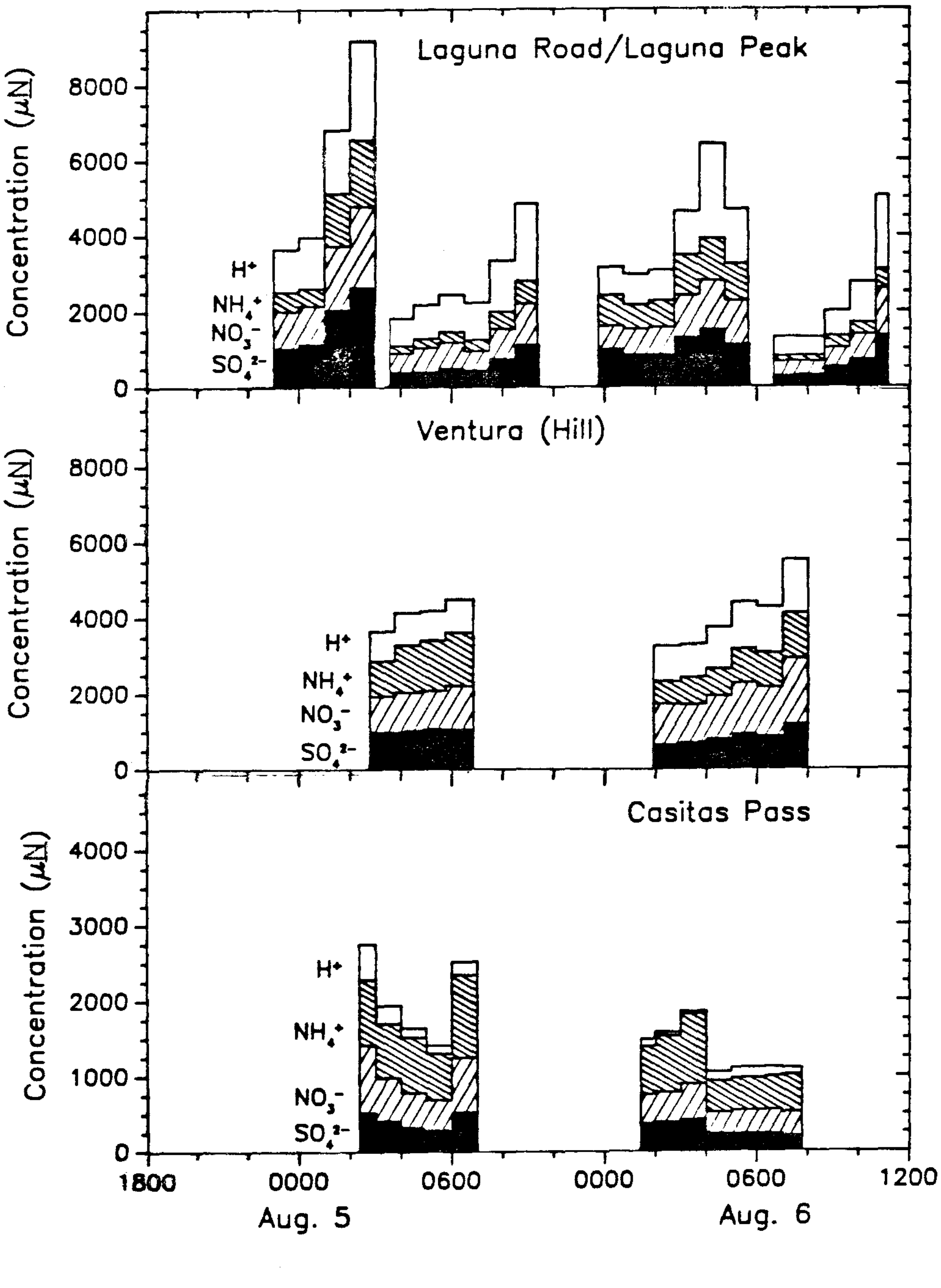

Figure 7.8 Concentrations of major ions in cloudwater samples collected at four sites along the coast of the Santa Barbara Channel on the mornings of August 5 and 6. Note the change in scale for the Casitas Pass samples

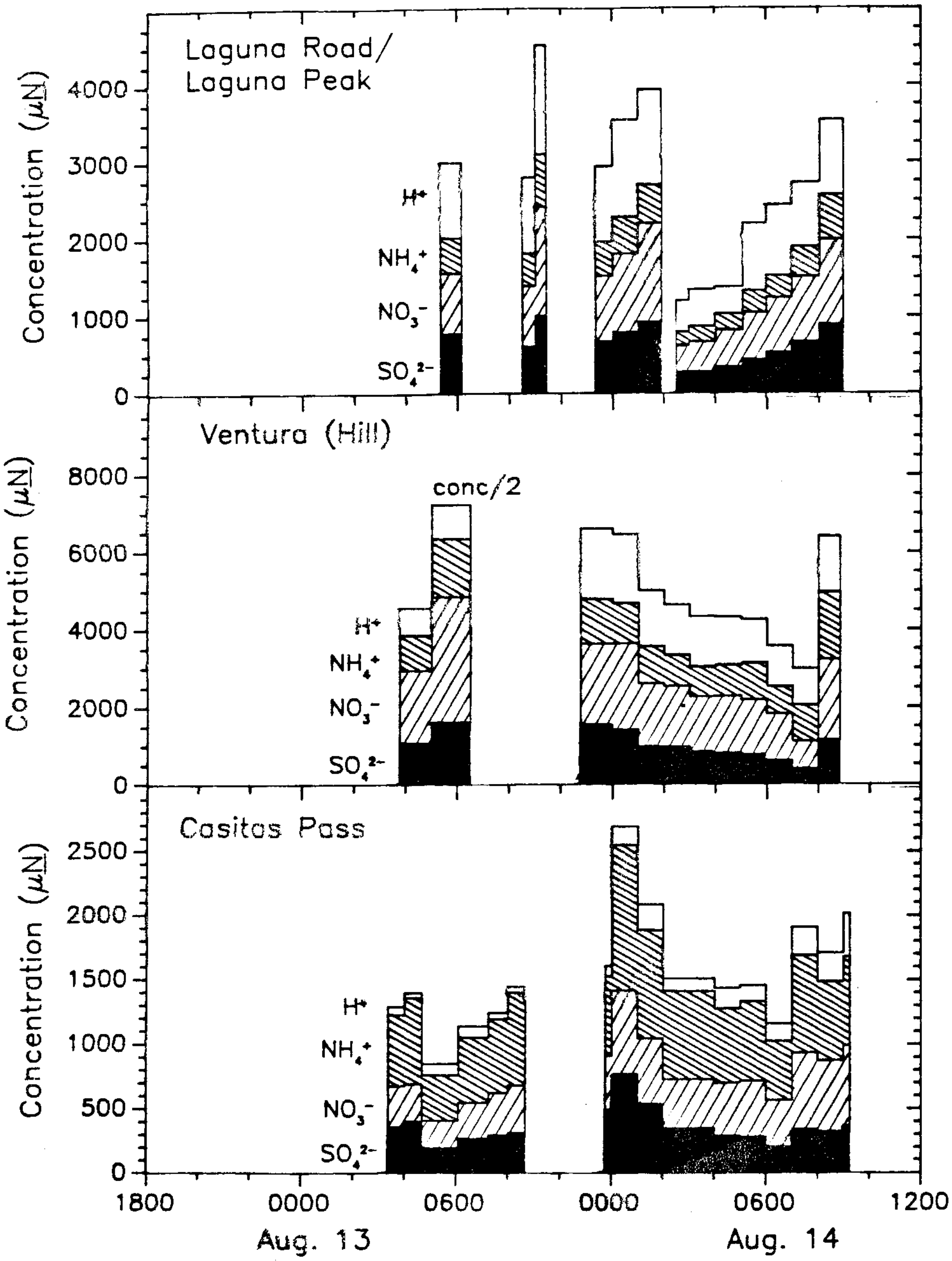

Figure 7.9 Concentrations of major ions in cloudwater samples collected at four sites along the coast of the Santa Barbara Channel on the mornings of August 13 and 14. Note the differences in scale for each site and the change in scale for the August 13 samples from Ventura.

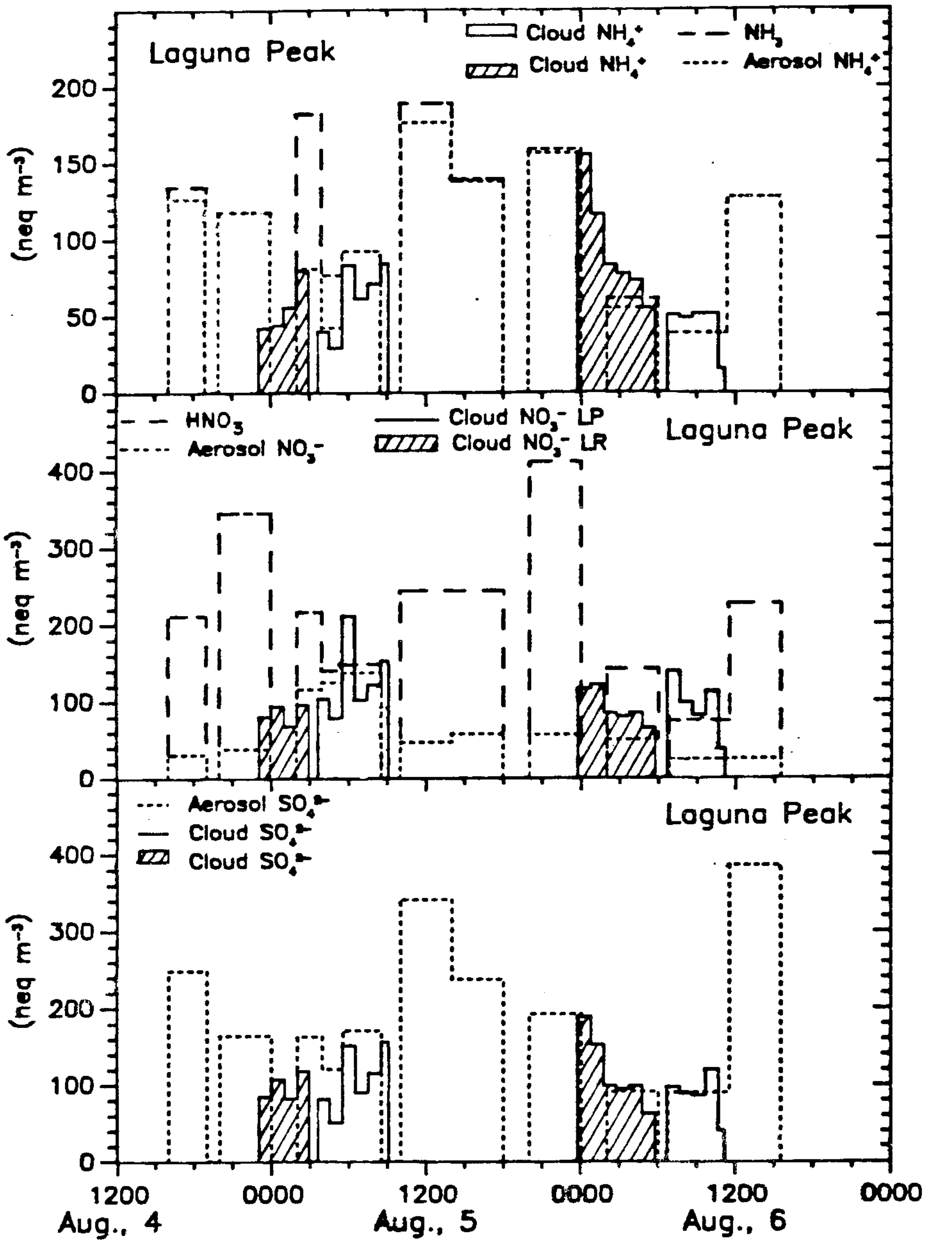

Figure 7.10 Aerosol and cloudwater loadings of major ions at Laguna Peak on August 4 – 6, 1986. Cloudwater loading is the product of aqueous–phase concentration and estimated LWC.

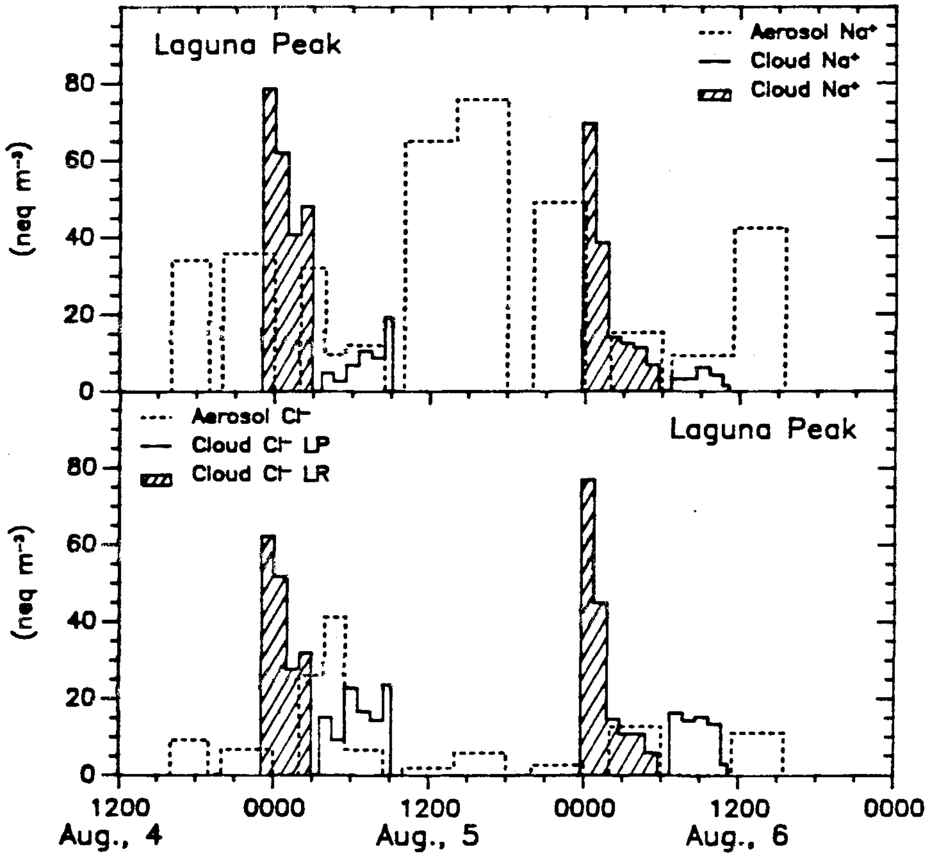

Figure 7.11 Aerosol and cloudwater loadings of sea salts at Laguna Peak on August 4 – 6, 1986. Cloudwater loading is the product of aqueous–phase concentration and estimated LWC.

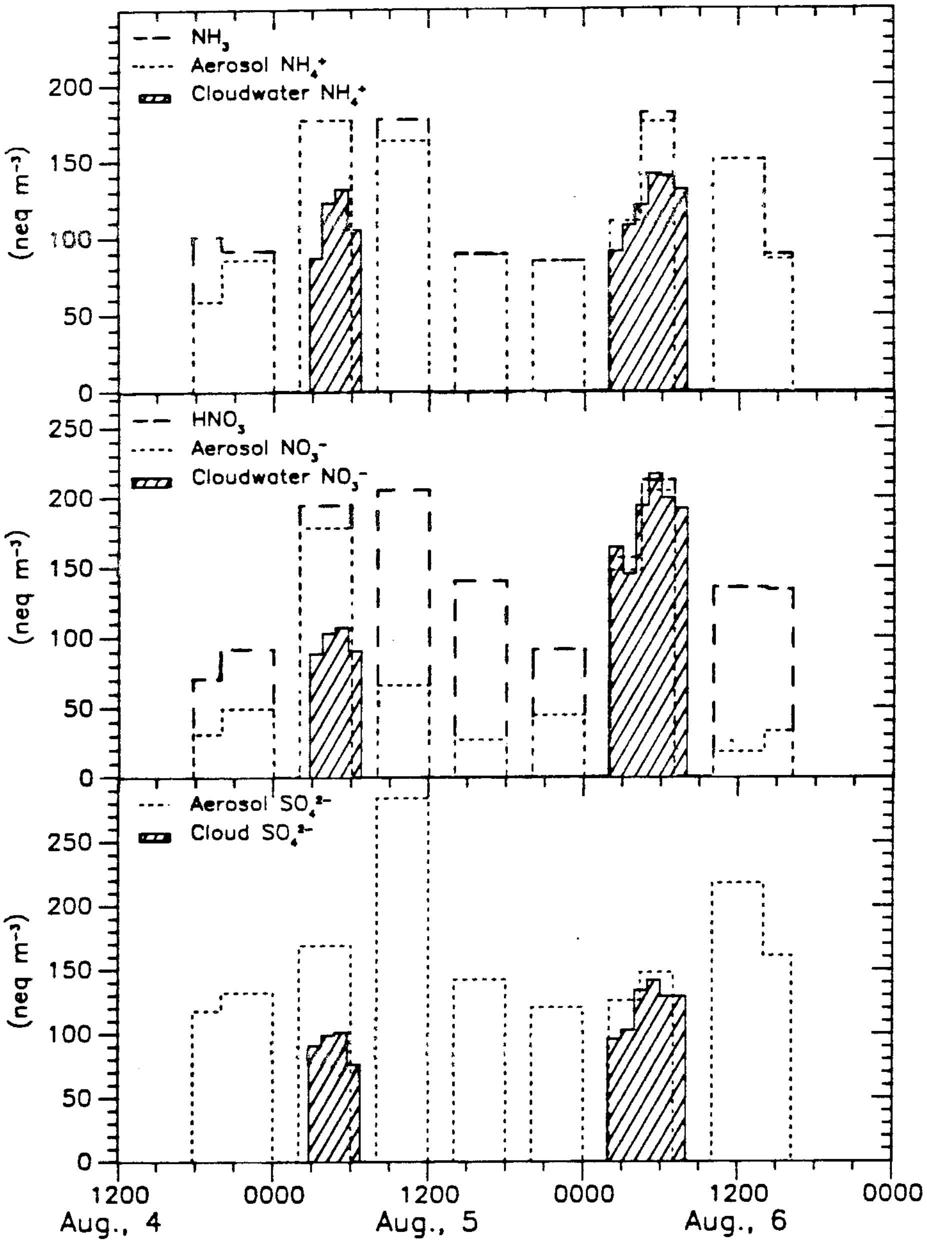

Figure 7.12 Aerosol and cloudwater loadings of major ions at Ventura on August 4 – 6, 1986. Cloudwater loading is the product of aqueous–phase concentration and estimated LWC.

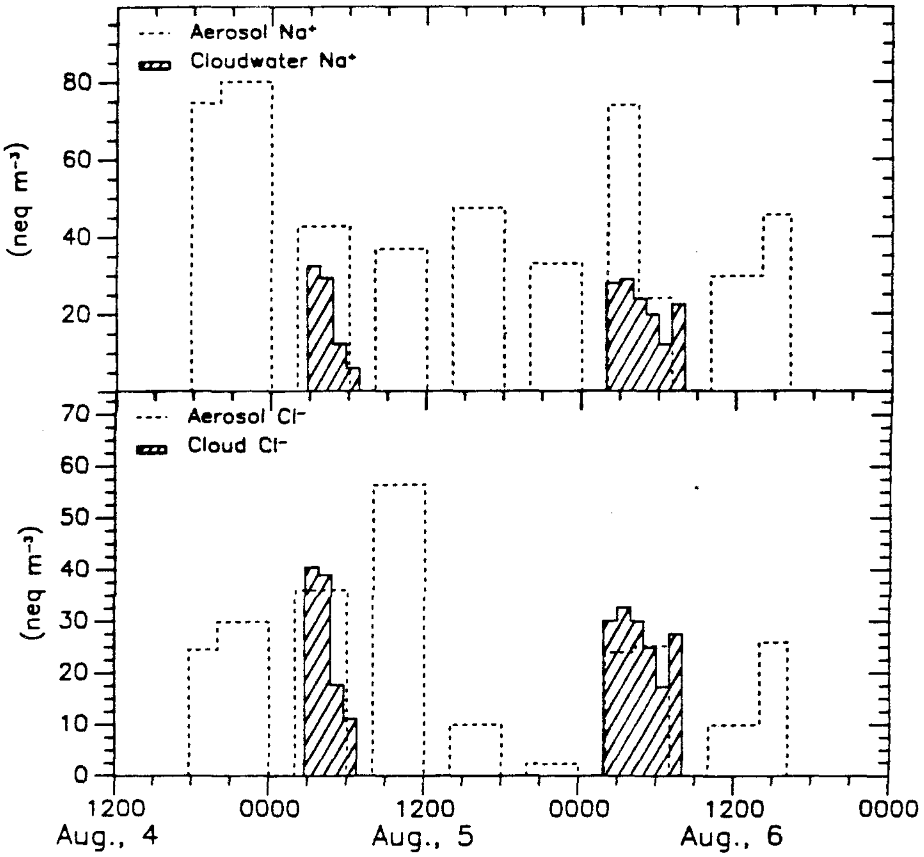

Figure 7.13 Aerosol and cloudwater loadings of sea salts at Ventura on August 4 – 6, 1986. Cloudwater loading is the product of aqueous–phase concentration and estimated LWC.

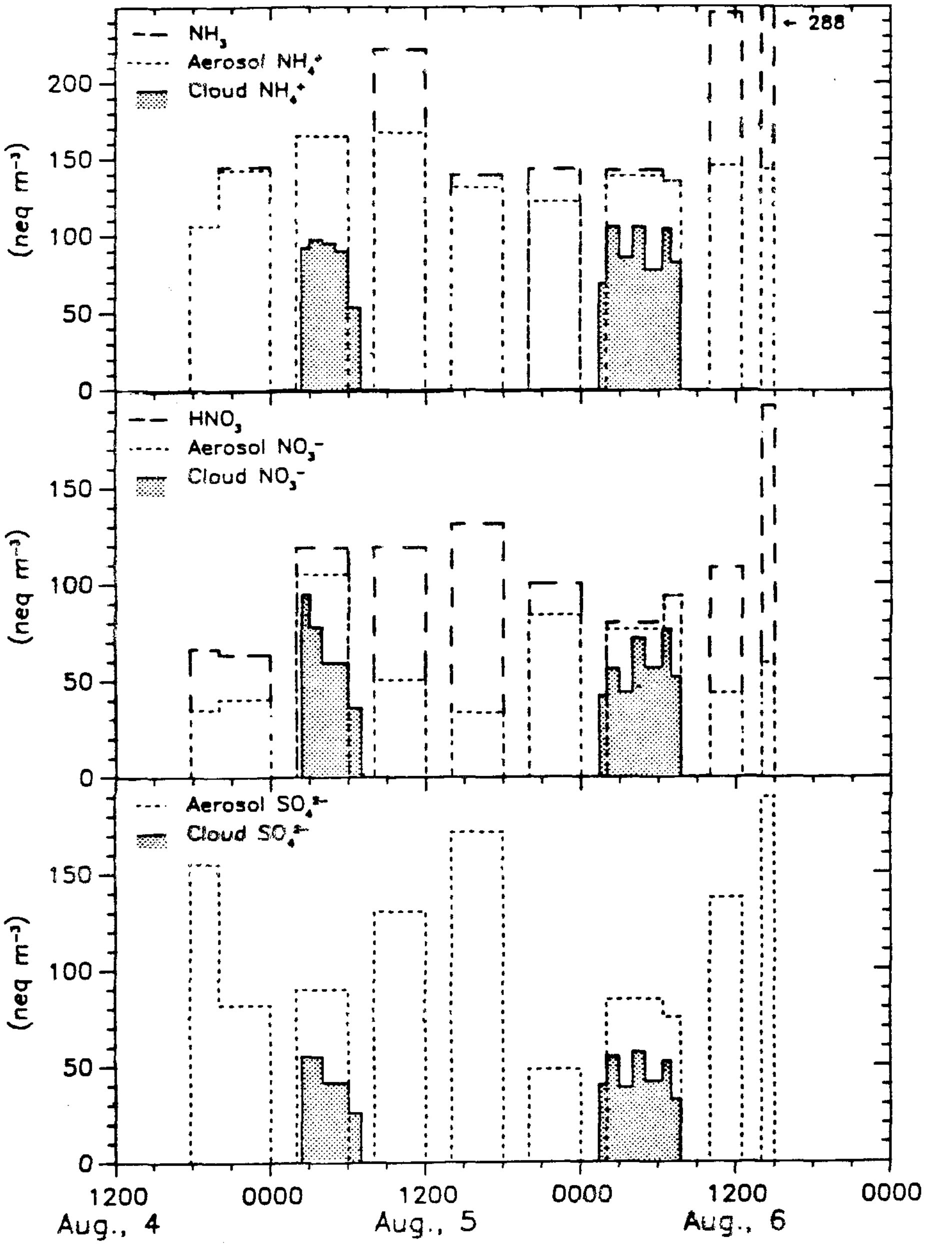

Figure 7.14 Aerosol and cloudwater loadings of major ions at Casitas Pass on August 4 – 6, 1986. Cloudwater loading is the product of aqueous–phase concentration and estimated LWC.

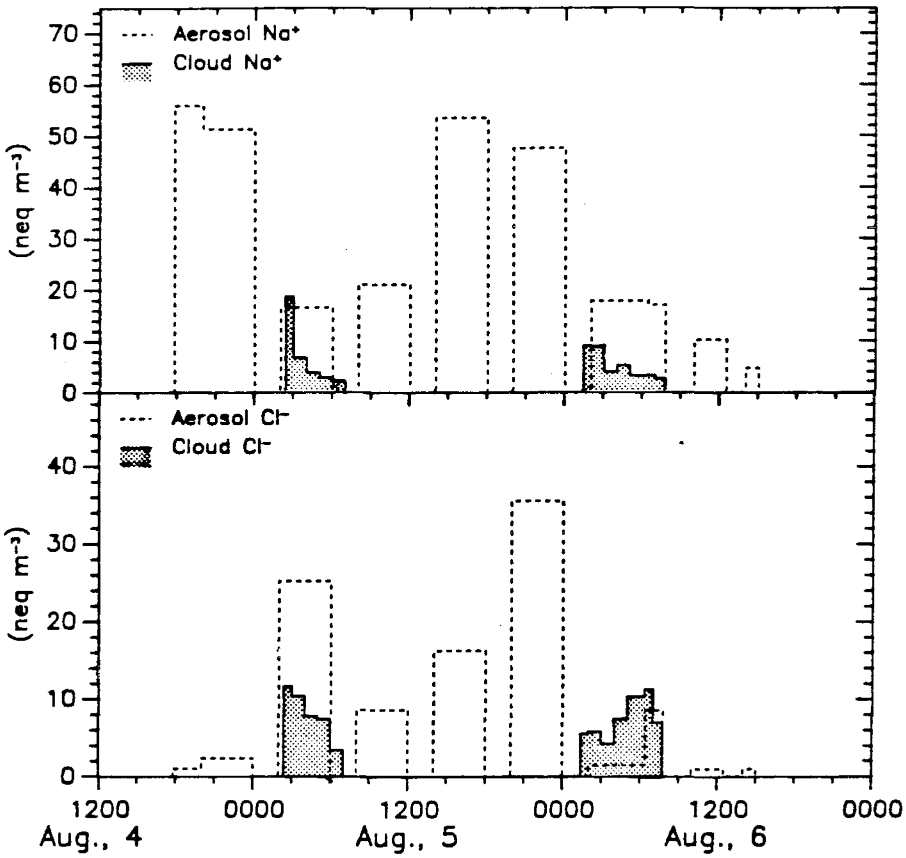

Figure 7.15 Aerosol and cloudwater loadings of sea salts at Casitas Pass on August 4 – 6, 1986. Cloudwater loading is the product of aqueous–phase concentration and estimated LWC.

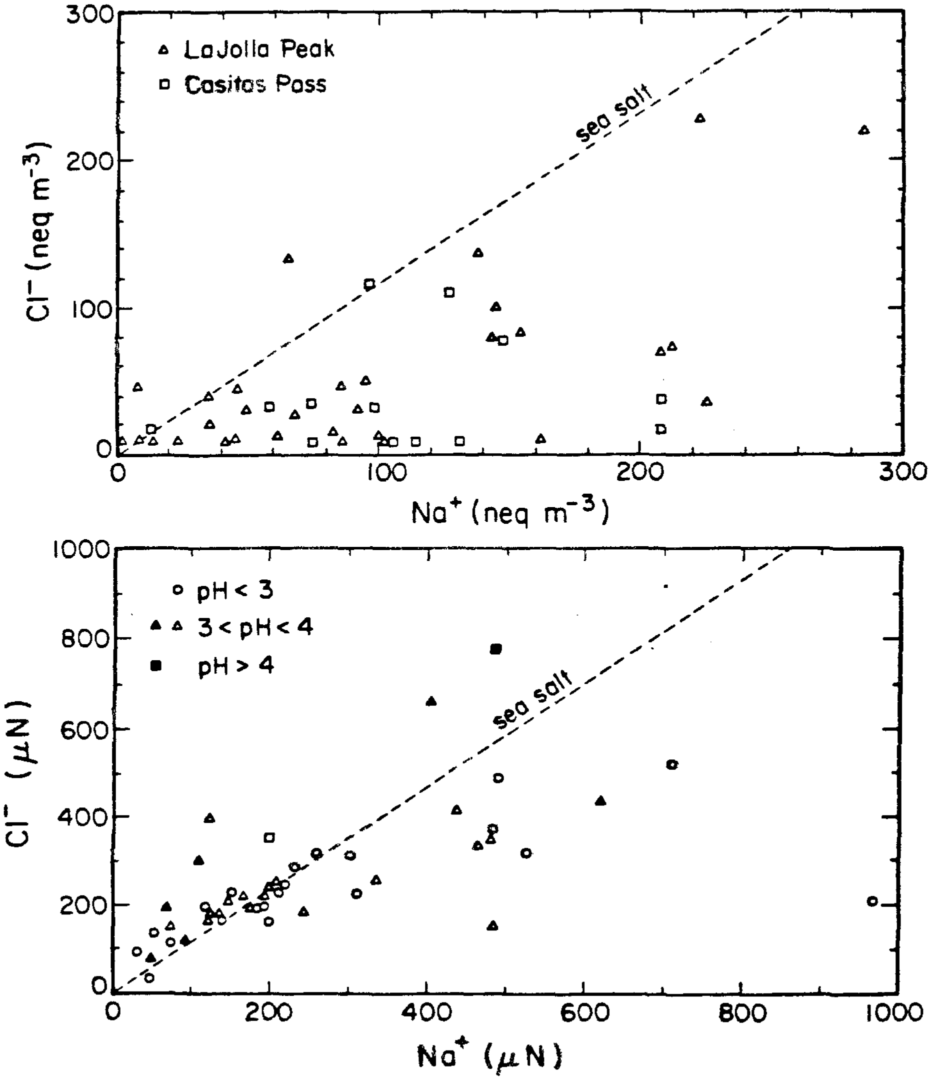

Figure 7.16 A. Plot of Cl^- concentration vs. Na^+ in aerosol samples collected at La Jolla Peak and Casitas Pass during July and August 1985
B. Plot of Cl^- concentrations vs Na^+ in cloudwater samples collected at La Jolla Peak (○,△) and Casitas Pass (▲,■).

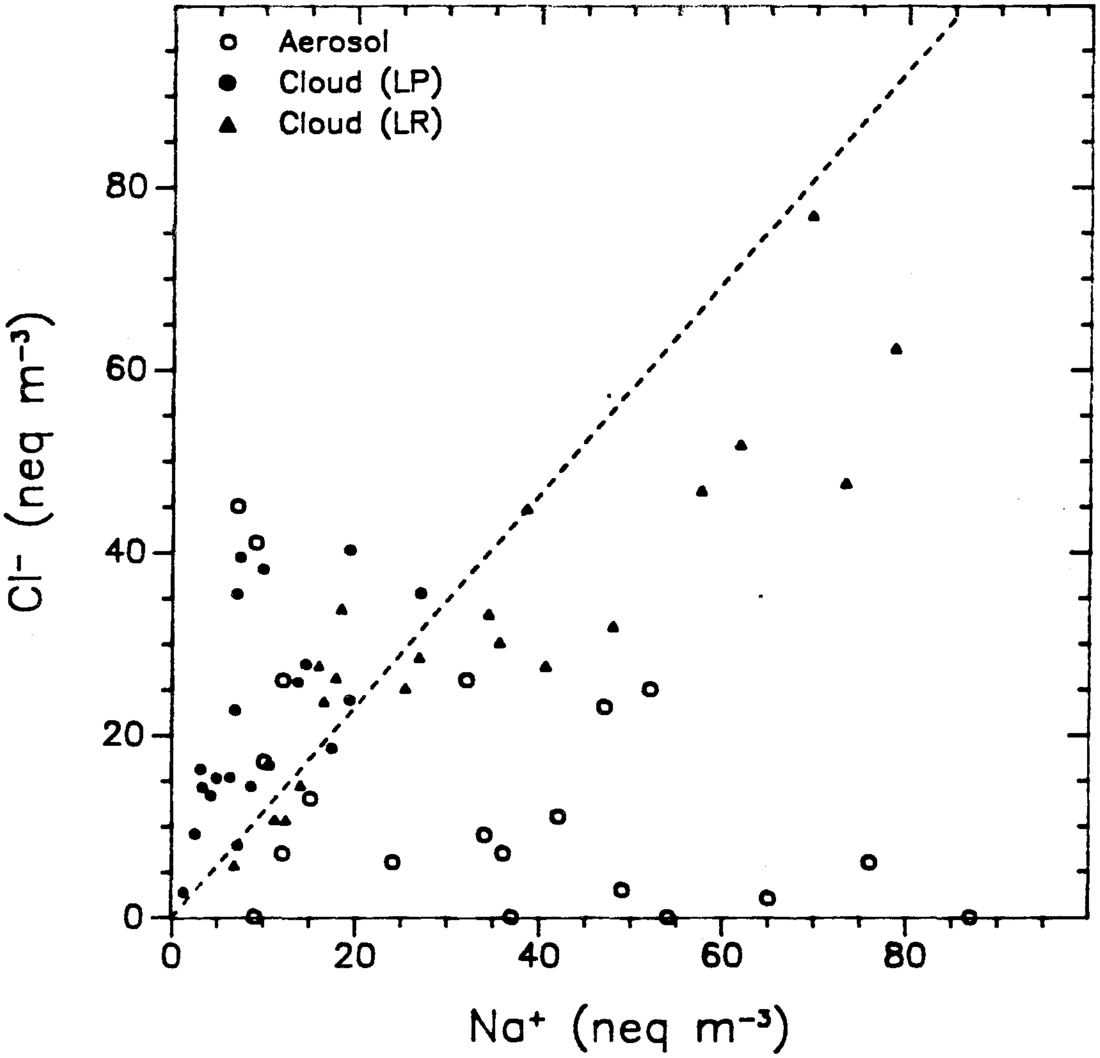

Figure 7.17 Plot of Cl^- concentrations vs Na^+ in aerosol and cloudwater samples from the upper and lower sites collected at Laguna Peak during July and August 1986. Cloudwater concentrations are given as loading, which is the product of aqueous–phase concentration and LWC.

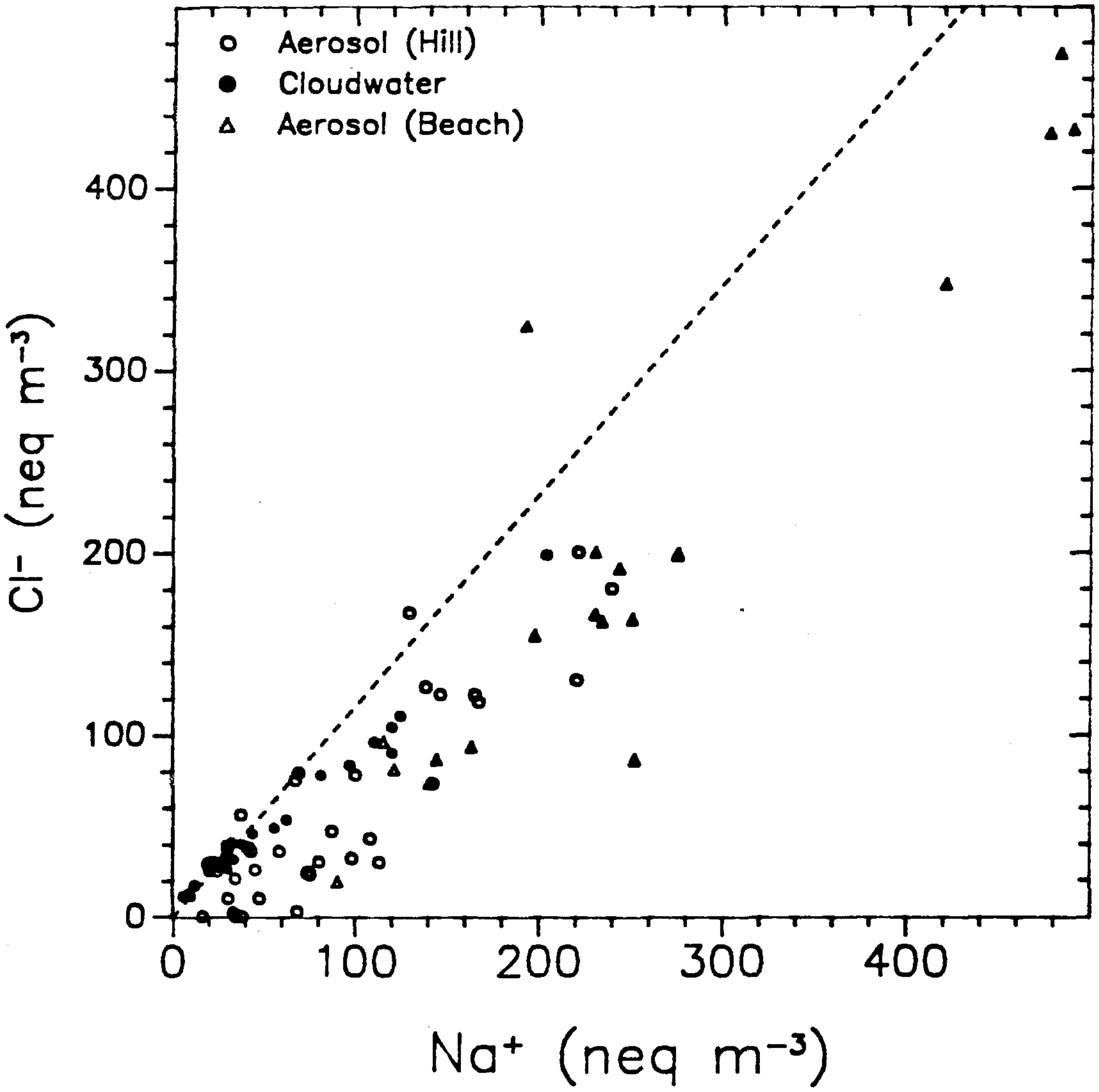

Figure 7.18 Plot of Cl^- concentrations vs Na^+ in aerosol and cloudwater samples collected at Ventura during July and August 1986. Cloudwater concentrations are given as loading, which is the product of aqueous–phase concentration and LWC.

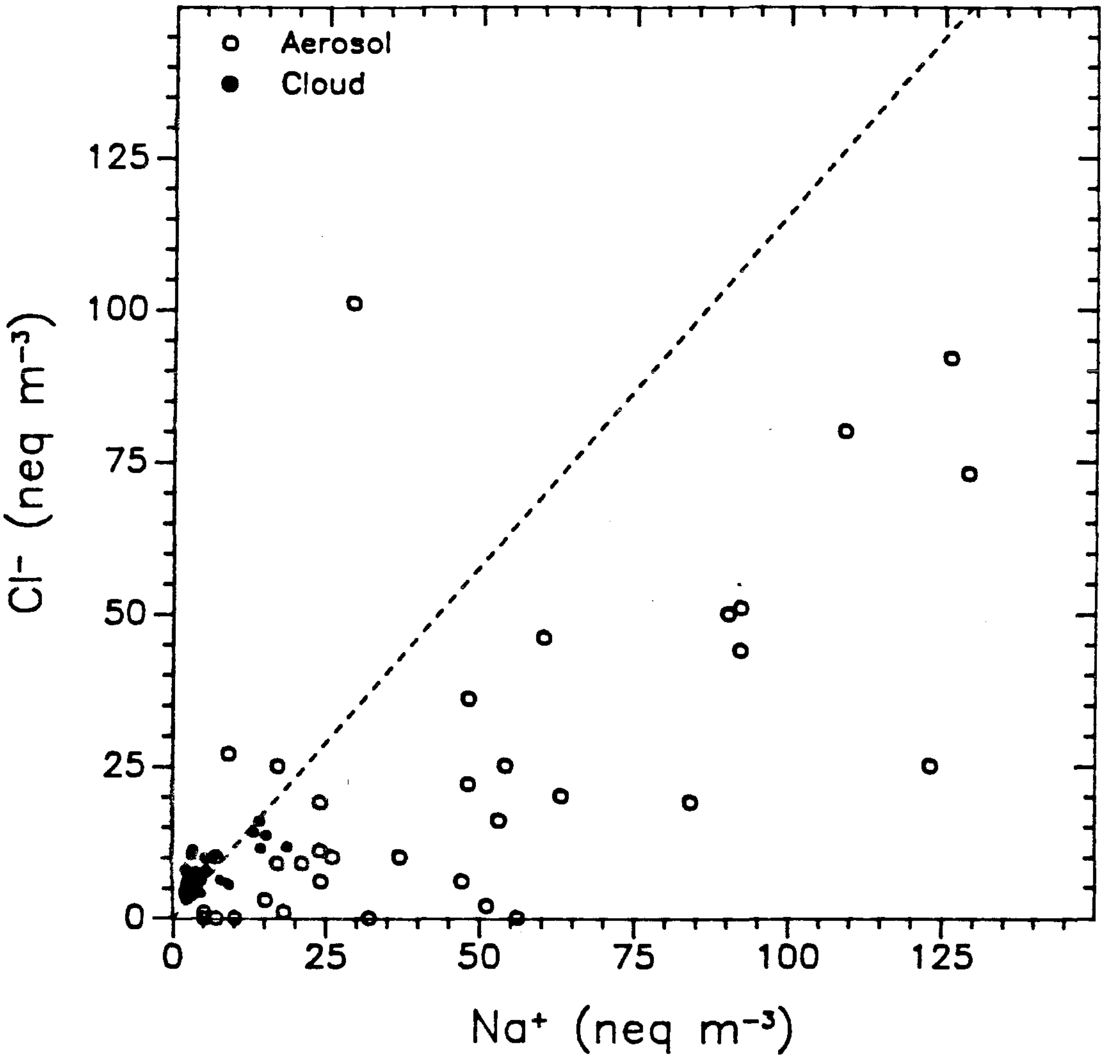

Figure 7.19 Plot of Cl^- concentrations vs Na^+ in aerosol and cloudwater samples collected at Casitas Pass during July and August 1986. Cloudwater concentrations are given as loading, which is the product of aqueous–phase concentration and LWC.

CHAPTER 8

CHEMICAL COMPOSITION OF COASTAL STRATUS CLOUDS: Dependence on Droplet Size and Distance from the Coast

by

J. William Munger, Jeff Collett, Jr.,
Bruce Daube, Jr., and Michael R. Hoffmann

Environmental Engineering Science
W. M. Keck Laboratories, 138–78
California Institute of Technology
Pasadena, CA 91125

Submitted to *Atmospheric Environment*:
December 9 1988

Abstract

The aerosol at elevated sites in the South Coast Air Basin in California is a mixture of sea salt and pollution–derived secondary aerosol. The influence of sea salt declines with increasing distance from the coast. Nitric acid appears to react with the NaCl in sea–salt aerosol to release $HCl_{(g)}$ and form $NaNO_3$ in the aerosol. At inland sites aerosol concentrations differ during onshore and offshore flow. The highest concentrations are observed during the day when the onshore flow transports pollutants to the sites, while lower concentrations were observed at night when drainage flows from nearby mountains influenced the sites. Variations in liquid water content are a major influence on cloudwater concentration.

Comparisons of the ionic concentrations in two size–segregated fractions collected during several sampling intervals suggest that there is a large difference between the average composition of the smaller droplets and that of the larger droplets. The concentrations of Na^+, Ca^{2+} and Mg^{2+} in the large droplet fraction were observed to be higher than in the small droplet fraction, while the concentrations of SO_4^{2-}, NO_3^-, NH_4^+, and H^+ were higher in the small droplet fraction. Chloride concentrations were nearly equal in both fractions. Differences in the composition of size–fractionated cloudwater samples suggest that large droplets are formed from sea salt and soil dust, which are large aerosol, and small droplets are formed on small secondary aerosol composed primarily of ammonium sulfate and ammonium nitrate. The concentrations of several components that exist partly in the gas phase (e.g. Cl^-, HCOOH, and CH_3COOH) appear to be independent of droplet size.

Introduction

Coastal stratus clouds are a major feature of the Los Angeles weather pattern. Cass (1979) noted a correlation between episodes of high SO_4^{2-} concentrations and the presence of cloud or fog. Previous studies by Waldman et al. (1985) and Richards et al. (1983) have indicated that stratus clouds above Los Angeles have high concentrations of NO_3^- and SO_4^{2-}.

The size–dependent composition of aerosol is well known. Soil dust and sea salt generally make up the large aerosol, while nitrate and sulfate, partially neutralized by ammonium, make up much of the sub–micron aerosol. If droplet size is dependent on the size of the condensation nucleus then the composition of droplets could depend on size as well. In Japan, Naruse and Maruyama (1971) observed a correlation between droplet size and nucleus mass. The larger droplets contained large sea–salt nuclei, while the smaller drops contained ammonium sulfate aerosol. Hudson and Rogers (1984) indirectly determined nucleus size by measuring the critical supersaturation (SS_{cr}) of nuclei from different size droplets. They found that the largest drops contained nuclei with low SS_{cr} (i.e. large mass). Noone et al. (1988) have recently provided evidence that solute concentration within cloud droplets can be a function of droplet size in coastal stratus clouds (Cheeka Peak Research Station, Washington). They reported that cloud droplets in the size range of 18 to 23 μm had solute mass 2.7 times that of droplets in the size range of 9 to 18 μm. Their results were consistent with the suggestion by Andreae et al. (1986) that in marine air the larger droplets are nucleated on dust or sea salt, while the smaller droplets form on excess (non–sea–salt) sulfate derived from the photoxidation of dimethyl sulfide. Collett et al. (1989) attributed differences in the composition of cloudwater samples collected by two collectors with different 50% lower droplet size cuts to size–dependent differences in droplet composition. Some of the theoretical aspects of size–dependent variations in droplet composition have been discussed by Perdue and Beck (1988).

In addition to an anticipated dependence of the chemical composition of the coastal stratus on droplet size, we also expected to see significant variations in composition as a function of distance from the coast. In order to examine these phenomena we developed a cloudwater sampler capable of size fractionation and we established cloudwater and aerosol sampling stations at three elevated sites in the Los Angeles air basin during a period of prolonged cloud cover. This effort overlapped in time with the Southern California Air Quality Study (SCAQS) of 1987.

Methods

· *Site Descriptions*

Three sites, San Pedro Hill, Henninger Flats, and Kellogg Hill (see Fig. 8.1), were operational during the period of June 13 to July 17, 1987. The San Pedro Hill site (elev. 450 m) was located at a radar and communications facility operated by the U. S. Air Force and the Federal Aviation Administration. San Pedro Hill is the easternmost hill of the ridge that forms the Palos Verdes Peninsula. The distance from the site to the ocean is 2.5 km; Los Angeles Harbor is 6 km east. The sampling equipment was placed at the edge of a flat grassy area. A steep hillside slopes away from the site, giving it unobstructed exposure from 70–270°.

Henninger Flats (elev. 780 m) is on a level bench partway up Mount Wilson in the San Gabriel Mountains, 7 km NE of Pasadena, and 45 km NE of the coastline. This site has been used in previous sampling programs (Waldman et al., 1985) and for a cloud/fog collector intercomparison (Hering et al., 1987). The Flats is an experimental forest area that has been planted with pine trees; the sampling equipment was located in a clearing a few hundred meters back from the edge. Because it is partially sheltered by the surrounding trees, cloud interception at the samplers is slightly delayed.

Kellogg Hill is 38 km E of downtown Los Angeles at an elevation of 370 m. It lies 50 km NE of the coastline. The sampling equipment was located in a fenced enclosure adjacent to a small building that housed radio transmission equipment. The building partially obstructed the sampler when winds were from the south to west, which is the prevailing daytime wind. The site was unobstructed in the direction of the prevailing night–time winds. Construction activity near the site increased aerosol concentrations of soil dust during the daytime.

· *Sampling Procedure*

Each site was equipped with a Caltech Active Strand Collector (CASC) with an automated fractionating sampler and a cloudwater sensor, shown in Figure 8.2 (Daube et al., 1987). The CASC collects droplets by inertial impaction on 510 μm Teflon strands. The 50% collection efficiency cutoff, predicted from impaction theory, is 3.5 μm (diameter) (Friedlander, 1977). A protective rain shield, which had its opening facing downward, was attached to the front of the collector to exclude large ($d > 200$ μm) sedimenting droplets. The cloudwater sensor, which is a miniature version of the CASC connected to a resistance grid, was used to turn the collector on when cloud was present. The cloudwater collected by the CASC was directed to the fractionating sampler. In the fractionating sampler, cloudwater accumulated in a reservoir until a liquid level sensor determined that 60 ml had been collected. The reservoir was then drained to a 60 ml polyethylene sample bottle held in a carousel. The carousel had a capacity of 20 bottles. When all 20 bottles had been filled, the level sensor was deactivated. Any further sample collected was retained in the reservoir. If its capacity was exceeded the sample drained out through an overflow tube. The reservoir and sample bottles were housed in a refrigerator. A printer recorded the times that the sampler came on and off and when the bottles were filled. Sampling periods varied from as short as 10 minutes to over an hour, depending on the liquid water content (LWC) of the cloud.

Also located at each site was an automated filter pack aerosol sampler. Open-faced Teflon filters (Gelman Zefluor, 1μm pore size) were used to collect total aerosol for inorganic analysis. $HNO_{3(g)}$ was collected on a nylon filter (Gelman Nylasorb) placed behind one Teflon filter. $NH_{3(g)}$ was collected on two oxalic acid impregnated glass fiber filters behind a second Teflon filter. A rain shield above the filter holders excluded debris and sedimenting droplets. These samples were intended to determine the total concentration of the measured ions in the atmosphere. Total concentrations are needed to evaluate temporal variations in concentration in the presence of fluctuating LWC. Sampling intervals were 3 – 4 hours and collection was timed to avoid sunrise and sunset when temperature and humidity would be changing rapidly. Because the collection intervals were controlled by a preset timer, it was not always possible to have sampling intervals coincide with the beginning and end of cloudy periods.

Because partitioning between the gas and aqueous phase may be disturbed by collection on a filter the data on concentrations of NO_3^-, HNO_3, NH_4^+, NH_3, and Cl^- may be invalid. However, the total concentrations, N(V) ($\equiv NO_3^- + HNO_3$) and N(–III) ($\equiv NH_4^+ + NH_3$) are not affected by artifact formation. The artifact problem will be most serious when a sampling interval extends past the end of a cloudy period and collected cloudwater is allowed to evaporate.

During the late afternoon or evening prior to an expected cloud event, the samplers were cleaned by rinsing the collection strands, sample tubing, and reservoir with distilled, deionized water (DDH_2O). After rinsing, the strands were sprayed again with DDH_2O, which was collected in the fraction collector as a system blank. Rinsing and blank collection were repeated the following morning whether cloudwater was collected or not. Major ion concentrations in the blank samples were small relative to the cloudwater samples indicating that contamination by the sampler did not affect the results (Munger 1989). Three sets of filters were loaded on the aerosol collector. A timer on the collector controlled the times that each filter set was run.

At San Pedro Hill, a size–fractionating inlet was used on the CASC for the period of 15–16 July, 1987. The rain shield was not used in conjunction with the size–fractionating inlet. Four rows of eight 12.7 mm Teflon rods, which have a 50% lower size cut of 16 μm (droplet diameter) at the sampling velocity of 9 m s^{-1} are arranged at the front of the inlet. Each row covers 46% of the cross–sectional area. Large droplets impact on the rods, while most droplets smaller than 15 μm pass through to be collected on the CASC strands in the main body of the collector. Water from the rods and strands is collected in separate bottles, which were emptied manually at the end of each sampling interval.

· *Analytical Procedures*

Samples were retrieved in the morning following a cloud event and transported to the lab at Caltech. The samples were weighed to determine their volume and the sample pH was measured with a Radiometer PHM82 pH meter using a combination electrode calibrated against pH 4 and 7 buffers. For selected samples small aliquots were removed and treated to stabilize reactive species. CH_2O was stabilized by addition of SO_3^{2-} (Dong and Dasgupta, 1987). Likewise, in a separate aliquot S(IV) was stabilized with CH_2O. Hydrogen peroxide was reacted with p–hydroxyphenylacetic acid in the presence of peroxidase to form a stable dimer (Lazrus et al., 1985). Carboxylic acids were preserved by addition of chloroform (Keene and Galloway, 1984).

The samples and preserved aliquots were stored in a refrigerator at 4 °C until analysis. Major anions were determined by ion chromatography with a Dionex AS4 or AS4A separator column and a micromembrane suppressor. The eluent was 2.8 mM HCO_3^-/ 2.2 mM CO_3^{2-}. The metallic cations were determined by atomic absorption spectrophotometry. An air/acetylene flame was used for Na^+ and K^+; N_2O/acetylene was used for Ca^{2+} and Mg^{2+} to minimize interferences. NH_4^+ was determined by flow injection analysis employing the indophenol blue method.

The stabilized CH_2O was determined by a modification of the Nash method for use with an autoanalyzer (Dong and Dasgupta, 1987) Hydrogen peroxide was added to eliminate S(IV), which interferes by forming an adduct with CH_2O. The absorbance of the colored product was measured at 410 nm. S(IV) was analyzed by the pararosaniline method (Dasgupta et al., 1980) adapted for flow injection analysis. Carboxylic acids were determined by ion exclusion chromatography (Dionex ICE–AS1) with dilute HCl as the eluent and by normal ion chromatography using $Na_2B_4O_7$ as the eluent.

The Teflon and oxalic acid–impregnated glass fiber filters were extracted in distilled deionized water (DDH_2O) on a shaker table. A small volume of ethanol was added to each Teflon filter prior to extraction to more effectively wet the filter surface. The nylon filters were extracted in HCO_3^-/CO_3^{2-} IC eluent. Composition of the extracts was determined by the same procedures used for the cloudwater samples, with the exception of additional buffer in the complexing reagent and oxalic acid in the rinse solution of the ammonia analysis to account for the effect of the oxalic acid. Complete details of the analytical procedures and estimates of their precision and accuracy are presented elsewhere (Munger, 1989).

Results

· *Aerosol Composition*

The aerosol and gas–phase data for San Pedro Hill, Henninger Flats, and Kellogg Hill are summarized in Tables 8.1 – 8.3. The samples are separated into day and night samples to account for the diurnal variation in wind direction at the sites. Onshore winds prevailed during the day; offshore drainage flows prevailed at night. Stratus clouds were more frequent and relative humidity was higher at night also. The major species present were NH_4^+, NO_3^-, and SO_4^{2-}. In many of the daytime samples

HNO_3 was equal to or greater than the NO_3^-. At night, HNO_3 accounted for a smaller fraction of the total N(V). In the presence of cloud, HNO_3 should be nearly 100% scavenged by the droplets. However, it is evident from looking at data for individual samples that there could have been evaporation of droplets to give artifact HNO_3, particularly in some of the samples collected at San Pedro Hill in the morning as the clouds dissipated. Evaporation of HCl is also possible under these circumstances. As noted above, the total concentration, N(V), is not affected by this artifact, thus trends in N(V) concentrations are real. In general, the concentrations of N(–III), N(V), and SO_4^{2-} increased with distance from the coast. Na^+, Cl^- and Mg^{2+} concentrations decreased away from the coast. The highest concentrations of NH_3 were observed at Kellogg Hill.

Day and nighttime concentrations at San Pedro Hill were similar. At Henninger Flats and Kellogg Hill there was a tendency towards higher concentrations in the daytime samples. This apparent trend was not statistically significant, however, because of the large degree of variability in the daytime concentrations.

Most of the samples showed a large Cl^- deficit when compared to the sea salt Na^+:Cl^- ratio for standard seawater (Weast, 1985) (see Fig. 8.3A). The averages in Tables 8.1 – 8.3 indicate that the Cl^- deficit is generally greater in the daytime.

Concentrations of the acidic anions, $NO_3^- + SO_4^{2-}$, exceeded those of NH_4^+ in all but one sample from San Pedro Hill (Fig. 8.4A). The overall acid–base balance of the atmosphere is indicated in Figure 8.4B which plots total acids against total bases (acids = $Cl^- + NO_3^- + SO_4^{2-} + HNO_3$; bases = $NH_4^+ + Na^+ + Ca^{2+} + Mg^{2+} + NH_3$). Other species such as S(IV) (including the sulfonate adducts), organic acids, and transition metals are not likely to be important to acid base balance. Measured values of S(IV) in selected cloudwater samples indicated it had negligible concentrations relative to the other ions. Observations at other locations indicate that the aerosol contains a very small fraction of the total organic acid concentration (Talbot et al., 1988). Furthermore, measured concentrations of organic acid in the cloudwater were small relative to the inorganic anions. Even if all the trace metals in cloud and fog water were dissolved, previous measurements (Munger et al., 1983) indicate they would be a minor component of the total ionic loading. The difference between the two sums is equivalent to total atmospheric alkalinity, as defined by Jacob et al. (1986). Most of the data plot along the 1:1 line, which indicates neutrality. The samples with the most excess acid are from Henninger Flats. Kellogg Hill had the samples with most excess base.

· ***Cloudwater Composition***

The weather pattern during June and July 1987 was ideal for cloudwater collection. Clouds formed nearly every night. During the sampling period, 242 samples from 18 cloud events were collected at San Pedro Hill. Because the sampling carousel could only hold 20 time–resolved samples, long cloud events with high liquid water content (LWC) were not sampled to the end.

Inorganic concentrations for the San Pedro Hill cloudwater samples are summarized in Table 8.4; data for organic species in selected samples are summarized in Table 8.5. Typical LWC values, as estimated from collection rate and the theoretical collection efficiency of the CASC, were $\simeq 0.1$ g m^{-3}. Cloudwater at San Pedro Hill was consistently acidic. The overall range of pH was 2.4 – 5.0; the volume–weighted average pH was 3.15. The major anions were NO_3^- and SO_4^{2-}; on an equivalent basis NO_3^- was in slight excess. In addition to H^+, the major cations were NH_4^+ and Na^+. Their ranking varied from event to event. Concentrations of CH_2O were typically 20 – 30 μM, while the concentrations of formic and acetic acid were found to be in the range of 12 – 43 μM and 6 – 31 μM, respectively. Hydrogen peroxide concentrations were found in the range of 4 – 72 μM while S(IV) was usually absent in samples for which it was determined. In addition to formaldehyde other aldehydes such as acetaldehyde (1 – 5 μM) glyoxal (1 – 10 μM), and methylglyoxal (4 – 8 μM) were identified and quantified in cloudwater collected at San Pedro Hill during this sampling program (Igawa et al., 1989).

Clouds intercepted Henninger Flats less frequently than at San Pedro Hill. Because of the difference in their elevations, clouds usually did not intercept both sites simultaneously. At Henninger Flats, 76 samples from 5 cloud events were obtained during the sampling period. Cloudwater from Henninger Flats was similar in chemical composition to that from San Pedro Hill (see Table 8.6). The range of pH was comparable at the two sites, but Henninger Flats had a slightly higher pH on the average. Henninger Flats cloudwater had higher concentrations of NH_4^+ and lower SO_4^{2-} and Na^+. Because of the lower SO_4^{2-}, the ratio of NO_3^- to SO_4^{2-} was greater at Henninger Flats. Stratus clouds did not penetrate far enough inland at low elevation to intercept the Kellogg Hill site.

In the majority of the cloudwater samples, Cl^- and Na^+ were present at the sea water ratio (see Fig. 8.3B), however, a Cl^- deficit (or Na^+ excess) was consistently observed in samples with $Na^+ > 750$ μN. The apparent Cl^- deficit in the average concentrations is due to the influence of the high concentration samples.

· *Temporal Variations*

Concentration vs. time profiles for 4 representative periods are shown in Figures 8.5 – 8.8. Gaps in the LWC trace indicate non–continuous sampling when the 20 bottles had been filled. Concentrations for the period 0400 –1300 on July 15 at San Pedro Hill are derived from the volume–weighted average of the two size–fractioned samples. Concentrations tended to decrease as LWC increased, and then increase again at the end of the event as LWC decreased. Some depletion was also apparent during long periods of stable LWC, such as the samples collected after 0700 on July 15 at San Pedro Hill and the second set of samples from Henninger Flats on July 16.

Most of the samples obtained at the two sites were collected during non-overlapping time periods. Often the stratus clouds would intercept one site on a given day and not the other. At other times, the clouds were observed to intercept the hillside at San Pedro during the period shortly after midnight, while interception at Henninger Flats did not begin until a few hours later. By this time, clouds were no longer intercepting the slopes of San Pedro Hill. The only event with simultaneous collection at both sites was on the night of July 16–17. This event, which was associated with drizzle in the L.A. Basin, was one of the most persistent during the study. Clouds were present at both sites the previous night, though the bottles at San Pedro Hill were full by 0244 on 16 July when continuous cloud interception began at Henninger Flats. The clouds did not completely clear during the day of July 16. Continuous cloud cover returned to both sites around 1740 the evening of July 16 and filled all 20 bottles by approximately 2300 on 16 July. Cloud interception continued without interruption until 0500 at both sites, followed by intermittent interception until mid–morning. This event had the lowest overall concentrations of major ions and the highest pH observed at San Pedro Hill. The pH and ion concentrations at Henninger Flats were close to their average values.

· *Size–fractionated Samples*

The size–fractionated cloud samples were collected during an extended cloud event at San Pedro Hill. Clouds initially intercepted the site at approximately 1900 on July 14 and remained until approximately 1300 on July 15. Twenty samples were collected between 1900 and 0000. Collection of size–fractionated samples began at 0400 and continued until 1200. A final one–hour unfractionated sample was collected from 1200 to 1300.

The overall concentration in the clouds when the size–fractionated samples were collected is indicated in Figure 8.6. The major ions are comparable to those at the beginning of the event and in the subsequent event. The sea salt ions were less than in the preceding and following samples. Figures 8.9 – 8.12 illustrate the major ions, sea salts and collection rates in the two fractions. The concentrations of all species increased concurrently around 0600 without appreciable change in collection rate. The sharp increase in the collection rate for large drops subsequent to this corresponded to a period of drizzle. Concentrations gradually decreased over the next several hours until the final samples when they rose again as LWC dropped.

Discussion

· *Inter–site and Temporal Variations*

The differences in chemical composition at the three sites are consistent with their locations. San Pedro Hill, being the closest to the ocean, is affected the most by sea salt. During the day, prevailing winds carry emissions of NO_x and SO_2 and their oxidation products, HNO_3 and $SO_4{}^{2-}$, inland where they impact Henninger Flats and Kellogg Hill. Higher N(–III) levels are obtained at Kellogg Hill, which is closest to the dairy feedlots in Chino (see Fig. 8.1). As noted above, the ratio of SO_4^{2-} to NO_3^- in cloudwater is higher at San Pedro Hill than at Henninger Flats. Modeling and measurements have previously indicated that N(V) concentrations increase in air parcels as they are transported from the coast to inland sites in the SCAB (Russel et al. 198?). In addition, local oil refinery emissions, which affect San Pedro Hill at night, when offshore winds prevail, may directly influence this ratio.

Aerosol concentrations at Henninger Flats and Kellogg Hill were generally less at night than during the day. Henninger Flats was frequently above the inversion at night, which could explain the low concentrations there. In addition, downslope flow from the adjacent mountains, which rise to 1800 m, could flush the site with cleaner air at night. Kellogg Hill, which also is near the San Gabriel Mountains, also may be affected by this mechanism. San Pedro Hill, on the other hand, is far from any higher ground and is not affected by clean–air drainage flows. The offshore winds that influence the site at night may have been influenced by primary emissions and secondary pollutants from throughout the South Coast Air Basin (SCAB). A sea breeze during the day normally would be expected to bring relatively clean air to San Pedro Hill. However, as Cass and Shair (1984) have pointed out, pollutants accumulate off the coast of Los Angeles due to the daily sea breeze/land breeze cycle. Thus, the onshore flow of the sea breeze may return pollutants that were carried out to sea by the previous night's offshore flow.

- ***Acid–Base Balance***

The routine observation of pH 3 cloudwater clearly indicates that the airmass in the portion of the SCAB affected by stratus clouds has excess acidity. The acid–base balance at San Pedro Hill and Henninger Flats (Fig. 8.4B) is generally consistent with this observation. Previous observations by Jacob et al. (1985) noted that coastal areas are generally deficient in acid–neutralizing capacity. Further inland, near the major sources of NH_3 (e.g. cattle feed lots and other agricultural activities), samples with excess alkalinity were collected. In the presence of excess acidity, sea salt aerosol readily loses $HCl_{(g)}$ if the humidity is <99% (Clegg and Brimblecombe, 1985). Apparent loss of Cl^- from aerosol samples has been frequently observed along the California coast (Jacob et al., 1985; Munger et al., 1989b). Due to the reaction between $HNO_{3(g)}$ and $NaCl_{(s)}$, NO_3^- replaces Cl^- in the NaCl–dominated aerosol and releases $HCl_{(g)}$. The emitted gas–phase HCl should be included in the acid base balance because it is efficiently scavenged by cloud droplets. In fact, unlike the aerosol samples most of the cloudwater samples did not have a Cl^- deficit.

It should be recognized that artifact formation may play a role in the observed Cl^- deficiency. Nitric acid could displace Cl^- from sea–salt aerosol collected on a filter. Nitric acid in cloudwater should not displace previously collected Cl^-, as long as the filter remains wet. If the filter dries out, however, HCl would likely be released. This may have occurred in some of the samples collected at San Pedro Hill during the morning hours. Direct measurements of HCl in the gas phase would be valuable to verify that Cl^- displacement is a real phenomena.

· ***Size–fractionated Cloudwater Samples***

Figure 8.13 illustrates the theoretical performance of the size–fractionating inlet calculated from impaction theory for spherical droplets on cylinders (Friedlander, 1977). The fraction of air actually sampled by the collector is a function the diameter and spacing of the collector elements as shown in the following relationship:

$$F_s = 1 - [1-\frac{D_c}{\Delta C}]^n$$

where F_s is the fraction of incoming air that is sampled, D_c is the diameter of an individual collection element, ΔC is the spacing of the elements, and n is the number of rows. The remaining air $(1-F_s)$ passes through the collector without interacting with the collection elements. The CASC contains 6 rows of 510 μm strands, spaced 1.8 mm apart, which yields an 86% sampling efficiency. The size–fractionating inlet contains 4 rows of 12.7 mm rods, spaced 25.4 mm apart, and samples 91% of the incoming air. The sampling efficiency, F_s, and collection efficiency, $\eta(d)$ (Fig. 8.13), are combined with droplet–size distribution curves generated from Best's (1951) formula to estimate the distribution of droplets in the collected fractions (Fig. 8.14).

At low LWC, where a higher proportion of the water is present in droplets too small to be collected by the rods, most of the water will be collected on the strands. With increasing LWC the mass median diameter increases and more sample is collected on the rods. Because the rods do not have a sharp lower size cut–off, there is considerable overlap in the portions of the droplet spectrum sampled by the rods and strands. Any differences observed in the composition of the two sample fractions, therefore, should be considered as a lower bound on the actual differences present.

Comparisons of the ionic concentrations in the two fractions collected during each interval suggest that there is a large difference between the average composition of the smaller droplets and that of the larger droplets. For every interval sampled, the concentration of Na^+ and Mg^{2+} in the large droplet fraction was observed to be higher than in the small droplet fraction. With the exception of one very low concentration sample, the same was true for Ca^{2+}. Concentrations of SO_4^{2-}, NO_3^-, NH_4^+, and H^+ (Fig. 8.9) were almost always higher in the small droplet fraction. Neither fraction had consistently higher Cl^- concentrations (Fig. 8.10); Cl^- was nearly equal in both fractions. The Cl^-:Na^+ ratio in the two fractions differs, however. In the large–droplet fraction, Na^+ and Cl^- are close to the seawater ratio, while the fine–droplet fraction has an excess of Cl^- relative to seawater. As noted above, Cl^- is removed from the sea salt aerosol by reaction with HNO_3. Gas–phase HCl should be scavenged as droplets form. Because the mass transfer and thermodynamics of HCl scavenging by growing droplets change dramatically over a their growth it is not possible to predict the relative fractions of HCl ultimately present in large and small droplets. It is, however, unlikely that HCl will be scavenged by droplets in the same proportion that it was originally present.

Comparison of the organic acid concentrations (Fig. 8.12) in the two fractions indicates little difference; this result would be expected if the clouds were in equilibrium with the surrounding air and the droplet pH did not vary appreciably with size. As noted previously the small droplets had a higher concentration of H^+, however, the difference in pH was <0.4 units. The calculated equilibrium partial pressures of each fraction are comparable (i.e. $C_{aq} = K_{h,i}P_i$). Over the observed cloudwater pH range of 3 to 3.6, the fractions of formic and acetic acid in the gas phase exceed 0.98 (Munger et al., 1989a). The behavior of HCOOH and CH_3COOH in these cloudwater samples is discussed further by Munger et al. (1989a). The CH_2O concentrations in the initial fractionated samples are equivalent, which is also consistent with equilibrium considerations. However, beginning at 0530 there was a spike in [CH_2O], [HCOOH], and [CH_3CO_2H] as well as the major inorganic ions. The organic acids appear to maintain their apparent equilbrium between the gas and aqueous phases, while the CH_2O showed a pronounced increase in the small–droplet fraction. This difference disappears over the subsequent three hours. The sharpness of the pulse suggests the passage of a pollutant plume or a major wind shift. The CH_2O data imply that the precursor nuclei for the smaller droplets contain formaldehyde that is not in equilibrium with the gas phase. The presence of α–hydroxymethanesulfonate (HMSA) and other aldehyde-bisulfite adducts could account for this apparent non–equilibrium behavior (Munger et al., 1986). At pH 3.5, the kinetics of aldehyde–bisulfite adduct dissociation is quite slow (Betterton et al., 1988), thus HMSA in the precursor aerosol would be retained in the droplet and measured analytically as CH_2O. The presence of detectable S(IV) during this period is consistent with this argument. Of special interest in this regard, S(IV) and H_2O_2 were not found to be present simultaneously in either size fraction.

The differences in concentration between the size fractions are consistent with the suggestion that large nuclei produce large droplets and small nuclei produce small droplets (Best, 1951; Mason and Chien: 1962; Hudson, 1984; Jensen and Charlson, 1984; Noone et al., 1988). For the size–dependent aerosol composition to be preserved in the droplets requires nucleation scavenging to be the dominant scavenging process. Because Na^+, Ca^{2+} and Mg^{2+} are associated with sea salt and soil dust (Seinfeld, 1986) they are found predominantly in the large droplets; while NH_4^+, SO_4^{2-}, and to some extent NO_3^-, which are mostly found in secondary aerosol, would be in the small droplets (Seinfeld, 1986). However, NO_3^-, which can exist in the gas phase or on large aerosol by exchange with Cl^-, would also be found to a substantial extent in large droplets. The presence of HNO_3 and presumably HCl serves to reduce the pH difference in the size fractions. In the absence of gaseous acids the large droplets formed on soil dust and sea salt would be expected to have much higher pH than the small droplets. Excess NH_3 in the gas phase would likewise alter the droplet–size dependence imparted by the aerosol composition.

Summary

Aerosol and cloudwater were sampled at three elevated sites in the South Coast Air Basin during the summer of 1987. Aerosol composition was a mixture of sea salt and pollution–derived secondary aerosol. The influence of sea salt declined with increasing distance from the coast. Abundant HNO_3 reacted with the NaCl in sea=salt aerosol to give $HCl_{(g)}$ and $NaNO_3$ in the aerosol. At inland sites aerosol concentrations differ during onshore and offshore flow. The highest concentrations were observed during the day when the onshore flow transports pollutants to the sites, while lower concentrations were observed at night when drainage flows from nearby mountains influenced the sites. Variations in liquid water content are a major influence on cloudwater concentration; however, steady declines in concentration also were observed during periods of stable liquid water content. These may be due to removal by drizzle, dilution by advection, or entrainment of cleaner air from aloft.

Differences in the composition of size–fractionated cloudwater samples suggest that large droplets are formed on large sea–salt and soil–dust aerosol, while small droplets are formed on small secondary aerosol composed of ammonium, sulfate, and nitrate. Components that exist partly in the gas phase (e.g. Cl^-, HCOOH, and CH_3COOH) did not appear to be size segregated. The exchange of HNO_3 for HCl on sea salt provides a means for Cl^- to associate with small droplets. Because Cl^- is removed from the sea salt aerosol during the day, the large droplets that form on these particles are deficient in Cl^-. Chloride is retained in the air mass and some ends up in the small droplets that formed on secondary aerosol.

Acknowledgements

This research was supported by the California Air Resources Board (Contract #A4–142–32). We thank the Federal Aviation Administration, Los Angeles County Fire Department and Pomona Dispatch for their cooperation in allowing us access to sampling sites. We thank Aram Kaloustian and Walter Chong for their assistance in the field and laboratory.

References

Andreae, M. O., Charlson, R. J., Bruynseels, F., Storms, H., Van Grieken, R. and Maenhaut, W. (1986) Internal mixture of sea salt, silicates, and excess sulfate in marine aerosols. *Science*, **295**, 683–685.

Best, A. C. (1951a) Drop–size distribution in cloud and fog. *Q. J. R. Met. Soc.* **77**, 418–426.

Best, A. C. (1951b) The size of cloud droplets in layer–type cloud. *Q. J. R. Met. Soc.* **77**, 241–248.

Betterton, E., Erel, Y., and Hoffmann, M. R. (1988) Aldehyde–bisulfite adducts. Prediction of some of their thermodynamic and kinetic properties. *Environ. Sci. Technol.* **22**, 92–98.

Cass, G. R., and Shair, F. H. 1984. Sulfate accumulation in a sea breeze/land breeze circulation system. *J. Geophys. Res.* **89**, 1429–1438.

Clegg, S. L. and Brimblecombe, P. (1985) Potential degassing of hydrogen chloride from acidified sodium chloride droplets. *Atmos. Environ.* **19**, 465–470.

Collett, J. L., Jr., Munger, J. W., Daube, B. D., Jr., and Hoffmann, M. R. (1988) A comparison of two cloudwater/fogwater collectors: the rotating arm collector and the Caltech active strand collector. submitted to *Atmos. Environ.*

Dasgupta, P. K., DeCesare, K. and Ullrey, J. C. (1980) Determination of atmospheric sulfur dioxide without tetrachloromercurate (II) and the mechanism of the Schiff reaction, *Anal. Chem.* **52**, 1912–1922.

Daube, B. C., Jr., Flagan, R. C., and Hoffmann, M. R. (1987) *Active Cloudwater Collector* United States Patent # 4,697,462, Oct. 6, 1987.

Dong, S. and Dasgupta, P. K (1987) Fast flourimetric flow injection analysis of formaldehye in atmospheric water, *Environ. Sci. Technol.* **21**. 581.

Friedlander, S. K. (1977) *Smoke, Dust and Haze, Fundamentals of Aerosol Behavior.* John Wiley and Sons, New York.

Hering, S. V., Blumenthal, D. L., Brewer, R. L., Gertler, A., Hoffmann, M., Kadlecek, J. A., and Pettus, K. (1987) Field intercomparison of five types of fogwater collectors. *Environ. Sci. Technol.* **21**, 654–663.

Hudson, J. G. and Rogers, C. F. (1984) Interstitial CCN measurements related to mixing in clouds. *Proc. 9th Int. Cloud. Physics. Conf.* August 21–28, TalinnUSSR.

Hudson, J. G. (1984) Ambient CCN and FCN measurements, in ***Hygroscopic Aerosols***, L. H. Ruhnke and A. Deepak, eds., A. Deepak Publishing, Hampton, VA.

Igawa, M., Munger, J. W. and Hoffmann, M. R. (1989) Analysis of aldehydes in cloud and fogwater samples by HPLC with a postcolumn reaction detector. *Environ. Sci. Technol.* in press.

Jacob, D. J., Waldman, J. M., Munger, J. W., and Hoffmann, M. R. (1985) Chemical composition of fogwater collected along the California coast. *Environ. Sci.* Technol. **19**, 730–736.

Jacob, D. J., Munger, J. W., Waldman, J. M., and Hoffmann, M. R. (1986) The H_2SO_4–HNO_3–NH_3 system at high humidities and in fogs: I. Spatial and temporal patterns in the San Joaquin Valley of California. *J. Geophys. Res.* **91**, 1073–1088.

Jensen, J. B. and Charlson, R. J. (1984) On the efficiency of nucleation scavenging. *Tellus*, **36B**, 367–375.

Keene, W. C. and Galloway, J. N. (1984) Organic acidity in precipitation of North America, *Atmos. Environ.* **18**, 2491–2497.

Lazrus, A., Kok, G. L., Gitlin, S. N., Lind, J. A., and McLaren, S. E. (1985) Automated fluorometric method for hydrogen peroxide in atmospheric precipitation, *Anal. Chem.* **57**, 917–922.

Mason, B. J. (1971) ***The Physics of Clouds***, 2nd Ed., Oxford University Press, London.

Mason, B. J. and Chien, C. W. (1962) Cloud–droplet growth by condensation in cumulus. Q. *J. R. Met. Soc.* **88**, 133–138.

Munger, J. W. (1989) *The Chemical Composition of Fogs and Clouds in Southern California* Ph.D. Thesis, California Institute of Technology, Pasadena, CA.

Munger, J. W., Jacob, D. J., Waldman, J. M., and Hoffmann, M. R. (1983) Fogwater chemistry in an urban atmosphere. *J. Geophys. Res.* **88,** 5109–5121.

Munger, J. W., Tiller, C. T., and Hoffmann, M. R. (1986) Determination of hydroxymethanesulfonate in fog water. *Science*, **231**, 247–249.

Munger, J. W., Collett, J., Jr., Daube, B. C., Jr., and Hoffmann, M. R. (1989a) Carboxylic acids and carbonyl compounds in Southern California fogs. *Tellus*, in press.

Munger, J. W., Collett, J., Jr., Daube, B. C., Jr., and Hoffmann, M. R. (1989b) Chemical composition of intercepted stratus cloud along the Santa Barbara Channel coast. (submitted to *Environ. Sci. Technol.*)

Naruse, H. and Maruyama, H. (1971) On the hygroscopic nuclei in cloud droplets, *Papers in Meteor. and Geophys.* **22**, 1–21.

Noone, K. J., Charlson, R. J., Covert, D. S., Ogren, J. A., and Heintzenberg, J. (1988) Cloud droplets: solute concentration is size dependent. *J. Geophys. Res.* **93**, 9477–9482.

Perdue, E. M. and Beck, K. C. (1988) Chemical consequences of mixing atmospheric droplets of varied pH. *J. Geophys. Res.* **93**, 691–698.

Richards, L. W., Anderson, J. A., Blumenthal, D. L., McDonald, J. A., Kok, G. L., and Lazrus, A. L. (1983) Hydrogen peroxide and sulfur (IV) in Los Angeles cloud water, *Atmos. Environ.* **17**, 911–914.

Russell, A. G., and Cass, G. R. (1986) Verification of a mathematical model for aerosol nitrate and nitric acid formation and its use for control measure evaluation. *Atmos. Environ.* **18**, 1815–1817

Seinfeld, J. H. (1986) ***Atmospheric Chemistry and Physics of Air Pollution***, Wiley Interscience, New York.

Shair, F. H., Sasaki, E. J., Carlan, D. E., Cass, G. R., Goodin, W. R., Edinger, J. G. and Schacher, G. E. (1982) Transport and dispersion of airborne pollutants associated with the land breeze–sea breeze system. *Atmos. Environ.* **16**, 2043–2053.

Talbot, R. W., Beecher, K. M., Harriss, R. C., and Cofer, W. R., III (1988) Atmospheric geochemistry of formic and acetic acids at a mid–latitude temperate site. *J. Geophys. Res.* **93**, 1638–1652.

Waldman, J. M., Munger, J. W., Jacob, D. J., and Hoffmann, M. R. (1985) Chemical characterization of stratus cloudwater and its role as a vector for pollutant deposition in a Los Angeles pine forest. *Tellus* **37**, 91–108.

Weast, R. C. (ed.) (1985) *Handbook of Chemistry and Physics 66th Edition*, CRC Press, Boca Raton, FL, p. F–148.

Table 8.1. Summary statistics for aerosol and gas samples collected at San Pedro Hill during the period June 13 – July 17, 1988.

	Na^+	NH_4^+	Ca^{2+}	Mg^{2+}	Cl^-	NO_3^-	SO_4^{2-}	NH_3	HNO_3	N(–III)	N(V)
	neq m^{-3}							nmole m^{-3}			
						Day					
N	18	13	18	18	16	18	18	18	14	13	14
Min	0	7	0	0	0	7	22	0	0	36	7
Max	188	430	47	49	105	147	448	105	166	479	279
Avg	81	186	22	19	25	69	179	19	91	206	164
σ	65	122	10	16	33	37	106	28	57	131	74
						Night					
N	19	12	19	19	16	18	19	19	17	10	17
Min	0	0	0	0	0	6	32	0	0	71	12
Max	170	624	56	44	90	435	475	29	124	635	448
Avg	52	169	22	15	34	127	162	5	28	212	155
σ	46	183	12	13	31	118	121	9	31	180	129

Table 8.2. Summary statistics for aerosol and gas samples collected at Henninger Flats during the period June 13 – July 17, 1988.

	Na^+	NH_4^+	Ca^{2+}	Mg^{2+}	Cl^-	NO_3^-	SO_4^{2-}	NH_3	HNO_3	N(–III)	N(V)
	neq m^{-3}							nmole m^{-3}			
						Day					
N	9	9	9	9	9	9	9	9	8	9	8
Min	0	4	0	0	0	7	5	0	11	4	19
Max	134	838	93	54	29	442	533	99	897	916	1255
Avg	59	367	39	19	6	173	255	40	363	407	526
σ	46	284	31	15	11	136	195	40	317	310	450
						Night					
N	12	12	12	12	12	12	12	12	10	12	10
Min	4	3	0	0	0	9	5	0	13	3	22
Max	59	284	35	15	21	123	234	31	113	302	186
Avg	33	141	23	10	3	59	119	12	57	153	118
σ	18	87	12	5	6	35	70	11	29	93	56

Table 8.3. Summary statistics for aerosol and gas samples collected at Kellogg Hill during the period June 13 – July 17, 1988.

	Na^+	NH_4^+	Ca^{2+}	Mg^{2+}	Cl^-	NO_3^-	SO_4^{2-}	NH_3	HNO_3	N(–III)	N(V)
	neq m^{-3}							nmole m^{-3}			
	Day										
N	7	7	7	7	7	7	7	7	7	7	7
Min	8	9	62	12	0	10	7	0	6	8	16
Max	149	875	270	62	16	629	451	339	624	1063	1191
Avg	92	575	162	44	5	413	296	140	277	714	690
σ	48	302	60	16	6	204	156	120	185	353	358
	Night										
N	11	11	11	11	11	11	11	11	11	11	11
Min	44	139	40	11	0	91	94	0	9	279	133
Max	183	594	109	61	72	452	372	283	63	620	512
Avg	112	343	75	33	20	266	201	89	40	432	306
σ	43	167	21	16	24	118	80	82	19	128	128

Table 8.4. Concentrations in cloudwater samples collected at San Pedro Hill during the period June 13 – July 17, 1987.

	Vol	pH	Na^+	NH_4^+	Ca^{2+}	Mg^{2+}	Cl^-	NO_3^-	SO_4^{2-}	CH_2O	$-/+^*$	LWC
	(ml)		$\|\vdash$	$\longrightarrow$		μN	$\longleftarrow$		$\|$	μM		$g\ m^{-3}$
						14 June 1987						
N	15	15	15	15	15	15	15	15	15	0	15	15
Min	18	2.80	149	323	15	47	247	702	574	—	1.09	0.02
Max	68	3.28	734	744	88	214	787	1608	1407	—	1.19	0.11
Avg	48	3.02	506	501	58	149	538	1062	939	—	1.14	0.07
Vol Wt. Avg		3.02	468	466	54	139	502	991	880	—	—	0.06
						19 June 1987						
N	3	3	3	3	3	3	3	3	3	3	3	3
Min	26	3.18	3258	665	281	593	1654	1281	978	25	0.73	0.02
Max	36	3.33	3796	1237	460	731	1701	2137	1131	31	0.75	0.06
Avg	33	3.25	3486	909	353	652	1676	1674	1078	27	0.74	0.04
Vol Wt. Avg		3.25	3553	980	375	670	1682	1784	1102	—	—	0.04
						20 June 1987						
N	6	6	5	6	4	6	6	6	6	4	6	6
Min	9	3.11	1722	347	173	388	1379	498	749	21	0.73	0.03
Max	65	3.35	2574	605	272	715	1756	1402	1290	31	1.84	0.10
Avg	48	3.24	2024	478	225	476	1468	850	1032	24	1.06	0.06
Vol Wt. Avg		3.24	1812	470	127	444	1434	815	964	—	—	0.06
						21 June 1987						
N	3	3	3	3	3	3	3	3	3	2	3	3
Min	12	3.48	706	169	79	192	735	377	312	12	1.00	0.03
Max	66	3.55	995	295	142	253	837	915	447	14	1.07	0.17
Avg	47	3.52	841	228	108	215	793	590	373	13	1.04	0.09
Vol Wt. Avg		3.51	866	238	113	216	787	606	382	—	—	0.09
						22 June 1987						
N	9	9	9	9	9	9	9	9	9	7	9	9
Min	13	2.84	206	311	27	53	267	436	354	11	0.94	0.04
Max	62	3.43	1257	1126	243	311	978	1632	1478	27	1.09	0.12
Avg	56	3.21	462	552	79	120	485	827	641	16	1.01	0.08
Vol Wt. Avg		3.23	424	467	70	110	447	704	540	—	—	0.07

Table 8.4.(continued)

	Vol	pH	Na^+	NH_4^+	Ca^{2+}	Mg^{2+}	Cl^-	NO_3^-	SO_4^{2-}	CH_2O	$-/+^*$	LWC
	(ml)		‖⟶			μN		⟵	‖	μM		g m^{-3}
						23 June 1987						
N	20	20	20	20	20	20	20	20	20	0	20	20
Min	61	3.15	123	223	17	33	173	277	224	—	0.95	0.02
Max	66	3.62	452	528	95	131	505	1024	608	—	1.27	0.16
Avg	62	3.47	200	293	38	55	257	407	342	—	1.08	0.12
Vol Wt. Avg		3.49	185	277	34	50	241	371	324	—	—	0.10
						24 June 1987						
N	24	24	24	24	20	24	24	24	24	22	24	22
Min	17	2.53	189	462	30	56	309	1291	1119	18	1.09	0.02
Max	66	2.94	3148	2859	560	601	1613	5623	3246	51	1.51	0.25
Avg	56	2.76	794	1495	134	179	666	2627	1871	34	1.18	0.11
Vol Wt. Avg		2.78	553	1340	99	133	552	2226	1669	—	—	0.09
						25 June 1987						
N	23	23	23	23	23	23	23	23	23	15	23	21
Min	10	2.63	142	410	30	37	132	832	660	16	0.89	0.00
Max	68	3.11	1618	9383	1143	1151	2096	8191	5796	37	1.42	0.34
Avg	42	2.78	468	1702	138	135	402	2708	1874	26	1.18	0.18
Vol Wt. Avg		2.81	323	1072	73	73	254	2062	1365	—	—	0.11
						26 June 1987						
N	21	21	21	21	21	21	21	21	21	0	21	19
Min	32	2.99	28	423	8	10	43	454	387	—	0.79	0.08
Max	69	3.51	315	1979	164	86	223	2462	1971	—	1.36	0.29
Avg	55	3.31	89	1058	27	25	90	1044	794	—	1.11	0.21
Vol Wt. Avg		3.34	67	931	20	19	71	915	660	—	—	0.21
						01 July 1987						
N	6	6	7	7	7	7	7	7	7	0	6	6
Min	8	3.15	336	242	57	90	339	401	435	—	0.95	0.02
Max	29	3.23	912	638	215	248	745	1138	836	—	1.02	0.15
Avg	15	3.18	480	517	111	129	454	741	652	—	0.98	0.10
Vol Wt. Avg		3.18	440	555	108	120	415	754	671	—	—	0.04

Table 8.4.(continued)

	Vol	pH	Na^+	NH_4^+	Ca^{2+}	Mg^{2+}	Cl^-	NO_3^-	SO_4^{2-}	CH_2O	$-/+^*$	LWC
	(ml)		$\|\!\longrightarrow$			μN			$\longleftarrow\!\|$	μM		$g\ m^{-3}$
						03 July 1987						
N	14	14	14	14	14	14	14	14	14	0	14	14
Min	20	2.42	308	394	71	83	327	535	492	—	0.98	0.02
Max	62	3.30	683	2770	286	202	656	4656	3028	—	1.26	0.11
Avg	55	2.72	443	1652	128	124	466	2987	1900	—	1.16	0.07
Vol Wt. Avg		2.66	415	1675	119	116	445	2994	1892	—	—	0.06
						07 July 1987						
N	7	7	7	7	7	7	7	7	7	7	7	7
Min	23	3.14	235	266	28	53	284	332	384	12	1.07	0.03
Max	66	3.51	719	1108	127	156	821	1301	810	22	1.19	0.21
Avg	55	3.33	489	473	57	107	537	706	562	16	1.13	0.12
Vol Wt. Avg		3.31	412	470	52	91	453	713	555	—	—	0.10
						08 July 1987						
N	9	9	9	9	9	9	9	9	9	0	9	9
Min	4	2.81	59	88	20	15	71	172	143	—	1.07	0.00
Max	65	3.91	1365	2458	508	335	1055	3419	2647	—	1.27	0.25
Avg	53	3.09	485	866	130	117	415	1435	1044	—	1.15	0.13
Vol Wt. Avg		2.99	481	855	119	116	409	1435	1052	—	—	0.11
						13 July 1987						
N	2	2	2	2	2	2	2	2	2	0	2	2
Min	9	3.79	204	210	45	57	242	174	230	10	0.93	0.01
Max	36	3.83	223	240	52	57	264	217	230	—	1.10	0.05
						14 July 1987						
N	21	21	21	21	21	21	21	21	21	11	21	19
Min	29	3.13	64	129	13	19	95	112	182	5	0.94	0.12
Max	65	3.91	207	977	55	59	240	600	820	38	1.17	0.31
Avg	40	3.61	106	351	26	29	146	285	382	15	1.02	0.22
Vol Wt. Avg		3.63	97	295	22	26	138	235	319	—	—	0.21
						14 July 1987						
N	19	21	21	21	21	21	21	21	21	8	21	19
Min	37	3.23	40	131	10	13	57	167	212	6	0.95	0.05
Max	42	3.73	267	391	77	65	272	602	550	15	1.08	0.23
Avg	39	3.50	160	227	30	38	162	307	327	10	1.01	0.17
Vol Wt. Avg		3.52	175	210	29	40	173	277	311	—	—	0.14

Table 8.4.(continued)

	Vol	pH	Na^+	NH_4^+	Ca^{2+}	Mg^{2+}	Cl^-	NO_3^-	SO_4^{2-}	CH_2O	$-/+$*	LWC
	(ml)		$\|\longrightarrow$			μN			$\longleftarrow\|$	μM		g m^{-3}
						16 July 1987						
N	16	16	16	16	16	16	16	16	16	0	16	15
Min	12	2.64	22	328	14	8	40	190	219	—	0.93	0.02
Max	68	3.93	271	2161	236	100	357	2797	2438	—	1.12	0.24
Avg	51	3.12	119	727	110	43	155	854	992	—	1.06	0.14
Vol Wt. Avg		3.06	93	639	87	35	131	819	888	—	—	0.11
						17 July 1987						
N	20	20	20	20	9	9	20	20	20	0	20	18
Min	25	3.50	6	44	3	1	11	28	39	—	0.92	0.05
Max	56	4.98	92	504	47	28	98	300	376	—	1.23	0.26
Avg	49	4.09	35	136	14	10	43	125	161	—	1.09	0.16
Vol Wt. Avg		3.94	28	101	6	4	35	100	138	—	—	0.14
						All Samples 6–14 to 7–17–88						
N	240	242	241	242	225	231	242	242	242	80	241	227
Min	1	2.42	6	44	3	1	11	28	39	5	0.73	0.00
Max	69	4.98	3796	9383	1143	1151	2096	8191	5796	51	1.84	0.34
Avg	49	3.25	404	775	82	107	369	1185	917	23	1.09	0.14
Vol Wt. Avg		3.15	263	632	51	65	256	941	736	—	—	0.103

* $-/+ = \Sigma$anions / Σcations.

Table 8.5.Concentrations of organic acids, S(IV), HCHO, and H_2O_2 in cloudwater samples collected at San Pedro Hill

Vol	pH	Time	S(IV)	CH_2O	H_2O_2	HCO_2H^*	CH_3COOH^*
		start–stop	‖⟶		μM		⟵‖
7–15–87 Size–fractionated Sample from the Front Rods of the CASC							
68	3.34	4:33–5:00	0	10	10	19	11
71	3.27	5:00–5:30	0	16	0	21	13
71	3.26	5:30–6:00	0	27	0	40	19
74	3.29	6:00–6:30	6	29	0	37	18
112	3.42	6:30–7:00	6	16	0	26	11
121	3.42	7:00–7:30	6	13	0	17	9
136	3.44	7:30–8:00	0	13	4	19	9
122	3.49	8:00–8:30	0	13	10	18	10
116	3.52	8:30–9:00	0	13	16	20	9
64	3.40	10:30–11:00	0	18	49	33	13
7–15–87 Size–fractionated Sample from the Back Strings of the CASC							
29	3.42	4:33–5:00	0	11	9	16	10
28	3.28	5:00–5:30	0	13	0	18	11
31	3.10	5:30–6:00	6	26	0	34	17
28	3.08	6:00–6:30	10	55	0	38	22
38	3.24	6:30–7:00	5	25	0	32	20
39	3.35	7:00–7:30	0	17	0	18	9
38	3.38	7:30–8:00	0	16	3	19	9
30	3.42	8:00–8:30	0	17	6	19	10
32	3.47	8:30–9:00	0	14	11	23	10
30	3.25	10:30–11:00	0	21	39	40	17

Samples Collected from 7–7–87 to 7–14–87

Parameter	Vol	pH	S(IV)	CH_2O	H_2O_2	$HCOOH^*$	CH_3COOH^*
	(ml)		‖⟶		μM		⟵‖
N	21	21	—	20	16	21	21
Min	9	3.14	—	5	4	12	6
Max	59	3.83	—	38	72	43	31
Avg.	38	3.58	—	13	42	20	10

*This represents the total RCOOH (i.e. [RCOOH] + $[RCO_2^-]$).

Table 8.6.Concentrations in cloudwater samples collected at Henninger Flats during the period June 20 to July 17, 1987.

	Vol	pH	Na^+	NH_4^+	Ca^{2+}	Mg^{2+}	Cl^-	NO_3^-	SO_4^{2-}	CH_2O	$-/+^*$	LWC
	(ml)		$\|\vdash$	$\longrightarrow$		μN	$\longleftarrow$		$\|$	μM		$g\ m^{-3}$
20 June 1987												
N	6	6	6	6	6	6	6	6	6	6	6	6
Min	24	2.75	180	805	39	48	169	877	447	66	0.90	0.03
Max	65	3.59	1652	3509	454	435	975	4034	2028	91	1.04	0.09
Avg	48	3.15	542	1575	136	144	377	1879	885	76	0.99	0.05
Vol Wt. Avg		3.09	442	1418	106	118	327	1715	796	78	—	0.05
21 June 1987												
N	12	12	12	12	12	12	12	12	12	11	12	12
Min	7	2.62	183	603	42	49	161	787	36	53	0.76	0.01
Max	45	3.75	1553	3172	520	400	666	5472	2606	109	1.09	0.18
Avg	39	3.01	485	1583	138	129	308	2116	1084	68	0.98	0.08
Vol Wt. Avg		2.96	340	1368	89	90	259	1773	963	62	—	0.05
10 July 1987												
N	20	20	20	20	20	20	20	20	20	0	20	19
Min	29	2.88	48	671	47	20	91	735	368	—	0.81	0.01
Max	63	3.88	195	1760	167	99	214	2065	1094	—	1.08	0.17
Avg	37	3.24	82	1022	91	36	128	1076	589	—	0.96	0.10
Vol Wt. Avg		3.22	68	864	76	29	111	949	526	—	—	0.05
16 July 1987												
N	20	20	20	20	20	20	20	20	20	0	20	18
Min	9	2.68	5	324	7	2	18	284	137	—	0.46	0.01
Max	65	4.78	149	4085	397	77	115	1908	1474	—	1.33	0.40
Avg	58	3.36	43	1392	80	23	48	804	549	—	0.78	0.24
Vol Wt. Avg		3.48	27	740	27	10	35	525	346	—	—	0.14
17 June 1987												
N	18	18	18	18	18	18	18	18	18	0	18	17
Min	40	3.03	3	273	15	7	22	231	159	—	0.95	0.07
Max	65	3.94	273	2435	985	171	301	3319	2028	—	1.18	0.23
Avg	62	3.35	55	817	171	40	73	967	628	—	1.05	0.17
Vol Wt. Avg		3.31	46	752	136	34	63	897	572	—	—	0.15

Table 8.6.(continued)

	Vol	pH	Na^+	NH_4^+	Ca^{2+}	Mg^{2+}	Cl^-	NO_3^-	SO_4^{2-}	CH_2O	$-/+^*$	LWC
	(ml)		||—	—	→	μN	←	—	—||	μM		g m^{-3}
					All Samples 6–20 to 7–17–88							
N	76	76	76	76	76	76	76	76	76	17	76	72
Min	7	2.62	3	273	7	2	18	231	36	53	0.46	0.01
Max	65	4.78	1652	4085	985	435	975	5472	2606	109	1.33	0.40
Avg	50	3.25	166	1203	118	57	142	1206	689	71	0.94	0.14
Vol Wt. Avg		3.29	82	845	74	31	86	855	511	—	—	0.09

* −/+ = Σanions / Σcations.

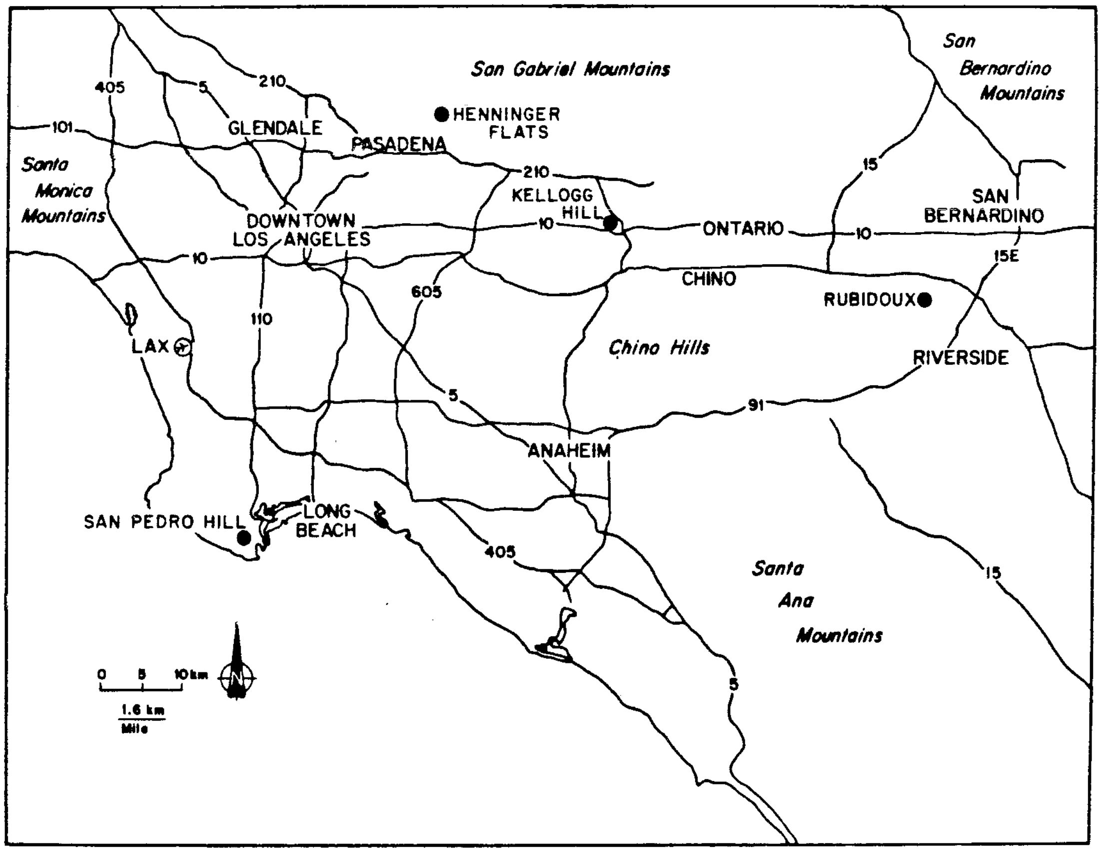

Figure 8.1 Map of the South Coast Air Basin. Major freeways and selected cities are shown. Sampling sites are indicated by •.

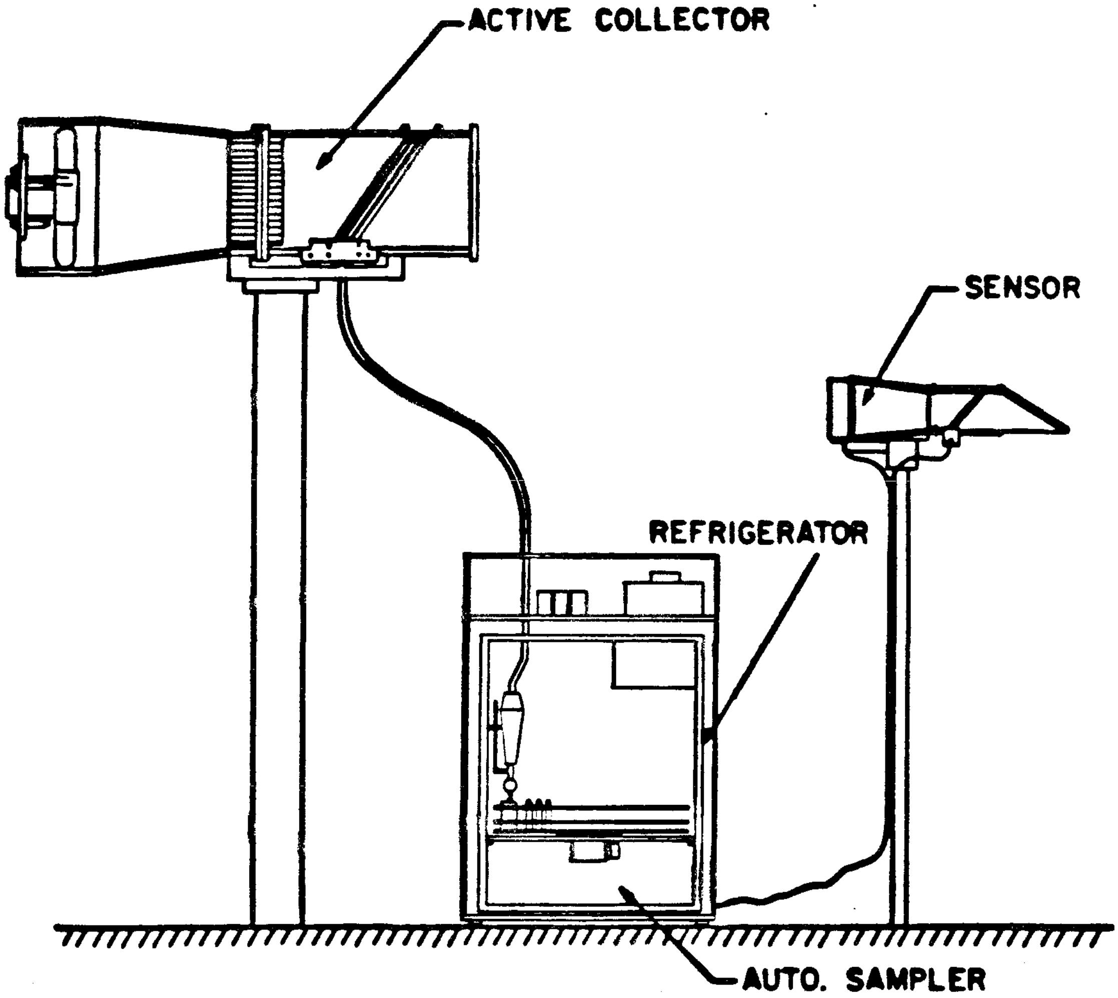

Figure 8.2 Diagram of the automated cloudwater collector system. Depicted in the figure are the CASC, a cloudwater sensor, and the fractionating collector, housed in a refrigerator.

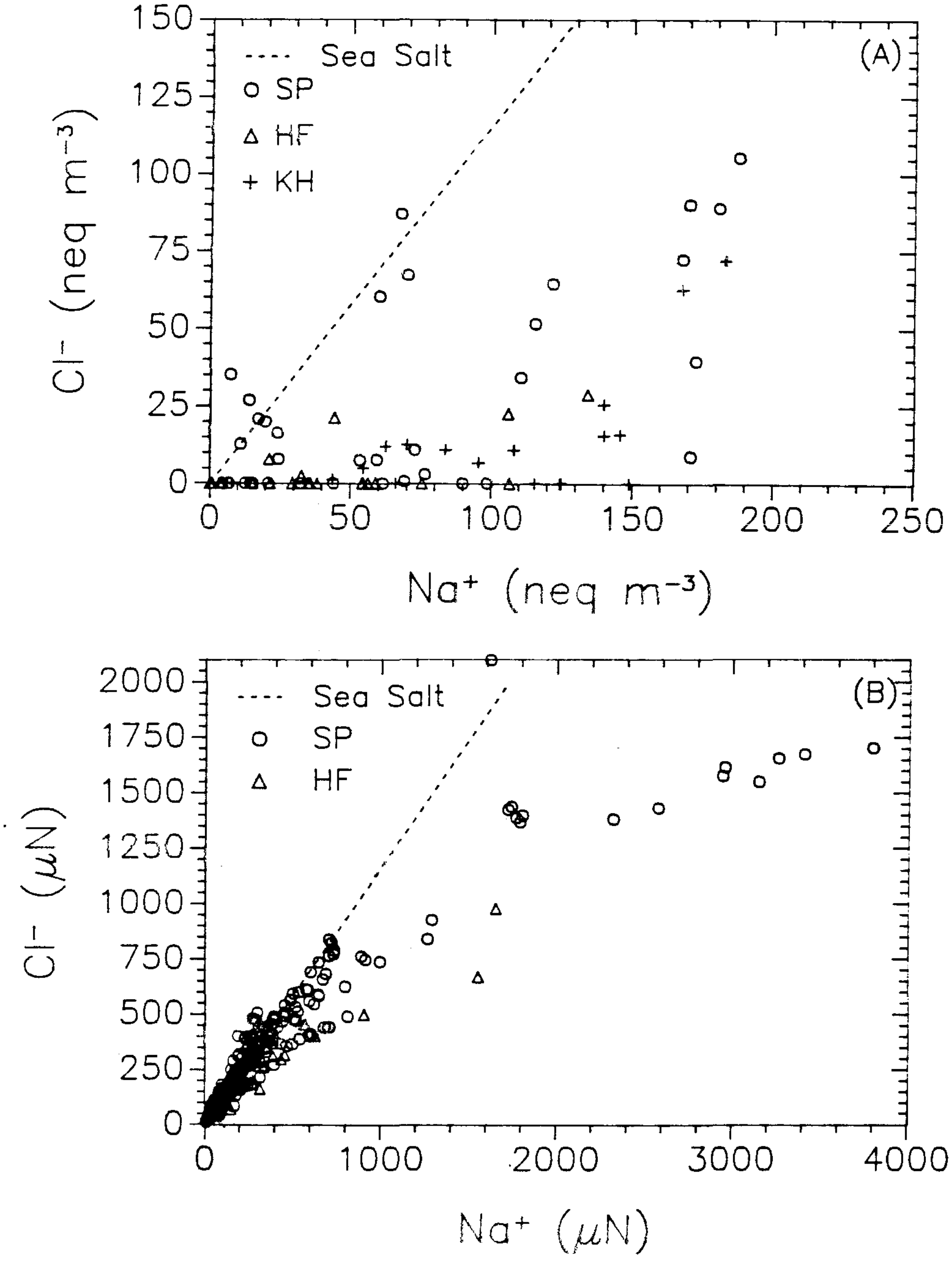

Figure 8.3 A) Cl^- concentrations in aerosol samples, plotted against Na^+, --- indicates the sea–salt ratio.

B) Same as A, but for cloudwater.

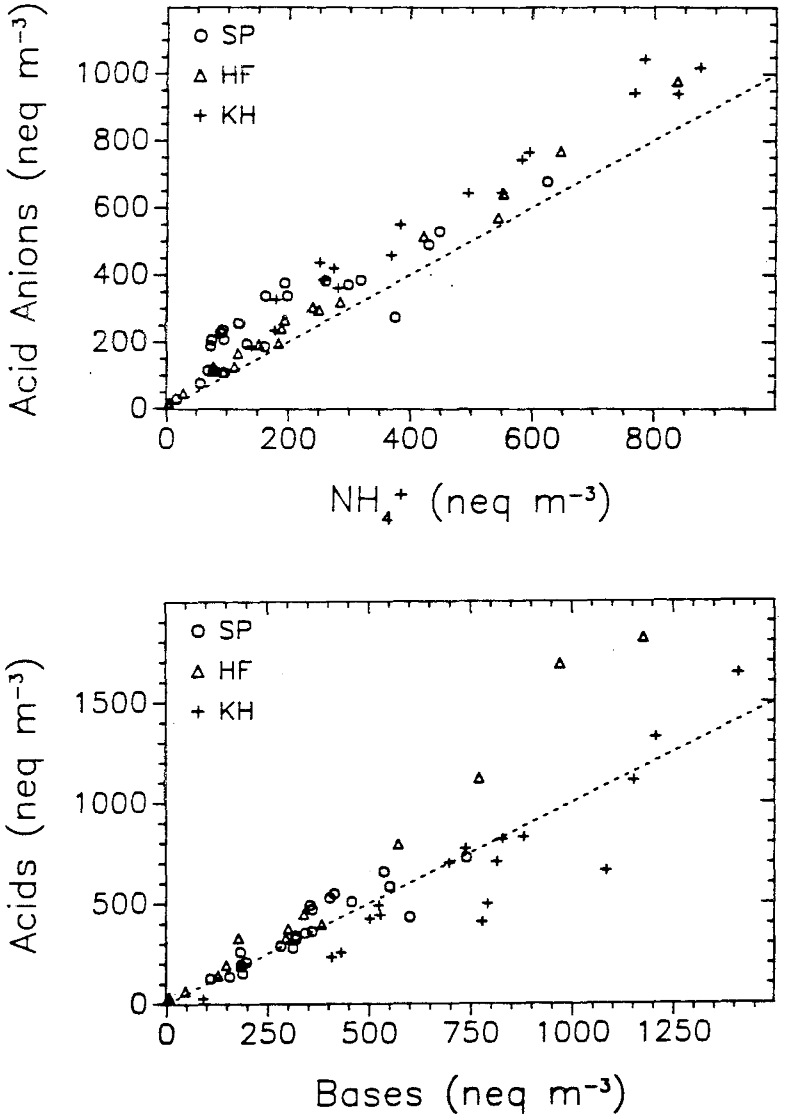

Figure 8.4 A) The sum, $NO_3^- + SO_4^{2-}$, plotted vs NH_4^+ in aerosol samples.

B) Total anions ($Cl^- + NO_3^- + SO_4^{2-} + HNO_3$) plotted vs total cations ($Na^+ + Ca^{2+} + Mg^{2+} + NH_4^+ + NH_3$) in aerosol and gas samples

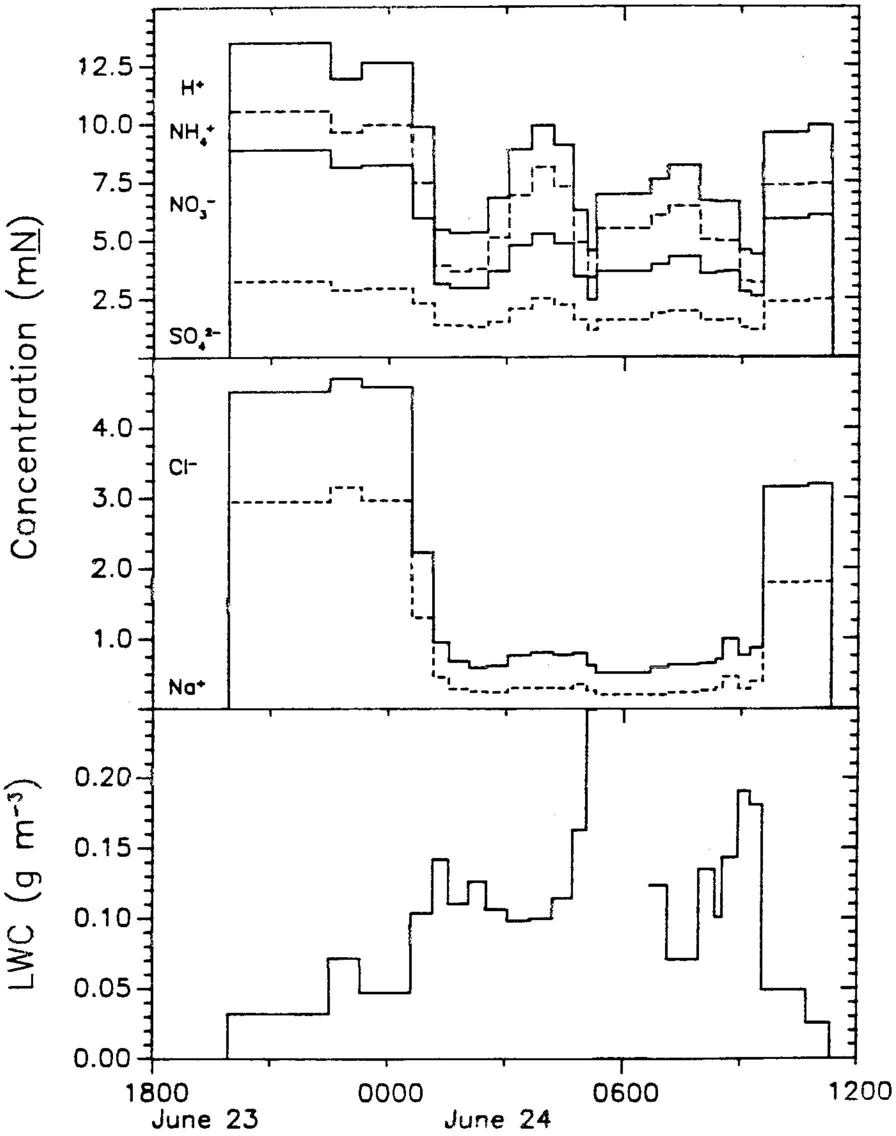

Figure 8.5 Concentrations of major ions and sea salts and LWC in cloudwater samples collected at San Pedro Hill on June 23 and 24, 1987. LWC is estimated from the sample collection rate and its theoretical efficiency.

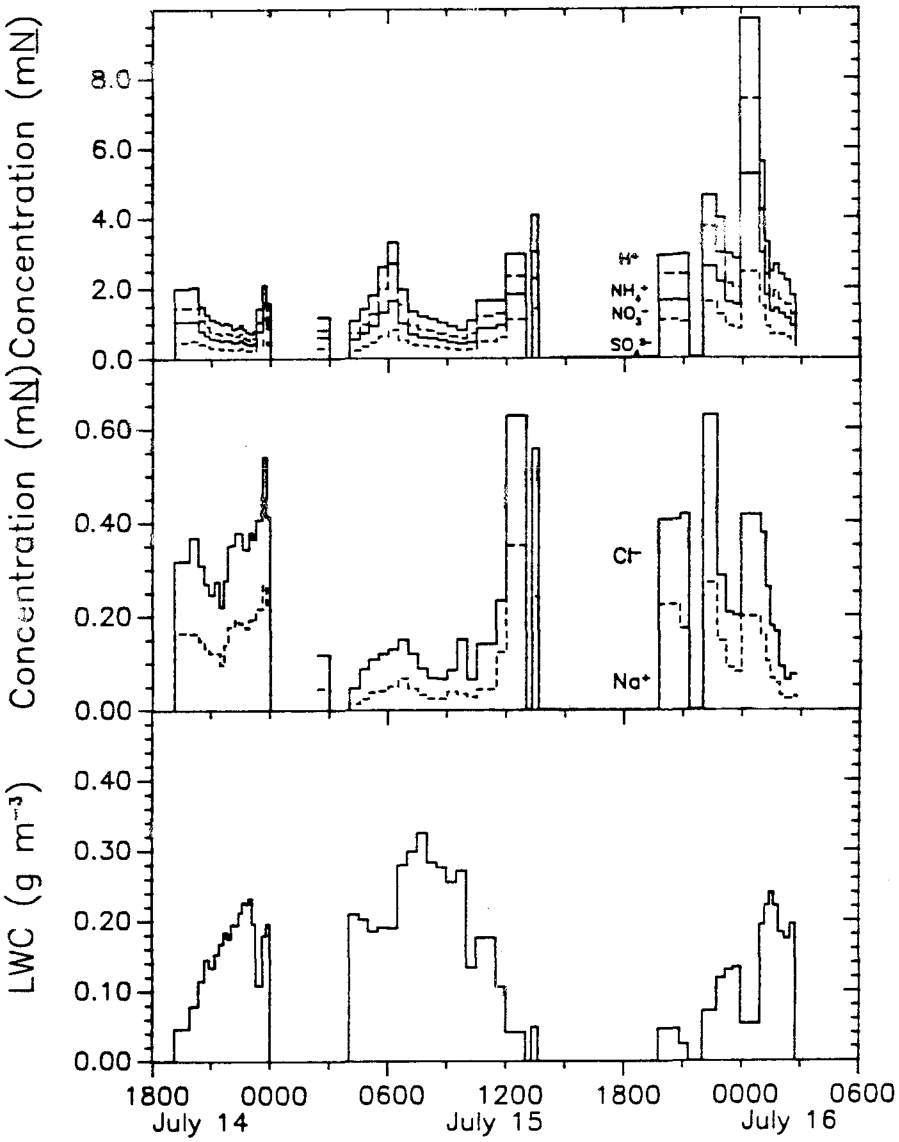

Figure 8.6 Concentrations of major ions and sea salts and LWC in cloudwater samples collected at San Pedro Hill over the period July 14 – July 16, 1987. LWC is estimated from the sample collection rate and its theoretical efficiency.

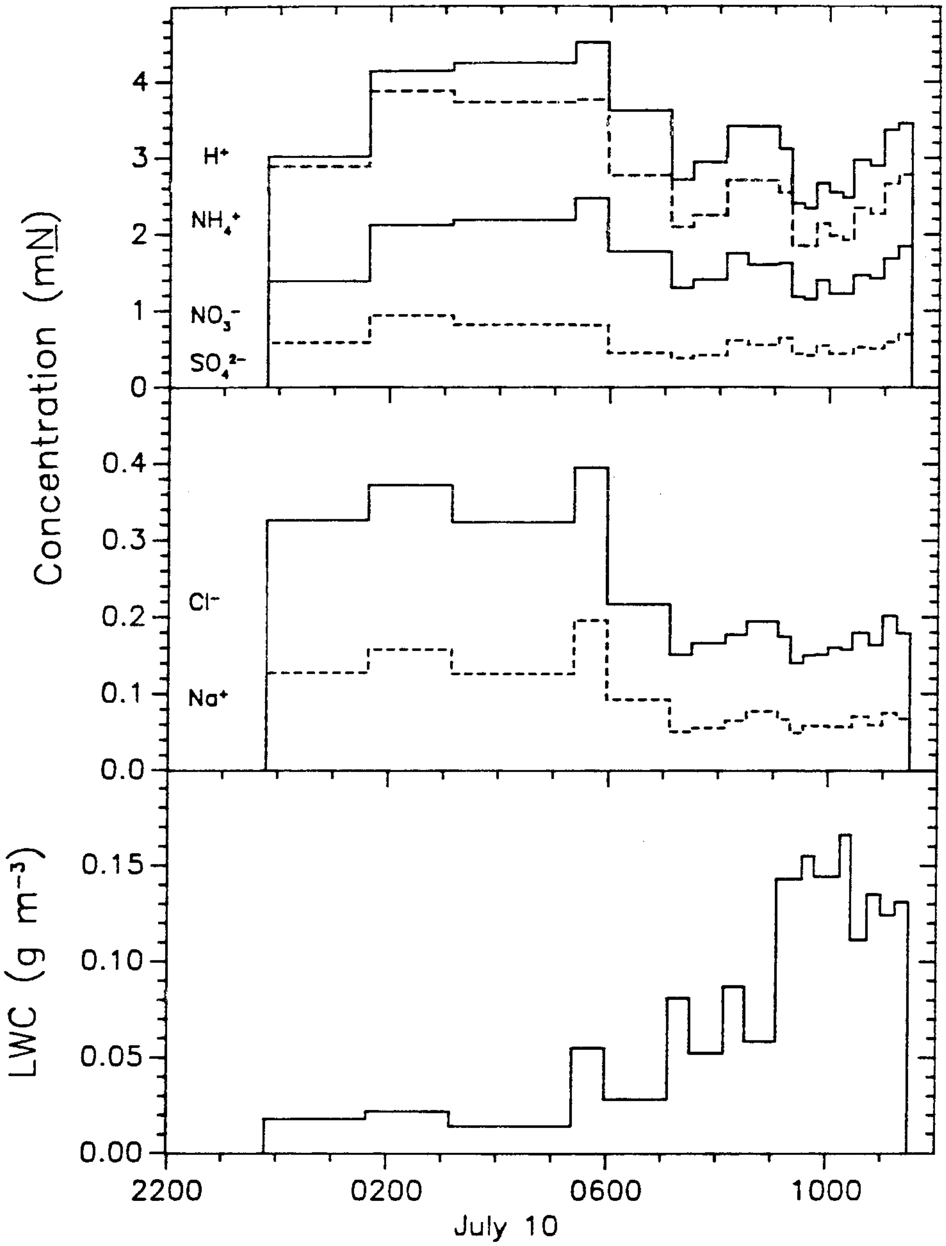

Figure 8.7 Concentrations of major ions and sea salts and LWC in cloudwater samples collected at Henninger Flats on July 10, 1987. LWC is estimated from the sample collection rate and its theoretical efficiency.

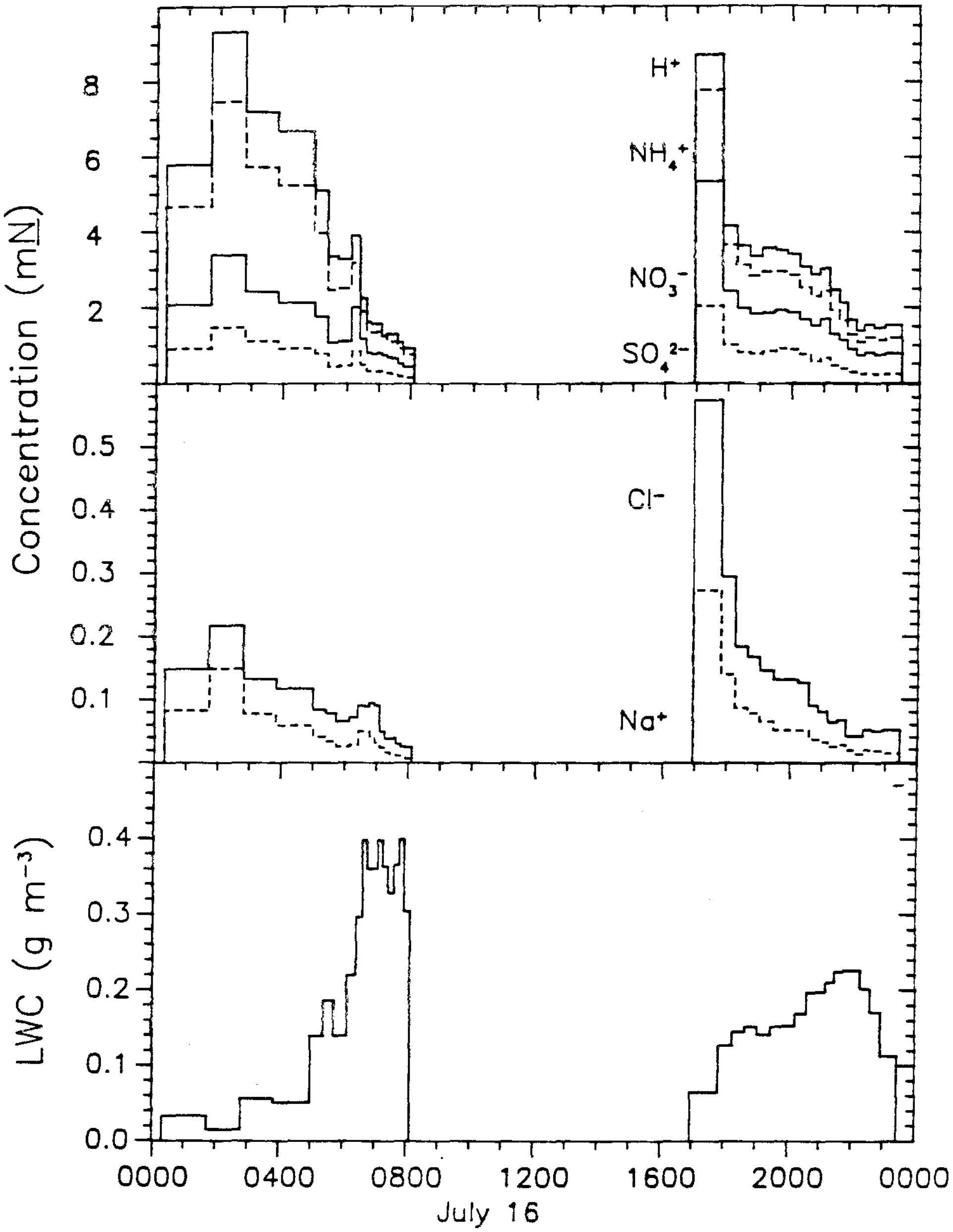

Figure 8.8 Concentrations of major ions and sea salts and LWC in cloudwater samples collected at Henninger Flats on July 16, 1987. LWC is estimated from the sample collection rate and its theoretical efficiency.

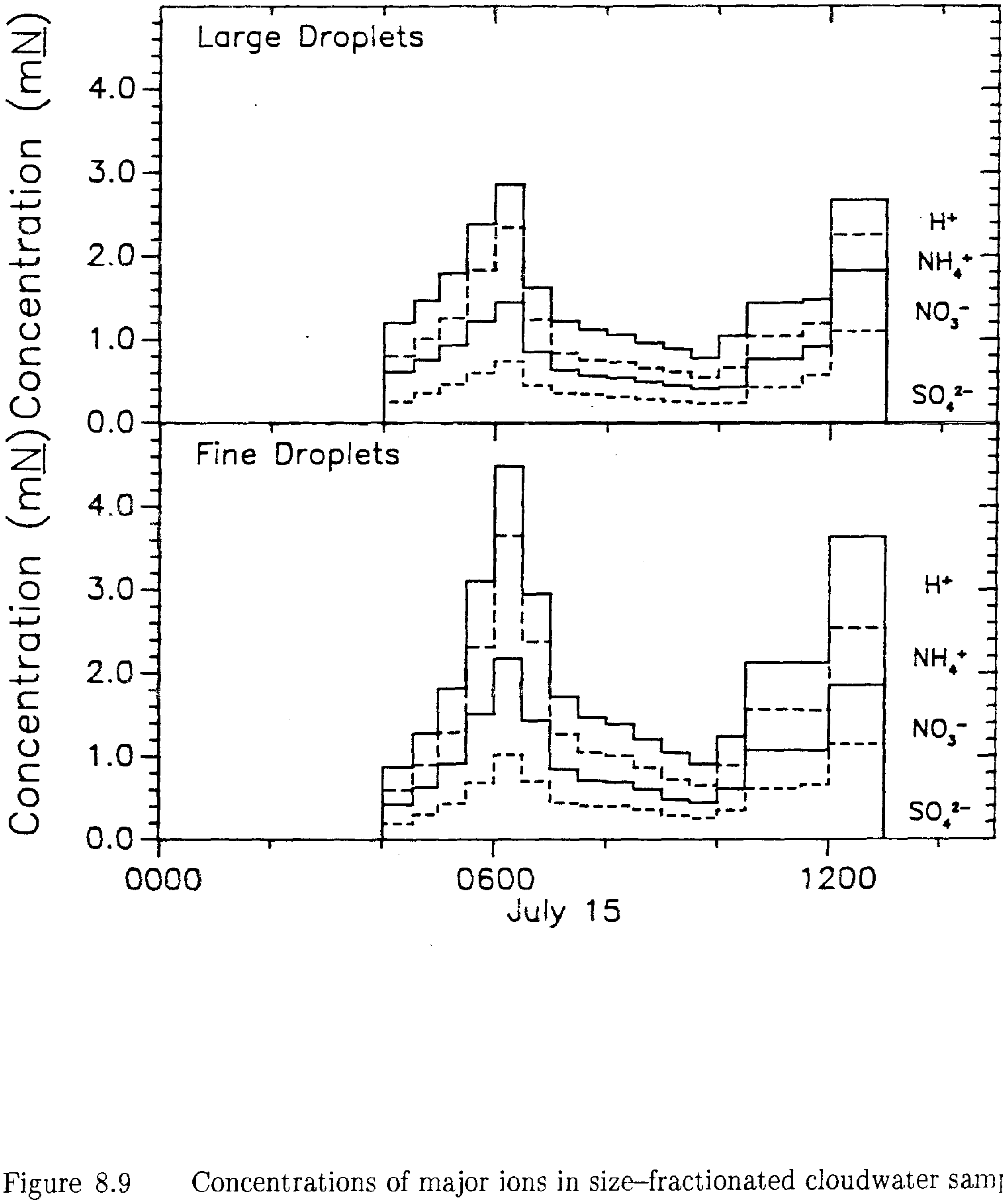

Figure 8.9 Concentrations of major ions in size-fractionated cloudwater samples collected at San Pedro Hill on the morning of July 15, 1987.

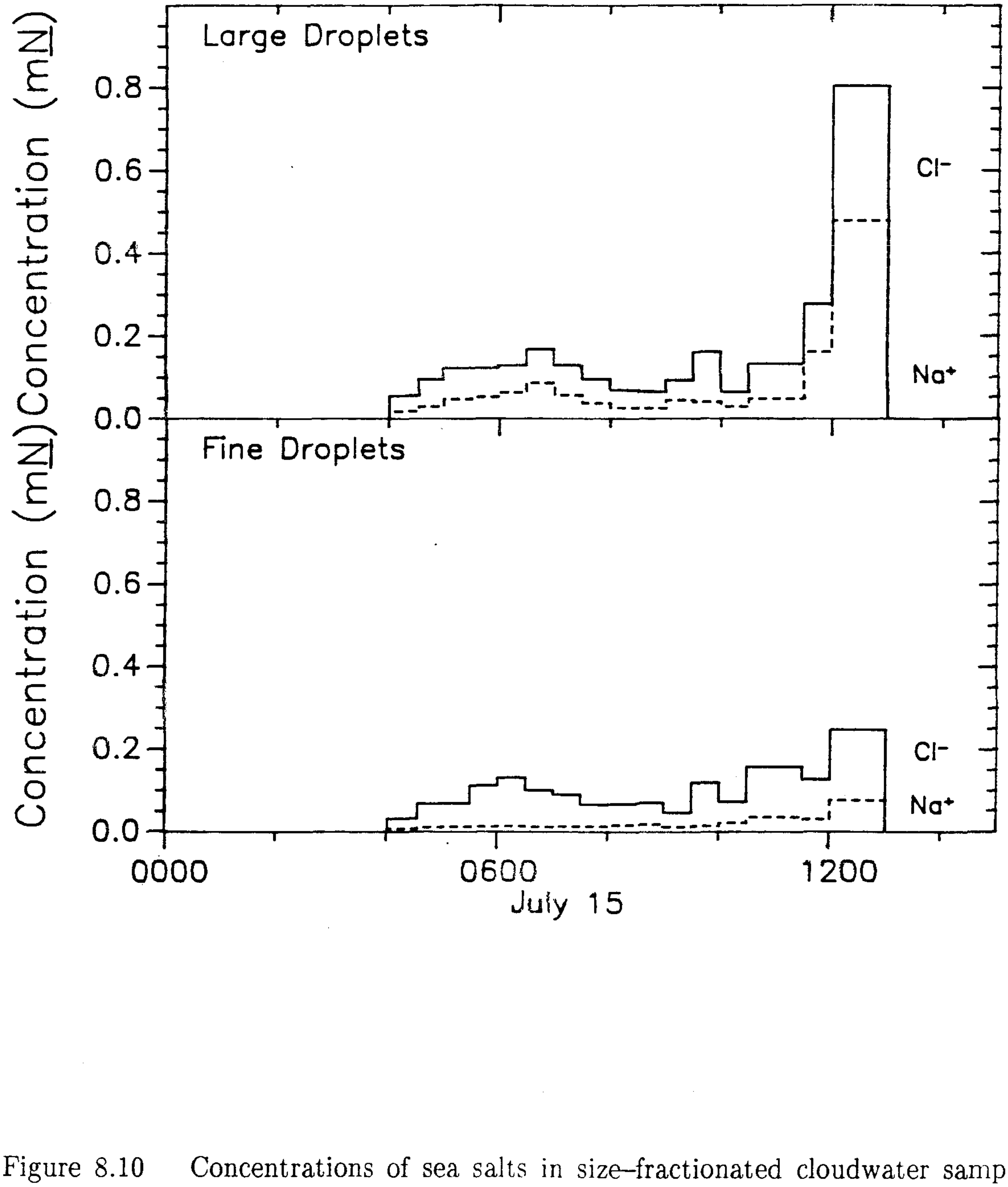

Figure 8.10 Concentrations of sea salts in size–fractionated cloudwater samples collected at San Pedro Hill on the morning of July 15, 1987.

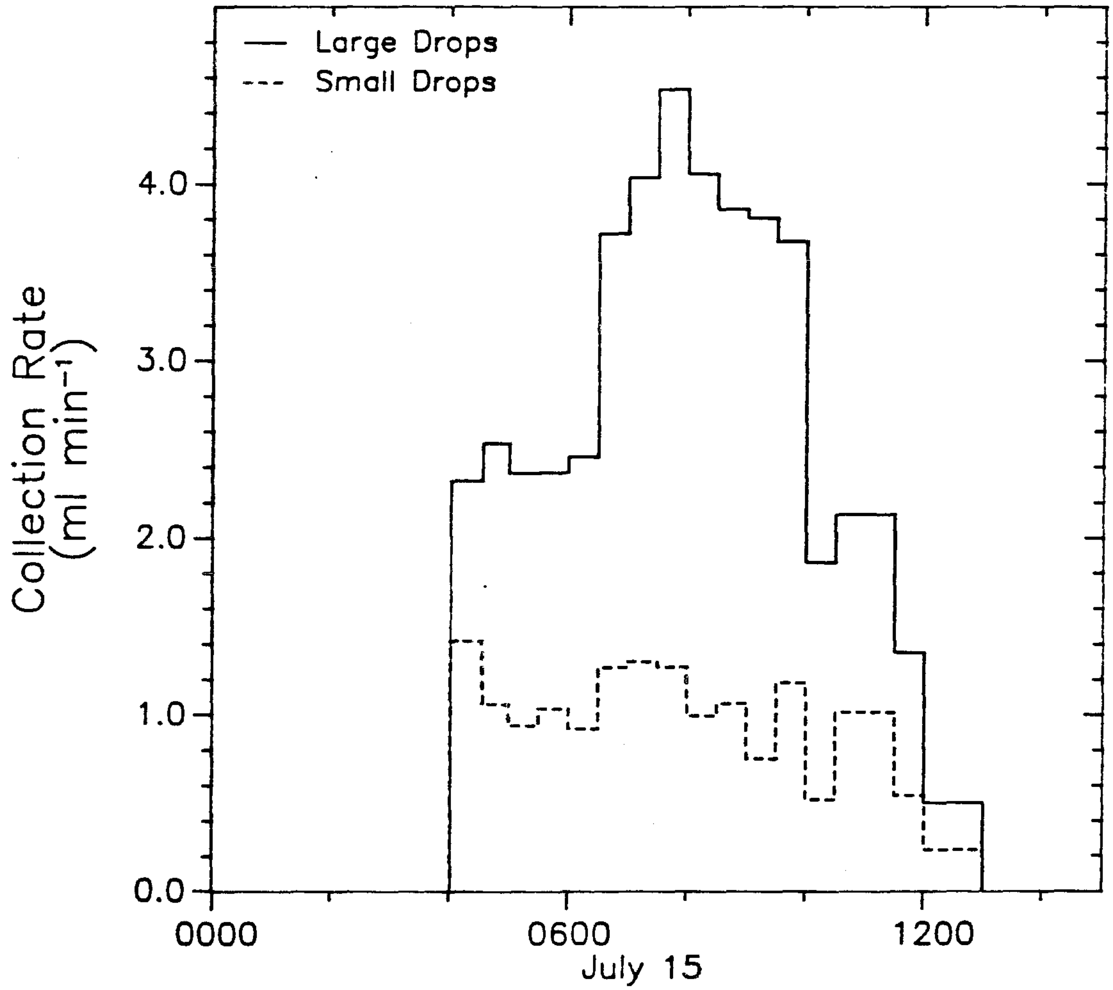

Figure 8.11 Collection rate for size–fractionated cloudwater samples collected at San Pedro Hill on the morning of July 15, 1987.

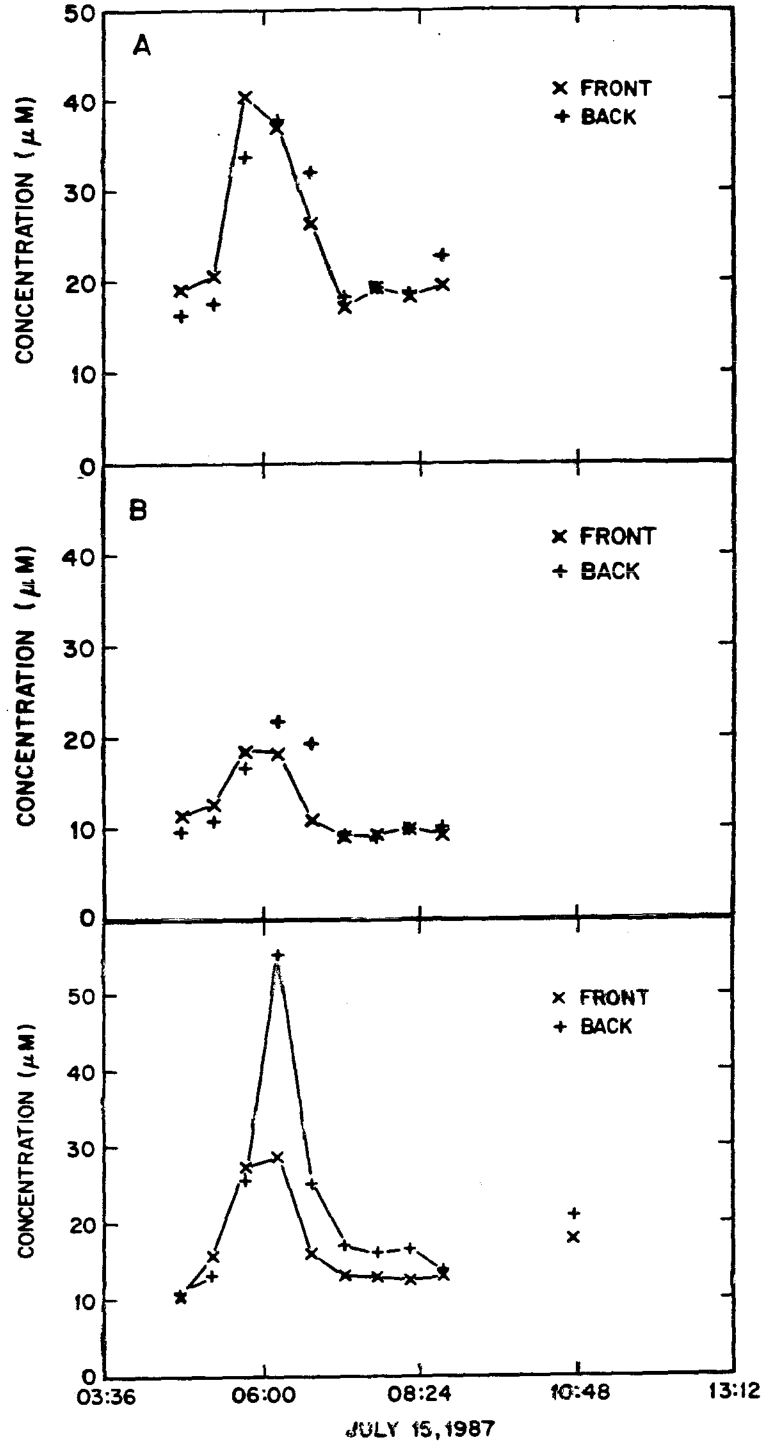

Figure 8.12 Formate (A), acetate (B), and formaldehyde (C) in size–fractionated cloudwater samples from San Pedro Hill. Large droplets are collected in the front fraction; small droplets are collected in the back fraction.

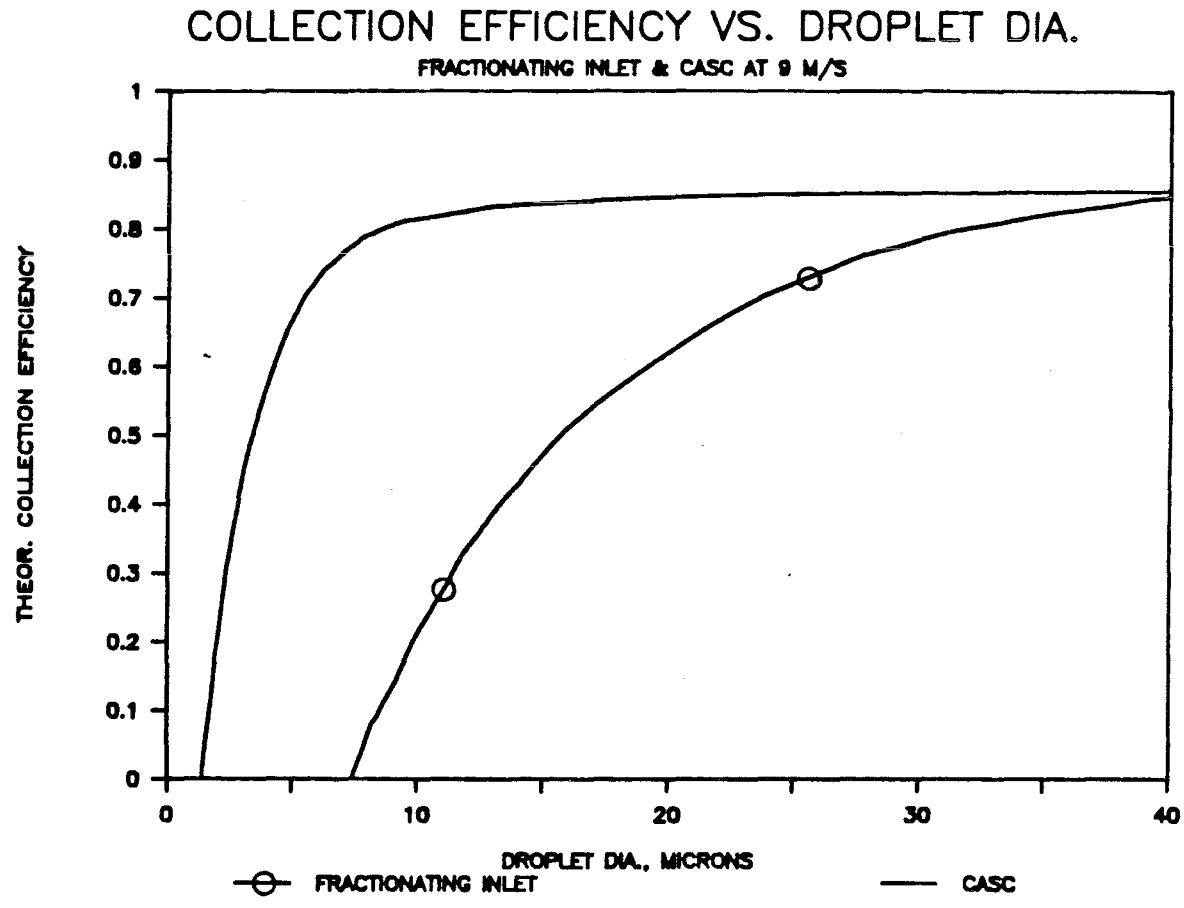

Figure 8.13 Theoretical collection efficiency, $\eta(d)$, vs droplet diameter for collection on the rods of the fractionating inlet and the strands of the CASC.

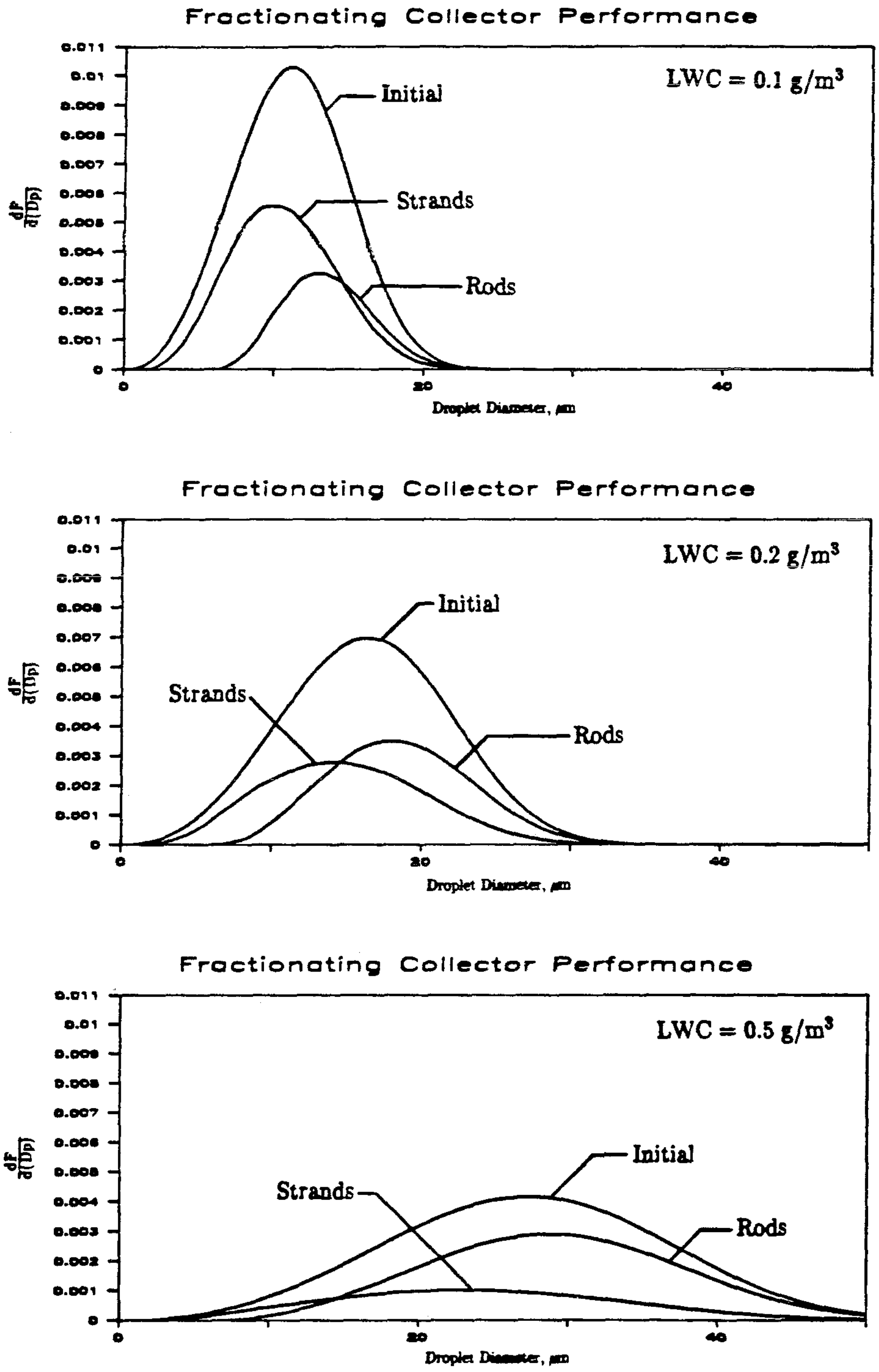

Figure 8.14 Collection of water on the fractionating inlet rods and CASC strands under three LWC conditions. Initial droplet-size distributions are given by Best's parameterized curves.

CHAPTER 9

SUMMARY, CONCLUSIONS,AND RECOMMENDATIONS FOR FUTURE RESEARCH

Summary of Observations and Conclusions

1. High concentrations of carboxylic acid were observed in fogs and clouds where pH was high or near sources of precursor hydrocarbons. Riverside California, which often has high pH fogwater and is near emission sources, had the highest concentrations observed in southern California.

2. The formation of hydroxymethanesulfonate (HMSA) contributes to high concentrations of CH_2O observed in fogwater. HMSA was measured directly in Bakersfield fogwater samples. Indirect evidence indicates it is present in fogwater from sites in Los Angeles and Riverside.

3. Reaction models predict that dicarbonyls should be present in the atmosphere. Oxidation of aromatic hydrocarbons and ozonolysis of isoprene are two important sources.

4. The spectra of 2,4,dinitrophenylhydrazine derivatives of glyoxal, methylglyoxal, and biacetyl were measured **in the solvent used for HPLC analysis**. Dicarbonyl hydrazones have an absorption maximum near 430 nm, which is higher than the maximum for hydrazones of normal aldehydes (360 nm). The distinct spectra of dicarbonyl–DNPH derivatives are an aid to their identification.

5. Glyoxal and methylglyoxal were measured in Riverside fogwater and Santa Barbara Channel cloudwater. Their concentrations were comparable to that of CH_2O. Biacetyl, $CH_3C(O)C(O)CH_3$, was also observed at low concentrations.

6. Fogwater collected at Riverside was highly concentrated. Ammonium concentrations ranged from 8 to 26 m**N**; NO_3^- ranged from 6 to 29 m**N**; and SO_4^{2-} ranged from 1.4 to 6.2 m**N**.

7. pH values in Riverside fogwater dropped to 2.3, despite the presence of excess NH_3 in the gas phase during the day. HNO_3 is the dominant acid. At night, reduced vertical mixing and drainage flows would isolate the sampling site from the NH_3 emission area. Continued production of HNO_3 via $NO_3\cdot$ and N_2O_5 pathways could then acidify the fog. Fog on the floor of the basin may still be in contact with the NH_3 emissions and would not be acidic. This mechanism implies that there could be a region of acidic fogwater on the slopes surrounding the Riverside/San Bernardino basin.

8. The preexisting aerosol is not completely scavenged by the radiation fog forming at Riverside. Scavenging efficiencies computed from fogwater loading and concurrent or prior aerosol samples are typically $< 50\%$. These radiation fogs never achieve high enough supersaturations to activate all of the aerosol.

10. Acid cloudwater was consistently observed in intercepted stratus clouds collected along the Santa Barbara Channel coast. Samples collected at Ventura and Pt. Mugu, which are immediately adjacent to the coast, were the most acidic. Casitas Pass, which is further inland, had somewhat less acidic cloudwater.

11. Nitrate was equivalent to or slightly greater than sulfate in the Santa Barbara Channel intercepted stratus clouds. The $NO_3^-:SO_4^{2-}$ equivalent ratio never exceeded 2, however. In contrast the ratio of NO_X to SO_2 in local emissions and

in the LA basin is greater than 2.

12. Concentrations of SO_4^{2-} and N(V) in the aerosol and gas phase are comparable over the length of the Santa Barbara Channel. A major portion of the N(V) was present as HNO_3 in the gas phase. Concentrations at a site above the inversion base were as high or higher than sites in the mixed layer. Sea–salt concentrations, however, decreased sharply with elevation and distance from the coast.

13. Cloudwater scavenging ratios less than 1 were observed in patchy or intermittent clouds. When the clouds were continuous, however, the scavenging ratio was near 1.

14. Chloride in aerosol samples from the Santa Barbara Channel was depleted relative to the sea salt ratio with Na^+, which is in accord with predictions that HCl is volatilized by exchange with HNO_3

15. Possible sources for acidity in the Santa Barbara Channel are oxidation of local emissions of NO_x and SO_2, or transport from Los Angeles.

16. Using an automated cloudwater sampling system, 245 samples from San Pedro Hill and 80 samples from Henninger Flats were obtained mid June to mid July, 1987.

17. Some of the variability in cloudwater chemical composition was explained by changes in cloud liquid water content. Changes in concentration were also observed during periods of relatively constant liquid water content. Removal

by drizzle may account for decreasing concentrations. Wind shifts, enhanced turbulence, or entrainment from aloft may account for increases in concentration.

18. A fractionating inlet was designed and constructed for use with the CASC. Droplets larger than $\simeq 16\ \mu m$ are collected on teflon rods at the mouth of the inlet. The remaining droplets pass through to the teflon strands and are collected there.

19. The size–fractionating inlet was used to collect intercepted stratus on San Pedro Hill. Ions associated with soil dust and sea salt (Ca^{2+}, Mg^{2+}, and Na^+) were enriched in the large droplet fraction. The secondary aerosol ions (NH_4^+, SO_4^{2-}, and to some extent H^+) were enriched in the small droplet fraction. Ions that are associated with gas-phase species (HCl and HNO_3) showed mixed behavior.

20. The Na:Cl ratio in the large droplet fraction was indistinguishable from the seawater ratio, while the ratio in the small droplets showed a Cl^- enrichment. Most of the sea salt aerosol ends up in the large droplets. Hydrogen chloride that has been volatilized from sea salt by exchange with HNO_3 is rescavenged by all droplets.

Recommendations for Future Research

Two areas for future research are the size–dependence of droplet chemical composition, and turbulent mixing processes in cloud and fog layers. A size–fractionating inlet has been developed for use with the Caltech Active Strand Collector. Samples collected from one coastal stratus cloud event indicate that large droplets are derived from large sea–salt and soil–dust aerosol and small droplets are formed from secondary ammonium sulfate and nitrate aerosol. Future work should refine the size–fractionating inlet in order to provide a sharper size cut and verify the performance of the inlet. A comprehensive experiment to determine the size dependence of droplet composition would include size–fractionated aerosol sampling, measurement of aerosol and droplet size distributions, cloud liquid water content. An adequate means for determining liquid water content in ground–based sampling is not presently available. Gravimetric methods for LWC determination do not allow sufficient time resolution to follow fluctuations in LWC from due to the turbulence in the cloud. Other locations, with different aerosol characteristics need to be investigated.

Results presented here and results of other studies indicate that entrainment from aloft is an important factor controlling cloud and fog chemical composition. Formation of HNO_3 via the $NO_2 + NO_3 \longrightarrow N_2O_5$ reaction is likely in the inversion layer above the cloud or fog. The mountains surrounding the Riverside basin and the coastal mountains in Los Angeles and the Santa Barbara Channel are ideal sites to study this phenomenon. A comprehensive experiment to identify the role of above–cloud reaction and entrainment mixing would include a vertical array of aerosol, gas, and cloudwater samplers and meteorological instruments.

Appendix A

ANALYTICAL METHODS AND QUALITY ASSURANCE

Table A.1. Analysis of liquid samples.

Species	Method
pH	Combination Electrode
Cl^-	Ion chromatography – HCO_3^-/CO_3^{2-} eluent
NO_3^-	"
SO_4^{2-}	"
NH_4^+	Indophenol blue – Flow Injection Analysis
Na^+	Flame Atomic Absorption Spectrometry
K^+	"
Ca^{2+}	"
Mg^{2+}	"
Fe	Graphite Atomization AAS
Mn	"
Pb	"
Cu	"
Ni	"
V	"
S(IV)	Pararosaniline – FIA
CH_2O	Nash Method
$C_1 - C_6$ Carbonyls	DNPH Derivative – HPLC
Carboxylic Acids	Ion Chromatography – $B_4O_7^{2-}$ eluent
	Ion Exclusion Chromatography – HCl eluent
α–OH sulfonates	Ion Pairing Chromatography
H_2O_2	POPA – flourescent dimer

Table A.2. Analysis of gas and aerosol samples.

Species	Filter	Method
	—— (aerosol) ——	
SO_4^{2-}	Teflon	H_2O extract – IC
NO_3^-	Teflon	"
Cl^-	Teflon	"
Na^+	Teflon	H_2O extract – Flame AAS
Ca^{2+}	Teflon	"
Mg^{2+}	Teflon	"
NH_4^+	Teflon	H_2O extract – indophenol FIA
	——— (gas) ———	
NH_3	Oxalic acid – imp. Glass	H_2O extract – indophenol FIA
HNO_3	Nylon	HCO_3^-/CO_3^{2-} extract – IC
HCOOH	Base – imp. Quartz	H_2O extract IC or IEC
CH_3COOH	Base – imp. Quartz	"
SO_2	Base – imp. Quartz	"

Standard Operating Procedures

Collector Cleaning

Prior to being deployed in the field the collectors will be dissassembled and cleaned thoroughly.

Remove strand cartridges and water accumulation trough.
Scrub strands, trough, and collector walls with non–ionic surfactant using a Kimwipe.
Soak small parts in distilled water.
Rinse collector walls with multiple aliquots of distilled water.
Reassemble collector and wash down with a final aliquot of distilled water.
Cover openings of collector to exclude dust.
Inspect sample tubing for visible soiling, replace if visibly soiled.
Rinse tubing with distilled water, cap ends with parafilm.
Soak sample collection bottles with distilled water.
Retain representative unused bottles from each sampling episode as blanks.
Disassemble sample reservoir and plumbing from fraction collector.
Soak all components in distilled water.
Inspect for soiling, scrub if necessary. Replace any components that can not be cleaned.

Sample analysis

All filter handling is to be performed in the cold room to minimize volatilization of collected material
Prepare extracted filters the evening before they will be analyzed
Transfer filter to specimen cup.
Add 200 µl of ethanol to teflon filters and allow to sit until translucent.
Add appropriate volume of distilled water (usually 10 ml)
Spike nylon filters with HCO_3^-/CO_3^{2-} Buffer.
Place cup with filter on shaker table and shake for 2 hours
Let extracted filters stand overnight and analyze the next day.

Quality Control Procedures

Quality control procedures that were followed during this study include regular analysis of blanks generated during each sampling period, replicate analyses of samples, and analysis of spiked samples to determine recovery. Our laboratory regularly participated in EPA Acid Rain Quality Assurance Audits for both aqueous acid rain samples and nitrate and sulfate on filter media. For ions with concentrations above our detection limits, the deviations between the observed and true values were less than 5%.

Precision and accuracy of the measurements were determined from the mean and standard deviation of repeated analyses of the same standard (Standard Methods). Two different concentration were evaluated levels in order to determine the dependence of precision and accuracy on concentration. Detection limits were estimated from analyses of blanks (or low standards). The detection limit is the concentration giving a signal 3 times the blank (or low standard) standard deviation. Following is a listing of expected precision, accuracy and detection limits for the major species. For gas–phase species the variance of the flow measurements is included in the estimates of precision and detection limit.

Table A.3
Precision, accuracy, and minimum detection limit

Aqueous Phase

Species	nominal conc. μN	Acc. μN	Prec. μN	RSD %	MDL μN
NH_4^+	20	0.28	0.58	2.92	1.75
Na^+	10.9	0.13	0.45	4.15	1.36
Ca^{2+}	12.5	–0.42	0.87	6.97	2.61
Mg^{2+}	10.25	0.30	0.48	4.66	1.43
Cl^-	20	0.26	2.04	10.20	6.12
NO_3^-	20	0.11	0.92	4.60	2.76
SO_4^{2-}	20	0.20	0.86	4.29	2.57
Cl^-	2	0.87	2.22	111.07	6.66
NO_3^-	2	0.31	0.35	17.71	1.06
SO_4^{2-}	2	0.26	0.38	19.13	1.15

Gas Phase (4 hour run)

Species	nominal conc. neq m^{-3}	Acc. neq m^{-3}	Prec. neq m^{-3}	RSD %	MDL neq m^{-3}
NH_4^+	69.42	0.96	2.90	4.18	8.70
Na^+	37.84	0.44	1.95	5.16	5.86
Ca^{2+}	43.39	–1.46	3.28	7.56	9.84
Mg^{2+}	35.58	1.04	1.99	5.61	5.98
Cl^-	69.42	0.90	7.40	10.65	22.19
NO_3^-	69.42	0.38	3.83	5.52	11.49
SO_4^{2-}	69.42	0.69	3.66	5.27	10.97
NH_3	69.42	0.96	2.90	4.18	8.70
HNO_3	69.42	0.38	3.83	5.52	3.69
Cl^-	6.94	3.02	7.71	111.07	23.13
NO_3^-	6.94	1.09	1.23	17.71	3.69
SO_4^{2-}	6.94	0.91	1.33	19.13	3.98

Appendix B

Chemical Composition and Meteorological Data for the Santa Barbara Channel Sampling During the Summers of 1985 and 1986

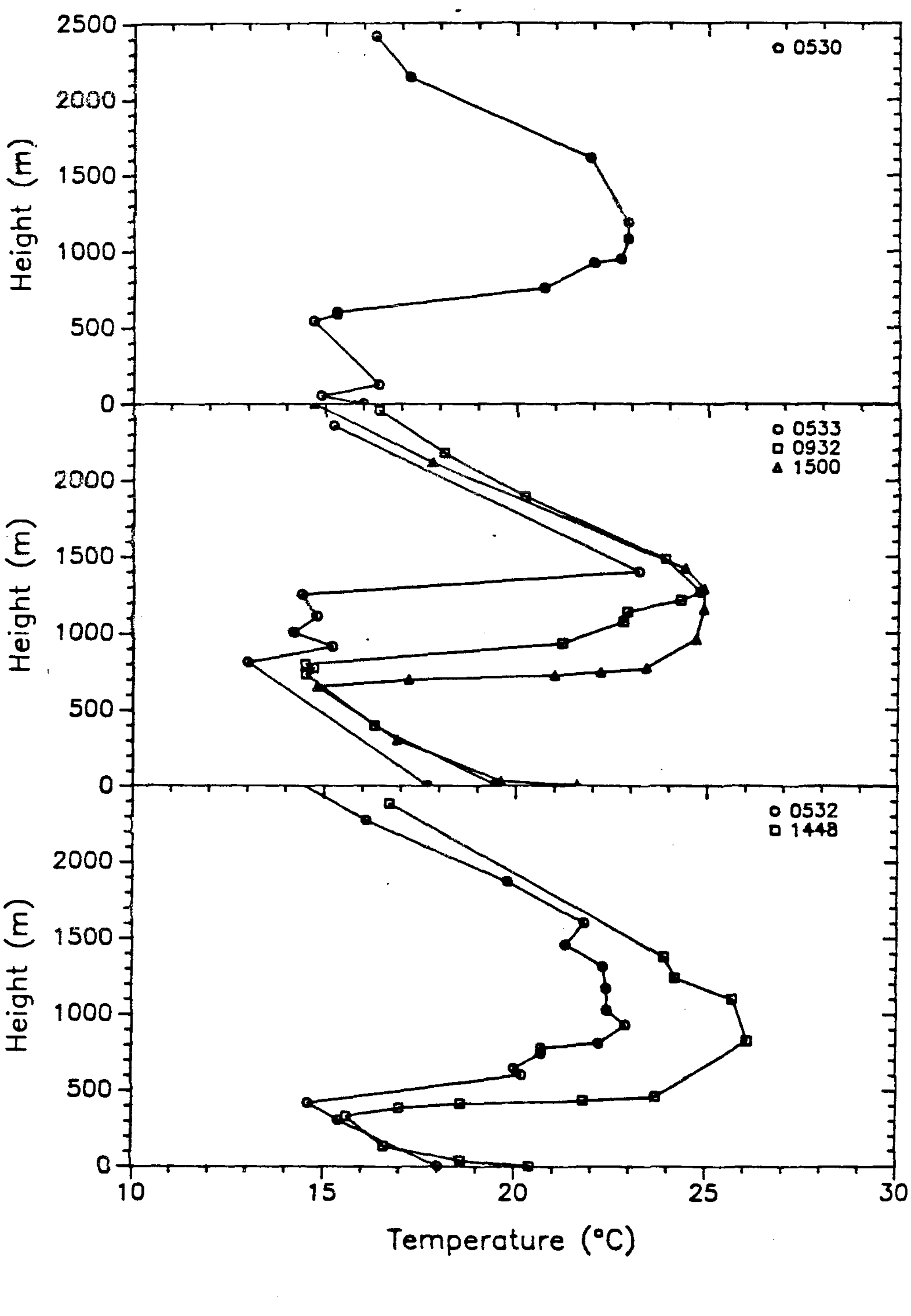

Figure B.1. Temperature profiles on July, 24, 25, and 26, 1985 taken at Point Mugu by rawinsonde. Stratus clouds were present during the late night and early morning of each day shown.

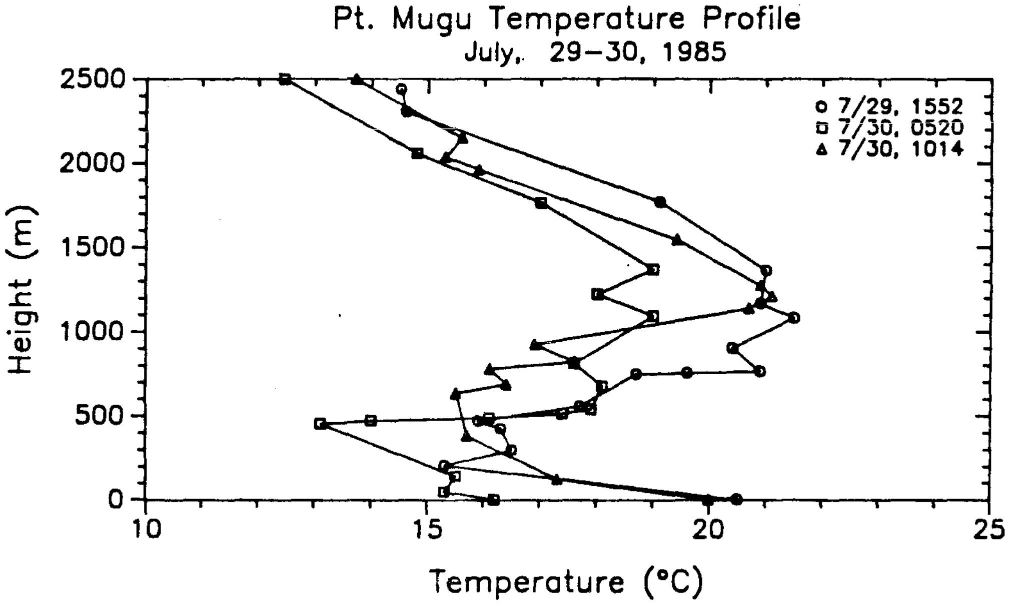

Figure B.2 Temperature profiles on July 29 and 30, 1985, taken at Point Mugu by rawinsonde. Thin stratus was present the morning of July 30 below the level of La Jolla Peak (500 m).

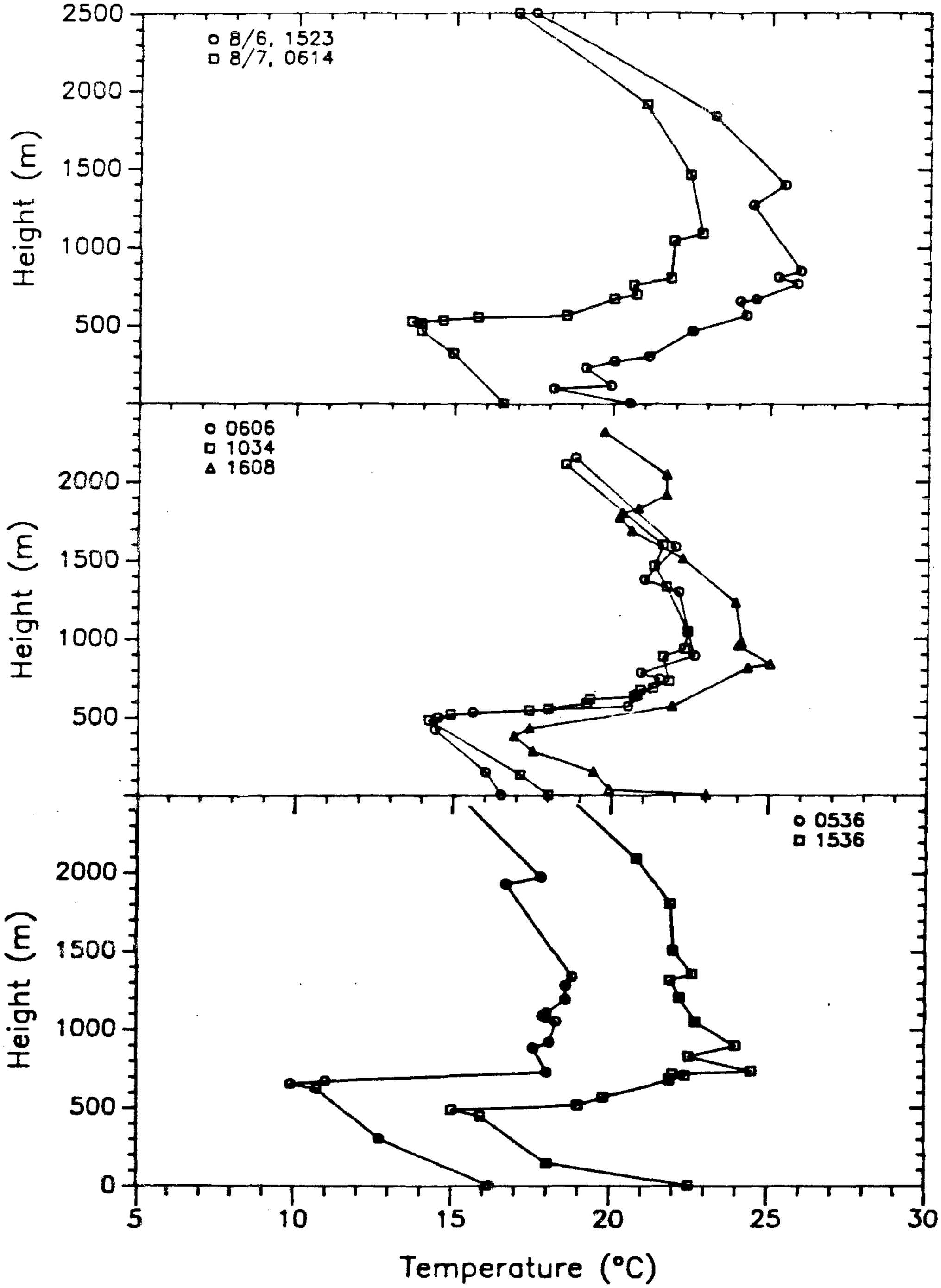

Figure B.3 Temperature profiles on August 7, 8, and 9, 1985 taken at Point Mugu by rawinsonde. Stratus clouds were collected at Casitas Pass on each of the mornings shown.

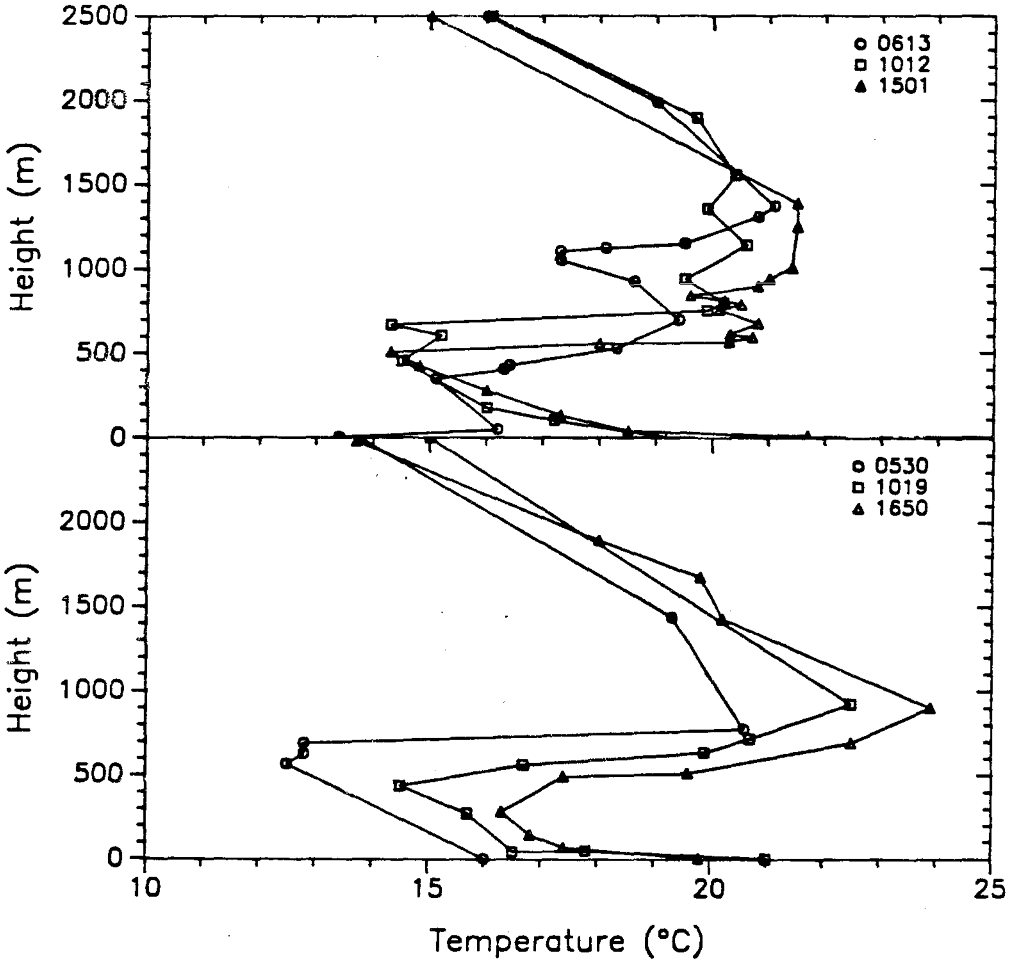

Figure B.4. Temperature profiles on August, 20 and 21, 1985 taken at Point Mugu by rawinsonde. Stratus cloud was present the morning of August 21.

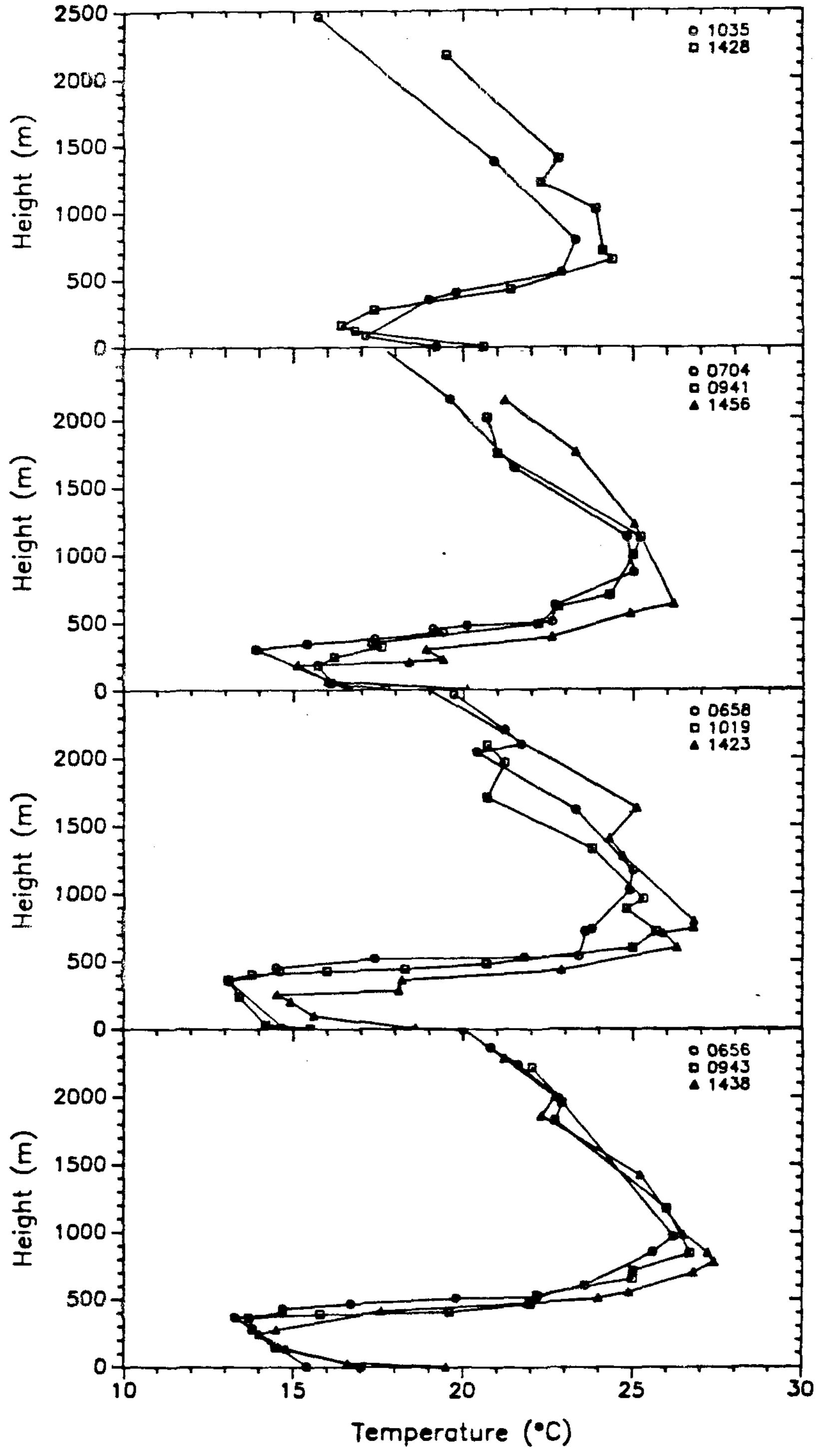

Figure B.5 Temperature profiles for the period July 29 – August 1, 1986 taken at Point Mugu by rawinsonde.

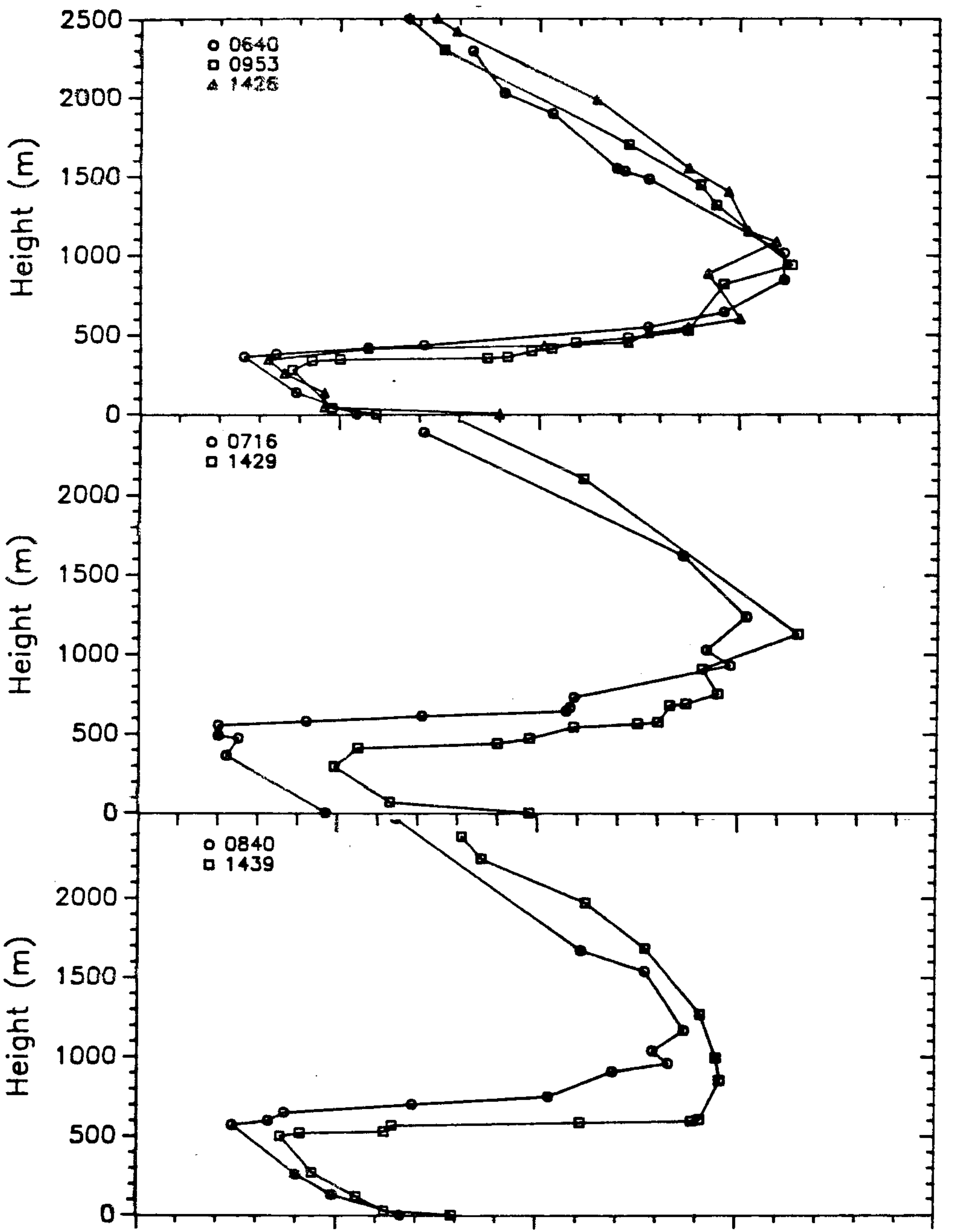

Figure B.6 Temperature profiles for the period August 12 – August 14 . 1986 taken at Point Mugu by rawinsonde.

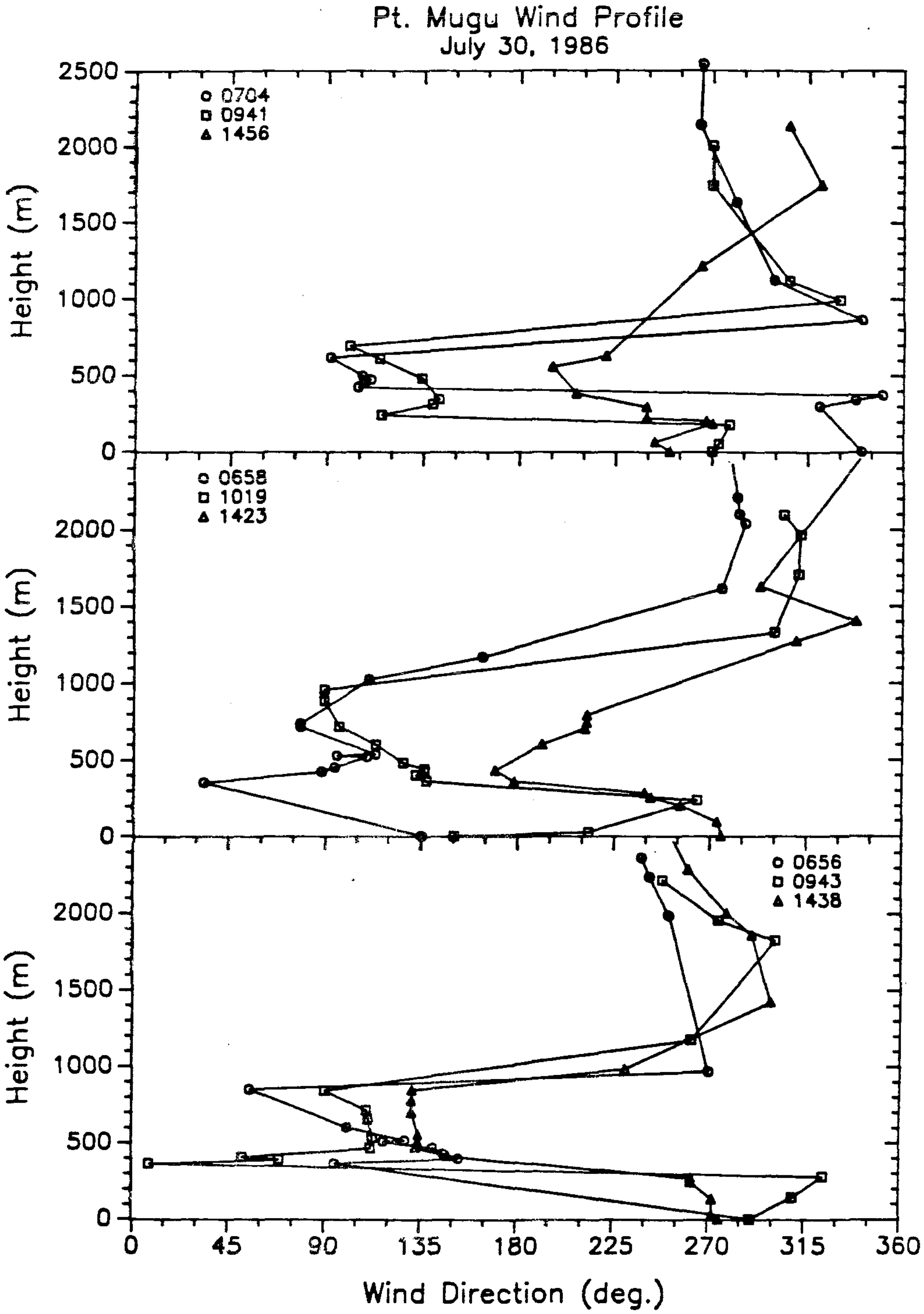

Figure B.7 Wind direction profiles taken at Point Mugu for the period July 30 – August 1, 1986.

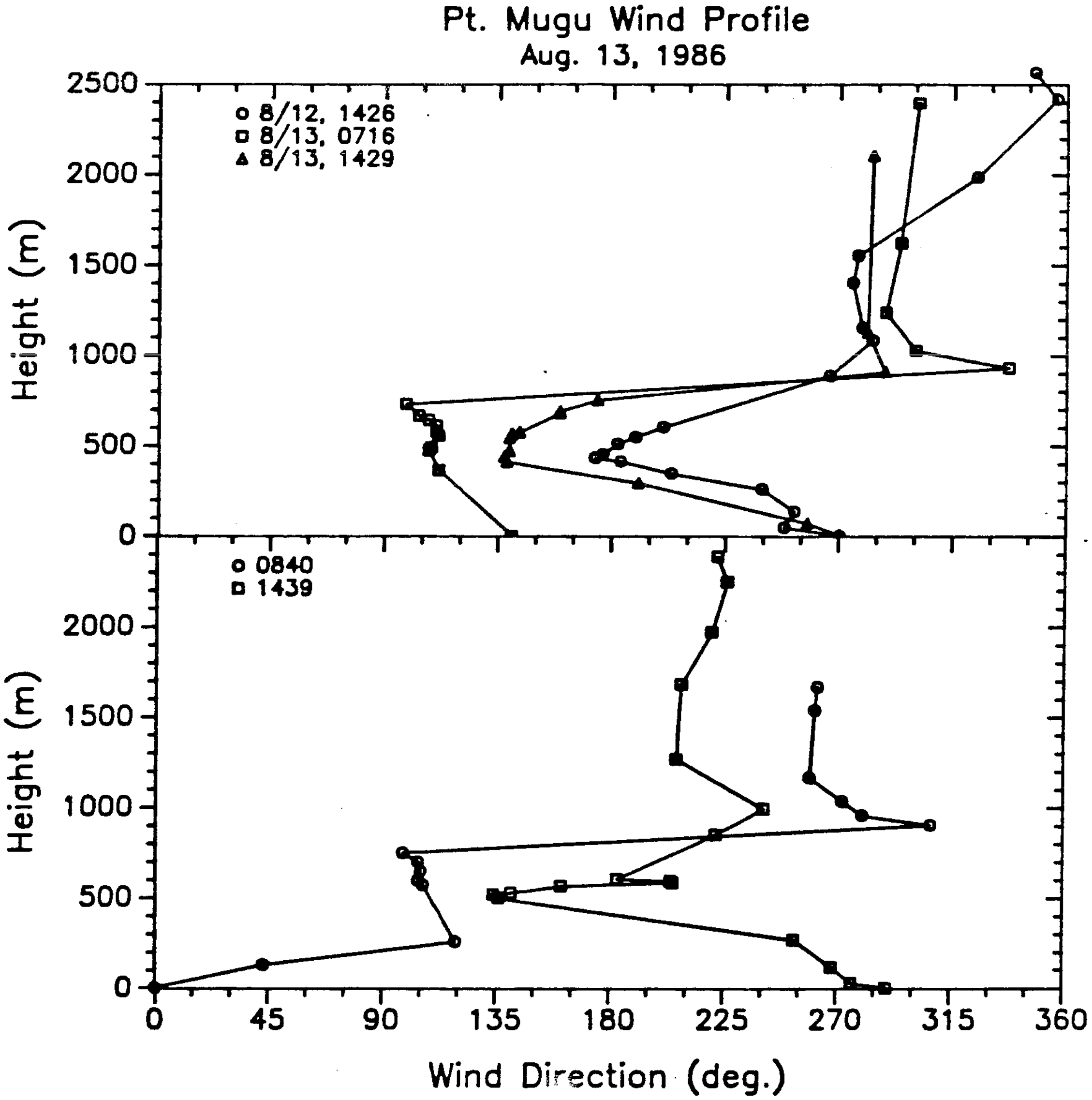

Figure B.8 Wind direction profiles taken at Point Mugu for the period August 13 – August 14, 1986.

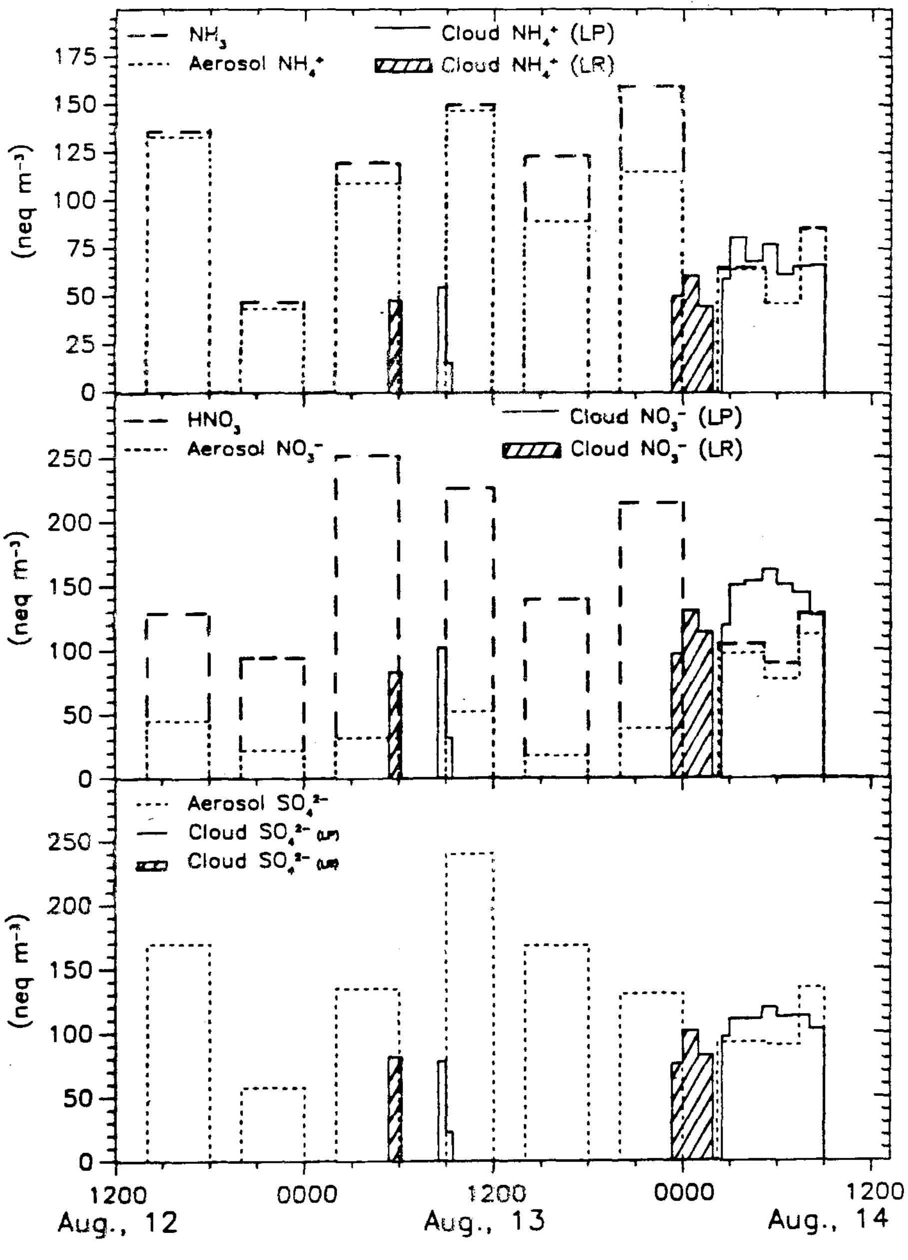

Figure B.9 Aerosol and cloudwater loadings of major ions at Laguna Peak on August 12 – 14, 1986. Cloudwater loading is the product of aqueous–phase concentration and estimated LWC.

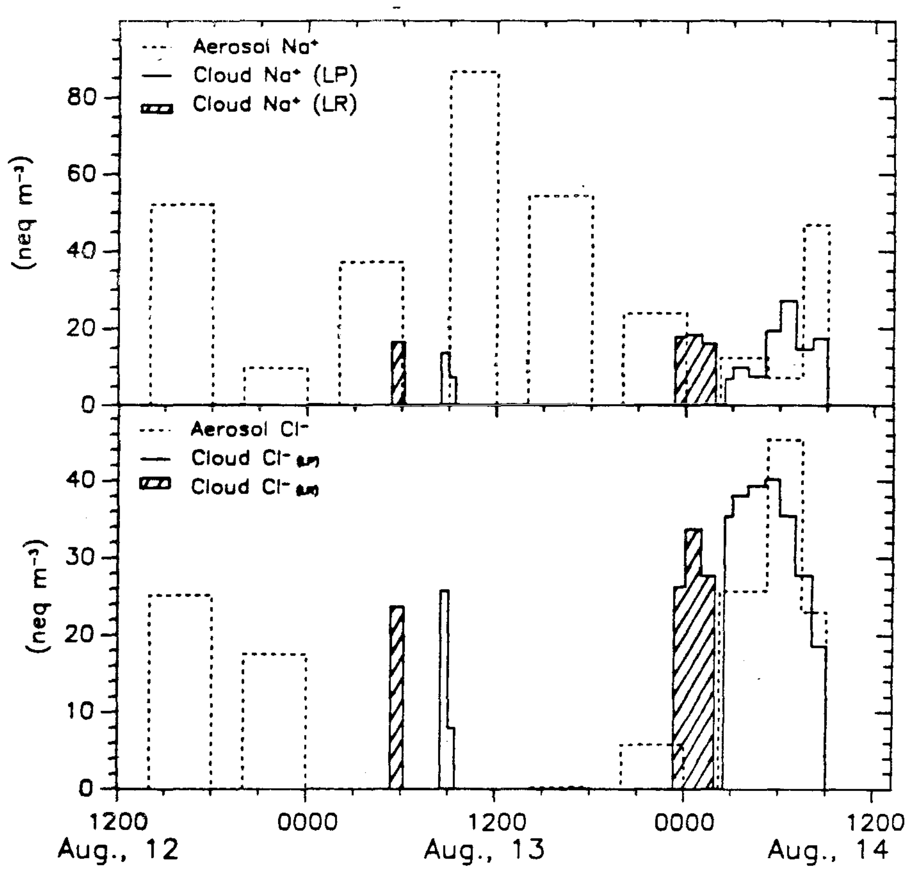

Figure B.10 Aerosol and cloudwater loadings of sea salts at Laguna Peak on August 12 – 14, 1986. Cloudwater loading is the product of aqueous–phase concentration and estimated LWC.

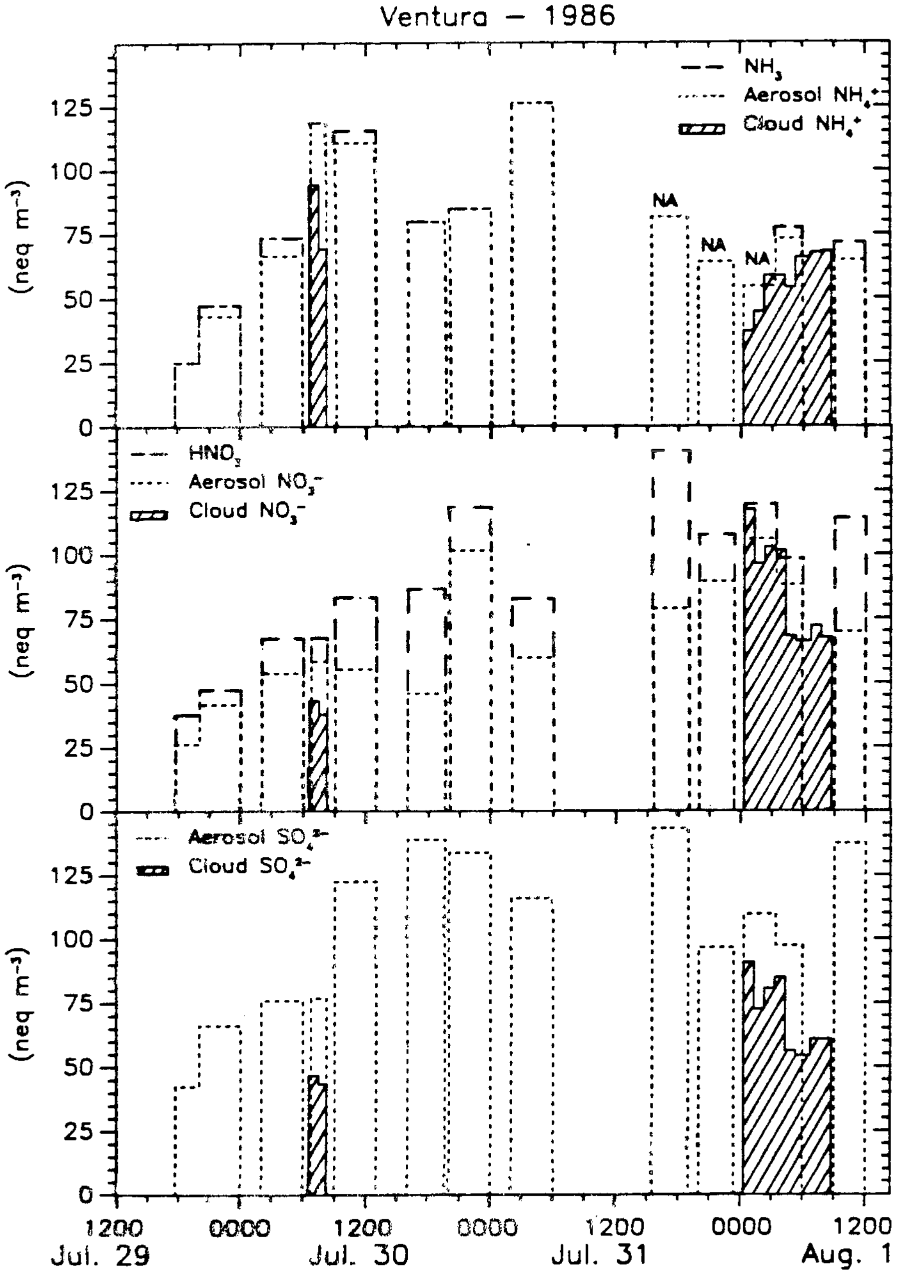

Figure B.11 Aerosol and cloudwater loadings of major ions at Ventura on July 29 – August 1, 1986. Cloudwater loading is the product of aqueous–phase concentration and estimated LWC.

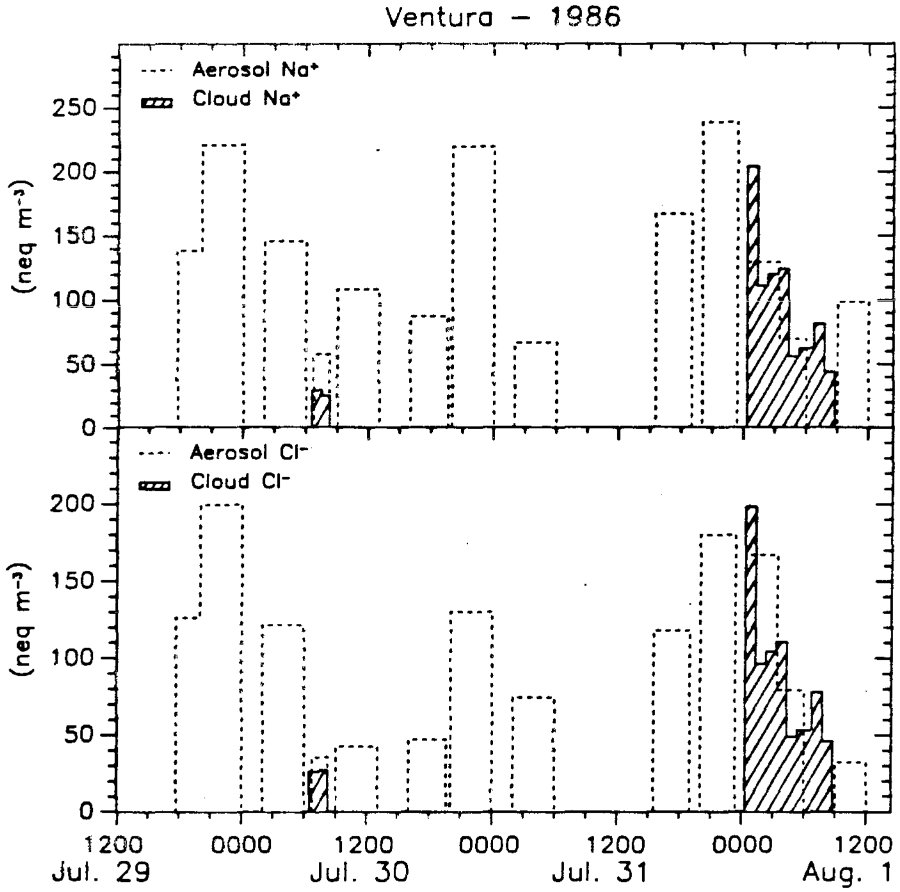

Figure B.12 Aerosol and cloudwater loadings of sea salts at Ventura on July 29 – August 1, 1986. Cloudwater loading is the product of aqueous–phase concentration and estimated LWC.

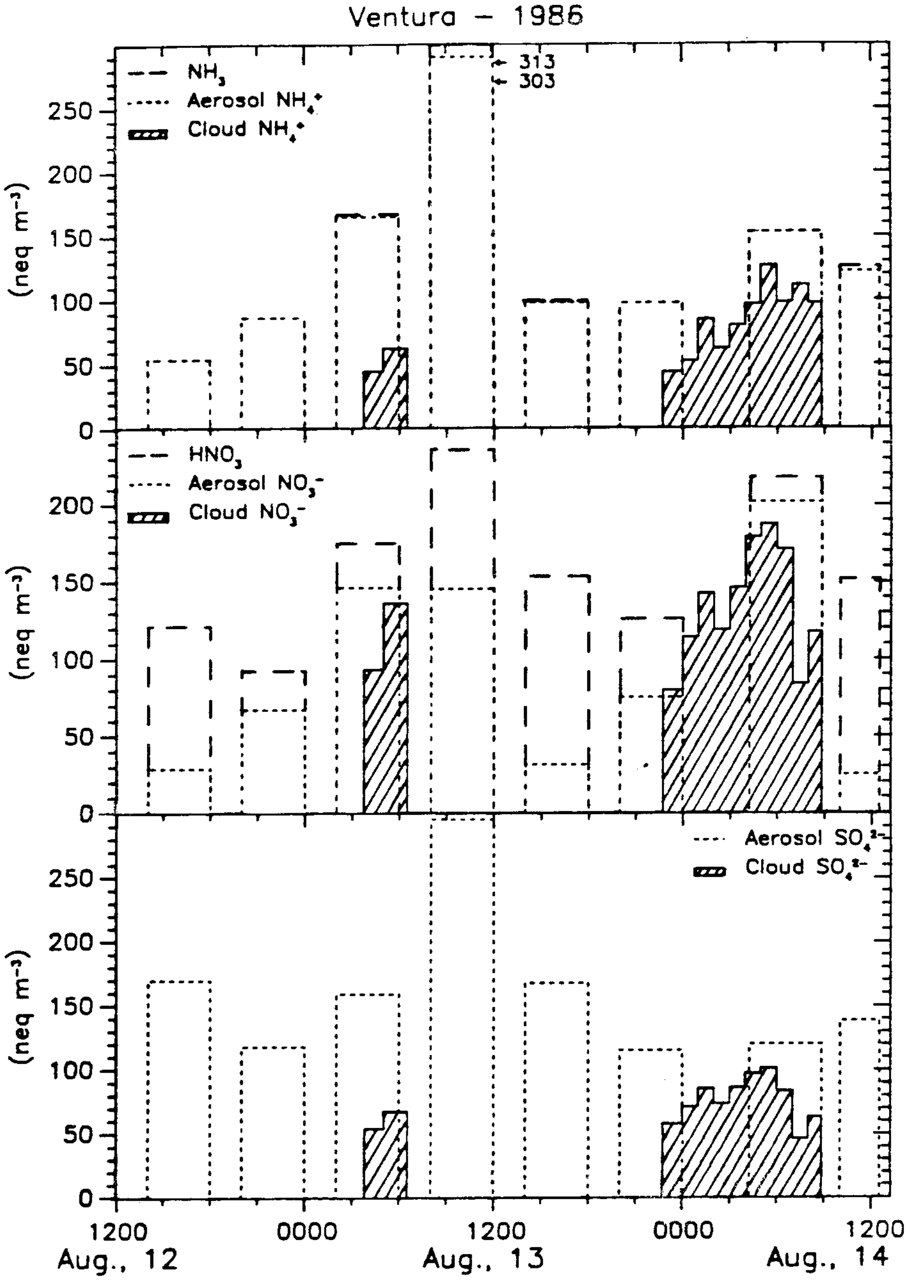

Figure B.13 Aerosol and cloudwater loadings of major ions at Ventura on August 12 – 14, 1986. Cloudwater loading is the product of aqueous–phase concentration and estimated LWC.

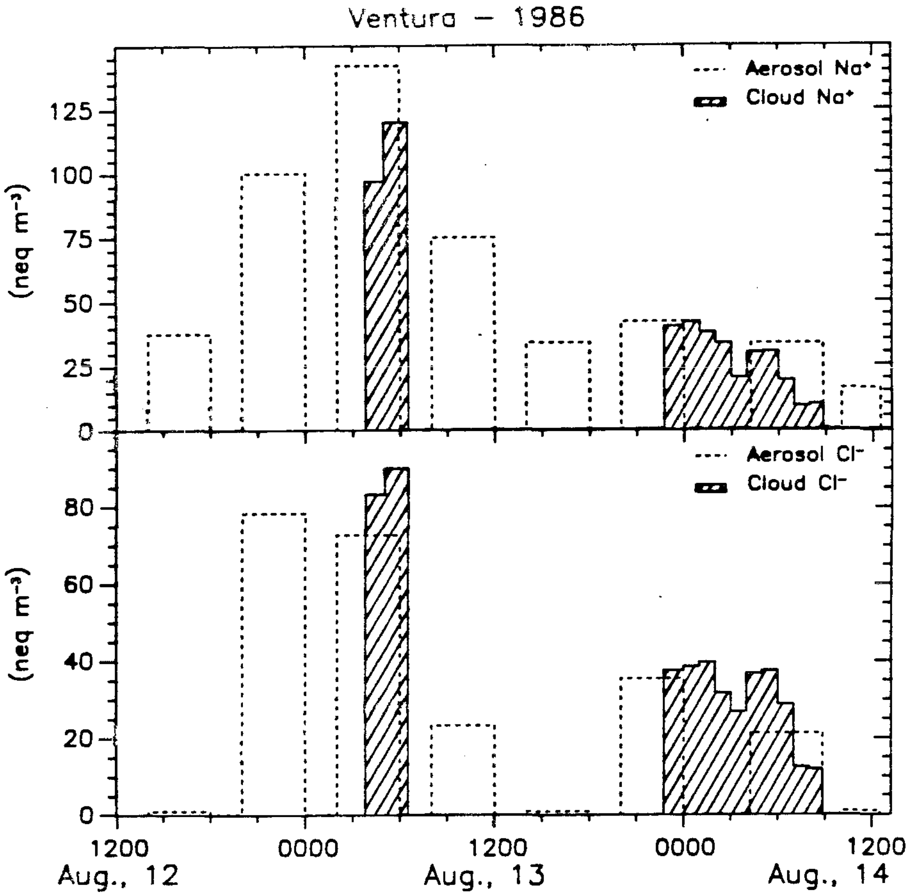

Figure B.14 Aerosol and cloudwater loadings of sea salts at Ventura on August 12 – 14, 1986. Cloudwater loading is the product of aqueous–phase concentration and estimated LWC.

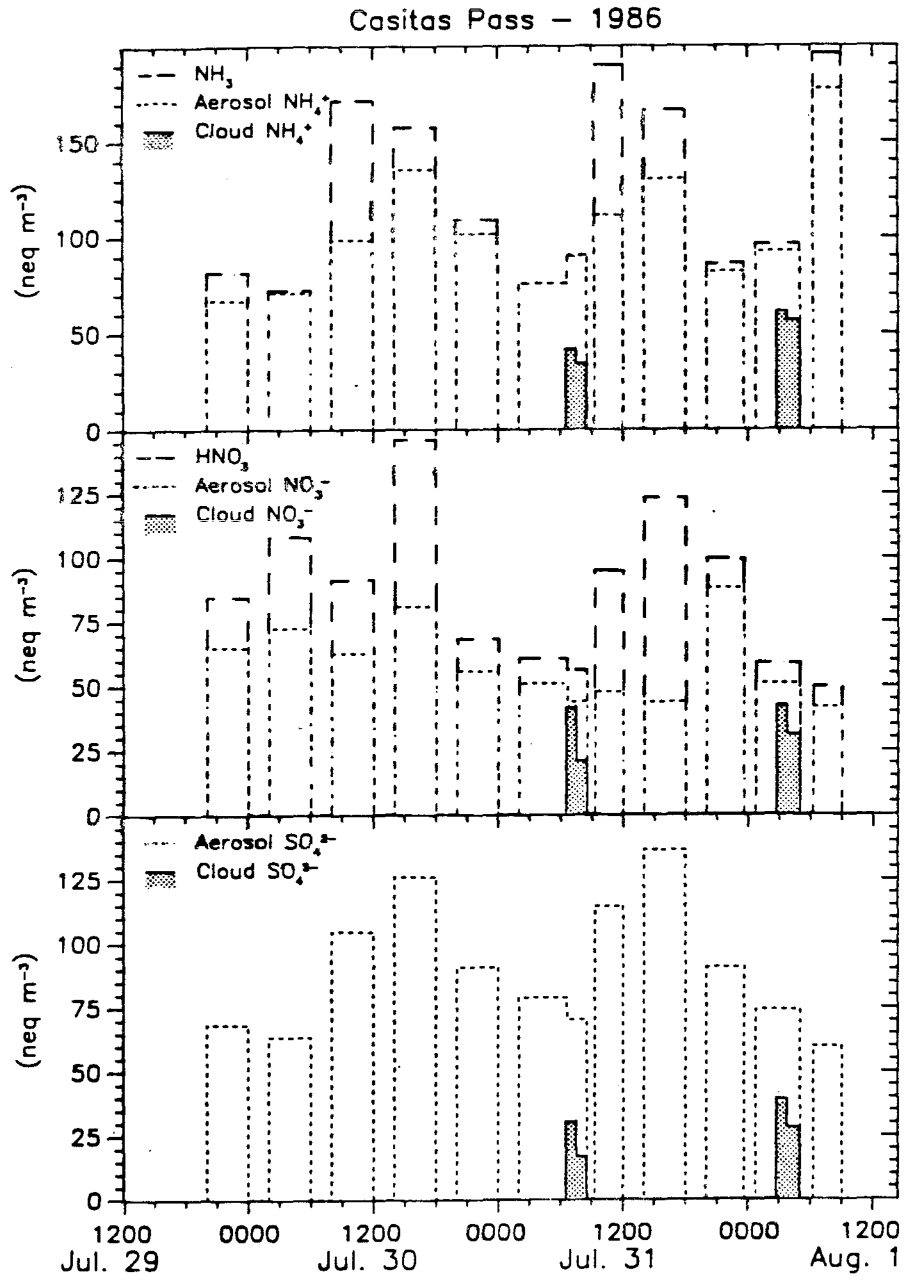

Figure B.15 Aerosol and cloudwater loadings of major ions at Casitas Pass on July 29 – August 1, 1986. Cloudwater loading is the product of aqueous–phase concentration and estimated LWC.

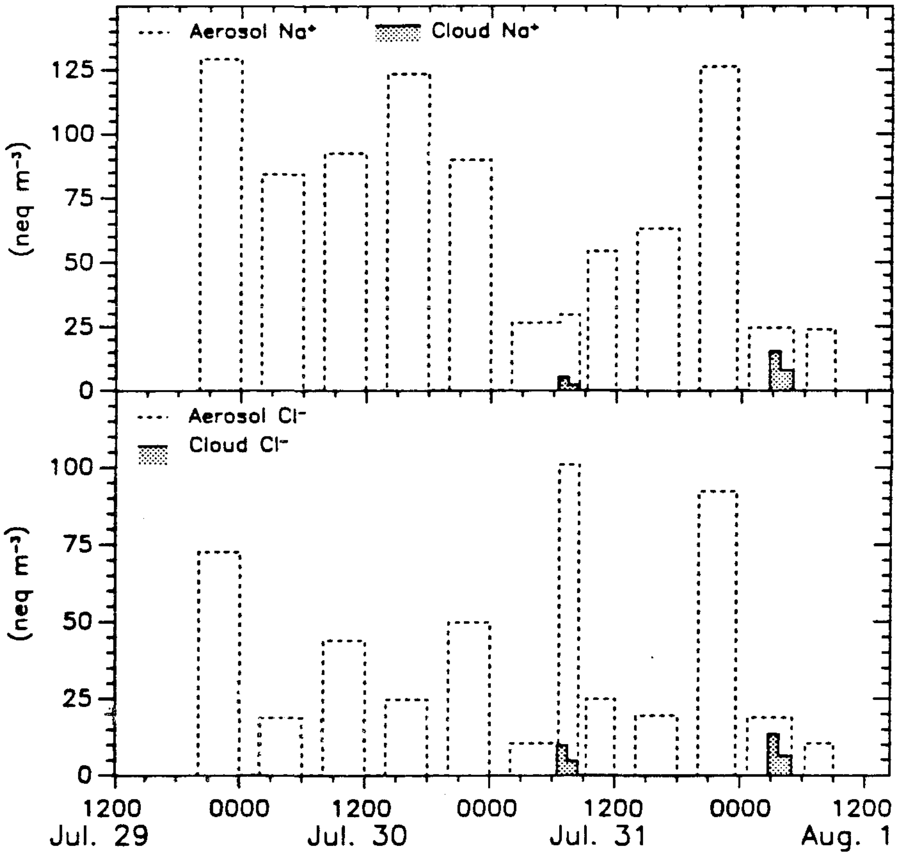

Figure B.16 Aerosol and cloudwater loadings of sea salts at Casitas Pass on July 29 – August 1, 1986. Cloudwater loading is the product of aqueous–phase concentration and estimated LWC.

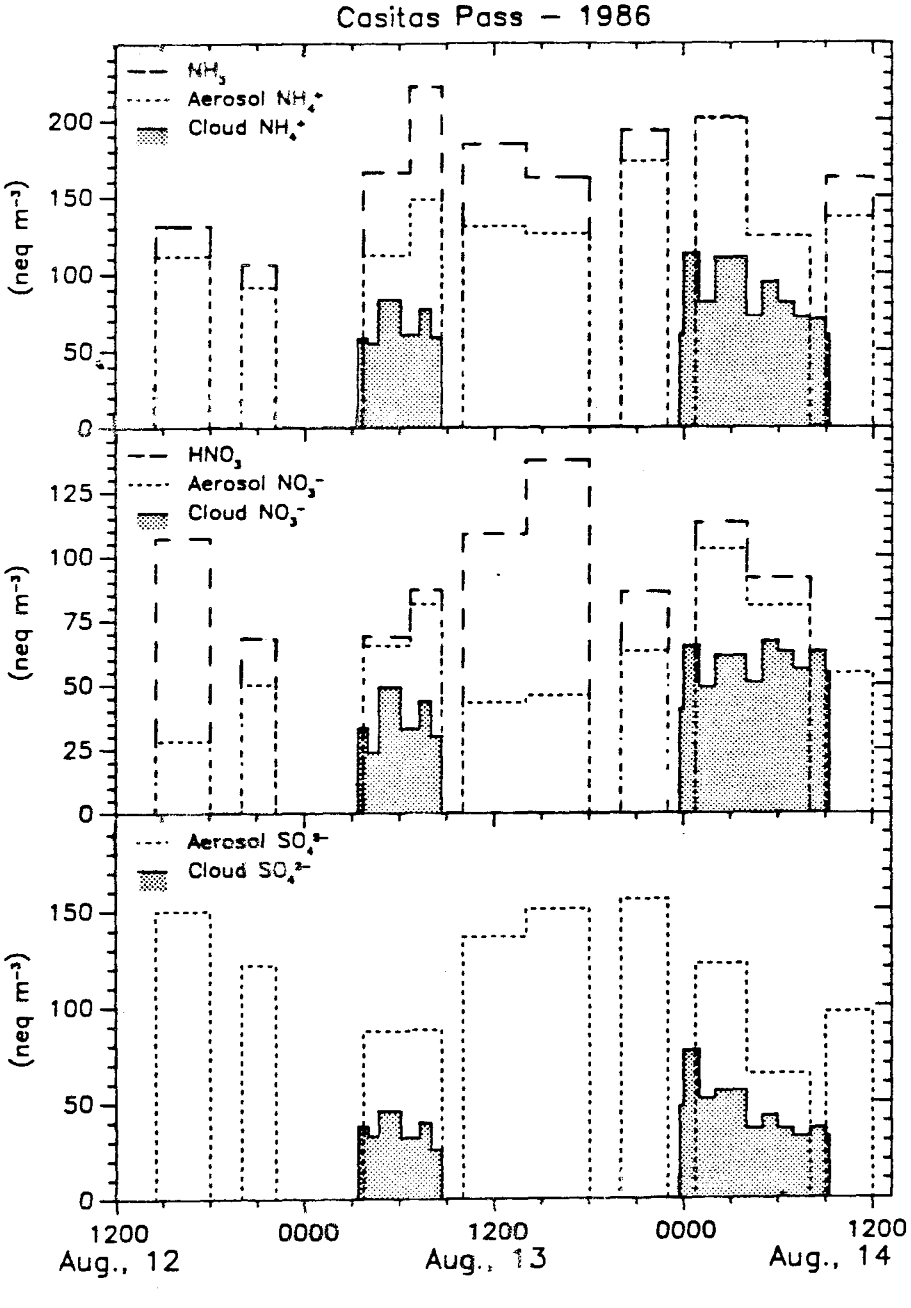

Figure B.17 Aerosol and cloudwater loadings of major ions at Casitas Pass on August 12 – 14, 1986. Cloudwater loading is the product of aqueous–phase concentration and estimated LWC.

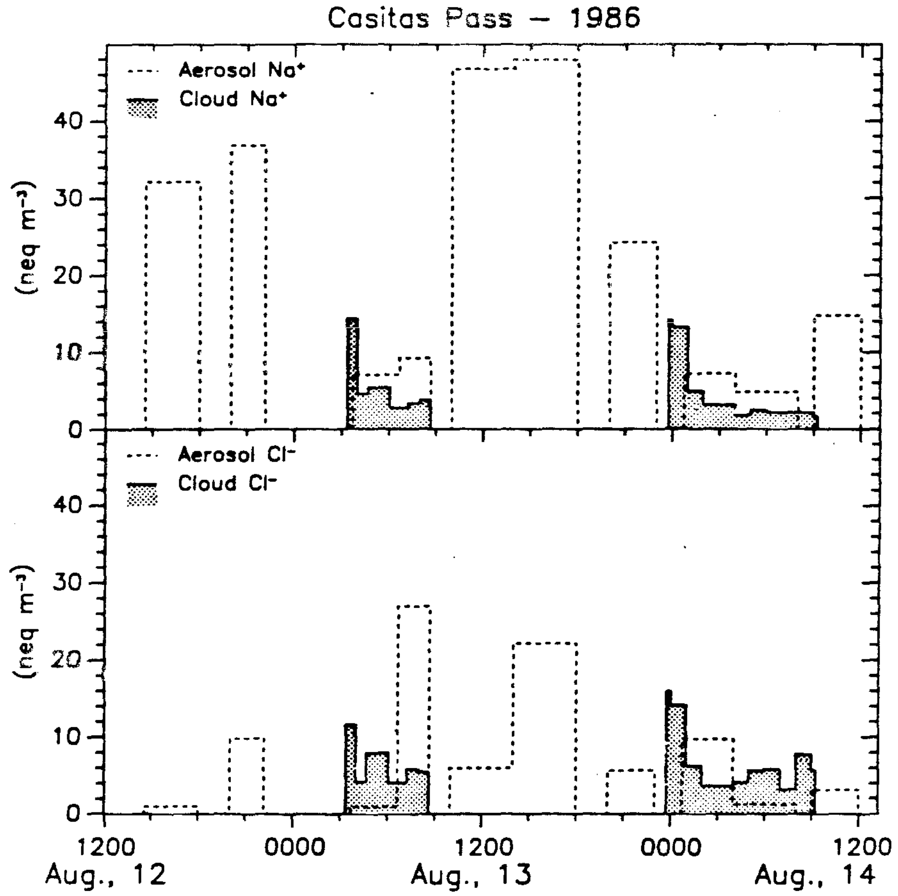

Figure B.18 Aerosol and cloudwater loadings of sea salts at Casitas Pass on August 12 – 14, 1986. Cloudwater loading is the product of aqueous–phase concentration and estimated LWC.

1985 LaJolla Peak Aerosol Concentrations

Date ID	Start	Stop	Na^+	NH_4^+	Ca^{2+}	Mg^{2+}	Cl^-	NO_3^-	SO_4^{2-}	NH_3	HNO_3
						neq m^{-3}				nmole m^{-3}	
07/23 A	12:00	15:54	99	62	7.3	18.4	4.1	59	173	66	101
07/24 A	02:30	05:53	14	65	3.9	2.7	0.0	24	107	19	61
07/24 B	06:00	09:33	4	52	0.0	0.8	0.8	22	53	36	94
07/25 A	12:00	15:52	41	73	6.9	5.6	16.6	38	132	22	119
07/26 A	12:00	15:52	23	78	1.7	4.1	0.0	16	176	12	4
07/27 B	03:30	06:20	1	18	16.8	0.0	0.0	31	71	31	NA
07/29 A	15:30	19:40	95	0	0.0	21.0	41.2	39	32	8	21
07/30 A	01:45	04:18	284	20	6.9	35.0	211	34	153	68	24
07/30 B	05:00	09:27	86	14	3.0	18.1	38.3	39	42	30	9
07/30 C	13:00	16:57	225	66	5.5	51.2	26.9	152	148	23	71
07/31 A	20:47	11:44	92	33	12.7	22.7	22.7	77	52	16	28
08/06 A	23:00	03:00	137	166	41.7	34.5	128	111	66	21	85
08/07 B	16:15	20:09	128	239	37.0	33.4	126	99	97	14	83
08/07 A	23:00	03:01	79	80	31.7	22.8	6.0	142	80	56	186
08/08 B	12:40	16:01	101	142	NA	30.1	0.0	68	304	7	386
08/14 B	02:00	05:55	NA	NA	NA	NA	107	95	67	19	34
08/19 A	17:02	20:02	45	34	0.0	9.7	2.2	40	34	33	37
08/20 A	12:00	15:56	65	48	1.1	13.9	124	34	63	8	82
08/21 A	00:11	04:10	8	14	10.6	8.1	36.3	29	81	8	30
08/21 B	04:25	07:51	162	33	15.7	6.8	1.7	153	111	4	37
08/26 A	16:00	19:07	86	95	37.4	23.5	1.3	72	129	29	77
08/28 A	14:40	21:19	61	46	17.5	20.3	4.5	57	57	42	99
08/29 A	00:00	03:59	35	43	31.9	12.9	11.9	32	36	66	97
08/29 B	12:00	15:52	118	51	31.6	30.3	34.0	65	58	89	97
08/30 A	00:00	04:07	46	44	26.7	16.0	34.8	39	36	58	110
09/03 A	14:30	18:31	144	12	6.4	35.1	92.4	19	46	21	11
09/04 A	00:00	03:52	35	21	0.0	12.5	31.6	11	40	27	5
09/04 B	12:00	15:55	142	6	0.0	28.7	71.1	24	62	25	13
09/16 A	16:15	19:25	153	38	22.3	42.0	75.4	67	62	26	22
09/17 A	00:00	03:53	68	26	16.7	18.7	17.6	58	72	15	31
09/17 B	13:00	16:59	109	22	5.4	24.3	28.0	71	61	37	62
09/18 A	00:00	05:44	50	11	0.0	13.4	22.4	23	39	14	9

NA indicates sample not analyzed

1985 Casitas Pass Aerosol Concentrations

Date ID	Start	Stop	Na^+	NH_4^+	Ca^{2+}	Mg^{2+}	Cl^-	NO_3^-	SO_4^{2-}	NH_3	HNO_3
						neq m^{-3}				– nmole m^{-3} –	
08/07 A	02:00	02:36	207	78	0.0	58.3	107	43	75	97	22
08/07 B	13:00	17:00	130	68	6.5	32.1	24.4	99	89	53	44
08/08 A	00:00	04:36	74	61	26.6	22.3	0.0	97	63	15	29
08/08 B	05:55	08:37	12	107	38.9	6.2	0.0	69	79	11	27
08/08 A	12:00	16:06	NA	NA	NA	NA	NA	NA	NA	21	136
08/09 B	00:00	03:45	96	65	32.4	26.4	9.1	122	109	8	25
08/09 C	06:00	09:12	57	185	43.2	20.6	0.0	148	141	28	43
08/14 A	00:00	04:00	100	35	34.6	32.7	75.0	52	61	12	16
08/14 B	12:00	16:12	113	22	3.4	28.4	26.8	73	59	37	28
08/28 A	16:30	19:30	207	68	38.6	55.0	50.0	172	95	94	24
08/29 A	14:20	15:56	105	57	40.6	22.4	14.6	82	53	115	163
09/03 A	16:20	19:48	146	0	2.9	31.0	101	10	43	0	11
09/04 A	16:00	19:36	73	7	19.7	19.0	23.8	34	55	31	15
09/05 A	00:00	04:00	195	38	33.3	54.2	115	110	77	16	18
09/16 A	19:30	23:12	116	46	5.4	37.8	123	126	85	22	23
09/17 A	03:30	06:36	126	98	30.4	35.2	37.4	153	97	20	23
09/17 B	14:00	18:12	NA	NA	NA	NA	NA	NA	NA	21	84
09/17 A	22:00	02:18	99	36	13.8	29.1	43.8	114	54	10	11

NA indicates sample not analyzed

1985 La Jolla Peak Cloudwater Concentrations
RAC Collector

Date ID	Start	Stop	Vol	pH	Na^+	NH_4^+	Ca^{2+}	Mg^{2+}	Cl^-	NO_3^-	SO_4^{2-}	$SO_{4\,xs}^{2-*}$
			(ml)						μN			
07/24 A	02:35	03:35	49	3.36	193	214	62	57	196	509	370	347
07/24 B	03:35	04:10	20	3.19	199	311	82	65	217	844	532	508
07/24 C	06:05	07:05	14	2.77	302	801	259	111	290	2260	1050	1013
07/24 D	07:07	08:10	17	2.56	710	882	192	236	495	2610	1500	1414
07/24 E	08:10	09:05	13	2.18	>300	873	102	153	1100	2750	1980	1905
07/24 A	23:02	00:00	36	3.38	480	253	77	125	322	481	225	167
07/25 B	00:02	01:00	48	3.26	464	196	106	116	309	600	537	481
07/25 C	01:02	02:00	53	3.26	259	192	136	72	272	449	433	402
07/25 D	02:02	03:00	58	3.28	243	210	42	64	161	370	310	281
07/25 E	03:02	04:00	70	3.01	335	333	53	88	234	687	481	440
07/25 F	06:00	07:00	18	2.42	310	719	52	92	202	1410	1080	1042
07/25 G	07:00	08:00	22	2.36	192	546	25	54	170	967	826	803
07/25 H	08:00	08:20	6	2.39	NA	632	69	92	242	1150	970	925
07/26 A	03:35	04:00	40	3.45	483	294	12	34	126	365	371	313
07/26 B	04:00	04:45	57	3.35	122	319	22	37	125	402	361	346
07/26 C	04:48	05:30	58	2.75	74	284	12	23	87	426	359	350
07/26 D	05:30	06:17	46	2.71	30	323	11	13	70	511	322	318
07/30 A	05:00	05:45	11	3.50	>870	310	76	816	1120	844	568	167
08/21 A	00:19	01:02	52	3.79	166	119	25	37	197	201	132	111
08/21 B	01:02	01:35	22	3.72	147	109	22	34	183	208	139	122
08/21 C	02:10	03:10	47	3.14	436	238	52	115	389	677	395	342
08/21 D	03:10	04:10	16	2.64	965	591	139	259	185	NA	1010	1046
08/21 F	05:10	06:10	34	2.81	211	402	51	46	203	1460	557	532
08/21 G	06:10	07:10	23	2.55	525	418	103	144	294	2540	1110	1046
08/21 H	07:10	07:50	1	2.21	NA	NA	NA	NA	NA	NA	NA	
09/17 A	00:00	00:45	15	3.46	1500	105	121	321	1030	558	358	177
09/17 B	03:15	04:00	4	NA	1550	>150	275	523	1210	1050	410	222
N			27	26	25	26	26	26	26	25	26	26
Min			1.1	2.18	30	105	10.5	12.5	70	201	132	111
Maximum			70	3.79	1550	882	275	816	1210	2750	1980	1905
Avg			31	2.98	396	372	83.8	143	363	973	630	566
Vol Wt Avg				2.95	301	308	57	86	247	681	472	436

1985 La Jolla Peak Cloudwater Concentrations (continued)
RAC Samples

Date ID	Start	Stop	S(IV)	CH_2O	H_2O_2	−/+
				μM		
07/24 A	02:35	03:35	0	13	19	1.08
07/24 B	03:35	04:10	0	16	4	1.19
07/24 C	06:05	07:05	1	29	11	1.10
07/24 D	07:07	08:10	3	44	5	0.95
07/24 E	08:10	09:05	2	50	4	NA
07/24 A	23:02	00:00	3	16	79	0.75
07/25 B	00:02	01:00	2	13	12	1.00
07/25 C	01:02	02:00	0	15	24	0.95
07/25 D	02:02	03:00	0	9	33	0.77
07/25 E	03:02	04:00	0	13	21	0.78
07/25 F	06:00	07:00	2	21	3	0.54
07/25 G	07:00	08:00	7	21	5	0.38
07/25 H	08:00	08:20	NA	NA	NA	NA
07/26 A	03:35	04:00	6	10	22	NA
07/26 B	04:00	04:45	0	13	12	0.92
07/26 C	04:48	05:30	0	16	12	0.40
07/26 D	05:30	06:17	0	17	6	NA
07/30 A	05:00	05:45	0	NA	21	NA
08/21 A	00:19	01:02	0	NA	22	1.03
08/21 B	01:02	01:35	0	NA	22	1.04
08/21 C	02:10	03:10	0	NA	15	0.93
08/21 D	03:10	04:10	0	NA	11	NA
08/21 F	05:10	06:10	0	NA	10	0.98
08/21 G	06:10	07:10	0	NA	5	0.98
08/21 H	07:10	07:50	NA	NA	NA	NA
09/17 A	00:00	00:45	NA	NA	NA	0.80
09/17 B	03:15	04:00	NA	NA	NA	NA
N			23	16	23	19
Min			0	9	3.2	0.38
Maximum			6.6	50	79	1.19
Arith Avg			1.1	19.8	16.4	0.70
Vol Avg			0.97	15.5	18.3	0.75

1985 La Jolla Peak Cloudwater Concentrations
CASC Collector

Date	ID	Start	Stop	Vol (ml)	pH	Na^+	NH_4^+	Ca^{2+}	Mg^{2+}	Cl^-	NO_3^-	SO_4^{2-}	$SO_{4\,xs}^{2-*}$
						μN							
07/25	B	00:02	01:00	143	3.22	207	224	51	86	229	427	500	475
07/25	C1	01:00	01:30	114	NA	124	223	41	52	153	362	436	421
07/25	C2	01:30	02:00	114	3.22	134	233	34	55	160	398	469	453
07/25	D	02:00	03:00	NA	3.26	121	236	36	39	138	327	349	334
07/25	E1	03:00	03:30	115	NA	138	260	33	41	144	365	317	300
07/25	E2	03:30	04:00	98	2.93	184	390	31	56	167	675	509	487
07/25	F	06:00	07:00	79	2.27	231	888	37	37	NA	NA	NA	
07/25	G	07:00	08:00	119	2.29	117	678	66	67	174	1140	1040	1026
07/25	H	08:00	08:20	19	2.21	151	716	32	45	204	1250	1190	1172
07/26	B	04:00	04:45	381	3.34	73	303	16	17	126	320	332	323
07/26	C	04:48	05:30	355	2.98	52	265	19	18	112	411	356	350
07/26	D	05:30	06:17	301	2.68	46	319	19	17	94	495	329	323
07/30	A	05:00	05:45	34	3.43	870	430	54	661	2200	949	717	611
08/21	A	00:19	01:02	208	3.70	175	134	30	23	168	225	172	
08/21	B	01:02	01:35	89	3.68	133	131	19	19	154	203	168	
08/21	C	02:10	03:10	23	NA	259	282	43	57	293	605	396	
08/21	D	03:10	04:10	103	2.68	488	525	67	113	463	745	894	
08/21	E	04:10	05:10	87	2.48	483	745	107	135	345	2230	1380	1322
08/21	F	05:10	06:10	150	2.63	198	568	53	38	138	1860	833	809
08/21	G	06:10	07:10	167	2.54	218	562	55	43	222	1990	922	895
08/21	H	07:10	07:50	31	2.2	781	NA	158	211	1370	4730	2000	1905
09/03	A	23:00	00:00	50	4.94	2980	795	256	775	909	378	734	373
09/04	B	00:00	01:00	56	4.85	2510	712	212	582	1050	325	653	349
09/04	C	01:00	03:00	49	4.27	764	1070	370	1110	738	732	1020	928
09/17	A	00:00	00:45	71	3.47	843	93	76	392	901	390	290	188
09/17	B	03:15	04:00	27	3.41	1270	260	140	356	1190	992	448	294
N				26	23	26	25	26	26	25	25	25	25
Min				19.4	2.21	46.1	92.9	15.8	17.3	94	203	168	151
Max				381	4.94	2980	1070	370	1110	2200	4730	2000	1905
Avg				128	3.16	521	442	79	194	474	901	658	594
Vol Wt Avg					2.83	248	345	44	81	253	647	484	454

1985 La Jolla Peak Cloudwater Concentrations (continued)
CASC Samples

Date	ID	Start	Stop	S(IV)	CH_2O	H_2O_2	−/+
					μM		
07/25	B	00:02	01:00	6	NA	36	0.96
07/25	C1	01:00	01:30	NA	NA	NA	NA
07/25	C2	01:30	02:00	NA	NA	NA	0.95
07/25	D	02:00	03:00	NA	NA	NA	0.81
07/25	E1	03:00	03:30	NA	NA	NA	NA
07/25	E2	03:30	04:00	NA	NA	NA	0.72
07/25	F	06:00	07:00	NA	NA	5	NA
07/25	G	07:00	08:00	5	NA	3	0.39
07/25	H	08:00	08:20	0	NA	4	0.37
07/26	B	04:00	04:45	0	13	10	0.89
07/26	C	04:48	05:30	0	14	5	0.62
07/26	D	05:30	06:17	4	15	9	0.37
07/30	A	05:00	05:45	0	NA	10	NA
08/21	A	00:19	01:02	0	NA	22	0.99
08/21	B	01:02	01:35	0	NA	21	1.02
08/21	C	02:10	03:10	0	NA	17	NA
08/21	D	03:10	04:10	0	NA	13	0.64
08/21	E	04:10	05:10	0	NA	12	0.82
08/21	F	05:10	06:10	0	NA	11	0.88
08/21	G	06:10	07:10	0	NA	5	0.83
08/21	H	07:10	07:50	0	NA	3	NA
09/03	A	23:00	00:00	NA	NA	NA	NA
09/04	B	00:00	01:00	NA	NA	NA	NA
09/04	C	01:00	03:00	NA	NA	NA	NA
09/17	A	00:00	00:45	NA	NA	NA	0.89
09/17	B	03:15	04:00	NA	NA	NA	1.07
N				15	3	16	17
Min				0	13	2.8	0.37
Max				6	15	36.3	1.07
Avg				1	14	11.6	0.67
Vol Wt Avg				0.96	—	11.9	0.63

1985 La Jolla Peak Cloudwater (RAC) Samples – Loading

Date Seq	Start	Stop	LWC	H^+	Na^+	NH_4^+	Ca^{2+}	Mg^{2+}	Cl^-	NO_3^-	SO_4^{2-}
			g m^{-3}	neq m^{-3}							
07/24 A	02:35	03:35	0.27	119	52	58	16.8	15.5	53.3	138	101
07/24 B	03:35	04:10	0.19	125	38	60	15.9	12.5	41.9	163	103
07/24 C	06:05	07:05	0.08	136	24	64	20.7	8.9	23.2	181	84
07/24 D	07:07	08:10	0.09	253	65	81	17.7	21.7	45.5	240	138
07/24 E	08:10	09:05	0.08	502	>4	66	7.8	11.6	83.6	209	150
07/24 A	23:02	00:00	0.20	85	98	52	15.7	25.5	65.7	98	46
07/25 B	00:02	01:00	0.27	151	127	54	29.1	31.8	84.7	164	147
07/25 C	01:02	02:00	0.30	167	79	58	41.5	21.8	82.7	136	132
07/25 D	02:02	03:00	0.33	174	80	70	13.8	21.1	53.3	122	103
07/25 E	03:02	04:00	0.40	392	134	134	21.3	35.3	93.8	275	193
07/25 F	06:00	07:00	0.10	384	31	73	5.3	9.3	20.4	142	109
07/25 G	07:00	08:00	0.12	537	24	67	3.0	6.7	20.9	119	102
07/25 H	08:00	08:20	0.09	375	NA	58	6.3	8.5	22.3	106	89
07/26 A	03:35	04:00	0.53	187	254	155	6.5	17.9	66.3	192	195
07/26 B	04:00	04:45	0.42	189	52	135	9.3	15.6	52.9	170	153
07/26 C	04:48	05:30	0.46	823	34	131	5.7	10.7	40.3	197	166
07/26 D	05:30	06:17	0.32	632	10	105	3.4	4.1	22.7	166	104
07/30 A	05:00	05:45	0.08	27	>12	26	6.4	68.5	94.1	71	48
08/21 A	00:19	01:02	0.40	65	66	48	9.9	14.6	78.9	80	53
08/21 B	01:02	01:35	0.23	43	33	25	5.0	7.6	41.3	47	31
08/21 C	02:10	03:10	0.26	189	114	62	13.6	30.0	102	177	103
08/21 D	03:10	04:10	0.09	197	83	51	12.0	22.3	15.9	NA	87
08/21 F	05:10	06:10	0.19	293	40	76	9.6	8.7	38.3	276	105
08/21 G	06:10	07:10	0.13	358	67	53	13.0	18.3	37.3	323	141
08/21 H	07:10	07:50	0.01	55	NA	NA	NA	NA	NA	NA	NA
09/17 A	00:00	00:45	0.11	37	161	11	12.9	34.3	110	60	38
09/17 B	03:15	04:00	0.03	NA	50	>1	8.8	16.7	38.7	34	13
N				26	25	26	26	26	26	25	27
Min				27	0.0	0.0	3.0	4.1	15.9	33.6	0.0
Max				823	254	155	41	69	110	323	177
Avg				250	69	68	13	19	55	155	92

1985 La Jolla Peak Cloudwater (CASC) Samples – Loading

Date Seq	Start	Stop	LWC	H^+	Na^+	NH_4^+	Ca^{2+}	Mg^{2+}	Cl^-	NO_3^-	SO_4^{2-}
			g m^{-3}	neq m^{-3}							
07/25 B	00:02	01:00	0.14	83	29	31	7.1	11.9	31.6	59	69
07/25C1	01:00	01:30	0.21	NA	26	47	8.7	11.0	32.6	77	93
07/25C2	01:30	02:00	0.21	128	29	50	7.2	11.7	34.1	85	100
07/25 D	02:00	03:00	NA	NA	NA	NA	NA	NA	NA	NA	NA
07/25E1	03:00	03:30	0.22	NA	30	56	7.0	8.9	31.0	78	68
07/25E2	03:30	04:00	0.18	215	34	71	5.7	10.3	30.6	124	93
07/25 F	06:00	07:00	0.07	397	17	66	2.7	2.8	NA	NA	NA
07/25 G	07:00	08:00	0.11	569	13	75	7.4	7.4	19.3	127	115
07/25 H	08:00	08:20	0.05	333	8	39	1.7	2.5	11.0	68	64
07/26 B	04:00	04:45	0.47	217	34	144	7.5	8.2	59.7	152	157
07/26 C	04:48	05:30	0.47	495	25	125	8.8	8.7	53.0	194	168
07/26 D	05:30	06:17	0.36	750	17	115	7.0	6.2	33.7	178	118
07/30 A	05:00	05:45	0.04	16	>37	18	2.3	27.8	92.4	40	30
08/21 A	00:19	01:02	0.27	54	47	36	8.0	6.1	45.5	61	47
08/21 B	01:02	01:35	0.15	32	20	20	2.8	2.9	23.4	31	25
08/21 C	02:10	03:10	0.22	NA	57	62	9.4	12.4	64.4	133	87
08/21 D	03:10	04:10	0.10	201	47	50	6.4	10.8	44.4	72	86
08/21 E	04:10	05:10	0.08	268	39	60	8.6	10.9	27.9	181	112
08/21 F	05:10	06:10	0.14	328	28	80	7.5	5.3	19.3	260	117
08/21 G	06:10	07:10	0.16	450	34	88	8.5	6.7	34.7	310	144
08/21 H	07:10	07:50	0.04	253	34	NA	7.0	9.3	60.3	208	88
09/03 A	23:00	00:00	0.05	1	137	37	11.8	35.7	41.8	17	34
09/04 B	00:00	01:00	0.05	1	131	37	11.0	30.3	54.6	17	34
09/04 C	01:00	03:00	0.02	1	18	25	8.5	25.5	17.0	17	23
09/17 A	00:00	00:45	0.09	30	74	8	6.7	34.5	79.3	34	26
09/17 B	03:15	04:00	0.03	13	42	9	4.6	11.7	39.3	33	15
N				22	25	24	25	25	24	24	24
Min				0.5	0.0	8.2	1.7	2.5	11.0	16.8	14.8
Max				750	137	144	12	36	92	310	168
Avg				220	39	56	7	13	41	106	80

1985 Casitas Pass Cloudwater Samples – Concentration

Date ID	Start	Stop	Vol (ml)	pH	Na^+	NH_4^+	Ca^{2+}	Mg^{2+}	Cl^-	NO_3^-	SO_4^{2-}	
					μN							
08/07 A	02:55	03:16	16	4.38	200	113	35	51	333	141	100	76
08/07 B	03:30	03:40	8	4.93	480	209	69	131	751	299	195	137
08/08 A	05:02	05:21	19	3.88	46	170	28	19	60	232	118	112
08/08 B	05:40	06:15	33	3.61	90	221	34	29	99	382	131	120
08/08 C	06:15	06:55	40	3.80	66	310	34	23	172	367	142	134
08/08 D	07:07	08:00	34	3.61	110	413	44	32	276	191	84	71
08/08 E	08:00	08:39	10	3.28	400	NA	149	108	628	956	422	374
08/09 A	06:00	07:00	13	3.36	620	847	268	222	411	1540	562	487
08/09 B	07:00	08:00	8	3.31	>1000	NA	362	842	1600	>2800	2150	1736
08/09 C	08:00	09:00	6	3.57	>1000	1450	672	637	155	401	162	0
N			10	10	10	8	10	10	10	10	10	10
Min			6	3.28	46	113	28	19	60	141	84	0
Max			40	4.93	>1000	1450	672	842	1600	>2800	2150	1736
Avg			19	3.77	401	467	169	209	448	451	407	325
Vol Wt Avg				3.75	>218	182	71	83	315	>414	206	165

1985 Casitas Pass Cloudwater Concentrations (continued)

Date ID	Start	Stop	S(IV)	CH_2O	H_2O_2	-/+
			μM			
08/07 A	02:55	03:16	NA	NA	NA	1.25
08/07 B	03:30	03:40	NA	NA	NA	1.32
08/08 A	05:02	05:21	0	NA	3	1.01
08/08 B	05:40	06:15	0	NA	7	0.95
08/08 C	06:15	06:55	0	NA	3	1.13
08/08 D	07:07	08:00	0	NA	12	0.64
08/08 E	08:00	08:39	0	NA	17	NA
08/09 A	06:00	07:00	0	NA	8	1.03
08/09 B	07:00	08:00	0	NA	NA	NA
08/09 C	08:00	09:00	NA	NA	NA	NA
N			7	0	6	7
Min			0	NA	3	0.64
Max			0	NA	17	1.32
Avg			0		8	1.05
Vol Wt Avg					6	

1985 Casitas Pass Cloudwater Samples – Loading

Date Seq	Start	Stop	LWC	H^+	Na^+	NH_4^+	Ca^{2+}	Mg^{2+}	Cl^-	NO_3^-	SO_4^{2-}
			g m^{-3}	neq m^{-3}							
08/07 A	02:55	03:16	0.25	11	50.8	28.7	9.0	12.9	84.6	35.8	25.5
08/07 B	03:30	03:40	0.27	3	128	55.6	18.3	34.8	199.8	79.6	51.8
08/08 A	05:02	05:21	0.32	43	14.9	55.1	9.1	6.2	19.4	75.3	38.2
08/08 B	05:40	06:15	0.31	76	27.8	68.3	10.4	9.0	30.6	118	40.5
08/08 C	06:15	06:55	0.33	53	21.8	103	11.2	7.5	57.2	122	47.3
08/08 D	07:07	08:00	0.21	52	23.5	88.4	9.5	6.9	59.0	40.9	18.1
08/08 E	08:00	08:39	0.09	45	34.0	NA	12.7	9.2	53.4	81.2	35.9
08/09 A	06:00	07:00	0.07	31	44.6	61.0	19.3	16.0	29.6	111	40.4
08/09 B	07:00	08:00	0.04	22	>7.0	NA	15.9	37.0	70.4	>20	94.6
08/09 C	08:00	09:00	0.03	9	>6.0	47.9	22.2	21.0	5.1	13.2	5.3

1986 Laguna Peak Cloudwater Concentration

Date ID	Start	Stop	Vol (ml)	pH	Na^+	NH_4^+	Ca^{2+}	Mg^{2+}	Cl^-	NO_3^-	SO_4^{2-}	SO_4^{2-*}
					μN							
08/05 A	03:33	04:30	210	3.14	24	195	13	9	74	504	395	392
08/05 B	04:30	05:30	131	3.05	21	238	11	8	75	639	410	407
08/05 C	05:30	06:30	327	3.01	22	273	6	7	75	693	496	493
08/05 D	06:30	07:30	218	3.01	52	300	10	15	82	500	439	433
08/05 E	07:30	08:30	166	2.87	56	460	16	17	92	790	744	737
08/05 F	08:30	09:05	88	2.69	137	599	27	39	169	1090	1110	1093
08/06 A	06:40	07:40	378	3.30	9	143	4	3	46	394	276	275
08/06 B	07:40	08:40	304	3.33	12	170	5	4	50	345	310	309
08/06 C	08:40	09:40	174	3.18	39	315	10	12	94	500	524	519
08/06 D	09:40	10:40	180	2.97	25	305	8	8	79	672	716	713
08/06 E	10:40	11:10	16	2.71	45	502	14	16	92	1250	1340	1335
08/13 A	08:30	09:00	69	3.01	106	425	23	31	200	792	607	594
08/13 B	09:00	09:25	10	2.85	318	686	73	88	350	1410	1010	972
08/14 A	02:30	03:00	186	3.39	20	171	7	8	102	344	279	277
08/14 B	03:00	04:00	423	3.32	25	205	8	9	97	381	280	277
08/14 C	04:00	05:00	346	3.46	23	211	7	10	122	475	342	339
08/14 D	05:05	06:00	265	3.06	72	286	15	24	149	601	442	433
08/14 E	06:00	07:00	227	3.04	128	290	18	32	167	710	528	513
08/14 F	07:00	08:01	185	3.08	85	388	19	27	163	848	665	655
08/14 G	08:05	09:00	113	3.01	151	578	27	40	161	1100	888	870
N			20	20	20	20	20	20	20	20	20	20
Min.				2.69	9	143	4	3	46	344	276	275
Max.				3.46	318	686	73	88	350	1410	1340	1335
Avg.				3.07	68	337	16	20	122	702	590	582
Vol Wt Avg.				3.16	47	276	11	15	105	579	472	466

1986 Laguna Peak Cloudwater Concentrations (continued)

Date ID	Start	Stop	S(IV)	CH_2O	H_2O_2	HFo	HAc	H^+	−/+
			μM						
08/05 A	03:33	04:30	0	15	2	24	14	724	1.01
08/05 B	04:30	05:30	0	18	0	26	16	891	0.95
08/05 C	05:30	06:30	0	18	0	25	15	977	0.98
08/05 D	06:30	07:30	0	18	1	28	17	977	0.75
08/05 E	07:30	08:30	0	17	1	36	19	1349	0.85
08/05 F	08:30	09:05	0	18	1	41	14	2042	0.83
08/06 A	06:40	07:40	0	20	2	40	13	501	1.08
08/06 B	07:40	08:40	0	20	3	48	14	468	1.07
08/06 C	08:40	09:40	0	26	5	58	23	661	1.08
08/06 D	09:40	10:40	0	33	6	63	26	1072	1.03
08/06 E	10:40	11:10	—	—	—	—	—	1950	1.06
08/13 A	08:30	09:00	0	7	2	37	19	977	1.02
08/13 B	09:00	09:25	—	—	—	—	—	1413	1.07
08/14 A	02:30	03:00	—	—	—	—	—	407	1.18
08/14 B	03:00	04:00	—	—	—	—	—	479	1.04
08/14 C	04:00	05:00	—	—	—	32	12	347	1.57
08/14 D	05:05	06:00	0	9	1	27	12	871	0.94
08/14 E	06:00	07:00	0	9	2	34	13	912	1.01
08/14 F	07:00	08:01	0	11	4	48	20	832	1.24
08/14 G	08:05	09:00	0	13	4	103	44	977	1.21
N			15	15	15	16	16	20	20
Min.			0	7	0	24	12	347	0.75
Max.			0	33	6	103	44	2042	1.57
Arith. Avg.			0	17	2	42	18	941	1.05
Vol Wt Avg.			0	12	1	32	14	775	1.02

1986 Laguna Peak Cloudwater Loading

Date Seq	Start	Stop	LWC	H^+	Na^+	NH_4^+	Ca^{2+}	Mg^{2+}	Cl^-	NO_3^-	SO_4^{2-}
			g m^{-3}	neq m^{-3}							
08/05 A	03:33	04:30	0.21	149.4	4.8	40.2	2.6	1.8	15.2	104.0	81.5
08/05 B	04:30	05:30	0.12	108.9	2.5	29.1	1.4	1.0	9.1	78.1	50.1
08/05 C	05:30	06:30	0.31	298.2	6.8	83.3	1.9	2.3	22.7	211.5	151.4
08/05 D	06:30	07:30	0.20	198.8	10.6	61.0	2.1	3.0	16.6	101.7	89.3
08/05 E	07:30	08:30	0.15	209.0	8.6	71.3	2.4	2.7	14.3	122.4	115.3
08/05 F	08:30	09:05	0.14	287.5	19.3	84.3	3.8	5.5	23.8	153.5	156.3
08/06 A	06:40	07:40	0.35	176.8	3.1	50.5	1.4	1.0	16.2	139.0	97.4
08/06 B	07:40	08:40	0.28	132.8	3.3	48.2	1.3	1.1	14.2	97.9	88.0
08/06 C	08:40	09:40	0.16	107.3	6.3	51.2	1.7	1.9	15.3	81.2	85.1
08/06 D	09:40	10:40	0.17	180.1	4.2	51.2	1.4	1.3	13.3	112.9	120.3
08/06 E	10:40	11:10	0.03	58.2	1.3	15.0	0.4	0.5	2.7	37.3	40.0
08/13 A	08:30	09:00	0.13	125.8	13.7	54.7	2.9	4.0	25.8	102.0	78.2
08/13 B	09:00	09:25	0.02	31.7	7.1	15.4	1.6	2.0	7.8	31.6	22.6
08/14 A	02:30	03:00	0.35	141.3	7.0	59.4	2.5	2.7	35.4	119.4	96.9
08/14 B	03:00	04:00	0.39	189.1	9.9	80.9	3.1	3.5	38.1	150.4	110.5
08/14 C	04:00	05:00	0.32	112.1	7.4	68.1	2.2	3.3	39.4	153.4	110.4
08/14 D	05:05	06:00	0.27	235.0	19.3	77.2	4.0	6.5	40.2	162.2	119.3
08/14 E	06:00	07:00	0.21	193.2	27.1	61.4	3.8	6.8	35.4	150.4	111.9
08/14 F	07:00	08:01	0.17	141.3	14.5	65.9	3.2	4.6	27.7	144.0	112.9
08/14 G	08:05	09:00	0.12	112.4	17.4	66.5	3.1	4.6	18.5	126.6	102.2
N			20	20	20	20	20	20	20	20	20
Min.			0.02	31.7	1.3	15.0	0.4	0.5	2.7	31.6	22.6
Max..			0.39	298	27.1	84.3	4.0	6.8	40	212	156
Arith. Avg.			0.21	159	9.7	57	2.3	3.0	21.6	119	97

1986 Laguna Peak Cloudwater Loading (continued)

Date Seq	Start	Stop	S(IV)	CH_2O	H_2O_2	HFo	HAc
			nmole m^{-3}				
08/05 A	03:33	04:30	0	3.05	0.37	4.93	2.97
08/05 B	04:30	05:30	0	2.21	0.00	3.18	1.93
08/05 C	05:30	06:30	0	5.59	0.13	7.54	4.61
08/05 D	06:30	07:30	0	3.64	0.22	5.60	3.50
08/05 E	07:30	08:30	0	2.63	0.08	5.57	2.94
08/05 F	08:30	09:05	0	2.51	0.15	5.78	2.03
08/06 A	06:40	07:40	0	7.02	0.53	14.20	4.62
08/06 B	07:40	08:40	0	5.79	0.82	13.53	4.09
08/06 C	08:40	09:40	0	4.25	0.80	9.35	3.72
08/06 D	09:40	10:40	0	5.46	0.97	10.57	4.38
08/06 E	10:40	11:10	0	0.00	0.00	0.00	0.00
08/13 A	08:30	09:00	0	0.93	0.22	4.80	2.43
08/13 B	09:00	09:25	0	NA	NA	NA	NA
08/14 A	02:30	03:00	0	NA	NA	NA	NA
08/14 B	03:00	04:00	0	NA	NA	NA	NA
08/14 C	04:00	05:00	0	NA	NA	10.4	3.7
08/14 D	05:05	06:00	0	2.43	0.23	7.4	3.3
08/14 E	06:00	07:00	0	1.86	0.44	7.2	2.8
08/14 F	07:00	08:01	0	1.85	0.66	8.2	3.4
08/14 G	08:05	09:00	0	1.53	0.51	11.8	5.1
N			20	20	20	20	20
Min.			0	0	0	0	0
Max.			0	7.02	0.97	14.2	5.09
Arith. Avg.			0	2.54	0.31	6.5	2.78

1986 Laguna Road Cloudwater Concentrations

Date ID	Start	Stop	Vol (ml)	pH	Na^+	NH_4^+	Ca^{2+}	Mg^{2+}	Cl^-	NO_3^-	SO_4^{2-}	SO_4^{2-*}
					μN							
07/30 A	23:45	00:00	43	3.41	456	1350	152	109	296	1110	806	751
07/31 B	00:30	01:30	125	3.49	304	1150	79	83	258	891	596	559
07/31 C	01:30	02:30	190	3.44	151	722	33	42	160	651	425	407
07/31 D	02:30	03:30	159	3.41	232	760	47	67	224	754	457	429
07/31 E	03:30	04:30	136	3.34	453	982	68	98	368	1050	604	549
07/31 F	04:30	05:10	68	3.36	266	821	47	73	264	867	498	466
08/04 A	23:00	00:00	88	2.95	957	512	132	217	758	978	1030	914
08/05 B	00:00	01:00	101	2.87	655	468	80	137	548	1000	1140	1061
08/05 C	01:00	02:00	43	2.77	1010	1390	142	239	684	1690	2040	1918
08/05 D	02:00	02:55	44	2.58	1070	1780	162	247	711	2140	2630	2501
08/05 A	23:45	00:45	204	3.13	365	816	36	88	404	612	996	952
08/06 B	00:45	01:45	194	3.09	212	639	21	52	247	674	842	816
08/06 C	01:45	02:45	125	3.09	119	709	21	28	124	722	846	832
08/06 D	02:45	03:45	77	2.94	171	1070	34	42	147	1110	1310	1289
08/06 E	03:45	04:45	70	2.60	170	1110	34	41	164	1300	1510	1489
08/06 F	04:45	05:45	60	2.84	119	974	24	29	102	1160	1110	1096
08/13 A	05:21	06:10	92	3.01	157	456	29	44	225	790	776	757
08/13 A	23:20	00:00	81	3.01	157	445	50	51	232	854	670	651
08/14 B	00:00	01:00	137	2.90	144	476	45	48	264	1020	793	776
08/14 C	01:00	01:55	87	2.91	180	504	59	61	312	1280	925	903
Minimum				2.58	119	445	21	28	102	612	425	407
Maximum				3.49	1070	1780	162	247	758	2140	2630	2500
Arith. Ave				3.06	367	857	65	90	325	1030	1000	956
Vol Wt Avg.				3.12	319	807	59	79	299	926	860	822

1986 Laguna Road Cloudwater Concentrations (continued)

Date Seq	Start	Stop	S(IV)	CH_2O	H_2O_2	HFo	HAc	H^+	−/+
			μM						
07/30 A	23:45	00:00	0	11	18	—	—	389	1.12
07/31 B	00:30	01:30	0	13	17	41	21	324	1.12
07/31 C	01:30	02:30	0	15	19	21	9	363	1.07
07/31 D	02:30	03:30	0	13	20	33	29	389	1.05
07/31 E	03:30	04:30	0	15	21	36	13	457	1.03
07/31 F	04:30	05:10	—	—	—	—	—	437	1.02
08/04 A	23:00	00:00	1	6	7	29	11	1122	1.08
08/05 B	00:00	01:00	0	6	4	34	13	1349	1.01
08/05 C	01:00	02:00	4	12	2	56	NA	1698	1.03
08/05 D	02:00	02:55	5	12	2	74	34	2630	1.09
08/05 A	23:45	00:45	12	11	0	24	7	741	1.02
08/06 B	00:45	01:45	6	9	0	30	13	813	0.99
08/06 C	01:45	02:45	3	7	1	34	8	813	1.01
08/06 D	02:45	03:45	2	11	2	47	10	1148	0.97
08/06 E	03:45	04:45	1	12	2	52	14	2512	1.31
08/06 F	04:45	05:45	0	15	4	51	16	1445	1.10
08/13 A	05:21	06:10	0	4	1	26	11	977	0.93
08/13 A	23:20	00:00	0	12	1	42	15	977	0.96
08/14 B	00:00	01:00	0	12	0	NA	NA	1259	0.95
08/14 C	01:00	01:55				44	14	1230	0.81
CHECK ME									
Min			0	4	0	21	7	324	0.81
Max			12	15	21	74	34	2630	1.31
Avg			2	11	7	40	15	1054	1.03
Vol Wt Avg			2	?	7	29	11	872	

1986 Laguna Road Cloudwater Loading

Date Seq	Start	Stop	LWC	H^+	Na^+	NH_4^+	Ca^{2+}	Mg^{2+}	Cl^-	NO_3^-	SO_4^{2-}
			g m^{-3}	neq m^{-3}							
07/30 A	23:45	00:00	0.16	62.4	73.2	216.7	24.4	17.5	47.5	178.2	129.4
07/31 B	00:30	01:30	0.12	37.8	35.5	134.2	9.2	9.7	30.1	104.0	69.5
07/31 C	01:30	02:30	0.18	64.4	26.8	129.9	5.8	7.4	28.4	115.4	75.4
07/31 D	02:30	03:30	0.15	57.7	34.4	112.8	7.0	9.9	33.2	111.9	67.8
07/31 E	03:30	04:30	0.13	58.0	57.5	124.6	8.6	12.5	46.7	133.3	76.7
07/31 F	04:30	05:10	0.10	41.6	25.3	78.2	4.5	6.9	25.1	82.5	47.4
08/04 A	23:00	00:00	0.08	92.2	78.6	42.1	10.8	17.8	62.3	80.3	84.6
08/05 B	00:00	01:00	0.09	127.2	61.7	44.1	7.5	12.9	51.7	94.3	107.5
08/05 C	01:00	02:00	0.04	68.1	40.5	55.8	5.7	9.6	27.5	67.8	81.9
08/05 D	02:00	02:55	0.04	117.8	47.9	79.7	7.3	11.1	31.9	95.9	117.8
08/05 A	23:45	00:45	0.19	141.1	69.5	155.4	6.8	16.7	76.9	116.5	189.6
08/06 B	00:45	01:45	0.18	147.2	38.4	115.7	3.7	9.5	44.7	122.0	152.5
08/06 C	01:45	02:45	0.12	94.9	13.9	82.7	2.4	3.3	14.5	84.2	98.7
08/06 D	02:45	03:45	0.07	82.5	12.3	76.9	2.5	3.0	10.6	79.8	94.1
08/06 E	03:45	04:45	0.07	164.1	11.1	72.5	2.2	2.7	10.7	84.9	98.7
08/06 F	04:45	05:45	0.06	80.9	6.7	54.5	1.3	1.6	5.7	65.0	62.2
08/13 A	05:21	06:10	0.11	102.7	16.5	47.9	3.1	4.6	23.7	83.1	81.6
08/13 A	23:20	00:00	0.11	110.8	17.8	50.5	5.7	5.8	26.3	96.8	76.0
08/14 B	00:00	01:00	0.13	161.0	18.4	60.9	5.7	6.2	33.8	130.4	101.4
08/14 C	01:00	01:55	0.09	109.0	15.9	44.6	5.2	5.4	27.6	113.4	81.9
Min			0.04	38	6.7	42.1	1.3	1.6	5.7	65.0	47.4
Max			0.19	164	78.6	217	24.4	17.8	77	178	190
Avg			0.11	96.1	35.1	88.9	6.5	8.7	32.9	102	95

1986 Laguna Road Cloudwater Loading (continued)

Date Seq	Start	Stop	S(IV)	CH_2O	H_2O_2	HFo	HAc
					neq m^{-3}		
07/30 A	23:45	00:00	0.00	1.73	2.89	0.00	0.00
07/31 B	00:30	01:30	0.00	1.47	2.01	4.83	2.45
07/31 C	01:30	02:30	0.00	2.62	3.44	3.79	1.65
07/31 D	02:30	03:30	0.00	1.88	2.89	4.84	4.27
07/31 E	03:30	04:30	0.00	1.95	2.64	4.59	1.70
07/31 F	04:30	05:10	0.00	0.00	0.00	0.00	0.00
08/04 A	23:00	00:00	0.09	0.48	0.53	2.40	0.92
08/05 B	00:00	01:00	0.00	0.60	0.33	3.17	1.19
08/05 C	01:00	02:00	0.15	0.48	0.10	2.25	0.00
08/05 D	02:00	02:55	0.23	0.55	0.09	3.31	1.52
08/05 A	23:45	00:45	2.25	2.13	0.00	4.58	1.39
08/06 B	00:45	01:45	1.16	1.67	0.07	5.50	2.28
08/06 C	01:45	02:45	0.32	0.83	0.13	3.98	0.89
08/06 D	02:45	03:45	0.11	0.79	0.11	3.36	0.73
08/06 E	03:45	04:45	0.07	0.81	0.12	3.39	0.91
08/06 F	04:45	05:45	0.00	0.81	0.24	2.83	0.90
08/13 A	05:21	06:10	0.00	0.43	0.09	2.75	1.20
08/13 A	23:20	00:00	0	1.39	0.07	4.82	1.70
08/14 B	00:00	01:00	0	1.47	0.06	0	0
08/14 C	01:00	01:55	NA	NA	NA	3.85	1.24
Min			0	0.4	0	2.25	0.73
Max			2.25	2.62	3.44	5.50	4.27
Ave			0.24	1.23	0.88	3.78	1.56

Ventura (Hill) Cloudwater Concentrations

Date ID	Start	Stop	Vol (ml)	pH	Na^+	NH_4^+	Ca^{2+}	Mg^{2+}	Cl^-	NO_3^-	SO_4^{2-}	SO_4^{2-*}
								µN				
07/30 A	06:30	07:30	188	4.92	171	539	65	43	150	247	267	246
07/30 B	07:30	08:15	107	4.24	189	520	57	47	203	284	325	302
08/01 A	00:20	01:20	97	3.13	2240	405	199	519	2180	1290	998	727
08/01 B	01:20	02:20	115	3.17	1030	416	91	225	896	898	676	551
08/01 C	02:20	03:20	122	3.16	1050	514	90	232	914	902	707	580
08/01 D	03:20	04:20	147	3.21	907	426	69	193	806	739	620	510
08/01 E	04:20	05:20	108	3.33	548	533	48	116	482	673	554	488
08/01 F	05:20	06:20	87	3.34	765	811	79	169	659	814	668	575
08/01 G	06:45	07:45	75	3.44	1160	966	198	267	1110	1030	870	730
08/01 H	07:45	08:45	76	3.43	611	960	217	147	642	948	855	781
08/05 A	02:45	03:45	100	3.11	349	931	62	47	435	952	976	934
08/05 B	03:45	04:45	106	3.07	295	1240	45	71	392	1040	998	962
08/05 C	04:45	05:45	107	3.11	121	1320	24	29	175	1070	1010	995
08/05 D	05:45	06:45	80	3.06	78	1400	26	23	146	1200	1010	1001
08/06 A	01:55	03:00	177	3.03	183	598	32	48	198	1080	630	608
08/06 B	03:00	04:00	158	3.06	196	734	25	48	222	985	700	676
08/06 C	04:00	05:00	182	2.96	139	712	18	32	176	1140	787	770
08/06 D	05:00	06:00	169	2.91	124	896	18	30	157	1370	897	882
08/06 E	06:00	07:00	164	2.92	78	913	25	24	112	1300	842	833
08/06 F	07:00	08:00	118	2.85	203	1190	157	69	250	1740	1170	1145
08/13 A	03:45	05:00	34	2.85	3880	1800	771	1010	3330	3730	2170	1701
08/13 B	05:00	06:30	33	2.75	5720	2990	1400	1450	4290	6480	3220	2528
08/13 A	22:45	00:00	51	2.74	1060	1160	297	254	989	2100	1530	1402
08/14 B	00:00	01:00	55	2.75	823	1030	281	199	757	2240	1400	1300
08/14 C	01:00	02:00	94	2.84	429	964	100	94	451	1620	973	921
08/14 D	02:00	03:00	81	2.89	440	814	87	95	415	1560	967	914
08/14 E	03:00	04:00	110	2.89	194	778	49	54	259	1420	839	816
08/14 F	04:00	05:00	130	2.91	248	798	51	65	304	1480	804	774
08/14 G	05:00	06:00	143	2.95	228	952	50	62	282	1410	762	734
08/14 H	06:00	07:00	150	2.98	135	698	31	38	204	1220	594	578
08/14 I	07:00	08:00	126	3.03	74	946	61	29	104	708	387	378
08/14 J	08:00	08:50	50	2.84	175	1730	209	69	208	2100	1130	1109
N			32	32	32	32	32	32	32	32	32	32
Min			33	2.74	74	405	18	23	104	247	267	246
Maximum			188	4.92	5720	2990	1400	1450	4290	6480	3220	2528
Avg			111	3.12	745	959	154	181	684	1430	948	858
Vol Wt	Avg.			3.05	471	833	87	112	463	1160	797	740

Ventura (Hill) Cloudwater Concentration (continued)

Date Seq	Start	Stop	S(IV)	CH_2O	H_2O_2	HFo	HAc	H^+	−/+
					μM				
07/30 A	06:30	07:30	0	13	2	—	—	12	0.80
07/30 B	07:30	08:15	0	18	0	—	—	58	0.92
08/01 A	00:20	01:20	0	8	6	40	6	741	1.07
08/01 B	01:20	02:20	0	6	6	31	3	676	1.00
08/01 C	02:2003:20		0	7	5	15	?–	692	0.97
08/01 D	03:20	04:20	0	5	6	35	16	617	0.97
08/01 E	04:20	05:20	0	10	11	33	14	468	0.99
08/01 F	05:20	06:20	0	7	11	52	30	457	0.93
08/01 G	06:45	07:45	0	7	8	54	16	363	1.01
08/01 H	07:45	08:45	0	8	0	—	—	372	1.05
08/05 A	02:45	03:45	0	6	5	—	—	776	1.08
08/05 B	03:45	04:45	0	9	5	—	—	851	0.96
08/05 C	04:45	05:45	0	11	6	—	—	776	0.99
08/05 D	05:45	06:45	0	13	6	—	—	871	0.98
08/06 A	01:55	03:00	0	19	29	—	—	933	1.06
08/06 B	03:00	04:00	0	17	19	—	—	871	1.01
08/06 C	04:00	05:00	0	12	0	—	—	1096	1.05
08/06 D	05:00	06:00	0	12	0	—	—	1230	1.05
08/06 E	06:00	07:00	0	15	0	—	—	1202	1.00
08/06 F	07:00	08:00	0	12	—	—	—	1413	1.04
08/13 A	03:45	05:00	—	—	—	—	—	1413	1.03
08/13 B	05:00	06:30	—	—	—	—	—	1778	1.03
08/13 A	22:45	00:00	0	27	17	92	28	1820	1.00
08/14 B	00:00	01:00	0	18	22	85	30	1778	1.06
08/14 C	01:00	02:00	0	19	22	74	173	1445	1.00
08/14 D	02:00	03:00	0	15	23	69	34	1288	1.07
08/14 E	03:00	04:00	0	21	24	64	24	1288	1.06
08/14 F	04:00	05:00	0	23	20	61	23	1230	1.08
08/14 G	05:00	06:00	0	11	18	64	23	1122	1.01
08/14 H	06:00	07:00	0	18	15	54	33	1047	1.03
08/14 I	07:00	08:00	0	14	12	60	27	933	0.58
08/14 J	08:00	08:50	0	23	10	96	45	1445	0.94
N			30	30	29	16	17	32	32
Min			0	5	0	?31	3	12	0.58
Max			0	27	29	96	173	1820	1.08
Avg			0	13	11	60	32	971	0.99
Vol Wt Avg.				13	10	56	30	896	

1986 Ventura (Hill) Cloudwater Loading

Date Seq	Start	Stop	LWC	H^+	Na+	NH_4^+	Ca^{2+}	Mg^{2+}	Cl^-	NO_3^-	SO_4^{2-}
			g m^{-3}	neq m^{-3}							
07/30 A	06:30	07:30	0.18	2.1	29.9	94.3	11.4	7.6	26.3	43.2	46.7
07/30 B	07:30	08:15	0.13	7.7	25.1	69.2	7.6	6.3	27.0	37.8	43.2
08/01 A	00:20	01:20	0.09	67.4	203.8	36.9	18.1	47.2	198.4	117.4	90.8
08/01 B	01:20	02:20	0.11	72.3	110.2	44.5	9.8	24.1	95.9	96.1	72.3
08/01 C	02:20	03:20	0.11	78.9	119.7	58.6	10.3	26.4	104.2	102.8	80.6
08/01 D	03:20	04:20	0.14	84.5	124.3	58.4	9.5	26.4	110.4	101.2	84.9
08/01 E	04:20	05:20	0.10	47.3	55.3	53.8	4.9	11.7	48.7	68.0	56.0
08/01 F	05:20	06:20	0.08	37.0	62.0	65.7	6.4	13.7	53.4	65.9	54.1
08/01 G	06:45	07:45	0.07	25.4	81.2	67.6	13.9	18.7	77.7	72.1	60.9
08/01 H	07:45	08:45	0.07	26.4	43.4	68.2	15.4	10.4	45.6	67.3	60.7
08/05 A	02:45	03:45	0.09	72.2	32.5	86.6	5.8	4.3	40.5	88.5	90.8
08/05 B	03:45	04:45	0.10	84.2	29.2	122.8	4.4	7.0	38.8	103.0	98.8
08/05 C	04:45	05:45	0.10	77.6	12.1	132.0	2.4	2.9	17.5	107.0	101.0
08/05 D	05:45	06:45	0.08	65.3	5.8	105.0	2.0	1.7	11.0	90.0	75.8
08/06 A	01:55	03:00	0.15	141.8	27.8	90.9	4.9	7.2	30.1	164.2	95.8
08/06 B	03:00	04:00	0.15	128.0	28.8	107.9	3.7	7.1	32.6	144.8	102.9
08/06 C	04:00	05:00	0.17	186.3	23.6	121.0	3.0	5.5	29.9	193.8	133.8
08/06 D	05:00	06:00	0.16	194.3	19.6	141.6	2.9	4.7	24.8	216.5	141.7
08/06 E	06:00	07:00	0.15	183.9	11.9	139.7	3.8	3.7	17.1	198.9	128.8
08/06 F	07:00	08:00	0.11	155.4	22.3	130.9	17.3	7.6	27.5	191.4	128.7
08/13 A	03:45	05:00	0.03	35.3	97.0	45.0	19.3	25.3	83.3	93.3	54.3
08/13 B	05:00	06:30	0.02	37.3	120.1	62.8	29.4	30.5	90.1	136.1	67.6
08/13 A	22:45	00:00	0.04	69.2	40.3	44.1	11.3	9.7	37.6	79.8	58.1
08/14 B	00:00	01:00	0.05	90.7	42.0	52.5	14.3	10.1	38.6	114.2	71.4
08/14 C	01:00	02:00	0.09	127.2	37.8	84.8	8.8	8.2	39.7	142.6	85.6
08/14 D	02:00	03:00	0.08	97.9	33.4	61.9	6.6	7.2	31.5	118.6	73.5
08/14 E	03:00	04:00	0.10	132.7	20.0	80.1	5.1	5.6	26.7	146.3	86.4
08/14 F	04:00	05:00	0.12	148.8	30.0	96.6	6.2	7.8	36.8	179.1	97.3
08/14 G	05:00	06:00	0.13	149.2	30.3	126.6	6.7	8.3	37.5	187.5	101.3
08/14 H	06:00	07:00	0.14	146.6	18.9	97.7	4.4	5.3	28.6	170.8	83.2
08/14 I	07:00	08:00	0.12	110.1	8.8	111.6	7.1	3.4	12.3	83.5	45.7
08/14 J	08:00	08:50	0.06	80.9	9.8	96.9	11.7	3.9	11.6	117.6	63.3
N			32	32	32	32	32	32	32	32	32
Min			0.02	2.1	5.8	36.9	2.0	1.7	11.0	37.8	43.2
Max			0.18	194	204	142	29.4	47.2	198	216	142
Avg			0.10	92.6	48.7	86.1	9.0	11.6	47.9	120	82.4

Ventura (Hill) Cloudwater Concentrations (continued)

Date Seq	Start	Stop	S(IV)	CH_2O	H_2O_2	HFo	HAc
			nmole m^{-3}				
07/30 A	06:30	07:30	0.0	2.3	0.3	NA	NA
07/30 B	07:30	08:15	0.0	2.4	0.0	NA	NA
08/01 A	00:20	01:20	0.0	0.7	0.6	3.7	0.6
08/01 B	01:20	02:20	0.0	0.7	0.6	3.3	0.4
08/01 C	02:20	03:20	0.0	0.8	0.5	NA	1.7
08/01 D	03:20	04:20	0.0	0.7	0.8	4.7	2.2
08/01 E	04:20	05:20	0.0	1.0	1.1	3.3	1.4
08/01 F	05:20	06:20	0.0	0.6	0.9	4.2	2.4
08/01 G	06:45	07:45	0.0	0.5	0.6	3.8	1.1
08/01 H	07:45	08:45	0.0	0.5	0.0	0.0	0.0
08/05 A	02:45	03:45	0.0	0.6	0.5	NA	NA
08/05 B	03:45	04:45	0.0	0.9	0.5	NA	NA
08/05 C	04:45	05:45	0.0	1.1	0.6	NA	NA
08/05 D	05:45	06:45	0.0	1.0	0.4	NA	NA
08/06 A	01:55	03:00	0.0	2.9	4.4	NA	NA
08/06 B	03:00	04:00	0.0	2.4	2.8	NA	NA
08/06 C	04:00	05:00	0.0	2.0	0.1	NA	NA
08/06 D	05:00	06:00	0.0	1.9	0.0	NA	NA
08/06 E	06:00	07:00	0.0	2.3	0.1	NA	NA
08/06 F	07:00	08:00	0.0	1.3	0.0	NA	NA
08/13 A	03:45	05:00	0.0	0.0	0.0	NA	NA
08/13 B	05:00	06:30	0.0	0.0	0.0	NA	NA
08/13 A	22:45	00:00	0.0	1.0	0.6	3.5	1.1
08/14 B	00:00	01:00	0.0	0.9	1.1	4.3	1.5
08/14 C	01:00	02:00	0.0	1.7	1.9	6.5	15.2
08/14 D	02:00	03:00	0.0	1.2	1.7	5.3	2.6
08/14 E	03:00	04:00	0.0	2.2	2.4	6.5	2.5
08/14 F	04:00	05:00	0.0	2.8	2.5	7.4	2.7
08/14 G	05:00	06:00	0.0	1.5	2.4	8.5	3.1
08/14 H	06:00	07:00	0.0	2.6	2.1	7.5	4.6
08/14 I	07:00	08:00	0.0	1.6	1.4	7.0	3.2
08/14 J	08:00	08:50	0.0	1.3	0.5	5.4	2.5
N			30	30	29	16	17
Min			0	0.5	0	3.3	0.4
Max			0	2.9	4.4	8.5	15.2
Avg			0	1.4	1.1	5.3	2.9

1986 Casitas Pass Cloudwater Concentration

Date	ID	Start	Stop	Vol (ml)	pH	Na^+	NH_4^+	Ca^{2+}	Mg^{2+}	Cl^-	NO_3^-	SO_4^{2-}	SO_4^{2-*}
									µN				
07/31	A	06:30	07:30	303	3.87	18	149	10	7	35	147	108	106
07/31	B	07:30	08:30	130	4.06	16	283	18	9	38	171	138	136
08/01	A	02:45	03:45	199	4.07	82	330	18	23	73	229	211	201
08/01	B	03:45	05:00	212	4.26	48	358	9	14	40	196	177	171
08/05	A	02:20	03:00	76	3.33	176	869	49	50	110	892	521	500
08/05	B	03:00	04:00	146	3.62	49	718	16	17	76	570	404	398
08/05	C	04:00	05:00	138	3.92	29	736	16	11	60	458	320	316
08/05	D	05:00	06:00	157	3.96	19	612	12	8	50	402	280	278
08/05	E	06:00	07:00	52	3.76	43	1090	27	17	68	729	523	518
08/06	A	01:25	02:00	68	4.02	83	636	25	27	51	386	369	359
08/06	B	02:00	03:00	152	4.32	62	748	19	19	41	394	387	380
08/06	C	03:00	04:00	99	4.52	42	930	16	14	45	474	419	414
08/06	D	04:00	05:00	272	3.92	21	418	9	7	29	283	225	222
08/06	E	05:00	06:20	258	3.85	17	429	9	6	57	310	230	228
08/06	F	06:20	07:00	167	3.91	14	448	8	6	48	326	224	222
08/06	G	07:00	07:46	135	4.07	16	502	11	7	42	314	197	195
08/13	A	03:21	04:00	73	4.21	137	552	48	40	110	317	359	342
08/13	B	04:00	04:20	29	4.42	57	669	26	21	51	290	401	394
08/13	C	04:40	06:05	356	4.06	23	354	12	9	34	209	195	192
08/13	D	06:05	06:55	105	4.07	23	508	11	9	34	278	268	265
08/13	E	07:15	08:00	108	4.32	26	575	32	14	44	326	297	294
08/13	F	08:00	08:40	58	4.34	47	721	48	22	67	369	314	308
08/13	A	23:45	00:00	26	4.11	146	618	170	49	164	417	496	478
08/14	B	00:00	01:00	107	3.84	132	1130	80	52	141	649	769	753
08/14	C	01:00	02:00	103	3.70	50	840	39	24	65	508	536	530
08/14	D	02:00	04:00	346	4.01	19	684	14	9	22	381	347	345
08/14	E	04:00	05:00	133	3.80	14	579	15	9	33	409	289	287
08/14	F	05:00	06:00	164	3.90	16	616	13	8	37	437	280	278
08/14	G	06:00	07:00	187	3.87	12	460	13	7	33	357	204	203
08/14	H	07:00	08:00	101	3.66	23	757	37	18	33	594	339	336
08/14	I	08:00	09:00	122	3.65	19	612	43	18	68	551	318	316
08/14	J	09:00	09:15	23	3.47	18	688	47	20	65	624	367	365
N				32	32	32	32	32	32	32	32	32	32
Min.					3.33	12	149	8	6	22	147	108	106
Max.					4.52	176	1130	170	52	164	892	769	753
Avg.					3.97	47	613	29	18	58	406	329	323
Vol Wt Avg					3.90	41	552	24	15	53	369	295	290

1986 Casitas Pass Cloudwater Concentrations (continued)

DateSeq	Start	Stop		S(IV)	CH2O	H2O2	HFo	HAc	H+
						μM			
07/31 A	06:30	07:30	0	6	4	NA	NA	135	0.91
07/31 B	07:30	08:30	0	7	5	24	9	87	0.83
08/01 A	02:45	03:45	0	5	3	17	8	85	0.94
08/01 B	03:45	05:00	0	5	3	20	10	55	0.85
08/05 A	02:20	03:00	0	11	16	57	14	468	0.94
08/05 B	03:00	04:00	0	8	10	23	14	240	1.01
08/05 C	04:00	05:00	0	8	7	18	7	120	0.91
08/05 D	05:00	06:00	0	8	6	16	8	110	0.96
08/05 E	06:00	07:00	0	8	6	27	11	174	0.97
08/06 A	01:25	02:00	0	9	7	21	10	96	0.93
08/06 B	02:00	03:00	0	8	6	25	9	48	0.91
08/06 C	03:00	04:00	0	9	4	32	14	30	0.91
08/06 D	04:00	05:00	0	8	5	17	10	120	0.93
08/06 E	05:00	06:20	0	9	5	21	9	141	0.99
08/06 F	06:20	07:00	0	8	6	16	9	123	0.99
08/06 G	07:00	07:46	0	8	6	21	10	85	0.89
08/13 A	03:21	04:00	0	3	3	29	8	62	0.91
08/13 B	04:00	04:20	0	4	3	31	9	38	0.91
08/13 C	04:40	06:05	0	4	6	19	6	87	0.90
08/13 D	06:05	06:55	0	5	5	25	7	85	0.91
08/13 E	07:15	08:00	0	NA	6	NA	NA	48	0.95
08/13 F	08:00	08:40	0	NA	8	NA	NA	46	0.83
08/13 A	23:45	00:00	0	9	NA	44	15	78	0.98
08/14 B	00:00	01:00	0	13	NA	58	4	145	1.01
08/14 C	01:00	02:00	0	10	NA	36	14	200	0.96
08/14 D	02:00	04:00	0	7	NA	23	11	98	0.91
08/14 E	04:00	05:00	0	8	NA	26	10	158	0.94
08/14 F	05:00	06:00	0	9	NA	27	10	126	0.96
08/14 G	06:00	07:00	0	10	NA	NA	NA	135	0.94
08/14 H	07:00	08:00	0	9	NA	NA	NA	219	0.91
08/14 I	08:00	09:00	0	11	NA	NA	NA	224	1.02
08/14 J	09:00	09:15	0	12	NA	NA	NA	339	0.95
N			32	30	22	25	25	32	32
Min.			0	3	3	16	4	30	0.83
Max.			0	13	16	58	15	468	1.02
Avg.			0	8	6	27	10	131	0.93
Vol Wt Avg			0	8	6	25	10	126	0.94

1986 Casitas Pass Cloudwater Loading

Date Seq	Start	Stop	LWC	H^+	Na^+	NH_4^+	Ca^{2+}	Mg^{2+}	Cl^-	NO_3^-	SO_4^{2-}
			g m^{-3}	neq m^{-3}							
07/31 A	06:30	07:30	0.28	38.2	5.2	42.2	2.7	2.0	9.8	41.6	30.6
07/31 B	07:30	08:30	0.12	10.5	1.9	34.2	2.1	1.1	4.6	20.7	16.7
08/01 A	02:45	03:45	0.19	15.8	15.3	61.4	3.4	4.4	13.6	42.6	39.2
08/01 B	03:45	05:00	0.16	8.7	7.6	56.6	1.4	2.2	6.3	31.0	28.0
08/05 A	02:20	03:00	0.11	49.6	18.7	92.1	5.2	5.3	11.7	94.6	55.2
08/05 B	03:00	04:00	0.14	32.6	6.7	97.6	2.2	2.3	10.3	77.5	54.9
08/05 C	04:00	05:00	0.13	15.5	3.8	94.9	2.1	1.4	7.7	59.1	41.3
08/05 D	05:00	06:00	0.15	16.1	2.8	90.0	1.8	1.1	7.4	59.1	41.2
08/05 E	06:00	07:00	0.05	8.5	2.1	53.4	1.3	0.8	3.3	35.7	25.6
08/06 A	01:25	02:00	0.11	10.4	9.1	69.3	2.7	2.9	5.5	42.1	40.2
08/06 B	02:00	03:00	0.14	6.8	8.8	106.2	2.7	2.7	5.8	55.9	55.0
08/06 C	03:00	04:00	0.09	2.8	3.9	85.6	1.5	1.3	4.2	43.6	38.5
08/06 D	04:00	05:00	0.25	30.5	5.3	106.2	2.3	1.8	7.4	71.9	57.2
08/06 E	05:00	06:20	0.18	25.6	3.1	77.6	1.5	1.1	10.3	56.1	41.6
08/06 F	06:20	07:00	0.23	28.8	3.3	104.8	1.9	1.3	11.2	76.3	52.4
08/06 G	07:00	07:46	0.16	14.0	2.5	82.3	1.8	1.1	6.9	51.5	32.3
08/13 A	03:21	04:00	0.11	6.5	14.4	58.0	5.1	4.2	11.5	33.3	37.7
08/13 B	04:00	04:20	0.08	3.1	4.6	54.2	2.1	1.7	4.1	23.5	32.5
08/13 C	04:40	06:05	0.24	20.5	5.5	83.2	2.8	2.1	8.0	49.1	45.8
08/13 D	06:05	06:55	0.12	10.0	2.7	59.9	1.3	1.1	4.0	32.8	31.6
08/13 E	07:15	08:00	0.13	6.4	3.4	77.1	4.3	1.9	5.9	43.7	39.8
08/13 F	08:00	08:40	0.08	3.7	3.8	58.4	3.9	1.7	5.5	29.9	25.4
08/13 A	23:45	00:00	0.10	7.5	14.2	59.9	16.5	4.8	15.9	40.4	48.1
08/14 B	00:00	01:00	0.10	14.5	13.2	113.0	8.0	5.2	14.1	64.9	76.9
08/14 C	01:00	02:00	0.10	19.2	4.8	80.6	3.7	2.3	6.2	48.8	51.5
08/14 D	02:00	04:00	0.16	15.7	3.1	110.1	2.3	1.4	3.6	61.3	55.9
08/14 E	04:00	05:00	0.12	19.7	1.7	71.8	1.8	1.1	4.1	50.7	35.8
08/14 F	05:00	06:00	0.15	19.3	2.4	94.2	2.1	1.2	5.6	66.9	42.8
08/14 G	06:00	07:00	0.18	23.6	2.1	80.5	2.3	1.2	5.8	62.5	35.7
08/14 H	07:00	08:00	0.09	20.6	2.2	71.2	3.5	1.7	3.1	55.8	31.9
08/14 I	08:00	09:00	0.11	25.5	2.1	69.8	4.9	2.1	7.8	62.8	36.3
08/14 J	09:00	09:15	0.09	29.1	1.5	59.2	4.1	1.7	5.6	53.7	31.6
N			32	32	32	32	32	32	32	32	32
Min.			0.05	2.8	1.5	34.2	1.3	0.8	3.1	20.7	16.7
Max.			0.28	49.6	18.7	113.0	16.5	5.3	15.9	94.6	76.9
Avg.			0.14	17.5	5.7	76.7	3.3	2.1	7.4	51.2	40.9

1986 Casitas Pass Cloudwater Loading (continued)

Date Seq	Start	Stop	S(IV)	CH_2O	H_2O_2	HFo	HAc
			nmole m^{-3}				
07/31 A	06:30	07:30	0.00	1.75	0.99	NA	NA
07/31 B	07:30	08:30	0.00	0.86	0.58	2.86	1.10
08/01 A	02:45	03:45	0.00	0.87	0.61	3.20	1.49
08/01 B	03:45	05:00	0.00	0.77	0.52	3.18	1.56
08/05 A	02:20	03:00	0.00	1.16	1.72	6.07	1.53
08/05 B	03:00	04:00	0.00	1.10	1.40	3.10	1.96
08/05 C	04:00	05:00	0.00	0.99	0.84	2.38	0.85
08/05 D	05:00	06:00	0.00	1.19	0.94	2.41	1.10
08/05 E	06:00	07:00	0.00	0.39	0.27	1.34	0.51
08/06 A	01:25	02:00	0.00	1.00	0.81	2.32	1.05
08/06 B	02:00	03:00	0.00	1.18	0.82	3.58	1.29
08/06 C	03:00	04:00	0.00	0.79	0.40	2.92	1.29
08/06 D	04:00	05:00	0.00	1.96	1.24	4.19	2.41
08/06 E	05:00	06:20	0.00	1.59	0.92	3.75	1.65
08/06 F	06:20	07:00	0.00	1.80	1.33	3.72	2.13
08/06 G	07:00	07:46	0.00	1.26	0.90	3.44	1.66
08/13 A	03:21	04:00	0.00	0.33	0.36	3.01	0.86
08/13 B	04:00	04:20	0.00	0.30	0.22	2.52	0.75
08/13 C	04:40	06:05	0.00	0.89	1.50	4.44	1.50
08/13 D	06:05	06:55	0.00	0.54	0.53	2.91	0.81
08/13 E	07:15	08:00	0.00	NA	0.83	NA	NA
08/13 F	08:00	08:40	0.00	NA	0.64	NA	NA
08/13 A	23:45	00:00	0.00	0.87	NA	4.28	1.41
08/14 B	00:00	01:00	0.00	1.26	NA	5.79	0.41
08/14 C	01:00	02:00	0.00	0.91	NA	3.47	1.35
08/14 D	02:00	04:00	0.00	1.19	NA	3.71	1.79
08/14 E	04:00	05:00	0.00	0.97	NA	3.16	1.24
08/14 F	05:00	06:00	0.00	1.32	NA	4.11	1.47
08/14 G	06:00	07:00	0.00	1.70	NA	NA	NA
08/14 H	07:00	08:00	0.00	0.86	NA	NA	NA
08/14 I	08:00	09:00	0.00	1.22	NA	NA	NA
08/14 J	09:00	09:15	0.00	1.01	NA	NA	NA
N			30	30	22	25	25
Min.			0	0.3	0.2	1.3	0.4
Max.			0	2.0	1.7	6.1	2.4
Avg.			0	1.1	0.8	3.4	1.3

Blank Corrected Aerosol Data for 1986 SBC study
Laguna Peak Aerosol concentrations: Summer, 1986

Date Seq	Start	Stop	Na^+	NH_4^+	Ca^{2+}	Mg^{2+}	Cl^-	$NO3^-$	SO_4^{2-}	NH_3	HNO_3	SO_2	Hfo	Hac
			neq m^{-3}								nmole m^{-3}			
08/04 A	16:00	19:00	34	126	14	6	9	31	249	8	180	247	192	132
08/04 B	20:00	00:00	36	118	13	8	7	39	164	0	306	283	5	3
08/05 A	02:00	03:40	32	81	37	8	26	116	163	101	101	228	141	175
08/05 B	03:55	05:30	9	42	19	1	41	125	120	34	14	237	80	81
08/05 C	05:31	08:30	12	91	10	3	7	138	171	0	11	263	85	76
08/05 D	10:00	14:00	65	176	22	15	2	47	342	13	197	250	165	126
08/05 E	14:01	18:00	76	137	14	16	6	58	237	1	185	274	179	153
08/05 F	20:00	00:00	49	156	17	11	3	57	193	2	355	156	178	92
08/06 A	02:00	06:00	15	55	11	3	13	51	92	6	92	—	122	92
08/06 B	06:45	11:10	9	39	12	1	0	24	90	0	50	161	103	86
08/06 C	11:30	15:30	42	127	5	7	11	25	386	0	202	224	157	147
08/12 A	14:00	18:00	52	133	32	13	25	45	170	3	84	102	102	68
08/12 B	20:00	00:00	10	44	16	3	17	22	58	3	72	96	80	116
08/13 A	02:00	06:00	37	109	22	8	0	32	135	10	220	298	113	97
08/13 B	09:00	12:00	87	147	16	17	0	52	240	3	173	192	105	102
08/13 C	14:00	18:00	54	89	12	13	0	18	168	34	122	140	100	99
08/13 D	20:00	00:00	24	115	12	6	6	39	130	45	176	200	126	122
08/14 A	02:12	05:00	12	64	6	2	26	97	92	1	7	14	40	61
08/14 B	05:13	07:00	7	46	49	5	45	77	90	0	12	19	58	77
08/14 C	07:25	09:00	47	86	47	5	23	112	135	0	16	27	66	79

Ventura – Hill Site – Aerosol Concentrations: Summer,1986

Date	Seq	Start	Stop	Na^+	NH_4^+	Ca^{2+}	Mg^{2+}	Cl^-	$NO3^-$	SO_4^{2-}	NH_3	HNO_3	SO_2	Hfo	Hac
				neq m^{-3}								nmole m^{-3}			
07/29	A	17:39	19:59	138	25	17	25	126	26	42	0	12	47	65	82
07/29	B	20:00	00:00	221	43	23	46	200	42	66	4	6	111	44	53
07/30	A	02:00	06:00	146	67	14	29	122	54	76	7	14	68	99	79
07/30	B	06:45	08:15	58	119	20	7	36	58	77	0	9	36	45	77
07/30	C	09:00	13:00	108	111	50	25	43	55	122	5	28	—	—	—
07/30	D	16:00	19:35	87	80	40	19	47	46	139	0	41	35	68	48
07/30	E	20:00	00:00	220	85	43	49	130	102	134	0	17	72	76	96
07/31	A	02:00	06:00	67	126	18	11	75	60	116	0	23	30	40	60
07/31	B	15:30	19:00	167	82	62	41	118	79	143	NA	61	73	66	65
07/31	C	20:00	23:23	239	64	52	53	180	89	97	NA	18	33	40	49
08/01	A	00:20	03:15	129	54	27	31	167	106	110	NA	14	35	48	48
08/01	B	03:25	06:00	69	73	12	15	79	88	97	4	10	105	38	46
08/01	C	09:00	12:00	98	65	36	20	32	70	137	7	45	42	99	108
08/04	A	17:45	19:30	75	59	21	10	24	31	118	42	40	50	260	96
08/04	B	20:00	00:00	80	86	25	18	30	49	132	6	42	39	140	75
08/05	A	02:00	06:00	43	177	10	9	36	178	169	0	16	137	140	73
08/05	B	08:00	12:00	37	164	25	9	56	66	284	14	139	84	100	100
08/05	C	14:00	18:00	47	89	19	11	10	27	142	0	113	28	113	95
08/05	D	20:00	00:00	33	85	11	8	2	45	121	0	47			
08/06	A	02:00	04:00	74	111	13	8	24	148	126	0	9	33	48	63
08/06	B	04:25	07:00	24	175	10	3	25	205	148	6	8	344	53	66
08/06	C	10:00	13:59	30	151	21	4	10	18	218	0	117	—	—	—
08/06	D	14:00	16:10	45	86	36	5	26	33	161	3	100	47	138	123
08/12	A	14:00	18:00	38	54	15	7	0	29	170	0	92	128	61	72
08/12	B	20:00	00:00	100	87	23	23	78	67	118	0	25	29	43	55
08/13	A	02:00	06:00	142	166	30	35	73	146	159	2	29	28	44	53
08/13	B	08:00	12:00	75	303	42	22	23	146	295	10	90	334	77	102
08/13	C	14:00	18:00	34	98	22	8	0	31	168	1	122	33	122	109
08/13	D	20:00	00:00	42	98	19	13	36	75	116	0	51	38	47	44
08/14	A	04:15	08:50	34	153	38	10	21	202	120	0	16	55	53	57
08/14	B	10:00	12:30	16	122	15	4	0	25	139	4	127	557	119	122
09/08	A	14:02	18:00	68	87	13	18	3	48	111	21	43	87	104	84
09/08	B	20:00	00:00	113	82	18	28	30	74	84	–8	25	67	86	60
09/09	A	02:00	06:00	165	56	15	41	122	63	77	19	11	123	46	36

Emma Wood State Beach Aerosol concentrations: Summer, 1986

Date	Seq	Start	Stop	Na^+	NH_4^+	Ca^{2+}	Mg^{2+}	Cl^-	$NO3^-$	SO_4^{2-}	NH_3	HNO_3	SO_2	Hfo	Hac
				neq m^{-3}								nmole m^{-3}			
07/23	A	12:00	16:00	490	63	57	98	432	93	108	32	28	—	83	110
07/23	B	20:00	00:00	1001	32	79	201	1051	49	77	21	8	—	40	25
07/24	A	02:00	06:00	115	41	36	31	96	33	45	82	6	—	62	68
07/29	A	17:01	19:59	477	43	31	94	430	37	114	0	6	—	45	17
07/29	B	20:00	00:00	967	52	58	183	834	44	130	1	4	—	33	19
07/30	D	20:00	00:00	483	86	35	105	474	99	159	0	15	—	29	11
07/31	A	02:00	06:00	275	125	27	63	199	104	159	0	35	—	35	22
07/31	B	08:00	12:00	230	129	24	49	200	90	163	0	28	—	46	30
07/31	C	14:35	18:00	275	98	24	59	198	67	159	0	51	—	62	46
07/31	D	20:00	00:00	564	52	33	112	493	86	148	2	9	—	26	13
08/01	A	02:00	06:00	420	119	26	86	347	114	167	0	23	—	42	35
08/01	B	09:45	13:00	250	127	23	55	163	88	155	3	40	—	62	47
08/04	A	17:30	19:30	197	65	20	39	154	45	150	37	24	—	—	—
08/04	B	20:00	00:00	234	85	25	53	162	75	159	0	39	—	—	—
08/05	B	08:45	12:00	144	210	15	34	86	86	261	8	144	—	152	136
08/05	C	14:00	18:00	230	102	21	57	166	79	226	0	75	—	100	104
08/05	D	20:00	00:00	163	89	25	39	93	86	153	0	49	—	41	21
08/06	A	02:00	06:00	90	146	9	19	19	81	176	21	112	—	55	48
08/06	B	08:00	12:00	140	178	21	34	73	68	249	2	133	—	111	89
08/06	C	14:00	15:45	121	80	5	21	81	53	160	2	49	—	95	89
09/08	A	14:00	18:00	243	78	15	61	191	57	121	35	20	—	79	58
09/08	B	20:00	00:00	252	101	31	63	86	77	111	35	5	—	92	51
09/09	A	02:00	06:00	192	60	29	67	324	52	95	35	5	—	41	27

Suspect runs

07/30	B	08:50	12:00	707	254	49	144	435	233	434	16	66	136	103	
07/30	C	14:00	18:00	162	79	16	31	98	51	136	0	33	50	37	
07/30	A	00:00	04:00	44	7	10	7	44	3	12	0	0	—	19	6
08/05	A	02:00	06:00	32	43	6	4	28	11	12	—	12	3		

West Casitas Pass Aerosol Concentrations: Summer, 1986

Date	Seq	Start	Stop	Na^+	NH_4^+	Ca^{2+}	Mg^{2+}	Cl^-	$NO3^-$	SO_4^{2-}	NH_3	HNO_3	SO_2	Hfo	Hac
				neq m^{-3}								nmole m^{-3}			
07/23	A	17:15	20:00	92	43	19	18	51	50	56	25	20	40	69	138
07/23	B	20:00	00:00	109	36	14	21	80	31	45	19	10	35	53	142
07/24	A	02:00	06:00	60	24	13	10	46	31	32	14	10	136	52	98
07/29	A	20:00	00:00	129	67	26	29	73	65	68	15	20	45	85	74
07/30	A	02:00	06:00	84	71	24	19	19	73	64	1	36	55	93	75
07/30	B	08:00	12:00	92	99	36	23	44	63	105	73	29	51	114	65
07/30	C	14:00	18:00	123	136	27	27	25	81	126	22	65	58	125	99
07/30	D	20:00	00:00	90	102	17	20	50	56	91	7	13	81	52	56
07/31	A	02:00	06:00	26	76	12	6	10	51	79	0	10	40	40	43
07/31	B	06:37	08:30	29	91	11	4	101	44	70	0	12	23	31	36
07/31	C	09:15	12:00	54	112	25	13	25	48	115	78	47	0	91	69
07/31	D	14:00	18:00	63	131	21	15	20	44	137	36	79	0	129	96
07/31	E	20:00	23:37	126	82	16	30	92	88	91	4	11	0	36	31
08/01	A	00:45	05:00	24	93	6	5	19	51	74	4	8	0	na	na
08/01	B	06:15	09:00	24	177	10	2	11	42	60	19	8	30	49	48
08/04	A	17:45	19:30	56	106	14	9	0	35	155	0	31	64	76	75
08/04	B	20:00	00:00	51	143	16	13	2	40	82	2	23	31	57	41
08/05	A	02:00	06:00	17	165	NA	4	25	105	90	0	14	26	35	31
08/05	B	08:00	12:00	21	168	11	4	9	51	130	54	68	31	78	64
08/05	C	14:00	18:00	53	132	16	11	16	34	172	8	98	38	136	114
08/05	D	20:00	00:00	48	123	14	10	36	84	48	21	16	37	53	70
08/06	A	02:00	06:00	18	139	8	3	1	77	85	3	4	11	27	60
08/06	B	06:25	07:46	17	135	9	3	9	94	75	0	0	23	45	71
08/06	C	10:00	12:30	10	146	11	3	0	43	137	100	65	48	73	82
08/06	D	14:00	15:00	5	144	25	0	0	59	189	145	133	199	180	208
08/12	A	14:30	18:00	32	111	19	7	0	28	150	20	79	180	96	107
08/12	B	20:00	22:10	37	91	17	7	10	50	122	15	18	46	54	69
08/13	A	03:41	06:00	7	112	6	0	0	65	87	54	4	25	24	40
08/13	B	06:40	08:40	9	148	9	2	27	81	88	74	6	17	34	46
08/13	C	10:00	13:59	47	131	21	10	6	43	136	54	65	35	98	66
08/13	D	14:00	18:00	48	125	16	10	22	46	151	36	91	36	151	98
08/13	E	20:00	23:00	24	173	35	9	6	63	156	20	23	23	49	48
08/14	A	00:45	04:00	7	201	7	3	10	103	122	1	10	57	25	25
08/14	B	04:00	08:00	5	124	5	1	1	80	65	0	11	18	28	37
08/14	C	09:00	12:00	15	136	15	3	3	55	97	25	NA	124	74	63
09/08	A	15:30	18:00	20	0	142	105	89							
09/08	B	20:00	00:00	29	0	27	50	42							
09/09	A	02:00	06:00	0	0	29	48	34							

El Capitan State Beach Aerosol concentrations: Summer, 1986

Date	Seq	Start	Stop	Na^+	NH_4^+	Ca^{2+}	Mg^{2+}	Cl^-	$NO3^-$	SO_4^{2-}	NH_3	HNO_3	SO_2	Hfo	Hac
								neq m^{-3}						nmole m^{-3}	
07/23	A	15:00	18:00	404	18	27	88	427	37	72	39	10	30	68	96
07/23	B	20:00	00:00	236	15	24	52	227	12	41	39	5	92	68	129
07/24	A	02:00	06:00	50	11	6	11	37	13	21	23	7	103	55	57
07/29	A	20:00	00:00	302	56	69	67	297	47	78	42	7	45	107	192
07/30	A	02:00	06:00	125	67	21	26	71	65	69	15	7	137	97	58
07/30	B	08:00	12:00	439	76	34	108	422	99	141	22	20	68	87	67
07/30	C	14:00	18:00	1079	97	85	215	867	133	289	2	29	67	98	81
07/30	D	20:00	00:00	261	97	43	60	237	61	111	15	12	77	76	136
07/31	A	02:00	06:00	142	117	18	29	116	67	98	6	21	71	58	61
07/31	B	20:00	00:00	335	108	58	73	286	108	130	NA	10	85	89	173
08/01	A	02:00	06:00	285	136	32	66	215	140	149	0	22	72	48	45
08/01	B	08:00	12:00	527	106	43	122	499	99	221	0	29	151	92	100

APPENDIX C

Chemical Composition of Cloudwater, and Aerosol Collected in the South Coast Air Basin During June – July, 1987

Concentrations in Aerosol Samples collected at San Pedro Hill
during the 1987 Summer SCAQS Project

Date Seq	Start	Stop	Na^+	NH_4^+	Ca^{2+}	Mg^{2+}	Cl^-	NO_3^-	SO_4^{2-}	NH_3	HNO_3
			neq m^{-3}							nmole m^{-3}	
06/19 A	01:00	05:00	170	119	25.1	44.3	90.2	142	113	0.0	15.5
06/19 B	06:00	09:00	188	74	15.9	42.4	105.4	81	124	0.0	26.6
06/19 C	09:00	12:00	181	93	22.1	46.3	88.9	103	133	0.0	27.1
06/19 D	20:00	00:00	115	94	24.8	33.5	51.5	102	104	14.5	28.4
06/20 A	02:00	06:00	60	73	17.2	29.5	60.2	94	93	2.9	10.7
06/20 B	08:00	12:00	168	89	17.8	45.2	72.3	99	127	0.0	23.6
06/23 A	20:00	00:00	110	NA	19.9	26.2	34.1	187	294	0.0	123.7
06/24 A	00:00	03:00	24	NA	14.4	2.5	7.9	51	37	0.0	–0.5
06/24 B	03:00	06:00	67	NA	27.2	18.6	86.9	435	475	0.0	12.9
06/24 C	07:30	08:00	13	318	16.1	6.7	0.0	43	340	0.0	106.8
06/24 D	10:00	14:00	171	194	18.4	19.1	8.8	108	267	0.0	140.5
06/24 E	14:00	18:00	173	162	34.9	48.8	39.5	147	188	38.4	131.8
06/24 F	20:00	00:00	59	447	17.5	26.0	7.6	211	317	0.0	46.7
06/25 A	01:15	05:00	32	297	17.0	6.3	NA	32	338	0.0	17.3
06/25 B	05:00	09:00	5	17	15.3	0.0	NA	7	22	19.1	–0.1
06/25 C	07:57	10:30	90	261	47.3	15.4	0.0	68	314	0.0	162.7
06/25 D	11:00	15:00	99	197	30.4	26.3	0.0	81	255	6.8	133.0
06/25 F	22:00	02:00	53	624	34.9	17.2	7.5	385	291	10.6	41.3
07/06 A	20:00	00:00	122	NA	23.8	26.4	64.4	189	131	0.0	—
07/07 A	00:00	04:00	70	NA	18.0	14.5	67.2	136	125	0.0	21.1
07/12 A	20:00	00:00	15	55	19.9	3.6	0.0	20	55	16.0	49.1
07/13 B	03:00	06:00	17	94	55.9	8.6	20.7	38	70	21.4	79.0
07/13 C	08:00	12:00	69	375	32.9	18.8	0.7	90	182	104.8	158.2
07/13 D	12:00	15:00	76	132	25.6	17.3	2.9	59	135	61.5	80.3
07/13 E	15:00	18:00	44	79	17.7	10.9	0.0	34	79	36.8	38.5
07/13 F	20:10	00:00	21	68	27.4	11.5	0.0	20	94	28.8	22.0
07/14 A	02:00	06:00	14	161	6.8	1.7	0.0	6	180	0.0	6.3
07/14 B	08:00	12:00	61	430	25.4	17.7	0.0	41	448	2.9	166.0
07/14 C	14:00	18:00	73	NA	28.9	16.6	10.8	57	179	45.4	79.9
07/14 D	20:00	00:00	11	0	15.8	3.7	12.7	NA	42	0.0	3.4
07/15 A	02:00	04:00	7	0	5.6	0.0	NA	23	32	0.0	5.9
07/15 B	04:00	06:00	0	NA	0.0	0.0	NA	86	96	0.0	0.9
07/15 C	06:00	08:00	20	NA	7.1	0.9	19.9	124	166	0.0	—
07/15 D	08:00	10:00	7	NA	19.0	0.0	35.0	46	82	0.0	—
07/15 E	10:00	11:30	0	NA	0.0	0.0	NA	16	75	0.0	—
07/15 F	14:00	18:00	24	NA	17.8	7.3	16.3	36	101	19.9	—
07/15 G	20:00	00:00	14	NA	38.8	8.3	26.8	137	200	0.0	—

Concentrations in Aerosol collected at Henninger Flats
during the 1987 Summer SCAQS Study

Date	Seq	Start	Stop	Na^+	NH_4^+	Ca^{2+}	Mg^{2+}	Cl^-	NO_3^-	SO_4^{2-}	NH_3	HNO_3
				neq m^{-3}							– nmole m^{-3} –	
06/19	A	01:00	05:00	5	3	0.1	0.0	0.0	9	5	0.0	12.8
06/19	B	06:00	09:00	0	5	0.0	0.0	0.0	8	5	0.0	10.9
06/19	C	09:00	12:00	1	4	1.4	1.4	0.0	7	7	0.0	17.5
06/24	A	02:00	06:00	33	77	24.3	11.8	2.3	51	74	2.9	65.4
06/24	B	06:00	10:00	36	117	12.5	13.9	0.0	63	102	0.0	161.5
06/24	C	10:00	14:00	134	838	71.3	53.6	28.7	442	533	78.5	812.2
06/24	A	17:00	20:00	107	551	63.9	23.2	0.0	193	446	24.5	479.1
06/24	B	20:00	00:00	59	239	28.3	13.8	NA	114	189	30.7	47.4
06/25	B	14:00	18:00	106	645	92.9	27.3	22.5	287	479	98.6	897.0
06/25	C	20:00	00:00	38	284	32.8	9.4	0.0	83	234	18.4	78.4
06/25	A	02:00	06:00	54	250	34.7	14.8	NA	77	217	10.6	69.4
06/26	A	02:00	06:00	44	188	34.6	12.9	21.2	65	174	20.7	112.7
07/06	A	20:00	00:00	56	193	30.9	13.7	0.0	123	141	0.0	63.1
07/07	A	02:00	06:00	29	75	16.4	7.6	0.0	46	66	0.0	28.4
07/07	B	08:00	12:00	75	421	46.3	22.4	0.0	202	311	6.8	277.8
07/12	A	20:00	00:00	21	93	33.5	9.3	7.8	28	81	26.8	72.9
07/13	A	02:00	06:00	4	27	2.9	4.0	0.0	12	33	9.1	17.4
07/13	B	08:00	12:00	21	183	27.9	13.7	0.0	99	96	91.7	251.2
07/14	A	20:00	00:00	35	151	27.7	13.2	NA	76	116	23.8	—
07/15	A	02:00	06:00	15	111	10.7	4.0	0.0	30	95	1.4	—
07/15	B	08:00	12:00	54	543	38.8	14.8	NA	254	313	58.5	—

Concentrations in Aerosol collected at Kellogg Hill
during the 1987 Summer SCAQS study.

Date Seq	Start	Stop	Na^+	NH_4^+	Ca^{2+}	Mg^{2+}	Cl^-	NO_3^-	SO_4^{2-}	NH_3	HNO_3
			neq m^{-3}							nmole m^{-3}	
06/19 A	01:00	05:00	183	178	73.4	60.3	72.1	190	136	283.0	9.5
06/19 B	06:00	09:00	168	273	95.8	60.8	62.7	226	191	192.2	16.0
06/19 C	09:00	12:00	8	9	62.3	12.0	0.0	10	7	0.0	6.1
06/24 A	02:00	06:00	140	581	64.6	41.9	15.6	452	291	0.0	59.8
06/24 B	06:00	10:00	145	767	153.6	59.8	15.8	582	359	26.8	152.2
06/24 C	10:00	13:50	149	875	192.8	61.6	0.0	567	451	131.9	624.0
06/24 D	20:00	00:00	124	250	78.3	35.8	0.0	234	203	34.6	52.7
06/24 E	02:00	06:00	125	594	109.3	25.6	0.0	392	372	26.8	63.1
06/25 B	20:00	00:00	84	279	51.3	28.2	10.9	191	167	58.5	52.3
06/25 C	02:00	06:00	62	549	40.1	11.1	12.0	372	271	34.6	43.4
06/25 D	08:00	12:00	66	838	116.3	32.2	0.2	496	441	154.9	385.8
06/25 A	08:00	12:00	115	784	179.0	48.8	NA	629	415	279.2	360.8
07/06 A	20:00	00:00	95	258	88.4	20.6	6.8	232	155	65.4	48.2
07/07 A	08:00	12:00	108	383	160.6	39.4	10.8	300	249	46.9	210.7
07/07 B	02:00	06:00	140	494	103.3	41.8	25.6	423	220	35.3	37.8
07/12 A	20:10	00:00	44	139	60.1	16.9	1.3	91	94	146.4	44.0
07/13 A	01:00	05:00	70	177	58.4	21.7	12.4	124	108	102.5	8.8
07/13 B	07:00	11:00	54	368	269.7	53.1	4.9	309	149	339.3	197.4

Concentrations in Cloudwater collected at San Pedro Hill
during the 1987 Summer SCAQS project

Date	Seq	Start	Stop	Vol (ml)	pH	Na^+	NH_4^+	Ca_2^+	Mg_2^+	Cl^-	NO_3^-	SO_4^{2-}
						μN						
6/13	1	20:43	21:22	49	3.28	516	471	88	119	474	855	678
06/13	2	21:22	21:52	53	3.19	369	377	52	166	407	743	661
06/13	3	21:52	23:19	68	3.18	592	496	74	178	558	904	781
06/13	4	23:19	00:20	62	3.08	587	588	70	184	609	957	924
06/14	5	00:20	00:56	48	2.89	688	562	80	214	681	1321	1215
06/14	6	00:56	01:41	56	2.80	647	555	71	190	587	1608	1329
06/14	7	01:41	02:45	57	2.85	706	625	78	202	762	1554	1296
06/14	8	02:45	03:13	47	3.07	731	495	75	214	771	962	899
06/14	9	03:13	03:46	51	3.09	440	376	43	119	465	796	722
06/14	10	03:46	04:09	42	3.00	361	402	38	95	400	893	872
06/14	11	04:09	04:31	44	3.06	265	379	27	64	327	819	736
06/14	12	04:31	04:59	53	3.12	149	323	15	47	247	702	574
06/14	13	04:59	05:40	34	2.98	263	477	27	82	400	993	870
06/14	14	05:40	06:16	34	2.91	536	648	55	155	599	1249	1125
06/14	15	06:16	07:13	18	2.82	734	744	77	208	787	1569	1407
06/19	4	04:48	05:22	36	3	3796	1237	460	731	1701	2137	1125
06/19	5	05:22	06:02	36	3	3405	827	318	634	1672	1603	1131
06/19	6	06:02	07:04	26	3	3258	665	281	593	1654	1281	978
06/20	1	00:29	01:44	59	3.11	2574	555	268	488	1430	1402	1094
06/20	2	01:44	02:28	62	3.14	1768	605	187	410	1384	1088	1046
06/20	3	02:28	03:25	65	3.26	2318	485	173	444	1379	716	783
06/20	4	03:25	04:02	65	3.35	1722	356		388	1421	518	749
06/20	5	04:02	04:42	30	3.35	1740	347		411	1435	498	1232
06/20	6	04:46	05:05	9	3.20		517	272	715	1756	877	1290
06/21	8	00:14	00:55	65	3.48	995	295	142	253	735	915	447
06/21	9	00:55	01:17	66	3.52	822	219	103	199	807	477	359
06/21	10	01:17	01:42	12	3.55	706	169	79	192	837	377	312
06/22	1	00:24	01:13	61	3.43	1257	353	243	311	978	1014	507
06/22	2	01:13	01:41	62	3.37	414	311	66	116	440	547	428
06/22	3	01:41	02:17	62	3.31	297	327	41	75	353	476	381
06/22	4	02:17	02:50	61	3.34	243	355	31	61	289	436	354
06/22	5	02:50	03:27	62	3.36	206	376	27	53	267	458	368
06/22	6	03:27	04:13	62	3.26	214	461	29	54	303	571	465
06/22	7	04:13	05:17	60	3.09	342	640	51	84	436	862	665
06/22	8	05:17	05:34	13	2.89	602	1025	109	168	689	1447	1121
06/22	9	06:00	07:16	60	2.84	578	1126	113	161	611	1632	1478
06/22	1	23:18	23:58	66	3.32	285	371	85	82	334	644	480
06/22	2	23:58	00:26	62	3.44	242	349	81	70	266	479	370
06/23	3	00:26	01:05	62	3.31	212	354	57	60	263	537	459
06/23	4	01:05	01:39	62	3.36	250	348	53	68	307	473	391
06/23	5	01:39	02:15	62	3.49	247	309	44	66	322	334	284
06/23	6	02:15	02:44	61	3.51	255	270	39	67	317	362	333

Concentrations in Cloudwater collected at San Pedro Hill
during the 1987 Summer SCAQS project

Date	Seq	Start	Stop	Vol	pH	Na$^+$	NH$_4^+$	Ca$_2^+$	Mg$_2^+$	Cl$^-$	NO$_3^-$	SO$_4^{2-}$
				(ml)		µN						
06/23	7	02:44	03:07	62	3.54	200	231	30	54	262	298	285
06/23	8	03:07	03:31	62	3.48	196	229	30	54	259	322	318
06/23	9	03:31	03:55	62	3.54	174	234	24	47	231	296	269
06/23	10	03:55	04:18	62	3.50	181	264	27	48	226	349	320
06/23	11	04:18	04:49	62	3.50	162	295	24	42	290	424	352
06/23	12	04:49	05:16	62	3.62	141	280	18	38	196	277	224
06/23	13	05:16	05:41	61	3.55	136	239	19	37	189	320	283
06/23	14	05:41	06:07	62	3.56	123	223	17	33	173	301	288
06/23	15	06:07	06:29	62	3.58	131	233	20	35	177	307	277
06/23	16	06:29	06:54	62	3.58	130	226	21	36	184	297	269
06/23	17	06:54	07:20	62	3.52	148	272	23	40	203	323	293
06/23	18	07:20	07:43	62	3.47	169	308	28	45	218	388	371
06/23	19	07:43	08:06	62	3.43	171	293	30	47	226	392	358
06/23	20	08:06	10:27	62	3.15	452	528	95	131	505	1024	608
06/23	1	19:55	20:47	30	2.53	2941	1659	527	561	1574	5623	3246
06/23	8	22:30	23:18	61	2.64	3148	1510	560	601	1548	5240	2846
06/23	9	23:18	00:21	53	2.57	2953	1725	505	577	1613	5267	2934
06/24	10	00:36	01:09	61	2.62	1289	1520	240	313	924	3617	2291
06/24	11	01:09	01:33	61	2.82	446	789	78	134	492	1770	1341
06/24	12	01:33	02:04	61	2.79	276	726	45	82	393	1586	1329
06/24	13	02:04	02:31	61	2.81	236	843	38	68	339	1667	1254
06/24	14	02:31	03:03	61	2.77	225	1443	48	68	386	2171	1493
06/24	15	03:03	03:38	61	2.71	295	2147	55	84	466	2715	2053
06/24	16	03:38	04:12	61	2.75	298	2859	60	86	505	2757	2501
06/24	17	04:12	04:42	61	2.75	284	2441	48	79	476	2618	2205
06/24	18	04:42	05:03	61	2.86	350	1465	50	96	441	1849	1561
06/24	19	05:03	05:17	62	2.94	249	966	30	65	360	1291	1119
06/24	20	reservoir		66	2.84	189	1748	33	57	309	2073	1538
06/24	20B	reservoir		64	2.83	194	1916	34	58	318	2108	1587
06/24	21	06:41	07:08	60	2.81	189	2088	36	56	400	2095	1853
06/24	22	07:08	07:56	60	2.76	230	2150	45	68	397	2340	1951
06/24	23	07:56	08:21	60	2.78	257	1448	46	71	390	2000	1540
06/24	24	08:21	08:32	20	2.78	294	1310	88	104	409	2100	1521
06/24	25	08:32	08:56	61	2.77	454	1272	107	136	539	2074	1588
06/24	26	08:56	09:14	61	2.88	273	462	—	67	478	1526	1224
06/24	27	09:14	09:33	61	2.92	385	595	—	91	477	1434	1125
06/24	28	09:33	10:42	60	2.65	1790	1457	—	377	1365	3521	2358
06/24	29	10:42	11:19	17	2.60	1803	1341	—	406	1396	3602	2452
06/24	1	19:39	23:02	11	2.66	1618	9383	1143	1151	2096	8191	5796
06/25	3	00:37	01:04	66	2.63	594	1855	200	135	400	3658	2438
06/25	4	01:04	01:33	66	2.67	810	1915	239	173	488	3481	2422
06/25	5	01:33	01:53	67	2.73	708	1242	193	159	440	2646	1815
06/25	6	01:53	02:07	67	2.72	395	724	77	81	270	1471	1105
06/25	7	02:07	02:20	67	3.09	244	470	43	53	176	832	662

Concentrations in Cloudwater collected at San Pedro Hill
during the 1987 Summer SCAQS project

Date	Seq	Start	Stop	Vol	pH	Na^+	NH_4^+	Ca_2^+	Mg_2^+	Cl^-	NO_3^-	SO_4^{2-}
				(ml)		μN						
06/25	8	02:20	02:31	67	3.11	205	410	38	50	157	845	711
06/25	9	02:31	02:42	67	3.11	270	429	55	61	184	870	741
06/25	10	02:42	02:56	67	3.04	177	509	30	40	132	891	660
06/25	11	02:56	03:12	67	2.87	158	1078	32	37	174	1805	1120
06/25	12	03:12	03:14	10	2.88	142	1031	33	37	162	1837	1095
06/25	13	03:16	03:41	68	2.74	171	1270	36	44	230	2583	1528
06/25	14	03:45	03:53	18	2.66	273	1753	57	66	276	3270	1896
06/25	15	03:57	04:06	26	2.67	289	1708	52	66	265	3020	1828
06/25	16	04:09	04:17	20	2.65	315	1631	60	72	281	4000	1854
06/25	17	04:20	04:27	23	2.70	224	1064	55	65	272	2823	1688
06/25	18	04:30	04:37	21	2.73	289	1423	54	69	295	2490	1702
06/25	19	04:39	04:45	13	2.71	434	1735	88	86	364	2888	2106
06/25	20	04:48	04:52	10	2.67	541	1779	113	105	386	3089	2185
06/25	21	04:55	05:04	19	2.65	611	1684	115	110	407	3233	2222
06/25	22A	reservoir		67	2.74	512	1955	90	91	476	2575	2234
06/25	22B	reservoir		44	2.76	520	1736	88	96	468	2362	2058
06/25	23	05:17	07:33	17	2.64	1266	2373	270	256	838	3435	3229
06/26	1	01:48	02:08	33	2.99	315	1979	164	86	213	2462	1528
06/26	2	02:08	02:19	39	3.26	113	1704	41	30	89	1445	1045
06/26	3	02:19	02:30	40	3.33	87	906	19	18	77	822	713
06/26	4	02:30	02:57	37	3.30	168	1035	43	39	84	1054	762
06/26	5	02:57	03:06	33	3.27	83	1363	22	24	43	912	645
06/26	6	03:06	03:15	36	3.36	49	1124	13	16	51	1015	747
06/26	7	03:15	03:24	32	3.39	67	1119	23	23	88	1096	810
06/26	8	03:24	03:39	64	3.42	103	1415	22	26	87	1113	823
06/26	9	03:39	03:53	68	3.48	41	879	17	16	55	814	590
06/26	10	03:53	04:04	39	3.48	98	593	19	24	106	572	534
06/26	11	04:04	04:24	66	3.51	114	479	27	30	94	489	461
06/26	12	04:24	04:43	65	3.47	59	423	12	17	58	454	387
06/26	13	04:43	05:00	69	3.43	41	478	11	13	51	560	393
06/26	14	05:00	05:14	64	3.40	28	585	9	11	49	718	482
06/26	15	05:14	05:27	63	3.38	33	709	8	10	47	750	496
06/26	16	05:27	05:45	69	3.24	46	943	10	13	64	1051	680
06/26	17	05:45	05:58	68	3.28	36	886	9	10	78	955	643
06/26	18	05:58	06:12	69	3.28	31	787	8	11	65	966	663
06/26	19	06:12	06:26	63	3.26	36	1026	13	12	66	1055	748
06/26	20A	reservoir		65	3.06	169	1977	38	43	196	1626	1553
06/26	20B	reservoir		69	3.00	160	1818	46	49	223	1998	1971
07/01	1	20:34	21:57	29	3.18	912	638	215	248	745	1138	836
07/01	4	22:07	22:10	8	3.15	618	613	159	176	544	936	775
07/01	8	22:33	22:39	13	3.15	386	522	97	108	366	722	658
07/01	10	22:51	22:56	10	3.18	336	496	79	90	339	682	585
07/01	11	22:59	23:08	17	3.19	372	566	88	99	378	704	666
07/01	13	23:19	23:24	11	3.23	348	545	80	90	351	605	609
07/01	20	reservoir			385	242	57	90	453	401	435	

Concentrations in Cloudwater collected at San Pedro Hill
during the 1987 Summer SCAQS project

Date	Seq	Start	Stop	Vol (ml)	pH	Na^+	NH_4^+	Ca_2^+	Mg_2^+	Cl^-	NO_3^-	SO_4^{2-}
						μN						
07/02	1	20:00	21:10	60	3.19	528	494	95	133	510	713	636
07/02	2	21:10	22:46	34	3.30	379	394	79	93	400	535	492
07/03	3	00:06	00:55	62	2.91	683	2132	286	202	438	3206	1546
07/03	4	00:55	01:32	61	2.99	345	2309	125	96	327	2325	1464
07/03	5	01:32	02:48	52	2.60	515	2770	209	158	532	4131	2562
07/03	6	02:51	03:50	61	2.47	487	2568	167	149	562	4656	3028
07/03	7	03:50	04:35	62	2.61	392	2156	118	110	488	3278	2305
07/03	8	04:35	05:12	60	2.67	377	1725	98	105	454	2748	1903
07/03	9	05:12	05:46	61	2.64	405	1557	100	115	479	2994	1959
07/03	10	05:46	06:22	60	2.63	308	1682	72	83	440	2924	2030
07/03	11	06:22	06:53	59	2.61	315	1195	71	83	365	2874	1691
07/03	12	06:53	07:25	58	2.58	355	1037	82	95	381	2973	1687
07/03	13	07:25	08:16	58	2.48	446	1426	110	124	491	3823	2340
07/03	14	08:16	09:08	20	2.42	672	1693	186	192	656	4631	2957
07/07	1	00:54	01:29	66	3.33	647	1108	127	145	582	1301	810
07/07	2	01:29	01:47	57	3.31	388	544	61	88	406	812	588
07/07	3	01:47	02:02	58	3.34	235	320	28	53	284	554	455
07/07	4	02:02	02:24	61	3.25	280	347	32	65	341	669	523
07/07	5	02:24	03:06	62	3.14	647	433	56	135	734	790	722
07/07	6	03:06	03:40	61	3.51	503	266	36	106	591	332	384
07/07	7	03:40	04:21	23	3.44	719	296	57	156	821	488	454
07/08	1	00:48	01:59	65	2.81	1365	2458	508	335	1055	3419	2647
07/08	2	01:59	02:26	57	2.87	798	1875	213	208	623	2446	1878
07/08	3	02:26	02:48	60	2.93	498	926	126	123	363	1557	1123
07/08	4	02:48	03:10	61	3.02	467	683	100	111	355	1211	932
07/08	5	03:10	03:31	59	3.08	287	431	54	65	290	915	686
07/08	6	03:31	03:54	56	3.12	314	424	56	70	353	901	606
07/08	7	03:54	04:18	60	3.04	274	428	45	61	294	1088	687
07/08	8	04:18	04:19	4	3.91	59	88	20	15	71	172	143
07/08	9	04:19	04:52	1	3.91							
07/08	10	04:52	04:52	59	3.00	303	481	51	68	331	1208	697
07/08	17	unknown		58	2.86	888	808	166	208	760	2142	1190
07/13	1	02:48	03:25	36	3.79	223	210	52	57	264	217	230
07/13	2	03:25	04:07	9	3.83	204	240	45	57	242	174	230
07/14	1	01:56	02:14	39	3.65	82	220	32	28	120	180	292
07/14	2	02:14	02:24	37	3.75	68	167	17	19	95	136	217
07/14	3	02:24	02:33	35	3.68	97	198	23	28	163	154	243
07/14	4	02:33	02:41	38	3.78	149	161	21	35	174	135	218
07/14	5	02:41	02:53	59	3.83	134	140	16	30	171	146	231
07/14	6	02:53	03:02	38	3.86	147	129	17	34	170	113	194
07/14	7	03:02	03:12	38	3.83	133	153	15	31	153	120	219
07/14	8	03:12	03:22	37	3.80	87	191	13	24	123	128	236
07/14	9	03:22	03:30	36	3.81	77	186	13	22	113	130	227
07/14	10	03:30	03:38	44	3.91	98	148	16	26	132	112	182

Concentrations in Cloudwater collected at San Pedro Hill
during the 1987 Summer SCAQS project

Date	Seq	Start	Stop	Vol	pH	Na^+	NH_4^+	Ca_2^+	Mg_2^+	Cl^-	NO_3^-	SO_4^{2-}
				(ml)		μN						
07/14	11	03:38	03:47	36	3.82	97	154	13	25	135	127	204
07/14	12	03:47	03:56	39	3.81	85	150	13	24	123	129	202
07/14	13	03:56	04:07	46	3.79	65	159	13	19	100	132	196
07/14	14	04:07	04:19	38	3.61	64	224	19	19	100	209	291
07/14	15	04:19	04:33	40	3.34	84	568	34	27	124	547	572
07/14	16	04:33	04:45	38	3.32	89	659	39	28	135	592	622
07/14	17	04:45	04:55	38	3.32	79	683	40	25	134	549	618
07/14	18	04:55	05:06	39	3.33	78	748	42	25	147	559	670
07/14	19	05:06	05:17	38	3.32	96	977	50	29	180	597	757
07/14	20	reservoir		65	3.14	204	694	55	57	240	600	820
07/14	21	reservoir		29	3.13	207	669	53	59	239	592	814
07/14	1	19:06	19:54	40	3.26	164	391	77	47	154	589	473
07/14	2	19:54	20:21	38	3.23	162	391	44	41	206	541	521
07/14	3	20:21	20:39	37	3.41	147	313	33	36	161	364	413
07/14	4	20:39	20:54	39	3.47	132	254	29	32	137	305	355
07/14	5	20:54	21:11	40	3.48	121	215	22	29	125	251	306
07/14	6	21:11	21:26	41	3.50	122	194	18	28	152	243	293
07/14	7	21:26	21:39	39	3.53	96	182	15	25	123	221	272
07/14	8	21:39	21:51	39	3.54	140	197	22	32	138	245	295
07/14	9	21:51	22:03	37	3.58	177	194	27	38	173	238	272
07/14	10	22:03	22:14	38	3.67	180	173	22	38	174	199	244
07/14	11	22:14	22:26	41	3.62	193	169	24	42	186	209	268
07/14	12	22:26	22:36	38	3.58	185	176	28	41	192	235	302
07/14	13	22:36	22:46	40	3.63	177	145	23	39	165	192	259
07/14	14	22:46	22:56	40	3.69	174	138	22	38	168	172	230
07/14	15	22:56	23:06	41	3.73	193	131	25	42	186	167	212
07/14	16	23:06	23:17	38	3.68	191	152	28	43	173	197	240
07/14	17	23:17	23:37	38	3.41	216	264	42	51	190	383	390
07/14	18	23:37	23:49	38	3.25	267	377	66	65	272	602	550
07/14	19	23:49	00:01	42	3.38	225	299	44	53	187	449	401
07/14	20A	reservoir			3.44	52	205	17	18	57	325	284
07/14	20B	reservoir			3.43	40	201	10	13	87	316	285
07/15	2	13:18	13:38	18	2.98	242	764	199	79	315	857	1417
07/15	3	19:45	20:50	54	3.28	224	754	197	76	181	565	1074
07/15	4	20:50	21:18	12	3.23	172	746	158	61	245	621	995
07/15	5	22:00	22:43	55	3.05	271	1141	236	100	357	1013	1583
07/15	6	22:43	23:09	55	3.00	145	828	134	51	139	927	1214
07/15	7	23:09	23:33	56	3.07	89	538	81	34	117	674	876
07/15	8	23:33	23:56	55	3.08	79	482	68	30	120	685	805
07/15	9	23:56	00:55	55	2.64	198	2161	235	71	217	2797	2438
07/16	10	00:55	01:11	55	2.86	157	1225	165	58	218	1528	1438
07/16	11	01:11	01:25	56	3.04	101	606	90	36	158	880	872
07/16	12	01:25	01:38	56	3.14	65	427	55	24	112	640	643
07/16	13	01:38	01:53	59	3.12	55	507	52	22	110	699	684
07/16	14	01:53	02:10	55	3.14	29	404	29	13	61	591	630

Concentrations in Cloudwater collected at San Pedro Hill
during the 1987 Summer SCAQS project

Date	Seq	Start	Stop	Vol (ml)	pH	Na^+	NH_4^+	Ca_2^+	Mg_2^+	Cl^-	NO_3^-	SO_4^{2-}
						μN						
07/16	15	02:10	02:28	56	3.16	22	391	21	10	40	547	548
07/16	16	02:28	02:44	56	3.27	28	330	31	12	47	448	438
07/16	17	Reservoir		68	3.93	24	328	14	8	47	190	219
07/16	2	15:35	16:07	55	3.56	84	284	—	—	84	249	259
07/16	3	16:07	16:19	55	3.74	33	160	—	—	50	147	215
07/16	4	16:19	16:45	25	3.67	33	142	—	—	44	167	203
07/16	5	17:40	18:30	55	3.50	92	207	—	—	98	280	277
07/16	6	18:30	19:02	27	3.64	63	187	27	22	70	231	248
07/16	7	19:14	19:37	56	3.51	75	242	47	28	88	295	329
07/16	8	19:37	19:49	56	3.55	52	126	—	—	55	145	295
07/16	9	19:49	20:03	26	3.86	35	98	13	11	39	116	170
07/16	10	20:03	20:18	56	4.06	24	80	9	7	30	96	114
07/16	11	20:18	20:33	55	4.14	20	70	8	7	28	84	93
07/16	12	20:33	20:50	56	4.15	20	66	9	7	27	77	104
07/16	13	20:50	21:04	56	4.30	19	56	8	6	25	53	74
07/16	14	21:04	21:25	56	4.48	16	66	—	—	23	43	58
07/16	15	21:25	21:43	55	4.58	10	80	—	—	21	37	69
07/16	16	21:43	22:04	56	4.32	8	71	—	—	14	35	77
07/16	17	22:04	22:23	56	4.46	9	53	—	—	11	34	60
07/16	18	22:23	22:40	55	4.98	6	47	3	1	13	28	39
07/16	19	22:40	22:53	56	4.75	11	44	5	3	14	30	55
07/17	20	reservoir		33	3.80	49	504	—	—	79	300	376
07/17	21	reservoir		34	4.65	45	134	—	—	56	60	98

Concentrations in Cloudwater collected at San Pedro Hill during the 1987 Summer SCAQS Study — continued

Date	Seq	Start	Stop	CH_2O	H_2O_2	HFo	HAc
				μM			
06/19	4	04:48	05:22	25			
06/19	5	05:22	06:02	31			
06/19	6	06:02	07:04	27			
06/20	1	00:29	01:44	31			
06/20	2	01:44	02:28	24			
06/20	3	02:28	03:25	21			
06/20	4	03:25	04:02	21			
06/21	8	00:14	00:55	14			
06/21	9	00:55	01:17	12			
06/22	1	00:24	01:13	11			
06/22	2	01:13	01:41	12			
06/22	3	01:41	02:17	15			
06/22	4	02:17	02:50	14			
06/22	5	02:50	03:27	15			
06/22	6	03:27	04:13				
06/22	7	04:13	05:17	20			
06/22	8	05:17	05:34				
06/22	9	06:00	07:16	27			
06/23	1	19:55	20:47	35			
06/23	8	22:30	23:18	26			
06/23	9	23:18	00:21	22			
06/24	10	00:36	01:09	26			
06/24	11	01:09	01:33	18			
06/24	12	01:33	02:04	19			
06/24	13	02:04	02:31	23			
06/24	14	02:31	03:03	30			
06/24	15	03:03	03:38	31			
06/24	16	03:38	04:12	49			
06/24	17	04:12	04:42	46			
06/24	18	04:42	05:03	31			
06/24	19	05:03	05:17	29			
06/24	20B	reservoir		47			
06/24	21	06:41	07:08	43			
06/24	22	07:08	07:56	45			
06/24	23	07:56	08:21	46			
06/24	24	08:21	08:32	51			

Concentrations in Cloudwater collected at San Pedro Hill during the 1987 Summer SCAQS Study — continued

Date	Seq	Start	Stop	CH_2O	H_2O_2	HFo	HAc
						μM	
06/24	25	08:32	08:56	36			
06/24	26	08:56	09:14	29			
06/24	27	09:14	09:33	30			
06/24	28	09:33	10:42	34			
06/25	3	00:37	01:04	35			
06/25	4	01:04	01:33	37			
06/25	5	01:33	01:53	31			
06/25	6	01:53	02:07	24			
06/25	7	02:07	02:20	16			
06/25	8	02:20	02:31	16			
06/25	9	02:31	02:42	17			
06/25	10	02:42	02:56	30			
06/25	11	02:56	03:12	30			
06/25	12	03:12	03:14				
06/25	13	03:16	03:41	34			
06/25	14	03:45	03:53				
06/25	15	03:57	04:06	28			
06/25	16	04:09	04:17				
06/25	17	04:20	04:27	22			
06/25	18	04:30	04:37	23			
06/25	19	04:39	04:45				
06/25	20	04:48	04:52				
06/25	21	04:55	05:04				
06/25	22A	reservoir		25			
06/25	22B	reservoir		24			
06/25	23	05:17	07:33				
07/07	1	00:54	01:29	20	4		
07/07	2	01:29	01:47	15	9		
07/07	3	01:47	02:02	14	18		
07/07	4	02:02	02:24	18	13		
07/07	5	02:24	03:06	22	54		
07/07	6	03:06	03:40	13	61		
07/07	7	03:40	04:21	12	72		
07/13	1	02:48	03:25	10	47	15	6
07/13	2	03:25	04:07	17	6		
07/14	1	01:56	02:14	9	16	8	
07/14	2	02:14	02:24				
07/14	3	02:24	02:33	8	14	8	
07/14	4	02:33	02:41				
07/14	5	02:41	02:53	5	13	6	
07/14	6	02:53	03:02				
07/14	7	03:02	03:12	6	13	6	
07/14	8	03:12	03:22				

Concentrations in Cloudwater collected at San Pedro Hill during the 1987 Summer SCAQS Study — continued

Date	Seq	Start	Stop	CH_2O	H_2O_2	HFo	HAc
				µM			
07/14	9	03:22	03:30	9	12	6	
07/14	10	03:30	03:38				
07/14	11	03:38	03:47	7	14	6	
07/14	12	03:47	03:56				
07/14	13	03:56	04:07	18	15	7	
07/14	14	04:07	04:19				
07/14	15	04:19	04:33	27	18	11	
07/14	16	04:33	04:45				
07/14	17	04:45	04:55	38	22	14	
07/14	18	04:55	05:06				
07/14	19	05:06	05:17	8	34	18	
07/14	20	reservoir		28	27	31	
07/14	21	reservoir					
07/14	1	19:06	19:54	15	31	43	22
07/14	2	19:54	20:21				
07/14	3	20:21	20:39	10	53	35	13
07/14	4	20:39	20:54				
07/14	5	20:54	21:11				
07/14	6	21:11	21:26	6	62	20	9
07/14	7	21:26	21:39				
07/14	8	21:39	21:51				
07/14	9	21:51	22:03	6	62	20	9
07/14	10	22:03	22:14				
07/14	11	22:14	22:26				
07/14	12	22:26	22:36	9	53	17	7
07/14	13	22:36	22:46				
07/14	14	22:46	22:56				
07/14	15	22:56	23:06	10	62	16	7
07/14	16	23:06	23:17				
07/14	17	23:17	23:37				
07/14	18	23:37	23:49	14	49	29	11
07/14	19	23:49	00:01				
07/14	20A	reservoir					
07/14	20B	reservoir		13	19	21	9